ЖУРНАЛ
ЭКСПЕРИМЕНТАЛЬНОЙ И ТЕОРЕТИЧЕСКОЙ
ФИЗИКИ
АКАДЕМИЯ НАУК СССР

SOVIET PHYSICS

JETP

Volume 36 (9) NUMBER 4

A Translation

of the

Journal of Experimental and Theoretical Physics

of the

Academy of Sciences of the USSR

Volume 36

OCTOBER, 1959

Published by the

AMERICAN INSTITUTE OF PHYSICS
INCORPORATED

SOVIET PHYSICS
JETP

A translation of the Journal of Experimental and Theoretical Physics of the USSR.

A publication of the

AMERICAN INSTITUTE OF PHYSICS

Governing Board

RALPH A. SAWYER, *Chairman*

Members:

WALTER S. BAIRD
JESSE W. BEAMS
RAYMOND T. BIRGE
R. H. BOLT
HARVEY BROOKS
J. W. BUCHTA
J. H. DILLON
VERNET E. EATON
HERBERT A. ERF
IRVINE C. GARDNER
S. A. GOUDSMIT
WINSTON E. KOCK
R. BRUCE LINDSAY
WALTER C. MICHELS
G. E. PAKE
R. RONALD PALMER
JOSEPH B. PLATT
RALPH A. SAWYER
H. D. SMYTH
JOHN STRONG
GEORGE E. UHLENBECK

Administrative Staff

ELMER HUTCHISSON
Director

HENRY A. BARTON
Associate Director

WALLACE WATERFALL
Secretary and Treasurer

THEODORE VORBURGER
Advertising Manager

RUTH F. BRYANS
Publication Manager

ALICE MASTRO
Circulation Manager

KATHRYN SETZE
Assistant Treasurer

EUGENE H. KONE
Director of Public Relations

EDWARD P. TOBER
Manager, Production and Distribution

W. C. KELLY
Director of Education Projects

EMILY WOLF
Office Manager

American Institute of Physics Advisory Board on Russian Translations

ROBERT T. BEYER, *Chairman*
J. GEORGE ADASHKO, FREEMAN DYSON, DWIGHT GRAY,
MORTON HAMERMESH, HAROLD F. WEAVER

Editor of SOVIET PHYSICS—JETP

J. GEORGE ADASHKO, 25 WEST 81ST ST., NEW YORK 24, NEW YORK

SOVIET PHYSICS—JETP is a monthly journal published by the American Institute of Physics and contains a complete translation of the JOURNAL OF EXPERIMENTAL AND THEORETICAL PHYSICS of the U.S.S.R. Academy of Sciences.

This translating and publishing project was undertaken by the institute in the conviction that dissemination of the results of researches everywhere in the world is invaluable to the advancement of science. The NATIONAL SCIENCE FOUNDATION of the United States has encouraged the project initially and is supporting it in large part by a grant.

The American Institute of Physics and its translators propose to translate faithfully all the material appearing in the original articles. The views expressed in the translations are therefore those of the original authors, and not those of the translators nor of the American Institute of Physics.

Volume 1 of SOVIET PHYSICS—JETP corresponds to Russian Volume 28 (1955). Two volumes are published annually, each of six issues. Each volume contains the translation of one volume of the JOURNAL OF EXPERIMENTAL AND THEORETICAL PHYSICS.

Beginning with Vol. 9 (36), the transliteration of the names of Russian authors follows British Standard 2979, which is being adopted in 1959 by a large number of scientific journals in the United States. The Library of Congress transliteration is followed in the earlier volumes.

Subscription Prices

Per Year (12 issues)

General:

United States and Canada	$75.00
Elsewhere	79.00

Libraries and non-profit degree-granting Institutions:

United States and Canada	$35.00
Elsewhere	39.00
Back Numbers	$ 8.00

Subscriptions should be addressed to the American Institute of Physics, 335 East 45th Street, New York 17, New York.

SOVIET PHYSICS, JETP is published monthly by the American Institute of Physics, Inc. Second Class postage paid at Ann Arbor, Michigan.

Copyright by American Institute of Physics 1959

SOVIET PHYSICS

JETP

A translation of the Journal of Experimental and Theoretical Physics of the USSR.

SOVIET PHYSICS JETP VOL. 36 (9) NO. 4, pp. 685-947 OCTOBER, 1959

OSCILLATIONS OF A PLASMA IN A MAGNETIC FIELD AT FREQUENCIES CLOSE TO THE CYCLOTRON FREQUENCY

V. N. LAZUKIN

Moscow State University

Submitted to JETP editor January 13, 1958

J. Exptl. Theoret. Phys. (U.S.S.R.) **36**, 969-975 (April, 1959)

A description is given of a method used to observe oscillations of a plasma in a longitudinal magnetic field at frequencies several times smaller than the ion cyclotron frequencies. The method makes it possible to observe the oscillation spectrum in the form of a series of narrow lines with very high signal-to-noise ratio. It is suggested that the observed oscillations are analogous to the waves known from the hydromagnetic analysis.

THE instabilities of plasmas in magnetic fields have been considered theoretically by many authors.[1] However a number of the questions in this field have not been answered in as much detail as might be desired. This situation is due to the fact that there is a large variety of complicated effects which make it essentially impossible to carry out a systematic theoretical investigation of the problem and the fact that the experimental data are very scanty and are not always amenable to theoretical interpretation. The latter circumstance arises from the difficulties involved in realizing the conditions of observation required by the theory. The instabilities of plasmas in magnetic fields are of the utmost importance, particularly as regards practical applications. In this connection the observations described below may be of interest. The results reported here are to be considered of preliminary nature only.

APPARATUS AND METHOD OF OBSERVATION

A diagram of the apparatus, which was originally intended for the observation of ion cyclotron resonances in helium plasmas and hydrogen plasmas, is shown in Fig. 1. The principle of operation is similar to that used for the observation

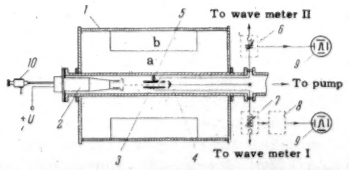

FIG. 1. Diagram of the apparatus. 1) solenoid: a) magnetizing winding, b) modulation winding; 2) ion source; 3) condenser; 4) collector; 5) proton probe; 6) magnetometer oscillator; 7) cyclotron resonance oscillator; 8) amplifier; 9) oscilloscopes; 10) needle valve for admitting gas.

nuclear magnetic resonance effects:[2,3] the absorption of radio frequency power by ions which rotate in a magnetic field is detected by the change in Q of an oscillator circuit. A powerful oil-cooled solenoid produces an axial magnetic field and the cold-cathode source is located at the axis of the field;* the source is a Penning discharge (Fig. 2). Collisions of ions extracted from the discharge chamber with gas molecules along the axis of the solenoid lead to the formation of a

*The source was designed by V. G. Gel'kovskiĭ and built under his direction at one of the Institutes of the Academy of Sciences, U.S.S.R.

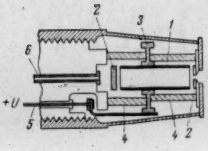

FIG. 2. Diagram of the ion source. 1) molybdenum cathode; 2) magnesium anodes; 3) rod cathode; 4) quartz insulators; 5) feed-through for cathode voltage; 6 gas inlet.

pinched plasma 3 — 5 mm in diameter and approximately 20 cm long. The pinch passes between the plates of a long plane condenser which is connected to the oscillator circuit; the plasma beam then strikes a collector which is connected to meters which measure the ion current and the electron current of the pinch. These measurements indicate that both currents are equal, varying from 10 to 35 μa depending on the mode of operation of the system. When the oscillator frequency coincides with the rotational frequency of ions of a given mass in the applied magnetic field a fraction of the radio frequency power is absorbed by the ions located between the plates of the condenser at a given instant of time. This absorption causes a reduction in the Q of the circuit and this effect is detected by the usual radio spectroscopy method: the magnetic field is modulated and the detected signal is applied to an oscilloscope whose sweep is synchronized with the modulation. On the outer side of one of the plates of the condenser there is a probe which is used to make proton measurements of the magnetic field strength. Measurements show that at the discharge (between the source and the collector) the field inhomogeneity is less than 1 — 1.5% (for fields of 2,000 to 3,000 oersteds); in the section occupied by the condenser the magnetic field variation is less than 0.25%. The magnetic field is modulated at 50 cps at an amplitude of 70 oersteds. A controlled leak (needle valve) of simple design is used to control the admission of gas into the system, making it possible to vary the pressure over wide limits and to maintain the pressure at a given value when desired.

The first observations in the hydrogen plasma showed that in addition to the very wide cyclotron resonances (due to the atomic and molcecular hydrogen ions) there were strong narrow signals (Fig. 3) which could be observed at lower values of the magnetic field. These lines are observed in groups, with different spacings between neighboring lines, with intensities which fall off uniformly with increasing frequency. It is also observed that similar signals appear on the screen of the oscilloscope used for the proton measurement of the magnetic field (Fig. 4). We believe that the observed signals, which are different

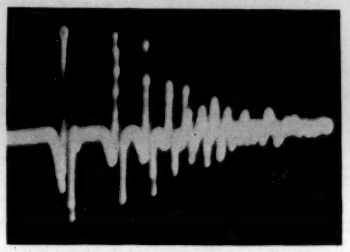

FIG. 3. Signals observed together with the cyclotron resonance signals in a hydrogen plasma. $p = 6 \times 10^{-4}$ mm Hg; H = 1276 oersteds; U = 560 v.

from the cyclotron resonance signals, are due to oscillations of the plasma. The alternating electric fields produced in the vicinity of the plasma as a result of these oscillations are picked up by the oscillator condenser used to detect the plasma resonance by the probe of the proton magnetometer, which operate as antennas; the oscillators themselves, under favorable conditions, act as narrow-band tunable receivers.

In order to obtain more meaningful measurements the following changes were made in the detection system. The condenser was replaced by antennas in the form of rods or loops: these antennas were oriented in different positions with respect to the beam. The antennas were placed at distances such that they could not be struck by electrons or ions from the beam. The antennas were connected to a narrow-band receiver or to a wide-band amplifier. In order to avoid the effect of the above-mentioned parasitic signals on the screen of the proton magnetometer oscilloscope the probe of this unit was shielded.

In the observations made with the first method, when the magnetic field modulation was applied signals similar to those shown in Fig. 3 were

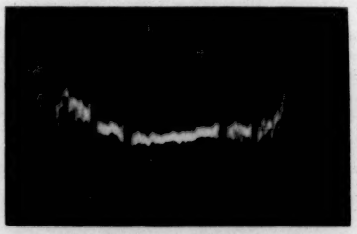

FIG. 4. View of the signals on the screen of the proton magnetometer oscilloscope. $p = 6 \times 10^{-4}$ mm Hg; H = 1180 oersteds; U = 530 v.

observed. In the observations made with the second method, in which no magnetic field modulation was used, reproducible periodic sinusoidal or saw-tooth curves were obtained on the screen. It was observed that the saw-tooth pulses of different intensity were produced only when the magnetic field modulation was applied in certain cases. The oscillation frequencies were measured by means of the receiver frequency meter or by making comparisons with a frequency standard. The intensities of the lines were determined by measurements of the heights of the signals on the screen of an oscilloscope to the input of which a current divider was connected.

RESULTS OF THE OBSERVATIONS

The signals shown in Fig. 3 were first observed in a hydrogen plasma at pressures of the order of 10^{-5} mm Hg (the pressure in the source discharge was a half an order of magnitude higher). Using the improved methods of detection described above it was possible to obtain a well-defined spectral pattern (Figs. 5 and 6) and to carry out the measurements reported here.

It was found that the signals were produced at pressures ranging from 10^{-1} to 10^{-5} mm Hg over a relatively narrow range of magnetic field values

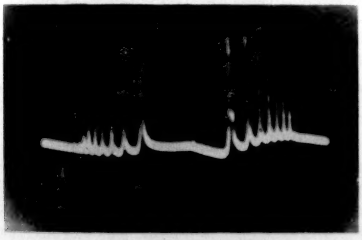

FIG. 5. Higher harmonics observed with a narrow-band receiver; $p = 2 \times 10^{-4}$ mm Hg, H = 1523 oersteds, U = 560 v; modulation amplitude 60 oersteds.

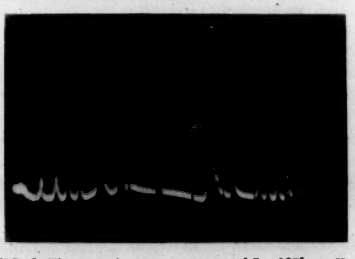

FIG. 6. The same but at a pressure of 5×10^{-3} mm Hg.

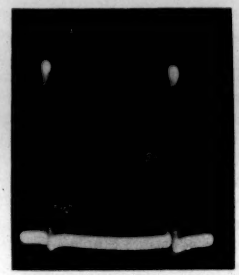

FIG. 7 One of the harmonics ($\nu = 1{,}440$ Mcs) of the oscillations in the field of 1,420 oersteds; $p = 5 \times 10^{-4}$ mm Hg; U = 650 v; modulation amplitude approximately 15 oersteds.

(900 to 1600 oersteds); no signals were observed beyond these limits. In the hydrogen plasma there are three clearly defined series of lines which are superimposed on each other but are very different in intensity. Within each series the intensity of the lines falls off approximately linearly with frequency; within a given series the lines are equally spaced. By varying the magnetic field with the detection system fixed at a given frequency or by tuning the detection system with the magnetic field fixed it is possible to observe the entire spectra. Several tens of lines are observed in the total spectrum. An idea of the shape of a line can be obtained from Fig. 7. In the region in which the signals are observed there is almost no noise but beyond this region the noise level is generally high. At certain values of pressure and magnetic field the intensity of the most sharply defined signals has a signal-to-noise ratio of $10^3 - 10^4$.

The measurements indicate that within the limits of the experimental accuracy the frequencies for lines of a given series are multiples of some base frequency. The intensities of the lines of the same series falls off approximately linearly while the intensity of nearby lines, associated with different series, is very different. In Table I

TABLE I

Line number	Frequency, Mcs	Relative intensity	Line number	Frequency, Mcs	Relative intensity
1	0.121	0.008	10	1.270	0.001
2	0.1816	0.012	11	1.453	0.650
3	0.242	0.005	12	1.815	0.540
4	0.363	1.000	13	2.172	0.453
5	0.484	0.003	14	2.541	0.365
6	0.544	0.003	15	2.912	0.244
7	0.726	0.880	16	3.270	0.140
8	0.908	0.002	17	3.643	0.048
9	1.088	0.740			

we show the frequencies of the first seventeen lines of the spectrum observed in a hydrogen plasma at a pressure of 2×10^{-4} mm Hg in a field of 1523 oersteds; estimates of the relative intensities are also given. It is apparent that the frequencies of the most intense lines are multiples of 0.363 Mcs, i.e., the frequency of the first line (line 4 of Table I), and that in addition to these harmonics there are much weaker lines whose frequencies do not fall in this series. These lines are to be associated with two other series in the spectrum. At pressures an order of magnitude lower, by a suitable choice of source cathode voltage it is possible to obtain still weaker lines; the frequencies of these lines are so close to the fundamental frequency that they are not considered multiples.

The frequencies of all lines are found to be highly dependent on the parameters characterizing the mode of operation of the system. The frequency increases nonlinearly with pressure. The relation between these quantities in the region of most rapid change is shown in Fig. 8. The dependence of frequency on the potential of the cathode in the source is almost linear, as is apparent from Fig. 9. At the present time, be-

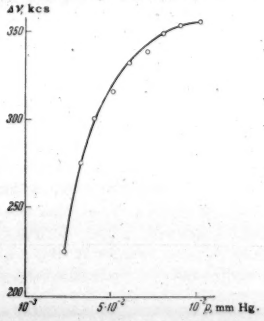

FIG. 8. Dependence of frequency on pressure. H = 1523 oersteds; U = 560 v.

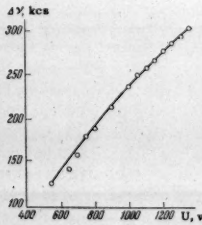

FIG. 9. Dependence of frequency on the potential of the cathode in the source. H = 1523 oersteds; $p \times 10^{-4}$ mm Hg.

FIG. 10. Dependence of the frequency difference between neighboring lines on magnetic field. $p = 5 \times 10^{-4}$ mm Hg.

cause of instrumental uncertainties it is impossible to determine the dependence of frequency on magnetic field; it is known, however, that the frequency increases very rapidly with field. The spacing between neighboring lines in the same series increases linearly with magnetic field (Fig. 10).

DISCUSSION OF THE RESULTS

Among the oscillation modes of a plasma in a magnetic field which are predicted by theory[4] there are oscillations at frequencies which are only slightly different from the ion cyclotron frequencies. Thus, Stix,[5] in considering the behavior of a plasma in a longitudinal magnetic field, has shown that it is possible to produce hydrodynamic Alfven waves,[6] which, at wavelengths much less than the wavelength of light in vacuum, degenerate into waves of frequency

$$\omega^2 = \omega_c \left(1 - \frac{\omega_p^2}{k^2 c^2}\right), \qquad (1)$$

close to $\omega_c = eH/m_i c$, the ion cyclotron frequency. Here ω_p is the ion plasma frequency and k is the wave number. The difference in frequency from the cyclotron frequency is due to the electric field in the plasma; this field gives rise to a centrifugal force which acts in addition to the force due to the magnetic field. The effect leads to a slowing down of ion rotation.

Essentially the same result has been derived by Ferraro[7] who has shown that in a rarified plasma there should be waves similar to the hydromagnetic waves at frequencies which approach a cyclotron frequency as the plasma density approaches zero. These waves are circularly polarized and can only exist in magnetic fields which are smaller than some critical value. The critical value is proportional to the square root of the product of the plasma density and the sum of the ion and electron masses.

It follows from the analyses of Stix and Ferraro

TABLE II

Frequency, Mcs	Proportionality number	Harmonic number and ion	Frequency, Mcs	Proportionality number	Harmonic number and ion
0.121	2	0; H_3^+	0.908	15	4; H_3^+
0.1815	3	0; H_2^+	1.088	18	4; H_1^+ 5; H_2^+
0.242	4	1; H_3^+			
0.363	6	0; H_1^+ 1; H_2^+ 2; H_3^+	1.270	21	6; H_2^+
			1.453	24	3; H_1^+
			1.815	30	4; H_1^+
0.484	8	3; H_3^+	2.170	36	5; H_1^+
0.544	9	4; H_2^+	2.540	42	6; H_1^+
0.726	12	1; H_1^+ 3; H_2^+ 5; H_3^+	2.910	48	7; H_1^+
			3.270	54	8; H_1^+
			3.640	60	9; H_1^+

that the difference in frequency between the described oscillations and the cyclotron oscillations should be very small for a rarified plasma. In this connection the difference observed in the present measurements is extremely significant; thus, in a field H = 1520 oersteds, ν_c = 2.3 Mcs while the frequency of the strongest harmonic which can be assigned to the atomic hydrogen ion is 0.363 Mcs, i.e., approximately six times smaller. This appreciable difference can be understood[4] if one notes that the ions move in a plane (perpendicular to the wave vector) which forms an angle φ with the direction of the magnetic field. This situation results in a frequency $\omega = \omega_c \cos \varphi$. If account is taken of the electric field the frequency should be determined by Eq. (1), with the right side multiplied by the factor $\cos \varphi$.

The theory does not exclude the possibility of the production in a plasma in a magnetic field of an oscillation spectrum of equally spaced lines:[8] $\omega = \omega_0 n$ $(n = 1, 2, 3 \ldots)$ where ω_0 is determined by the plasma density and the product of the magnetic field and electric field of the beam. However, as has been shown in the work cited, the frequencies given by this formula are 3 to 4 orders of magnitude lower than the observed frequencies.

If we assume that the observed lines are harmonics of a given fundamental it is possible to make a comparison of the experimental results with the theory so far as the dependence of frequency on ion mass is concerned.

If we assume $\omega = \omega_c \cos \varphi$, the departure from simple multiplicity shown in Table I is amenable to a simple explanation. Under the conditions of the present experiment the following ions should be present: H_1^+, H_2^+, and H_3^+. The frequencies associated with these ions should be in the ratio 2 : 3 : 6. The first harmonics should be in the ratio 4 : 6 : 12 etc. Consequently the entire spectrum should consist of lines whose frequencies go as the numbers 2 : 3 : 4 : 6 : 8 : 10 : 12 : 14 : 15 etc. In a number of cases the higher harmonics of the heavier ions will coincide with the lower harmonics of the lighter ions. Thus, the second harmonic of the H_3^+ ion and the first harmonic of the H_2^+ should coincide with the fundamental frequency of the H_1^+ ion. This effect leads to a departure from a uniform diminution of the line intensity with increasing frequency. The intensities of the first lines of the various ions should be different, corresponding to the different abundances of these ions in the plasma.

Applying these considerations to the data of Table I, we see (cf. Table II) that the frequencies of the observed lines are proportional to the numbers of the series enumerated above. From a comparison of the frequencies we may conclude that the first line (0.121 Mcs) is due to H_3^+ ion, the second line (0.1815 Mcs) is due to H_2^+ ion, the third line is the first harmonic of the H_3^+ ion while the fourth is the resultant of the superposition of the second harmonic of H_3^+ and the first harmonic of H_2^+ are the fundamental frequency of the H_1^+ ion and so on.

The differences in the intensities of the series of different ions also means that the lines of different series become lost in the noise background at different values of the harmonic number. Thus, the lines of H_3^+ are no longer observed after the second harmonic (0.484 Mcs) while the last observable harmonic of H_2^+ is the sixth (1.270 Mcs). On the other hand the lines of H_1^+ are observable up to the fifteenth harmonic.

If one assumes that the relative intensities of the lines in the spectrum makes it possible to estimate the relative abundances of various ions in the beam we may conclude that in the present case the fundamental effect in the plasma is due to H_1^+ ions and that the H_2^+ and H_3^+ content is only a fraction of a percent.

From the point of view of the explanation which has been proposed the oscillations and their dependence on ion mass obtained from the present experimental data represent a hydrogen mass spectrum; the apparatus which has been used is essentially a radio-frequency plasma mass spectrometer with a linear dispersion of approximately 1,000 cps per 1% relative difference of mass and a rather high resolving power.

The weak lines which are sometimes observed are possibly due to deuterium or to higher harmonics of the hydrogen mixtures. If this assumption is correct, with further improvement of this method of observation of plasma oscillations it may be possible to build a device which will be useful in mass spectrometry.

The author is highly indebted to V. G. Gel'kovskiĭ for his help in the construction of the apparatus and a number of valuable comments. The author is also indebted to Mechanic N. A. Matsuev and Technician N. I. Naumkin for their skill in the construction of this apparatus.

[1] L. Spitzer, Physics of Completely Ionized Gases, (Russ. Transl.) IIL, Moscow, 1957.

A. Guthrie, and R. K. Wakerling, The Characteristics of Electrical Discharges in Magnetic Fields, McGraw Hill, New York, 1949. See also Проблемы современной физики (Problems of Contemporary Physics), No. 11, 1952; No. 2, 1956; No. 7, 1955; No. 7, 1957; and No. 1, 1958, which contains a comprehensive bibliography.

[2] H. J. Woodford and I. H. Gardner, Rev. Sci. Instrl, **27**, 378 (1956).

[3] E. Andrew, Nuclear Magnetic Resonance, (Russ. Transl.) IIL, Moscow, 1957.

[4] S. I. Braginskiĭ, Dokl. Akad. Nauk SSSR **115**, 475 (1958). Soviet Phys. Doklady **2**, 345 (1957).

[5] T. H. Stix, Phys. Rev. **106**, 1146 (1957).

[6] H. Alfven, Cosmical Electrodynamics, Oxford, 1950 (Russ. Transl. IIL, Moscow, 1955).

[7] V. Ferraro, Proc. Roy. Soc. (London), **A233**, 310 (1955), see also Проблемы современной физики (Problems of Contemporary Physics), No. 7, 1957.

[8] Chao K'ei-Hua, Dissertation, Moscow State Univ. 1958.

Translated by H. Lashinsky
194

STRUCTURE OF THE CORE AND OF THE CENTRAL REGION OF AN EXTENSIVE AIR SHOWER AT SEA LEVEL

S. N. VERNOV, Ya. S. BABETSKIĬ, N. N. GORYUNOV, G. V. KULIKOV, Yu. A. NECHIN, Z. S. STRUGAL'SKIĬ, and G. B. KHRISTIANSEN

Nuclear Physics Institute, Moscow State University

Submitted to JETP editor August 13, 1958

J. Exptl. Theoret. Phys. (U.S.S.R.) **36**, 976-984 (April, 1959)

Experimental data on the lateral distribution of the energy flux of the electron-photon and nuclear-active components in the core and central region of extensive air showers are presented. It has been found that appreciable fluctuations in the lateral distribution of the energy flux of the electron-photon and nuclear-active components occur in the core of the showers and, apparently, in the central region as well. The data indicate the existence of a specific correlation between the lateral distribution of the energy flux of the electron-photon component and the lateral distribution of the energy flux of the nuclear-active component in an individual shower.

In a preceding article,[1] a new method of studying extensive air showers (EAS) has been described. It consists of a study of each recorded shower at various depths in its passage through dense matter, which, when the substance used is suitably chosen, makes it possible to observe the various shower components simultaneously.

The method had been applied to the study of the core of EAS, and preliminary experimental results were presented. A fuller report on the experimental data on the energy flux of the electron-photon and nuclear-active components of individual extensive air showers is given in the present article. The measurements were carried out by means of the array for comprehensive study of EAS, operating at Moscow State University.

1. EXPERIMENTAL SETUP

Data on the energy flux of the electron-photon and nuclear-active components were obtained by means of an array consisting of a large number of ionization chambers placed in two layers under composite absorbers made of lead and graphite. A detailed description of the chamber array is given in reference 1.

The use of an array consisting of a large number of ionization chambers of comparatively small dimension (25 cm) and covering a large area (4 m^2) makes it possible to determine the position of the axis of each recorded shower with an error much smaller than the dimensions of the array. Thus, the array permits one to detect the passage of a shower axis through the array and to investigate the phenomena accompanying such an event.*

The position of the chamber array with respect to the hodoscope counters of the array for comprehensive study of EAS is shown in Fig. 1.

The presence of a large number of hodoscope counters both near the chamber array and at large distances from it make it also possible to use the chambers to obtain data on the energy flux of the electron-photon and nuclear-active components of EAS at large distances from the axis.

2. RESULTS OF MEASUREMENTS

During the time of operation of the ionization chamber array together with the full array (1800 hours), about 18,000 showers were recorded with a number of particles N in the range of 10^3 to 10^6, and with the axis incident at distances up to 30 m from the ionization chamber array.

The experimental results obtained contain detailed data on the structure of each individually recorded shower. In view of the limited dimensions of the chamber array, most detailed data on the structure of an individual shower are ob-

*An array of ionization chambers under an absorber has also been used for the study of high-energy nuclear-active component in reference 2. However, the setup used there was, for instance, not suitable for studying the correlation between the incidence of a shower axis on the array and the incidence of a high-energy nuclear-active particle, since the accuracy in determining the axis position from the hodoscope counters was of the order of the size of the chamber array.

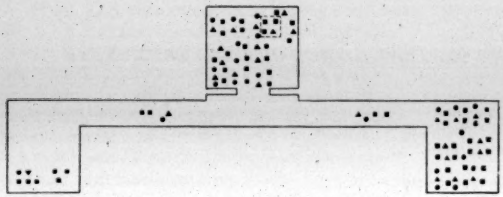

FIG. 1. Position of the ionization chamber array with respect to the hodoscope counters of the array for comprehensive study of EAS: ■ – trays of 12 counters with area 330 cm² each; ▲ – trays of 24 counters with area 100 cm² each ● – trays of 24 counters with area of 24 cm² each. The area occupied by the chamber array is denoted by the dashed line.

tained at comparatively small distances from the axis, in the so-called core region. The experimental results given below are deduced only from a part of available material.

The following method of selection of the cores of showers of various size was used. For the selection of shower cores of small-size showers, a systematical reduction of data obtained during 160 hours of operation of the array was carried out. With the selection system used (see reference 1), this corresponds to the recording of about 3000 events. The majority of these correspond to the passage of cores of showers of very small size, and also to the periphery of large showers. The ionization produced then in the first row of ionization chambers corresponds to the passage of a small number of relativistic particles and is comparable to the lower threshold of recording.

For the discussion to follow, we selected events where the ionization produced in the first row of chambers correspond to the passage of 200 and more relativistic particles through the volume of the chambers, and where the number of discharged hodoscope counters amounted to 20 out of 240 placed above the chamber array. A total of 146 such events was recorded. From these, events were then selected with a marked gradient of particle density over the first row of chambers and over the hodoscope counters placed near the chambers. Whenever in one, or in a few adjacent chambers, the ionization produced was larger than the ionization in neighboring chambers, and whenever an analogous region of maximum particle density was observed also by means of the hodoscope counters, then such an event was interpreted as an incidence of the axis of an extensive air shower upon the system. We found 55 such events, which correspond mainly to showers with a total number of particles N between 6×10^3 to 2×10^4.

For the selection of the cores of EAS of medium size, the data obtained during another period of 170 hours of array operation was systematically reduced. These cases were considered where the ionization in the first row of chambers corresponded to the passage of 500 and more relativistic particles and where the number of struck hodoscope counters amounted to 40 and more, out of 240 placed above the ionization chambers. In such a way, 40 events of incidence of EAS axes with total number of particles N between 1.5×10^4 and 4×10^6 were detected.

Finally, for the selection of the cores of showers of larger size, the data of the ionization chamber array obtained during 1000 hours of operation was analyzed systematically. Events were selected in which the ionization in the first row of chambers was larger than that corresponding to 2000 relativistic particles and where the EAS triggered the master system C_6 (see reference 1). In this way, the incidence upon the ionization chamber system of 28 axes of EAS with total number of particles N from 1×10^5 to 2×10^6 was detected.

It should be noted that the above criteria for the selection of events in which a core of an EAS of a given size fell upon the ionization chamber array, are confirmed by a further detailed analysis of these events. In fact, as will be seen below, the ionization produced in the first row of chambers in the passage of the shower axes of a given size group was in all cases, many times smaller than that which was needed for the selection of showers of these size groups. As far as the requirement of the discharge of a given number of counters is concerned, it is determined by the required shower size under the assumption that the shower axis falls upon the ionization chamber array and that the lateral distribution of particle density is given by the standard function

$$\rho(r) \approx 2 \cdot 10^{-3} N / r \quad \text{for } r < 10 \text{ m}.$$

In order to obtain information on the energy flux at large distances from the shower axis, again only a part of the experimental data was used. Owing to the sharp decrease of the energy flux density with increasing distances from the axis, showers of sufficiently large size with a number of particles $N > 10^5$ were chosen. For this purpose, data of the hodoscope counters were

TABLE I

ΔN	n							
	<0.8	0.8—1.2	1.2—1.6	1.6—2.0	2.0—2.4	2.4—2.8	2.8—3.2	3.2—3.6
$1.0 \cdot 10^5$—$5.0 \cdot 10^5$	0	6	10	5	0	0	1	0
$1.5 \cdot 10^4$—$6.5 \cdot 10^4$	1	2	15	12	1	0	1	0
$5 \cdot 10^3$—$1.5 \cdot 10^4$	2	3	8	6	5	3	0	1
$5 \cdot 10^2$—$5 \cdot 10^3$	3	11	33	23	6	3	2	1

reduced for 190 hours of the operation of the array, and 300 showers with total number of particles N from 10^5 to 10^6 and with the axis falling at distances of up to 30 m from the ionization chamber array were selected. In the selection of a shower from the hodoscope data, the discharge of not less than 120 counters out of 240 placed above the ionization chamber array was required.

The recorded 130 events of incidence of the cores of EAS on the array were submitted to a detailed analysis, first from the point of view of the lateral distribution of the energy flux of the electron-photon component.

The flux of electrons and photons near the axes of the studied showers is so large that even for the least dense showers one should obtain a continuous distribution of ionization in the first row of chambers. For all 130 cases, the lateral distribution of ionization was constructed with respect to the point chosen as a shower axis, and under the assumption of a circular symmetry. This construction was carried out in the following way: In order to find the shower axis, the center of gravity method[3] was used. The indeterminacy in the position of the axis amounts then to the linear dimensions of a single chamber, i.e., to 25 cm. Concentric circles were drawn with the axis as center, forming a system of rings. Ionization in each ring was then computed. If a given ring contained only a part of a chamber, the contribution of the chamber was assessed in the following way: the ionization produced in the whole chamber was multiplied by the ratio of the area of the part belonging to a given ring to the area of the whole chamber. In order to obtain the energy flux density, the ionization was divided by the ring area. It should be noted that the most accurate distribution of the energy flux is obtained when the shower axis fell near the center of the chamber array since, in that case, one obtains a total azimuthal picture of the whole shower. This may be important for showers of small size in which the number of π^0 mesons produced in the core is not so large as to ensure a circular symmetry of the shower.

In the majority of cases (90%) out of the 130 events analyzed, the distribution of the energy flux density can be represented by a single power law in the distance range under consideration

$$\rho_E(r) \sim r^{-n}.$$

The distribution of the exponents n is given in Table I, where a part of the reduced material is used (82 events).

It can be seen from the table that the lateral distribution of the energy flux of the electron-photon component near the shower axis is subject to large fluctuations: the exponent n assumes values from 1 to 3. It should be noted that the character of these fluctuations is identical for showers of different size.

The flux of nuclear-active particles is even near the shower axis insufficient to obtain a picture of the distribution of the high-energy nuclear-active component in the core of each individual shower. The lateral distribution of the energy flux of the nuclear-active component and the energy spectrum of nuclear-active particles in the shower core were therefore obtained statistically for several shower groups differing in the structure of the electron-photon component (see Table I). The lateral distribution of the energy flux of the nuclear-active component for two groups of showers ($0.8 < n < 1.2$ — group 1; $1.8 < n < 2.2$ — group 2) is given in Fig. 2.* The average lateral distribution of the energy flux of the electron-photon component for these groups is also shown in the figure. A characteristic correlation in the form of these distributions may be observed; a slow decrease of the energy flux of nuclear-active component corresponds to a fast decrease of the energy flux of the electron-photon component with the distance from the axis, and vice versa for a slower decrease of electron-photon component, a faster decrease of the energy flux of the nuclear-active component is observed.

In connection with the above, it is of interest to compare the energy spectrum of nuclear-active

*The position of the shower axis in the second row of chambers was determined from their position in the first layer, and from the angle of incidence (see reference 1).

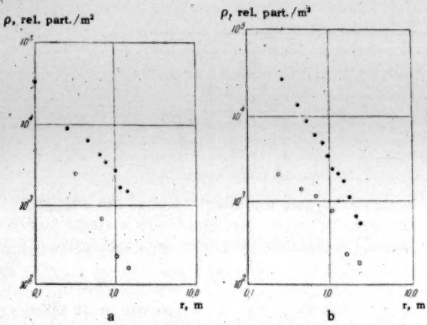

FIG. 2. Lateral distribution of the energy flux of the electron-photon and nuclear-active components in showers with different structure of the core: a – showers of group 1 for $0.8 < n < 1.2$ (see Table I); ● – electron-photon component (slope $\sim 1/r^{1.1}$); ○ – nuclear-active component (slope $\sim 1/r^2$); b – showers of group 2: ● – electron-photon component (slope $\sim 1/r^{1.5}$); ○ – nuclear-active component (slope $\sim 1/r$). $\bar{N} = 10^5$, number of showers used – 8.

particles in the core of showers of the first and second groups. Corresponding data are shown in Fig. 3. The energy spectrum of nuclear-active particles in showers of both groups is found to be identical.*

The 130 cases of incidence of a shower core upon the ionization chamber array discussed were further analyzed individually from the point of view of the absolute value of the energy flux contained in the core. The energy of the electron-photon component can be clearly determined for each individual case by the means of the following method: For each of the 130 showers, we have a lateral distribution of the energy flux density of the electron-photon component. In the majority of showers, the flux density is determined up to the distance of 1.5 m. We can therefore determine the energy flux of the electron-photon component in a circle with radius 1.5 m and with center coinciding with the shower axis for the majority of showers. The distribution of the absolute values of the energy flux is given in Fig. 4. It can be seen that the energy flux of the electron-photon component normalized to a given shower size is subject to marked deviations from the average value. This may be observed both in showers of the group 1 and in showers of the group 2 (the

*It should be noted that the identification of high-energy nuclear-active particles from ionization bursts produced by them in the chambers was carried out taking into account the lateral divergence of particles over the area occupied by the chambers (for details, see reference 1).

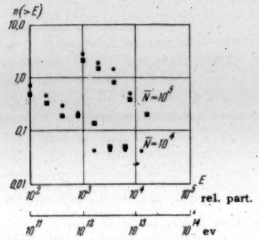

FIG. 3. Energy spectrum of nuclear-active particles in shower cores: ● – group 1 and ■ – group 2; x axis represents the energy of the nuclear-active particles expressed in the number of relativistic particles and in electron volts, the y axis represents the number of particles with energy larger than a given value in the core of showers with total number of particles indicated in the graph. In constructing the graph, it was assumed that the number of nuclear-active particles $n(>E) \sim N$, where N is the total number of particles in the shower.

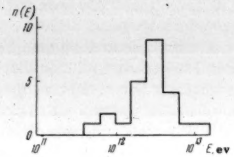

FIG. 4. Distribution of the absolute value of the energy flux of the electron-photon component in a circle with radius 1.5 m with center at the axis for showers with $\bar{N} = 10^5$ (for groups 1 and 2 together). It was assumed that $n(E) \sim N$.

distributions were also constructed for separate groups).

A comparison of the average energy flux of the electron-photon component in the showers of the groups 1 and 2 is presented in Table II. It can be seen from the table that the average energy flux in the core is the same for the groups 1 and 2.

The determination of the absolute energy flux of the nuclear-active component in each individual shower, even in those of the largest size recorded, is difficult since the number of nuclear-active particles is small and the dimensions of the chamber array are comparable to the average deviation of these particles from the shower axis.

TABLE II

$\bar{N}$	Group	$E_{e\text{-}p}$, ev	$E_{n\text{-}a}$, ev	Number of showers
$1.0 \cdot 10^5$	1	$2.2 \cdot 10^{12}$	$5.0 \cdot 10^{12}$	8
	2	$3.3 \cdot 10^{12}$	$5.4 \cdot 10^{12}$	8
$1.0 \cdot 10^4$	1	$4.0 \cdot 10^{11}$	$1.7 \cdot 10^{12}$	11
	2	$5.0 \cdot 10^{11}$	$2.0 \cdot 10^{12}$	15

The average energy flux of the nuclear-active component for groups 1 and 2 was determined separately. These data are also given in Table II. It is found that the energy flux of the nuclear-active component in showers of the first and second groups is the same.

The correlation between the average energy flux of the nuclear-active component and the energy flux of the electron-photon component in the core is illustrated by Table III. The absolute value of the energy flux of the electron-photon component and the corresponding ratio of the burst size in the second layer to the burst size in the first layer of ionization chambers are given in the table. Group 1 comprises showers with an energy flux of the electron-photon component larger, and group 2 smaller, than the average. It can be seen that the energy flux of the nuclear-active component varies little with the change of the energy of the electron-photon component.

TABLE III

Group	Energy flux of the e-p component in a circle with radius r = 1.5 m N = 10^5	Ratio of the burst in the lower layer of chambers to the burst in the upper layer (shower axis within the limits of ionization chambers)
1 (11 showers)	$4.7 \cdot 10^4$	0.13
2 (12 showers)	$1.8 \cdot 10^4$	0.31

As has been mentioned above, because of the limited dimensions of the chamber array it was necessary to use a statistical approach, for the study of the structure of central regions of the showers at distances larger than 1.5 m from the axis. Data on the lateral distribution of the energy flux of the electron-photon component was obtained in such a way.

The 300 showers mentioned above with a number of particles N between 10^5 and 10^6 were used to obtain the distribution of the energy flux of electron-photon and nuclear-active components. Thanks to the large shower size, the comparatively large threshold of recording pulses from ionization chambers, equal to 5 to 10 relativistic particles, did not introduce any errors in the determination of the energy flux of the electron-photon components, even at distances up to 30 m. The flux of the energy of the nuclear-active component may, however, be underestimated because of the threshold.

The data obtained are shown in Fig. 5. Data on the lateral distribution of the energy flux in the shower core obtained for 28 showers of large size with $N > 10^5$ particles (for $r = 0.1 - 2$ m) are also shown in the figure.

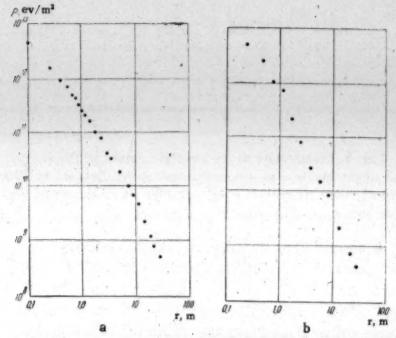

FIG. 5. Lateral distribution of the energy flux for showers with $N = 10^5$ particles: a – electron-photon component in the distance range from 0.1 – 30 m; b – nuclear-active component in the distance range from 0.2 – 30 m.

The lateral distribution of the energy flux of the electron-photon components can be approximated by a power law

$$\rho_{E_{e\text{-}p}} \sim 1/r^{1.35} \text{ for } 0.1\,\text{m} < r < 2.0\,\text{m},$$

$$\rho_{E_{e\text{-}p}} \sim 1/r^{2} \quad \text{for } 2.0\,\text{m} < r < 30\,\text{m}.$$

The lateral distribution of the energy flux of nuclear-active component can be given by the law

$$\rho_{E_{na}} \sim 1/r^{2} \text{ for } 0.2\,\text{m} < r < 30\,\text{m}.$$

In order to find out to what degree the energy flux at large distances from the axis deviates from the average value, the distribution of the energy fluxes of the electron-photon component at a given distance from the shower axis was constructed, normalized to $\overline{N}$. This distribution is given in Fig. 6. It can be seen from the figure that the energy flux at a given distance from the axis deviates from the average flux much more markedly than it could be expected for Poisson fluctuations only.

3. CONCLUSION

The experimental data given above indicate clearly the presence of substantial fluctuations of the absolute energy flux of the electron-photon and nuclear-active components in the core of individual showers and in the lateral distribution of these fluxes. This fluctuation can be followed especially clearly for the electron-photon component. In a shower with a given total number of particles, the absolute value of the energy flux of the electron-photon component in the core can vary by an order of magnitude, and the distribution of the flux density can vary as $1/r$ to $1/r^3$.

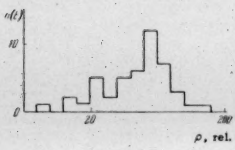

Fig. 6. Distribution of the absolute values of the energy flux of the electron-photon component at the distance of 10 m from shower axis with $\bar{N} = 10^8$ particles. In constructing the distribution, it is assumed that $n(E) \sim N$.

It should also be noticed that fluctuations in the absolute value of the flux are independent of the fluctuations in the distribution of the flux density. This follows both from the direct considerations as well as from the value of the average energy of the electron-photon component in the core of EAS of groups 1 and 2, which are identical. Obviously, it is highly improbable that such fluctuations would be of a purely electromagnetic nature and were connected with the fluctuations in the development of the electron-photon cascade in air and the lead placed above the first row of chambers. These fluctuations must be naturally ascribed to the features of the nuclear cascade process.

The fluctuations of the ionization produced in the passage of the core of an individual shower observed in the second row of ionization chambers cannot obviously be interpreted directly as fluctuations in the energy flux of the nuclear-active component in the core. The reason is that fluctuations in the development of the nuclear cascade in the absorbers screening the second row of ionization chambers can be themselves sufficiently large, so that a different part of the energy of the nuclear-active particle will be transferred to the electron-photon component recorded by the chambers. On the other hand, as has been stated above, fluctuations are possible which are connected with the on the average comparatively large deviation of the nuclear-active high-energy particles from the shower axis. A statistical approach is therefore advisable.

As was seen from the data given in Sec. 2, in a shower with a given total number of particles N, the energy flux of the nuclear-active component is subject to fluctuations simultaneously with the energy flux of the electron-photon component, and the fluctuations of the lateral distributions of the energy flux of both components are connected by a definite correlation.

In showers of group 1, the lateral distribution of the energy flux of the nuclear-active component is rather steep. In showers of group 2, a slow variation of the density flux is observed up to 1 m with a sharp decrease following. At the same time, the energy spectrum of the nuclear-active particles and the absolute energy flux of the nuclear-active component in the core are approximately the same for both groups.*

In connection with the observed fluctuation and their features, a problem arises as to whether they exist only in the shower core, where a cascade consisting of a small number of high-energy particles is present, or whether they are characteristic of the shower as a whole. A direct observation of fluctuations in the energy flux density of the electron-photon component not only in the shower core but also at distances 10 m from the axis (see Fig. 6) shows that the second possibility seems to be very probable.

It should be noted that the above remark, as well as that about the correlation between the lateral distribution of the electron-photon and nuclear-active components, is based on the determination of the averages of the measured variables. The determination of the dispersion of the mean value can be carried out only by using a statistically large amount of material. Therefore, for a final solution of this problem, reduction of additional experimental material is necessary.

The authors would like to express their gratitude to G. T. Zatsepin and I. P. Ivanenko for valuable advice and discussion of results.

[1] Vernov, Goryunov, Zatsepin, Kulikov, Nechin, Strugal'skiĭ, and Khristiansen, J. Exptl. Theoret. Phys. (U.S.S.R.) **36**, 669 (1959). Soviet Phys. JETP **9**, 468 (1959).

[2] Dmitriev, Kulikov, and Khristiansen, Suppl. Nuovo cimento **8**, 587 (1958).

[3] Abrosimov, Goryunov, Dmitriev, Solov'eva, Khrenov, and Khristiansen, J. Exptl. Theoret. Phys. (U.S.S.R.) **34**, 1077 (1958); Soviet Phys. JETP **7**, 746 (1958).

Translated by H. Kasha
195

*The total of experimental data cannot be explained without assuming the existence of a specific correlation in the angular distribution of π^0 mesons and secondary nuclear-active particles in the elementary acts of the nuclear cascade process. It is namely necessary to assume that, for all small angular deviation of produced π^0 mesons, a large angular deviation of the secondary nuclear-active particles with the energy of the same order occurs and vice versa. This problem, however, needs further detailed analysis.

DETERMINATION OF CHARGED PARTICLE MASS FROM SCATTERING AND RESIDUAL RANGE IN MULTIPLATE CLOUD CHAMBERS

F. R. ARUTYUNYAN

Physics Institute, Academy of Sciences, Armenian S.S.R.

Submitted to JETP editor August 15, 1958

J. Exptl. Theoret. Phys. (U.S.S.R.) **36**, 985-991 (April, 1959)

The method of determining the mass of a charged particle from its scattering and residual range in multiplate cloud chambers is experimentally checked by using it to determine the masses of protons, μ and π mesons identified independently (from momentum-range data). The proton, μ- and π-meson masses derived from the corresponding multiple Coulomb scattering curves are in good agreement with the correct values.

1. INTRODUCTION

A method of determining the mass of a charged particle from its scattering and residual range in multiplate cloud chambers has been proposed and described by Annis et al.[1] The present work is an experimental test and study of the possibilities of this method by using it to determine the masses of protons, μ and π mesons which had been previously identified by an independent technique. Our preliminary data have already been published.[2]

When a charged particle is stopped inside a cloud chamber after being scattered in several plates a mean value for the experimental scattering angle can be computed. This mean angle can also be calculated from the theoretical distribution of multiple Coulomb scattering angles. The mean scattering angle and the rms scattering angle are the most frequently used characteristics of the scattering curve. However, instead of using the scattering angle θ it is convenient to work with $\eta = \theta R^{\alpha}$,[1] where R is the residual range of the particle and $\alpha = 0.55$, which is the same constant for all elements. The theoretical distribution of η and the angular distribution coincide except for the scale factor R^{α}.

The mean and rms values of η given in reference 3 are

$$\langle \eta \rangle = A_1 (m_e/m)^{1-\alpha}, \quad (1)$$

$$\langle \eta^2 \rangle^{1/2} = A_2 (m_e/m)^{1-\alpha}, \quad (2)$$

where the coefficients A_1 and A_2 depend on the material and thickness of the scattering plates and the angular distribution function for multiple scattering. Ter-Mikaelyan[3] gives values of these coefficients for lead plates 7 and 4 mm thick taking finite nuclear size into account. Table I gives the values of A_1 and A_2 for the 7-mm plates which were calculated for finite nuclear size, for a point nucleus by Molière[4] and for the normal distribution of scattering angles.

We calculated A_1 and A_2 for copper plates only from the scattering curve for a point nucleus because in the case of copper finite nuclear dimensions are of negligible significance in the investigated momentum and angular ranges.

A sufficiently large number of observed angles for particles of the same type enables us to compute the mean and rms values of η and the particle mass m from (1) and (2).

2. EXPERIMENTAL RESULTS AND DISCUSSION

In order to test the given procedure for determining particle masses we used data on proton, μ- and π-meson scattering in lead plates 7 and 4 mm thick and copper plates 5 and 2 mm thick, given in references 5 and 6, respectively. We also used data on μ-meson scattering in 4-mm copper plates which have been obtained by Kirillov-Ugryumov et al.[7]

For our purposes we selected particles which traversed at least four plates of the total number

TABLE I

A	For finite model of nucleus[3]				For point model of nucleus	Normal distribution of scattering angles
	β=0.50	0.61	0.7825	0.8554		
A_1	520	532	550	561	611	566
A_2	655	672	694	711	776	708

TABLE II

n	Plate material	Type of particle		
		Protons	μ mesons	π mesons
3—6	Pb	1500	465	169
	Cu	145	546	103

of 7 plates in the cloud chamber. Table II gives the total of selected protons, μ and π mesons. The value of η was determined from the scattering angle and residual range for each scattering event individually. The values for each type of particle were grouped, and $\langle\eta\rangle_{exp}$ and $\langle\eta^2\rangle^{1/2}_{exp}$ were calculated separately for protons, μ and π mesons, after which (1) and (2) were used to determine the masses.

Certain features of the experiment strongly enhance the theoretical values of A_1 and A_2 which are given in Table I. For example, when the experimental geometry is taken into account (different angles are registered with different probabilities for scattering in the volume bounded by the instrument) we obtain an increased expectation number for large-angle scattering and thus derive larger values of A_1 and A_2. We have given a detailed analysis of all these corrections in an earlier communication[6] and now regard these improved values of A_1 and A_2 as the computed values. For example, for the scattering curve taking finite nuclear size into account with 7-mm lead plates the computed values for μ mesons are $A_1 = 593$ and $A_2 = 766$, while for a point nucleus they are $A_1 = 665$ and $A_2 = 849$. The computed values of A_1 and A_2 for protons, μ and π mesons differ because the corrections vary with the type of particle.

Table III gives the proton, μ- and π-meson masses obtained in experiments with lead and copper plates separately. The μ- and π-meson masses calculated by two methods (using $\langle\eta\rangle$ and $\langle\eta^2\rangle^{1/2}$), from the scattering curve, taking finite nuclear size into account (for lead plates) and for a point nucleus (for copper plates), are in good agreement with the true masses. The μ- and π-meson masses calculated from the scattering curve for a point nucleus in the case of lead plates are much too high and are incompatible with the masses calculated from the scattering curve for a finite nucleus.

We note that when we calculate the μ- and π-meson masses from uncorrected values of A_1 and A_2 (Table I) the masses calculated from the corresponding curves are much too low (for example, $(157 \pm 5)\,m_e$ for the μ meson).

The proton mass calculated from the scattering curve for a finite nucleus when lead plates are used is only 0.6 ± 0.015 of the correct mass by the $\langle\eta^2\rangle^{1/2}$ method and only 0.734 of the correct mass by the $\langle\eta\rangle$ method. The calculations for a point nucleus gives a value which is close to the correct proton mass but still a little smaller.

In reference 5, where we presented our results on proton scattering, we showed that the

TABLE III

Particles	Method	Theory*	Lead plates 7 and 4 mm thick		Copper plates 5.4 and 2 mm thick	
			No. of scattering events, N	Mass, m_e	No. of scattering events, N	Mass, m_e
μ-mesons	$\langle\eta^2\rangle^{1/2}$	1	2337	201±7	—	—
		2	2337	267±9	2740	210±6
	$\langle\eta\rangle$	1	2337	211	27	
		2	2337	262	2740	223
π-mesons	$\langle\eta^2\rangle^{1/2}$	1	818	286±16		
		2	818	386±21	528	287±19
	$\langle\eta\rangle$	1	818	289	—	—
		2	818	363	528	294
Protons	$\langle\eta^2\rangle^{1/2}$	1	6187	1106±22		
		1′	6177	1243±25		
		2	6187	1675±34	580	1760±115
		2′	6177	1843±37		
	$\langle\eta\rangle$	1	6187	1352		
		1′	6177	1425		
		2	6187	1770	580	1805
		2′	6177	1855		

*1 – from the scattering curve for a finite nucleus, 2 – from the scattering curve for a point nucleus.

experimentally observed proton scattering-angle distribution is in good agreement with the multiple Coulomb scattering curve for a point nucleus. This results from the combined effects of the finite nuclear size and elastic nuclear scattering. Finite nuclear size and diffraction scattering are two mutually compensating factors, as a result of which the experimental scattering-angle distribution for protons can be well represented by the Coulomb scattering curve for a point nucleus. At large angles the experimental values lie above the Coulomb scattering curve for a point nucleus. When we cut off large scattering angles, which result from nuclear scattering, the proton mass can be calculated from the values of A_1 and A_2 computed from the Coulomb scattering curve for a point nucleus, since we do not possess values of A_1 and A_2 which take nuclear scattering into account.

The proton mass obtained, after the large-angle cutoff ($\theta \geq 30°$), from the scattering curve for a point nucleus is in excellent agreement with the correct value. When finite nuclear size is taken into account the proton mass is smaller than the correct value (these mass values are indicated by 2′ and 1′ in Table III). Table III also gives the proton mass calculated for copper plates for a point nucleus, which are in good agreement with the correct mass within the limits of statistical error.

We have published our results on π-meson scattering in reference 6. Diffraction scattering of π-mesons also occurs but affects the multiple-scattering part of the curve only slightly and the experimental angular distribution for π-mesons is in good agreement with the multiple Coulomb scattering curve for a finite nucleus. Diffraction scattering of π-mesons occurs only at large angles. The π-meson mass given in Table III was calculated from the scattering curve for a finite nucleus neglecting large angles.

In determining the masses of nuclear-active particles from scattering and residual range we therefore first exclude large angles, which are associated with nuclear scattering, and then calculate the masses of the particles from their scattering curves.

When the number of scattering events n is small, which occurs for a single stopping particle, the data must be treated more rigorously. To obtain a better estimate of the particle mass m we must know the distribution of η_2, the rms of η. Olbert[8] has obtained a formula for the distribution of η_2, from which normal angular distribution it follows that

$$\eta_{2\,\text{most prob}} = \left(\frac{n-1}{n}\right)^{1/\alpha} \rho, \tag{3}$$

where

$$\rho = A_2 (m_e/m)^{1-\alpha} \tag{4}$$

and A_2 is taken for the normal approximation. But since $\eta_{2\,\text{most prob}}$ depends on ρ it is evident that for a mixture of particles with different ρ (different masses) the resultant distribution may consist of distinct parts. However, since $\eta_{2\,\text{most prob}}$ depends only on the number n of the scattering events and this number is not the same for different trajectories, for each proton, μ- and π-meson trajectory the quantity

$$\xi = \left(\frac{n}{n-1}\right)^{1/\alpha} \eta_2 = \left(\frac{1}{n-1} \sum_{i=1}^{n} \eta_i^{\alpha}\right)^{1/\alpha}, \tag{5}$$

was set up separately, the most probable value of which depends only on ρ ($\xi_{\text{most prob}} = \rho$).

We can thus separate particles of different masses by means of the distribution function of ξ:[1]

$$G_n(\xi, \rho)\, d\xi = \left(\frac{n-1}{2\rho^3}\right)^{1/\alpha} F_n\left[\left(\frac{(n-1}{2\rho^3}\right)^{1/\alpha} \xi\right] d\xi, \tag{6}$$

where

$$F_n(\chi)\, d\chi = (2/\Gamma(n/2))\, \chi^{n-1} \exp(-\chi^2)\, d\chi$$

is the χ^2 distribution for n degrees of freedom. The maximum of this functions corresponds to the most probable value of the mass m.

Statistical errors of the masses are calculated from the formulas in reference 1. The average number of scatterings on each trajectory is $\bar{n} = 4$ for protons and $\bar{n} = 5$ for mesons.

The experimental distributions of ξ for protons, μ- and π-mesons and the corresponding theoretical curves of $G_n(\xi, \rho)$ with lead plates inside the chamber are given in Fig. 1a. Fig. 1b gives the distributions for lead and copper plates combined. The horizontal axis represents values of $\nu_\mu = \xi/\rho_\mu$, where ρ_μ is the value of ρ for μ-mesons calculated from (4).

The angular distribution for multiple Coulomb scattering of μ and π mesons in the given momentum range for the case of a finite nucleus and lead plates is well approximated by a normal distribution curve.[3] Fig. 1 shows that the experimental and theoretical values for μ and π mesons are in good agreement.

For protons there is a large discrepancy between the experimental distribution of ξ and the theoretical curve $G_n(\xi, \rho)$ (Fig. 1a and b) which shows that the function $G_n(\xi, \rho)$ calculated for a normal distribution of scattering angles cannot be used for comparison with the actual non-

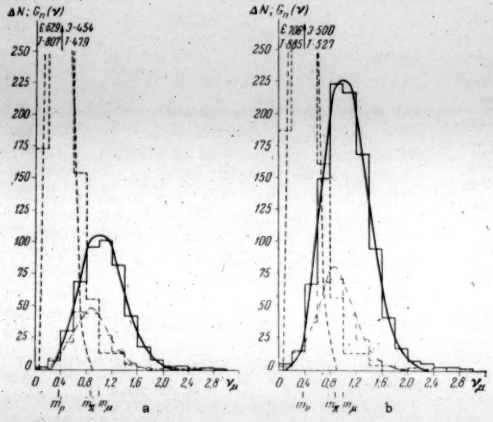

FIG. 1. Distribution of ξ for protons and mesons and corresponding theoretical curves $G_n(\xi, \rho)$: a – for lead plates and b – for lead and copper plates combined, with n = 3 to 6. Protons – dashed lines; μ and π mesons together – solid lines; π mesons separately – dot-dash lines. E and T – experimental and theoretical values of the ordinates instead of their graphical representation.

TABLE IV

n	Material	Type of particle: Protons	Type of particle: μ mesons	Type of particle: π mesons
20—25	Pb	300	93	34
	Cu	29	109	21
40—50	Pb	450	47	17
	Cu	15	55	11

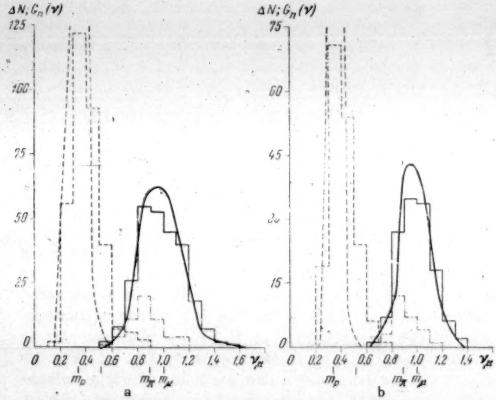

FIG. 2. Distribution of ξ for protons and mesons and corresponding theoretical curves $G_n(\xi, \rho)$: a – for n = 20 to 25; b – n = 40 to 45; for lead and copper plates combined. Protons – dashed lines; μ and π mesons combined – solid lines; π mesons separately – dot-dash lines.

normal distribution of proton scattering angles.

Annis et al[1] have plotted a similar distribution for protons and π-mesons, assuming that all values of ξ to the left of the intersection of $G_n(\xi, \rho)$ curves can be assigned to protons and all values to the right to π mesons. It is clear from Fig. 1 that the area to the right of the intersection of the $G_n(\xi, \rho)$ curves for protons and mesons contains a considerable number of ξ values for protons; by cutting these off the authors of reference 1 would necessarily obtain an excessively large proton mass. Moreover, by using values of A_1 and A_2 calculated for scattering from a finite nucleus (which was not done quite correctly, and we have already shown that such values cannot be used to determine the proton mass), they obtained a proton mass which approximates the correct mass more or less. On the other hand, by cutting off small values of ξ for π mesons the mass obtained for these particles was too low.

As the number of scatterings along an individual trajectory increases the mass determination becomes more accurate. In order to determine the number n of scattering events along a single trajectory which would permit complete separation of protons and mesons, the values of η for the same type of particle were put into groups of 20 – 25 at 40 – 50 in succession (without any selection) and ξ was obtained for each of these groups separately; the numbers of these groups are given in Table IV.

The experimental distributions of ξ for n =

$20-25$ and $n = 40-50$ and the corresponding theoretical $G(\xi, \rho)$ curves for protons and mesons are shown in Fig. 2a and b from data for lead and copper plates combined; the ξ distributions for μ and π mesons are here combined.

Protons and mesons are separated practically completely with $n = 20-25$.

In conclusion the author wishes to thank Professor A. I. Alikhanyan, M. L. Ter-Mikaelyan and M. I. Daĭon for their interest and participation in a discussion of the results.

[1] Annis, Bridge, and Olbert, Phys. Rev. **89**, 1216 (1953).

[2] Arutyunyan, Daĭon, and Ter-Saakyan, Izv. Akad. Nauk Armenian SSR **11**, 71 (1958).

[3] M. L. Ter-Mikaelyan, J. Exptl. Theoret. Phys. (U.S.S.R.) **36**, 253 (1959). Soviet Phys. JETP **9**, 171 (1959).

[4] G. Molière, Z. Naturforsch. **3a**, 78 (1948); **2a**, 133 (1947).

[5] F. R. Arutyunyan, J. Exptl. Theoret. Phys. (U.S.S.R.) **34**, 800 (1958), Soviet Phys. JETP **7**, 552 (1958).

[6] A. I. Alikhanyan and F. R. Arutyunyan, J. Exptl. Theoret. Phys. (U.S.S.R.) **36**, 32 (1959). Soviet Phys. JETP **9**, 23 (1959).

[7] Kirillov-Urgyumov, Dolgosheĭn, Moskvichev and Morozova, J. Exptl. Theoret. Phys. (U.S.S.R.) **36**, 416 (1959), Soviet Phys. JETP **9**, 290 (1959).

[8] S. Olbert, Phys. Rev. **87**, 319 (1952).

Translated by I. Emin
196

LATERAL DISTRIBUTION OF THE ENERGY FLUX OF THE ELECTRON-PROTON COMPONENT OF EXTENSIVE AIR SHOWERS

V. A. DMITRIEV, G. V. KULIKOV, E. I. MASSALSKIĬ, and G. B. KHRISTIANSEN

Nuclear Physics Institute, Moscow State University

Submitted to JETP editor September 15, 1958

J. Exptl. Theoret. Phys. (U.S.S.R.) **36**, 992-1000 (April, 1959)

Measurements are reported on the lateral energy flux distribution of the electron-photon component of extensive air showers with a total number of particles between 1×10^4 to 2×10^6 at sea level. The lateral distribution of the energy flux in the central region of the shower is found to agree with the calculations based on the cascade theory with age parameter of $s = 1.2$. It is shown that the energy flux of the electron-photon component decreases with the distance from the shower axis slower than the energy flux of the nuclear-active component.

The energy carried by the electron-photon component in the central region of the showers is estimated.

INTRODUCTION

NUMEROUS experiments have been devoted to the study of the electron-photon component of extensive air showers (EAS).* In the majority of these, the lateral distribution function of electrons was studied, but only in few experiments[3,4,5] were the energy characteristics of the soft component investigated.

In the present experiment, the energy flux of the electron-photon component was measured by means of studying the ionization produced by it in a substance with high Z. As is well known, the total energy of the electron-photon component is ultimately dissipated on ionization of the medium and, consequently, if the area under the transition curve of the ionization is known, then one can determine the value of the energy flux carried by the electron-photon component:

$$\rho_E = \int_0^\infty n(t)\,\beta dt,$$

where $n(t)$ is the number of particles at the depth t, and β is the mean energy loss per radiation length. In order to obtain the transition curve, the ionization produced by the electron-photon component under layers of lead of various thickness was studied, using large ionization chambers.

The use of ionization chambers with large area makes it possible to substantially increase the statistical accuracy of the results, and to study the energy flux of the electron-photon component over a wide range of shower sizes and of distances from the shower axis. Preliminary results of the experiment are given below. The measurements were carried out between June 1957 and February 1958, using the array for comprehensive study of EAS operating at present at Moscow State University.

DESCRIPTION OF THE APPARATUS

For the study of the electron-photon component of EAS, cylindrical ionization chambers, 25 cm in diameter and 1 m long, with a total effective area of 3 m^2, were used. The chambers were filled with high-purity argon to a pressure of 5 atmos. The thicknesses chosen for the lead absorbers were 2, 4, and 6 cm; in a part of the experiments, the absorber above the chambers was removed. A lead layer 1 cm thick was placed below the chambers. Thus, the chambers were surrounded on all sides by absorbers made of the same substance (see Fig. 1). During almost the whole period of operation of the array, absorbers of various thicknesses were placed above the different chambers. In this way, data about ionization under two different thicknesses of lead were obtained simultaneously for a single shower. The study of a large size range of the showers (1×10^4 to 2×10^6) and, simultaneously, a large range of distances from the shower axis (1 to 50 m, see below) necessitates the recording of ionization varying by a factor of 10,000. This required suitable electronic apparatus which could record

*For bibliography see references 1 and 2.

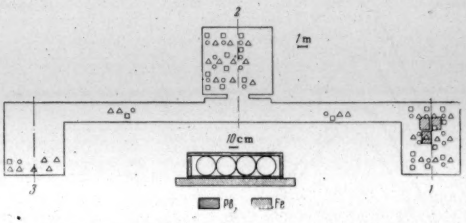

FIG. 1. Plan of the array cross section of the detector. Trays containing 24 counters with area: Δ – 330 cm², ○ – 100 cm², and □ – 18 cm² each.

pulses over an amplitude range of 10^4. For work with a small number of chambers, this problem was solved as described in reference 6 by using a linear amplifier and several pulse-height analyzers. In the present array, where the number of recording channels equals 12, non-linear amplifiers are used. In order to widen the range amplitude, the amplification factor for pulses of large amplitude is decreased by means of an additional feedback loop which is connected automatically by the unblocking of a diode, a method used for the first time by Magee, Bell and Jordan.[7] Recently, this method of widening the dynamic range has become widespread. Three such amplifiers, with an amplification factor of 10 before connecting the additional feedback loop, are used in each of the channels. The amplifiers are designed for amplifying negative pulses and are therefore followed by an inverter with a gain varying from 2 to 4. The pre-amplifier and the pulse-height analyzer are the same as used previously.[6] The maximum gain of the whole channel is set to be equal to 10^5 for the central region, and to 4×10^5 for the study of the periphery of showers. The accuracy of the output-pulse amplitude measurement depends on the value of the latter. The mean accuracy of the measurement is ~30%. The accuracy of measuring small amplitude pulses is limited by the noise whoch amounts to ~ $\frac{1}{3}$ of the signal produced by the passage of a single relativistic particle through the chamber (~20 μv). This makes it possible to measure particle densities in the ionization chambers commencing with $\rho = 0.5$ m^{-2}.

The axis location and the number of particles in an individual shower were determined from the values of the charged particle density at various points in the plane of observation. 2000 Geiger-Müller counters with area of 330 cm², 100 cm², and 18 cm² were used for measurements of the charged-particle densities. Each counter was connected to a hodoscope cell HK-7. The counters were placed in three enclosures (see Fig. 1). The showers were selected by master systems placed in each of the enclosures. In the enclosures 1 and 2, the master system gives a signal for each coincidence of signals from six groups of counters with an area of 0.132 cm² each. In the enclosure 3, getting an output signal from the master system requires a coincidence of not less than three counters with an area of 100 cm² each out of 24 counters placed under 10 cm of lead and of signals from two groups of air counters with an area of 0.26 m² (Cocconi core selector). Data on the ionization chambers and hodoscopes is recorded for every signal from the selection systems.

The axes of the showers recorded by the array fell in regions surrounding the selection systems.* In practice, the axes of showers with $N \geq 10^5$ are distributed continuously along the enclosure up to a distance of 60 m from the chambers. Analysis of the hodoscope data is carried out by the usual method,[9] and makes it possible to determine the total number of particles in the shower N and the distance R from the shower axis to the chamber. For a shower axis falling inside one of the hodoscope points (in an enclosure), the accuracy of determination of N amounts to 20%, and that of R to the order of 1 m.[10] The accuracy becomes worse with increasing distance of shower axis from the line joining the hodoscope points.

RESULTS

All recorded showers were individually analized and classified according to the following groups with respect to the number of particles N:

$$N_1 < 1 \cdot 10^4; \quad 1 \cdot 10^4 \leqslant N_2 < 3 \cdot 10^4; \quad 3 \cdot 10^4 \leqslant N_3 < 1 \cdot 10^5;$$
$$1 \cdot 10^5 \leqslant N_4 < 3 \cdot 10^5; \quad 3 \cdot 10^5 \leqslant N_5 < 1 \cdot 10^6 \text{ and } N_6 \geqslant 10^6.$$

The mean number of particles in each group was determined as follows: $\overline{N}_2 = 2 \times 10^4$; $\overline{N}_3 = 5.6 \times 10^4$; $\overline{N}_4 = 2 \times 10^5$; $\overline{N}_5 = 5.7 \times 10^5$. Showers of each group were then classified with respect

*The size spectrum of showers selected by such systems and their lateral distribution are described in a number of articles (see references 3, 4, and 8).

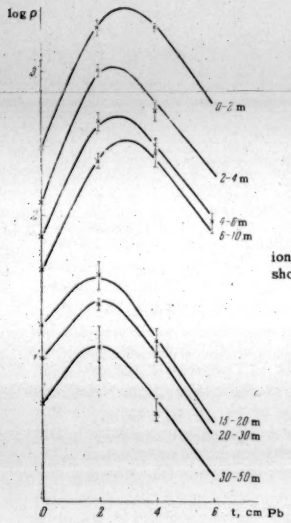

FIG. 2. Transition ionization curves for showers of group N_4.

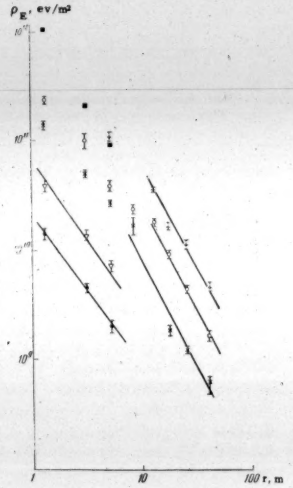

FIG. 3. Energy flux density of the electron-photon component in showers of the groups: ● – N_1; ▽ – N_2; × – N_3; ○ – N_4; ■ – energy flux of the electron-photon and nuclear-active components in showers of the group N_4.

to the distance of the axis of each shower from the chamber. A statistical analysis made it possible to find the mean value of the particle density under the lead absorbers of different thickness for each of the distance intervals 0 – 2; 2 – 4; 4 – 6; 6 – 10; 10 – 15; 15 – 20; 20 – 30; and 30 – 50 m. Cascade curves for the above distance ranges were then constructed for each $\overline{N}_1$. At a depth larger than 8t (where t is the radiation unit), the curves were constructed using a constant absorption coefficient for photons in lead ($\mu_t = 0.24$). A family of such curves for showers of the group N_4 is shown in Fig. 2. The curves were drawn so that, using a semi-logarithmic scale, they run into straight lines smoothly at t = 8.* The energy-flux density ρ_E carried by the electron-photon component was determined from the area under the curves. The integral determining was split into two terms

$$\rho_E = \int_0^\infty n(t)\beta dt = \int_0^{t=8} n(t)\beta dt + \int_0^\infty \beta n(t=8)\exp(-\mu_t t)\,dt.$$

The value of the first term was determined graphically by computing the area under the curves, and the second term from the value of density for t = 8.

Data on the energy-flux density of the electron-photon component in showers with different values of N as a function of the distance is given in Fig. 3. The role of the nuclear-active component and of μ mesons is discussed below.

The electron lateral-distribution function of a shower is independent of N, and its form has been well studied.[10] Using the data on the energy-flux density and electron density, one can obtain the value of the mean energy carried by one electron in a shower. The values obtained are given in Fig. 4. The values of the mean energy have, within the limits of accuracy, been found to be independent of N, and the data were therefore averaged over all showers.

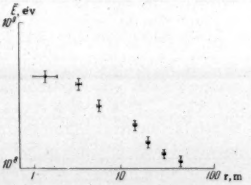

FIG. 4. Average energy per electron at various distances from axis.

If the energy-flux density is known, then it is possible to determine the value of the energy carried by the electron-photon component in a circle of a given radius:

$$E_{e\text{-}p}(\leqslant R, N) = \sum_i \rho_E(r_i, N)\Delta s_i,$$

where the summation is carried over all ranges of the smaller radius. In Fig. 5, the obtained

*This may, in principle, lead to an underestimate of the energy of the electron-photon component at small distances from the axis (in the range 0 – 2 m).

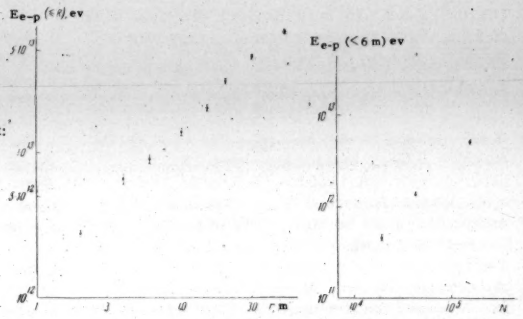

FIG. 5. Energy of the electron-photon component: a – as a function of radius for a shower of the group N_s; b – in a circle with radius R = 6m, for different number of particles in the shower.

values of energy in a circle with radius R are given for showers of the group N_5 as a function of the radius. The value of the energy in a circle with radius 6 m for showers with different number of particles is also given in the figure.

In determining the energy of the electron-photon component from ionization under various thicknesses of lead, it is necessary to account for the contribution of the nuclear-active and μ meson components. The energy of the nuclear-active component in the central region of the showers is substantially larger[10] than the energy of the electron-photon component. At distances of the order of 2 – 4 m from the axis, the energy density of the nuclear-active component is about five times larger than the energy density of the electron-photon component. For larger thicknesses of lead, a large fraction of the energy E_0 of the nuclear-active component is transferred to μ_0 mesons. Using assumptions analogous to those of reference 10, this amounts to 0.03 E_0 for t = 4 cm Pb and to 0.08 E_0 for t = 6 cm Pb. However, the contribution of electrons produced by the π^0 mesons to the total value of ionization is decreased by the fact that the cascades from π^0 mesons have no chance of developing sufficiently in lead since they originate in the depth of the absorber, while the cascades from electrons and photons of the shower start on the boundaries of the absorbers. For the estimate of this factor, the average cascade produced by the first nuclear interaction in lead was calculated. Cascade curves of photons produced by π^0 mesons were approximated, following I. P. Ivanenko,[11] by the first three terms of the Laguerre polynomial series. This leads to approximations of the type

$$n(t) = e^{-\gamma t}(at + bt^2 + ct^3).$$

Numerical values of the coefficients were taken from reference 11 for $\epsilon_0 = 118$. It was found that the number of electrons in such a cascade, for thicknesses of less than 4 cm Pb, decrease by a factor of more than two compared with the number of electrons in the electron-photon cascade of the same energy. Thus, for a lead thickness of 4 cm, only 1 to 1.5% of the energy of the nuclear-active component will, on the average, be added to the electron-photon component determined from the area under the ionization curve up to the depth of 4 cm. With increasing thickness of lead, the contribution of electrons from the nuclear cascade will increase, since the development of the nuclear cascade is much slower than that of the electron-photon cascade.[12] For the estimate of the energy of the electron-photon component, only the data up to 4 cm Pb were used near the shower core. As has been mentioned, beyond 4 cm Pb the curves were drawn with a constant absorption coefficient. It may be seen from the calculation given above that the contribution of the nuclear-active component is then small (less than 10%, even for the central region of showers).

The contribution of the μ mesons component to the energy flux can be estimated in the following way: The total number of μ mesons in the central region of the shower (R < 6 m) amounts to 1% of the number of electrons. Hence, the total number of μ mesons in a circle with radius 6 m will be

$$N_\mu = 10^{-2} \int_0^{R=6} \frac{kN}{r} 2\pi r dr = 7.3 \cdot 10^{-4} N,$$

where N is the total number of electrons in the shower, and $k = 2 \times 10^{-3}$. The average contribution of μ mesons to the energy determined from ionization is not larger than the total ionization energy loss of μ mesons, i.e., the loss for the production of δ electrons and for collisions with a small energy loss. For μ mesons of the shower,

$(dE/dx)_{ion} = 2 \times 10^6$ ev/g for lead. Up to the depth of 4 cm, the μ mesons ionization energy loss is therefore given by the formula

$$\Delta E'_\mu = (dE/dx)_{ion}\, tN_\mu.$$

If one accounts for depths larger than 4 cm Pb, the energy lost by μ mesons increases. For the depths larger than $t = 4$ cm, the curves were continued with a constant slope, and the contribution of μ mesons for such depths is therefore determined from the value of loss for $t = 4$ cm. The total value of the energy due to ionization loss of μ mesons amounts to $E_\mu = 1.1 \times 10^5$ N ev. It may be seen from a comparison with Fig. 5 that

$$\Delta E_\mu (<6\text{m}) \sim 0.005\, E_{e\text{-}p} (<6\text{ m}.)$$

At a distance $r \sim 50$ m, the relative number of μ mesons increases by a factor of about two, and the contribution to the ionization produced remains negligible.

DISCUSSION OF RESULTS

The data obtained (see Fig. 3) permits us to state that the form of the lateral distribution function of the electron-photon energy flux is independent of the number of particles in the shower. In the central region of the shower $1 < r < 8$ m, the function may be approximated by a power law with an exponent $n = 1.5 \pm 0.2$, while at distances larger than 10 m, the exponent is $n = -2 \pm 0.3$. Using the log-log scale, the straight lines representing the above relations given in Fig. 3. A comparison of the value obtained for the energy density with the results of the experiments[3,4] for showers with the same number of particles shows that the data of these experiments are, in this respect, in agreement with our results.

In order to test the agreement of the results with the predictions of the cascade theory, the calculations of the lateral distribution function of the energy flux near the shower axis ($0.5 < r < 6$ m) were carried out by the method given by Guzhavin and Ivanenko.[13] In reference 13 the integral lateral-distribution functions of electrons of various energies are given for various values of the age parameter s, in addition to the lateral distribution functions of photons of various energies (for $s = 1$); $f_\beta(x, s)$ and $f_\gamma(x, s)$, where $x = Er/E_s$, $E_s = 21.3$ Mev. This made it possible to calculate the mean energy of electrons (and photons) as a function of r, obtaining

$$\bar{E}_\beta = \int_{E_{min}}^{\infty} E \frac{d}{dE} f_\beta(x, s)\, dE \Bigg/ \int_{E_{min}}^{\infty} \frac{d}{dE} f_\beta(x, s)\, dE$$

$$= \frac{E_s}{r} \int_{x_{min}}^{\infty} x f'_\beta(x, s)\, dx \Bigg/ \int_{x_{min}}^{\infty} f'_\beta(x, s)\, dx.$$

For an accurate determination of $\bar{E}$, the lower limit of integration should be made equal to zero. However, the functions f are calculated neglecting ionization loss, and are therefore correct for $E > \beta$. However, a comparison of the electron lateral distribution function with $E \geq 0$ obtained by Nishimura[1,2] and the curves with the distribution functions of particles with $E \geq E_{min}$ shows that, in the central region of the shower ($r < 6$ m at sea level), the number of particles with $E < E_{min} = 1 \times 10^8$ ev is not larger than 10%. Consequently, the contribution of particles with $E < E_{min}$ to the energy flux carried by the electron photons in that region is smaller than 10%. One can therefore find the mean energy of particles with $E \geq 1 \times 10^8$ ev at various distances and, using the known lateral distribution of electrons and photons with $E \geq 1 \times 10^8$ ev, find the distribution of the energy-flux density with the above accuracy as a function of distance. It should be noted that the values of the mean energy obtained will, in general, be higher. The above mentioned calculations were carried out for three values of s; $s = 1$, $s = 1.3$, and $s = 1.5$. Since the form of the lateral distribution functions of photons for $s \neq 1$ is not given, we assume then, for $s = 1.3$ and 1.5, that the ratio of the mean energies of electrons and photons for different values of s is the same as $s = 1$.

It was found that, at distances $0.5 \leq r < 6$ m in a shower characterized by the value $s = 1$, this function can be approximated by a power function with the exponent $n = -1.73$. For $s = 1.3$, the exponent is $n = -1.6$; while, for $s = 1.5$, it is $n = -1.45$. One can therefore maintain that the data on the lateral distribution of the energy flux of the electron-photon component do not contradict the value of the parameter $s = 1.2$ obtained for the average shower from the form of the lateral distribution function. A comparison of the obtained data with the results of investigations[8,10] shows directly that the energy-flux distribution of the nuclear-active component is much narrower than the energy flux of the electron-photon component.

The value of the average energy given in Fig. 4 was also compared with the results of our calcu-

lations (see above). It was found that, for $s = 1.3$, the average energy per electron as a function of distance in the same region of the shower can be described by a power law with an exponent $n = -0.65$. It was found experimentally that the average energy changes at a slower rate, $n \approx -0.5$, and that, the value of the average energy is markedly less than that calculated for $r = 3$ m (by a factor of 2.5). However, as has been stated above, the average energy near the shower axis may be slightly underestimated, and the calculated value overestimated.

To compare our results with those of Matano et al.,[5] Fig. 3 includes points (squares) corresponding to the total energy flux of the two components (nuclear-active and electron-photon) near the axis of a shower with $\overline{N} = 2 \times 10^5$. Data on the energy flux of the nuclear-active component are taken from reference 10. The decrease of the total energy flux near the shower axis can be described by a power function with $n = -2.0$. The value of the energy obtained by us for $r = 5$ m agrees closely with the data of reference 5, but the increase of the energy density near the axis given there is steeper. However, Matano et al. did not carry out an analysis of individual showers. Instead, the axis location of showers was estimated from the value of the mean energy observed in each case. If a spread of energy values at a given distance existed in the real shower, then such a method would lead to steeper increase of energy near the shower axis. In our experiment, we determined the place of incidence of the shower independently, and therefore, in principle, obtained the average value of the energy at a given distance from the axis.

The values of the electron-photon component in a circle with radius $R = 6$ m given in Fig. 5 show that the energy flux is proportional to the total number of particles in the shower N. Data on the energy of electron-photon component in a circle with a radius of 50 m are also given in Fig. 5. However, only a little over half of the shower particles is contained in such a circle. It follows from Fig. 4 that the average energy per electron at distances larger than 50 m is smaller than 10^8 ev. Assuming that for large distances $\overline{E} = \beta$, we find that $70 - 80\%$ of the total energy of the electron-photon component is contained in a circle with $R = 50$ m. If we represent the energy carried by the electron-photon component by the expression $E_{e-p} = aN$, then $a \approx 1.7 \times 10^8$ ev $\approx 2.5\beta$.

CONCLUSIONS

1. The form of the lateral distribution function of the energy flux of the electron-photon component of EAS has been obtained. The function is a power law with the following exponents:

$$n = -1.5 \pm 0.2 \text{ for } 1\text{ m} < r < 8\text{ m},$$
$$n = -2.0 \pm 0.3 \text{ for } 10\text{ m} < r < 50\text{ m}.$$

2. It was found that the lateral distribution function of the energy of the electron photon component in showers with total number of particles $N = 10^4 - 10^6$ is independent of the shower size.

3. The lateral distribution of the energy flux of the electron-photon component is not in disagreement with the theoretical distribution obtained from the cascade theory for $s = 1.2$.

4. About 75% of the total energy of the electron-photon of EAS is contained in a circle with 50 m radius.

The authors would like to thank S. N. Vernov and G. T. Zatsepin for their great help, and I. P. Ivanenko for discussion of the results obtained. They would also like to thank V. I. Artemkin, L. A. Dikarev, V. N. Sokolov, K. I. Solov'ev, and D. S. Stel'makh, who took part in the measurements and in the analysis of the data.

[1] K. Greisen, Progress in Cosmic Ray Physics **3**, Amsterdam, 1956.

[2] G. Cocconi, Handbuch der Physik **45**, 1958.

[3] Ivanovskaya, Kulikov, Rakobol'skaya, and Sarycheva, J. Exptl. Theoret. Phys. (U.S.S.R.) **33**, 358 (1958), Soviet Phys. JETP **6**, 276 (1958).

[4] Danilova, Dovzhenko, Nikol'skiĭ, and Rakobol'skaya, J. Exptl. Theoret. Phys. (U.S.S.R.) **34**, 541 (1958), Soviet Phys. JETP **7**, 374 (1958).

[5] Matano, Miura, Oda, Suga, Tanahashi, and Tanaka, Nuovo cimento **8**, Suppl. 2, 668 (1958).

[6] Bekkerman, Dmitriev, Molchanov, Khristiansen, and Yarigin, Приборы и техника эксперимента (Instruments and Meas. Engg.), No. 4 (1958).

[7] Magee, Bell, and Jordan, Rev. Scient. Instr. **23**, 30 (1952).

[8] Dmitriev, Kulikov, and Khristiansen, Nuovo cimento **8**, Suppl. 2, 587 (1958).

[9] Abrosimov, Goryunov, Dmitriev, Solov'eva, Khrenov, and Khristiansen, J. Exptl. Theoret. Phys. (U.S.S.R.) **34**, 1077 (1958), Soviet Phys. **7**, 746 (1958).

[10] Abrosimov, Dmitriev, Kulikov, Massal'skiĭ, Solov'ev, and Khristiansen, J. Exptl. Theoret.

Phys. (U.S.S.R.) **36**, 751 (1958), Soviet Phys. JETP **9**, 528 (1959).

[11] I. P. Ivanenko, Dokl. Akad. Nauk SSSR **107**, 819 (1956), Soviet Phys. "Doklady" **1**, 231 (1956).

[12] Zatsepin, Krugovykh, Nikol'skiĭ, and Murzina, J. Exptl. Theoret. Phys. (U.S.S.R.) **34**, 298 (1958), Soviet Phys. JETP **7**, 207 (1958).

[13] V. V. Guzhavin and I. P. Ivanenko, Dokl. Akad. Nauk SSSR **113**, 533 (1957); **115**, 1089 (1957), Soviet Phys. "Doklady" **2**, 131 (1957); **2**, 407 (1957).

Translated by H. Kasha
197

DETERMINATION OF THE IONIZATION POTENTIAL OF URANIUM BY A SURFACE IONIZATION METHOD

I. N. BAKULINA and N. I. IONOV

Leningrad Physico-Technical Institute, Academy of Sciences U.S.S.R.

Submitted to JETP editor September 18, 1958

J. Exptl. Theoret. Phys. (U.S.S.R.) 36, 1001-1005 (April, 1959)

A method is described for determining the difference in ionization potentials for two different atomic species which are ionized simultaneously on a heated metal surface. The method has been verified by measuring the ionization potentials of sodium and lithium. The method has been used to measure the difference in ionization potentials of uranium and lithium. The ionization potential of uranium is found to be 6.08 ± 0.08 volts. At high temperatures the positive ion currents for sodium, lithium, and uranium are found to vary in accordance with the theoretical expressions for surface ionization.

THE most precise values of the ionization potentials of atoms (V) are obtained from atomic spectra. In a number of cases, however, for instance the rare earths and uranium, atomic spectroscopy has not yet furnished reliable values of V. In the present paper we describe a method for determining the difference in ionization potentials for any two atomic species which can be ionized on a heated metallic surface. The method is based on a comparison of the ion currents of the two elements which are ionized simultaneously on the same heated surface; this scheme has been used by us earlier[1] for determining the difference in electron affinities for atoms which are capable of forming negative ions by means of surface ionization.

Usually surface ionization is investigated with heated polycrystalline filaments of refractory metals. It is known that the surfaces of such filaments exhibit an inherent nonuniformity in work function — different grains have work functions which differ significantly.[2] The adsorption of contaminating atoms on the surface may lead to an increase in the nonuniformity in contact effects at the surface. If the intensity of the electric field E which extracts ions from the surface is sufficient to compensate for the contact field of these localized regions the ion emission of the surface is the simple sum of the ion currents for all such localized regions.* The work function of all the regions lies within the limits $\varphi_{k\,min}$ and $\varphi_{k\,max}$. It has been shown,[3] that if the following condition is satisfied:

$$\varepsilon(V-\varphi_{k\,max}-\sqrt{\varepsilon E})\gg kT \qquad (1)$$

the surface ionization coefficient β of such a nonuniform surface is

$$\beta=n^+/n=A\exp\{(\varepsilon/kT)(\sqrt{\varepsilon E}-V)\}\times\sum_k f_k\exp(\varepsilon\varphi_k/kT). \qquad (2)$$

Here n is the number of atoms which strike the surface per second, n^+ is the number of positive ions which are extracted from the surface per second; A is the ratio of the partition functions of the ions and atoms; f_k is the area of all regions of the k-th type which have a work function φ_k; T is the temperature of the surface and ϵ is the charge of the electron.

Assuming that two atomic species are ionized simultaneously on the same surface, using Eq. (2) we obtain the ratio of ion currents $I = \epsilon n^+$

$$I_1/I_2=(A_1n_1/A_2n_2)\exp\{(\varepsilon/kT)(V_2-V_1)\} \qquad (3)$$

or

$$\log(I_1/I_2)=\log(A_1n_1/A_2n_2)+5040\,(V_2-V_1)\,T^{-1}. \qquad (4)$$

If the condition in (1) is satisfied the ion-current ratio I_1/I_2 is independent of the state of the surface and the intensity of the ion accelerating field E.

Equations (3) and (4) may be used to determine the difference in ionization potentials $\Delta V = V_2 - V_1$ of two elements. Knowing the ionization potential of one of the elements it is then possible to deter-

*We start from the considerations of Langmuir, who assumes that the work function φ_k of a region of the k-th type is constant over the surface of the region and changes discontinuously at the boundaries of the region. For our purposes the exact distribution of the work function $\varphi(x, y)$ over the surface is not important.

mine the ionization potential of the other. Two methods can be used for this purpose: the ratios n_1/n_2 and I_1/I_2 can be determined experimentally at different values of T and the quantity $\Delta V = V_2 - V_1$ calculated from Eq. (3) or the quantities n_1 and n_2 can be held constant throughout the experiment and the function $\log I_1/I_2 = f(1/T)$ determined, thereby making it possible to determine ΔV from the slope of the curve. The quantities A_1 and A_2 remain essentially constant for small variations of T and are known for the majority of elements.

Equation (2) can also be written in the form

$$I = \varepsilon n A^* \exp[(\varphi^* + \sqrt{\varepsilon E} - V)\varepsilon / kT], \qquad (5)$$

where $A^* = A\Sigma_k f_k \exp[(\epsilon/kT)(\varphi_k - \varphi^*)]$ is a weak function of T. For small variations of T the quantity A^* is essentially constant. In this case the curve $\log I = f(1/T)$ should be a straight line, the slope of which should yield the quantity $\varphi^* + \sqrt{\epsilon E} - V$. If φ^* is the same for ionization of different elements on the same surface the condition in (1) is actually satisfied.

METHOD OF MEASUREMENT

In order to make separate measurements of the ion currents for the two atoms and to exclude effects due to easily ionized contaminants the experiments are carried out in a magnetic-sector mass spectrometer. The filament on which surface ionization is investigated serves as the ion source of the mass spectrometer.

The atoms of the elements being compared are directed onto the filament H (Fig. 1) through symmetrically arranged slits S_1 and S_2 from two evaporators E_1 and E_2. Slits S_1 and S_2 can be closed independently by means of slides. The ions from the filament are accelerated by means of an electric field (the potential difference between the filament and the accelerating electrode is 600 — 1,000 volts) in the direction of the input slit (S) of the mass spectrometer and the ion beam, which is mass resolved in the magnetic field, strikes the detector. The ion currents are measured with a type EMU-3 electrometer amplifier, sometimes in conjunction with a secondary-electron multiplier. During the measurements the vacuum in the device is never worse than 10^{-6} mm Hg. Before the measurements are made the filament is baked; the filament temperature is measured with an optical pyrometer.

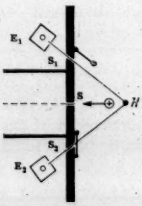

FIG. 1

In order to check the method ΔV was measured in sodium and lithium, the ionization potentials of which are well-known (5.14 and 5.40 volts respectively). Since it is possible that (1) is not satisfied for ionization of Na on W, the ionization of sodium and lithium was studied on tantalum filaments. Having convinced ourselves from this work that the method was satisfactory we then determined the difference in ionization potentials for uranium and lithium. The effect was studied with tungsten filaments in the latter elements.

The reason for using tungsten instead of tantalum to measure the ionization potentials for lithium and uranium is the following. Uranium is rather strongly adsorbed by surfaces and remains on these surfaces even when heated to 2300° K and higher. When tantalum or tungsten is covered by uranium the work function of these materials is reduced sharply. In order to guarantee the maximum purity of the surface for the range of values of T it is necessary to carry out the measurements of $I = f(t)$ at the highest possible temperatures. When tungsten is used it is possible to raise T up to 2800° K To reduce contamination of the surface by uranium in the operating temperature range it is convenient to reduce the number of uranium atoms which strike the filament; however this procedure obviously leads to a reduction in ion current. By using an electron multiplier as a preamplifier the sensitivity is increased by two orders of magnitude; in some of the experiments this increase allows us to make a corresponding reduction in the intensity of the molecular beams from the ovens.

We have not studied ionization in the pure metals, but rather in halogen salts NaCl, LiCl, LiF, UCl_4 and UF_4, which are simpler for experimental purposes. It is assumed that at the operating temperatures complete reduction of the metals obtains at the surface. A great deal of attention is given to the problem of making the intensity of the molecular beams constant. The evaporating ovens have a thermal intertia and the heating elements are supplied by high-capacity storage batteries. Before the measurements the

ovens are pre-heated for long periods of time.

The measurements are carried out by the following two methods.

First method. The oven temperature is established at 2250° K for tantalum and 2650° K for tungsten. Successive measurements are made of the current of F^- ions for ionization of LiF and UF_4 (the molecular beams are shut off by the oven slides) or the chlorine isotopes in the case of NaCl—LiCl and LiCl—UCl_4; the additivity of the currents when both slides are opened and the stability of the currents are checked. In making the calculations, in accordance with Eq. (4) it is assumed that the ratio n_1/n_2 is equal to the ratio of the negative ion currents of chlorine for the NaCl—LiCl case or ¼ of the ratio of the negative ion currents for UCl_4—LiCl and UF_4—LiF. Then the magnetic and accelerating electric fields are reversed and at the same temperature T measurements are made of the positive ion currents I_1 and I_2. In all the subsequent measurements at other values of T the stability of the molecular beams is checked periodically at 2250° K for tantalum and 2650° K for tungsten.

Second method. In this case measurements are made of the dependence of the positive ion currents on T and graphs of the function $\log (I_1/I_2) = f(1/T)$ are plotted. The values of n_1 and n_2 and the intensities of the molecular beams are monitored by measuring the currents of positive ions at T equal to 2250° K for Ta and 2650° K for W; the currents are measured before and after the measurements at each temperature.

RESULTS OF THE MEASUREMENTS

Curves of the function $\log (I_T/I_{2250}) = f(1/T)$ are shown in Fig. 2 for ionization of Li and Na on tantalum; it is apparent from these curves that, in agreement with Eq. (5), the experimental points lie on a straight line in the temperature range from 1700 to 2375° K. From the slope of the straight lines we find $\varphi^* + \sqrt{\epsilon E} - V$ is 0.53 volts for Na and 0.83 volts for Li. In both cases this gives agreement with the limits of experimental accuracy for the values of $\varphi^* + \sqrt{\epsilon E}$ (to 4.61 and 4.57 volts).

All the lines have been plotted from the experimental data, using a least-squares fit. Approximately 85 determinations were made of the differences in ionization potentials of lithium and sodium $V_{Li} - V_{Na}$ by the first method in different samples of tantalum for values of T between 1600 and 2115° K (with different values of the intensities of the molecular beams of NaCl and LiCl). The spread in the values of ΔV is found to lie between 0.23 and 0.28 volts while the mean arithmetic value of 85 determinations yields $V_{Li} - V_{Na} = 0.25 \pm 0.02$ volts.

In addition two series of measurements were made by the second method in the temperature range between 1700 and 2375° K. An example of a curve $\log (I_1/I_2) = f(1/T)$ is shown in Fig. 3. The values of ΔV calculated from ten curves lie between the limits of 0.19 and 0.32 volts. The average of all the values is found to be $V_{Li} - V_{Na} = 0.26 \pm 0.05$ volts. The results obtained by both methods are in agreement with the spectroscopic data for these elements.

In making a comparison of the ion currents U – Li we cannot use the first method because of the difficulty of making an accurate determination of the ratio of ion currents I_U/I_{Li} in this case. In determining I_U/I_{Li} it is necessary to make corrections for the difference in the ion-electron emission coefficients for U^+ and Li^+ at the first dynode of the multiplier and for the difference in the transmission of the mass spectrometer in the passage of ion beams which differ so greatly in mass.

In Fig. 4 we show the function $\log (I_T/I_{2650}) = f(1/T)$ for Li and U for ionization of the salts LiF and UF_4 on tungsten in the temperature region between 2100 and 2800° K. In all cases the straight lines reproduce the behavior of the experimental functions. In Fig. 5 is shown the curve $\log (I_{Li}/I_U) = f(1/T)$; the slope of this curve can be used to calculate $V_U - V_{Li}$.

Varying the experimental conditions we carried out five series of measurements of the temperature dependence of the ion currents in the ioniza-

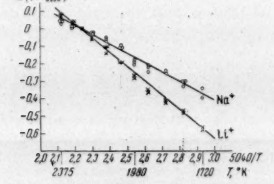

FIG. 2

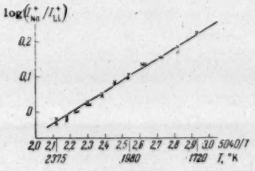

FIG. 3

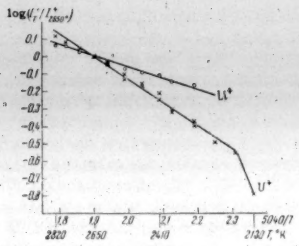

FIG. 4

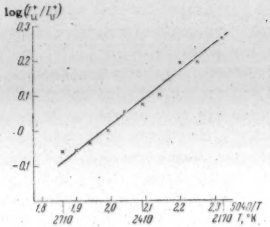

FIG. 5

tion of $UF_4 - LiF$ and one in the ionization of $UCl_4 - LiCl$; the appropriate curves were plotted. The differences $V_U - V_{Li}$ determined from the slope lie between 0.57 and 0.83 volts while the average value if $V_U - V_{Li} = 0.68 \pm 0.08$ volts. Whence the ionization potential of the uranium atom is

$$V_U = 5.40 + 0.68 = 6.08 \pm 0.08\ \text{V}.$$

The uncertainty in the determination of ΔV stems from the estimate of the accuracy of the determination by Eq. (4). Actually the ratio of the ion currents in the mass spectrometer is measured with an accuracy which is probably no better than 10 – 20%. The basic reason for the reduction in the accuracy of the current measurements is the small uncontrollable shift of the filament with respect to the input slit of the mass spectrometer as the temperature is changed. The molecular beam intensity is maintained with an accuracy of several percent during the experiments. The accuracy in the measurement of T, which is carried out by means of an optical pyrometer, is 2 – 3%.

Our assumption as to the complete dissociation of the molecules of the alkali-halide salts on tungsten and tantalum surfaces is rather well justified by all of the work which has been carried out on the surface ionization of these salts. The reduction of the uranium and certain other rare metals from the halogen salts at high temperatures is used in metallurgy in order to obtain pure metals. The agreement of the experimental relations $I = f(T)$ in Figs. 2 and 4 with Eq. (5) appears as additional evidence for the complete dissocation of the salts used in the present work.

[1] I. N. Bakulina and N. I. Ionov, Dokl. Akad. Nauk SSSR **105**, 680 (1955); **116**, 41 1957, Soviet Phys. "Doklady" **2**, 423 (1957).

[2] G. N. Shuppe, Электронная эмиссия металлических кристаллов (Electron Emission in Metal Crystals) Tashkent, 1957.

[3] Z. Ya. Zandberg, J. Tech. Phys. (U.S.S.R.) **28**, 2434 (1958), Soviet Phys. JTP **3**, 2233 (1959).

[4] Z. Ya. Zandberg and N. I. Ionov, J. Tech. Phys. (U.S.S.R.) **28**, 2444 (1958), Soviet Phys. JTP **3**, 2243 (1959).

Translated by H. Lashinsky
198

PRODUCTION OF STRANGE PARTICLES IN THE INTERACTION BETWEEN 9-Bev PROTONS AND EMULSION NUCLEI

N. I. KOSTANASHVILI* and O. A. SHAKHULASHVILI†

Joint Institute for Nuclear Research

Submitted to JETP editor September 20, 1958

J. Exptl. Theoret. Phys. (U.S.S.R.) **36**, 1006-1011 (April, 1959)

The frequency of production of strange particles by the collision of high energy protons with photoemulsion nuclei is examined.

A study of the dependence of the frequency of production of strange particles on the energy of the primary particles was undertaken in the laboratory of the Joint Institute for Nuclear Research. The preliminary results of this work are given below.

The emulsion stack, consisting of 100 pellicles of type BR-450, was bombarded with 9 Bev protons in the proton synchrotron of the Joint Institute for Nuclear Research. The volume of the emulsion chamber was $10 \times 10 \times 4.5$ cm. The pellicles are scanned by areas, and nuclear disintegrations caused by the primary protons are located. For the detection of hyperons and K mesons, one observed the tracks of singly-charged particles found among the disintegrations. The indicated tracks were traced up to their stopping point, decay, nuclear interaction, or exit from the chamber. The identification of strange particles was made by their characteristic appearance in decay and nuclear capture.

The comparatively small dimensions of the stack prevented the investigation of particles with long ranges outgoing at large dip angles. To study high-speed particles the initial nuclear splittings were chosen near that edge of the stack which was turned toward the primary current. Secondary particles satisfying the following three conditions were traced:

(a) The outgoing particle is in the forward hemisphere. (This does not cause the loss of strange particles, because they, as will be later evident, are fundamentally outgoing in the forward direction.)

(b) The length of the horizontal component of the track in one pellicle is ≥ 3 mm, corresponding to a dip angle $\leq 7.5°$. (This condition also excludes a large quantity of slow protons and deuterons formed in the decay of excited nuclei.)

(c) The ionization is not less than 1.6 times the ionization of the primary proton. (From this, the velocity of the particle $\beta \leq 0.64$.)

When the above conditions are satisfied, the probability of recording the decay of a hyperon inside the stack is $\geq 85\%$. In such a manner, 1920 stars were got in thirty pellicles from the center part of the stack, and 670 tracks of secondary particles were traced. Six strange particles were found, three hyperons and three K^+ mesons. In addition, one ovserved in one case a sharp break (about 160°) in the track of a strongly ionized particle, which might have corresponded either to the large-angle scattering of a proton or to the decay of a hyperon to a proton. The absence of a change of ionization before and after the break and also the insufficient length of the track ($\sim 2200\mu$) prevented identifying the particle. The results of these tracings are the following:

Total number of measured prongs	670
Prongs without visible events at their ends	494
Strange particles	6
$\pi^\pm$ mesons	19
Number of secondary reactions*	53
Number of tracks leaving the stack	94

It can be seen that, on an average, one strange particle corresponds to 100 secondary particles. Just such a magnitude was got in the work of Edwards et al.[1] carried out with π^- mesons having energies ~ 4.5 Bev. In references 2 and 3, covering work done with cosmic rays, one strange particle appears, on an average, for every 250 or 300 ordinary particles. However, a rigorous

*On leave from the Tbilisi State University.

†On leave from the Institute of Physics of the Academy of Sciences of the Georgian S.S.R.

*All the tracks of secondary particles were followed to their stopping place or exit from the stack. No strange particles were found in these cases.

comparison of the various results is not possible due to some differences in the conditions of examination and choice of the particles.

The large magnitude of the ratio of the number of strange particles to the number of $\pi^{\pm}$ mesons, $(N_{\Sigma,K}/N_{\pi^{\pm}}) \sim 1/3$, is remarkable. In an analogous work[3] the ratio $\sim 1/10$. It must be emphasized that these numbers refer only to the slow secondary particles outgoing in the forward direction.

For the evaluation of the cross section for production of slow strange particles by the photoemulsion nuclei, it is essential to know the cross section for star-formation and the frequency of appearance of strange particles, calculated for one star. In Fig. 1 the distribution of stars according to the number of black and gray prongs is depicted, both for stars found by track scanning (solid lines) and for those found by area scanning (dotted lines). The comparison of the solid and dotted histograms allows one to make a small correction, connected with the unobserved small-angle disintegrations, to the number of prongs. To determine the frequency of appearance of the strange particles, it is necessary to know the spatial distribution of particles having velocities $\beta \leq 0.64$ and a range, $l \geq 3$ mm. If we suppose that this is of the form $1 + a \cos \psi$, it follows from the experimental data that $a \sim 1$. Under these conditions the frequency of appearance of strange particles (for $\beta \leq 0.64$ and $l \geq 3$ mm) is about 0.042 per star. From the composition of elements in the NIKFI emulsion[4] and from the magnitude of the free range for the inelastic interaction of protons of energies ~ 9 Bev with photoemulsion nuclei, one gets a magnitude of ~ 460 millibarn for the star-formation cross section. This leads to the cross section for the production of slow strange particles, $\sigma_{\Sigma,K} \sim 20$ millibarn.

Besides the method described for distinguishing hyperons and heavy mesons, other events which could be strange particles are located in the area scanning: two-pronged stars, decays of various types and nuclear captures. The corresponding particles were traced in the reverse direction to find their parent disintegrations. In such a way 24 strange particles were found, a large part of which were formed in stars produced by primary protons. The collected data for all the strange particles found are given in Tables I and II.

From the tables it follows that the majority of strange particles are outgoing in the direction of the forward hemisphere. We note also that all the π mesons formed in the decay of a Σ hyperon in flight are outgoing backwards in the center of mass system (except for hyperon No. 8, whose parent star was produced by a neutral particle).

Stars formed by primary protons and containing slow strange particles, found in the area search, have a somewhat increased number of gray and black prongs, N_h. In fact, for this group of stars we have $\langle N_h \rangle = (12.5 \pm 2.1)$ and $\langle n_s \rangle = (2.9 \pm 0.5)$; for the same time for ordinary stars, formed by primary protons, $\langle N_h \rangle = (8.3 \pm 0.5)$ and $\langle n_s \rangle = (3.4 \pm 0,1)$.[5] This fact evidently means that the production of hyperons and heavy mesons stems predominantly from the heavy nuclei of the photoemulsion. An analogous remark was made in a series of other papers (see, for example, reference 6).

In the stars containing strage particles, all the other prongs were also traced. The production of a second strange particle was observed in three cases, in one of which a pair of K mesons (K^+

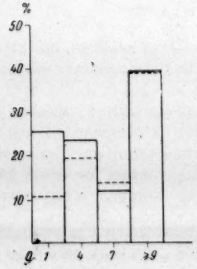

FIG. 1

TABLE I. Heavy mesons

No.	Particle	Type of parent star	Production angle of K meson, deg	K meson range, Mev	No.	Particle	Type of parent star	Production angle of K meson, deg	K meson range, Mev
1[1]	K^+	5+3 p	54	14	10[3]	K^+	11+0 p^*	—	21.8
2[2]	K^+	22+3 p	8	56.6	11[4]	K^+	6+1 p	49	57.1
3	K^+	14+7 p	48	22.5	12	τ^+	21+4 p	72	12.8
4	K^+	4+4 p	41	4.4	13	τ^+	21+0 p	44	30.7
5	K^+	7+0 π	—	54	14[3]	K^-	6+1 p	20	50.6
6[3]	K^+	4+0 p^*	—	59	15	K^+	Entered the stack from below		
7	K^+	6+5 p	86	50.4	16	K^+	Entered the stack from below		
8[3]	K^+	3+0 p^*	—	17.3	17	K^+	Entered the stack from below		
9	K^+	14+1 p	91	52.3					

[1]Formed in a pair with hyperon No. 4 (see Table II).
[2]Formed in a pair with hyperon No. 5 (see Table II).
[3]Stars with p* produced by secondary charged particles.
[4]Formed in a pair with K meson No. 14.
[5]The method adopted for the strange particle search does not guarantee that the ratio obtained for the number of K^+ and K^- mesons corresponds to reality.

TABLE II. Hyperons

	Primary					Secondary		
No.	Particle	Type of parent star	Production angle, deg	Length of hyperon path, mm	Energy	Particle	Range, mm	Center of mass exit angle, deg
1	Σ^-	$4+3p$	42	53.2	217	π^-	15.3	168
2	$\Sigma^\pm$	$21+1p$	84	16.5	96	$\pi^\pm$	—	113
3	$\Sigma^\pm$	$18+5p$	89	0.80	~42	$\pi^\pm$	—	~121
4	Σ^+	$5+3p$	20	28.6	800	π^+	11.5	154
5	Σ^-	$22+3p$	29	16.8	115	π^-	33.2	155
6	$\Sigma^\pm$	$2+1p$	37	10.6	~67	$\pi^\pm$	—	~120
7	Σ^+	$12+4p$	91	4.4	37	$\pi^\pm$	—	51
8	$\Sigma^\pm$	$8+0n$	—	4.8	~55	π^+	—	~82
9	$\Sigma^\pm$	$15+6p$	47	4.5	~90	$\pi^\pm$	—	~102
10[1]	Λ^0	$18+2p$	3	0.164	140	—	—	—
11[2]	Λ^0	—	133	—	20	—	—	—
12[2]	Λ^0	—	152	—	36	—	—	—
13[2]	Λ^0	—	19	—	112	—	—	—
14[2]	Λ^0	—	77	—	35	—	—	—
15[3]	Hf	$11+4p$	90	0.020	—	—	—	—
16[4]	Hf	$22+3p$	63	0.284	—	—	—	—

[1]Decayed beside parent star.

[2]The production angle of the Λ^0 hyperon changed relative to the direction of the primary protons.

[3]Mesonic decay.

[4]Non-mesonic decay.

and K^-) was formed. In the other two, a hyperon and K^+ meson were found.

The kinetic energies and production angles were measured for all Σ hyperons formed in stars produced by primary protons. The corresponding points are plotted in Fig. 2, which shows also the limiting curves for energies and angles of Σ hyperons formed in the reaction

$$P + N \rightarrow \Sigma + K + N. \qquad (1)$$

The solid curve corresponds to a rigid target nucleus, the dotted one takes into account internal nuclear motion. The possibility of producing various numbers of π mesons in reaction (1) can be accounted for only by the restriction that limiting curves for such reactions must lie within the solid and dotted curves shown in Fig. 2. Therefore, the presence of the points distributed outside of the limiting curves shows that the production of the hyperons considered must be connected, at least partly, with reactions more complicated than reaction (1). Here two possibilities must be considered:

(a) The hyperons are possibly formed by some kind of secondary particle, for example, a π meson, in its interaction with nucleons of the parent nucleus (see, for example, reference 6).

(b) The hyperons are originally formed in a type (1) reaction but in their further passage through the parent nucleus they can experience interactions leading to changes of energy and direction of motion.

Apparently both these possibilities are realized.

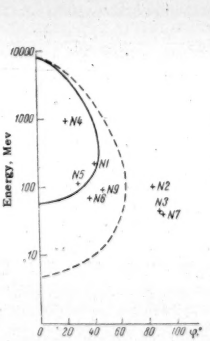

FIG. 2

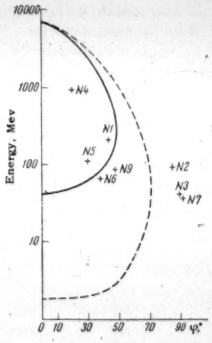

FIG. 3

Actually, a kinematic analysis shows that, taking into account the intranuclear motion of the target nucleon, both cases of pair production of a Σ hyperon and a K^+ meson agree with the scheme

$$\pi + N \rightarrow \Sigma + K. \qquad (2)$$

On the other hand, it is apparently impossible to connect the formation of hyperons no. 2, 3 and 7 with reaction (2). In Fig. 3 the limiting curves for Σ's formed in reaction (2) are given. The solid line again corresponds to a rigid target nucleus, the dotted line includes intranuclear motion. The energy of the π meson chosen is 8 Bev, which corresponds to the maximum possible energy for

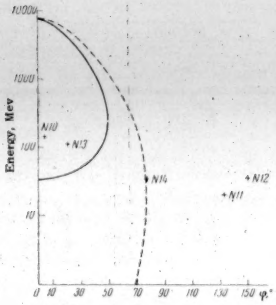

FIG. 4

π's produced by protons with E ~ 9 Bev.* The direction of production of the π is calculated as coinciding with the direction of motion of the primary proton (see reference 7). It follows from Fig. 3 that hyperons 2, 3 and 7 fall outside the region enclosed by the limiting curves. It is natural to suppose that they experienced interactions inside the parent nucleus.†

Analogous reasoning can be carried out for Λ particles, some of which are observed to be produced at such large angles as 133° and 152°. The corresponding data, together with their limiting curves, is shown in Fig. 4 for the reaction

$$P + N \to \Lambda^0 + K + N. \qquad (3)$$

If we look at the reactions in which Λ^0 particles are formed through intermediate pions of high energy (close to 8 Bev), then even in this case the formation of Λ^0 particles 11 and 12 is kinematically impossible.

The authors thank M. I. Podgoretskiĭ for his guidance, V. I. Veksler and M. Ya. Danysh for their participation in discussions, and also Z. P. Golovin, T. A. Zhuravlev, A. M. Kucher, T. N. Mikheev, and N. A. Protsenko for their part in the scanning and measurements.

*When the π-meson energy decreases, the regions enclosed by the limiting curves shrink. The same applies to the reactions of the type $\pi + N \to \Sigma + K + n\pi$.

†Of course, the formation of hyperons through the absorption of slow K^- mesons inside the parent nucleus is not excluded.

[1] Edwards, Engler, Friedlander, and Kamal, Nuovo cimento **5**, 1188 (1957).

[2] Daniel, Krishnan, Mitra, and Pal, Nuovo cimento Supplement **12**, 231 (1954).

[3] Dahanayake, Francois, Fujimoto, Jredale, Waddinton, and Yashin, Nuovo cimento **1**, 888 (1955).

[4] M. F. Rodicheva, Журн. науч. и прикл. фотогр. и кинем. (J. of Sci. and Appl. Photogr. and Cinematogr.) in press.

[5] Bogachev, Van Shu-fen', Gramenitskiĭ, et al. Атомная энергия (Atomic Energy) **4**, 281 (1958).

[6] Besson, Crusard, Fouche, Hennessy, Kayas, Parikh, and Trilling, Nuovo cimento **6**, 1168 (1957).

[7] Bayatyan, Gramenitskiĭ, Nomofilov, Podgoretskiĭ, and Skzhipchak, J. Exptl. Theoret. Phys. (U.S.S.R.) **36**, 690 (1959), Soviet Phys. JETP **9**, 483 (1959).

Translated by W. Ramsay
199

MEASUREMENT OF THE NEUTRON HALF-LIFE

A. N. SOSNOVSKIĬ,* P. E. SPIVAK, Yu. A. PROKOF'EV, I. E. KUTIKOV, and Yu. P. DOBRYNIN*

Submitted to JETP editor September 29, 1958

J. Exptl. Theoret. Phys. (U.S.S.R.) **36**, 1012-1018 (April, 1959)

The half-life of the neutron was measured and found to be equal to 11.7 ± 0.3 minutes.

1. INTRODUCTION

THE free neutron is the simplest beta-emitting nucleus, and a quantitative knowledge of its half-life can give useful information in the explanation of the form of the beta interaction. Interest in this question has increased lately, and demands have arisen for accurate determinations of the half-life of the neutron. However, a more accurate measurement of this important constant involves considerable experimental difficulties, and up to now it has been measured to an accuracy of only 10 — 15%. The present work was undertaken with the goal of significantly improving this accuracy.

Determinations of the half-life of the neutron have been carried out in the U.S.A.[1-3] and in the U.S.S.R.[4] In these works the slow decay protons formed in the powerful neutron beams of a nuclear reactor were accelerated to 10 — 15 kev and were detected either directly[2,4] or by their coincidences with decay electrons.[1,3] In all these cases the accelerating electrode was placed near the beam, and the decay protons were "drawn out" of it by a field. For the determination of the half-life it was necessary to calculate what part of the total number of protons being created in some particular part of the beam were detected in the experiment. However, the result of the calculations was also determined, under the conditions of the experiment, by the spectrum of the decay protons. Experimentally, this spectrum is still insufficiently known,[4,5] and its theoretical form depends strongly on the possible choice of the beta interaction, which is also still insufficiently checked by experiment. Therefore, in experiments with an accelerating electrode alongside the beam the half-life measurements have a systematic uncertainty, connected with the poor knowledge of the proton spectrum, which significantly decreases the accuracy of these experiments.

Such experiments at first produced rather rough estimates of the half-life. Thus Snell, Pleasonton, and McCord gave values from 10 to 30 min,[1] Robson reported 9 to 25 min,[2] and Spivak and Sosnovskiĭ reported 8 to 15 min.[4] In later work Robson got 12.8 ± 2.5 min[3] and Spivak and Sosnovskiĭ 12.0 ± 1.5 min.[4] The latest values were obtained by an arrangement in which the beam was located in the field accelerating the protons, as before; the experiment was set up, however, so that the number of protons picked up by the detector were exactly equal to the number of protons created in a rigorously determined part of the beam. The half-life found in this experiment was free from the uncertainty connected with the proton spectrum.

In the present work the half-life is also determined by directly-measured quantities and by purely geometrical factors which can be accounted for exactly. This was possible thanks to the fact that the decay protons, before coming into the accelerating field, passed through a system of diaphragms. Although the number of protons N_p picked out by these diaphragms was only a small part of the whole quantity formed in the effective part of the beam, these protons enter the accelerating field with small angular dispersion. This allows one to fully focus them on the entrance aperture of the detector with relatively little effort. Therefore, in the formula for the half-life of the neutron,

$$T = kJ \ln 2 / N_p, \qquad (1)$$

where J is the integral of the neutron density over the beam cross-section, the coefficient k depends only on the geometrical conditions of the experiment and the distribution of neutrons in the beam.

2. DESCRIPTION OF THE APPARATUS

The measurements were carried out on a beam of neutrons from the RFT reactor. A longitudinal section of the apparatus is displayed in a schematic diagram (Fig. 1). A well-collimated neutron beam with a diameter of 80 mm passed through the vacuum chamber 1, in which a vacuum

*Deceased.

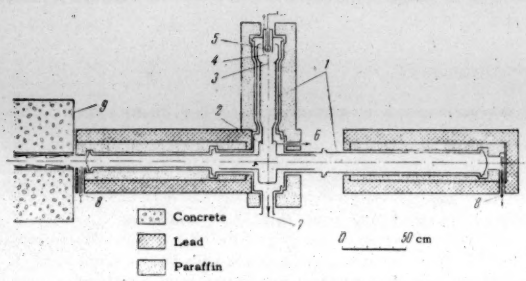

FIG. 1. Schematic diagram of the apparatus. 1 – apparatus shell, 2 – diaphragm, 3 – diaphram with grid, 4 – spherical grid, 5 – proportional counter, 6 – high voltage electrode, 7 – diffusion pump outlet, 8 – monitors, 9 – reactor shield.

of $\frac{1}{2} \times 10^{-6}$ mm is maintained. A hollow electrode 6, which was given a positive potential of 20 kv, was placed in the chamber. The decay protons appearing in the beam opposite to diaphragm 2 (diameter, 78 mm) passed through into this electrode (in which a field existed) and up to grid 3 (diameter, 100 mm). The diaphragm 2 and the grid 3 were distant, respectively, 13.6 and 82.1 cm from the axis of the beam. Beyond grid 3 the decay protons came into a region where the electric field between the grounded spherical grid (3 cm radius) and the high-voltage electrode accelerated them and focussed them onto detector window 5. The accelerating field was very nearly spherical so that the motion of the protons in it could be easily calculated. The calculations showed that a potential of just 10 kv ensured that all the protons passing through diaphragm 3 were collected at the detector window. The characteristics of the focusing system were examined in special trials in which one investigated the dependence of the number of protons both on the size of the charge and on the placement of detector 5 and the dimensions of the entrance window 3. The results of these trials affirmed the calculation and provided full confidence in that, for 20 kv — the potential which was actually used, to assure a better relation to background effects — all the decay protons coming into the focusing field were definitely collected at the detector window.

For the proton count one used a Geiger-proportional counter, whose construction and characteristics are described in detail in reference 4. The counter window (16 mm diameter) was covered by a thin film of collodion (0.07 μ thick), which was backed from the vacuum side by a tungsten grid (wire diameter, 2.5 μ; spacing, 0.5 mm). A second grid (wire diameter, 20 μ, spacing, 0.9 mm) was placed on the other side of the film to shield the effective volume of the counter from charges collected on the film.

Since four grids were placed between the creation point of the decay protons and the counter effective volume, part of the protons were absorbed by them and did not reach the counter. If the counter recorded n_p protons, then

$$n_p = \alpha N_p,$$

where N_p is the quantity of protons hitting counter 3, and α is the transmissivity of all the grids.

Grid 3, covering the entrance window of the focusing system, was made out of wires of 20 μ diameter in a square mesh 4 mm on a side. The geometrical transmissivity of such a grid is close to 0.99. In actuality it was even closer to unity because of the "hanging" of the field onto the relatively coarse mesh. Therefore we did not take into account the absorption in this grid, including it instead in an increase of the error in α. The geometrical transmissivity (for normal incidence) of the spherical grid 4 was 0.913, and those of the grids at the counter window were 0.950 and 0.978. From this, the transmissivity of all grids for normally incident protons was 0.848. The value for the largest possible angles of inclination of the protons from the normal was a bit smaller than this, 0.838. Since the protons were incident on the grids at angles spread between these two extreme values, the value $\alpha = 0.843 \pm 0.006$ was taken for the general transmissivity of all the grids.

3. MEASUREMENT OF THE BEAM NEUTRON DENSITY

The neutron density was determined by the activation of sodium targets, whose cross section follows the 1/v law,[6] and by the activation of gold targets, applying corrections for the neutron resonance effect.

The absolute number of β electrons for Au^{198}, gotten by the 4π counter method, was a supporting measurement for both methods. The neutron den-

sity measurement by activation of gold was carried out with two targets, one of which was prepared by evaporation in vacuum, in the form of a thin layer of gold (0.06 mg/cm^2) on a metallized collodion film. The other, thicker one (40 mg/cm^2) consisted of precisely weighed gold foil.

The absolute number of decays from the thin target, measured by the spherical counter, and the relative activity of both targets, measured by the gamma radiation on a scintillation counter, made possible the determination of the neutron density, after making the corrections for neutron resonance. The corrections were got by the measured cadmium ratio values for gold and the 1/v detector; they were 2.84 and 23.4, respectively.

The determination of the neutron density by activation of the sodium target was made by measuring the intensity of its emitted gamma rays with a scintillation counter; the coefficient of proportionality between the neutron density ρ and the measured velocity of the gamma rays was found by a separate experiment. In this experiment the sodium target was placed in a collimated beam of thermal neutrons, whose density had been found by the absolute number of decays as described above for gold. The relation of the measured neutron density to the gamma activity of the sodium target, measured by the same scintillation counter, gave the value of the constant of proportionality.

In this experiment the correction for the neutron resonance effect in gold was insignificant (0.7%), since the cadmium ratios, measured with thermal neutrons for Na and Au, were 4000 and 150. So one could be confident that the error in the neutron density determined by the sodium activation was fixed only by the errors in the gold cross-section, $\sigma_{abs} = (98 \pm 1.5) \times 10^{-24}$ cm^2 (reference 7) for E = 0.025 ev, and by those in the absolute measurements with the 4π counter ($\pm 0.5\%$) and in the relative measurements with the scintillation counter ($\pm 0.5\%$). The error for the gold cross-section includes 0.5×10^{-24} cm^2 for deviation from 1/v.

The results of the neutron density measurements by the activation of gold and sodium in the center of the same beam in which the half-life measurements were made coincided within limits of $\pm 0.5\%$. These density measurements gave a value of $\rho = 2.17 \times 10^3$ neutrons/cm^3, $\pm 1.8\%$.

The integral of the density J, which enters in relation (1), was determined by the activation of the gold foil, which was placed across the beam, completely blocking it. The foil, therefore, was completely cut to pieces and the scintillation detector miscounted its activity. Therefore the relation of these pieces to the specific activity of the central piece was determined. The application of this relation to the value of the neutron density ρ in the center of the beam gave the wanted value of the integral of the neutron density, $J = (7.68 \pm 0.15) \times 10^4$ neutrons/cm.

4. DETECTION OF THE DECAY PROTONS

As already mentioned, the decay protons were detected with a proportional counter, the end of which was covered by a thin film. The counter was filled with pure carbon tetrafluoride at a pressure of 10 mm of mercury, so that the range of protons with energies about 20 kev was contained within the counter.

The decay protons were counted directly but did not coincide with the number of electrons, so that their number was determined as the difference in count when the accelerating potential was turned on and then off. One had to reckon with the fact that the inclusion of the accelerating potential led to some increase of the count even in the absence of the neutron beam. Investigation of this effect showed[4] that it was caused by the detection of H_1^+ ions coming from the apparatus. Polishing and oxidizing the aluminum high-voltage electrode and other parts, measures prompted by the experience of past work, allowed us to make this effect much smaller than the count of the decay protons.

The count of H_1^+ ions fell slowly as the equipment stood under vacuum, but such ions were always observed in a freshly pumped-out apparatus; using this fact, it was possible to carry out a series of controlled experiments. It was found primarily that the magnitude of the effect depended neither on the degree of irradiation of the apparatus nor on whether the neutron beam passed through the chamber or was shut off from it. This allowed us to determine, for the shut-off beam, the effect of the H_1^+ ions as the difference in counts with and without accelerating potential.

Besides this, when the number of H_1^+ ions was large, one could construct — for a chosen multiplier — an integral curve for the distribution of momenta and set the discriminator level to a value corresponding to the plateau of this distribution (Fig. 2, dotted line). In counting the decay protons, the number of protons and, even more so, the number of H_1^+ ions was not large and the scheme previously set up (for the H_1^+ ions) was repeated and periodically checked with the aid of

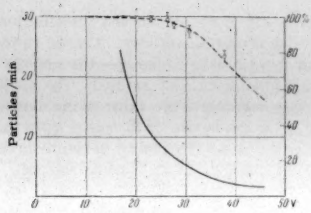

FIG. 2. Integral distribution of pulse amplitudes of H^+ ions – dotted curve; dependence of the background on the discriminator level – solid curve; o – decay protons (control values).

alpha particles from a source (Am^{241}) that could be moved within the vacuum chamber. This was also convenient because it appeared that the integral curves of the momentum amplitude distribution for alpha particles and H_1^+ ions coincided with good accuracy, if for the alpha count the amplifier strength was decreased as necessary.

The gas multiplication factor of the counter was preserved unchanged through the long hours of the experiment by the use of a grid to shield the charges on the film, by stabilizing the supply, by the nature of the gas used, and by the large ballast volume joined to the counter.

Since the measurements were rather lengthy, two extra ionization chambers, their stability controlled by the activation of copper targets, were used to detect fluctuations in beam intensity. The counting procedure for the decay protons is illustrated in the table, where several measurement cycles, each consisting of four short trials, are shown. Twenty-five measurement cycles were carried out, and the decay proton count was found to be 29.6 ± 0.4 protons/min. This value was reconciled with the results of the monitor chambers, with which the beam neutron density was determined. The deviations of the results of the individual cycles are in good agreement with the statistical error for the average values.

The measurements were carried out for discriminator levels somewhat higher than necessary to count all the decay protons, but the background effect correlation was much more favorable for this setting than for a lower discriminator level.

The results obtained, together with some control values measured for large biases are shown in Fig. 2. From this figure it is evident that the extrapolation to zero bias could be done rather exactly, since the error, (1.5 ± 0.5)%, was small. The extrapolated value for the number of protons was $N_p = 30.0 \pm 0.4$ protons/min; taking into account the transmissivity of the grids ($\alpha = 0.843$) we get $N_p = 35.6 \pm 0.54$ protons/min.

As to systematic errors, notice must be taken of the danger involved in the circumstance that the decay protons have to travel a rather long distance, about 80 cm, before they enter the accelerating field. However, loss of protons in this way, by scattering and charge exchanges in collisions with residual gas molecules – pressures were 1 or 2×10^{-6} mm of mercury (measured directly in the chamber) – could take place only for the insignificant soft part of the proton spectrum, even for the worst conceivable cross-section value; the proton loss can hardly have exceeded several tenths of a percent.

Besides, the protons scattered into small angles on the sides of the electrode could hit the aperture of diaphragm 3 and raise the count somewhat, but only if this effect was not compensated for by proton charge exchange during scattering.

The measurements described above were carried out with a large quantity of thin diaphragms placed inside the electrode between diaphragms 2 and 3. We repeated the measurements, using the same accuracy, with the diaphragms removed, when the potential scattering surface for the protons was almost a hundred times greater. The agreement of the results showed that the effect discussed actually did not occur.

5. DETERMINATION OF THE COEFFICIENT k

The value of the coefficient k in formula (1) is determined by the geometrical conditions of the experiment and by the neutron density distribution in the plane perpendicular to the beam axis.

Neutron beam on			Neutron beam off			Number of decay protons in one min
Number of counts in 20 min			Number of counts in 20 min			
Accelerating voltage on	Accelerating voltage off	Decay proton and hydrogen ions	Accelerating voltage on	Accelerating voltage off	Hydrogen ions	
864	280	584	81	47	34	27.5
874	249	625	66	54	12	30.65
917	263	654	80	62	18	31.8
859	280	579	58	58	0	28.95
823	213	610	80	56	24	29.3

To carry out the calculation, involving a numerical integral, the effective volume of the beam was cut up into 900 elements in the form of long parallelopipeds along the beam, each having a transverse cross section in the form of a square, 0.3×0.3 cm. The number of decay protons incident on the aperture of the focusing system from the i-th element is proportional to the product $P_i L_i$, where P_i is the neutron density of the i-th element and L_i its geometrical "weight." The total number of protons incident on the counter from the whole beam volume is proportional to $\Sigma P_i L_i$. This quantity, referred to ΣP_i, is the unknown.

The "weights" L_i, which depend only on the geometrical conditions of the experiment, were calculated with an electronic computer.

The neutron density distribution was determined from the activation of a gold foil. For this, the gold foil was cut up into 900 squares, which coincided with the cross sections of the volume elements used for the numerical integration, and the specific activity of each, which was proportional to P_i, was determined. Figure 3 illustrates the neutron density distribution in the beam.

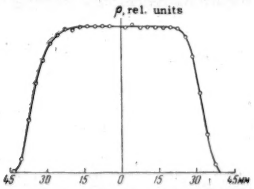

FIG. 3. Neutron density distribution over the beam diameter.

The coefficient k was determined with the help of a computer and found to be 7.87×10^{-13} cm. The value of d depends only insensitively on the form of the density dependence. For example, changing the density distribution by substituting a similar one for a somewhat smaller beam diameter (70 mm) leads to a value $k = 7.84 \times 10^{-3}$ cm. The error in the calculation of k was found to be due, in the main, to the inaccuracy in the given geometry of the apparatus and did not exceed some tenths of a percent.

6. RESULTS OF THE MEASUREMENTS

Substitution of the values of J, N_p, and k in Eq. (1) give for the half life of the neutron the value*

$$T = (11.7 \pm 0.3) \text{ min.}$$

*Here, as in all the other cases, the reduced mean-square error is used.

The reduced lifetime of the neutron is thus $fT = 1180 \pm 40$.*

For tritium, a value $fT = 1132 \pm 40$ (reference 9) was cited in the literature until recently. Not long ago the mass difference for H^3 and He^3 was measured, and from those data it follows that for tritium, $fT = 1132 \pm 40$ (reference 10). Thus it appears that the fT of the neutron and that of tritium are, with good accuracy, identical. If use is made of the conection between the quantity fT and the ratio of the constants G_{GT} and G_F, then comparing the fT of the neutron and of O^{14}, $fT = 3103 \pm 62$ (reference 11), we get

$$G_{GT}^2 / G_F^2 = 1.42 \pm 0.08.$$

The authors are grateful to Academician I. V. Kurchatov for his continuing interest in the work. We want to express our gratitude to the mathematical group, in the persons of M. R. Shura-Bura, E. S. Kuznetsov, and their co-workers I. G. Krutikova, V. N. Toroptseva, and O. B. Moskalev, for their indispensable computer work, and also to the group operating the RFT reactor.

[1] Snell, Pleasonton, and McCord, Phys. Rev. **78**, 310 (1950).

[2] J. M. Robson, Phys. Rev. **78**, 311 (1950).

[3] J. M. Robson, Phys. Rev. **83**, 349 (1951).

[4] A. N. Sosnovskiĭ and P. E. Spivak, Physical Research, Reports of the Soviet delegation to the International Conference on the Peaceful uses of Atomic Energy, U.S.S.R. Acad. Sci. Press (1956).

[5] J. M. Robson, Phys. Rev. **100**, 933 (1955).

[6] Harris, Muelhause, and Thomas, Phys. Rev. **79**, 11 (1950).

[7] D. J. Hughes and J. A. Harvey, Neutron Cross Sections, McGraw-Hill, N. Y., 1955.

[8] B. S. Dzhelepov and L. N. Zyryanova, Влияние электрического поля атома на бета-распад (The Influence of the Atomic Electric Field on Beta Decay), U.S.S.R. Acad. Sci. Press (1956).

[9] O. Kofoed-Hansen and A. Winther, Kgl. Danske Videnskab. Selskab, Mat.-fys. Medd. **30**, no. 20 (1956).

[10] M. Goldhaber, Proceedings, 1958 Annual International Conference on High Energy Physics at CERN, 233, Geneva (1958).

[11] J. B. Gerhard, Phys. Rev. **109**, 897 (1958).

Translated by W. Ramsay
200

*The value of f is calculated from the tables of Dzhelepov and Zyryanova.[8]

LOW ENERGY POSITRONS FROM THE μ^+-e^+ DECAY

A. O. VAĬSENBERG

Submitted to JETP editor October 8, 1958

J. Exptl. Theoret. Phys. (U.S.S.R.) **36**, 1019-1021 (April, 1959)

The value $\rho = 0.72 \pm 0.10$ was obtained for the Michel parameter by analyzing available data on the spectrum of low-energy positrons emitted in μ^+-e^+ decays in photographic emulsions.

IN the study of the anisotropy in the directions of emission of positrons from the π^+-μ^+-e^+ decay[1,2] some indications appeared for low-energy positrons ($\lesssim 20$ Mev) of a μ-e correlation which was larger than predicted by the two-component neutrino theory.[3] Because of this the study of the positron distribution in the low-energy region of the spectrum became of interest. It should be noted that in this region those radiative corrections to the spectrum are of greatest importance which depend on the covariant involved in the decay interaction and they affect the spectrum shape as well as the μ-e correlation. Consequantly this low energy region of the spectrum may be a source of information on the type of covariant involved in the μ-e decay interaction. However this region of the spectrum is poorly known. If measurements are carried out by electronic methods and the mesons are stopped in a layer of dense matter, the spectrum of slow electrons will be strongly distorted by initial energy losses and by scattering. In photoemulsions or in chambers, where the entire electron track from the decay point is available for study, the above mentioned difficulty does not occur; however the statistical accuracy of such measurements is usually low.

Vaĭsenberg et al.[1] measured the spectrum of 1100 positrons by their multiple scattering in emulsion. Analogous spectra,[4-9] published in recent years, contain a total of 1850 particles. Thus data is available on 2950 positrons where the energy of all the positrons was measured by the same method under approximately the same conditions, and therefore this composite spectrum may be studied in the low energy region. Such a study permits a relatively accurate determination of the Michel parameter ρ. This is possible because the low-energy region is most sensitive to the value of this parameter. From the expression for the positron spectrum as given by the four-fermion interaction

$$P(\varepsilon)\,d\varepsilon \sim 4\varepsilon^2 [3(1-\varepsilon) + 2\rho(4/3\,\varepsilon - 1)]\,d\varepsilon \qquad (1)$$

(here ϵ is the positron energy in units of maximum energy) it is easy to show that as ρ varies from 0 to 0.75 the relative number of low energy particles

$$\eta_{<\varepsilon} = \int_0^{\varepsilon} P(\varepsilon)\,d\varepsilon \quad (\varepsilon \leqslant 0.3 - 0.4)$$

changes by approximately a factor of two. On the other hand those characteristics of the spectrum that are determined by high energy particles depend on ρ only slightly. Thus, for example, the above-mentioned change in ρ changes the average energy of the decay electrons merely from 0.6 to 0.7. Another circumstance favorable to the determination of ρ is the fact that the low-energy region is least affected by the spread in the scattering measurements and by bremsstrahlung in the emulsion. This can be seen from the figure, where we show the positron spectrum for $\rho = 0.75$, and the same spectrum washed out by the spread in the measurements and by bremsstrahlung in the emulsion under our experimental conditions. For ϵ less than $0.3 - 0.4$ the two spectra differ by very little.

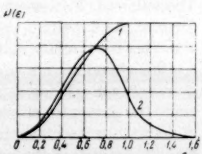

Positron spectrum from the $\mu^+ \to e^+$ decay for $\rho = 3/4$ (ε – positron energy, $p(\varepsilon)$ – decay probability): 1 – theoretical spectrum, 2 – same spectrum washed out by instrumental errors.

The experimental data are shown in the table. The second column gives the total number of particles in the spectrum and the fourth column gives the number of particles in energy intervals near the beginning of the spectrum. These data are subject to two corrections. In the first place, low-energy electrons are strongly scattered and leave the emulsion, so that the number of tracks of a given length depends upon the energy. This effect was estimated by Davies et al.[8] and by

Reference	Number of particles in spectrum	Energy interval	Number of low energy particles	Number of particles after corrections	ρ
[1]	1100	0—0.1	2		
		0.1—0.2	16	51	0.69±0.15
		0.2—0.3	46		
		0.3—0.4	96	71	0.48±0.14
[4]	405	0—0.26	22	18	0.41±0.30
[5,6,7,8]	1161	0—0.1	2		
		0.1—0.2	14	42	0.95±0.12
		0.2—0.3	36		
		0.3—0.4	88	71	0.60±0.13
[9]	286	0—0.14	3		
		0.14—0.24	8	15	0.83±0.23
		0.24—0.33	8		
		0.33—0.43	18	15	0.94±0.24

Bramson et al.,[9] and using their results we deduced the relevant corrections; they are not greater than a few percent in magnitude for the very lowest energies. Secondly, there are corrections due to the "washing out" of the spectrum (see figure). For our measurements in the energy interval from 0 to 0.4 this correction amounts to nearly 20%. The same correction was applied to the measurements of the other authors. This is justified by the smallness of the correction as well as by the fact that for low energies this correction should be approximately the same in all measurements, performed by the same method, of tracks of approximately the same distribution in length.

After integration we obtain from Eq. (1) the following expression for ρ:

$$\rho = 3(4-3\varepsilon)/8(1-\varepsilon) - 3\eta_{l<\varepsilon}/8(\varepsilon^3-\varepsilon^4). \qquad (2)$$

In the sixth column of the table we give ρ, calculated in this manner, for the indicated energy intervals. The values of ρ lie in the interval from 0.41 to 0.95. However, as can be shown by applying the χ^2 test, they are in sufficiently good agreement with each other. Indeed, the extreme values of ρ are accompanied by large statistical errors. The average value, weighted according to the error, is $\rho = 0.72 \pm 0.06$.

Beside the statistical error one must consider the uncertainty in the determination of the scattering constant for electrons is emulsion. The existing data permit us to conclude that this constant is known accurate to 2 or 3%. A three-percent change in this constant corresponds to a ten-percent change in the value of ρ. Another source of error is to be found in the corrections that were applied. This error, however, is not too important since it amounts to only half the statistical error. Consequently the indicated statistical error should be multiplied by about 1.5 to take into account the uncertainty in the scattering constant. In conclusion we obtain

$$\rho = 0.72 \pm 0.10.$$

This value of ρ agrees well with the most precise determination known[10] in which, however, the main contribution comes from particles at the high energy end of the spectrum. Therefore it may be said that in the low energy region which we studied the spectrum shape is in agreement with that predicted by the two-component neutrino theory, which in the absence of radiative corrections gives the value 0.75 for ρ.

[1] Vaĭsenberg, Smirnit-skiĭ, Kolganova, Minervina, Pesotskaya, and Rabin, J. Exptl. Theoret. Phys. (U.S.S.R.) **35**, 645 (1958), Soviet Phys. JETP **8**, 448 (1959).

[2] Barmin, Kanavets, Morozov, and Pershin, J. Exptl. Theoret. Phys. (U.S.S.R.) **35**, 542 (1958), Soviet Phys. JETP **8**, 374 (1959).

[3] L. Landau, Nucl. Phys. **3**, 127 (1957).

[4] Babayan, Marutyan, Matevosyan, and Sarinyan, J. Exptl. Theoret. Phys. (U.S.S.R.) **35**, 561 (1958), Soviet Phys. JETP **8**, 387 (1959).

[5] Bonetti, Levi Setti, Panetti, Rossi, and Tomasini, Nuovo cimento **3**, 33 (1956).

[6] C. Castagnoli, Padua Conference (1957).

[7] C. Mabboux-Stromberg, Ann. phys. **9**, 441 (1954).

[8] Davies, Lock, and Muirhead, Phil. Mag. **40**, 1250 (1949).

[9] Bramson, Seifert, and Havens Jr, Phys. Rev. **88**, 304 (1952).

[10] L. Rosenson, Phys. Rev. **109**, 958 (1958).

Translated by A. M. Bincer
201

MAGNETO-OPTICAL RESONANCE IN NICKEL AT INFRARED FREQUENCIES

G. S. KRINCHIK and R. D. NURALIEVA

Moscow State University

Submitted to JETP editor October 9, 1958

J. Exptl. Theoret. Phys. (U.S.S.R.) **36**, 1022-1024 (April, 1959)

Resonance absorption of infrared light in nickel has been detected by a magneto-optical method. The resonance wavelength of $4 \pm 0.5\,\mu$ corresponds to the reorientation energy of the electron spin magnetic moment in the exchange field of a ferromagnet.

RECENT measurements of the magneto-optical characteristics of nickel in infrared, visible, and ultraviolet light[1-3] have made it possible to detect resonance effects in the region of 1 and $5\,\mu$. The first of these resonances is due, apparently, to electron transitions between the 3d and 4s bands. Such a possibility was predicted theoretically in a formulation of the quantum theory of magneto-optical phenomena.[4*]

More interesting is the second resonance, observed at $5\,\mu$. Firstly, such low-energy transitions cannot be investigated by the x-ray method or by the method of discrete electron energy losses. Secondly, the natural frequency of this resonance corresponds to the energy of spin flip in the molecular field of the ferromagnet, and we may be dealing here with exchange resonance. We therefore undertook more precise measurements in the region of second resonance.

In this investigation we measured, as previously, the change in the intensity of reflected light upon reversal of magnetization of the ferromagnet. The principal apparatus used for such measurements is described in reference 2. Light, polarized in the plane of incidence (p wave) is reflected from the specimen and strikes one of the junctions of a vacuum thermocouple. A portion of the light from the same source is aimed with a system of mirrors onto the second, compensating junction of the thermocouple. Before each measurement, the intensities of the two beams are equalized. When the magnetization of the specimen is reversed, the intensity of the first beam changes by an amount $2\Delta I$, which is registered by an M21/4 galvanometer connected to the output of an FEOU-15 photoelectron-optical amplifier. Knowing the intensity of the light reflected from the specimen, we obtain the relative change in the intensity of the light during magnetization, $\delta = \Delta I/I$.

The specimen was a mechanically polished plate of electrolytic nickel, $40 \times 40 \times 3$ mm, placed between the poles of a small electromagnet. The specimen was magnetized to saturation, i.e., the so-called equatorial magnetization was produced. This effect can be analyzed phenomenologically by assuming the ferromagnet to be a gyrotropic medium. The dielectric-constant tensor is then

$$[\varepsilon] = \begin{vmatrix} \varepsilon & -i\varepsilon M & 0 \\ i\varepsilon M & \varepsilon & 0 \\ 0 & 0 & \varepsilon_0 \end{vmatrix}.$$

For a gyromagnetic medium, the magnetic permeability has a similar form. The magneto-optical parameter $M = M_1 - iM_2$ is a constant of the substance and determines the magnitudes of all the magneto-optical effects. M_1 and M_2 can be determined from two independent measurements made on any magneto-optical effect for light of a given frequency. In reference 1 the following formula was obtained for the relation between δ and M_1 and M_2

$$\delta = 2 \sin 2\varphi\,(M_1 A - M_2 B)/(A^2 + B^2), \qquad (1)$$

where $A = \epsilon_2 \cos^2\varphi - q$, $B = \epsilon_1 \cos^2\varphi - 1 + p$, $p = \epsilon_1 \sin^2\varphi/(n^2+k^2)^2$, $q = \epsilon_2 \sin^2\varphi/(n^2+k^2)^2$, $\epsilon_1 = n^2 - k^2$, $\epsilon_2 = 2nk$, and φ is the angle of incidence. Bonetti et al.[5] considered the general case of a bi-gyrotropic medium and obtained an analogous formula for a gyromagnetic medium.

Figure 1 shows the measured values of δ for nickel at various angles of light incidence. Each point on the curve was obtained by averaging 40 readings. The mean-squared measurement er-

*In connection with this, it would be desirable to find an analogous resonance at ultraviolet frequencies, where the presence of inter-band electron transitions in nickel were established by the x-ray method and by the method of discrete electron energy losses. However, progress in the ultraviolet region down to $0.3\,\mu$ is still insufficient to observe the expected resonance with certainty.[3]

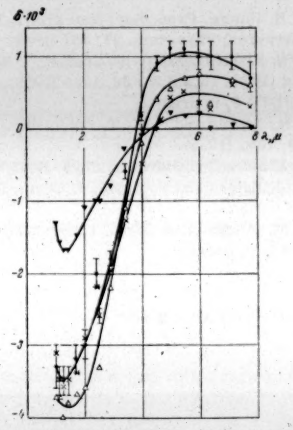

FIG. 1. Variation of the intensity of reflected light during magnetization of nickel, for various angles of incidence: • – 85°, Δ – 80°, × – 75°, ▼ – 60°.

ror, which was determined for all cases, is shown for only one of the curves.

A singularity is observed on these curves in the region from 4 to 8 μ: the effect reverses its sign and reaches a considerable magnitude. This is particularly interesting since, according to (1), δ is inversely proportional to n^2 and k^2, while n and k increase strongly with increasing wavelength.

Figure 2 shows curves of M_1 and M_2, calculated by formula (1) for the values of δ obtained at $\varphi = 75°$ and $\varphi = 85°$. The values of n and k used in these calculations were determined from the curves for ϵ_1 and ϵ_2, obtained in reference 6. This is the principal source of the possible systematic errors, since the optical constants of our specimen may differ greatly from the foregoing ones. As a check, measurements were made on less pure, non-electrolytic nickel, and the results, although lower, were qualitatively the same. As can be seen from the curves of Fig. 2, the resonance region is clearly shown, although the error in the determination of M_1 and M_2 increases with increasing λ. The resonant frequency can be determined from the position of the maximum of M_2, i.e., it equals $4 \pm 0.5\,\mu$. At this frequency M_1 apparently reverses its sign.

The origin of the observed resonance is still not clear. One can assume that it is due either to electronic transitions between 3d and 4s bands, or to spin reorientation in the volume under the influence of the light wave. The first explanation

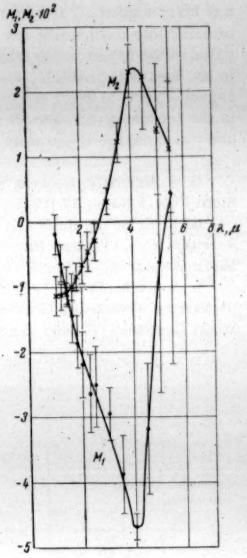

FIG. 2. Real and imaginary components of the magneto-optical parameter of nickel in the infrared region.

is generally accepted and the theory based on it gives the required order of magnitude for the magneto-optical effects.[4] However, the value of the transition energy in our case is ~0.3 ev, while theoretical estimates of this energy, made from the widths of the energy bands, give a value of several electron volts. The second explanation leads directly to a correct numerical value of the resonant frequency,[1] but no further comparison with experiment can yet be made for lack of a theory. The calculation of the exchange resonance on the base of a model of two interacting "sublattices" of s and d electrons gave too small a value for the effect,[1] and exchange resonance in a ferromagnet with one sublattice is generally considered impossible.[7] But it has been shown recently[8] that resonant absorption of light should be observed at the exchange frequency in

λ, μ	n	k	λ, μ	n	k
1	2.6	5.3	3.5	4.7	11.8
1.2	2.9	6.0	4.0	4.8	13.4
1.4	3.1	6.7	4.5	4.8	15.5
1.6	3.3	7.3	5.0	4.9	17.6
1.8	3.6	7.9	5.5	5.1	19.0
2.0	3.7	8.5	6.0	5.4	20.6
2.25	3.9	9.2	6.5	5.8	21.8
2.5	4.0	9.3	7.0	6.1	23.0
3.0	4.4	10.4			

any ferromagnet. Further calculations will show whether this mechanism can ensure the observed value of the effect in the infrared region. If this is so, then it is possible, with the aid of the observed effect, to study the exchange interaction in the ferromagnets, and, in particular, to measure the exchange integral by direct methods.

[1] G. S. Krinchik, Вестник МГУ (Bull. Moscow State Univ.) No. 6, 87 (1957).

[2] G. S. Krinchik and R. D. Nuralieva, Физика металлов и металловед. (Physics of Metals and Metal Research) **7**, No. 5 (1959).

[3] G. S. Krinchik and I. S. Stroganova, Физика металлов и металловед. (Physics of Metals and Metal Research) **7**, 460 (1959).

[4] H. R. Hulme, Proc. Roy. Soc. **135**, 237 (1932); P. N. Argyres, Phys. Rev. **97**, 334 (1955).

[5] G. S. Krinchik and M. V. Chetkin, J. Exptl. Theoret. Phys. (U.S.S.R.) **36**, 1924 (1959), Soviet Phys. JETP **9**, in press.

[6] J. R. Beattie and G. K. T. Conn, Phil. Mag. **46**, 989, 1002 (1955).

[7] C. Kittel and C. Herring, Phys. Rev. **77**, 725 (1950), J. Kaplan and C. Kittel, J. Chem. Phys. **21**, 760 (1953).

[8] N. M. Potapkov, J. Exptl. Theoret. Phys. (U.S.S.R.), in press.

Translated by J. G. Adashko
202

ANOMALOUS ELECTRON SCATTERING AND THE EXCITATION OF PLASMA OSCILLATIONS

M. D. GABOVICH and L. L. PASECHNIK

Institute of Physics, Academy of Sciences, Ukrainian S.S.R.

Submitted to JETP editor October 10, 1958

J. Exptl. Theoret. Phys. (U.S.S.R.) **36**, 1025-1033 (April, 1959)

We have studied the interaction of an electron beam with an independently formed plasma, an interaction leading to an appreciable change in the electron energy and to the excitation of plasma oscillations. The observed data can qualitatively be interpreted by assuming that the electrons form clusters and that these clusters interact coherently with the plasma.

THE phenomenon of the so-called anomalous scattering, which consists in that electrons passing through a plasma experience a strong interaction leading, in particular to the occurrence of anomalously fast electrons, was already described by Langmuir.[1] In a careful study Merrill and Webb[2] established the connection between this phenomenon and the plasma oscillations and in a number of later papers further experimental studies of this effect were made[3-6] or attempts were made to interpret Merrill and Webb's experiments.[7-10] Notwithstanding the progress made in both directions, this problem has not lost its urgency and a further elucidation of it is not only required as far as an additional analysis of the physical phenomena is concerned, but also with respect to obtaining new experimental data.

The method applied in the present research enabled us to analyze more thoroughly the electron beam which passes through the plasma. It was also more flexible since it allowed us to change independently the plasma parameters and those of the electron beam passing through the plasma. This possibility was, for instance, already present in the work of Polin and Gvozdover[11] and of Looney and Brown,[3] but was not used in the direction in which we are interested.

THE METHOD

The apparatus studied was a glass tube T (Fig. 1) which had a lateral branching tube O. Using a liquid-mercury cathode and a system of anodes, one can form a plasma in the mercury vapors along the tube T. By changing the current I_a in the circuit of one of the anodes, we could change the concentration of charges of this plasma, usually within the range from 1×10^9 to 1.5×10^{11} cm^{-3}. We took care that that part of the apparatus which contained the liquid-mercury cathode was removed from the plasma region studied; the liquid cathode was in the coldest position and at constant temperature, so that condensation of mercury at other, hotter places was avoided; the mercury vapor pressure was $p \approx 10^{-3}$ mm Hg.

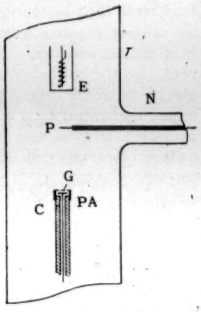

FIG. 1. Diagram of part of the experimental apparatus. E – oxide heater cathode; PA – probe analyzer; G and C – grid and collector of the probe analyzer.

As an electron source we could use a tungsten filament, a tantalum heater cathode, or an oxide heater cathode E. In that part of our research which is described here we used mainly an oxide cathode. By applying an appropriate potential difference between the anode and the emitter E, we could introduce an electron beam into the plasma. The notation used in the following, for instance, E = 50 v, means that the cathode potential relative to the anode was −50 v; the energy of the electrons entering the plasma was in fact less by 2 v (anode drop).

In all similar investigations[1,2,4,5,11] the analysis of the velocity of the velocity of the electrons passing through the plasma was performed by plotting

the normal probe characteristics. Since in that case the division between the fast primary electrons and the "plasma electrons" is impeded and since at high energies of the primary electrons a strong distortion may arise due to the secondary emission from the probe, we employed for such an analysis a modulation of the electron beam in conjunction with use of probe-analyzer PA. The latter consisted of a collector C and a grid G (diameter 1.5 mm, wire diameter 10 μ, width of the square mesh of the grid 50 μ) which screened it from the plasma. A relatively small negative grid potential U_{ac} produces an overlap of it with the ionic film and a delay of the main flow of the plasma electrons. A sufficiently large positive collector potential (for instance +100 v relative to the grid) does not allow the positive ions from the plasma to fall upon the collector; the collector potential was so chosen that a change in it did not produce a change in the collector current. On the collector may impinge: fast primary electrons which cannot be delayed by the grid for a given potential U_{ac}, a small fraction of the plasma electrons, and some fraction of the secondary electrons knocked out of the grid. The last two components of the collector current are weakly affected by the characteristics, and even less in the case of a modulation of the electron beam. The above-mentioned low-frequency modulation was realized in such a way that the cathode E periodically, during 1/40 sec, was at a chosen negative potential, and during the next 1/40 sec at a potential close to the plasma potential. The current in the collector circuit was in that case measured by means of a narrow-band smplifier (frequency 20 cps, band width 2 cps) and all effects connected with the unmodulated plasma in the main discharge were not affected by the characteristics. In Fig. 2, curves 1 and 2 show the dependence of the collector current on the retarding grid potential $PA - U_{ac}$ obtained for a small value of the electron beam current I_e, when there is no anomalous scattering. The fact that the collector current becomes equal to zero for a potential less than 50 v can be explained by the contact potential difference between the grid and the oxide cathode. The drop in potential between the loops of the grid was estimated, and in the most unfavorable case was not more than 1 or 2 v. For small retarding potentials of the grid ($U_{ac} < 20$ v) the behavior of the characteristic was discontinuous, for obvious reasons. The probe-analyzer with a grid of the given geometry could therefore not be used for small beam energies. In that case, and also in other cases when the PA cannot be used for

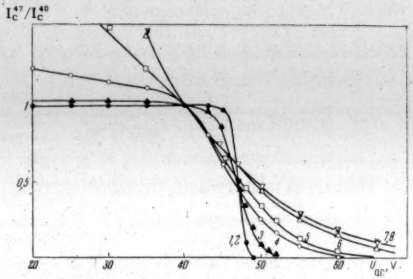

FIG. 2. Dependence of the current in the collector (PA) circuit on the potential of the grid of that probe (I_a = 0.5 amp, E = 50 v, l = 50 mm). 1 – I_e = 0.05; 2 – I_e = 0.8; 3 – I_e = 1.2; 4 – I_e = 1.65; 5 – I_e = 2.25; 6 – I_e = 3.8; 7 – I_e = 6; 8 – I_e = 13 ma.

different reasons, one can use a normal cylindrical probe P with simultaneous modulation of the electron beam. The modulation by itself allows us to separate the probe current of primary electrons (more exactly, the current of the primary beam and the modulated components of the plasma currents) from the probe current, which is connected with the unmodulated plasma of the main discharge.

To indicate the oscillations and to measure their frequency, it was most useful to use a double-wire line connected to the cylindrical probe P (length 5 mm, diameter 150 μ). The latter served also for a measurement of the plasma parameters.

In conclusion we note that both probes were movable and could be placed at any point in space, and their position could be fixed with an accuracy of 0.2 mm. By means of a small motor one could give the probe P a continuous, uniform motion and determine the spatial distribution of the intensity of the oscillations by an EPP-09 recording instrument with a synchronized moving tape.

ANOMALOUS SCATTERING. THE LIMITING CURRENT

In Fig. 2 the delay characteristics are given for different beam currents I_e (E = 50 v, I_a = 0.5 amp) corresponding to a particle concentration $n = 1.6 \times 10^{10}$ in the plasma. The ordinates of all curves are normalized at the point U_{ac} = 40 v. The probe-analyzer was at a distance l = 50 mm from the cathode. When the beam current is small, say I_e = 0.05 – 0.8 ma or less, all curves lie on one another (curves 1, 2). When, for the same beam currents, the particle concentration in the plasma of the main discharge is increased to $n \approx 1 \times 10^{11}$, the form of the characteristics is not changed.

Only beginning with the above-mentioned maximum concentration can one notice in the characteristics a small increase in loss, which can be assumed to be the result of a diffractive scattering connected with Coulomb interaction, as an estimate shows. More important effects were observed when the beam current was increased. As is clear from Fig. 2, starting from some value of the current I_e (curve 3), there appear electrons undergoing a large loss and also electrons with an energy appreciably higher than their original energy (Langmuir[1] was the first to show that these effects set in at large beam currents).

The strong interactions observed at large currents I_e are accompanied by a diffractive scattering of the beam. The particular curves of Fig. 2 were treated as follows. The dependence on the beam current of the ratio of the probe currents for a value U_{ac} near the threshold and one somewhat less [for E = 50 v, the ratio I_c (U_{ac} = 47 v) to I_c (U_{ac} = 40 v)] was determined. Starting with some value of the beam current I_e, the value of this ratio rises steeply and the corresponding value of I_e is a limiting current I_{lim}. It is of interest to determine the dependence of the limiting current on the beam parameters and the parameters of the plasma with which the beam interacts. The data obtained are given in the table. These data correspond to an electron energy E = 50 v. The most important consequence of this table is the independence of the limiting current on the charged-particle concentration in the plasma. We note that for a cathode diameter of 5 mm and E = 50 v a beam with a current I_e = 1.0 ma produces along its track a plasma with a concentration of charges $n \approx 5 \times 10^8$ cm^{-3}, so that the independence of I_{lim} from I_a, which we have established, corresponds to a wide range of values for the charged particle concentration in the plasma. The table discloses some dependence of the limiting current density on the cathode diameter, but since the measurements were performed only on cathodes of three different diameters, it is premature to insist on this sort of dependence. An analysis of similar curves shows that the magnitude of the limiting current increases approximately linearly with the electron energy.

The problem of the spatial location of the region where the observed anomalous scattering takes place is of interest. We cannot use the probe-analyzer in that case, since near the cathode it shows a strong perturbing action on the plasma. We therefore used the probe P simultaneously with modulation of the electron beam. By taking the probe characteristics at different distances from the cathode, we could plot $I_c(55)/I_c(40) = f(l)$, where $I_c(55)$ and $I_c(40)$ are the currents at the probe for grid potentials U_{ac} of 55 and 40 v respectively (electron energy E = 50 v), and l is the distance from the cathode. Such a dependence is given in Fig. 3 for different beam currents I_e, all above the limiting current.

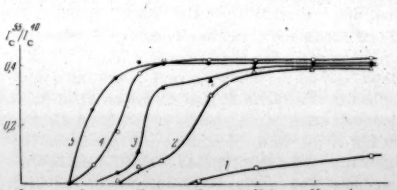

FIG. 3. Dependence of the relative number of anomalously fast electrons on the position of the probe (I_a = 0.5 amp, E = 50 v). 1 – I_e = 1.6; 2 – I_e = 3.8; 3 – I_e = 7.4; 4 – I_e = 12.4; 5 – I_e = 30 ma.

It follows from this figure that an increase of the electron energy occurs in a certain zone. When the beam current I_e is increased, this zone approaches the cathode and its width decreases. We could detect this zone by a somewhat different method and establish that it possesses a structure, for instance, it may consist of two separate zones.

The foregoing characteristics of the delay due to the observed diffractive scattering of the beam enable us to analyze the electrons only as far as the normal velocities are concerned and cannot serve to determine the total energy losses of the electrons. A specially developed method, which will be described elsewhere, made it possible to determine that for electron beam energies E = 50 to 125 v and for a current larger than the limiting value the average total energy loss of the electrons through the interaction with the plasma is 10 to 20%.

In conclusion we note that when the beam current is larger than the limiting value, one can observe an increase in the noise level in the plasma.

Type of cathode and its diameter, mm	I_a = 0.05 amp, n ≈ 1.6·10^9		I_a = 0.5 amp, n ≈ 1.6·10^{10}		I_a = 5 amp, n ≈ 1.6·10^{11}	
	I_{lim}, ma	j_{lim}, ma/cm^2	I_{lim}, ma	j_{lim}, ma/cm^2	I_{lim}, ma	j_{lim}, ma
Oxide, 3	0.9—1.1	12.7—15.5	0.6—0.8	8.5—11.3	0.5—0.7	7—9.9
" 5	1—1.2	5.1—6.1	0.8—1.2	4.1—6.1	1.1—1.6	5.6—8.2
" 10	7—9	8.9—11.5	6—8	7.6—10	5.6—6.6	7.6—10
Ta, 5	0.7—1.1	3.6—5.6	1—1.3	5.1—6.7	0.6—1.5	3.1—7.7

It was impossible to establish "monochromatic" oscillations in the general case.

EXCITATION AND QUENCHING OF PLASMA OSCILLATIONS

The occurrence of anomalously fast electrons can be explained by the production of microwave oscillations. However, in the general case one does not succeed in establishing monochromatic oscillations, as was mentioned above. To find such oscillations the condition $I_e > I_{lim}$ is necessary, but not sufficient. Only by an appropriate choice of I_e and E one can find such conditions that monochromatic oscillations are produced. In those cases one observed an easily expressed oscillation zone, the position and width of which depend both on the beam current (this was established in reference 2) and on the charged-particle concentration in the plasma of the main discharge. In Fig. 4 we show the spatial distribution of the intensity of the oscillations for different beam currents, and in Fig. 5 similar curves for different currents in the main discharge, I_a. In the legends to the figures we have also given the relative intensities of the peaks (I_{osc}). It is clear that an increase in the beam current strength as well as an increase in the current of the main discharge causes the vibration zone to come closer to the cathode and also to become narrower. A complete analogy with the influence of these parameters on the width and position of the scattering zone (see Fig. 3) was observed. It follows from Fig. 5 that an increase in the charge-particle concentration leads to a decrease in the intensity of the monochromatic oscillations produced. In Fig. 6 we have given the dependence of the intensity of the vibrations and their wavelength on the current of the main discharge I_a. This figure shows the quenching of the oscillations when the plasma is intensified and at the same time verifies the correspondence of the observed wavelengths (experimental points) with the ones calculated from the equation $\lambda = 2\pi c/\omega$, where

$$\omega = \{(4\pi e^2/m)(n_b + n_{pl})\}^{1/2}, \qquad (1)$$

and $(n_b + n_{pl})$ denotes the concentration measured while the beam passed through the plasma. If we substitute in Eq. (1) the concentration of charged particles measured without the beam we

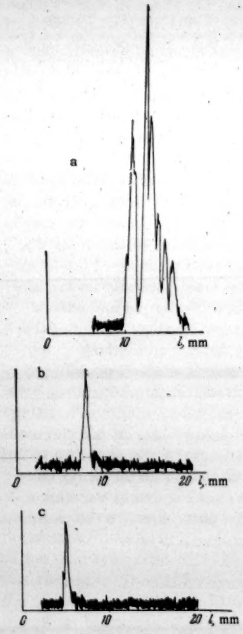

FIG. 4

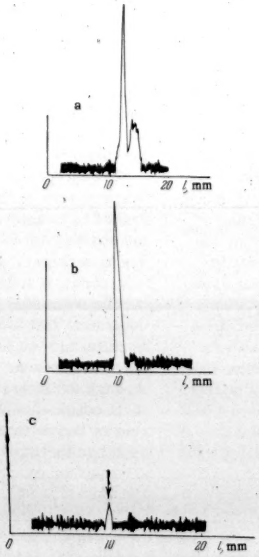

FIG. 5

FIG. 4. Spatial distribution of the oscillation intensity for different electron beam currents (I_a = 10 ma, E = 40 v). a – beam current I_e = 13.5 ma, oscillation intensity I_{osc} = 200; b – I_e = 33 ma, I_{osc} = 300; c – I_e = 68 ma, I_{osc} = 100.

FIG. 5. Spatial distribution of the oscillation intensity for different currents in the main discharge (I_e = 13.5 ma, E = 40 v). a – I_a = 100 ma, I_{osc} = 60; b –, I_a = 400 ma, I_{osc} = 12; c – I_a = 600 ma, I_{osc} = 2.

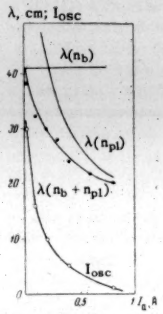

FIG. 6

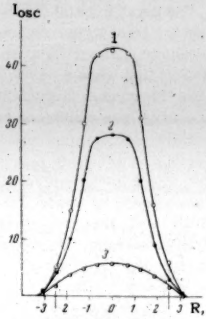

FIG. 7

FIG. 6. Dependence of the wavelength and the oscillation intensity on the current of the main discharge (I_e = 20 ma, E = 28 v).

FIG. 7. The radial distribution of the oscillation intensity in the beam passing through the plasma for different currents of the main discharge (I_e = 20 ma, E = 28 v). 1 – I_a = 0.01; 2 – I_a = 0.1; 3 – I_a = 0.5 amp.

obtain the curve for $\lambda(n_{pl})$. If the concentration were determined by the plasma produced by the beam itself, the line $\lambda(n_b)$ would be obtained.

In Fig. 7 we show the radial distribution of the oscillations for different currents of the main discharge. It is clear that the oscillations are strongly damped in the direction of the periphery of the beam.

INFLUENCE OF AN EXTERNAL MAGNETIC FIELD

The application of an external magnetic field parallel to the direction of the electron beam reduces somewhat the magnitude of the limiting current. For instance, at H = 0, E = 75 v, I_{lim} = 1.4 ma, and at H ≈ 100 to 200 oe, $I_{lim} \approx 0.6$ ma. If prior to application of the magnetic field conditions were such that oscillations with a well defined wavelength were observed, the field causes a steep decrease in the intensity of these oscillations, until it is totally impossible to observe them for H ≈ 30 – 50 oe.

DISCUSSION OF THE RESULTS

The facts stated above, together with those already known, make it possible to give the following picture of the interaction of the beam with a plasma.

In accordance with the prevalent point of view[2,5,8] we shall imagine that near the emitter E at the boundary of the plasma there is a localized modulating voltage of amplitude ΔU. According to the simplest klystron theory the velocity modulation of the electrons leads to a localization of electron clusters at the position

$$l_{osc} = mv_0^3/e\omega\Delta U = mv_0^3\lambda/2\pi ce\Delta U, \qquad (2)$$

where v_0 is the initial electron velocity, ω the modulation frequency, and $\lambda = 2\pi c/\omega$ the measured wavelength of the electromagnetic oscillations. To verify the applicability of Eq. (2) to our case we plotted the dependence of the position of the localization of the center of the oscillation zone l_{osc} on the wavelength λ. Such a plot is given in Fig. 8; to obtain this we varied λ by changing the main-discharge current I_a. Here is also plotted the dependence of the position of the scattering zone on λ (curve 2). As also in the experiments of Merrill and Webb,[2] the oscillation zone is slightly shifted with respect to the scattering zone. In Fig. 9 we have given the dependence $l_{osc} = f(\lambda)$; to obtain this we varied λ by changing the beam current. In all cases one could observe a linear dependence $l_{osc} = f(\lambda)$, corresponding to Eq. (2). A comparison of the slope of these curves with (2) enables us to estimate the unknown ΔU. From Fig. 8, ΔU = 3.9 v (E = 28 v); from Fig. 9, ΔU = 3.7 v (E = 28 v) and ΔU = 5.7 v (E = 41 v). As we have stated, there exists a complete analogy between the behavior of the oscillation zone and the scattering zone in those experiments where no monochromatic oscillations are produced. Using our data on the anomalous scattering, one can construct the dependence of the distance from the cathode

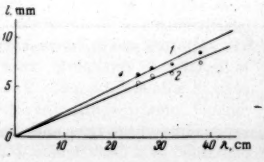

FIG. 8. The dependence of the position of the oscillation zone (1) and of the scattering zone (2) on the wavelength of the observed electromagnetic oscillations (I_e = 20 ma, E = 28 v).

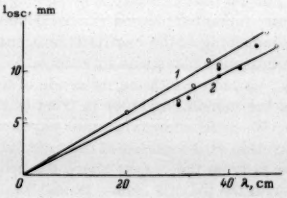

FIG. 9. The dependence of the position of the scattering zone on the wavelength for electron energies of (1) E = 41 v and (2) E = 28 v.

to the scattering zone l_1 on the quantity $\lambda_{eq} = 2\pi c/\omega$ where ω is the frequency of the plasma oscillations; the latter, and hence λ_{eq} can be evaluated using Eq. (1) from the experimentally determined particle concentration in the plasma. The result of such a treatment is given in Fig. 10. The slope of the straight line enables us to determine $\Delta U = 5.1$ v ($E = 50$ v). The value of ΔU cannot be determined in our experiments independently. We can only refer to reference 12 where, by direct measurements, the existence of a variable microwave field with an amplitude of several volts was proved. It seems to us to be incorrect to compare ΔU with the spread in the electron energy determined at large distances, as was done in reference 5.

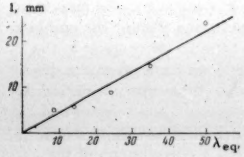

FIG. 10. The dependence of the position of the scattering zone on the wavelength which is equivalent to the given plasma concentration ($I_e = 5$ ma, $3 = 50$ v).

From the data stated above we conclude that the ideas of the importance of phase focusing can be applied to all cases of anomalous scattering, independent of whether or not monochromatic oscillations are observed. In either case the modulation of the electron beam takes place near the cathode with a frequency equal to the natural frequency of the plasma and a consequent formation of clusters leading to a strong interaction (vide infra). The difference between them consists only in the fact that when monochromatic oscillations are observed the phase relations are satisfied and the necessary inverse coupling is maintained constantly, whereas in the other case this does not occur. The quenching of the monochromatic oscillations described above (spreading of the frequency spectrum) can be explained by a disturbance to the necessary feedback and of the phase relations occurring when a sufficiently intensive plasma is introduced.

This quenching of the oscillations occurring when an intensive plasma is introduced is, apparently, connected with the influence of the latter on the modulating layer in front of the cathode. We shall show in another paper that the separation of the region of the modulation of the beam from the region where the beam interacts with the plasma makes it possible to observe in the plasma not the quenching of the oscillations, but their amplification and plasma resonance.

The experimental data given here show that a strong interaction occurs in the region where the electrons bunch into clusters. It is well known[13] that when a particle of charge q and mass M passes through a plasma it undergoes an energy loss which can be evaluated from the formula

$$\frac{d\varepsilon}{dx} = \frac{\omega^2 q^2}{v_0^2} \ln \frac{1.23\, m v_0^3 M}{eq\omega\,(m+M)}, \qquad (3)$$

where ω is the plasma eigenfrequency, v_0 the particle velocity (the formula in this form is valid for $v_0 < eq/\hbar$). If we assume, for instance, $\omega = 1 \times 10^{10}$ sec^{-1}, and $q = e = 4.8 \times 10^{-10}$esu, $M = m$, $v_0 = 2.5 \times 10^8$ cm sec^{-1}, then $d\epsilon/dx = 3.5 \times 10^{-3}$ ev cm^{-1}. The individual interaction of the electrons with the plasma can thus not explain the experimentally observed loss.

If we assume that in these experiments a coherent interaction with the plasma occurs[4] of clusters containing a charge $q = Ne$, where N is the number of electrons in a cluster then the change in energy per electron will be described by the formula

$$\frac{d\varepsilon}{dx} = \frac{\omega^2 e^2 N}{v_0^2} \ln \frac{1.23\, m v_0^3}{Ne^2\omega}. \qquad (4)$$

The number of electrons in a cluster can be estimated as $N = \pi jS/e\omega$ where j is the beam current density and S the cross section for coherently interacting particles in the cluster. If we take $jS \approx I_{lim} \approx 1$ ma and $\omega = 1 \times 10^{10}$ then $N \approx 2 \times 10^6$, and the quantity $d\epsilon/dx$ turns out to be comparable with the experimentally observed magnitude ($d\epsilon/dx \approx 600$ ev cm^{-1}).

The extension of the scattering zone we shall take to be equal to the wavelength of the plasma oscillations $\Delta x \approx \lambda_{pl} \approx 2\pi v_0/\omega$. The change in the electron energy can then be estimated as follows:

$$\Delta\varepsilon \approx \frac{\omega^2 e^2 N}{v_0^2} \lambda_{pl} \ln \frac{1.23\, m v_0^3}{Ne^2\omega}. \qquad (5)$$

If $S > S_c$, where S_c is the cathode surface area, the quantity $\omega^2 N\lambda_{pl} \neq f(\omega)$. The quantity $\Delta\epsilon$ turns thus out to be independent of the particle concentration in the plasma. This is in accordance with the independence of the limiting current on the plasma intensity, established by us. Expression (4) enables us to explain also the increase of the limiting current with increasing initial energy of the particles.

The numerical comparisons given here cannot, of course, pretend to give a quantitative explanation of the observed facts. Indeed, the phenomenon is very complicated and can, in particular, not be

considered to be uniform; this is illustrated by our observations with a probe and visually of an angular divergence of the beam (for $I_e > I_{lim}$) behind the spot where the clusters are localized and by the splitting of the beam into separate rays.[15] However, it seems to us that the considerations given above enable us to combine a large number of experimental facts into one idea about the importance of a bunching of electrons in clusters and about the coherent interaction of the latter with the plasma.

The authors express their gratitude to N. D. Morgulis for discussions of the results of this paper.

[1] I. Langmuir, Phys. Rev. **26**, 585 (1925).

[2] H. J. Merrill and H. W. Webb, Phys. Rev. **55**, 1191 (1939).

[3] D. H. Looney and S. C. Brown, Phys. Rev. **93**, 965 (1954).

[4] G. Wehner, J. Appl. Phys. **22**, 761 (1951).

[5] T. R. Neill and K. G. Emeleus, Proc. Roy. Irish Acad. **A53**, 197 (1951).

[6] Kojima, Kato, and Hagiwara, J. Phys. Soc. Japan **12**, 1276 (1957).

[7] D. Bohm and E. P. Gross, Phys. Rev. **79**, 992 (1950).

[8] A. A. Vlasov, Теория многих частиц, (Many-Particle Theory) GITTL, 1950.

[9] M. Sumi, J. Phys. Soc. Japan **9**, 88 (1954).

[10] P. A. Sturrock, Proc. Roy. Soc. **A242**, 277 (1957).

[11] V. Polin and S. D. Gvozdover, J. Exptl. Theoret. Phys. (U.S.S.R.) **8**, 436 (1938).

[12] Gabor, Ash, and Dracott, Nature **176**, 916 (1955).

[13] A. I. Akhiezer and A. G. Sitenko, J. Exptl. Theoret. Phys. (U.S.S.R.) **23**, 161 (1952).

[14] V. I. Veksler, Атомная энергия (Atomic Energy) **2**, 427 (1957); English abstract in J. Nucl. En. **5**, 265 (1957).

[15] Allen, Bailey, and Emeleus, Brit. J. Appl. Phys. **6**, 320 (1955).

Translated by D. ter Haar
203

He^3 *CRYOSTATS*

V. P. PESHKOV, K. N. ZINOV' EVA, A. I. FILIMONOV

Institute for Physical Problems, Academy of Sciences, U.S.S.R.

Submitted to JETP editor October 16, 1958

J. Exptl. Theoret. Phys. (U.S.S.R.) **36**, 1034-1037 (April, 1959)

Systems are described which permit the attainment and maintenance of temperatures below 1° K through pumping on He^3 vapor. Temperatures down to 0.3° K have been obtained over a volume of approximately 1 cm^3 within a transparent glass system. Temperatures of 0.5° K and higher have been maintained in the presence of a heat influx of 7×10^{-4} W in a continuously-operating metal apparatus containing 140 cm^3 of liquid He^4.

As is well-known, experiments at temperatures between 1 and 4.2° K are carried out in cryostats, Dewars of liquid He^4 subjected to pumping being customarily used for this purpose. At temperatures below T_λ = 2.18° K, however, helium becomes a superfluid, and a film of liquid helium begins to flow rapidly along the Dewar walls to the region of higher temperatures, where it evaporates. This circumstance complicates greatly the attainment of extremely low temperatures by pumping on the helium vapor. The record low temperature for He^4, 0.71° K, was reached by Keesom[1] in 1932, using for removal of the vapor a pump of 675 *l*/sec capacity. Ten years later the same result was obtained by Lazarev and Esel'son,[2] who pumped away the He^4 vapor through a diaphragm having a very small aperture (0.05 mm in diameter), using for this purpose a pump of relatively small capacity, 15 *l*/sec. Temperatures below 0.7° K have not been obtained at all by these means.

The extremely rare helium isotope He^3 does not become superconducting even at the lowest temperatures; its use in systems for the attainment of low temperatures by vapor pumping is therefore highly effective.

At the present time there are, both here and in other countries,[3,4] a number of low-temperature establishments in which He^3 is used as a working substance for obtaining temperatures substantially below 1° K. The present paper is concerned with the description of two such systems in use at the Institute for Physical Problems.

The first of these systems is represented schematically in Figure 1b, together with the apparatus for the production of low temperatures. This same apparatus is illustrated separately in Figure 1a. The system consists of the double Dewar 1 filled with He^4, within which is situated a smaller, transparent glass Dewar 2, containing liquid He^3 and having a volume of approximately 3 cm^3. The He^3 vapor is pumped off through a thin-walled steel tube 3, 15 mm in diameter, which is joined to the inner Dewar by means of the copper seal 4. A screen 5, in contact with the liquid He^4 bath, is placed inside the copper coupling to pro-

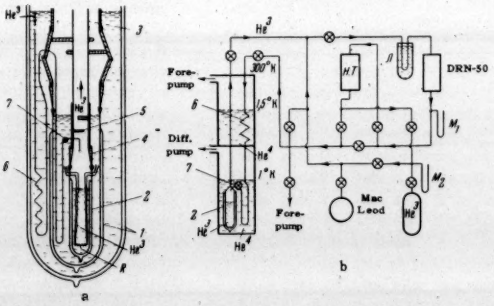

FIG. 1

vide shielding against radiation from above.

Pumping is provided by means of a DRN-50 mercury diffusion pump (Fig. 1b), of 30 l/sec capacity, operating with a forepressure of 25 – 30 mm Hg. A cold trap cooled with liquid nitrogen is connected to the input of the DRN-50. The output of the pump is coupled to a coiled tube 6 immersed in the liquid He^4 bath and connected through the valve 7 with the innermost Dewar. The coil passes in succession through the outer and inner He^4 Dewars in which temperatures of 1.5 and 1°K, respectively, are maintained with the aid of separate pumps. Due to the low temperature of the He^4 bath, the DRN-50 mercury pump can be operated without a forepump, having at its output a pressure approximately equal to the vapor pressure of He^3 at 1°K; i.e., 8 – 10 mm Hg. For use in the attainment of limitingly low temperatures, as well as in the event of a high temperature in the surrounding bath, a mechanical mercury Toepler pump NT as developed by Danilov[5] is connected in series following the diffusion pump. A mercury manometer M_1 permitting measurement of the He^3 pressure up to 200 mm Hg is installed at the output side of the DRN-50. The He^3, condensed and cooled to 1°K in the coil, is transferred as needed into the He^3 Dewar 2 through the valve 7. At the end of the experiment the He^3 is pumped into a gas cylinder, the DRN-50 and mechanical mercury Toepler pumps being used for this purpose. Control of the quantity of He^3 collected is accomplished with the aid of a mercury manometer M_2 having a 760 mm Hg scale. The system containing the He^3 is carefully tested for vacuum-tightness.

The lowest temperature reached with this apparatus was 0.3°K (p = 0.002 mm Hg). The temperature of the liquid He^3 was determined by means of a resistance thermometer R of 30 μ phosphor-bronze wire. The thermometer was calibrated in advance against the He^3 vapor pressure as measured with a MacLeod gauge. In the lowest temperature region the resistance thermometer was calibrated against the magnetic susceptibility of potassium chrome alum. For the temperature determinations we employed the scale of Sydoriak and Roberts.[3] The possibility of periodically adding liquid He^3 made it feasible to work uninterruptedly with this system at a low temperature for a period of 8 – 10 hours, using a single charge of gaseous He^3 (approximately 3 l). With the pumps shut down, the warm-up of the liquid from 0.3 to 1°K occupied no less than three hours.

The second type of system, used for obtaining low temperatures over a greater volume, is illustrated in Figure 2. The layout of the system is fundamentally similar to that shown in Figure 1b, with the exception that the Toepler pump is replaced by a NVG-2 oil pump[6] developed at NIVI. The gaseous He^3 condenses in a coil 1 (2 × 0.3 mm in diameter, 5 m long) situated in the liquid He^4 bath, and is introduced through an opened valve 2 and a smaller coil 3 into the He^3 collector 4. The coil 3 is formed from a 200 mm length of 0.2 mm i.d. capillary tubing.

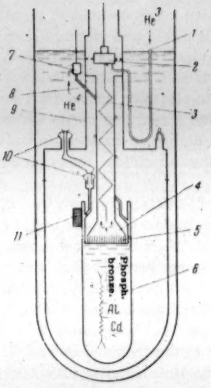

FIG. 2

The He^3 flowing through the smaller coil is further cooled by the vapors from the liquid evaporating below. The valve 2, in contact with the surrounding bath, serves at the same time as a shield for radiation coming from above. The He^3 collector 4 is in the form of a copper vessel soldered to a thin-walled stainless steel tube 12 × 0.2 mm in diameter and 100 mm long. The upper end of the tube is soldered into the body of the apparatus. To the bottom of the He^3 container is soldered a strip 5 of copper 5 mm wide and 0.3 mm thick, in the form of a spiral with a spacing of 0.2 mm between the turns. This increase in the surface area of the collector in contact with the boiling He^3 is needed for better transfer of cold from the coldest surface layer of the He^3 to the walls of the collector. (In the first version of the apparatus, without this increased surface area, sudden increases in the temperature were observed as the He^3 was cooled, due to boiling up of the lower layers of the liquid). The volume of the cylindrical portion of the collector was 2.5 cm^3. A copper bulb 6 of approximately 200 cm^3 capacity was soldered to the He^3 collector. Liquid He^4 was transferred from the bath into the bulb 6

through a valve 7 and a German silver tube 8 (2 × 0.3 mm in diameter and 160 mm long). The He^3 collector and bulb were isolated from the helium bath by means of a vacuum jacket 9. Copper-glass seals 10, with platinum wires (0.3 mm in diameter) sealed into the glass, and connected to each other with 0.1 mm diameter constantan wire, were used to carry twelve electrical leads through the vacuum jacket.

A screen 11 containing activated charcoal (1.5 gm) was fastened to the outer wall of the bulb, within the vacuum jacket. The jacket was filled with He^4 at a pressure p = 0.5 mm Hg, at room temperature, and then sealed off. The presence of He^4 within the jacket reduced the cooling time for the bulb and He^3 collector. At a low temperature the He^4 in the jacket was adsorbed by the charcoal. The time required for cooling the bulb, from the moment pumping was begun on the He^4 bath (T = 4.2°) until a temperature T = 0.5°K was reached, including the filling of the bulb with He^4 and the condensation of the He^3, did not exceed one hour. The time for cooling the He^3 collector and the bulb, with the latter containing liquid He^4, from T = 1.15°K to T = 0.5°K, was 5 — 10 minutes.

Pumping on the He^3 vapor was carried out with the aid of the DRN-50 mercury diffusion pump and an NVG-2 forepump. The temperature of the bulb could be set at 0.5°K or higher by adjusting the rates at which the He^3 was introduced and its vapor pumped away, with the aid of the valve 2. With continuous circulation of the He^3, work could be continued as long as the liquid in the outer bath was not completely boiled away (5 — 10 hr). When the bulb was cooled down without liquid He^4, the temperature could be reduced as far as 0.35°K. The principal leakage of heat into the bulb came from the bath, through the helium in the tube 8. The temperature of the helium bath was maintained at 1.15°K. It should be noted that if an additional valve is installed on the bulb 6 and the tube 8 is evacuated, then for small heat inputs it is possible to obtain a temperature of 0.35°K with the bulb completely filled with liquid He^4. The temperature within the bulb 6 was determined from the He^3 vapor pressure with the pump shut off, and also from the resistance of a thermometer of 30 μ phosphor bronze placed inside it. The resistance thermometer was calibrated in advance against the He^3 vapor pressure and the magnetic susceptibility of potassium chrome alum, and, over the temperature range 0.3 — 1.1°K, had a practically linear temperature dependence. In addition, the superconducting transition points of wires of pure aluminum, 50 μ in diameter, and cadmium, 67 μ in diameter, connected in series with the thermometer, served as standard points with which the temperature measurement could be checked each time.

The systems described above make it possible to experiment conveniently over the temperature region from 0.3 to 2°K.

[1] W. H. Keesom, Leid. Commun. 219a, 1 (1932), Proc. Roy. Acad. (Amsterdam) **35**, 136 (1932).

[2] B. G. Lazarev and B. N. Esel'son, J. Exptl. Theoret. Phys. (U.S.S.R.) **12**, 549 (1942).

[3] S. G. Sydoriak and T. R. Roberts, Phys. Rev. **106**, 175 (1957); **93**, 1418 (1954).

[4] G. Seidel and P. H. Keesom, in Low Temperature Physics and Chemistry, J. R. Dillinger, editor; Univ. of Wisconsin, 1958. p. 218.

[5] I. B. Danilov, Приборы и техника эксперимента (Instruments and Meas. Engg.) **1**, 93 (1956).

[6] Symposium on the Interchange of Advanced Experiments in the Field of Technology and Organization of Production, MRTP, U.S.S.R. 1955, p. 55.

Translated by S. D. Elliott
204

SOVIET PHYSICS JETP VOLUME 36 (9), NUMBER 4 OCTOBER, 1959

MEASUREMENT OF THE RESISTANCE OF HIGH PURITY TIN AT HELIUM TEMPERATURES

V. B. ZERNOV and Yu. V. SHARVIN

Institute for Physical Problems of the Academy of Science, U.S.S.R.

Submitted to JETP editor October 16, 1958

J. Exptl. Theoret. Phys. (U.S.S.R.) **36**, 1038-1045 (April, 1959)

The resistance of a number of single crystals of tin of various purity has been measured. The resistance was deduced from the moment of the forces acting on the specimen in a rotating magnetic field. The anisotropy and temperature dependence of the resistance between 4.2 and 3.73°K was measured and the residual resistance determined. For the purest specimen the residual resistance was about 3.7×10^{-11} ohm-cm, which corresponds to an electron mean free path of about 3 mm.

MEASUREMENT of the residual resistance of metals at low temperatures is widely used as a convenient method of checking the overall impurity concentration, especially when other methods become insufficiently sensitive ("spectrally-pure" metals).

The residual resistance method is in turn limited in sensitivity because electrons are scattered at lattice defects which are not connected with the chemical impurities.

Electrons are scattered: 1) by inter-crystallite boundaries if the specimen is not a single crystal; 2) by dislocations and other lattice imperfections; 3) by the external boundaries of the specimen. If the metal consists of a mixture of several isotopes, there must also be an "isotopic" residual resistance due to the change of zero-point vibrations of the lattice produced by the randomness of the isotope distribution.

If single crystal specimens of large enough dimensions are used, the first source of scattering is absent and the third can be considered a small correction. The experimental determination of the contributions to the residual resistance of the second and, especially, the last scattering mechanism is a much more difficult problem.

Measurements on specimens of the highest purity, such as those described below, make it possible to set an upper limit to the magnitude of these effects. We also determined the temperature variation of resistance for tin at helium temperatures, and its anisotropy.

EXPERIMENTAL METHOD

The usual dc potentiometric method of measuring resistance was not suitable for the extremely small resistivities to be measured. Also, fixing the leads would have introduced impurities and deformed the specimens.

We adopted a method which does not require the fixing of contacts, but depends on the measurement of the moment of the forces acting on a spherical specimen in a rotating magnetic field.

This method has been developed by Regel'[1] who used a frequency of 50 kcs for the rotating field. For our experiments the frequency had to be much less because at 50 kcs the field penetration depth in our samples would only be tenths of a millimeter, which is small compared both with the specimen size and with the electron mean free path. This would complicate the calculations and reduce the accuracy of the measurements.

The apparatus used is shown schematically in Fig. 1. The spherical specimen 1, of diameter 12.6 mm, was hung on the torsion balance by a quartz fiber. In most of the experiments the torsion constant of the fiber was 0.17 dyne-cm. The lower part of tube 9, which housed the balance, was enclosed by the liquid helium bath. The vapor pressure of a small quantity of liquid helium at the bottom of tube 9 served to measure the specimen temperature. The specimen was in a horizontal magnetic field, produced by the Helmholtz coils 14, which rotated about a vertical axis.

The magnitude of the field has to be chosen so that neither the Hall effect nor the magneto-resistance effect have any influence. For the purest specimens the field was 1.5 to 2.5 oe, and the effect of the magnetic field on the results only became noticeable beyond 5 oe for these specimens. Two Helmholtz coil systems (not shown in the figure) compensated the earth's magnetic field.

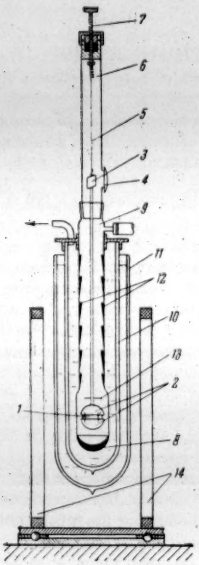

FIG. 1. 1 – specimen; 2 – quartz cups; 3 – mirror; 4 – window and lens; 5 – quartz fibre; 6 – spring protecting the quartz fibre from breaking under shock; 7 – torsion head; 8 – lining of soft material; 9 – glass tube, protecting the balance from convection currents in the liquid helium; 10 – liquid-helium Dewar; 11 – liquid-nitrogen Dewar; 12 – layer of black paper for shielding the specimen from radiation; 13 – thin aluminium shield; 14 – Helmholtz system of coils on a rotating table.

The whole apparatus was carried on a massive foundation, with the Dewar vessel and rotating coil separately supported.

It can easily be shown[1,2] that if the frequency of rotation of the field is sufficiently small for the field in the specimen to differ little from the external field, the resistance of an isotropic spherical specimen is given, to a first approximation, by the simple relation

$$\rho = 10^{-9}(4\pi^3/15)(R^5H^2/TM), \qquad (1)$$

where ρ is expressed in ohm-cm, R is the sphere radius in cm, H the rotating field strength in oersteds, T the period of rotation of the field in seconds and M the moment of the forces acting on the specimen, in dyne-cm. This approximation is valid for $\delta \gg R$, where $\delta = \sqrt{10^9\rho T}/2\pi$ is the field penetration depth. The error is less than 1% below $R/\delta = 0.7$.

In our experiments the period of rotation was 400 to 500 sec and R/δ was not more than 0.5 for the specimens with the smallest resistance. We verified experimentally that the moment M varied linearly with the speed of rotation over the range of speeds used.

Although the condition of slow rotation speed, required for applying Eq. (1), was fulfilled, this equation was only suitable for rough calculations in our case because A) the specimens were single crystals and therefore had anisotropic properties and B) the electron mean free paths were large at helium temperature (~1 mm). The relevant corrections were made in the following way.

A. One must first take into account the anisotropy in the electrical resistance of tin, the resistance parallel to the fourfold symmetry axis $\rho_\parallel$, being greater than $\rho_\perp$, the resistance in any direction perpendicular to the axis (tin has a tetragonal lattice).

Allowance must also be made for the departure of the specimen from a spherical shape due to anisotropy of the coefficient of thermal expansion. Single crystal specimens cast in a spherical glass former which departed from sphericity by less than 5 μ, became slightly flattened ellipsoids of revolution on cooling to helium temperature.

If the field rotates sufficiently slowly the calculation is straightforward. For an ellipsoidal specimen with semiaxes a, b, and c (b = c), in which the principal axes of the resistance tensor coincide in direction with the axes of the ellipsoid, and dH/dt is perpendicular to a, the moment of the forces becomes

$$M = 10^{-9}\frac{4\pi^3}{15}\frac{a^5H^2}{T}\frac{2k^4}{\rho_\parallel + k^2\rho_\perp}, \qquad (2)$$

where $k = b/a$. If $\rho_\parallel = \rho_\perp$ this formula, after slight rearrangement, agrees with the relation for isotropic ellipsoids of revolution found by Gans.[2]

For our specimens $k = 1 + \epsilon$, where $0 < \epsilon \ll 1$. As ϵ is small we obtain the approximate relation

$$\bar{\rho} = 10^{-9}\frac{4\pi^3}{15}\frac{a^5H^2}{TM}(1 + 4\varepsilon) - \varepsilon\rho_\perp, \qquad (3)$$

where $\bar{\rho} = (\rho_\parallel + \rho_\perp)/2$. With our method of measurement this quantity is the most convenient parameter for comparing one specimen with another. In determining the moment M, which enters into Eq. (3), the fourfold axis of the crystal was placed vertical, i.e., parallel to the axis of the balance. Besides the essential quantities H, T, and M, it is also necessary, for applying Eq. (3), to know: a) the lengths of the semi-axes of the specimen at helium temperature, and b) the magnitude of $\rho_\perp$,

although it can be seen from (3) that the accuracy required in ρ is not very great.

a) The specimen dimensions at helium temperature were determined from measurements at room temperature (the accuracy was $\pm 2\mu$) and data on the coefficient of expansion of single crystals of tin at room temperature,[3,4] which were extrapolated to low temperatures according to Grüneisen's rule (according to the temperature dependence of the specific heat). It was assumed that the ratios of the expansion coefficients along different axes are independent of temperature. As an example, these calculations gave for specimen No. 5 axial lengths 12.619 and 12.526 mm ($\epsilon = 7.4 \times 10^{-3}$).

The value of ϵ at helium temperature can also be obtained directly with the apparatus, if the specimen is made superconducting. As a magnetic field does not penetrate into a superconductor, a mechanical moment will act on an ellipsoid in an external steady field. Naturally, the field must not destroy the superconductivity. If the specimen is fixed to the balance so that the fourfold axis is horizontal, then the moment of the force is a maximum, M^s_{max}, when the angle between the field direction and the axis is 45°. If $\epsilon \ll 1$

$$\varepsilon = M^2_{max} / 0.15\, H^2 a^3. \qquad (4)$$

The value of ϵ, obtained in this way, agreed well with the extrapolation method described. For the same specimen No. 5, Eq. (4) gave $\epsilon = 7.7 \times 10^{-3}$.

b) The measurement of $\rho_\perp$ was made, in a rotating magnetic field, with the specimen hung in the same way as for determining ϵ, i.e., with the axis horizontal. The deflection of the mirror is then not constant, since the angle between the field and the fourfold axis varies with the rotation of the field. The suspension system carries out oscillations with a period T/2. The largest deflection occurs when the field is perpendicular to the specimen axis. The currents then flow everywhere perpendicular to the axis, and $\rho_\perp$ can be derived from the greatest deflection of the mirror, using the equation

$$\rho_\perp = 10^{-9} \frac{4\pi^3}{15} \frac{a^5 H^2 k^4}{T M_{max}} \approx 10^{-9} \frac{4\pi^2}{15} \frac{a^5 H^2}{T M_{max}} (1 + 4\varepsilon). \qquad (5)$$

The deflection is a minimum when the field is parallel to the axis and is then equal to the stationary deflection in the case of the axis being vertical, as it should be since Eqs. (2) and (3) hold for M_{min}.

In determining $\rho_\perp$ we neglected the effect of the inertia and damping of the balance, in a magnetic field, on the amplitude of oscillation of the suspended system. For our conditions, when the period τ of free oscillation in zero field was only 0.05 T and the damping in the magnetic field was near critical, the error involved is small. By solving the differential equation for the motion of the balance in a rotating magnetic field, this error is found to be proportional to $(\tau/T)^2$ and is only 1 or 2% of the amplitude of oscillation of the pointer in the rotating field.

B. The corrections for the long electron mean free path, l, were made in the following way. As the scattering of electrons at the boundaries of the metal appears to be diffuse, a surface layer of the specimen, with thickness of the order of l, has a higher effective resistance ρ_{eff} than the interior of the specimen. It is not difficult to solve numerically the problem of the magnetic moment of a sphere, for which ρ depends on R, placed in a slowly rotating field. As $l \ll R$, Sondheimer's formula[14] for a plane can be used for $\rho_{eff}(R)$. We neglected the anisotropy in conductivity and took $\rho l = 1.05 \times 10^{-11}$ ohm-cm for tin from Chambers' data.[15]

The corrections calculated in this way are considerable (8 — 14% for the purest specimens) as a result of which the large mean free path is the greatest source of error in our measurements. The overall accuracy in the absolute values of $\bar{\rho}$ are about 5%, while the random errors in individual measurements (due to irregularities in rotation of the field, vibration of the balance etc) are less than 0.5%.

MEASUREMENT RESULTS

Table I shows the results of measurements of the resistance of a number of single crystal specimens of increasing purity. The resistances of the purest specimens, Nos. 4 — 6, depend appreciably on temperature in the helium region (see Table II).

For specimen No. 6 $\bar{\rho}_{20°C} / \bar{\rho}_{4.2°K}$ was 1.0×10^5, but $\bar{\rho}_{20°C} / \bar{\rho}_{3.75°K} = 1.4 \times 10^5$. Owing to the superconducting transition at 3.73° K, the residual resistivity of these specimens could not be determined. The values of residual resistivity given in Table I, were obtained by extrapolating the temperature dependence of resistance to T = 0. Over the range of our measurements (4.2 to 3.73° K) the dependence of $\bar{\rho}$ on T fits the relation $\bar{\rho} = \bar{\rho}_0 + \bar{b}T^n$ with n = 5 (see Table II). If we take n = 5 and derive the values of $\bar{\rho}_0$ and $\bar{b}$ by the method of least squares, the scatter of the points from the curve is not more than 0.2%. If n is taken as 4, the corresponding de-

TABLE I

Specimen No.	Impurity concentration according to analysis, % by weight	Further purification: Heating in vacuo, t°C	Further purification: Zone melting; number of passes	Temperature, T °K	$\rho \times 10^{10}$ ohm-cm at T°K	$\rho_{\parallel}/\rho_{\perp}$ at ~4.2°K	$\rho \times 10^{10}$ ohm-cm	$(\bar{\rho}_{20^\circ C}/\bar{\rho}_0) \times 10^{-4}$	Estimated impurity concentration after purification, %
1	0.1	1000	10	4.23	42±3 %	1.3±5%	41	2.95***	$7 \cdot 10^{-3}$
2	0.002	1000	—	4.22	13.7±3%	1.30±4%	12.8	9.5	$2 \cdot 10^{-3}$
3	0.002*	1200—1400	—	4.22	6.4±5%	1.40±5%	5.5	24.2	$8 \cdot 10^{-4}$
4	0.002	1200—1400	43	4.215	1.68±5%	--	0.77	157	$1 \cdot 10^{-4}$
5	0.002	1200—1400	43	4.227	1.67±5%	1.56±7%	0.75	162	$1 \cdot 10^{-4}$
6	0.1	1200—1400**	166	4.216	1.23±5%	1.5±7%	0.37	330	$< 6 \cdot 10^{-5}$
				3.75	0.87±6%				

*The value determined by analysis is not shown. Preliminary measurements gave $\rho_{4.2}/\rho_{20^\circ C} = 1 \times 10^{-4}$ for this kind of tin, i.e., the impurity concentration ~0.002%.

**Purification consisted of double electrolysis, heating and zone melting, and was carried out by N. N. Mikhaĭlov in the Technical Section of the Institute for Physical Problems, as were the purifications of the other specimens.

***For all specimens $\bar{\rho}_{20^\circ C} = 1.21 \times 10^{-5}$ ohm-cm.[4]

TABLE II. $\bar{\rho}(T)$ for specimen No. 5

$\bar{\rho}_{calc} \times 10^{10} = 0.753 + 6.762 \times 10^{-4} T^5$ ohm-cm

T°K	$\rho_{meas} \times 10^{10}$ ohm-cm	$\rho_{calc} \times 10^{10}$ ohm-cm
4.227	1.668	1.666
4.192	1.629	1.628
4.120	1.554	1.556
4.062	1.500	1.501
3.992	1.435	1.439
3.883	1.351	1.350
3.730	1.243	1.241

partures reach 0.5 to 0.6% and take on a systematic appearance. Van den Berg[5] has found that the resistance of single crystals of tin obeys the relation $\rho = \rho_0 + bT^5$ between 4.2 and 10° K, but the value of b which he found is 35% greater than ours. It is possible that this difference is due to a difference in crystal orientation, which was not determined by van den Berg.

From our measurements of $\rho_{\parallel}/\rho_{\perp}$ for specimens Nos. 5 and 6 at 4.2 K (see Table I) it follows that the anisotropy in b is considerable, with $b_{\parallel}/b_{\perp} = 1.5$ to 1.6. At room temperature $\rho_{\parallel}/\rho_{\perp} = 1.45$ (Bridgman[4]). The value $\rho_{\parallel}/\rho_{\perp} = 1.3$ for the least pure specimens (Nos. 1 and 2) presumably represents the anisotropy of the residual resistance for these specimens. Faber and Pippard[9] found $(\rho_{\parallel}/\rho_{\perp})_0 = 1.14$ for tin with indium impurity. The difference from our data for specimens No. 1 and 2 must presumably be ascribed to the different impurities.

The value of $\bar{\rho}_0$ which is given in Table I was, for all our specimens, calculated on the basis of the data for specimen No. 5, given in Table II.

The accuracy with which $\bar{\rho}_0$ can be determined is, clearly, small in view of the uncertainties in the theory of the temperature dependence of resistance. If we assume that there is also a term proportional to T^2 in the expression for the resistivity (due to electron-electron collisions), and its upper limit is determined from the possible errors of measurement, then we obtain an uncertainty in $\bar{\rho}_0$ for specimens No. 4 and 5 of about 10 to 15%. For specimen No. 6 the uncertainty in $\bar{\rho}_0$ reaches 20 to 30%. It would be difficult to obtain values of $\bar{\rho}_0$ of any reliability for tin specimens of even lower resistivity, using this method.

Returning to the causes of the residual resistance in our specimens, we should point out that lattice defects, unconnected with impurities, make no significant contribution in specimens 1—5, since specimen No. 6 was produced with a significantly lower residual resistance.

We carried out special experiments to make sure that accidental damage to the specimen did not influence the results. For example, dropping a specimen onto the floor from a height of 1.5 m produced no noticeable increase in $\bar{\rho}_0$. In general, mechanical deformation did not affect $\bar{\rho}_0$ appreciably. We give in Table III some values of ρ for a specimen initially shaped with a chisel, then recrystallized, hammered and turned in a lathe and finally heated. It can be seen from the table that the maximum increase in ρ_0 is not more than a factor of ten.

TABLE III. Influence of various treatments on resistance (in 10^{-10} ohm-cm)

Specimen treatment	$\rho_{4.2°K}$	ρ_0	ρ_0/ρ_0 single crystal
Initial shaping	3.5	2.6	3.35
Single crystal	1.69	0.78	1
Violently hammered and turned at 20°C	8.3	7.4	9.5
After 40 hrs at 20°C	7.3	6.4	8.2
Heating for 8 hrs at 220–225°C. (The specimen consisted of 10–20 crystals with dimensions 4–8 mm)	2.3	1.4	1.8

The residual resistance of specimens 1 – 5 must, therefore, be due to chemical impurities. In the last column of Table I we give rough values for the total impurity concentration C in parts per cent, using the relation $C \approx 20\,\bar{\rho}_0 / \bar{\rho}_{20°C}$, which is based on data in the literature for the residual resistance of tin with small impurities of In, Bi, and Sb, and also for some specimens with known total impurity concentrations (see Fig. 2). This calculation only gives an upper limit to the impurity concentration in the purest specimen, No. 6, since a significant fraction of its residual resistance could be due to "non-chemical" lattice imperfections. The possible imperfections are vacancies and other defects, produced in the lattice as a result of thermal motion at high temperatures and retained on quenching the specimen (see Lazarev and Ovcharenko,[16] who studied the residual resistance of quenched gold and platinum wires), and also isotopic disorder, mentioned above. It is difficult to evaluate the part played by these factors with sufficient accuracy. As tin has a high boiling point (~2500° C) and a low melting point, we may expect the concentration of vacancies on our specimens to be insignificant (10^{-4} to 10^{-8} %, according to rough calculation if we take the heat of formation of vacancies to be ¼ the heat of vaporization, as found by Lazarev and Ovcharenko). It is not impossible that such a vacancy concentration has a noticeable effect on the resistance of specimen No. 6. This is even more so for the isotopic source of resistance. Natural tin consists of a mixture of many isotopes with atomic weights ranging from 112 to 124. Pomeranchuk[17] has given a theoretical estimate of the electron mean free path in an isotopically impure metal, and for tin this comes to 1 – 10 mm, while in specimen No. 6 the mean free path at 0° K is 3 mm.

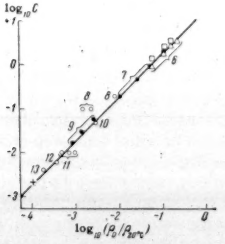

FIG. 2. The dependence of the residual resistance of tin on impurity concentration C (in % by weight). ● – Sn+ In, Δ – Sn + Sb, □ – Sn + Bi, ○, + – upper limit of concentration according to the suppliers' analysis or from the conditions of preparation (+ – our measurements on specimen No. 2). The numbers against the points indicate the literature references.

We would like to express our thanks to N. N. Mikhaĭlov, director of the Technical Department of the Institute for Physical Problems, who carried out the purifications, to I. Ya. Pomeranchuk for informing us of his results prior to publication, and to A. I. Shal'nikov for his interest and valuable advice.

[1] A. R. Regel', J. Tech. Phys. (U.S.S.R.) **18**, 1511 (1948).
[2] R. Ganz, Z. Math. u. Physik **48**, 1 (1903).
[3] B. G. Childs and S. Weintroub, Proc. Phys. Soc. **B63**, 267 (1950).
[4] P. W. Bridgman, Proc. Amer. Acad. Arts. Sci. **60**, 305 (1925).
[5] G. J. van den Berg, Physica **14**, 111 (1948).
[6] Budnick, Lynton, and Serin, Phys. Rev. **103**, 286 (1956).
[7] A. B. Pippard, Phil. Trans. Roy. Soc. **A248**, 97 (1955).
[8] Aleksandrov, Berkin, and Lazarev, Физика металлов и металловед. (Physics of Metals and Metal Research) **2**, 100 (1956).
[9] T. E. Faber, Proc. Roy. Soc. **A219**, 75 (1953).
[10] L. Rinderer, Z. Naturforsch. **10a**, 174 (1955).
[11] H. K. Onnes and W. Tuyn, Comm. Leid. Suppl. 58 (1926).
[12] E. S. Borovik, Dokl. Akad. Nauk SSSR **69**, 767 (1949).
[13] E. R. Andrew, Proc. Phys. Soc. **A62**, 77 (1949).
[14] E. H. Sondheimer, Advan. in Phys. **1**, 1 (1952).
[15] R. G. Chambers, Proc. Roy. Soc. **A215**, 481 (1952).
[16] B. G. Lazarev and O. N. Ovcharenko, Dokl. Akad. Nauk SSSR **100**, 875 (1955).
[17] I. Ya. Pomeranchuk, J. Exptl. Theoret Phys. (U.S.S.R.) **33**, 992 (1958), Soviet Phys. JETP **8**, 693 (1959).

Translated by R. Berman
205

MILLISECOND HALF-LIFE ISOMERS PRODUCED IN REACTIONS INVOLVING 14-Mev NEUTRONS

V. L. GLAGOLEV, O. M. KOVRIZHNYKH, Yu. V. MAKAROV, and P. A. YAMPOL'SKIĬ

Submitted to JETP editor October 21, 1958

J. Exptl. Theoret. Phys. (U.S.S.R.) **36**, 1046-1057 (April, 1959)

The short-lived γ-radiation produced by pulsed irradiation of 43 elements with 14.5-Mev neutrons was investigated. Nine isomer activities with half-lives ranging from 10^{-3} to 10^{-1} sec were detected in Mg, Al, Ge, As, Y, In, Pb and Bi. The half-lives and γ-ray energies were measured and in some cases the isomer production cross sections were estimated. Besides the Pb^{207m} and Bi^{208m} activities all other isomer activities were produced in the neutron reactions for the first time. As a result it has been possible to identify a number of the isomers and to discuss the possible decay schemes.

1. INTRODUCTION

THE present paper is concerned with a search for and preliminary investigation of nuclear isomers with half-lives of 10^{-3} to 10^{-1} sec produced in reactions with 14-Mev neutrons. Part of the experiments described below was designed to establish or make more accurate measurements on the types of reactions which could explain the γ radiation with millisecond half-lives observed earlier.[1-5]

We carried out experiments on the lighter elements, for although the existence of isomer states is theoretically possible in several of these only a few have actually been found. The heavy and medium elements are of interest because the reaction (n, 2n) at 14-Mev neutron energies has a large cross section and therefore the mechanism whereby this reaction takes place should provide a large yield of isomers.[1]

We investigated the following 43 elements (Li, C, Na, Mg, Al, S, Ca, Sc, Ti, V, Mn, Co, Ni, Zn, Ga, Ge, As, Se, Br, Rb, Cu, Fe, Sr, Y, Zr, Nb, Mo, Pd, Cd, In, Sn, Te, La, Ce, Ta, W, Au, Hg, Tl, Pb, Bi, Th, U) and the effect was found for eight (Mg, Al, Ge, As, Y, In, Pb and Bi). The energies and the half-lives of the activities were measured and an estimate was made of their production cross-sections. The negative results obtained with 35 elements cannot be considered final and the measurements should be continued under improved experimental conditions and better measurement methods.

2. APPARATUS AND METHODS OF MEASUREMENT

1. Neutron monitor, determination of γ-radiation energy and half-lives of the isomer activities. The experiments concerned the γ-radiation spectra and the half-lives of the isomers produced in reactions with neutrons, and an estimate was made of the cross sections of several reactions that produce neutrons. The γ-radiation was recorded during the intervals between neutron pulses.

Neutrons were obtained from the reaction T (d, n) He^4 using 500-kv accelerating system previously described.[6] The unsorted ion beam was incident upon a thick tritium-zirconium target. The neutron pulse was produced by applying a square wave pulse of anode voltage to the ion source. The square wave was obtained by discharging a capacitor through a shaping circuit consisting of four resonant networks. The capacitor discharge circuit was closed by a photoelectric relay operated by a light signal from the low voltage end of the accelerator. The pulse repetition frequency was about 1 pulse per second. The target received a rectangular pulse of ion current with a duration of 1.3 milliseconds and amplitude up to 2 ma; under these conditions 2×10^7 neutrons were emitted per current pulse.

The neutron monitor consisted of a type FEU-19M photomultiplier tube with scintillation screen sensitive to neutrons (ZnS on Plexiglas). Pulses obtained from the photomultiplier were applied to the input of the PS-10,000 ("Floks") apparatus. The average pulse count rate, controlled by the neutrons, was of the order of 10 per second (10 pulses for 1 pulse of ion current). Pulses due to possible discharges in the accelerator could interfere with the measurements, so that for this reason the "Floks" scaler was shut off by a special circuit[7] and was switched on for 8 millisec by means of a photo relay operating from the same light signal as the photo relay of the ion source. It was during this time interval that the ion current pulse took place. The "Floks" sensitivity was set so as to discriminate against pulses

caused by Co^{60} γ radiation. This made it possible to control the sensitivity of the equipment. With such a choice of sensitivity, discrimination was had also against pulses associated with the long period activities produced in the scintillation material when it was radiated with neutrons during the period of continuous operation of the accelerator. The ratio of yield for the reactions studied and for the reaction $Cu^{63}(n, 2n)Cu^{62}$ to the monitor count was reproducible within limits of ±10%. The absolute calibration of the neutron beam, required for an evaluation of the reaction cross section, was carried out with copper indicators using the yield from the reaction $Cu^{63}(n, 2n)Cu^{62}$, the cross section for which is known.[8] The copper cross section was taken equal to 500 millibarns.

Measurements of the γ radiation from the isomers were carried out by means of a NaI(Tl) crystal (diameter, 29 mm, h = 13 mm in a standard duraluminum container) with a type FEU-S photomultiplier. Pulses from the multiplier were applied to an analyzer with a grey wedge.[9] This device made it possible to obtain a photograph of the amplitude distribution of the pulses in a relatively short time interval. The resolving time of the device was 3×10^{-6} sec, the linear portion of the oscilloscope screen being 40 mm long. At the maximum sensitivity, input pulses with amplitude of 1 v produced a deflection of about 40 mm on the screen.

In addition, the pulses from the FEU-S were applied to a single channel amplitude analyzer,[10] which made it possible to count the pulses in a chosen portion of the amplitude spectrum. The resolving time of the analyzer was 0.8×10^{-6} sec. The amplifier, which was linear up to 120 v, had a rise time of 5×10^{-8} sec. The bandwidth could be changed in several steps from 0.5 to 3 v. By means of this analyzer we obtained the spectra of the isomer radiation produced after pulsed irradiation of the samples by neutrons. The results of these measurements were utilized to estimate the isomer yield cross section.

To determine the half-life of an isomer, the analyzer was set to the photo peak of the investigated line, so as to reduce the contribution of the background to the total count. The shaped pulses arriving from the amplitude analyzer were fed to a 16-channel time analyzer.[11] The channel bandwidth was variable from 0.1 to 4×10^{-5} sec and the resolving time of the channel was 0.8×10^{-6} sec. The time analyzer was switched in by the leading edge of the ion current pulse of the accelerator, and the count was started in the first channel with the particular time delay with respect to this leading edge chosen for each experiment. The photomultiplier, which was normally cut off by a negative voltage on its first focusing electrode, was switched in during the measurements. As a result, the photographs obtained with the grey wedge show a spectrum of the pulses, whose time distribution was studied, with a reduced contribution from the pulse background.

The equipment was carried out by means of γ lines of known energy: Zn^{65} — 1.118 kev, Cs^{134} — 800 and 600 kev, Cr^{51} — 323 kev, Hg^{203} — 279 kev, and Ce^{141} — 144 kev. With the crystal and photomultiplier used in this work, resolution of the Zn^{65} line was 7%. The position of the light peak was found not to vary with the intensity of radiation, right up to counting speeds of 3×10^4 pulses per second (integrated count). The intensity did not exceed this value in our experiments.

With pulsed operation, when the FEU-S was shut off and then turned on for definite periods of time after intensive pulsed neutron bombardment of the crystal and specimen, we observed a change both in sensitivity and resolution of the photomultiplier. When the photomultiplier was exposed for 300 μsec, the resolution became somewhat worse but for a period of exposure equal to about a millisecond and more the resolution did not change.

When determining the energy of the radiation studied, the source calibration lines were obtained either under the same conditions of photomultiplier operation as for irradiation of the samples, or simultaneously with the photomultiplier operation, so as to be able to account for possible changes of sensitivity in the operation of the FEU under pulsed conditions. The sensitivity of type FEU-S photomultiplier, when operated continuously after being turned on, was increased approximately 10% by the light from the crystal irradiated by the γ-source, and after 20 or 30 minutes reached a value that remained constant to within 1 or 2% during its subsequent operation. After cessation of the radiation, the sensitivity of the photomultiplier did not change significantly over a period of an hour.

A block diagram of the equipment is given in Fig. 1. The entire apparatus enabled us to measure the half-lives of isomers with a duration from 2 milliseconds up to 1 second and energies from 100 kev to 1.5 Mev.

The arrangement of the target, sample, and crystal is shown in Fig. 2. The tritium target was placed on the bottom of a steel cup (thick-

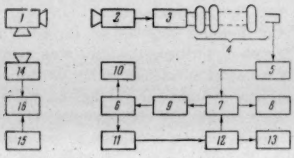

FIG. 1. Block diagram of the equipment: 1–pulsed radiator, 2–photorelay, 3– pulsed ion source, 4–linear accelerator, 5–delay network, 6–photomultiplier FEU-S with cathode follower[NaI(Te) crystal], 7–sixteen-channel time analyzer, 8–sixteen scalars, 9–circuit for shutting off FEU-S, 10–analyzer with gray wedge, 11–amplifier, 12–single channel differential discriminator, 13–scalar type PS-10,000, 14–photorelay and circuit for turning the "Floks" on, 15–photomultiplier FEU-19M with cathode follower (scintillation-screen – ZnS on Plexiglass), 16–scalar PS-10,000, "Floks."

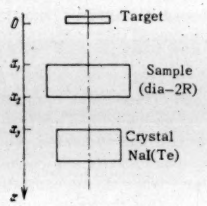

FIG. 2. Experiment geometry.

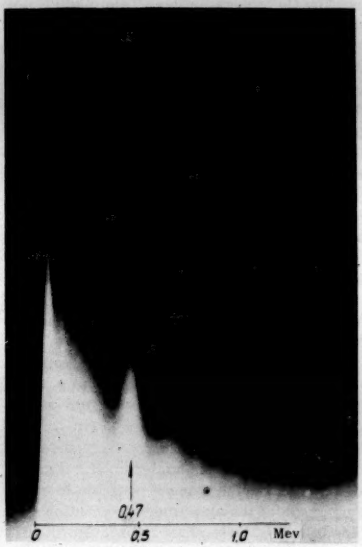

FIG. 3. Background spectrum in absence of sample, obtained by starting the exposure 4 millisec after start of neutron pulse. Monitor count, 11,600.

ness of walls and bottom 1 mm) and the samples were placed between the target and the crystal used to detect the γ radiation. The distance from crystal to sample $(x_2 - x_3)$ was 3.0 cm, the distance x_3 from the target to the crystal was varied from 5.5 to 9 cm, depending on the intensity of the radiation being studied. In the vicinity of the target the amount of scattering materials was reduced to the least amount possible. In the first experiments, we observed intense γ radiation with E = 470 kev, $T_{1/2}$ = 20 millisec, due, as further experiment showed, to aluminum and producing a background which interfered with the study of other materials. For this reason, aluminum parts of the equipment were replaced by steel and Plexiglas wherever possible. A typical background spectrum is shown in Fig. 3. During operation a shutter could be set over the tritium target to cut off the current reaching the target. In this case the current pulse started the recording equipment but no neutrons were present. Experimental conditions were chosen such that the equipment recorded only the pulses associated with neutrons (x-rays, background due to stray electrical pickup, etc.).

Experiments were performed in the following order. The background γ-radiation was measured with the gray-wedge analyzer with no specimen between target and crystal. The sample was then set in place and the γ-radiation spectrum was again obtained under the same conditions as the background spectrum. If new lines (other than those of the background) appeared, their energy was measured. After this, by means of the single channel amplitude analyzer, we selected a section of the spectrum containing the new line and, using the time analyzer, measured the time distribution of pulses both with the sample and without it. To obtain satisfactory statistics, several hundred neutron pulses were used. By analysis of the time distribution of γ-radiation pulses we obtained the half-lives for the isomer activities.

As has been pointed out above, γ-radiation spectra were obtained for a number of elements with the aid of the single-channel amplitude analyzer. In these experiments the exposure times of the FEU-S were chosen in accordance with the half-life to permit the measured activity to decay completely during the measurement time interval. The amplitude analyzer channel was switched over automatically after the monitor had counted a definite number of pulses. Recording was accom-

plished by means of 16 scalers which were simultaneously switched in when an analyzer channel was switched over.

2. Estimates of the Isomer Production Cross Sections. We carried out additional experiments on some elements to enable us to evaluate isomer production cross sections. In view of the fact that the mean neutron yield was not large ($\sim 10^7$ neutrons per sec over a solid angle of 4π), we used samples of rather large dimensions and placed them near the tritium-zirconium target. In this case, the dimensions of target, samples, and crystal were comparable with the distances between them. Cylindrical specimens were used in these measurements (2R = 4.5 cm and 2R = 10 cm). The formula for the cross section was derived by relating the number of neutrons passing through a circular section of specimen of thickness dx at a distance x from the target, with the number of pulses at the photopeak due to the γ quanta emitted by this layer. The first of these quantities was measured by means of a copper indicator (copper foil 33.6 mg/cm^2, diameter 2R, located at a distance x from the target during irradiation by neutrons); the second was determined by model experiments in which the irradiation of the layer dx was represented by the γ radiation of a thin γ emitter of known power located in the same position between sheets of the material under study. Here we measured the effectiveness of the spectrometer $\epsilon(x, E)$ at the photopeak, with allowance for specimen absorption. By integration of the effects produced by each layer dx we obtained the full count n of peaks in the spectra of the isomer radiation, a count connected with the cross section σ for isomer production through the following formula:

$$\sigma = \sigma_{Cu}\, nMB(x_2 - x_1) \Big/ \nu P \int_{x_1}^{x_2} \xi(x)\, \varepsilon(x, E)\, dx. \qquad (1)$$

Here σ_{Cu} is the cross section for the $Cu^{63}(n, 2n)Cu^{62}$ reaction, M is the molecular weight of the specimen, P the weight of the specimen taking into account the isotopic composition, ν the monitor count when the sample is irradiated, B a factor that accounts for the decay in isomer activity, x_1 and x_2 are shown in Fig. 2, and $\xi(x)$ is a function that accounts for the number of neutrons that have passed through the layer dx:

$$\xi(x) = n_{Cu} M_{Cu}\, B_{Cu} / \gamma_{Cu} P_{Cu} \eta \mu, \qquad (2)$$

where n_{Cu} is the reading of counter AC-2, around which a copper foil was wrapped to count the positrons of the Cu^{62} decay after pulsed irradiation by neutrons, η is a factor that accounts for the absorption in the foil and the absorption in the counter walls (44.5 mg/cm^2 aluminum), μ is a geometrical factor (we assumed the solid angle of the counter to be equal to 2π, therefore $\mu = 0.5$), the rest of the quantities being those of Eq. (1) but refering to experiments with the copper indicator. $\xi(x)$ was measured for several distances x for two values of 2R. A graph of these results is given in Fig. 4.

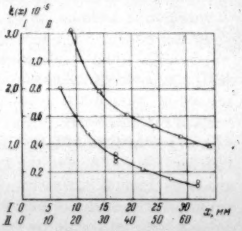

FIG. 4. The function $\xi(x)$. The abscissa gives the distance from the tritium target to the copper indicator. Δ – sample diameter 10 cm, ⊙ – sample diameter 4.5 cm.

For the measurement of $\epsilon(x, E)$, thin γ-ray sources of diameter 2R were required. By means of a counter with a known dependence of sensitivity on γ-radiation energy,[12] supplied to us by V. N. Sakharov, we measured the power of Ce^{141}, Hg^{203}, Cr^{51}, Au^{198}, Zn^{65} compounds, which could be considered as point sources in the measurements. After this, the activities of the sources were uniformly distributed in thin layers around circles of diameter 2R. The completed compounds were placed between sheets of Mg, Al, In, and Pb at various distances from the crystal in a manner such as to retain the geometry of Fig. 2. The value of $\epsilon(x, E)$ was determined as the ratio of total count at the peaks to the number of γ quanta emitted by the source. Figure 5 shows the spectrometer effectiveness for E = 0.411 Mev (Au^{198}) for an aluminum sample. Values of $\epsilon(x, E)$, interpolated by energy, were substituted in the integral of formula (1). For the heavy elements we used here the results of measurements of $\epsilon(x, E)$ on In and Pb, while for the light elements we used the measurements on Al and Mg.

In evaluating the cross-section we did not take into account the dependence of σ_{Cu} on neutron energy. Work was carried out on an unsorted

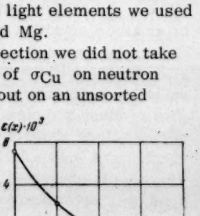

FIG. 5. Spectrometer effectiveness at the Au^{198} line (E_γ = 9.411 Mev), taking into account the absorption in $(x_2 - x)$ cm of aluminum. Point 0 corresponds to a distance of 3 cm to the crystal. Abscissa is $(x_2 - x)$, cm Al.

Specimen	Energy of γ rays, Mev	Half-life, millisec	Cross-section,	Suggested reaction
Mg	0.47±0.01	20±1	0.08	$Mg^{24}(n, p)\ Na^{24m}$
Al	0.47±0.01	20±1	0.04	$Al^{27}(n, \alpha)\ Na^{24m}$
Ge	0.17±0.01	16±1	0.3	—
As	0.28±0.01	17±1	0.13	$As^{75}(n, n')\ As^{75m}$
Y	0.24±0.01	14±1	—	$Y^{89}(n, n')\ Y^{89m}$ or $Y^{89}(n, 2n)\ Y^{88m}$
In	0.32±0.01	42±2	0.8	$In^{115}(n, 2n)\ In^{114m}$
Pb	0.48±0.01; 0.94±0.02	5±0.5	—	$Pb^{206}(n, 2n)\ Pb^{205m}$
	0.58±0.01; 1.04±0.03	$8\cdot10^2\pm1.5\cdot10^2$	1.5	$Pb^{208}(n, 2n)\ Pb^{207m}$ $Pb^{207}(n, n')\ Pb^{207m}$
Bi	0.48±0.01; 0.86±0.02	2.7±0.3	0.6	$Bi^{209}(n, 2n)\ Bi^{208m}$

deuteron beam of unknown composition. The errors in the quantities entering into the cross-section formula were: $\xi(x)$ — around 10%, $\epsilon(x, E)$ — around 10% for $E_\gamma \sim 1$ Mev and around 15% for $E_\gamma \sim 100$ kev; the ratio of the photopeak areas to the monitor count, with allowance for some arbitrariness in separating the peaks of the pulse spectrum, could be repeated with an accuracy up to 10 to 15%. The factor B in formula (1), for $T_{1/2}$ on the order of several milliseconds, was known to an accuracy of 10%, while for the long half-lives the accuracy was 1 to 2%. The probable maximum error in the cross section was 40 to 50%. It is for this reason that we consider our measurements of cross-section as estimates.

3. RESULTS OF MEASUREMENTS

The results of our measurements are given in the table.

Bismuth. To check the accuracy of our equipment, we investigated the isomer activity known to us from previous work in our laboratory, which involved the bombardment of bismuth by 14 Mev neutrons.[1] In reference 1 the measurements of γ-radiation energy were quite rough, and we therefore first made a more accurate measurement of this quantity. The radiation spectrum of a sample of bismuth (weight 962 g, diameter 100 mm, distance to the tritium target 24 mm) was obtained by an analyzer with a gray wedge. The photomultiplier was exposed for 24 millisec, 4 millisec after the start of the neutron pulse. One of the spectrum photographs obtained is shown in Fig. 6. Two γ lines are clearly visible. The energies of these lines, determined from several photographs, are 0.48 ± 0.01 and 0.86 ± 0.02 Mev. The results presented here and below are averaged over several experiments, while the errors are the mean deviations from these results.

The half-life was determined by means of the time analyzer, with the single channel discriminator set to each of the two γ lines of the spectrum. Measurements on both lines gave $T_{1/2}$ = 2.7 ± 0.3 millisec. To ascertain whether the 0.48-Mev line belongs to the bismuth spectrum and is not the sum of a background 0.47-Mev line and a Compton-effect 0.86-Mev line, we performed the following experiment. The channel of the pulse analyzer was first set to that point in the pulse distribution at which there is a Compton peak with energy 0.86 Mev, and then to the 0.48-Mev line. A count was taken for equal monitor indications. At these same conditions, we measured the background radiation. It turned out that the

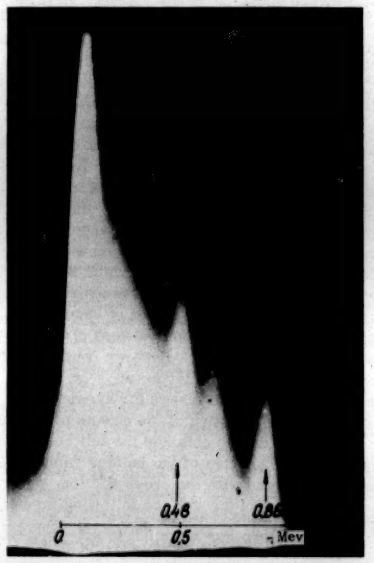

FIG. 6. Spectrum of Bi specimen. Two lines are seen, corresponding to energies of 0.48 and 0.86 Mev. The photomultiplier was exposed for 24 millisec, 4 millisec after start of neutron pulse.

difference in count caused by the radiation of Bi was twice as great at the 0.48-Mev line as at the Compton peak, which proves the actual existence of two γ lines.

The results obtained agree with the data in previously published papers. In the bombardment of bismuth by fast neutrons,[1] radiation with $T_{1/2}$ = 2.4 millisec was found and ascribed to Bi^{208}. In the irradiation of bismuth by γ quanta in the 24-Mev betatron,[4] an isomer activity was found with $E_\gamma = 500 \pm 20$ and (930 ± 30) kev and $T_{1/2} = (2.7 \pm 0.3)$ millisec. On bombarding bismuth with 20-Mev protons[2] an activity was found with $T_{1/2} = (3.0 \pm 1)$ millisec. In the same work, upon bombardment of lead by protons, radiation was observed with $E_\gamma = 0.7$ Mev and with approximately the same $T_{1/2} = (2.0 \pm 0.5)$ millisec. According to our measurements, carried out on the 0.86-Mev line, the cross section for the bismuth isomer production was estimated to be 0.6×10^{-24} cm^2. This comprises ~ 0.3 of the cross section for the reaction $Bi^{209}(n, 2n)Bi^{208}$, for which statistical theory gives 2.2×10^{-24} cm^2. An estimate of the multipole nature of the transitions based on the Montalbetti[13] nomogram, for the measured energies and periods, does not determine which of these transitions is the first in the cascade. Thus, for a transition energy of 0.48 Mev, an M3 transition is possible (the nomogram yields for this energy $T_{1/2} \sim 45 \times 10^{-3}$ sec, which in view of the low accuracy of the nomogram, is close to the measured period). For an energy of 0.86 Mev, the same M3 transition is possible ($T_{1/2} \sim 10^{-3}$ sec). In view of the fact that M3 transitions are the most common for odd-odd nuclei, it is possible to suggest that in this case the first transition to take place in the cascade is M3. Here, regardless of which transition takes place in the ground state, the difference in moments of the ground and first excited state cannot be greater than 3. To explain the large probability of isomer production in the reaction $Bi(n, 2n)Bi^m$ and the small yield of this isomer in the reaction $Pb(p, n)Bi^m$ observed in reference 2, we can assign, for example, a spin of 9 to the (480 + 860) kev level.

The possibility of the Bi^{209m} isomer production was not analyzed in detail, but existing results make it possible to assign a lower probability to this possibility.

Magnesium and aluminum. For a number of light alloys with $A < 30$, in which filling of the $p_{3/2}$ and $d_{3/2}$ shells occurs, two odd nucleons give rise to a configuration with a large value of spin in the ground state [for example $Bi^{10}(3^+)$, $Na^{22}(3^+)$, $Na^{24}(4^+)$, $Al^{26}(5^+)$, $Al^{28}(3^+)$]. If low lying excited levels with moments 0 and 1 exist for these configurations, these states will be isomeric. Indeed, a long-lived isomer of Al^{26m} has recently been found.[14] Existence of a millisecond Na^{22m} isomer is also theoretically possible. However, many experimental attempts to find the isomer Na^{22} have so far led to negative results.[4]

In view of the great interest presented by the possibility of the existence of isomers in so many light nuclei, we investigated Na^{24m}, which can be obtained either by the radiative capture of slow neutrons by Na^{23}, or in the reactions $Al^{27}(n, \alpha)Na^{24}$ and $Mg^{24}(n, p)Na^{24}$.

A sample of metallic aluminum (weight 159 g, diameter 44 mm, distance from target 58 mm) was irradiated in the direct neutron beam. In the γ-radiation spectrum we found a line of (0.47 ± 0.01)-Mev line with a measured half-life of (20 ± 1) millisec. The cross-section for the production of a 0.47-Mev level was estimated to be 0.04×10^{-24} cm^2.

The found γ line was ascribed to an isomer state Na^{24m}. In view of the fact that the cross section for the reaction $Al^{27}(n, \alpha)Na^{24}$ is 0.12×10^{-24} cm^2,[8] the ratio of the cross section for production of an isomer state to the reaction cross section is ~ 0.3.

To check the correctness of the isomer identification we irradiated metallic magnesium (weight 100 g, diameter 44 mm) under the same conditions. The measured half-lives were the same as in the case of aluminum. The cross-section for Mg is 0.08×10^{-24} cm^2.

In reference 15, Na^{24m} was identified through study of the decay of Ne^{24} ($E_\gamma = (472 \pm 5)$ kev, $5 \leq T_{1/2} \leq 50$ millisec).

These results, as well as the circumstance that a 0.47-Mev line is observed in the irradiation of Na^{23} by thermal neutrons,[16] confirm our assumption that the observed γ radiation is associated with the production of the Na^{24m} isomer in the (n, α) and (n, p) reactions with Al and Mg.

Germanium. Pulsed irradiation of a specimen of metallic germanium (weight 17 g, thickness 3 mm, distance to tritium target 27 mm) was accompanied by γ radiation with $E_\gamma = (0.17 \pm 0.01)$ Mev and a $T_{1/2} = (16 \pm 1)$ millisec. In spite of the intense background, the line that appears during the irradiation of germanium in the spectrum obtained by means of an analyzer with a gray wedge, is distinctly visible. The cross section for production of a 0.17-Mev metastable level is estimated to be 0.3×10^{-24} cm^2.

FIG. 7. Spectrum of As. The 0.28 Mev line, not found in the background spectrum, is quite pronounced. The photomultiplier was exposed for 134 millisec, 4 millisec after start of neutron pulse. Monitor count – 21,400.

We assume that the radiation found, as well as the radiation observed previously in the irradiation of Ga by protons,[3] belong to one of the isomers of Ge or Ga.

Arsenic. Among the elements with atomic numbers from 60 to 80, a considerable number of isomers is known. For this reason, an investigation of millisecond isomers, for a number of such nuclei, is of particular interest.

Upon irradiation of a sample of metallic arsenic (weight of sample, 43 g, distance to tritium target, 40 mm), we observed a short-lived γ activity with an energy of 0.28 ± 0.01 Mev. This spectrum is shown in Fig. 7. Along with the new line 0.28-Mev line, a background line is also seen at 0.47 Mev. Half-life measurements for the 0.28-Mev line gave $T_{1/2} = (17 \pm 1)$ millisec. The graph for the determination of the period is given in Fig. 8.

An estimate of the cross section for the production of isomers in this reaction gave a value of 0.13×10^{-24} cm^2. The spectrum obtained with the one-channel differential discriminator used to estimate the cross section is shown in Fig. 9. The found γ activity apparently belongs to As, which is formed by the reaction $As^{75}(n, n')As^{75m}$, in good agreement with the results obtained by other authors. As a matter of fact, it has been shown in reference 18 that the γ radiation with $E_\gamma = 0.28$ Mev, which accompanies K capture by Se^{75}, is a delayed radiation with $T_{1/2} = (18 \pm .5)$ millisec and may be ascribed to the isomer As^{75m}.

In the irradiation of As in a 24 Mev betatron,[4] an activity was obtained with $E_\gamma = (305 \pm 15)$ kev and $T_{1/2} = (12 \pm 3)$ millisec. The γ-radiation found[3] upon irradiation of Ge by 20-Mev protons with $T_{1/2} = (17.5 \pm 2)$ millisec and $E_\gamma = 0.31$ Mev evidently also belongs to As^{75m}, which is produced in the $Ge^{76}(p, 2n)As^{75m}$ reaction.

Yttrium. A sample of yttrium oxide Y_2O_3 pressed into the shape of a disc with diameter 44 mm (weight 20 g, distance to tritium target, ~ 20 mm) was irradiated. At first an attempt was made to find the well known isomer Y^{88m},[19,4] with $T_{1/2} = 0.37$ millisec and $E_\gamma = 393$ kev. However, we did not succeed in finding it since the minimum delay after the start of neutron pulse could not be made less than 2 millisec (the neu-

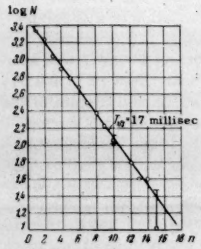

FIG. 8.

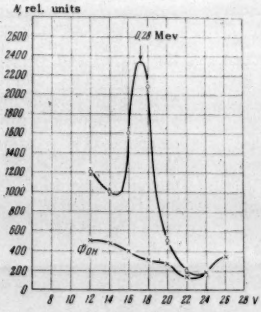

FIG. 9.

FIG. 8. Decay of As ($E_\gamma = 0.28$ Mev). Bandwidth of channel = 7.95 millisec. Abscissa – channel number. Ordinate – logarithm of difference between counts with and without specimen.

FIG. 9. Spectrum of As obtained with the single channel discriminator. Bandwidth of channel – one volt. Abscissa – discrimination voltage. Ordinate – channel count referred to 2000 monitor pulses. This spectrum is used to estimate the cross section.

tron pulse did not have a sufficiently steep trailing edge), and our equipment did not allow us to measure activities with so short a period.

For photomultiplier exposure times of ~100 millisec it was possible to find activities with $E_\gamma = (0.24 \pm 0.01)$ Mev and $T_{1/2} = (14 \pm 1)$ millisec. This same isomer activity ($E_\gamma = 0.2$ Mev and $T_{1/2} = 13$ millisec) was evidently observed earlier, when yttrium was irradiated by fast protons.[3] From an analysis of the cross reactions it follows that this is either the isomer Y^{89m} obtained in inelastic scattering of neutrons and protons, or the isomer Y^{88m} obtained by us in the reaction $Y^{89}(n, 2n)Y^{88m}$ and by Lel'punskiĭ et al.[3] in the reaction $Y^{89}(p, pn)Y^{88m}$. From Montalbetti's nomogram it follows that the E3 transition corresponds to this isomer.

The assumption that the observed γ radiation belongs to Y^{88m} and that the 240-kev level in the scheme of reference 17, shown in Fig. 10, has a moment (1^+), evidently is in disagreement with reference 19, since it is difficult to explain the absence of β decay of Zr^{88} at this level. Moreover, another unexplained fact is the absence of this activity in the irradiation of strontium by fast protons [$Sr^{88}(p, n)Y^{88}$][3] and of yttrium by γ quanta [$Y^{89}(\gamma n)Y^{88}$].[4] If, on the other hand, we assign to the 240-kev level of Y^{88m} a moment (7^+), then these difficulties disappear: the β decay of Zr^{88} is strictly forbidden at this level, while the probability of exciting the (7^+) level in the reactions $Sr^{88}(p, n)Y^{88}$ and $Y^{89}(\gamma, n)Y^{88}$ is small because the Sr^{88} spin is 0^+, while the Y^{89} spin is $\frac{1}{2}^-$. In this case we can also explain the relatively large yield of isomers in the (n, 2n) and (p, pn) reactions: the average moment of the residual nucleus may be ≥ 4, which will lead to a large probability of transitions to the 7^+ level. For this reason, it seems to us that the assumption about Y^{88m} deserves serious attention and should be very thoroughly studied.

Indium. Upon irradiating a sample of indium (weight 54 g, diameter 40 mm, distance to target 24 mm) we observed a γ-activity with energy

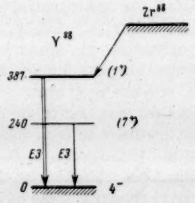

FIG. 10. Level scheme for Y^{88}.

(0.32 ± 0.01) Mev and a half-life (42 ± 2) millisec. The cross section estimated from the measurements with the single-channel analyzer comes to 0.8×10^{-24} cm.

The following circumstance is of interst. A known regularity is noted when we study the tabulated data on the decay of the odd-odd isotopes of indium. In In^{110} and In^{112} we observe an M3 isomer transition, while in In^{114} and In^{166} the transition of the E4 type. If we plot $\log(\tau A^2)$ as a function of E_γ for this type of transition, the experimental points will in general lie on a straight line. If we pass such a straight line through the points for In^{110} and In^{112}, we find that there may be an M3 type transition in In^{114} with energy 0.3 Mev and a half-life of some tens of millisec. Bearing this in mind we can assume that we have observed the radiation of In^{114} which is obtained from the reaction $In^{115}(n, 2n)In^{114}$. The experimental point fits rather well the straight line drawn through the known points for In^{110} and In^{112}. To explain the large isomer-production cross section one should assume that the γ transitions from the highly excited states which have a large moment after emission of two neutrons take place, basically, at the 8^+ isomer level which is 320 kev away from the known 5^+ level.[17]

The assumption that the observed radiation belongs to In^{114} is confirmed also by the results of other workers. When Cd was irradiated by 20 Mev protons, a γ-activity was observed[3] with $E_\gamma = 0.28$ Mev and $T_{1/2} = (47 \pm 10)$ millisec. An analysis of thresholds shows that the most probable reaction is $Cd^{114}(p, n)In^{114}$.

As a result of a photonuclear reaction, an activity was produced[5] with $E_\gamma = (0.312 \pm 0.01)$ Mev and $T_{1/2} = (45 \pm 10)$ millisec. Evidently the reaction that took place was $In^{115}(\gamma, n)In^{114}$.

In conclusion, let us note that the magnitude of half life estimated from the Montalbetti nomogram for In^{114} and the M3 transition, is equal to 25×10^{-3} sec and is sufficiently close to the one observed by us.

Lead. During irradiation of a metallic lead specimen (weight 1448 g, diameter 100 mm, distance to target 24 mm) we observed a short-lived activity with a complicated spectrum. To determine the nature of this activity we obtained the γ-radiation spectrum of lead for various delays after the start of the neutron pulse. If the photomultiplier is exposed for 60 millisec and a 4-millisec delay is used, we can distinguish in the spectrum of Fig. 11 four γ lines: $E_{\gamma_1} = (0.48 \pm 0.01)$ Mev; $E_{\gamma_2} = (0.58 \pm 0.01)$ Mev; $E_{\gamma_3} = (0.94 \pm 0.02)$ Mev and $E_{\gamma_4} = (1.04 \pm 0.03)$ Mev. How-

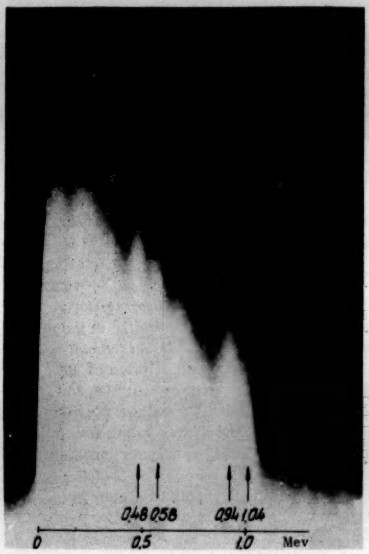

FIG. 11. Spectrum of Pb. Photomultiplier exposed for 60 millisec with 4 millisec delay after start of neutron pulse.

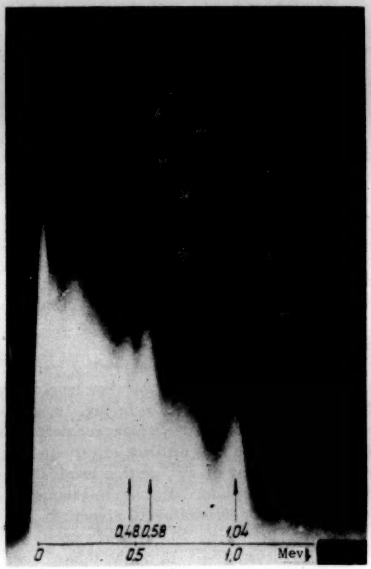

FIG. 12. Spectrum of Pb. Photomultiplier exposed for 60 millisec with 35 millisec delay from start of neutron pulse.

ever, if we expose the photomultiplier for the same period of time but use a delay of 35 millisec (Fig. 12), we can see clearly only two lines, γ_2 and γ_4, which belong to the known lead isomer Pb^{207} ($T_{1/2} = 0.8$ sec). The intensity of the γ_1 and γ_3 lines is greatly reduced in this case and therefore they have considerably shorter half-lives than γ_2 and γ_4.

Measurements of the half-lives showed that the lines with $E_\gamma = 0.48$ and 0.94 Mev have $T_{1/2} = (5 \pm 0.5)$ millisec, while the lines with $E_\gamma = 0.58$ and 1.04 Mev have a half-life of (0.8 ± 15) sec. The latter result is in good agreement with the data in the literature pertaining to the study of the Pb^{207m} isomer (for example, in reference 20, $E_\gamma = 0.50$ and 1.0 Mev and $T_{1/2} = 0.9$ sec). To decide whether the 0.48-Mev line belongs to lead and whether it occurs in the cascade with the 0.94-Mev line, we performed an experiment similar to the one described above for bismuth. The measurements showed that both lines, with an activity of 5 millisec, have approximately equal intensities.

Let us note that this activity has not been observed previously in lead bombarded by neutrons. In reference 2 a γ radiation with energy ~ 0.9 Mev and a similar period ($T_{1/2} = 6.5$ millisec) was noted upon irradiation of Tl by protons. Comparing these data, we ascribed the isomer activity to Pb^{205}, obtained in our work from the reaction $Pb^{206}(n, 2n)Pb^{205m}$ and obtained in reference 3 by the reaction $Tl^{205}(p, n)Pb^{205m}$.

The existence of the Pb^{205m} isomer was predicted by Pryce[21] as the result of a theoretical computation of the Pb^{205} levels, based on the shell model. The energy predicted for the transition, 0.4 ± 0.2 Mev, and the half-life of several milliseconds do not contradict our data, but according to Pryce's calculation this transition must take place at a level of 703.3 kev with a moment of $^7/_2^-$ and, therefore, is accompanied by γ radiation of this energy or less.

From our estimates, the cross section for the production of isomers with 0.8 sec activity, at the 1.04 Mev line, is 1.5×10^{-24} cm^2.

In conclusion we consider it our pleasant duty to express our gratitude to O. I. Leĭpunskiĭ for his significant aid to the work, to O. B. Likin, N. M. Meleshin, N. K. Parshenkov, V. A. Shabashov for the development and the adjustment of the equipment, and also to Yu. Ya. Lapitskiĭ, A. V.

Gusev, V. S. Ionov, and D. F. Veprintsev, for faultless operation of the pulsed-neutron equipment.

[1] Yampol'skiĭ, Leĭpunskiĭ, Gen, and Tikhomirov, Izv. Akad. Nauk SSSR, Ser. Fiz. **19**, 338 (1955), Columbia Tech. Transl. p 312.

[2] Leĭpunskiĭ, Miller, Morozov, and Yampol'skiĭ, Dokl. Akad. Nauk SSSR **108**, 935 (1956), Soviet Phys. "Doklady" **1**, 505 (1957).

[3] Leĭpunskiĭ, Morozov, Makarov, and Yampol'skiĭ, J. Exptl. Theoret. Phys. (U.S.S.R.) **32**, 393 (1957), Soviet Phys. JETP **5**, 305 (1957).

[4] S. H. Vegors, Jr. and P. Axel, Phys. Rev. **101**, 1067 (1956).

[5] S. H. Vegors, Jr. and R. B. Duffield, Bull. Am. Phys. Soc. **1**, 206 (1956).

[6] Lapitskiĭ, Levintov, Slivkov, and Shamshev, J. Tech. Phys. (U.S.S.R.) **26**, 733 (1956), Soviet Phys. JTP **1**, 714 (1957).

[7] V. A. Shabashov and M. F. Ivakin, Отчет ИХФ АН СССР (Report, Inst. Chem. Phys. Acad. Sci. U.S.S.R.) 1956.

[8] Y. Chinjiro, J. Phys. Soc. of Japan **12**, 443 (1957).

[9] O. B. Likin, Приборы и техника эксперимента (Instruments and Meas. Engg.) No. 2, 326 (1958).

[10] Yu. V. Makarov and N. M. Meleshin, Отчет ИХФ АН СССР (Report, Inst. Chem. Phys. Acad. Sci. U.S.S.R.) 1957.

[11] Yu. V. Makarov, Отчет ИХФ АН СССР (Report, Inst. Chem. Phys. Acad. Sci. U.S.S.R.) 1957.

[12] V. N. Sakharov, Атомная энергия (Atomic Energy) **7**, 61 (1957).

[13] R. Montalbetti, Canadian J. Phys. **30**, 660 (1952).

[14] Kawanag, Mills, and Sherr. Phys. Rev. **97**, 248 (1955). T. H. Handley and W. S. Lyon, Phys. Rev. **99**, 755 (1955).

[15] B. J. Dropesky and A. W. Schardt, Phys. Rev. **102**, 426 (1946).

[16] H. T. Motz, Phys. Rev. **90**, 355 (1953).

[17] B. S. Dzhelepov and L. K. Peker, Схемы распада радиоактивных изотопов (Decay Schemes of Radioactive Isotopes) Acad. Sci. Press, 1957.

[18] A. W. Schardt, Bull. Am. Phys. Soc. **1**, 85 (1956).

[19] Hyde, Florence, and Larsh, Phys. Rev. **97**, 1255 (1955).

[20] E. C. Campbell and M. Goodrich, Phys. Rev. **78**, 640 (1950).

[21] M. H. L. Pryce, Nucl. Phys. **2**, 226 (1956).

Translated by M. E. Zaret
206

EFFECT OF ATOMIC ORDERING ON EXCHANGE INTERACTION IN THE Fe_3Pt *ALLOY*

K. P. BELOV and Z. D. SIROTA

Moscow State University

Submitted to JETP editor October 22, 1958

J. Exptl. Theoret. Phys. (U.S.S.R.) **36**, 1058-1062 (April, 1959)

The magnitude of the shift of the Curie point due to pressure and spontaneous deformation of the lattice is computed from the data on the measurement of the temperature dependence of magnetostriction in an alloy close to Fe_3Pt. It has been found that these quantities decrease with atomic ordering in the alloy. It is concluded that atomic ordering in the Fe_3Pt not only changes the magnitude of exchange interaction but also the nature of its dependence on the interatomic distance.

1. The alloys of the system Fe-Pt are characterized by a number of extremely interesting magnetic properties. Compounds close to Fe_3Pt display unusually sharp ferromagnetic anomalies in the thermal expansion coefficient[1] and strong magnetostrictive properties.[2] The manner in which both these properties manifest themselves depends on the heat treatment the alloys are subjected to, because atomic ordering takes place in this process. At the same time, a considerable change occurs in the Curie temperature. In alloys containing a large amount of Pt, i.e., those close in composition to $FePt_3$ and having suitable atomic ordering, antiferromagnetism is observed.[3] All of these considerations make the Fe-Pt alloys extremely interesting subjects in which to study the effect of atomic ordering in the lattice on the character of the exchange interaction.

We have undertaken in the present paper an investigation of the influence of atomic ordering on magnetostriction which accompanies the paraprocess in alloys close to Fe_3Pt in composition. In an earlier paper one of the authors showed[4] that on the basis of an investigation of this magnetostriction (especially in connection with measurements made in the vicinity of the Curie point) it is possible to obtain information on the character of the dependence of the exchange interaction on the interatomic distance. For this reason the main attention in our work has been directed to the magnetostriction of the paraprocess in the alloy indicated, without going into all its other magnetic properties.

2. For this investigation, we chose an alloy containing 58% of Pt by weight, 42% Fe by weight, close in its stoichiometric composition to Fe_3Pt. The Kurnakov point for this alloy occurs in the vicinity of 900 or 1000°C.

The alloy was prepared, in the form of a small rod of length 150 mm and diameter 3 mm in an induction furnace, by pulling the melt in a quartz tube in vacuum. The rod was subjected to a homogenizing anneal at a temperature of 1020°C with subsequent water quench, which fixed the non-ordered state. The ordered state was produced by annealing at 600°C (below the Kurnakov point) with various periods of heat treatment (20 minutes, 1 hour 20 minutes, 4 hours 20 minutes, 12 hours).

After each anneal, magnetostriction vs. temperature curves were obtained by using a remote wire strain gauge, which has been previously described in detail (see, for example, reference 4). Curves of the magnetization as a function of the temperature were also obtained. The precision of magnetostriction and magnetization measurements was ±5% and ±2% respectively.

3. Figure 1 shows the curves of magnetostriction as a function of the temperature for a sample

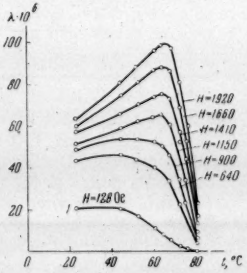

FIG. 1. Dependence of magnetostriction on the temperature in an alloy of 58% Pt, and 42% Fe (by weight) in the quenched condition (in water at 1020°C).

in the ordered state (water quenched at 1020°C) obtained in various magnetic fields. The appearance of these curves is characteristic for the magnetostriction of the paraprocess: as the temperature increases the magnetostriction of the paraprocess increases and reaches a maximum in the vicinity of the Curie point. As the degree of ordering increases (with various durations of anneal at 600°C) the character of the curves changes (see Figs. 2 and 3). Along with the magnetostriction of the paraprocess, magnetostriction appears as a concomitant to the processes of displacement and rotation; the latter is reduced monotonically with an increase in temperature and practically approaches zero at the Curie point. Superposition of both types of magnetostriction leads to a "saddle shaped" type of curve which is quite evident in Figs. 2 and 3. As the degree of ordering increases the magnetostriction of displacement and rotation becomes predominant while the magnetostriction of the paraprocess is reduced. Simultaneously the Curie point moves up from 70° to 170°C.

In Fig. 4 we have the curves of magnetostriction as a function of the square of the specific magnetization for an alloy annealed over a period of 1 hour 20 minutes at 600°C. It is evident that in the region of the paraprocess λ is a linear function of σ^2. An analogous dependence is observed in the sample for other degrees of ordering as well as in the non-ordered state. Curves of this shape make it possible to determine not only the magnitude of the spontaneous magnetization σ_S (by extrapolating the straight portions of the curves in Fig. 4 down to the abscissa) but, as has been shown in reference 5, we can also determine the magnitude of the spontaneous deformation of the lattice λ_S (by the extrapolation of the straight portions of Fig. 4 to the ordinate axis — see dashed lines). Figure 5 shows λ_S as a function of σ_S^2. Both quantities λ_S and σ_S^2 were determined by the method given above. The results of the measurements correspond to conclusions drawn from thermodynamics (see reference 6), according to which

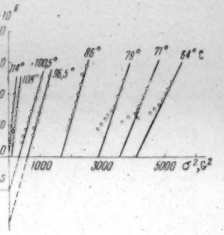

FIG. 4. Magnetostriction as a function of the square of the specific magnetization in an alloy consisting of 58% Pt and 42% Fe (by weight) after anneal at 600°C (1 hour 20 minutes).

$$\lambda_s = {}^1/_6 \gamma \sigma_s^2, \qquad (1)$$

where γ is the coefficient for the spontaneous deformation of the lattice. It follows from Fig. 5 that the largest value for γ is obtained for an alloy in the non-ordered state. The coefficient γ, and therefore the magnitude of the spontaneous lattice deformation, become smaller as the degree of ordering in the alloy increases.

4. Making use of the thermodynamic theory for ferromagnetic transformation[6] and data obtained from measurements on the magnetostriction as a function of temperature in the vicinity of the Curie point, we can compute the magnitude of

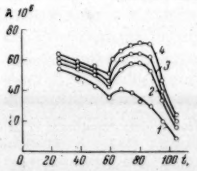

FIG. 2. The same as Fig. 1, but after anneal at 600°C (for 20 Min.): 1 – at H = 900, 2 – at 1410, 3 – at 1660, 4 – at 1920 oersteds.

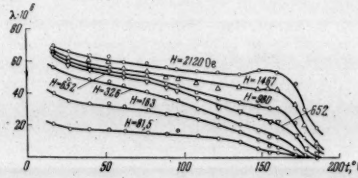

FIG. 3. The same as in Fig. 1 after anneal at 600°C (12 hours).

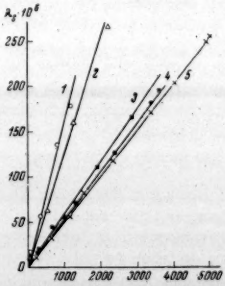

FIG. 5. Spontaneous lattice deformation as a function of the square of the spontaneous magnetization in an alloy containing 58% Pt by weight, 42% Fe by weight, for various degrees of atomic ordering: 1 – quenched condition, 2 – anneal for 20 min., 3 – anneal for 1 hour 20 min., 4 – anneal for 4 hours 20 min., 5 – anneal for 12 hours.

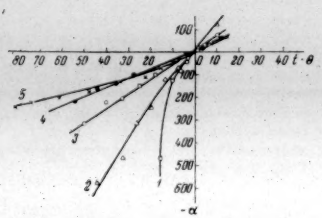

FIG. 6. Thermodynamic coefficient α as a function of the temperature in the vicinity of the Curie point for an alloy containing 58% Pt and 42% Fe (by weight), for various degrees of ordering: 1 – quenched condition, 2 – anneal for 20 min., 3 – anneal for 1 hour 20 min., 4 – anneal for 4 hours 20 min., 5 – anneal for 12 hours.

the temperature shift of the Curie point as a function of the pressure:

$$d\Theta / dP = -\gamma / \alpha'_\Theta. \qquad (2)$$

Here γ can be determined from relation (1), and α'_Θ is the derivative of the thermodynamic coefficient α with respect to temperature obtained from the curves of the true magnetization in the vicinity of the Curie point (see, for example, reference 6). Figure 6 shows the curves of $\alpha(T)$ obtained for our alloy for various degrees of ordering. The quantity α'_Θ may be determined by passing a tangent to the curve for $\alpha(T)$ as the point $\alpha = 0$. Substituting γ and α'_Θ in formula (2) we can determine the value of $d\Theta/dP$ for our specimen. In Fig. 7 we note that $d\Theta/dP$ falls off as a function of ordering, while Θ itself increases.

5. The value of $d\Theta/dP$ can serve as a quantitative characteristic of the variation of the exchange integral with volume or interatomic distance.[4] As a matter of fact, if we bear in mind that $\Theta = zA/2k$, where A is the exchange integral, z is the coordination number for the lattice, k is the Boltzmann constant, and $\kappa = -d\omega/dP$ (κ is the compressibility coefficient, ω is the relative volume change), we can write

$$d\Theta / dP = (-z\kappa / 2k)(dA / d\omega). \qquad (3)$$

From this it follows that the larger the quantity $d\Theta/dP$ the stronger is the dependence of A in the present ferromagnetic material on ω or on the interatomic distance ($dA/d\omega$ is the "curvature" of the exchange integral if we neglect the s-d exchange interaction).

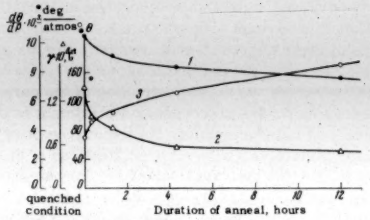

FIG. 7. 1 – effect of Curie point shift on the pressure, $d\Theta/dP$, 2 – coefficient γ, which determines the magnitude of the spontaneous lattice deformation, 3 – the Curie temperature Θ, all vs. the degree of ordering.

In accordance with the above, the curvature of the exchange integral for our alloy is especially large in the non-ordered condition; the curvature is reduced in the transition to the ordered state or to a partial atomic order. A large magnitude for the "curvature" of the exchange integral in the non-ordered alloy Fe_3Pt must give rise to large values of spontaneous lattice deformation and as a consequence of the latter to considerable ferromagnetic anomalies in the thermal expansion. This has indeed been found to be true experimentally.[1]

[1] Kussman, Auwarter, and Rittenberger, Ann. Physik **4**, 176 (1948).

[2] Akulov, Ali-Zade, and Belov, Dokl. Akad. Nauk SSSR **15**, 815 (1949). A Kussman and G. Rittenberger, Ann. Physik **7**, 173 (1950). E. Klokholm and F. J. Donahoe, J. Frank. Inst. **264**, 59 (1957).

[3] J. Grangle, Nature **181**, 644 (1958).

[4] K. P. Belov, Упругие тепловые и электрические явления в ферромагнетиках, 2-е изд., (Elastic, Thermal, and Electrical Phenomena in Ferromagnetics) 2nd ed., Gostekhizdat (1957).

[5] K. P. Belov and I. K. Panina, Dokl. Akad. Nauk SSSR **111**, 985 (1957), Soviet Phys. Doklady **1**, 732 (1957).

[6] K. P. Belov, Usp. Fiz. Nauk **65**, 207 (1958).

Translated by M. E. Zaret
207

SOVIET PHYSICS JETP VOLUME 36 (9), NUMBER 4 OCTOBER, 1959

THE MAGNETIZATION AND MAGNETOCALORIC EFFECT OF MANGANESE PHOSPHIDE

I. G. FAKIDOV and V. P. KRASOVSKIĬ

Institute of the Metal Physics, Academy of Sciences, U.S.S.R.

Submitted to JETP editor October 23, 1958

J. Exptl. Theoret. Phys. (U.S.S.R.) **36**, 1063-1067 (April, 1959)

The magnetocaloric effect and magnetization of manganese phosphide (MnP) were investigated at various field strengths in the temperature region of magnetic transformations. As contrasted with Guillaud, we found that the magnetic transformation temperature was not dependent on the magnetic field strength. The character of the dependence of magnetocaloric effect on the temperature and magnetic field strength and also the temperature dependence of the spontaneous magnetization indicate the existence of a Curie point at 22° C.

The results obtained are discussed from the viewpoint of the s-d exchange model of ferromagnetism.

INTRODUCTION

GUILLAUD'S[1] measurements have shown that the temperature dependence of the magnetization of the monophosphide of manganese (MnP) follows a T^2 law at low temperatures. The saturation magnetization is not large and the magnetic moment per atom of manganese comes to 1.2 μ_B. On the basis of these data, Guillaud suggests the existence in manganese phosphide of an anti-ferromagnetic interaction between the manganese atoms. He breaks down the crystal lattice of MnP into two sub-lattices one of which consists of the Mn_I atoms with electron state $3d^7$, and the other consisting of Mn_{II} in a $3d^5 4s^2$ state. The magnetic moments of the Mn_I atoms, equal to 3 μ_B, are oriented antiparallel to the moments of Mn_{II} with value 5 μ_B. As a result of such an orientation the magnetic moments of the manganese atoms in various electronic states provide a resultant moment equal to 1 μ_B per atom. The temperature of magnetic transformation Θ_f found by Guillaud is equal to 25° C. By his assertion, the magnitude of Θ_f is strongly dependent on the intensity of the external magnetic field.[2,3]

Measurements carried out by us on the temperature dependence of the electrical resistivity of MnP show that the curve of the function $\rho = \rho(t)$ has a singular point at 22° C. The character of the singular point is analogous to the kind which usually occurs in ferromagnetic substances at the transition through the Curie point. Moreover, measurements of the effect of the magnetic field on the resistance of the same compound have confirmed the assumed presence of a second-order phase transformation in the vicinity of t = 22° C (Curie point), which followed from measurements of the electrical conductivity. However, a definite conclusion about the character of the magnetic transformation could only have been made on the basis of an investigation of the magnetocaloric effect in MnP.

Altogether, the measurements of the magnetocaloric effect, when considered with the measurements of the magnetization isotherms, make it possible to establish the temperature dependence of spontaneous magnetization in the vicinity of the magnetic transformation.

PREPARATION OF SAMPLE AND METHOD OF MEASUREMENT

As raw materials for obtaining manganese phosphide we used red phosphorus and manganese obtained electrolytically by sublimation in vacuo. The mixture of manganese and phosphorus powders was mixed in a quartz vessel which was then pumped down in a vacuum system to a pressure of 10^{-6} mm of Hg.

To obtain a sufficiently uniform alloy the vessel was kept in an oven at 650° C for 50 hours. The alloy was allowed to cool down with the oven. From the alloy thus obtained a sample was prepared in the shape of an ellipsoid with axes equal to 12 and 6 mm respectively. The sample was cemented to a thin glass rod which was held inside a silvered glass tube. The latter was placed into a copper chamber over which thermostatically controlled water was allowed to circulate, and it was held

between the poles of an electromagnet. Measurements of the heat effect, Δt, were carried out in vacuum at a pressure of 10^{-4} mm Hg., which was attained by means of an adsorption type pump in which activated charcoal was used as the adsorbent.

For the measurement of temperature, as well as the change in temperature during magnetization and demagnetization of the sample, a thermistor with a time constant of the order of hundredths of a second was used. The thermistor was inserted into the sample, approximately down to the middle, through a hole 0.8 mm in diameter. A magnetic field of intensity up to 20,000 oersteds showed no effect on the thermistor resistance. The thermistor was calibrated at temperatures of 0.2 and 100° C. The parameters of the thermistor were $R\ (0°C) = 4736\,\Omega$ and $B = 2409°K$. The resistance-temperature coefficient for the thermistor at room temperature (20° C) was $\alpha = 2.8\%/°C$. The thermistor resistance was measured with an MTV bridge to an accuracy of 0.02 ohms. The temperature stability of the sample was not less than 0.001°. The sensitivity of the measuring equipment changed with the sample temperature because of the nonlinearity of the thermistor temperature coefficient, and was not less than 0.001° per mm.

The use of a thermistor for the measurement of the magnetocaloric effect has some advantages over the measurement of small temperatures Δt by means of thermocouples. In addition to the considerable increase in sensitivity of the measuring equipment obtained by the use of a thermistor, its use in a bridge circuit makes it possible to eliminate the ballistic throw which always occurs when thermocouples are used.

The magnitude of the heat effect, Δt, was measured both during magnetization of the sample and during demagnetization. The change in sample temperature during magnetization was always very closely equal to the change in temperature of the sample during demagnetization.

Measurements of the magnetization isotherms were carried out on the same sample in the vicinity of the Curie point. These measurements were obtained ballistically. The sample was magnetized in the field of an electromagnet and then was pulled out of the search coil through a hole in one of the magnet pole shoes.

The magnetization of the sample was computed from the formula

$$\sigma = \frac{C\alpha}{Sn\,(4\pi - N)},$$

where σ is the magnetization, C is the value for one galvanometer division in maxwells/mm, α is the deflection in mm, S is the sample cross section area in cm^2, n is the number of turns in the search coil, and N is the demagnetizing factor.

DISCUSSION OF RESULTS

We have investigated the dependence of the magnitude of the magnetocaloric effect on the intensity of magnetic field at various temperatures in the vicinity of the temperature of magnetic transformation, along with investigating the magnetization isotherms for a sample of MnP. Figure 1 depicts the magnitude of the Δt effect as a function of the sample temperature. As is evident, all the curves have a maximum near 22° C. The position of this maximum along the axis of temperatures is independent of the magnitude of magnetic field intensity. This temperature is the Curie point for the manganese monophosphide investigated by us. The strong dependence of the Curie point on the magnetic field intensity noted by Guillaud was not found by us either in the investigation of the magnetocaloric effect or when we studied the influence of magnetic field on the electrical resistance of a whole series of manganese alloys with various amounts of phosphorus.

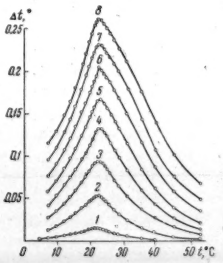

FIG. 1. Temperature dependence of the magnetocaloric effect, Δt, for various magnetic field intensities: 1 – at 1000, 2 – 3000, 3 – 5000, 4 – 7000, 5 – 9000, 6 – 11,000, 7 – 13,000, and 8 – 15,000 oersteds.

Figure 2 shows the dependence of the temperature effect, Δt, on the square of the magnetization. As is well known,[4,5] by extrapolating the linear portions of these curves we can determine the magnitude of the spontaneous magnetization at a given temperature. It should be pointed out that the extent of the linear portion of these curves is rapidly shortened with a reduction in temperature, which complicates the process of extrapolation. For this reason, to obtain sufficiently accurate values of spontaneous magnetization at lower temperatures, it is necessary to use field strengths of the order of 20,000 oersteds which were not available to us.

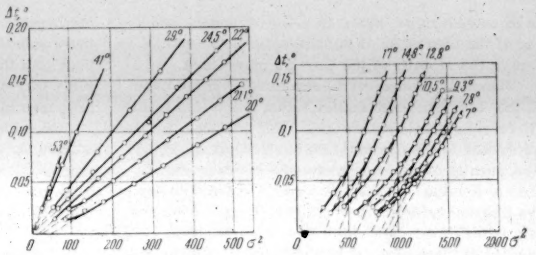

FIG. 2. Dependence of magnetocaloric effect, Δt, on the square of the magnetization at various temperatures.

The value of the spontaneous magnetization σ_S was determined from the curves of the magnetocaloric effect, Δt, as a function of the square of the magnetization σ^2, which were obtained at various temperatures above and below the Curie point (see Fig. 2). Curve 1 in Fig. 3 depicts the temperature as a function of the spontaneous magnetization σ_S. The value of σ_0 for manganese phosphide MnP is taken from Guillaud's paper.[1]

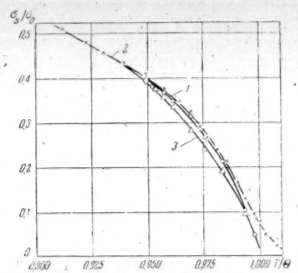

FIG. 3. Spontaneous magnetization as a function of temperature. Curve 1 – from magnetocaloric effect data, 2 – from the data of "line of equal magnetization," 3 – by the method of "thermodynamic coefficients."

The temperature dependence of the spontaneous magnetization can also be determined by working over the data obtained from the magnetization isotherms in the vicinity of the paraprocess. Firstly, the temperature dependence of σ_S may be determined by extrapolating the isotherms of the true magnetization down to zero magnetic field, $H = 0$, and also by the method proposed by Weiss and Forrer, called the method of " line of equal magnetization." The results of analyzing the curve of true magnetization by the "line of equal magnetization" method are given in curve 2 of Fig. 3.

Belov[6-8] has recently used the "method of thermodynamic coefficients" to investigate the temperature dependence of the spontaneous magnetization for a whole series of ferromagnetic alloys and ferrites. This method is based on the analysis of the curves of true magnetization by means of the thermodynamic equation

$$H = a\sigma + b\sigma^3, \qquad (1)$$

where a and b are thermodynamic coefficients. This equation, at a value of $H = 0$, provides an expression for the spontaneous magnetization in the vicinity of a Curie point from the relation $\sigma_S^2 = -a/b$. This method makes it possible to determine the Curie point as well, if we take $a = 0$ at $T = \Theta_f$.

The results of working over the data of measurements of the MnP magnetization by Belov's method are shown in curve 3 of Fig. 3. It is worth noting the rather good coincidence of the curves for σ_S/σ_0, obtained by three different methods. A comparison of these curves indicates that curves 1 and 3, obtained by magnetocaloric-effect measurements and by the method of "thermodynamic coefficients" both drop off sharply to the temperature axis, whereas curve 2 obtained by the method of "line of equal slope" drops off more smoothly. As curve 2 drops off it forms a "tail" of spontaneous magnetization. This "tail" is rather short (on the order of 20) for manganese phosphides. For temperatures higher than 42° C, the magnetization isotherms appear as straight lines.

The Curie temperature determined by the method of "thermodynamic coefficients" is equal to 21.1° C; this corresponds to the value of Curie temperature obtained from the magnetocaloric effect.

It thus becomes evident that the magnetization of manganese phosphide for the para process region near the Curie point is quite satisfactorily described by the thermodynamic relation (1).

The quantity ξ which appears in the well known formula

$$(\sigma_s/\sigma_0)^2 = \xi(1 - T/\Theta).$$

is of considerable importance for an understanding of the character of the magnetic transformation in the vicinity of the Curie temperature.

Vlasov and Vonsovskiĭ have shown, on the basis of the s-d exchange model,[10] that $\xi > 3$ for metallic ferromagnetic substances. For ferrites $\xi < 3$, according to the computation carried out by Vlasov. The results of our measurements given in Fig. 4 lead to a value $\xi = 3.4$, according to the data for the magnetocaloric effect (curve 1), and $\xi = 3.0$ according to the data obtained when using the method of "line of equal magnetization" (curve 2), i.e., the values of ξ are close to those obtained from the "quasi-classical" theory of ferromagnetism. We must therefore conclude that from the paramagnetic standpoint manganese phosphide resembles the metallic ferromagnetic materials more closely than it does the ferrites.

It should be emphasized that in the paramagnetic region, according to the data of reference 11 and from our measurements, the susceptibility follows the Curie-Weiss law and does not have the hyperbolic form characteristic of ferromagnetic substances. This makes it possible to suppose that the manganese phosphide, MnP, is possibly ferromagnetic, and not ferrimagnetic as was proposed by Guillaud.

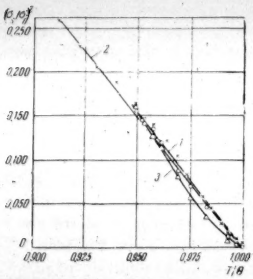

FIG. 4. Square of spontaneous magnetization as a function of temperature. Experimental point designation corresponds to Fig. 3.

The authors express their gratitude to K. B. Vlasov for supplying us with the results of his computations and for valuable discussions, and also to V. N. Novogrudskiĭ for participating in the measurements.

[1] Ch. Guillaud, Compt. rend. **224**, 266 (1947).
[2] Ch. Guillaud, Compt. rend. **235**, 468 (1952).
[3] Ch. Guillaud, Revs. Modern Phys. **25**, 119 (1953).
[4] P. Weiss and R. Forrer, Ann. Phys. **10**, 5, 153 (1926).
[5] H. Potter, Proc. Roy. Soc. **A146**, 362 (1934).
[6] K. P. Belov and A. N. Goriaga, Физика металлов и металловед. (Physics of Metals and Metal Res.) **2**, 3 (1956).
[7] K. P. Belov and A. N. Goryaga, Izv. Akad. Nauk SSSR, Ser. Fiz., **21**, 1038 (1957) [Columbia Tech. Transl. p. 1043].
[8] Belov, Bol'shova, and Elkina, Izv. Akad. Nauk SSSR, Ser. Fiz. **21**, 1047 (1957) [Columbia Tech. Transl. p. 1051].
[9] K. P. Belov and Ya. Pachess, Физика металлов и металловед. (Physics of Metals and Metal Res.) **4**, 48 (1957).
[10] S. V. Vonsovskiĭ and K. B. Vlasov, J. Exptl. Theoret. Phys. (U.S.S.R.) **25**, 327 (1953).
[11] L. Bates, Phil. Mag. **8**, 714 (1929).

Translated by M. E. Zaret
208

INTERACTION BETWEEN $10^{11} - 10^{12}$ ev PARTICLES AND IRON NUCLEI

N. L. GRIGOROV, V. S. MURZIN, and I. D. RAPOPORT

Institute of Nuclear Physics, Moscow State University

Submitted to JETP editor November 4, 1958

J. Exptl. Theoret. Phys. (U.S.S.R.) **36**, 1068-1079 (April, 1959)

The following characteristics of the elementary interaction between $10^{11} - 10^{12}$ ev cosmic ray particles and iron nuclei were studied at elevation 3860 m by means of apparatus which determined the "primary" particle energy: a) the inelastic cross section, b) the degree of inelasticity of the interaction, c) the distribution function of energy transferred to π^0 mesons and certain other properties.

1. INTRODUCTION

AFTER the fundamental work of Powell and his coworkers[1] showed that interactions between cosmic rays and atomic nuclei produce pions, detailed investigations of interactions with high-energy cosmic rays were conducted to determine the meson-producing mechanism, particularly the energy dependence of the processes involved and the nature of the "primary" particles. Some experiments which aimed to select primary particles of specified energies (mainly in the stratosphere) made use of the geomagnetic effect, while other experiments employed cloud chambers placed in a magnetic field. Since the earth's magnetic field has practically no effect on particles with a few tens of billions of electron volts the use of the geomagnetic effect to select primary particles is practically confined to energies below about 20×10^9 ev. A cloud chamber in a magnetic field is only slightly more advantageous. Thus the study of interactions with particles possessing 10^{11} to 10^{12} ev and above requires new methods of measuring primary particle energies.

During recent years extensive use has been made of nuclear emulsions to determine primary particle energies from the emission angles of secondary particles created in nuclear reactions with primary particles. However the degree of reliability of this method has still not been determined and experimental verification of the results requires some independent means of measuring primary particle energies.

In a search for such means we have made use of the fact that strong interactions between nuclei and high-energy nuclear-active particles (the N component) are followed by the absorption of the primary particle and of all its descendants in relatively thin layers of matter of the order 1000 g/cm^2. The energy of a primary particle is ultimately expended for the ionization of atoms in the medium where absorption occurs. Therefore when we measure the total number of ion pairs produced in a layer of the order 1000 g/cm^2 through the absorption of a single primary particle, knowledge of the energy ϵ required to produce a single ion pair makes it easy to determine the energy E_0 of a particle entering the absorber:

$$E_0 = \epsilon \int_0^{x_0} I(x)\,dx, \qquad (1)$$

where $I(x)\,dx$ is the ionization in a layer of thickness dx g/cm^2 at depth x g/cm^2 and x_0 is the total thickness of the absorber.

This technique for determining energies resembles calorimetric measurements and the apparatus that we have accordingly designed for the purpose[2] will be called an "ionization calorimeter." In practice ionization is not measured along a continuous line through the absorber but at discrete levels $x_1, x_2, \ldots, x_n$ under layers of finite thickness. From the ionization $I(x_i)$ measured under layers of thickness x_i we can plot a smooth $I(x)$ curve to be used in (1) for the determination of E_0. It is evident that the accuracy of E_0 will increase with the number of layers. In order to reduce the minimum number of layers in an ionization calorimeter required for satisfactory accuracy of E_0 it is desirable to use an absorbing material in which the mean free path for nuclear interaction and the electron-photon cascade range are of the same order. The thickness of layers between adjacent ionization detectors should be of the order 6 or 8 cascade units.

Special mention must be made of the fact that as the primary particle energy E_0 increases it

is determined more accurately by an ionization calorimeter. This results from the fact that with increasing E_0 a relatively smaller fraction of the energy is transferred to strongly ionizing products of nuclear disintegrations, whose energy is measured with small efficiency by our apparatus. We estimate the accuracy of E_0 at about 30% in the vicinity of 10^{11} ev.

It is evident that the ionization calorimeter, which is of relatively simple construction, can easily be combined with other techniques for observing particles. For example, in a cloud chamber placed above an ionization calorimeter we can observe the elementary interaction of a particle of known energy and study various properties of this interaction (dependence on the atomic weight of the nucleus and primary particle energy) at $\sim 10^{11}$ or 10^{12} ev. In a magnetic field the cloud chamber also permits analysis of secondary particles.

At the time when we raised an ionization calorimeter to an elevation of 3860 m an auxiliary large cloud chamber was still not ready. Therefore our published data pertain only to processes which can be studied with only a single ionization calorimeter. It will be seen that an investigation of the dynamics of electron-nuclear cascades in dense matter (by using a large number of detectors which register ionization independently of each other) not only provides a reliable primary particle energy measurement in each individual instance but also enables us to investigate such properties of an elementary event as a) the degree of elasticity of the interaction between the primary particle and absorber nuclei in the ionization calorimeter, b) the degree of inelasticity of secondary-particle interactions, c) the secondary-particle energy spectrum, d) the distribution of the energy fraction which is transferred to π^0 mesons in a primary-particle interaction, e) the cross section for inelastic interactions between primary particles and absorber nuclei and its dependence on the primary particle energy.

2. APPARATUS

The ionization calorimeter used in our experiments was a large assembly of seven layers of iron alternating with six rows of pulse ionization chambers (Fig. 1, I-VI). A more detailed description has been given in reference 2. A single ionization detector was formed by connecting three chambers in parallel. Each detector was connected to an amplifier with a dynamic range of 800, and was sensitive enough for the reliable

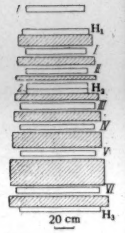

FIG. 1. Schematic cross section of setup. I – VI) rows of ionization chambers; 1, 2) rows of telescopic counters; $H_1 - H_3$) boxes with hodoscopic counters.

registration of 5 to 10 relativistic particles passing through it simultaneously. Signals from the amplifiers were fed to oscilloscopes mounted in a separate assembly, the construction and operation of which have been described in reference 3. Also, signals from the amplifiers were fed to a sum circuit which combined all pulses from a single row of ionization chambers. Pulses were recorded by photographing the oscilloscope screens at the instant when all oscilloscope beams were triggered by a master signal. Altogether 105 ionization chambers were used, forming 35 independent detectors. The total thickness of iron between rows of ionization chambers was 650 g/cm^2 and the total thickness of the iron assembly was 750 g/cm^2.

In addition to the ionization chambers the apparatus included three boxes of gas-discharge tubes which served as hodoscopic counters (H_1, H_2, H_3). Each box contained two rows of counters, the axes of counters in one row being perpendicular to the axes in the other row. The hodoscopic counters were glass tubes 70 to 90 cm long, 2 cm in diameter with an Aquadag anode and filament of 100 μ diameter. These counters were filled with pure argon to ~ 100 mm Hg and were subjected to a voltage pulse of 2×10^{-5} sec duration at the instant when coincident discharges occurred in the two boxes of telescopic counters (1 and 2). The hodoscopic counters were connected to MTX-90 neon bulbs, which were photographed independently.

The hodoscopic counters enabled us to determine the air-shower accompaniment of high-energy nuclear-active particles (box H_1), and the direction of the electron-nuclear cascade core within the ionization calorimeter absorbing material in a plane parallel to the chamber axes (boxes H_2 and H_3).

Two rows of telescopic counters (1 and 2) served mainly to produce a master signal with the minimum delay required for control of the hodoscopic counters (when the pulse to the gas-

discharge tubes was delayed by not more than 2×10^{-6} sec they exhibited 94% efficiency in the recording of charged particles). The neon bulbs of the hodoscope were photographed only at the instants when a high-energy particle struck the ionization calorimeter; the pulse which triggered the oscilloscope beams simultaneously applied a voltage to the anodes of the neon bulbs, in the hodoscope.

The master signal was produced as follows. All simultaneous ionization pulses from each row of ionization chambers were summed, as has already been mentioned. The resultant signal was fed to a selector, which was triggered when a few rows of ionization chambers simultaneously produced resultant signals above a predetermined threshold V_{thr}. A master pulse resulted from simultaneous triggering of the selector and discharges in both rows of telescopic counters. Our data were obtained through the simultaneous triggering of any two or more rows of chambers, in which case V_{thr} was equivalent to 250 relativistic particles traversing the mean chords of the chambers.

The requirement of simultaneous ionization > V_{thr} in two rows of chambers considerably reduced the number of events resulting from low-energy nuclear disintegrations, and a sufficiently high value of V_{thr} insured the registration of nuclear-active particles with energies of about 10^{11} ev and higher.

3. TREATMENT OF RESULTS

Pulses from the ionization chambers were fed to a multi-channel oscilloscope and were photographed on motion picture film which also recorded the electronic calibration of all amplifying channels. The first step in the treatment of these data was the measurement of ionization-chamber pulse heights and the determination of the ionization produced in each chamber. The ionization was converted to the number of relativistic particles passing through the chambers whenever required. The results were used to plot a diagram showing the distribution of ionization along a row of chambers and the absorber depth for each separate case. Typical diagrams are shown in Fig. 2. These diagrams were used to determine the angle of incidence of the primary particles.

A picture of the triggered hodoscopic counters was obtained at the same time. This could be done in two projections to determine the shower inclination in a projection along the ionization chamber axes. These diagrams helped to determine whether a significant fraction of shower energy passed through the side walls of the ionization calorimeter.

4. RESULTS

The majority of events registered by our selection scheme were induced by nuclear-active particles from the atmosphere, but our apparatus also efficiently registered electrons and photons (the latter accompanied by charged particles) as well as air showers and muon bursts.

In the present paper we analyze 110 instances in which more than 250 relativistic particles passed through any two rows of ionization chambers. A division was made into a few groups depending on the character of the observed events. The ionization was sometimes distributed more or less uniformly along the first two or more rows, falling off rapidly with depth; these instances were interpreted as air showers, of which 17 were recorded. In a number of instances the ionization in the chambers revealed a distinct core, with the ionization versus depth curve in good agreement with electromagnetic cascade theory.[4] When such an event took place at the edge of our absorber (shown by large ionization in the first row) there was strong reason to attribute it to an electron or

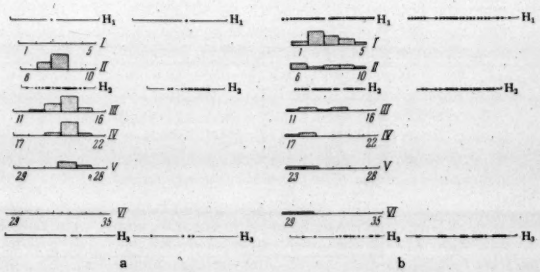

FIG. 2. Distribution of ionization in the ionization calorimeter for a – incident nuclear-active particle, b – air shower. The positions of rows of ionization chambers are indicated by the numerals I – VI. The numerals 1 – 35 denote individual ionization detectors. The heights of the rectangles represent the ionization recorded by these detectors, in relative units. The dots show the arrangement of triggered hodoscopic counters.

photon. A shower originating within the absorber suggests production through muon bremsstrahlung (in the case of two showers).

It should be noted that whenever the interaction of a nuclear-active particle with a nucleus resulted in the entire energy being transferred to π^0 mesons the event was attributed to an electron or a muon depending on the point of origin. This might somewhat reduce the mean energy losses that we determined for pion production. All other observed events showed a distinct core (Fig. 2a) and varying shapes of the ionization versus depth curves, all of which were considerably broader than electron-photon cascade curves and often showed secondary maxima within the absorber or slow falling-off of ionization with depth.

These curves are evidence of secondary interactions in the apparatus and of additional energy transfer to the electron-photon component under considerable depths of matter. We classified such events as nuclear interactions with primary particles and selected them for analysis.

In most instances a comparison of ionization hodoscope and counter data enabled us to determine whether the shower core passed through the side of the apparatus; such showers were excluded from the data. Thirty-two showers were selected with cores within the solid angle of the ionization hodoscope (see the table). These were distributed as follows: Four showers possessed a "structure," with two cores separated by 25 to 40 cm. In the three cases when the energy of both particles could be determined the energy ratios were 1:2, 1:5 and 2:3. Ten nuclear-active particles had energy $\geq 10^{12}$ ev and 22 were between 10^{11} and 10^{12} ev.

No.	Particle energy, 10^{11} ev	Angle to vertical, deg	Point of first interaction, g/cm²	Number of particles in first maximum	Number of particles in second maximum	Number of particles accompanying electron*	Remarks
1	10.0	23	<50	2300	>1200	≥11	
2	>1.0	<10	~0	270	—	≥15	Structured shower; a single particle is analysed
3	1.5	19	~0	430	—	11	
4	1.4	?	~0	580	330	6	
5	1.7	≥17	~0	~300	420	≥20	
6	4.8	22	50	1550	—	≥25	Energy of accompanying particles** ~4.5×10^{10} ev
7	4.0	15	<50	40	230	3	
8	7.8	14	<50	1470	1000	8	
9	4.0	~15	30	1250	—	—	
10	16.0	10	50	31.0	~1500	11	
11	3.0	23	100—200	490	~300	~20	Energy of accompanying particles** ~9×10^{10} ev
12	2.5	20	50	340	440	—	
13	3.0	<10	100	880	—	—	
14	0.7	24	~0	360	—	~20	Structured shower; a third maximum exists with $n_s = 50$
	0.5	24	100	220	275		
15	9.7	20	300	1550	—	—	
16	3.5	22	<50	200	1500	—	
17	3.5	0	~0	3200	1150	>25	Structured shower
	15.0	0	50	970	—		
18	5.2	25	0	1280	~500	10	
19	3.4	<10	<50	910	—	~30	Energy of accompanying particles** ~ 10^{10} ev
20	13.0	20	150	5300	370	~30	Energy of accompanying particles** > 10^9 ev
21	4.0	<10	80	1200	200	?	Energy of accompanying particles** > 10^9 ev
22	11.0	0	50	2340	960	?	
23	2.4	0	<50	460	370	?	
24	25.0	0	0	6000	—	?	
25	10.0	15	<50	1850	—	5	
26	3.2	0	100—200	850—1300	—	6	
27	15.0	12	50—100	4000	1300	15	
28	22.5	<10	50—100	7600	—	>30	Structured showers
	46.0	<10	≤50	18000	—		
29	1.6	18	150	400	450—600	1	
30	2.5±0.2	13	180	430	~400	—	
31	2.0	25	0	220	365	1	
32	10.0	10	125	3500	—	~15	Energy of accompanying particles** ~ 2×10^9 ev

*The number of accompanying particles is given without the generating particle.

**The energy of the accompanying particles was estimated by means of data from the first row of ionization chambers.

In six cases there were no accompanying charged particles; in one of these cases the energy was about 10^{12} ev.

5. DISCUSSION OF RESULTS

An analysis of the results collected in the table and of the nuclear-cascade curves (of which examples are given in Fig. 3) leads to a number of conclusions concerning the properties, and interactions with matter, of nuclear-active particles with $10^{10}-10^{12}$ ev.

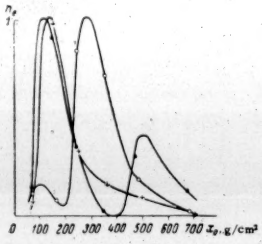

FIG. 3. Examples of nuclear-cascade curves. The vertical axis gives the number of electrons in arbitrary units (normalized to the maximum); the horizontal axis represents absorber thickness. + – nuclear-cascade curve in first group, • and o – nuclear-cascade curves in second group.

1. Interaction Cross Section

Until recently the cross section for interactions between high-energy particles and nuclei could not be measured because of the low intensity of cosmic-ray particles with $\geq 10^{11}$ ev as well as methodological difficulties. The greatest progress was made by Williams, who measured the cross section for the interaction between iron and ~ 50-Bev nucleons.[5]

Our apparatus can determine the cross section for interactions between nuclei and nuclear-active particles above $5 \times 10^{10}-10^{11}$ ev. We can record any nuclear interaction in which more than 3 – 5% of the primary-particle energy is transferred to the soft component (at $\sim 10^{11}$ ev).

We determined the interaction mean free path of nuclear-active particles (principally nucleons) in iron, observing the distribution of cascade origins as a function of absorber thickness. The number of interactions occurring below a layer of thickness x is given by

$$N = N_0 \exp(-x/L),$$

where L is the interaction mean free path. Figure 4 is a semi-logarithmic plot of the number of interactions occurring below x thickness as a function of x.

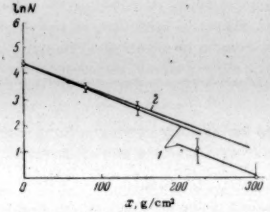

FIG. 4. Number of interactions occurring below thickness x of iron absorber as a function of x: 1 – direct experimental data without corrections, 2 – after corrections for neutrons.

The experimental results require some comment. The placing of telescopic counters under a thick layer of matter introduces discrimination into the observed events. As already mentioned, ~ 80% of all nuclear-active particles are accompanied by soft electrons as they enter the apparatus. These electrons trigger the first row of telescopic counters. Therefore our apparatus will also register neutrons which have undergone interactions above the second row of telescopic counters. The second row of counters is not triggered when neutrons interact with nuclei below it (since the soft-electron accompaniment is absorbed in the iron) and the event is not registered. Figure 3 gives the experimental data and the results of a correction for uncounted neutrons in the lower layers. This correction was based on the hypothesis that the discontinuity of the experimental straight line 1 in Fig. 4 for $x \geq 200$ g/cm² resulted from the omission of primary neutrons.

For the purpose of increasing the statistical information needed to determine the cross section we also used interactions of particles with from 7×10^{10} to 3×10^{11} ev which were registered above a lower threshold (47 events). The mean free path was determined using the only nuclear interactions whose core was included in the solid angle of the apparatus. These data yielded the interaction mean free path $L = 92^{+20}_{-12}$ g/cm², which is close to the value corresponding to the geometric nuclear cross section $r_0 = 1.4 \times 10^{-13}$ cm ($L_{geom} = 105$ g/cm²). The interaction mean free path can sometimes be reduced when two nuclear-active particles simultaneously impinge on the apparatus close enough to form a single common core. In such cases the shower will be regarded as originating at the point where one of the particles first experiences a collision and the mean free path will be reduced. Improved statistics will hereafter make it possible to select single particles striking the apparatus unaccompanied by showers, thus ex-

cluding the possibility of reducing the mean free path in this manner. However, at $10^{11} - 10^{12}$ ev we have no reason to expect the frequent appearance of very close pairs of nuclear-active particles.

2. Average Inelasticity of Interactions Between $10^{11} - 10^{12}$ ev Particles and Iron Nuclei

The experimental results can be used to determine the average inelasticity $\bar{\alpha}$ of interaction between nuclear-active particles and iron nuclei. $\bar{\alpha}$ can be evaluated by analyzing the average curve of the ionization $\bar{I}(x)$ produced in iron by a particle with given energy E_0. It will be seen that the average curve is based on only the mean properties of the interaction: $\bar{\alpha}$ — the mean fraction of its energy which is lost by a primary nucleon in a single pion-producing interaction, and β/L_π, where $\bar{\beta}$ is the mean fraction of the energy lost by a pion in a single interaction which produces the electron-photon component and L_π is the interaction mean free path of pions (or more precisely, of all secondary particles differing in nature from the primary particles).

We have calculated the nuclear-cascade curves for different values of the inelasticity $\bar{\alpha}$, obtaining our result for $\bar{\alpha}$ by comparing the average experimental curve with the family of calculated curves.

Our apparatus registered electrons resulting from the development of an electron-photon cascade produced by gamma quanta from π^0-meson decay. If the number of quanta with energy from ϵ to $\epsilon + d\epsilon$ resulting from π^0 decay in a layer dx is $n_\gamma(\epsilon, x)\,d\epsilon\,dx/L$, the number of electrons at depth x_0 is given by

$$dn_e = \int_0^{E_0} F(\varepsilon, x_0 - x)\, n_\gamma(\varepsilon, x)\, d\varepsilon dx / L, \qquad (2)$$

where $F(\epsilon, x_0 - x)$ is the cascade curve for a photon with energy ϵ. Since $F(\epsilon, x_0 - x)/\epsilon$ depends very slightly (logarithmically) on ϵ, we obtain

$$dn_e = \frac{dx}{L}[F(\bar{\varepsilon}, x_0 - x)/\bar{\varepsilon}] \int_0^{E_0} \varepsilon n_\gamma(\varepsilon, x)\, d\varepsilon.$$

But $\int_0^{E_0} \epsilon n_\gamma(\epsilon, x)\, d\epsilon$ is the total energy of quanta liberated in a layer dx at depth x and is equal to the combined energy E_{π^0} of π^0 mesons produced in this layer. This total energy is

$$E_{\pi^0}(x)\,dx/L = [S_n(x)\,\bar{\alpha}_{\pi^0}/L + S_\pi(x)\bar{\beta}/L_\pi]\,dx,$$

where $S_n(x)$ and $S_\pi(x)$ are the energy flux of the nucleon and pion components at depth x; α_{π^0} and $\bar{\beta}$ are the corresponding mean energy fractions transferred by π^0 mesons to nucleons and charged mesons; L_π is the meson interaction mean free path. The Total number of electrons which can be observed at depth x_0 is given by

$$n_e(x_0) = \int_0^{x_0} E_{\pi^0}(x)\,[F(\bar{\varepsilon}, x_0 - x)/\bar{\varepsilon}]\,\frac{dx}{L}. \qquad (3)$$

We must now calculate the variation with depth of the energy flux of nuclear-active particles. The thickness of the absorber is reckoned from the point where the primary particle undergoes an interaction. Using the notation $\bar{\alpha}_{\pi^0} = \bar{\alpha}/3$, we can write the following equations for the variation with depth of the energy flux (assuming that π^0 mesons receive $\frac{1}{3}$ of the energy transferred to all π mesons):

$$dS_n = -\bar{\alpha}S_n dx/L;\quad dS_\pi = \left(\frac{2}{3}\bar{\alpha}S_n/L - \bar{\beta}S_\pi/L_\pi\right)dx.$$

These equations are solved subject to the boundary conditions (at $x = 0$)

$$S_n = (1 - \bar{\alpha})E_0;\quad S_{\pi^+} = 2\bar{\alpha}E_0/3;\quad S_{\pi^0} = \bar{\alpha}E_0/3.$$

The results are

$$S_n(x) = (1 - \bar{\alpha})E_0 \exp(-\bar{\alpha}x/L).$$

$$S_\pi(x) = \frac{\frac{2}{3}\bar{\alpha}E_0}{3\left(\bar{\alpha}/L - \bar{\beta}/L_\pi\right)} \times \left\{\left(\frac{1}{L} - \frac{\bar{\beta}}{L_\pi}\right)\exp\left(-\frac{\bar{\beta}x}{L_\pi}\right) - \frac{1-\bar{\alpha}}{L}\exp\left(-\frac{\bar{\alpha}x}{L}\right)\right\}. \qquad (4)$$

After substituting these expressions in (3) and performing a numerical integration we obtain the number of electrons $n_e(x_0)$ at different absorber levels. The following circumstances must be kept in mind in connection with the integration:

1. $F(t, \bar{\epsilon})/\bar{\epsilon}$ depends very slightly (logarithmically) on $\bar{\epsilon}$. We have therefore neglected the variation with depth of the mean gamma quantum. As the cascade curve we used the curve for photons with $\epsilon = 4.5 \times 10^9$ ev which was obtained in reference 4.

2. β/L_π can be determined experimentally. A computation shows that the average curve $\bar{I}(x) \sim \bar{n}_e(x)$ depends only on the average properties of $\bar{\alpha}$ and $\bar{\beta}/L$. $\bar{\beta}/L$ can be determined from the experimental curve

$$\bar{\beta}/L_\pi = -\,d\bar{I}(x)/\bar{I}(x)\,dx \quad \text{for } x \gg L.$$

Assuming $\bar{\beta}/L = \frac{1}{3}L$, which is our experimental result, we are left with only one unknown parameter, which can be determined by comparing the average curve with the calculations.

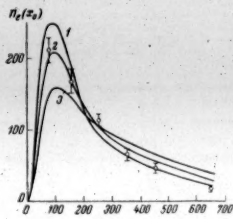

FIG. 5. Comparison of experimental results with the computed average nuclear-cascade curve: 1) $\bar{\alpha} = 1.0$, 2) $\bar{\alpha} = 0.75$, 3) $\bar{\alpha} = 0.5$

Figure 5 represents the calculations for different energy fractions transferred to pions. The experimental data shown here were converted to values for $E_0 = 10^{11}$ ev, which was used in the calulations.

To determine the average experimental curve, which our apparatus would give automatically if all interactions began at the same depth and pertained to the same primary particle energy, we proceeded as follows. All nuclear-cascade curves for $E_0 \geq 10^{11}$ ev were areally normalized to the same energy $E_0 = 10^{11}$ ev. (This reflects the assumption that the shape of the average nuclear-cascade curve is independent of E_0, at least in the range $10^{11} - 10^{12}$ ev.) Following the normalization the starting points of all experimental curves were superposed and the ordinates were added. The resulting average curve $n_e(x)$ corresponds to the assumptions used in the calculation.

The experimental result is in best agreement with an energy fraction $\bar{\alpha}$ from 0.75 to 1 and, apparently, $\bar{\alpha} > 0.5$. The inadequate statistical accuracy of our results prevents greater certainty. Under great thicknesses of matter an appreciable fraction of the energy may possibly be expended for the production of strongly ionizing particles which are not registered by our apparatus. In that event the averaged experimental curve at great depths will be steeper, thus simulating an increase of the energy loss fraction.

Some investigators[6] have noted the interesting fact that interactions between high-energy nucleons ($\sim 10^{10}$ ev and higher) and light nuclei are accompanied by low fractional energy losses. We have found that at $E_0 > 10^{11}$ ev interactions with iron nuclei are accompanied by a high degree of inelasticity. We expect that in the near future our apparatus will supply us with direct data on the relation between the inelasticity and the atomic weight of the target nucleus.

6. FLUCTUATIONS OF THE ENERGY TRANSFERRED TO π^0 MESONS

Our technique enables us in principle to determine the fraction of energy α_{π^0} transferred to π^0 mesons by nucleons in each individual collision of a nucleon with a nucleus, and thus to study the fluctuations in the transfer of energy to π^0 mesons.

In determining α_{π^0} we assumed that the principal contribution to ionization in the first few rows of ionization chambers comes from electrons arising from π^0 mesons produced in the first event. By measuring the area under the initial part of the ionization curve (which is most instances resembles the electron-photon cascade curve) we can calculate the energy transferred to π^0 mesons in the first event. At the same time we must take into account the fraction of electrons resulting from secondary nuclear interactions in the first few layers.

In the case of the first group of nuclear-cascade curves (Fig. 3) the ionization contribution of secondary interactions can be calculated quite accurately since these interactions are entirely responsible for the gradually descending part of each curve. This part can be extrapolated to the point of the first interaction by using the calculation in the preceeding section, thus giving the contribution of secondary nuclear collisions.

In determining α_{π^0} for curves of the second group difficulties arise when the second maximum is close to the first. In such cases the contribution of secondary interactions in each individual event was taken to be the average for this group; this occurred in $\frac{1}{3}$ of all instances. α_{π^0} could be determined more reliably when the maxima were sufficiently separated. Figure 6 shows the distribution of values of α_{π^0} in 29 interactions which were obtained by the described procedure. From this histogram it appears that the average energy transferred to π^0 mesons is $\sim 0.4 \pm 0.1$ of the primary particle energy, which is close to the most probable value of α_{π^0}. The distribution may be distorted because some of the maxima of the secondary and primary interactions are unresolved. This increases the fraction of the area

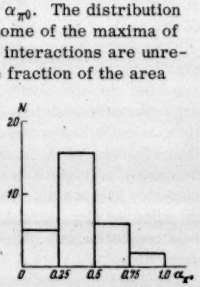

FIG. 6. Fraction of primary-particle energy transferred to π^0 mesons. N represents the number of events.

under the initial part of the nuclear-cascade curve and raises the value of α_{π^0}. Therefore the distribution shown in Fig. 6 is the distribution of fluctuations in the transfer of energy to π^0 mesons on a segment of the particle track which is $\sim 1/3$ to $1/2$ of the nuclear-component range. This distribution apparently does not differ strongly from that of α_{π^0} in a single event. The difference consists in an increased number of events with large energy loss (due to the aforementioned effect) and a small reduction of the number with low energy loss ($\alpha_{\pi^0} < 6.25$). The latter reduction results from the fact that some events with low energy loss may occur close to secondary interactions with large energy transfer which mask the former events. The corresponding correction is easily estimated to be not more than 5% of all instances (30% of all transfers of small amounts of energy).

7. ABSORPTION OF ENERGY FLUX OF NUCLEAR-ACTIVE PARTICLES UNDER GREAT THICKNESSES OF IRON

The ionization produced by the entire spectrum of primary nuclear-active particles at depth x_0 can be represented by

$$I(x_0) \sim \int_0^{x_0} \frac{dx}{L} \exp(-x/L)\, n_e(x_0 - x,\ E_0) \frac{dN}{dE_0},$$

where $n_e(x_0 - x)$ is given by (3). Since the range of the electron-photon component is smaller than that of the nuclear-active component the two components will be in equilibrium at great depths. The number of electrons $n_e(x)$ is proportional to the energy transferred to pions in one gram of absorber material, so that when the soft component is in equilibrium with the nuclear component the variation, with depth x, of the soft-component intensity will be determined only by the variation with depth of the energy E_{π^0} transferred to π^0 mesons in one gram of absorber, i.e., in the long run, the variation with depth x of the energy flux of the nuclear component.

The ionization produced in our apparatus principally by electrons will therefore vary under large absorber thickness with the same range as the energy flux of the nuclear-active component. In sections 5 and 6 it was shown that nucleons lose a large fraction of their energy through meson production in a single event. This means that the nucleons are rapidly absorbed and that under large thicknesses of matter the nuclear-active component will consist mainly of mesons, in which case we can determine β/L_π.

To determine the experimental curve of $I(x_0)$ we added all nuclear-cascade curves, which had previously been reduced to the same energy through areal normalization. (This normalization led to the equating of statistical weights of the different events.) The resulting curve of $I(x_0)$ is shown in Fig. 7.

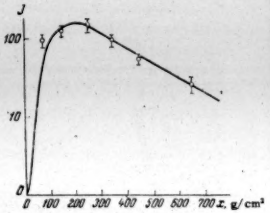

FIG. 7. Ionization I produced at different depths x of an iron absorber by nuclear-active particles with energy $E_0 > 10^{11}$ ev.

The curve is characterized by very slow reduction of the energy flux of the nuclear-active component with depth. This reduction can be described by the absorption mean free path $L_{abs} = 240$ g/cm^2 if we neglect corrections for neutron-induced showers (at depths > 200 g/cm^2). Corrections increase the absorption mean free path to 270 g/cm^2, so that the absorption mean free path of the energy flux is about three times the nucleon interaction mean free path.

The given result is easily accounted for by the hypothesis that deep within the absorber most of the energy is concentrated in high-energy pions which in each nuclear-interaction mean free path transfer $1/3$ of their energy to π^0 mesons. The absorption mean free path is then given by L_{abs}, which is equal to $3L_{int}$ according to our experiments.

The results were obtained with the assistance of V. S. Kaftanov and graduate students Yu. G. El'kin and V. I. Lobodenko, whom the authors wish to thank.

[1] Brown, Camerini, Fowler, Heitler, King, and Powell, Phil. Mag. **40**, 862 (1949).

[2] Grigorov, Murzin, and Rapoport, J. Exptl. Theoret. Phys. (U.S.S.R.) **34**, 506 (1958), Soviet Phys. JETP **7**, 348 (1958).

[3] Grigorov, Murzin, Rapoport, and Savin, Приборы и техника эксперимента (Instruments and Measurement Engg.) No. 6, 109 (1958).

[4] I. P. Ivanenko and B. E. Samosudov, J. Exptl. Theoret. Phys. (U.S.S.R.) **35**, 1265 (1958), Soviet Phys. JETP **8**, 884 (1959).

[5] A. E. Brenner and R. Williams, Phys. Rev. **106**, 1020 (1957).

[6] Vernov, Grigorov, Zatsepin and Chudakov, Izv. Akad. Nauk SSSR Ser. Fiz. **19**, 493 (1955) (Columbia Tech. Transl. p. 445).

Translated by I. Emin
209

OBSERVATION OF THE $\pi^0 \to e^- + e^+ + e^- + e^+$ *DECAY*

Yu. A. BUDAGOV, S. VIKTOR, V. P. DZHELEPOV, P. F. ERMOLOV, and V. I. MOSKALEV

Joint Institute for Nuclear Research

Submitted to JETP editor December 25, 1958

J. Exptl. Theoret. Phys. (U.S.S.R.) **36**, 1080-1084 (April, 1959)

An event of charge-exchange scattering, $\pi^- + p \to \pi^0 + n$, with subsequent decay, $\pi^0 \to e^- + e^+ + e^- + e^+$, was detected on a photograph taken in a hydrogen diffusion chamber located in a magnetic field and bombarded with 160-Mev π^- mesons. One decay of this type was detected per 2500 π^0-meson decays of the usual $\pi^0 \to 2\gamma$ type. The π^0-meson mass is estimated as 141 ± 8 Mev. In the rest system of the π^0 meson, the angle between the electrons and positrons of the pairs are 7° and 12°, and the angle between the planes of the pair does not exceed 37°. Other possible explanations of the observed event seem to be very improbable.

INTRODUCTION

It is known that in addition to decaying in the usual manner

$$\pi^0 \to 2\gamma \qquad (1)$$

approximately one out of 80 π^0 mesons decays by the scheme proposed by Dalitz[1]

$$\pi^0 \to e^- + e^+ + \gamma. \qquad (2)$$

Such a decay can be interpreted as the internal conversion of one of the γ quanta in the field of the other γ quantum. Another possible process is double internal conversion of the gamma quanta, leading to the decay of the π^0 meson into two electron-positron pairs:

$$\pi^0 \to e^- + e^+ + e^- + e^+. \qquad (3)$$

Kroll and Wada[2] theoretically estimated the probability of decay (3), relative to the usual decay (1), to be 3.47×10^{-5} (if the π^0-meson spin is zero). All particles produced when the π^0-meson decays according to (3) are charged, and are thus readily recorded by diffusion or bubble chambers. The observation of such decays in a chamber can therefore yield much important information on the properties of the π^0 meson. Thus, by measuring the momenta of all four particles (by measuring the radii of curvature in a magnetic field), we can determine the mass of the π^0 meson, while the spin and parity of the π^0 meson can be found by direct experiment from a study of the angular correlation between the planes of both pairs. However, in view of the exceedingly low probability, a systematic experimental investigation of process (3) involves certain difficulties. We know of only one description of such a decay in the literature. Hodson, Ballam, Arnold, et al.,[4] in a study of the production of heavy unstable particles in cosmic rays (by means of a controllable cloud chamber), discovered an event, the kinematics of which agrees with the decay $K^+ \to \pi^+(\mu^+) + \pi^0 + Q$, $\pi^0 \to e^- + e^+ + e^- + e^+$. Since only sixty $V^\pm$ decays were recorded in this investigation, and furthermore since π^0 mesons were produced only in some of these events, the probability of observing a decay of type (3) was very small. The authors themselves remark that the appearance of a decay of type (3) under the conditions of their experiment, in which not one event of the more probable decay (2) was observed, is an unusual statistical fluctuation. The angles between the electrons and positrons of the pairs, in the event described in reference 4, were so small (0.5 and 1.7 deg in the laboratory system), that the angle between the planes of the pairs could not be determined.

We describe in this article an event of charge-exchange scattering, $\pi^- + p \to \pi^0 + n$, with subsequent decay $\pi^0 \to e^- + e^+ + e^- + e^+$, registered in a diffusion chamber (Fig. 1).

CONDITIONS OF THE EXPERIMENT

A photograph of the decay described was obtained in an investigation of the scattering of π^- mesons by protons, using a diffusion chamber filled with hydrogen at a pressure up to 25 atmos.[5] The inside diameter of the chamber was 380 mm, and the height of the sensitive volume was 6 to 7 cm, at a temperature gradient of 7 deg/cm. The chamber was placed in a 9000-gauss dc magnetic field, uniform to within ±3.5% over the height of the sensitive volume and to within ±2.5% over the

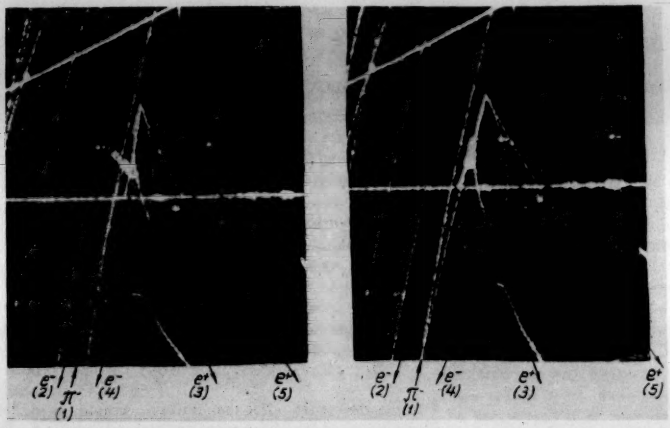

FIG. 1. Stereophotograph of an event of charge-exchange scattering $n^- + p \to \pi^0 + n$ with subsequent decay $\pi^0 \to e^- + e^+ + e^- + e^+$, obtained with the aid of a hydrogen diffusion chamber.

radius. The topography of the magnetic field was plotted with a magnetometer operating on the Hall-effect principle and calibrated by the proton-resonance method.* The photographs were taken with a stereo camera with two GOI (State Optical Institute) "Gelios-37" lenses of 62 mm focal length, on Pankhrom-Kh 35-mm film of speed 1000 GOST units. The "Gelios-37" objectives were corrected for the distortion arising when photographing through the 25-mm thick glass upper windows of the chamber; their resolution at the center of the field of view was 50 lines/mm. The base of the stero camera was 120 mm long, and the taking distance was approximately 1 m.

The camera was exposed in a beam of π^- mesons with an average energy of 160 Mev, obtained from the synchrocyclotron of the Joint Institute for Nuclear Research. The beam intensity was maintained such as to produce on each photograph an average of 30 to 40 π^--meson tracks. Approximately 90,000 stereo-photographs were obtained in the series of exposures. The scanning of these photographs disclosed the aforementioned case of $\pi^- + p \to \pi^0 + n$, $\pi^0 \to e^- + e^+ + e^- + e^+$, along with 1400 cases of elastic scattering of π^- mesons by protons and 26 cases of charge-exchange scattering with subsequent decay $\pi^0 \to e^- + e^+ + \gamma$. In a previous communication[6] we reported the results of processing 14 $\pi^0 \to e^- + e^+ + \gamma$ decay events.

PROCESSING AND RESULTS

As can be seen from Fig. 1, which is a stereo photograph of the analyzed case, the track (1) of one of the π^- mesons, passing through the chamber, stops inside the sensitive volume and four particles, with ionization close to minimum, are emitted into the rear hemisphere. Two of these (3, 5) are positively charged, and the other two (2,4) are negative.

We processed this case by the re-projection method. The construction and principal characteristics of the re-projector are analogous to those described in reference 7. The following were measured directly on the re-projector: 1) the radii of curvature of all five tracks, 2) the angles α between the incident π^- meson and each decay particle, 3) the azimuth angles β of each decay particle; 4) the depth angles γ, i.e., the angles between the direction of particle motion and the horizontal plane. Figure 2 shows schematically the angles α, β, and γ for one decay particle.

The radii of curvature of the tracks were measured with templates as well as by the coordinate method, using the UIM-22 microscope. Both methods yielded the same results, within the limit of errors. The accuracy of measure-

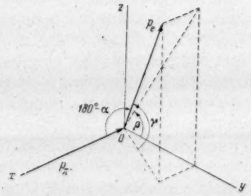

FIG. 2

*We are grateful to D. P. Vasilevskaya and Yu. N. Denisov for allowing us the use of this instrument.

ment of the radius of curvature of each track depends on the value of the curvature and on the length and direction of the track in space. The particle momenta, determined from the measured radii and depth angles γ, were corrected for the inhomogeneity of the magnetic field ($\sim 2\%$) and shrinkage of the film ($\sim 1\%$). In the coordinate method, corrections necessitated by the distortion of the optical system and by the fact that the image on the film is a conical projection of the actual track, were disregarded as small. Estimates have shown that the measurement results are practically unaffected by multiple scattering of particles by the gas in the chamber or by bremsstrahlung.

TABLE I

No. of track; particle	Radius of curvature, cm	Momentum, Mev/c
1, π^-	105±5	272±16
2, e^-	20±4	72±18
3, e^+	3.75±0.15	13.9±0.7
4, e^-	4.2±0.1	15.8±0.5
5, e^+	29±3	100±13

Table I lists the values of the radius of curvature, averaged over measurements made by the re-projection and coordinate methods on two frames of a stereo pair; the corresponding particle momentum is also listed. The errors given for the radii are the maximum measurements errors. Total errors, which reflect both the inaccuracies in the measurements of the radii of curvature and depth angles, and the indeterminacies connected with the introduced corrections, are given for the momenta.

The ionization density produced by the particles in the chamber was estimated visually; it did not exceed $1\frac{1}{2}$ times minimum for all particles. Comparison of the obtained particle momenta with their ionization shows that all decay particles are electrons.

Table II gives the measured values of the angles α, β, and γ. The accuracy in the angle measurements is ±1%. The corrections necessitated by film shrinkage are negligibly small.

From the measured electron momenta and angles α and β, it is easy to calculate the direction and magnitude of the total momentum of all four electrons, $P_t = 147 \pm 26$ Mev/c; $\alpha = 153 \pm 2$ deg, and the total energy of all electrons is 202 ± 32 Mev. It follows from the kinematics of the process $\pi^- + p \rightarrow \pi^0 + n$ at a π^--meson kinetic energy of 166 ± 14 Mev (corresponding to a measured π^--meson momentum of 272 ± 16 Mev/c), that the π^0 meson emitted at an angle of 153 ± 2 deg should have a momentum of 163 ± 7 Mev/c and a total energy of 212 ± 6 Mev. Kinematically therefore, the four electrons are equivalent to the neutral pion from the reaction $\pi^- + p \rightarrow \pi^0 + n$, emitted at an angle 153 ± 2 deg.

TABLE II

No. of track; particle	α, deg	β, deg	γ, deg
2, e^-	138	84	42
3, e^+	138	94	42
4, e^-	127	—56	—41
5, e^+	128	—48	—36

The relatively large errors in the values of the total energy and total momentum of the four electrons permits only a rough estimate of the neutral-pion mass. However, taking into account certain kinematic relations between the neutral-pion mass and the measured values of momenta and angles, one can obtain a better value for the π^0-meson mass, namely 141 ± 8 Mev. Within the limit of measurement errors, this is in agreement with the presently accepted mass value, 135 Mev.

Table III gives the angles between the particles and the planes of the pairs, calculated in the laboratory system and in the rest system of the π^0 meson; the electron momenta in the rest system of the π^0 meson are also given. To calculate these quantities, we assumed accuracy limits for the particle-momentum measurements, within the limits indicated in Table I, to correspond kinematically to a π^0-meson mass of 135 Mev.

In the reference system where the π^0 meson is at rest, the decay particles form two electron-positron pairs with small angles between the electrons and positrons (Table III) and with equal and opposite momenta; the momentum projections on the coordinate axes are balanced to a high degree of accuracy. (In principle, it is possible to con-

TABLE III

Number of track; particle	Laboratory system		π^0-meson rest system		
	Angle ϑ between particles, deg	Angle Φ between planes, deg	Momentum Mev/c	Angle ϑ between particles, deg	Angle Φ between planes, deg
2, e^-	6.5±1	75±10	56.1	7±2	<37
3, e^+			11.9		
4, e^-	6.5±1.5		9.0	12±4	
5, e^+			58.7		

sider the analyzed case as that of π^0-meson decay into two electron-positron pairs with angles of emission close to 180 deg. According to Dalitz,[1] however, that two such wide-angle pairs appear as the result of internal conversion is approximately 400 times less probable than the appearance of pairs with angles ~10 deg.)

In view of the effect that the angles of emission θ between the pair particles are relatively small, the angle between the planes of the pair can be determined only very roughly. Calculations show that in the rest system of the π^0 meson this angle does not exceed 37 deg, although angles close to 90 deg are more probable for the pseuco-scalar meson.

POSSIBLE EXAMPLES OF ANOTHER INTERPRETATION

Let us examine several other possible explanations for the observed event.

a) Let a π^0 meson, produced through charge-exchange decay, by the usual scheme (1), into two gamma quanta that are then converted into electron-positron pairs at so close a distance from the π^0-meson decay point, that this distance cannot be resolved on the photograph. The probability of both gamma quanta from the π^0-meson decay converting in the chamber hydrogen at a distance not exceeding 1 mm (width of track ~0.5 mm) is 2.2×10^{-12}. Since approximately 1400 events of elastic π^--p scattering have been registered in all the scanned films, and since the ratio of the cross sections of charge-exchange and elastic π^--p scattering is 1.8 at these energies,[6] the total number of π^0 mesons decaying in the chamber is 2500. Thus, the probability of observing the conversion of both gamma quanta at a distance less than 1 mm amounts to 5.5×10^{-9} in our experiment.

b) If the π^0 meson decays as in scheme (2) and then the gamma quantum is converted less than 1 mm from the point of π^0-meson decay, the probability of observing such an event in our experiments amounts to 4.7×10^{-5}.

c) The kinetic energy of the π^- meson (166 ± 14 Mev) exceeds somewhat the threshold of the reaction $\pi^- + p \rightarrow \pi^0 + \pi^0 + n$ (160 Mev). We can therefore observe an event analogous to that considered here if the two π^0 mesons produced in this reaction decay as per scheme (2). A rough estimate, in which the cross section of the foregoing reaction is taken to be 7×10^{-30} cm^2 and calculated for a π^--meson energy of 260 Mev,[8] shows the probability of observing such an event to be much less than 9×10^{-5}. Another argument against such an interpretation is the exceedingly good agreement between the kinematics of the observed event and the kinematics of decay (3).

d) According to the estimates of Kroll and Wada, only one π^0 meson in 29,000 decays by scheme (3). Consequently, the probability of observing such a decay in our experimental data amounts to approximately 0.09. A comparison of this value with estimates a), b), and c), and also the good agreement with the kinematics, leave no doubts regarding the reliability of observation of the $\pi^0 \rightarrow e^- + e^+ + e^- + e^+$ decay.

CONCLUSION

As noted previously, a definite angular correlation exists between the pair planes in the decay of a π^0 meson into two electron-positron pairs. A study of this correlation permits a direct determination of the spin and parity of the π^0 meson. The correlation function has the form

$$W(\varphi) \sim 1 + \lambda \cos 2\varphi,$$

where φ is the angle between the pair planes. Kroll and Wada have found that for zero π^0-meson spin the correlation coefficient λ is ± 0.19, with the plus and minus signs pertaining to the even and odd π^0 mesons, respectively. The correlation is much stronger here than the correlation between the planes of the pairs produced by the gamma quanta from the decay $\pi^0 \rightarrow 2\gamma$.[9,10] Joseph[3] has analyzed the angular correlation for a π^0-meson spin and parity $2^\pm$, and has shown that in this case $|\lambda| < 0.19$.*

Thus, even in the most favorable case, $|\lambda| = 0.19$, one must observe a rather large number of decays as per scheme (3) (on the order of several hundred) if any definite conclusions are to be drawn from the experimental data regarding the spin and parity of the π^0 meson. Although such an experiment is unusually laborious, it can be made quite realizable by increasing the efficiency of recording such decays by observing the stopping of slow π^- mesons in a hydrogen bubble chamber.

In conclusion, the author express their gratitude to D. V. Shirkov for discussing several problems connected with this research, and also to L. I. Krasnoslobdtseva, T. S. Sazhneva, and Yu. L. Saikina for scanning the films.

[1] R. H. Dalitz, Proc. Phys. Soc. **A64**, 667 (1951).

[2] N. M. Kroll and W. Wada, Phys. Rev. **98**, 1355 (1955).

*We are indebted to Dr. D. W. Joseph for providing us with a preprint of his paper.

[3] D. W. Joseph, Preprint, 1958.

[4] Hodson, Ballam, Arnold, Harris, Rau, Reynolds, and Treiman, Phys. Rev. **96**, 1089 (1954).

[5] Budagov, Viktor, Dzhelepov, Ermolov, and Moskalev, Материалы совещания по камерам Вильсона, диффузионным и пузырьковым камерам, ОИЯИ, Дубна, 1958. (Transactions of the Conference on Cloud, Diffusion, and Bubble Chambers, Joint Inst. for Nucl. Res., Dubna, 1958).

[6] Budagov, Viktor, Dzhelepov, Ermolov, and Moskalev, J. Exptl. Theoret. Phys. (U.S.S.R.) **35**, 1575 (1958), Soviet Phys. JETP **8**, 1101 (1959).

[7] Vasilenko, Kozodaev, Sulyaev, Filimonov, and Shcherbakov, Приборы и Техника Эксперимента (Instrum. and Meas. Engg.) No. 6, 1957.

[8] J. Franklin, Phys. Rev. **105**, 1101 (1957).

[9] C. N. Yang, Phys. Rev. **77**, 722 (1950).

[10] E. Karlson, Arkiv för Fysik **13**, 1 (1958).

Translated by J. G. Adashko
210

CONTRIBUTION TO THE THEORY OF FERROELECTRIC POLARIZATION CURVES

N. S. AKULOV

Submitted to JETP editor June 6, 1958

J. Exptl. Theoret. Phys. (U.S.S.R.) **36**, 1085-1087 (April, 1959)

The principles of a polarization theory for single- and many-domain ferroelectric crystals possessing one or two Curie points are developed for weak, strong, and medium fields at various temperatures. In contrast to the magnetization-curve theory previously developed, it is assumed that rotation can be neglected in the first approximation. The various refinements can be introduced in a way similar to that employed in the magnetization-curve theory.

THE theory of electrification curves for ferroelectrics should be formulated with account of the results of the theory of magnetization curves of ferromagnets.[1] Sometimes, however, one begins with the theory formulated by Becker in 1930, in which inversion processes (shifting of the domain boundaries) are not taken into account. According to this theory, if one starts with an S-shaped curve (Fig. 1), the Barkhausen jump should not occur anywhere except at points C or C′. In this case the coercive force E_C' is determined by the segment DC′. In 1931 – 1933[1] we showed that this theory is inadequate in principle and in practice. Actually (as indicated, for example in reference 1) the Barkhausen jump can occur at any point δ or in the segment RC (or R′C′), which indeed determines the value of E_C. This is due to the existence of inversion (displacement of the domain boundaries), in addition to rotation processes and the paraprocess.

If these concepts are carried over to the theory of ferroelectric electrification curves it becomes necessary to develop a new theory of coercive force and its temperature dependence, differing in principle from the single-domain theory (in spite of the attractiveness of this theory because of its great simplicity).[2] In solving this problem, we are able at the same time to formulate a theory of susceptibility in weak and strong fields. Owing to the existence of the rotation and inversion processes, and of the paraprocess we have accordingly for the susceptibility $\kappa = \kappa_r + \kappa_i + \kappa_p$, with κ_r small for Rochelle salt. To calculate κ_i and κ_p at various values of T, we start with the relation we have derived for the temperature dependence of the electrification curve[3]

$$E = -a(T-\Theta_1)^{\nu}(\Theta_2-T)^{\mu}P + BP^3 + CP^5, \qquad (1)$$

where P and E are the polarization and the electric field, Θ_i are the Curie points, a and B are parameters, and ν and μ are integers. In the case of a single Curie point, $\mu = 0$.

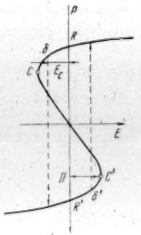

FIG. 1

This formula can be obtained most simply in the following manner:[3] we expand the work of electrification into a series (even) in powers of P

$$\int_0^P E\,dP = \tfrac{1}{2}AP^2 + \tfrac{1}{4}BP^4 + \tfrac{1}{6}CP^6 + \ldots \qquad (2)$$

The quantity A is expanded in powers of the differences $T-\Theta_1$ and $\Theta_2 - T$

$$A = A_0 + C_1(T-\Theta_1)^{\alpha} + C_2(\Theta_2-T)^{\beta} - a(T-\Theta_1)^{\nu}(\Theta_2-T)^{\mu} + \ldots \qquad (2')$$

But A = 0 at the Curie points for here $(P)_{E=0} = 0$. Equation (1) follows from (2) and (2′).

In addition, we should know the dependence of the domain energy U on the positions of the boundaries between domains. Let x be the displacement of the boundary from the equilibrium position. Then, expanding in powers of x and P, we have

$$U_i = x^2P(c_1\sigma + c_0P), \qquad (3)$$

where c_0 is the sum of two terms, one linear and

the other quadratic in σ, the internal elastic stress. A formula of this type is applicable to various types of domain energy (electrostriction, spontaneous electrification, and energy of the domain boundaries). Consequently, we obtain an analogous formula for the total energy, too. In the general case we should also take into account the types of energy which are proportional to other powers of P. In the first approximation it is enough, however, to restrict oneself to Eq. (3).

Taking into account the energy of the external field ($U_a = -2PEx$), we obtain for the equilibrium condition, $\partial(U_i + U_a)/\partial x = 0$, the following equation

$$E = x(c_0 P + c_1 \sigma). \tag{4}$$

Let n be the number of plane domains per cubic centimeter. We then obtain for the initial electric susceptibility

$$\varkappa_i = 2nxP/E. \tag{5}$$

From (4) and (5) we get

$$\varkappa = 2nc_0', \quad c_0' = P/(c_0 P + c_1 \sigma), \tag{6}$$

i.e., the susceptibility of inversion at $\sigma \to 0$ is independent of the temperature. The situation is different with the susceptibility of the paraprocess. We consider first fields considerably weaker than the coercive force. We then obtain for the point E = 0

$$\varkappa_p = dP/dE = 1/2A. \tag{7}$$

Thus we have from (2), (6), and (7), for the total susceptibility in weak fields at $\nu = \mu = 1$,

$$\varkappa = \varkappa_0 + 1/2a(T - \Theta_1)(\Theta_2 - T), \tag{8}$$

where

$$\varkappa_0 = \varkappa_i + \varkappa_p.$$

According to (1), we have for the case of strong fields at $\nu = \mu$ (for $\Theta_1 < T < \Theta_2$ and $c = 0$)

$$\varkappa' = P/E = 2\sqrt{(T - \Theta_1)(\Theta_2 - T)}/E(\Theta_2 - \Theta_1), \tag{9}$$

where κ' is the susceptibility in the absence of rotation and inversion.

At the Curie points themselves, P depends

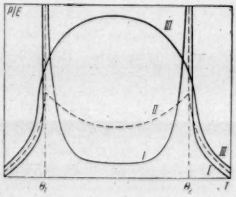

FIG. 2

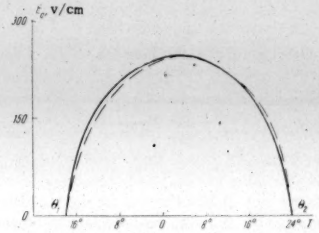

FIG. 3. Solid line– theoretical data; dotted–experimental data.

strongly on E. Indeed, we get from (1) and (2)

$$P = (E/B)^{1/3}. \tag{10}$$

Supplementing (9), we readily find by the method of successive approximation the value of P for temperatures near Θ_1 and Θ_2. As a result we obtain a curve of type III (Fig. 2).

The types of susceptibility curves obtained in weak fields (I) and in strong ones (II) are also shown in Fig. 2. The experiment yields a family of curves of this type.

Let x_c be the critical boundary displacement corresponding to the Barkhausen jump. We then obtain for the coercive force, from (4),

$$E_c = c_0 x_c P, \tag{11}$$

i.e., according to (2) and (1), we have (for $\nu = \mu$)

$$E_c = 2E_{st}\sqrt{(T - \Theta_1)(\Theta_2 - T)}/(\Theta_2 - \Theta_1), \tag{12}$$

where E_{st} pertains to the point $T = (\Theta_1 + \Theta_2)/2$. As can be seen from Fig. 3, Eq. (4) is in good agreement with the experimental data of Bradford[3] (reference 4, p. 576). We assume that the discrepancy between the experimental data of various authors is due to insufficient stabilization of the temperature, and also to the presence of dielectric viscosity.

[1] N. S. Akulov, Z. Physik **81**, 790 (1933).

[2] W. P. Mason, Piezoelectric Crystals and their Application to Ultrasonics, (Russ. Transl.) IIL, 1952, p 221, Van Nostrand, N. Y., 1950.

[3] N. S. Akulov, Сб. Применение ультраакустики к исследованию вещества (Anthology, Application of Ultrasonics to Investigations of Matter) No. 2, p. 279, 1958.

[4] W. C. Cady, Piezoelectricity, (Russ. Transl.) IIL, 1950, p. 546, Fig. 137, McGraw-Hill, New York, 1946.

Translated by J. G. Adashko
211

NEW DISPERSION RELATIONS IN QUANTUM FIELD THEORY

L. A. KHALFIN

Submitted to JETP editor June 17, 1958

J. Exptl. Theoret. Phys. (U.S.S.R.) **36**, 1088-1092 (April, 1959)

Some new dispersion relations are obtained between the modulus and the phase shift of the forward scattering amplitude. In contrast to the usual dispersion relations between the real and imaginary parts of the forward scattering amplitude, the present relations do not depend on the detailed behavior (degree of increase or decrease) of the forward scattering amplitude at infinite energy. In connection with the deduced dispersion equations the question of possible existence of zeros in the forward scattering amplitude in its region of analyticity is investigated.

1. In order to make clear the main ideas in the derivation of the new dispersion relations, we shall study a model. With appropriate technical improvements this model could be applied to realistic theories.

Let $f(E)$ be the forward scattering amplitude defined by the Fourier integral*

$$f(E)=\int_{-\infty}^{\infty}\tilde{F}(t)e^{iEt}dt\equiv\psi(E)e^{i\varphi(E)} \tag{1}$$

of a causal function $\tilde{F}(t)$, i.e., a semi-finite function:

$$\tilde{F}(t)=\begin{cases}F(t), & t>t_0\\ 0 & t<t_0\end{cases}\qquad t_0\leqslant 0. \tag{2}$$

In the case when the limit of semi-finiteness $t_0 = 0$ we say that $\tilde{F}(t)$ is microcausal, and when $t_0 < 0$ we say that $\tilde{F}(t)$ is macrocausal.[1] In the derivation of the usual dispersion relations one makes use of the condition of microcausality.[1]

The function $f(E)$ satisfies the following symmetry condition:†

$$f(E)=f^*(-E) \tag{3}$$

and from the "optical" theorem we have[1]

$$\operatorname{Im} f(E)=\frac{k}{4\pi}\sigma(E),\quad E\in[\mu,\infty), \tag{4}$$

Here $\sigma(E)$ is the total scattering cross section and $k^2 = E^2 - \mu^2$, where μ is the rest mass of the particle.

As is well known, relations of the type (1), (3), or (4) may be derived rigorously starting from only the most fundamental physical principles (in particular, the causality principle) and, most important, without any specific assumptions about the (unknown) form of the interaction operator. The function $\tilde{F}(t)$, of course, does depend on the specific structure of the interaction operator.

The derivation of the usual dispersion relations is based on the analyticity of $F(E)$ in the upper half plane $\operatorname{Im} E > 0$, which follows from the semi-finiteness of $\tilde{F}(t)$. However, in the derivation of the usual dispersion relations between $\operatorname{Re} f(E)$ and $\operatorname{Im} f(E)$, it is necessary to make additional assumptions about the behavior of $f(E)$ as $|E|\to\infty$.[1,2-9] It is important to note that the behavior of $f(E)$ as $|E|\to\infty$ does not, in general, follow from the fundamental physical principles used to obtain the basic relation (1). When studying the behavior of $f(E)$ as $|E|\to\infty$ one must start from a specific form for the interaction operator.[10,11] This is most unsatisfactory since it is believed that it is exactly at these infinitely high energies that present day theories are inconsistent (and therefore the interaction operators known at present are inconsistent also).

Therefore the usual dispersion relations cannot be used directly to verify the fundamental physical principles experimentally; the failure of the usual dispersion relations* may also be due to an incorrect assumption about the behavior of $f(E)$ as $|E|\to\infty$.

2. For those functions $f(E)$ which are in the Lebesgue class L^2† (i.e., are square-integrable) one obtains from the causality principle (micro- as well as macro-causality) not only analyticity

*The Fourier integral (1) is defined, generally speaking, for the class of generalized functions.[2]

†For the sake of simplicity we consider the case when the particles are described by a neutral field.

*Dispersion relations are a necessary but not sufficient (!) condition for the validity of the fundamental physical principles.

†This is the class of functions f(E) considered by Oehme.[6]

of $f(E)$ in the upper half plane $\mathrm{Im}\, E > 0$ but also the criterion of physical realizability in quantum field theory:[12]

$$\int_{-\infty}^{\infty} \frac{|\log \psi(E)|}{1+E^2}\, dE < \infty. \tag{5}$$

From Eq. (5) follow, in particular, definite restrictions on the behavior of $f(E)$ as $|E| \to \infty$, namely

$$|f(E)| = \psi(E) \geqslant A \exp\{-\gamma |E|^q\}, \tag{6}$$

where $A > 0$, $\gamma > 0$, $q < 1$, i.e., $f(E)$ cannot decrease too rapidly.

On the other hand $f(E)$ cannot increase too rapidly as $|E| \to \infty$ since it follows in any case from the analyticity of $f(E)$ that

$$|f(E)| = \psi(E) \leqslant A_1 \exp\{\gamma_1 |E|^{q_1}\}, \tag{7}$$

where $A_1 > 0$, $\gamma_1 > 0$, $q_1 < 1$. Furthermore, it can be shown[1] that $f(E)$ can increase or decrease as $|E| \to \infty$ only as a polynomial in E.

3. On the basis of the analyticity of the forward scattering amplitude $f(E)$ in the upper half plane $\mathrm{Im}\, E > 0$ and on the basis of the criterion of physical realizability (5) and (6), and the condition (7) we obtain by methods analogous to those used in quantum decay theory[13-15] the desired dispersion relations between $\log \psi(E)$ and $\varphi(E)$, which do not depend on the degree of increase or decrease of $f(E)$ as $|E| \to \infty$:

$$\varphi(E) = -\frac{(E-E_0)^m}{\pi} \mathrm{P} \int_0^{\infty} \frac{\log \psi(E')\,[(E'+E)(E'+E_0)^m + (-1)^{m+1}(E'-E)(E'-E_0)^m]}{(E'^2-E^2)(E'^2-E_0^2)^m}\, dE'$$

$$+ \varphi(E_0) + \frac{(E-E_0)}{1!}\frac{d\varphi(E_0)}{dE_0} + \cdots + \frac{(E-E_0)^{m-1}}{(m-1)!}\frac{d^{m-1}\varphi(E_0)}{dE_0^{m-1}} - \sum_k \tan^{-1}\frac{2(E-E_k^{(1)})E_k^{(2)}}{(E-E_k^{(1)})^2 - E_k^{(2)2}}$$

$$+ \sum_k \left\{ \tan^{-1}\frac{2(E_0-E_k^{(1)})E_k^{(2)}}{(E_0-E_k^{(1)})^2-(E_k^{(2)})^2} + \cdots + \frac{(E-E_0)^{m-1}}{(m-1)!}\frac{d^{m-1}}{dE_0^{m-1}} \tan^{-1}\frac{2(E_0-E_k^{(1)})E_k^{(2)}}{(E_0-E_k^{(1)})^2 - E_k^{(2)2}} \right\}; \quad m \geqslant 2. \tag{8}$$

If $f(E)$ increases or decreases as a polynomial[1] as $|E| \to \infty$ then it can be shown, making use of the symmetry condition (3), that the following much simpler dispersion relation is valid:

$$\varphi(E) = -\frac{2E}{\pi} \mathrm{P} \int_0^{\infty} \frac{\log \psi(E') - \log \psi(E)}{E'^2 - E^2}\, dE'$$

$$- \sum_k \tan^{-1}\frac{2(E-E_k^{(1)})E_k^{(2)}}{(E-E_k^{(1)})^2 - E_k^{(2)2}}. \tag{9}$$

In Eqs. (8) and (9) the summation over k is a summation over the possible zeros of the function $f(E)$ in the upper half plane $E_k = E_k^{(1)} + iE_k^{(2)}$; $E_k^{(2)} > 0$; and $\psi(E)$ and $\varphi(E)$ are the differential forward scattering cross section and the phase shift of the forward scattering amplitude respectively. They are given in terms of experimentally measureable quantities by

$$\psi(E) = \{[\mathrm{Re}\, f(E)]^2 + [\mathrm{Im}\, f(E)]^2\}^{1/2},$$

$$\varphi(E) = \tan^{-1}[\mathrm{Im}\, f(E) / \mathrm{Re}\, f(E)],$$

$$\varphi(E) = \tan^{-1}\frac{\mathrm{Im}\, f(E)}{(|\psi(E)|^2 - [\mathrm{Im}\, f(E)]^2)^{1/2}}. \tag{10}$$

The symbol P indicates that the integrals are principal value integrals at the points $E' = E$ as well as $E' = E_0$.

The dispersion relations (8) and (9), in contrast to the usual ones,[1,2-8] are valid for any degree of increase or decrease of the forward scattering amplitude $f(E)$ as $|E| \to \infty$. The dispersion relations (9), as opposed to the relations (8), do not require the knowledge of the derivatives of the phase shift, which constitutes a distinct advantage from the point of view of accuracy of the experimental data.

4. The main problem arising in the application of the new dispersion relations (8), (9) is in the determination of the possible zeros of the forward scattering amplitude $f(E)$ in the upper half plane $\mathrm{Im}\, E > 0$. The complete solution of this problem differs for particles with vanishing ($\mu = 0$) or with finite ($0 < \mu < \infty$) rest mass.

It can be shown, using criterion (5) and condition (7), that $f(E)$ is a function of completely regular increase and in class A in the upper half plane $\mathrm{Im}\, E > 0$.[16] Consequently one has, from the theorem by A. Pflyuger,[16] convergence of the series

$$\sum_k \left| \mathrm{Im}\, \frac{1}{E_k} \right| < \infty \tag{11}$$

(here E_k are the zeros of the analytic function $f(E)$ in the upper half plane) and the existence of the density

$$\Delta_f = \lim_{|E| \to \infty} n_f(|E|)/|E|, \tag{12}$$

where $n_f(|E|)$ is the number of zeros of $f(E)$ in a semicircle of radius $|E|$. The convergence of (12) means that "almost all" possible zeros of the forward scattering amplitude $f(E)$ lie in the

neighborhood of the real axis. It is seen from Eqs. (8) and (9) that the zeros that lie close to the real axis $E_k^{(2)} \to 0$ make a vanishingly small contribution to the dispersion relations.

5. The results obtained above concerning the possible zeros of the forward scattering amplitude $f(E)$ in the upper half plane $\operatorname{Im} E > 0$ are based on the same fundamental physical principles that are used in the proof of dispersion relations.[1]

These results can be made considerably more precise if use is made of the additional natural physical assumption that the total cross section $\sigma(E)$ differs from zero for all finite $E \in [\mu, \infty]$,

$$\sigma(E) \neq 0. \tag{13}$$

Using Eq. (4) we obtain from the additional condition (13) for particles with zero rest mass $\mu = 0$

$$\operatorname{Im} f(E) \neq 0, \quad E \in [0, \infty), \tag{14}$$

and for particles with finite rest mass $\mu > 0$

$$\operatorname{Im} f(E) \neq 0, \quad E \in [\mu, \infty). \tag{15}$$

On the basic of the fundamental theorem on the number of zeros of an analytic function[17] it is not difficult to see that the existence of zeros in $f(E)$ in the upper half plane $\operatorname{Im} E > 0$ corresponds to the vanishing of $\operatorname{Im} f(E)$ in isolated points E_i and, further, that $\operatorname{Re} f(E)$ should alternate in sign at neighboring points E_i.

Hence, using Eq. (14), we obtain the following final result for particles with zero rest mass $\mu = 0$. For such particles the forward scattering amplitude $f(E)$ either does not vanish at all in the upper half plane $\operatorname{Im} E > 0$ if $\operatorname{Re} f(0)$ and $\operatorname{Re} f(\infty)$ have the same sign, or has one simple zero $E_1 = iE_1^{(2)}$ if $\operatorname{Re} f(0)$ and $\operatorname{Re} f(\infty)$ have opposite signs.

On the other hand for particles with finite rest mass $0 < \mu < \infty$ it can be shown, using the fundamental theorem[17] and the condition (15), that the forward scattering amplitude $f(E)$ has only a finite number of zeros in the upper half plane $\operatorname{Im} E > 0$. To obtain more precise results one generally speaking needs to know the behavior of $f(E)$ in the nonphysical* region $E \in (-\mu, \mu)$. At that it is only necessary to know those values of $|E_i| < \mu$ for which $\operatorname{Im} f(E)$ vanishes and to know the sign of $\operatorname{Re} f(E)$ at these points E_i.

*For the π-meson-nucleon scattering, for example, the behavior of f(E) in the nonphysical region is known.

In connection with the dispersion relations derived above the following mathematical problem is of interest:[15] to find the necessary and sufficient criteria which must be satisfied by the analytic function — the forward scattering amplitude $f(E)$ — for $\infty > |E| \geq \mu$ in order that it have no zeros in the upper half plane $\operatorname{Im} E > 0$.

[1] Bogolyubov, Medvedev, and Polivanov, Вопросы теории дисперсионных соотношений, (Problems in the Theory of Dispersion Relations), FMI, 1958.

[2] N. N. Bogolyubov and N. S. Parasyuk, Dokl. Akad. Nauk SSSR **109**, 717 (1956).

[3] Gell-Mann, Goldberger, and Thirring, Phys. Rev. **95**, 1612 (1954).

[4] M. Goldberger, Phys. Rev. **99**, 979 (1955).

[5] Goldberger, Miyazawa, and Oehme, Phys. Rev. **99**, 986 (1955).

[6] R. Oehme, Phys. Rev. **100**, 1503 (1955); **102**, 1174 (1956).

[7] A. Salam, Nuovo cimento **3**, 424 (1956).

[8] A. Salam and W. Gilbert, Nuovo cimento **3**, 607 (1956).

[9] W. Gilbert, Phys. Rev. **108**, 1078 (1957).

[10] R. Arnowitt and G. Feldman, Phys. Rev. **108**, 144 (1957).

[11] K. Symanzik, Nuovo cimento **5**, 659 (1957).

[12] L. A. Khalfin, Dokl. Akad. Nauk SSSR **111**, 345 (1956); Soviet Phys. "Doklady" **1**, 671 (1956).

[13] L. A. Khalfin, Dokl. Akad. Nauk SSSR **115**, 277 (1957), Soviet Phys. "Doklady" **2**, 340 (1957).

[14] L. A. Khalfin, J. Exptl. Theoret. Phys. (U.S.S.R.) **33**, 1371 (1957), Soviet Phys. JETP **6**, 1053 (1958).

[15] L. A. Khalfin, О некоторых задачах теории функций комплексного переменного в квантовой теории распада физических систем, доклад на IV Всесоюзной конференции по теории функций комплексного переменного. (On Some Problems in the Theory of Functions of a Complex Variable in Quantum Theory of the Decay of Physical Systems, Report at the IV All-Union Conference on the Theory of Functions of a Complex Variable), M., 1958 (in press).

[16] B. Ya. Levin, Распределение корней целых функций, (Distribution of Roots of Entire Functions), GITTL, 1956.

[17] V. I. Smirnov, Курс высшей математики (Course in Higher Mathematics), vol. 3, part 2, GITTL, 1948.

Translated by A. M. Bincer
212

POLARIZATION IN PAIR PRODUCTION BY CIRCULARLY POLARIZED QUANTA

I. G. IVANTER

Scientific Information Institute, Academy of Sciences, U.S.S.R.

Submitted to JETP editor July 12, 1958

J. Exptl. Theoret. Phys. (U.S.S.R.) **36**, 1093-1097 (April, 1959)

An analysis is given of the cross section formulas for bremsstrahlung and pair production by photons on a Coulomb center; the formulas are derived in the Born approximation without taking into account screening and recoil and for fixed polarization of all the particles. Transformations have been found which allow one to obtain some of the formulas from the others, and by means of them formulas have been derived for pair production by circularly-polarized quanta.

1. For the case of elliptically polarized light the polarization vector may be written in the following form

$$\mathbf{e} = (\mathbf{e}_1 + i\delta\,\mathbf{e}_2)(1+\delta^2)^{-1/2}, \tag{1}$$

where $|\delta|$ differs from unity provided that the polarization is not circular. In this formula $\mathbf{e}_1$ and $\mathbf{e}_2$ are unit polarization vectors along two mutually perpendicular directions in a plane which is perpendicular to the momentum of the quantum, δ is a real number. On expanding (1) into a plane-polarized and a circularly-polarized wave we obtain

$$\mathbf{e} = |\delta|/\sqrt{1+\delta^2}\;[\mathbf{e}_1 + i(\delta/|\delta|)\,\mathbf{e}_2] + (|\delta|-1)\,\mathbf{e}_1/\sqrt{\delta^2+1}. \tag{2}$$

The cross section for the production of a pair with prescribed polarization must be of the form

$$\sigma = \sigma_A \frac{1}{4}\frac{2\delta^2}{1+\delta^2} + \sigma_B \frac{1}{4}\frac{2(2\delta^2-3|\delta|+1)}{1+\delta^2} + \sigma_C \frac{1}{2}\frac{2\delta^2}{1+\delta^2} + \sigma_{C'}\frac{1}{2}\frac{2\delta^2}{1+\delta^2} + \sigma_D \frac{2\delta^2}{1+\delta^2} + \sigma_E \frac{2(2\delta^2-3|\delta|+1)}{1+\delta^2}. \tag{3}$$

In the foregoing the following notation has been adopted: σ_A is the cross section given by the Bethe-Heitler formula[1] for the production of pairs of unpolarized particles by unpolarized γ quanta; σ_B is the cross section for the production of pairs of unpolarized particles by γ quanta which are plane-polarized in the $\mathbf{e}_1$ direction;[2,5] the ratios σ_C/σ_A and $\sigma_{C'}/\sigma_A$ give respectively the degree of polarization of electrons and positrons (or of μ^-- and μ^+-mesons) in the case of pair production by circularly-polarized γ quanta. The ratios σ_D/σ_A and σ_E/σ_A give the "degree of correlation of polarization" of positive and negative particles in the cases of unpolarized and plane-polarized γ quanta respectively.

The bremsstrahlung formula is of a form similar to formula (3):

$$\sigma' = \frac{\sigma'_A}{4}\frac{2\delta^2}{1+\delta^2} + \sigma'_B\frac{2(2\delta^2-3|\delta|+1)}{1+\delta^2} + \sigma'_C\frac{2\delta^2}{1+\delta^2}\frac{1}{2} + \sigma'_{C'}\frac{2\delta^2}{1+\delta^2} + \sigma'_D\frac{2\delta^2}{1+\delta^2}\frac{1}{2} + \sigma'_E\frac{2(2\delta^2-3|\delta|+1)}{1+\delta^2}. \tag{4}$$

In this case a quantum is radiated with polarization given by formula (1), while σ'_i have the following meaning: σ'_A is the bremsstrahlung cross section for an unpolarized electron summed over the polarizations of the γ quanta (Bethe-Heitler formula);[1] σ'_B is the bremsstrahlung cross section for radiation of a given linear polarization from an unpolarized electron,[2-5] the ratios $\sigma'_{C'}/\sigma'_A$[5] and σ'_C/σ'_A give respectively the degree of circular polarization in the case when the final or the initial electron is polarized; the ratios σ'_D/σ'_A and σ'_E/σ'_A give the "degree of correlation of polarizations" in the case of emission of an unpolarized or a linearly-polarized quantum respectively.

The difference in the coefficients in formulas (4) and (3) arises because it is necessary to take into account the fact that in the first case an averaging was carried out in the calculations, while in the other case a summation over the spins and the polarizations of the quanta was performed.

All the subsequent investigation is carried out in the Born approximation.

The formulas for σ_B, σ'_B, σ_A, σ'_A, σ'_C have been obtained and investigated a long time ago;[1-5] the formulas for $\sigma'_{C'}$, σ_C, $\sigma_{C'}$ may be easily obtained by introducing new variables (and making use of symmetry properties) from the formula for the circular polarization of bremsstrahlung by polarized electrons obtained in the paper by Vysotskiĭ et al.[5] The formulas for σ'_D, σ_D, σ_C, σ'_C

have been obtained earlier in special cases.[6,7] In the general case the expressions for σ'_D, σ_D, σ_E and σ'_E were obtained in Claesson's paper,[8] but since in deriving them McVoy's method[6,7] was used, the expressions obtained are of such an awkward form that it is possible to utilize them only by using an electronic computer.

Let us first of all investigate the question of the possibility of a direct derivation of the formulas for bremsstrahlung from the formulas for pair production, and conversely, in the case of fixed polarizations. In order to do this we shall investigate the expressions for the square of the modulus of the matrix element for both these processes.

In the case of pair production

$$|M|^2 = \frac{e^2}{32\omega E_- E_+}\frac{1}{(1+\delta^2)}\,\mathrm{Sp}\left\{\left[\frac{\hat{a}_q(-\hat{p}_+ + \hat{k} + m)\hat{e}}{2(p_+k)} + \frac{\hat{e}(\hat{p}_- - \hat{k} + m)\hat{a}_q}{2(p_-k)}\right](-\hat{p}_+ + m)(1 - i\gamma_5\hat{S}^-)\left[\frac{\hat{a}_q(\hat{p}_- - \hat{k} + m)\hat{e}}{2(p_-k)} + \frac{\hat{e}(-\hat{p}_+ + \hat{k} + m)\hat{a}_q}{2(p_+k)}\right](1 - i\gamma_5\hat{S}^-)(\hat{p}_- + m)\right\}. \quad (5)$$

In the foregoing and also in subsequent material the following notation has been used: the index "+" refers to the positron (μ^+ meson), the index "−" refers to the electron (μ^- meson), $E_{(\pm)}$, ω denote the energy and $p_{(\pm)}$, k denote the 4-momentum of a positively or a negatively charged particle and of a γ quantum. The projection operators for the electron and positron polarization are of the form

$$S^{\pm} = \{(\mathbf{p}_{\pm}, \mathbf{J}_{\pm})/m;\ \mathbf{J}_{\pm} + (\mathbf{p}_{\pm}, \mathbf{J}_{\pm})\,\mathbf{p}_{\pm}/m(E_{\pm} + m)\}, \quad (6)$$

J is the spin direction.

The square of the modulus of the matrix element for pair production (5) goes over into the square of the modulus for bremsstrahlung on making the following substitution:

$$p_+ \to -p_1; \quad p_- \to p_2; \quad k \to -k, \quad (7a)$$

$$S^+ \to S^1; \quad S^- \to S^2. \quad (7b)$$

Thus from the four-dimensional expressions for the cross sections of the one process we can obtain the four-dimensional expressions for the cross sections of the other process. However, it may be seen from expression (6) for the projection operators that if one makes the substitution (7a) in (6) then in this case we have $S^- \to S^2$, but S^+ does not go over into S^1. In order to find the transformation under which it is possible to obtain from the three-dimensional expressions for the one process the three-dimensional expressions for the other process, we note that expression (5) for the square of the modulus of the matrix element for pair production goes over into itself under the transformation

$$k \to -k; \quad p_+ \rightleftarrows -p_-; \quad S_+ \rightleftarrows S_-; \quad \mathbf{e} \rightleftarrows \mathbf{e}^*. \quad (8)$$

A similar transformation for the square of the modulus of the matrix element for bremsstrahlung may, however, also be carried out in three-dimensional form, since when the transformation:

$$k \to -k; \quad p_1 \rightleftarrows p_2; \quad S^1 \rightleftarrows S^2; \quad \mathbf{e} \rightleftarrows \mathbf{e}^* \quad (9a)$$

is carried out then automatically the transformation

$$\mathbf{J}_1 \rightleftarrows \mathbf{J}_2, \quad (9b)$$

occurs, and therefore the following transformation is at once realized

$$\mathbf{e} \rightleftarrows \mathbf{e}^*; \quad k \to -k; \quad p_1 \rightleftarrows p_2; \quad \mathbf{J}_1 \rightleftarrows \mathbf{J}_2. \quad (10)$$

However, in expression (5) one may carry out another replacement in addition to (8), in which the spin directions of the electron and the positron are directly interchanged, viz. the following replacement takes place

$$k \to k; \quad p_- \rightleftarrows p_+; \quad S^- \rightleftarrows S^+, \quad (11)$$

which differs in the signs of p_+, p_-, k from the replacement (8). Indeed, only such terms in (5) differ from zero which contain an even number of factors: $\hat{p}_+$; $\hat{p}_-$; $\hat{S}^-$; $\hat{S}^+$; $\hat{k}$; therefore the following two cases are possible:

1) The term contains one of the spin projection operators ($\hat{S}^-$ or $\hat{S}^+$). Then under the replacement (11) it will change sign. But such terms may appear only in expressions corresponding to circular polarization, and moreover one must also take into account the fact that in the replacement $\mathbf{e} \rightleftarrows \mathbf{e}^*$ these (and only these) expressions have an additional change of sign, and therefore the term will not change its sign.

2) The term contains both projection operators. In this case the requirement that the square of the absolute value of the matrix element should be real leads to the result that the expressions which contain the first power of δ (cf (1)) cannot appear in such terms, and therefore in the replacement $\mathbf{e} \rightleftarrows \mathbf{e}^*$ the sign does not undergo an additional change, and since in this case there is a change of sign in an even number of factors (four-momenta), then the term does not change sign in this case also. But under the transformation (11) a replacement of spins

$$\mathbf{J}_+ \rightleftarrows \mathbf{J}_-,$$

also occurs, and therefore expression (5) turns

out to be symmetric with respect to the replacement

$$k \to k; \quad p_+ \rightleftarrows p_-; \quad \mathbf{J}_- \rightleftarrows \mathbf{J}_+, \tag{12}$$

since it is equivalent to the replacement (8).

We emphasize that if in the expression for bremsstrahlung we introduce a replacement similar to (10),

$$k \to -k; \quad p_1 \rightleftarrows p_2; \quad \mathbf{J}_1 \rightleftarrows \mathbf{J}_2 \tag{13}$$

(without replacing $\mathbf{e}$ by $\mathbf{e}^*$), then the expressions corresponding to circular polarization will change sign (the other expressions will not change sign).

We also note another property of the projection operators: if $\mathbf{J}$ is the transverse polarization, then any arbitrary transformations of p in S will not change S. But if $\mathbf{J}$ is a longitudinal polarization, then when the (four-dimensional) momentum p changes sign the longitudinal polarization will also change sign. We can make use of this last fact in order to obtain special cases of formulas for the correlation of polarizations.

We emphasize that although all the considerations presented below apply to the case of the absence of screening, the symmetry properties of the formulas are retained also for the case of complete screening at ultra-relativistic energies.

2. The expression for σ'_C, containing circular polarization was obtained in the general case in the paper by Vysotskiĭ, Kresnin, and Rozentsveig:[5*]

$$\sigma'_C = \frac{m}{2E_1 |\mathbf{q}'|^4} \times \left\{ \left(\frac{\mathbf{p}_1}{\varkappa_2} + \frac{\mathbf{p}_2}{\varkappa_2} \quad [\mathbf{k} \times [\mathbf{k} \times (\mathbf{p}_1 - \mathbf{p}_2)]] \right) \left(\mathbf{J}_1, \frac{\omega \mathbf{p}_1 + E_1 \mathbf{k}}{\varkappa_1} + \frac{\omega \mathbf{p}_1 - E_1 \mathbf{k}}{\varkappa_2} \right) + \frac{1}{2} m^2 \omega \left[\frac{\varkappa_1}{\varkappa_2} - \frac{\varkappa_2}{\varkappa_1} + \frac{4\omega}{m^2} \left(\frac{E_1}{\varkappa_1} + \frac{E_2}{\varkappa_2} \right) \right] \times \left(\mathbf{J}_1, \frac{E_2}{\varkappa_2} (\omega \mathbf{p}_1 - E_1 \mathbf{k}) + \frac{E_1}{\varkappa_1} (\omega \mathbf{p}_2 - E_2 \mathbf{k}) \right) \right\} N_b \frac{\delta}{|\delta|}; \tag{14}$$

where ϑ_1, ϑ_2 are the angles between $\mathbf{k}$ and $\mathbf{p}_1$ or $\mathbf{p}_2$; N_b is a factor which takes into account the number of states:

$$N_b = \frac{4Z^2\alpha^3 \, d\omega \, do_1 \, do_2}{(2\pi)^2 \omega} \frac{|\mathbf{p}_2|}{|\mathbf{p}_1|}.$$

We carry out the replacement (13) in expression (14). In doing this both now and everywhere later naturally the replacement is not carried out in N. In making this replacement it is necessary to change the sign in front of the whole expression as was mentioned earlier. Then for the quantity $\sigma'_{C'}$ corresponding to circular polarization and for a fixed polarization of the final electron we obtain the following expression

$$\sigma'_{C'} = -\frac{1}{2} N_b \frac{\delta}{|\delta|} \frac{m}{2E_2 |\mathbf{q}'|^4} \left\{ \left(\frac{\mathbf{p}_2}{\varkappa_1} + \frac{\mathbf{p}_1}{\varkappa_2}, \ [\mathbf{k}\,[\mathbf{k}, \mathbf{p}_2 - \mathbf{p}_1]] \right) \times \left(\mathbf{J}_2, \frac{\omega \mathbf{p}_2 + E_2 \mathbf{k}}{\varkappa_2} + \frac{\omega \mathbf{p}_2 - E_2 \mathbf{k}}{\varkappa_1} \right) + \frac{1}{2} m^2 \omega \left[\frac{\varkappa_2}{\varkappa_1} - \frac{\varkappa_1}{\varkappa_2} + \frac{4\omega}{m^2} \left(\frac{E_2}{\varkappa_2} + \frac{E_1}{\varkappa_1} \right) \right] \times \left(\mathbf{J}_2, \frac{E_1}{\varkappa_1} (\omega \mathbf{p}_2 - E_2 \mathbf{k}) + \frac{E_2}{\varkappa_2} (\omega \mathbf{p}_1 - E_1 \mathbf{k}) \right) \right\}. \tag{15}$$

To obtain the expression for σ_C we shall carry out in formula (15) the replacement $\mathbf{p}_+ \to -\mathbf{p}_-$; $\mathbf{p}_- \to \mathbf{p}_2$; $\mathbf{k} \to -\mathbf{k}$; $\mathbf{J}_2 \to \mathbf{J}_-$ [which in the present case is equivalent to the replacement (7a), (7b)]

$$\sigma_C = \frac{N_p \delta (-1) m}{|\delta| 2E_- |\mathbf{q}|^4} \left\{ \left(\frac{\mathbf{p}_-}{\varkappa_-} - \frac{\mathbf{p}_-}{\varkappa_+}, \ [\mathbf{k}\,[\mathbf{k}, \mathbf{p}_- + \mathbf{p}_+]] \right) \times \left(\mathbf{J}_-, \frac{-\omega \mathbf{p}_- - E_- \mathbf{k}}{\varkappa_+} - \frac{\omega \mathbf{p}_- - E_- \mathbf{k}}{\varkappa_-} \right) - \frac{1}{2} m^2 \omega \left[\frac{\varkappa_+}{\varkappa_-} - \frac{\varkappa_-}{\varkappa_+} + \frac{4\omega}{m^2} \left(\frac{E_-}{\varkappa_+} + \frac{E_+}{\varkappa_-} \right) \right] \left(\mathbf{J}_-, \frac{E_+}{\varkappa_-} (\omega \mathbf{p}_- - E_- \mathbf{k}) + \frac{E_-}{\varkappa_+} (\omega \mathbf{p}_+ - E_+ \mathbf{k}) \right) \right\}. \tag{16}$$

Here

$$\varkappa_- = -2E_- \omega (1 - V_- \cos \vartheta_-);$$

$$\varkappa_+ = -2E_+ \omega (1 - V_+ \cos \vartheta_+); \quad \mathbf{q} = \mathbf{p}_- + \mathbf{p}_+ - \mathbf{k};$$

$$N_p = 4Z^2\alpha^3 |\mathbf{p}_+| |\mathbf{p}_-| dE_+ \, do_+ \, do_- / (2\pi)^2 \omega^3.$$

We shall obtain the expression containing positron polarization from (15) by making use of the replacement (12)

$$\sigma'_C = \frac{N_p \delta (-1) m}{|\delta| 2E_+ |\mathbf{q}|^4} \left\{ \left(\frac{\mathbf{p}_+}{\varkappa_+} - \frac{\mathbf{p}_-}{\varkappa_-}, \ [\mathbf{k}\,[\mathbf{k}, \mathbf{p}_+ + \mathbf{p}_-]] \right) \times \left(\mathbf{J}_+, \frac{-\omega \mathbf{p}_+ - E_+ \mathbf{k}}{\varkappa_-} - \frac{\omega \mathbf{p}_+ - E_+ \mathbf{k}}{\varkappa_+} \right) - \frac{1}{2} m^2 \omega \left[\frac{\varkappa_-}{\varkappa_+} - \frac{\varkappa_+}{\varkappa_-} + \frac{4\omega}{m^2} \left(-\frac{E_+}{\varkappa_-} + \frac{E_-}{\varkappa_+} \right) \right] \times \left(\mathbf{J}_+, \frac{E_-}{\varkappa_+} (\omega \mathbf{p}_+ - E_+ \mathbf{k}) + \frac{E_+}{\varkappa_-} (\omega \mathbf{p}_- - E_- \mathbf{k}) \right) \right\}. \tag{17}$$

The author wishes to thank I. Yu. Kobzarev for discussing certain questions associated with the present work.

*Quite recently the paper by Fronsdal and Uberall was published[10] which contains a part of the results already obtained previously[5] and in agreement with them.

[1] A. I. Akhiezer and V. B. Berestetskiĭ, Квантовая электродинамика (Quantum Electrodynamics), Gostekhizdat, Moscow, 1953 (English Transl., U.S. Dept. Comm.).

[2] M. M. May and G. C. Wick, Phys. Rev. **81**, 628 (1951). M. M. May, Phys. Rev. **84**, 265 (1951).

[3] R. L. Gluckstern and M. H. Hill, Phys. Rev. **90**, 1030 (1953).

[4] L. N. Rozentsveĭg, J. Exptl. Theoret. Phys. (U.S.S.R.) **31**, 520 (1956), Soviet Phys. JETP **4**, 455 (1957).

[5] Vysotskiĭ, Kresnin, and Rozentsveĭg, J. Exptl. Theoret. Phys. (U.S.S.R.) **32**, 1078 (1957), Soviet Phys. JETP **5**, 883 (1957).

[6] K. W. McVoy, Phys. Rev. **106**, 828 (1957).

[7] K. W. McVoy and F. J. Dyson, Phys. Rev. **106**, 360 (1957).

[8] A. Claesson, Ark. f. fysik **12**, 569 (1957).

[9] H. A. Tolhoek, Revs. Modern Phys. **28**, 277 (1956).

[10] C. Fronsdal and H. Uberall, Nuovo cimento **8**, 165 (1958).

Translated by G. Volkoff
213

A NEW CLASS OF REPRESENTATIONS OF THE FULL LORENTZ GROUP

G. A. SOKOLIK

Submitted to JETP editor July 14, 1958; resubmitted September 24, 1958

J. Exptl. Theoret. Phys. (U.S.S.R.) **36**, 1098-1102 (April, 1959)

All representations of the full Lorentz group are found. It is shown that these representations reduce to direct products of spinors belonging to three classes. An attempt is made to interpret isotopic spin in terms of the generalized parity operator without introducing new degrees of freedom.

It is shown that the connection between spin and statistics may not hold for spinors which transform according to commuting representations.

IN the paper by Gel'fand and Tsetlin[1] the possibility was noted of representing the group of space-time reflections by matrices which commute in the case of spinor representations and which anti-commute in the case of representations corresponding to particles of integral spin.

The author has shown[2] that the Dirac equation is invariant with respect to the commuting spinor representation of the Lorentz group only in the extended eight-dimensional form. In this connection it was noted that the doubling of dimensionality obtained in this way may be interpreted as the introduction of isotopic spin. This gives rise to the possibility of obtaining the isotopic doublet without introducing new degrees of freedom only by means of generalizing the representation of the full Lorentz group, while the majority of the attempts to interpret isotopic spin undertaken recently were based on the generalization of the Lorentz group itself (cf. for example, reference 3).

Thus, it appears to be possible to classify elementary particles according to the representations of the group of space-time reflections. In this case the parity operator will play the role of isotopic spin. In connection with this the problem arises of finding all the irreducible representations of the full Lorentz group. In this way we shall obtain all the invariants and pseudoinvariants expressed in terms of polylinear combinations of three kinds of spinors. In other words, the solution of this problem will make it possible to carry out the classification of interactions of elementary particles (conserving or nonconserving parity) in terms of the representations of the full Lorentz group. This problem is of particular interest in connection with the fusion theory, according to which all the particles reduce to one or several spinor particles,[4] and also in connection with attempts of creating a single nonlinear field theory taking into account various types of fundamental spinors.[5] The normal and the anomalous (commuting and anticommuting)[1] representations of the full Lorentz group are effectively specified by means of the contracted direct product of the following three spinor representations:

$$T_{01}=\begin{pmatrix}0 & I\\ I & 0\end{pmatrix};\qquad T_{10}=\begin{pmatrix}0 & iI\\ iI & 0\end{pmatrix};\qquad T_{11}=\begin{pmatrix}iI & 0\\ 0 & iI\end{pmatrix}, \quad (1)$$

$$T_{01}=\begin{pmatrix}0 & I\\ I & 0\end{pmatrix};\qquad T_{10}=\begin{pmatrix}0 & -I\\ I & 0\end{pmatrix};\qquad T_{11}=\begin{pmatrix}I & 0\\ 0 & -I\end{pmatrix}, \quad (2)$$

$$T_{01}=\begin{pmatrix}0 & -iI\\ iI & 0\end{pmatrix};\qquad T_{10}=\begin{pmatrix}0 & iI\\ iI & 0\end{pmatrix};\qquad T_{11}=\begin{pmatrix}I & 0\\ 0 & -I\end{pmatrix}. \quad (3)$$

The representation (1) is normal, while the representations (2) and (3) are anomalous. The operators T_{01}, T_{10}, T_{11}, which satisfy the relations $T_{10}T_{11} = T_{01}$; $T_{10}T_{01} = T_{11}$, operate on the bispinors $(x_1x_2\bar{x}_1\bar{x}_2)$, with T_{01}, T_{10}, T_{11} corresponding to reflections of space, time and space-time respectively. The representations are determined up to a factor of modulus 1. As was shown in reference 2, the spinors transforming according to formulas (3) may be interpreted in terms of the five-dimensional rotation group.

We note that the spinors (1) may be regarded as spinors of the first kind with respect to spatial reflections, and of the second kind with respect to time reflections.[6,7] The representations of the full Lorentz group are given[6] by multiplying the spinor representations $(\frac{1}{2}, 0)$ and $(0, \frac{1}{2})$.

By expanding the generating polynomials D^{+}_{jk} and D^{-}_{jk}:

$$D^{+}_{jk}=(u_1x_1+u_2x_2)^{2j}(v_1\bar{x}_1+v_2\bar{x}_2)^{2k},$$

$$D^{-}_{jk}=(u_1x_1+u_2x_2)^{2j}(v_1\bar{x}_1+v_2\bar{x}_2)^{2k}\begin{vmatrix}x_1x_2'-x_2x_1'\\ \bar{x}_1\bar{x}_2-\bar{x}_2\bar{x}_1\end{vmatrix},$$

we obtain the quantities Y^{jk}_{mp} and Z^{jk}_{mp} which transform according to the representations D^{+}_{jk} and $D^{+}_{\bar{j}\bar{k}}$:

$$Y^{jk}_{mp} = x_1^{j+m} x_2^{j-m} \bar{x}_1^{k+p} \bar{x}_2^{k-p},$$

$$Y^{kj}_{pm} = x_1^{k+p} x_2^{k-p} \bar{x}_1^{j+m} \bar{x}_2^{j-m},$$

$$Z^{jk}_{mp} = x_1^{j+m} x_2^{j-m} \bar{x}_1^{k+p} \bar{x}_2^{k-p} (x_1 x_2' - x_2 x_1'),$$

$$Z^{kj}_{pm} = x_1^{k+p} x_2^{k-p} \bar{x}_1^{j+m} \bar{x}_2^{j-m} (\bar{x}_1 \bar{x}_2' - \bar{x}_2 \bar{x}_1').$$

Let us examine the case D^{+}_{jk} and $D^{+}_{\bar{k}\bar{j}}$. For spinors which transform according to formulas (1), (2), and (3), we have

$$T_{01} = \begin{pmatrix} 0 & I \\ I & 0 \end{pmatrix}; \quad T_{10} = \begin{pmatrix} 0 & i^{2(k+l)} \\ i^{2(k+l)} & 0 \end{pmatrix};$$

$$T_{11} = \begin{pmatrix} i^{2(k+l)} & 0 \\ 0 & i^{2(k+l)} \end{pmatrix}, \tag{4}$$

$$T_{01} = \begin{pmatrix} 0 & I \\ I & 0 \end{pmatrix}; \quad T_{10} = \begin{pmatrix} 0 & (-I)^{2k} \\ (-I)^{2j} & 0 \end{pmatrix};$$

$$T_{11} = \begin{pmatrix} (-I)^{2j} & 0 \\ 0 & (-I)^{2k} \end{pmatrix}, \tag{5}$$

$$T_{01} = \begin{pmatrix} 0 & (-i)^{2j} i^{2k} \\ (-i)^{2k} i^{2j} & 0 \end{pmatrix}; \quad T_{10} = \begin{pmatrix} 0 & i^{2(j+k)} \\ i^{2(j+k)} & 0 \end{pmatrix};$$

$$T_{11} = \begin{pmatrix} (-I)^{2j} & 0 \\ 0 & (-I)^{2k} \end{pmatrix} \tag{6}$$

respectively. The representations (5) and (6) are anomalous in the case when one of the jk is integral, while the other one is half-integral; in all other cases these representations are normal. The representation (4) is always normal.

Let us examine the improper representation D^{-}_{jk} and $D^{-}_{\bar{k}\bar{j}}$. It may be easily shown that Z^{jk}_{mp} transforms according to formulas (4), (5), and (6), if $x\bar{x}$ and $x'\bar{x}'$ transform according to (1), (2), and (3). In the case when $x\bar{x}$ transforms according to (1), while $x'\bar{x}'$ transforms according to (2), the representation D^{-}_{jk}, $D^{-}_{\bar{k}\bar{j}}$ is specified by the anticommuting operators

$$T_{10} = \begin{pmatrix} 0 & -I \\ I & 0 \end{pmatrix}; \quad T_{01} = \begin{pmatrix} 0 & I \\ I & 0 \end{pmatrix}; \quad T_{11} = \begin{pmatrix} I & 0 \\ 0 & -I \end{pmatrix}. \tag{7}$$

We see that in this case the representation of the full Lorentz group specified by the direct product of spinors of different type decomposes into two representations of the proper group related by reflection even in the case when $j = k$. When $x\bar{x}$ and $x'\bar{x}'$ transform according to (1) and (3) or (2) and (3), respectively, the following representations hold

$$T_{01} = \begin{pmatrix} 0 & -i \\ i & 0 \end{pmatrix}; \quad T_{10} = \begin{pmatrix} 0 & i \\ i & 0 \end{pmatrix}; \quad T_{11} = \begin{pmatrix} I & 0 \\ 0 & -I \end{pmatrix}, \tag{8}$$

$$T_{01} = \begin{pmatrix} 0 & i^{2k} \\ (-I)^{2k} & 0 \end{pmatrix}; \quad T_{10} = \begin{pmatrix} 0 & (-I)^{2j} i^{2k} \\ i^{2k} & 0 \end{pmatrix};$$

$$T_{11} = \begin{pmatrix} (-I)^{2k} & 0 \\ 0 & (-I)^{2j} \end{pmatrix}. \tag{9}$$

In the last case the operators commute when kj are integral or half-integral, and anticommute if 2j and 2k have opposite parity.

The representation of the full Lorentz group may also be specified by the generating polynomials

$$B^{+}_{jk} = (u_1 x_1 + u_2 x_2)^{2j} (v_1 \bar{x}_1 + v_2 \bar{x}_2)^{2k},$$

$$B^{-}_{jk} = (u_1 x_1 + u_2 x_2)^{2j} (v_1 \bar{x}_1 + v_2 \bar{x}_2)^{2k} \begin{vmatrix} x_1 x_2' - x_2 x_1' \\ \bar{x}_1 \bar{x}_2' - \bar{x}_2 \bar{x}_1' \end{vmatrix}. \tag{10}$$

In this case the basis of the representation is specified by the products of the monomials

$$Z^{jk}_{mp} = x_1^{j+m} x_2^{j-m} \bar{x}_1^{k+p} \bar{x}_2^{k-p},$$
$$\bar{Z}^{jk}_{mp} = \bar{x}_1^{j+m} \bar{x}_2^{j-m} x_1^{k+p} x_2^{k-p},$$
$$Z^{kj}_{pm} = x_1^{k+p} x_2^{k-p} \bar{x}_1^{j+m} \bar{x}_2^{j-m},$$
$$\bar{Z}^{kj}_{pm} = \bar{x}_1^{k+p} \bar{x}_2^{k-p} x_1^{j+m} x_2^{j-m},$$
$$Z^{00} = x_1 x_2' - x_2 x_1', \quad \bar{Z}^{00} = \bar{x}_1 \bar{x}_2' - \bar{x}_2 \bar{x}_1',$$

where x and x′ behave in the same way under rotations. If x and x′ transform according to (1) and (2), Z^{jk}_{mp} $\bar{Z}^{jk}_{mp}$ and Z^{kj}_{pm} $\bar{Z}^{kj}_{pm}$ transform according to the following representations:

$$T_{01} = \begin{pmatrix} 0 & I \\ I & 0 \end{pmatrix}; \quad T_{10} = \begin{pmatrix} 0 & (-I)^{2j} i^{2k} \\ i^{2k} & 0 \end{pmatrix};$$

$$T_{11} = \begin{pmatrix} i^{2k} & 0 \\ 0 & (-I)^{2j} i^{2k} \end{pmatrix} \tag{11}$$

and

$$T_{01} = \begin{pmatrix} 0 & I \\ I & 0 \end{pmatrix}; \quad T_{10} = \begin{pmatrix} 0 & (-I)^{2n} i^{2j} \\ i^{2j} & 0 \end{pmatrix}; \quad T_{11} = \begin{pmatrix} i^{2j} & 0 \\ 0 & (-I)^{2k} i^{2j} \end{pmatrix}.$$

The representations obtained above are anomalous for j and k having half-integral values respectively and are normal in all other cases. By considering x and x′ as transforming according to (2), (3) and (1), (3), it may be shown in general that in the case when $x\bar{x}$ transform according to the normal representations while $x'\bar{x}'$ transform according to anomalous representations the resulting representation of B^{+}_{jk}, $B^{+}_{\bar{k}\bar{j}}$, is anomalous if j or k is half-integral and is normal in all other cases. If both spinor representations are anomalous then B^{+}_{jk}, $B^{+}_{\bar{k}\bar{j}}$ is anomalous only when one of the numbers j, k is integral and the other one is half-integral.

In conclusion we note that both new variants of the representation of the full Lorentz group (the commuting spinor and the anticommuting boson representations) lead to a doubling of the dimensionality of the ψ-function.

As an example we shall consider two pseudoscalar irreducible representations

$$Z^{(0)} = x_1x_2 - x_2x_1, \quad \overline{Z}^{(0)} = \bar{x}_1\bar{x}_2 - \bar{x}_2\bar{x}_1, \qquad (12)$$

which transform according to the Pauli matrices

$$T_{10}=\begin{pmatrix}0&-1\\1&0\end{pmatrix}; \quad T_{10}=\begin{pmatrix}0&1\\1&0\end{pmatrix}; \quad T_{11}=\begin{pmatrix}1&0\\0&-1\end{pmatrix}. \qquad (13)$$

The representation obtained above may be used to describe a scalar particle which may exist in states with different parities. In order to do this we shall go over to another representation

$$T=\begin{pmatrix}1&1\\1&-1\end{pmatrix}; \quad T'_{ik}=T^{-1}T_{ik}T,$$

$$T_{10}=\begin{pmatrix}0&-1\\1&0\end{pmatrix}; \quad T_{01}=\begin{pmatrix}1&0\\0&-1\end{pmatrix}; \quad T_{11}=\begin{pmatrix}0&1\\1&0\end{pmatrix}. \qquad (14)$$

In this case we have the doublet

$$\psi=\psi'^{+}L\psi, \quad \Phi=\psi'^{+}C\psi, \qquad L=\begin{pmatrix}0&0&0&-1\\0&0&1&0\\0&-1&0&0\\1&0&0&0\end{pmatrix},$$

$$C=\begin{pmatrix}0&0&0&1\\0&0&-1&0\\0&-1&0&0\\1&0&0&0\end{pmatrix}, \qquad \psi=\begin{bmatrix}x_1\\x_2\\\bar{x}_1\\\bar{x}_2\end{bmatrix},$$

which may be interpreted as one of the K-meson isotopic doublets $[K^0K^+]$ or $[-K^{0*}K^-]$.

With reference to the spinor particles we see that in accordance with (2) the Dirac equation $\gamma_i\partial\psi/\partial x_i + m\psi = 0$ is invariant with respect to (3), while the equation $\gamma_i\partial\psi/\partial x_i + m\gamma_5\psi = 0$ is invariant with respect to (2). The normal representation gives the eight-dimensional Dirac equation

$$\Gamma_i\partial\Psi/\partial x_i + m\Psi = 0, \quad \Gamma_i=\begin{pmatrix}\gamma_i&0\\0&-\gamma_i\end{pmatrix}.$$

The spinor Ψ may be expressed in terms of x_1x_2 and $\bar{x}_1\bar{x}_2$ in the following manner. $\Psi = \Pi \times Z$ where

$$\Pi=\begin{pmatrix}x_1\\x_2\\\bar{x}_1\\\bar{x}_2\end{pmatrix}, \qquad Z=\begin{pmatrix}Z^{(0)}\\\overline{Z}^{(0)}\end{pmatrix}.$$

It may be easily shown that in the case of spinors which transform according to the normal representation, time reversal is equivalent to charge conjugation. Indeed, if $\psi = C\psi^*$, where $CD^*C = -D$

$$\gamma_ip_i = D=\begin{pmatrix}0&0&\partial_4+\partial_3&\partial_1-i\partial_2\\0&0&\partial_1+i\partial_2&\partial_4-\partial_3\\\partial_4-\partial_3&-\partial_1+i\partial_2&0&0\\-\partial_1-i\partial_2&\partial_4+\partial_3&0&0\end{pmatrix};$$

$$p_i\equiv\partial_i\equiv\partial/\partial x_i.$$

On the other hand $\gamma_4D_{-t}\gamma_4 = -D_t$ with $\psi' = \gamma_4\psi$. Consequently the operation TC in the case of the normal spinor representation preserves the Dirac equation and, thereby, also the Lagrangian $\mathcal{L} = \tilde{\psi}^*(D\psi + m\psi)$; here $\tilde{\psi}^*$ and ψ are not subjected to the anticommutation condition as in the case of the anomalous spinor representations.[8]

Thus the normal spinors are quantized according to Bose statistics.[2] The argument presented above is applicable to the Dirac equation interacting with the electromagnetic field

$$\gamma_i(\partial/\partial x_i - ieA_i)\psi + m\psi = 0; \qquad \Box A_i = j_i/c,$$

since $j = \psi^*\gamma_i\psi$ and A_i transform under reflections like $\partial/\partial x_i$. I wish to thank O. A. Germogenova and A. M. Brodskiĭ for valuable suggestions and fruitful discussions.

[1] I. M. Gel'fand and M. L. Tsetlin, J. Exptl. Theoret. Phys. (U.S.S.R.) **31**, 1107 (1956), Soviet Phys. JETP **4**, 947 (1957).

[2] G. A. Sokolik, J. Exptl. Theoret. Phys. (U.S.S.R.) **33**, 1515 (1957), Soviet Phys. JETP **6**, 1170 (1958).

[3] G. A. Sokolik, Dokl. Akad. Nauk SSSR **114**, 6 (1957).

[4] M. A. Markov, Гипероны и K-мезоны (Hyperons and K-mesons), Joint Institute for Nuclear Research, Dubna-Moscow, 1957.

[5] W. Heisenberg, Revs. Modern Phys. **29**, 269 (1957).

[6] E. Cartan, Theory of Spinors (Russ. Transl.) IIL, Moscow, 1947.

[7] A. M. Brodskiĭ and D. D. Ivanenko, J. Exptl. Theoret. Phys. (U.S.S.R.) **9**, 1279 (1959), Soviet Phys. JETP this issue, p. 907.

[8] J. Schwinger, Phys. Rev. **82**, 914 (1951).

Translated by G. Volkoff
214

DISPERSION RELATIONS AND CHEW-LOW TYPE EQUATIONS FOR INELASTIC MESON PROCESSES IN THE FIXED SOURCE CASE

W. ZOELLNER

Joint Institute for Nuclear Research

Submitted to JETP editor August 26, 1958

J. Exptl. Theoret. Phys. **36**, 1103-1109 (April, 1959)

The static dispersion relations and Chew-Low equations are established for the process $\pi + N \rightarrow n\pi + N$. It turns out that for this process one can obtain physically different dispersion relations and Chew-Low equations, depending on how the variables are chosen.

THE progress in theoretical π-meson physics of the last few years has been achieved mainly by means of the theory of dispersion relations and by means of the so-called Chew-Low equations. There exists a connection between these two theories. This has already been investigated by several authors.[1,2] In the present paper we will establish the dispersion relations and the Chew-Low equations for the process $\pi + N \rightarrow n\pi + N$ in the fixed-source approximation.

As in the case of elastic scattering one has to utilize the causality conditions in order to establish the dispersion relations. Utilizing the Bogolyubov formalism[3] it is possible to introduce the causality conditions in an explicit manner in the static case[4] to which we shall restrict ourselves. This is as is well known not possible in the formalism of Wick, Chew, and Low.[5]

In setting up the dispersion relations we employ the retarded and advanced transition amplitudes of the considered process. Since there does not hold an "optical theorem" for the case $n > 1$ and because of the appearance of the unphysical region it seems that it is not possible to apply the dispersion relations in an exact fashion. Therefore we shall go over from the static dispersion equations to the appropriate equation of the Chew-Low type.

Depending on the way how one fixes the variables in the case $n > 1$, one can obtain different dispersion relations. Presumably the exact solutions to these different dispersion relations will coincide.

On the other hand it turns out that the results obtained by using approximations definitely depend on the choice of variables. This is also true for the different Chew-Low type equations which correspond to the different dispersion relations. It should be mentioned that these differences are due to physical reasons and are not connected in any way with the frequently discussed nonuniqueness of the solutions to the Chew-Low equations (see references 6 and 7). We shall not consider this point in the present paper.

1. STRUCTURE OF THE S MATRIX

An element of the S matrix of the process $\pi + N \rightarrow n\pi + N$ can be written in the form

$$S_{n,1} = \langle s', \mathbf{q}_n, \ldots, \mathbf{q}_1 | S | s, \mathbf{q}_0 \rangle = \frac{v_n \ldots v_0 \mathbf{q}_n \ldots \mathbf{q}_0}{(2\pi)^{3(n+1)/2}(2^{n+1}E_n \ldots E_0)^{1/2}}$$

$$\times (-i)^n i \int dt_n \ldots dt_0 e^{i\{E_n t_n + \ldots + E_1 t_1 - E_0 t_0\}}$$

$$\times \langle s' \left| \frac{\delta^n [(\delta S/\delta\varphi_0(t_0))S^+]}{\delta\varphi_n(t_n)\ldots\delta\varphi_1(t_1)} \right| s \rangle, \qquad (1)$$

where $\mathbf{q}_0$ is the momentum of the incoming π mesons and $\mathbf{q}_n \ldots \mathbf{q}_1 \ldots$ are the momenta of the outgoing mesons; each of the momenta $\mathbf{q}_n$ is understood to form a scalar product with the corresponding $\delta S/\delta\varphi$; $v_i = v(|\mathbf{q}_i|)$ is the Fourier transform of the smeared out fixed nucleon, and $\varphi_i(t_i)$ can be written in the form

$$\varphi_i(t_i) \equiv \varphi_{\gamma_i \rho_i}(t_i)$$

$$= \frac{-i}{(2\pi)^{3/2}} \int \frac{d\mathbf{q}_i}{\sqrt{2E_i}} q_{\gamma_i} v_i \left\{ a_{\rho_i}^{(+)}(\mathbf{q}_i) e^{iE_i t_i} - a_{\rho_i}^{(-)}(\mathbf{q}_i) e^{-iE_i t_i} \right\} \qquad (2)$$

and is essentially the field operator of the i-th π meson.

Owing to the assumption of a fixed and smeared out nucleon, (2) depends only on the time variable.

Between the π meson creation and annihilation operators and the operator S there hold the following commutation relations:

$$[a_\rho^{(-)}(\mathbf{q}),\ S] = -\frac{i}{(2\pi)^{3/2}} \frac{v q_\gamma}{\sqrt{2E}} \int e^{-iEt} \frac{\delta S}{\delta\varphi_{\gamma\rho}(t)} dt,$$

$$[S,\ a_\rho^{(+)}(\mathbf{q})] = +\frac{i}{(2\pi)^{3/2}} \frac{v q_\gamma}{\sqrt{2E}} \int e^{+iEt} \frac{\delta S}{\delta\varphi_{\gamma\rho}(t)} dt. \qquad (3)$$

The pseudoscalar nature of the π mesons leads to the well known factors in (1) and (3). They are of no particular importance for our purposes.

In order to bring the matrix element of the considered process to the form (1) one has to utilize the stationary character of

$$S|\alpha\rangle = |\alpha\rangle, \tag{4}$$

where $|\alpha\rangle$ is either the vacuum or a one-particle state. This way one can immediately express the S matrix element in terms of the retarded transition amplitude. For this purpose we utilize the translational invariance of the expression and write $S_{n,1}$ in the following form:

$$S_{n,1} = -2\pi i\delta(E_n + \ldots + E_1 - E_0)$$
$$\times \frac{v_n \ldots v_0}{(2^{n+1}E_n \ldots E_0)^{1/2}}\, T^{ret}_{n,1}(E_n, \ldots, E_1; E_0),$$
$$T^{ret}_{n,1}(E_n, \ldots E_1;\ E_0) =$$
$$= \frac{\mathfrak{q}_n \ldots \mathfrak{q}_0}{(2\pi)^{3(n+1)/2}}(-i)^n i \int dt_n \ldots dt_1 e^{i(E_n t_n + \ldots + E_1 t_1)}$$
$$\langle s' \left| \frac{i\delta^n[(\delta S/\delta\varphi_0(0))S^+]}{\delta\varphi_n(t_n)\ldots\delta\varphi_1(t_1)} \right| s\rangle. \tag{5}$$

Starting with the Hermitian conjugate of the matrix element $S_{n,1}$ we find for the advanced transition amplitude

$$T^{av}_{n,1}(E_n, \ldots, E_1;\ E_0)$$
$$= \frac{\mathfrak{q}_n \ldots \mathfrak{q}_0}{(2\pi)^{3(n+1)/2}}(-i)\, i \int dt_n \ldots dt_1 e^{i(E_n t_n + \ldots + E_1 t_1)}$$
$$\times \langle s' \left| \frac{-i\delta^n[(\delta S^+/\delta\varphi_0(0))S]}{\delta\varphi_n(t_n)\ldots\delta\varphi_1(t_1)} \right| s\rangle. \tag{6}$$

The causality conditions can be expressed in our static case in the following two ways:

$$\delta\left(\frac{\delta S}{\delta\varphi(0)}S^+\right)\Big/\delta\varphi'(t') = 0 \qquad \text{for } t' < 0,$$
$$\delta\left(\frac{\delta S^+}{\delta\varphi(0)}S\right)\Big/\delta\varphi'(t') = 0 \qquad \text{for } t' > 0. \tag{7}$$

From this it follows that

$$T^{ret}_{n,1} = 0 \quad \text{for } t_l < 0, \quad l = 1, \ldots n;$$
$$T^{av}_{n,1} = 0 \quad \text{for } t_l > 0, \quad l = 1, \ldots, n, \tag{8}$$

which is the justification for the terms "advanced" and "retarded."

The conditions (8) will allow to establish dispersion relations.

2. DISPERSION RELATIONS

We consider the expressions (5) and (6) to be functions of n complex variables $E_l = a_l + ib_l$ ($l = 1 \ldots n$). One sees from the causality conditions (7) that $T^{ret}_{n,1}(E_n, \ldots E_1; E)$ is an analytic function of E_l for Im $E_l > 0$ while $T^{av}_{n,1}(E_n, \ldots \ldots E_1; E)$ is analytic for Im $E_l < 0$.

In order to establish the behavior of the functions $T^{ret}_{n,1}$ and $T^{av}_{n,1}$ for real values of the arguments we consider the difference of these functions which is proportional to the antihermitian part of the transition amplitude, $A_{n,1}$. For this we exchange $(\delta S^*/\delta\varphi_0)S$ in $T^{av}_{n,1}$ by $-S^*(\delta S/\delta\varphi_0)$ and perform explicitly the functional derivative. Then we obtain the following expression (here E_l are real)

$$T^{ret}_{n,1} - T^{av}_{n,1} = 2iA_{n,1}$$
$$= \frac{\mathfrak{q}_n \ldots \mathfrak{q}_0}{(2\pi)^{3(n+1)/2}}(-i)^n i \int dt_n \ldots dt_1 e^{i(E_n t_n + \ldots + E_1 t_1)}$$
$$\times \mathfrak{S}i\left\{-\langle s' \left| \frac{-i\delta S^+}{\delta\varphi_n} \frac{i\delta^n S}{\delta\varphi_{n-1}\ldots\delta\varphi_0} \right| s\rangle \right.$$
$$+\langle s' \left| \frac{i\delta^n S}{\delta\varphi_0\ldots\delta\varphi_{n-1}} \frac{-i\delta S^+}{\delta\varphi_n} \right| s\rangle - \langle s' \left| \frac{-i\delta^3 S^+}{\delta\varphi_n\delta\varphi_{n-1}} \frac{i\delta^{n-1}S}{\delta\varphi_{n-2}\ldots\delta\varphi_0} \right| s\rangle$$
$$+\langle s' \left| \frac{i\delta^{n-1}S}{\delta\varphi_0\ldots\delta\varphi_{n-2}} \frac{-i\delta^2 S^+}{\delta\varphi_{n-1}\delta\varphi_n} \right| s\rangle$$
$$-\ldots - \langle s' \left| \frac{-i\delta^n S^+}{\delta\varphi_n\ldots\delta\varphi_1} \frac{i\delta S}{\delta\varphi_0} \right| s\rangle$$
$$\left. +\langle s' \left| \frac{i\delta S}{\delta\varphi_0} \frac{-i\delta^n S^+}{\delta\varphi_1\ldots\delta\varphi_n} \right| s\rangle \right\}. \tag{9}$$

Here $\mathfrak{S}$ is a symmetrization operator defined by the following relations:

$$\mathfrak{S}f(n;\ n-1, \ldots, 1)$$
$$= f(n;\ n-1, \ldots, 1) + f(n-1;\ n, n-2, \ldots, 1) + \ldots;$$
$$\mathfrak{S}f(n,\ n-1;\ n-2, \ldots, 1)$$
$$= f(n, n-1;\ n-2, \ldots, 1)$$
$$+ f(n, n-2;\ n-1, n-3, \ldots, 1) + \ldots$$
$$\ldots + f(n,\ 1;\ n-2, \ldots, 2, n-1)$$
$$+ f(n-1, n-2;\ n, n-3, \ldots, 1) + \ldots$$
$$\ldots + f(n-1, 1;\ n, n-3, \ldots, 2, n-2)$$
$$+ \ldots + f(2, 1;\ n, \ldots, 3).$$

In an analogous fashion one can write down at once expressions for $\mathfrak{S}f(n, \ldots, k;\ k-1, \ldots, 1)$.

Utilizing the translational invariance of the matrix elements one can write (9) as a sum of terms of the following form (we take as an example the fourth term of (9))

$$2\pi i \sum_i \mathfrak{S}\delta(E_n + E_{n-1} + E_i)$$
$$\times T_{n-1,i}(-E_0, E_1, \ldots, E_{n-2}; E_i) T^+_{i,2}(E_i, -E_{n-1}, -E_n),$$

where

$$T_{n-1,i}(-E_0, E_1, \ldots, E_{n-2}; E_i)$$

$$= \frac{q_0 \ldots q_{n-2}}{(2\pi)^{3(n-1)/2}} (-i)^{n-2} i \int dt_1 \ldots dt_{n-2} e^{i(E_1 t_1 + \ldots E_{n-2} t_{n-2})}$$

$$\times \langle s' \left| \frac{i\delta^{n-1} S}{\delta\varphi_0 \ldots \delta\varphi_{n-2}} \right| s, i \rangle.$$

We now introduce new variables for the E_l

$$E_l = \nu_l E, \quad l = 1, \ldots, n, \quad E_0 = E;$$

$$\sum_{l=1}^{n} \nu_l = 1, \quad \nu_l = \text{const} \quad (\text{real}) \tag{10}$$

(on the nonuniqueness of this choice of variables and its consequences see Sec. 4). Then $T^{ret}_{n,1}$ and $T^{av}_{n,1}$ are analytic functions in the upper and lower half of the complex E-plane respectively.

If we now consider only strong interactions in our process then the energy E_i can assume only the values $E_i = 0$ and $E_i \geq \mu$ where μ is the mass of the π meson. As a consequence of this the difference $T^{ret}_{n,1} - T^{av}_{n,1}$ has at $E = 0$ a δ-function singularity and equals zero for $0 < |E| < \mu$. One can thus make the following statement: $T^{ret}_{n,1}(E, \nu)$ and $T^{av}_{n,1}(E, \nu)$ define in the complex E plane a single analytic function which has branch cuts only on the real axis and has there one δ-function singularity (see Fig. 1).

FIG. 1

One can apply the Cauchy theorem to this function thus obtaining dispersion relations. Assuming that $A_{n,1}(E, \nu)$ decreases for $E \to \infty$ like $1/E$ or faster these have the form

$$D_{n,1}(E_n, \ldots, E_1; E) = \frac{1}{\pi} P \int_{-\infty}^{+\infty} \frac{A_{n,1}(\varepsilon, \nu)}{\varepsilon - E} d\varepsilon. \tag{11}$$

For negative energies the integral can be obtained from the relations

$$T_{n,1}(-E_n, \ldots, -E_1; -E) = P_{s's} T^{+}_{1,n}(E; E_1, \ldots, E_n)$$
$$= P_{s's} T^{*}_{n,1}(E_n, \ldots, E_1; E).$$

where $P_{s's}$ — operator exchanging initial and final spin and isospin of the nucleon.

Finally, writing explicitly the one-nucleon term we obtain for the process $\pi + N \to n\pi + N$ the dispersion relation

$$D_{n,1}(E_n, \ldots, E_1; E) = \frac{1}{\pi} P \int_{\mu}^{\infty} \left\{ \frac{A_{n,1}(\varepsilon, \nu)}{\varepsilon - E} + \frac{P_{s's} A^{+}_{n,1}(\varepsilon, \nu)}{\varepsilon + E} \right\} d\varepsilon$$
$$+ \sum_{s_i} \Im \left\{ \frac{1}{E_n} (T^{+}_{1,0} T_{0,n} - T_{n,0} T^{+}_{0,1})_{\varepsilon=0} \right.$$
$$+ \ldots + \frac{1}{E_n + E_{n-1}} (T^{+}_{2,0} T_{0,n-1} - T_{n-1,0} T^{+}_{0,2})_{\varepsilon=0}$$
$$\left. + \frac{1}{E} (T^{+}_{n,0} T_{0,1} - T_{1,0} T^{+}_{0,n})_{\varepsilon=0} \right\}. \tag{12}$$

The summation is over the spin and isospin indices of the nucleon in the intermediate state.

The physical region of the integration (11) begins at the point $E_\pi = \mu/\bar{\nu}$ where $\bar{\nu} = \min(\nu_1, \ldots, \nu_n)$. Therefore the inequality $E_\pi \geq n\mu$ always holds, the equal sign applying when the outgoing mesons all have equal energy. One sees from this that except in the case of elastic scattering ($n = 1$) there always exists a large unobservable region in the dispersion integral. It therefore is appropriate to bo over from the dispersion relation to the corresponding equation of the Chew-Low type.

3. EQUATIONS OF THE CHEW-LOW TYPE

If one knows the dispersion relation for any process in the fixed nucleon approximation one can immediately obtain the Chew Low type equation for this process.

To this end we insert into the dispersion relation the explicit expression for the antihermitian part of the transition amplitude. The expression thus obtained can be easily integrated because of the δ-function. In our case we shall this way obtain an explicit expression for $D_{n,1}(E, \ldots, E_1; E)$. Utilizing

$$T_{n,1} = D_{n,1} + iA_{n,1} \quad \text{и} \quad \frac{1}{x \pm i\delta} = P\frac{1}{x} \mp i\pi\delta(x)$$

one can immediately write down the following relation:

$$T_{n,1}(E_n, \ldots, E_1; E)$$
$$= -\sum_i \Im \left\{ \frac{(T^{+}_{1,i}(\varepsilon_n; E_i) T_{i,n}(E_i; -\varepsilon_{n-1}, \ldots, -\varepsilon_1, \varepsilon))_{\varepsilon_n = E_i}}{E_i - E_n - i\delta} \right.$$
$$+ \frac{(T_{n,i}(-\varepsilon, \varepsilon_1, \ldots, \varepsilon_{n-1}; E_i) T^{+}_{i,1}(E_i; -\varepsilon_n))_{\varepsilon_n = -E_i}}{E_i + E_n + i\delta}$$
$$+ \frac{(T^{+}_{2,i}(\varepsilon_n, \varepsilon_{n-1}; E_i) T_{i,n-1}(E_i; -\varepsilon_{n-2}, \ldots, -\varepsilon_1, \varepsilon))_{\varepsilon_n + \varepsilon_{n-1} = E_i}}{E_i - E_n - E_{n-1} - i\delta}$$
$$+ \frac{(T_{n-1,i}(-\varepsilon, \varepsilon_1, \ldots, \varepsilon_{n-2}; E_i) T^{+}_{i,2}(E_i; -\varepsilon_{n-1}, -\varepsilon_n))_{\varepsilon_n + \varepsilon_{n-1} = -E_i}}{E_i + E_n + E_{n-1} + i\delta}$$
$$+ \ldots + \frac{(T^{+}_{n,i}(\varepsilon_n, \ldots, \varepsilon_1; E_i) T_{i,1}(E_i; \varepsilon))_{\varepsilon = E_i}}{E_i - E - i\delta}$$
$$\left. + \frac{(T_{1,i}(-\varepsilon; E_i) T^{+}_{i,n}(E_i; -\varepsilon_1, \ldots, -\varepsilon_n))_{\varepsilon = -E_i}}{E_i + E + i\delta} \right\}. \tag{13}$$

In view of the equality

$$\frac{\delta S}{\delta\varphi} S^{+} - S^{+} \frac{\delta S}{\delta\varphi} = \frac{\delta S^{+}}{\delta\varphi} S - S \frac{\delta S^{+}}{\delta\varphi}$$

one can replace on the right hand side $T^{+}_{m,k}(E_m; E_k) \rightleftarrows T^{+}_{m,k}(E_m; E_k)$ (this not identical with hermitian conjugation).

Equations (12) and (13) are symmetrical with respect to the outgoing mesons and, furthermore, have the required crossing symmetry. The terms of (13) correspond to the diagrams shown in Fig. 2 (for the case $n = 3$).

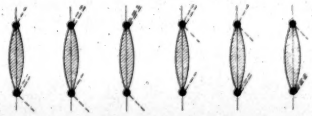

FIG. 2

4. THE PROCESS $\pi + N \rightarrow 2\pi + N$

We now shall show by means of the example $\pi + N \rightarrow 2\pi + N$ what are the consequences of the choice (10) of the variables.

For this purpose we compare the results of the present paper with those of Zoellner et al.[4] where the choice had been made

$$E_1 = (E + \Delta)/2, \quad E_2 = (E - \Delta)/2. \qquad (14)$$

In both cases we have two variables of which one has to be kept constant in order to establish dispersion relations. This can be done in several ways (particularly in the case of $n\pi$ mesons). In reference 4 the differnce $E_1 - E_2 = \Delta$ was kept constant while in the present paper this was done with their ratio $E_1/E_2 = \nu_1/\nu_2$.

This possibility of choosing different variables has both a mathematical and a physical meaning. It was shown in reference 4 that the choice (14) for the variables leads to limiting conditions for the existence of the dispersion relation or of the Chew-Low equation since the region on the real axis where $T^{ret} = T^{av}$ exists only for $|\Delta| < 2\mu$.

However, as can be seen from the present work, there do not exist such limiting conditions for the ν_l if the choice (10) has been made (even in the case of arbitrary n).

In fixing the variables one has to make sure that the analyticity of the amplitude is guaranteed and that the symmetry of the system is not disturbed. For example, if one chooses the variables in the form $E_2 = \text{const} = c$ and $E_1 = E - c$, then one finds that part of the spectrum of the amplitude A does not depend on E due to the presence of terms of the type $\sim \sum_i \delta(E_i \pm E_2)(E_i \geq \mu)$. It is thus impossible, within the framework of the present model, to establish exact relations for D (dispersion relations) or for T (Chew-Low type equations).

This way one can obtain for the process $\pi + N \rightarrow n\pi + N$ (with $n \geq 2$) in the fixed nucleon case different dispersion relations and Chew-Low type equations which differ from each other by the different ways of choosing the $(n-1)$ appearing parameters.*

One can suppose that the final results of an exact evaluation of the different dispersion relations (which, obviously, for $n > 1$ is practically impossible to achieve) will be identical. However, this cannot be assumed for the approximate expressions following from the respective dispersion relations or Chew-Low type equations. So, for example, the one-nucleon terms in reference 4 have the form† $T_{1,1}(\Delta)$ while here they are $T_{1,1}(0)$.

The common characteristic of all these variants of the dispersion relations and Chew-Low equations is that in all expressions the energy is conserved. This is due to the circumstance that always the hermitian part of the transition amplitude is expressed as a dispersion integral over the antihermitian part.

In references 9 — 11, Chew-Low equations have been obtained for the process $\pi + N \rightarrow 2\pi + N$ where the utilized quantities did not lie on the energy shell. The authors, for example, assumed that the argument of the amplitude of the elastic process (the one-nucleon term) lies in the observable energy region. In the here considered case where energy conservation is always required the argument of the one-nucleon term lies in the unobservable region of the process and has to be calculated by means of the dispersion relations for the case of elastic scattering. The results of the corresponding computations will be published in a subsequent paper.

The author expresses his thanks to A. A. Logunov for numerous discussions and suggestions.

[1] A. A. Logunov and A. N. Tabkhelidze, Сообщения АН ГрузССР, (Commun. Acad. Sci. Georgian S.S.R.) **18**, 19, 533 (1957).

[2] R. E. Norton and A. Klein, Phys. Rev. **109**, 584 (1958).

*In the relativistic case the number of variables is still considerably larger (see, e.g., reference 8).

†In several expressions of reference 4, the symbols used differ from those in the present paper.

[3] N. N. Bogolyubov and D. V. Shirokov, Введение в теорию квантованных полей (Introduction to the Quantum Theory of Fields), Moscow, 1957.

[4] Zoellner, Chrustaljow, Serebrjakow, and Lesnow, Z. Naturforsch. **13**, 449 (1958).

[5] G. C. Wick, Revs. Modern Phys. **27**, 339 (1955).

[6] Castillejo, Dalitz, and Dyson, Phys. Rev. **101**, 453 (1956).

[7] F. J. Dyson, Phys. Rev. **106**, 157 (1957).

[8] W. Zoellner, Dokl. Akad. Nauk (U.S.S.R.) **123**, 838 (1957), Soviet Phys."Doklady" **3**, 1222 (1958).

[9] J. Franklin, Phys. Rev. **105**, 1101 (1957).

[10] L. S. Rodberg, Phys. Rev. **106**, 1090 (1957).

[11] R. Omnes, Nuovo cimento **5**, 983 (1957); **6**, 780 (1957).

Translated by M. Danos
215

WALL PROBE IN A MAGNETIC FIELD

I. K. FETISOV

Submitted to JETP editor Setember 5, 1958

J. Exptl. Theoret. Phys. (U.S.S.R.) **36**, 1110-1118 (April, 1959)

The current flowing to a wall probe in a strong magnetic field is computed in the case when the motion of the electrons can be considered free along the magnetic field and diffuse across the field.

SPIVAK and Reikhrudel',[1] in a series of articles, have extended the Langmuir theory of probe measurements to include the case of a weak magnetic field (~ 10 oe), when the condition $\rho_e \gg a$ is satisfied (ρ_e is the Larmor radius of the electron, and a is the dimension of the probe).

In a magnetic field H, the electron moves along a circle of radius $\rho_e = mvc/eH$ (e, m, and v are the charge, mass, and velocity of the electron, respectively). The center of the circle moves in space only because of the collisions between the electron and other particles, or under the influence of the plasma fields. After each collision the center of the circle is displaced on the average by ρ_e. As a result, ρ plays the role of effective mean free path in a direction perpendicular to the magnetic field. In fields of ~ 1000 oe, the value of ρ is $\sim 10^{-3}$ cm and it is impossible to satisfy the condition $\rho_e \gg a$, since the dimension of the probe is usually ~ 1 mm. For this reason, the Spivak-Reikhrudel' theory cannot be used to interpret probe data on discharges in strong magnetic field. Nevertheless, the Larmor radius of positive ions is usually noticeably greater than the dimension of the probe, and the magnetic field can be neglected in calculating the ion current.

Bohm, Barhop, and Massey[2] examined in detail the question of the ion current flowing in the presence of a strong magnetic field into a negatively-charged probe. According to reference 2, the ion flow is independent, within 20%, of the ion temperature, as long as the latter is lower than the electron temperature. The following formula is given for the total current:

$$J = 0.4 n_0 S \sqrt{2kT/M},$$

where S is the probe area, M the ion mass, and n_0 the electron concentration outside the layer. The criterion of the validity are the inequalities $\rho_+ \gg a$ and $\lambda_+ \gg a$, which are readily satisfied in low-pressure discharges. This formula should therefore give the correct order of magnitude of the ion current.

As to the electron portion of the probe characteristic, Bohm, Barhop, and Massey,[2] in view of the difficulty in its interpretation, restricted themselves only to a positively-charged probe, which repels the ions. Their premises are equivalent to the assumption of a plasma of infinite extent along the direction of the magnetic field.

The case most frequently encountered in practice is the reverse, when the length of the plasma along the magnetic field is $l \lesssim \lambda_e$, where λ_e is the range of the electron along the magnetic field. It is absolutely impossible to neglect in this case the finite extent of the plasma in this direction.

A compensated ion beam is used in many physical setups. One of the methods used to investigate the properties of the ion beam is the probe method. The theory of probe measurements in compensated ion beams is therefore of definite practical interest. In the first part of this paper we calculate the current into the probe in the limiting case, when the concentration of the slow ions is negligibly small compared with the concentration of the fast ions of the beam. In the second part we calculate the current into the probe for the opposite limiting case, when the concentration of the slow ions is high. This case corresponds to a discharge plasma. The motion of the electrons along the magnetic field is assumed free, $\lambda_e > 1$, and the transverse motion is assumed diffuse with a diffusion coefficient D.

I. PROBE MEASUREMENTS IN A COMPENSATED ION BEAM

1. Statement of the Problem

A quasi-neutral plasma, produced by ionization of the residual gas by fast ions from the beam, is located between conducting planes AB and CD, (Fig. 1). The density of the current of fast ions is constant along z. The magnetic field H is directed perpendicular to the planes that bound the plasma. The plasma is infinite in the direction perpendicular to the magnetic field.

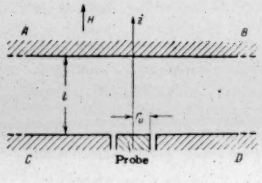

FIG. 1. Geometry of the problem.

Located in one of the planes (CD, Fig. 1) is a probe, which is a disk of radius r_0, the surface of which is perpendicular to the magnetic field. The potential of the probe is measured relative to the potential of plane CD. To be specific, we consider a case when the plane AB is negative relative to CD. In this case the plasma electrons cannot fall on AB. The case in which both planes are of the same potential can be considered in an analogous manner.

The electron current $\mathbf{j}$ satisfies the equation

$$\operatorname{div} \mathbf{j} = Q, \tag{1}$$

where Q is the ionization density. In a cylindrical coordinate system with the z axis passing through the center of the probe and directed along the magnetic field, we can rewrite (1) as

$$\nabla_\perp j_\perp + \partial j_z / \partial z = Q. \tag{2}$$

The properties of the plasma change little in the z direction, except for the thin layer at the walls, of thickness on the order of the Debye radius. Integration of Eq. (2) with respect to z yields

$$l\nabla_\perp j_\perp = -j_z|_{z=0} + Ql. \tag{3}$$

It is obvious that a change in the probe potential produces an axially symmetrical change in the current $\mathbf{j}$; Eq. (3) can therefore be averaged over the azimuth angle. This yields

$$\frac{l}{r}\frac{dr j_r}{dr} = -j_z|_{z=0} + Ql. \tag{4}$$

The density of the electron current on the wall, in the presence of a potential barrier, is: outside the probe ($r > r_0$)

$$j_z|_{z=0} = (nv/4)\, e^{-U_{pl}/T}, \tag{5}$$

and inside the probe ($r \le r_0$)

$$j_z|_{z=0} = (nv/4)\, e^{-(U_{pl}-U_s)/T}. \tag{6}$$

Here n is the concentration of the electrons, equal to the concentration of the fast ions, T is the electron temperature in volts, U_{pl} is the potential of the plasma relative to the wall, $U_{pl} > 0$, and v is a certain velocity, which coincides with the mean velocity of random motion of the electrons in the case of Maxwellian distribution.

We denote the current corresponding to $U_{pr} = 0$ by j_z^0:

$$j_z^0 = (nv/4)\, e^{-U_s/T}, \tag{7}$$

where U_0 is the potential of the unperturbed plasma.

Using (5), (6), and (7), we can rewrite (4) as

$$\frac{l}{r}\frac{dr j_r}{dr} = -j_z^0 - \frac{nv}{4} e^{-U_s/T}\left(e^{-(\varphi - U_{pr})/T} - 1\right) + Ql, \tag{8}$$

where $\varphi = U_{pl} - U_0$ is the perturbation of the plasma potential when a potential U_{pr} is applied to the probe.

Inserting into (8) an expression for j_r in terms of the coefficient of diffusion of the electrons across the magnetic field,

$$j_r = -D\frac{\partial n}{\partial r} + \frac{D}{T} n \frac{\partial U_0}{\partial r} + \frac{D}{T} n \frac{\partial \varphi}{\partial r}, \tag{9}$$

and attributing the terms that do not contain φ to j_z^0, i.e., putting

$$j_z^0 = \frac{lD}{r}\frac{\partial}{\partial r} r \frac{\partial n}{\partial r} - \frac{lD}{r}\frac{\partial}{\partial r} r \frac{n}{T}\frac{\partial U_0}{\partial r} + Ql, \tag{10}$$

we obtain for $r \le r_0$

$$\frac{d^2\varphi}{dr^2} + \frac{1}{r}\frac{d\varphi}{dr} = Tk^2\left(1 - e^{-(\varphi - U_{pr})/T}\right) \tag{11}$$

and for $r > r_0$

$$\frac{d^2\varphi}{dr^2} + \frac{1}{r}\frac{d\varphi}{dr} = Tk^2\left(1 - e^{-\varphi/T}\right), \tag{12}$$

where

$$k^2 = (v/4Dl)\, e^{-U_s/T}. \tag{13}$$

Let us estimate the value of k^2. Comparing (13) and (7), we have

$$k^2 = j_z^0/nDl.$$

If a is the characteristic length over which the drop in n, U_0, and T takes place, then, taking (10) into account,

$$k^2 \sim \frac{1}{a^2} + \frac{U_0}{Ta^2} + \frac{Q}{Dn} \sim \frac{U_0}{Ta^2} + \frac{Q}{Dn}. \tag{14}$$

The probe current is

$$J = \int_0^{r_0} 2\pi r j_z|_{z=0}\, dr$$

$$= \int_0^{r_0} 2\pi r \frac{nv}{4} e^{-U_s/T}\left(e^{-(\varphi - U_{pr})/T} - 1\right) dr + J_0. \tag{15}$$

Here J_0 is the probe current when $U_{pr} = 0$. Using (11), we get

$$J - J_0 = -2\pi nDl \frac{x_0}{T} \frac{d\varphi}{dx}\Big|_{x=x_0}, \quad (16)$$

where $x = kr$ and $x_0 = kr_0$. To find $d\varphi/dx$, it is necessary to solve Eqs. (11) and (12) with suitable boundary conditions. These equations can be generally solved only numerically. In particular cases, however, results can be obtained without resorting to numerical methods.

2. Low Probe Potentials

The most simple case for which an approximate solution of (11) and (12) is possible when the probe potential is low. Since $|\varphi| \leq U_{pr}$ always, we have also $|\varphi - U_{pr}|/T \ll 1$ when $|U_{pr}| \ll T$, and $\exp\{-(\varphi - U)/T\}$ can therefore be expanded into a series, with accuracy to first-order quantities. Solving the resultant equations and substituting the expression obtained for φ in (16), we obtain for the probe current

$$J - J_0 = 2\pi nDl \frac{K_1(x_0) I_1(x_0)}{I_0(x_0) K_1(x_0) + I_1(x_0) K_0(x_0)} x_0 \frac{U_{pr}}{T}, \quad (17)$$

where $I_n(x)$ is the Bessel function of imaginary argument and $K_n(x)$ is the MacDonald function.

The probe thus has a linear characteristic at low probe potentials. It must be noted that for low probe potentials the solution is valid for all values of $x_0 = kr_0$. At large values of x_0 we obtain, using the asymptotic values of the functions I_0, I_1, K_0, and K_1,

$$J - J_0 = \pi nDlkr_0 U_{pr}/T. \quad (18)$$

It follows from (18) and (17) that the probe current is proportional to the probe radius at large kr_0 and to the square of the radius at small kr_0. This is due to the fact that the potential barrier decreases essentially at the edge of the probe, and the electrons therefore spill out over the ring near the edge of the probe, without being able to reach its inner parts. If the probe dimension kr_0 is sufficiently small, the electrons spill out over the entire probe area.

3. The General Case

Equations (11) and (12) were solved approximately for the limiting cases of small ($kr_0 \ll 1$) and large ($kr_0 \gg 1$) probes. The physical meaning of the concepts "small" and "large" probe is as follows. If there is no ionization near the probe ($Q = 0$) or if it is very small, and if U_0/T is relatively small, then, considering (14) and the fact that $r_0/a \ll 1$, we get $kr_0 \ll 1$. This is the case of a small probe. But if Q is sufficiently large, and the coefficient of transverse diffusion, D, is small, corresponding to a strong magnetic field, the second term will be large and $kr_0 \sim r_0\sqrt{Q/Dn} \gg 1$, which is the condition of a large probe. Approximate solutions of Eqs. (11) and (12), and consequently the probe currents, were found for these two cases. For intermediate probe dimensions, these solutions were interpolated over the probe dimensions for each U_{pr}/T.

Figure 2a shows a plot of j vs. the probe dimension x_0 for various probe potentials, with the probe current determined from the following formula:

$$J - J_0 = 0.4\pi nDlj. \quad (19)$$

The dotted curves delimit the interpolation region. For comparison, Fig. 2b shows the dependence of the current on the probe dimension x_0 (in the same units) for the Lngmuir case.

It follows from these results that at small probe dimensions, no matter what the probe potential, the probe current, as in the Langmuir case, is proportional to the square of the probe radius, i.e., the density of the electron current is more or less uniform over the probe. If the probe is large, when $x_0 \gg 1$, the probe current, unlike the Langmuir case, is proportional to first power of x_0, i.e., the density of the electron current is large essentially on the periphery of the probe, and is small near its center.

At sufficiently high negative probe potentials the dependence of the probe current on the probe potential is nearly exponential. This permits de-

FIG. 2. Dependence of probe current on probe dimensions: a – in the presence of a magnetic field, b – in the absence of a magnetic field. Curve 1) $U_{pr}/T = 0.3$; 2) $U_{pr}/T = 1$; 3) $U_{pr}/T = 2$; 4) $U_{pr}/T = 4$; 5) $U_{pr}/T = 6$; 6) $U_{pr}/T = 8$; 7) $U_{pr}/T = 10$.

termination of the electron temperature by the Langmuir method.

Using the curves of Fig. 2 and Eq. (19), and knowing T, we can determine x_0. If x_0 is known, the coefficient of transverse electron diffusion, D, can be determined from (19). Using Eq. (13) for k, we can determine U_0 from x_0.

II. PROBE MEASUREMENTS IN GAS-DISCHARGE PLASMA

4. Statement of the Problem

We consider the limiting case, when the concentration of the slow ions is large compared with the concentration of the fast ions in the plasma discharge.

The plasma consists of electrons with a temperature T and of slow ions with a temperature T_+, with $T_+ \ll T$. The slow ions are formed by ionization of the residual gas by external sources, by fast ions, and by electrons; they also arise through ion charge exchange. In this case the change produced in the plasma potential by a change in the probe potential is limited to a small quantity, on the order of T_+. The potential of the plasma, U_0, can therefore be considered constant with sufficient degree of accuracy, inasmuch as $T_+ \ll T$ and $U_0 > T$. A change in the probe potential will influence the ion and electron concentration. The gometry of the problem remains the same.

Under these assumptions, Eq. (3) holds for the electron current. On the other hand

$$j_\perp = -D\nabla_\perp n + \frac{D}{T} n \nabla_\perp U_0. \tag{20}$$

We put $n = n_0 + \nu$, where n_0 is the electron concentration at $U_{pr} = 0$ and ν is the change in electron concentration due to the change in the probe potential U_{pr}.

The ionization density may be a function of the electron concentration n, provided the electron temperature is sufficiently high. We assume $Q(n) = \beta + \alpha n$, where β is the ionization density due to external ionization sources, such as the discharge radiation and α is the coefficient of ionization by the electrons.

Inserting into (3) the value of $j_\perp$ from (20) and Q, and attributing the terms not containing ν to the probe current density j_z^0 at $U_{pr} = 0$, i.e., putting

$$j_z^0 = lD\nabla_\perp^2 n_0 - \frac{lD}{T} \nabla_\perp n_0 \nabla_\perp U_0 - \frac{lD}{T} n_0 \nabla_\perp^2 U_0 + \beta l + \alpha n_0 l, \tag{21}$$

we get

$$j_z|_{z=0} - j_z^0 = \alpha \nu l + lD\nabla_\perp^2 \nu - \frac{lD}{T} \nabla_\perp \nu \nabla_\perp U_0 - \frac{lD}{T} \nu \nabla_\perp^2 U_0. \tag{22}$$

Considering that the change in electron concentration ν, produced by a change in the probe potential, is axially symmetric, we average Eq. (22) over the azimuth. The third term in (22) then vanishes. It is easy to show that $\overline{\nabla_\perp^2 U_0} \cong \nabla_\perp^2 U_0(0)$, with sufficient accuracy. We shall henceforth denote this quantity by $\nabla_\perp^2 U_0$. Thus

$$j_z|_{z=0} - j_z^0 = \alpha \nu l + Dl\nabla_\perp^2 \nu - \frac{Dl}{T} \nu \nabla_\perp^2 U_0. \tag{23}$$

On the other hand,

$$j_z|_{z=0} = \frac{(n_0 + \nu)\, v}{4} e^{-(U_e - U_{pr})/T}, \tag{24}$$

$$j_z^0 = \frac{n_e v}{4} e^{-U_e/T}. \tag{25}$$

Insertion of (24) and (25) into (23) results in an equation for ν:

$$\nabla_\perp^2 \nu - \left(\frac{1}{T} \nabla_\perp^2 U_0 - \frac{\alpha}{D} + \frac{v}{4Dl} e^{-(U_e - U_{pr})/T}\right) \nu = \frac{n_e v}{4Dl} e^{-U_e/T} \left(e^{U_{pr}/T} - 1\right). \tag{26}$$

Equation (26) has been derived for the region over the probe, i.e., for $r \leq r_0$. Outside the probe ($r > r_0$) it is necessary to put in (26) $U_{pr} = 0$. This yields

$$\nabla_\perp^2 \nu - \left(\frac{1}{T} \nabla_\perp^2 U_0 - \frac{\alpha}{D} + \frac{v}{4Dl} e^{-U_e/T}\right) \nu = 0. \tag{27}$$

To find the electron component of the current into the probe by integrating $J_z|_{z=0}$, it is necessary to find ν in accordance with Eq. (24).

5. Electron Current in Probe

A. Absence of Ionization. In the region above the probe, ν changes substantially at distances $\sim r_0$, while U_0 changes substantially at distances on the order of a, where $a \gg r_0$ is the characteristic length for the potential. It is therefore possible to neglect the term $\nu\nabla_\perp^2 U_0/T \sim U_0\nu/Ta^2$ as compares with $\nabla_\perp^2 \nu \sim \nu/r_0^2$ for $r \leq r_0$, provided U_0/T is not too large.

We introduce

$$\omega^2 = k^2 + \frac{1}{T} \nabla_\perp^2 U_0, \tag{28}$$

where k^2 is determined from (13). Taking this into account, Eqs. (26) and (27) yield for ν, in the region $r \leq r_0$:

$$\nabla_{\perp}^2 \nu - \nu k^2 e^{U_{pr}/T} = \frac{n_0 v}{4Dl} e^{-U_{pr}/T} (e^{U_{pr}/T} - 1) \quad (29)$$

and for $r > r_0$

$$\nabla_{\perp}^2 \nu - \omega^2 \nu = 0. \quad (30)$$

From (13) and (25) we find $j_z^0 = k^2 n_0 D l$. Making use of (21), we get

$$k^2 = \frac{\nabla_{\perp}^2 n_0}{n_0} - \frac{\nabla_{\perp} n_0}{n_0} \frac{\nabla_{\perp} U_0}{T} \sim \frac{1}{a^2}.$$

Consequently $kr_0 \sim r_0/a \ll 1$. Solving (29) and (30), we obtain the distribution of electron concentration. After inserting ν into (24) and integrating with respect to r from $r = 0$ to $r = r_0$, we obtain the final equation for the electron current in the probe:

$$J_- - J_-^0 = \frac{4J_-^0}{kr_0} \sinh \frac{U_{pr}}{2T} \times \frac{K_1(\omega r_0) I_1(ke^{U_{pr}/2T} r_0)}{I_0(ke^{U_{pr}/2T} r_0) K_1(\omega r_0) + \frac{k}{\omega} e^{U_{pr}/2T} I_1(ke^{U_{pr}/2T} r_0) K_0(\omega r_0)}, \quad (31)$$

where J_-^0 is the probe current at $U_{pr} = 0$. It follows from (28) that ω and k are of the same order of magnitude. We can therefore simplify (31) by expanding $K_0(\omega r_0)$ and $K_1(\omega r_0)$ in series.

B. Presence of Ionization. In this case $\alpha \neq 0$ and $\beta \neq 0$. An estimate of the value of k^2 yields for this case

$$k^2 \approx \beta/Dn_0 + \alpha/D + 1/a^2 \approx \beta/Dn_0 + \alpha/D,$$

since $1/\alpha^2 \ll \beta/Dn_0 + \alpha/D$ for sufficiently small D. We can therefore disregard terms of order $1/a^2$. Equations (26) and (27) become for this case

$$\nabla_{\perp}^2 \nu - \omega_1^2 \nu = n_0 k^2 (e^{U_{pr}/T} - 1) \quad (32)$$

for $r \leq r_0$, and

$$\nabla_{\perp}^2 \nu - \omega_2^2 \nu = 0 \quad (33)$$

for $r > r_0$. Here

$$\omega_1^2 = k^2 e^{U_{pr}/T} - \alpha/D; \quad \omega_2^2 = k^2 - \alpha/D. \quad (34)$$

After finding ν and inserting it into the current equation, we obtain

$$J_- - J_-^0 = J_-^0 (e^{U_{pr}/T} - 1) \left[1 - \frac{k^2}{\omega_1^2} e^{U_{pr}/T} + \frac{2e^{U_{pr}/T} K_1(\omega_2 r_0) I_1(\omega_1 r_0) k^2/\omega_1^2}{\omega_1 r_0 [I_0(\omega_1 r_0) K_1(\omega_2 r_0) + (\omega_1/\omega_2) K_0(\omega_2 r_0) I_1(\omega_1 r_0)]} \right]. \quad (35)$$

It must be noted that this result differs from the expression for the electron current in the probe in the Langmuir case by the factor in the square brackets. The value of this factor depends on the actual mechanism of electron production and on the value of the coefficient of transverse diffusion.

If only external ionization is present, i.e., $\alpha = 0$, $\beta \neq 0$, we have $\omega_1^2 = k^2 \exp(U_{pr}/T)$ and $\omega_2^2 = k^2$. Equation (35) then coincides with (31), but it must be recognized that in this case $k^2 \approx \beta/Dn_0$ is not small when D is small.

If there is no external ionization, we can no longer neglect terms on the order of $1/a^2$ and $\omega_2^2 \approx 1/a^2$, and therefore $\omega_2 r_0 \approx r_0/a$ is always small.

6. Ion Current in Probe

In the preceding computations (Secs. 4 and 5) it is assumed that the probe is negative relative to the plasma, and there is no potential barrier for the ions. Therefore, a change in the probe potential causes a change in the probe ion current through a change in the electron concentration and the associated quasi-neutral ion concentration. The ion current in the probe is given by[3]

$$J_+ = 2\pi v_+ \int_0^{r_*} n_+ r dr, \quad (36)$$

where $v_* = 0.345\sqrt{2T/M}$, M is the ion mass, and T is the electron temperature. But we have by Poisson's equation

$$n_+ = n_- - (1/4\pi e^2) \nabla^2 \varphi.$$

Therefore, considering the axial symmetry of φ, we get

$$J_+ = J_+^0 + 2\pi v_+ \int_0^{r_*} \nu r dr - \frac{v_+}{2e^2} r_0 \left. \frac{d\varphi}{dr} \right|_{r=r_*}. \quad (37)$$

Here φ is the change in the plasma potential produced by the change in the probe potential due to the violation of quasi-neutrality.

The correction to the ion current, necessitated by the violation of quasi-neutrality of the plasma, can be found approximately in the following manner. We can write for the ion concentration $n_* = n_0 \exp(-\varphi/T_*)$ and obtain from the quasi-neutrality condition $n_0 + \nu = n_* = n_0 \exp(-\varphi/T_*)$. Therefore $\varphi = -T_* \ln(1 + \nu/n_0)$.

Making use of this result, we get

$$J_+ - J_+^0 = v_+ \left[2\pi \int_0^{r_*} \nu r dr + \frac{T_+}{T} r_0 \lambda^2 \frac{2\pi dv/dr|_{r=r_*}}{(1 + \nu/n_0)_{r=r_*}} \right], \quad (38)$$

where $\lambda^2 = T/4\pi e^2 n_0$ is the Debye length. The second term in (38) is the correction to the ion current, necessitated by the fact that n_* and $n_- = n_0 + \nu$ are not exactly equal, i.e., necessitated by the violation of quasi-neutrality of the plasma upon change in the probe potential. The correc-

tion should be small compared with the principal term. If the probe potential is very high, then $\nu|_{r=r_0} \to -n_0$ and the correction may prove to be not small. This indicates that one cannot calculate the concentration $n_0 + \nu$, as was done above, and the change in the plasma potential must be taken into account.

When calculating the correction to the current, we inserted into the expression for φ a value of ν calculated without allowance for the change in the plasma potential. It is easy to show that the correction computed in this manner is greater than the true correction.

7. Probe Characteristic

Under experimental conditions, one measures the total probe current, $i_{pr} = J_- - J_+$. The expressions for J_- and J_+ were given above. It is of interest to examine several limiting cases:

1. Only external ionization exists, i.e., $\alpha = 0$ and $\beta \neq 0$. In this case $k^2 = \beta/Dn_0$ can be large when D is small. Using the asymptotic expression for the Bessel function, we obtain for sufficiently high probe potentials

$$i_s \to J_-^0 + (2/kr_0)J_-^0. \qquad (39)$$

The second term is the electron current due to diffusion. In the case of a probe with large kr_0, we see from the results obtained that the electron current, $J_- - J_-^0$, is proportional to the probe radius at high probe potential. An explanation for this was given above.

2. There is no external ionization, the ionization is proportional to the electron concentration, $\alpha \neq 0$, and $\beta = 0$. In this case $k^2 = \alpha/D > 1$ at sufficiently small D. If $kr_0 > 1$ it turns out that i_{pr}, at sufficiently large U_{pr}/T, is less than J_-^0. This becomes understandable if it is taken into account that $kr_0 > 1$ corresponds to small diffusion, and that in this case the ionization is proportional to the electron concentration. It sufficiently high probe potentials, the electron concentration over the probe drops to zero, and the external diffusion, which places the electrons over the probe, is small. The ion current into the probe is therefore zero, and the electron current starts dropping.

3. If ionization is present in the case of greatly hindered diffusion, i.e., at small D and correspondingly large kr_0, the electron concentration over the probe increases considerably when the probe potential is negative, and this leads to violation of the quasi-neutrality condition and to a substantial change in the plasma potential. Under these conditions, the results obtained no longer helod, for it has been assumed in the derivation that the plasma potential changes by an amount proportional to T_+ and that $T_+ \ll T$. This case should be investigated separately.

On the other hand, if the diffusion is not very small, i.e., kr_0 is small, the diffusion will again not let the electron concentration rise over the probe. The quasi-neutrality will therefore not be violated. The results obtained above will remain in force.

The expressions obtained for the probe current make it possible to determine, from the experimental probe characteristic, the principal parameters of the plasma and the coefficient of diffusion D.

The author thanks O. B. Firsov and A. V. Zharinov for interest in the work, for valuable advice, and for participating in a discussion of the results.

[1] G. V. Spivak and E. M. Reikhrudel', J. Exptl. Theoret. Phys. (U.S.S.R.) **6**, 816 (1936); **8**, 319 (1938); **10**, 1408 (1940).

[2] Bohm, Burhop, and Massey. Collection: The Characteristics of Electrical Discharges in Magnetic Fields, Ed. by A. Guthrie and R. K. Wakerling, New York, 1949, ch. 2.

[3] O. B. Firsov, J. Tech. Phys. (U.S.S.R.) **26**, 445 (1956), Soviet Phys. JTP **1**, 431 (1956).

Translated by J. G. Adashko
216

ON THE ANALYSIS OF HIGH-ENERGY SHOWERS

Ya. I. GRANOVSKIĬ and I. Ya. CHASNIKOV

Nuclear Physics Institute, Academy of Sciences, Kazakh S.S.R.

Submitted to JETP editor September 6, 1958

J. Exptl. Theoret. Phys. (U.S.S.R.) **36**, 1119-1122 (April, 1959).

The double-valued dependence of the shower particle energy on the angle of emission in the laboratory system is explained. A method is suggested for a more precise determination of γ_c taking into account the energy and angular distribution of shower particles.

THE dependence of the energy of shower particles on their angle of emission in the laboratory system of coordinates (l.s.)[1] has been analyzed by Huzita.[2] The resulting double-valued dependence is interpreted as a consequence of two or more collisions taking place in the interaction between the primary particle with the nucleons of the target nucleus.

If this conclusion is accepted, then the dependence should be multi-valued for other showers, especially when the primary is multiply charged. However, for a shower produced by a multi-charged particle (a case found and analyzed in our laboratory) the dependence $pv = f(1/\sin\theta)$ (where p and v are the momentum and velocity of the particle and θ is the spatial angle of emission in l.s.), is also found to be double-valued (see Fig. 1, curves A and B). The double-valued dependence is also observed for the shower described by Boos et al.,[3] produced in a nucleon-nucleon collision.

The observed character of the dependence of the energy of shower particles on the angle of their emission in certain showers can probably be explained by kinematic considerations without any assumptions concerning the mechanism of interaction of the primary particle with one or several nucleons of the target nucleus.

In the observed high-energy showers (jets), there are no shower particles emitted in the backward direction in the l.s. This indicates that, in such cases,

$$V_c > V^*, \qquad (1)$$

where V_c is the velocity of the center-of-mass system (c.m.s.) and V^* is the velocity of the shower particles in c.m.s. From the Lorentz transformation, we have

$$E^* = \gamma_c(E - pV_c\cos\theta), \qquad \gamma_c = 1/\sqrt{1-V_c^2}$$

and it follows that

$$\frac{E}{m} = \frac{E^*/m\gamma_c \pm V_c\cos\theta\,\sqrt{(E^*/m\gamma_c)^2 - (1-V_c^2\cos^2\theta)}}{1-V_c^2\cos^2\theta}, \qquad (2)$$

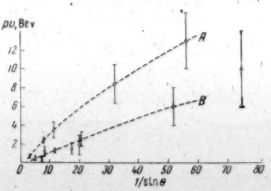

FIG. 1. Dependence on the energy of shower particles on their angle of emissions in the l.s. for a shower produced by multiply charged particles.

where $E(E^*)$—is the energy of the shower particle in l.s. (c.m.s.), and m is the particle mass (π meson). Under condition (1) one should take both signs in formula (2). Assuming various values of $a = E^*/m\gamma_c$, one can construct the graph of the dependence $y = E/m$ on $x = 1 - V_c^2\cos^2\theta = \sin^2\theta + \gamma_c^{-2}\cos^2\theta$ according to formula (2). A family of such curves is shown in Figs. 2 and 3; the value of the parameter a is indicated on the curves. In formula (2), the sign + is taken for those particles for which $0 < \theta^* < \theta_0^*$, and the sign − for $\theta_0^* < \theta^* < \pi$ (where θ_0^* is the angle in c.m.s. corresponding to the limiting angle in l.s.) For $\theta^* = \theta_0^*$, we have $x = \sqrt{a}$ and $y = 1/\sqrt{x}$. On a logarithmic scale, $y = 1/\sqrt{x}$ is represented by a straight line (Figs. 2 and 3) below which lie the points corresponding to particles with an angle $\theta^* > \theta_0^*$. If, in the shower under study, there are no such particles, then all experimental points on the graph are above the limiting straight line, and there is no double-valued dependence $E(\theta)$ in the l.s.

From the Lorentz transformation, we have

$$E = \gamma_c(E^* + p^*V_c\cos\theta^*) \qquad (3)$$

It follows that the points corresponding to particles emitted at the angle $\theta^* = 90°$ fall on one curve

$$y = \gamma_c^2 a. \qquad (4)$$

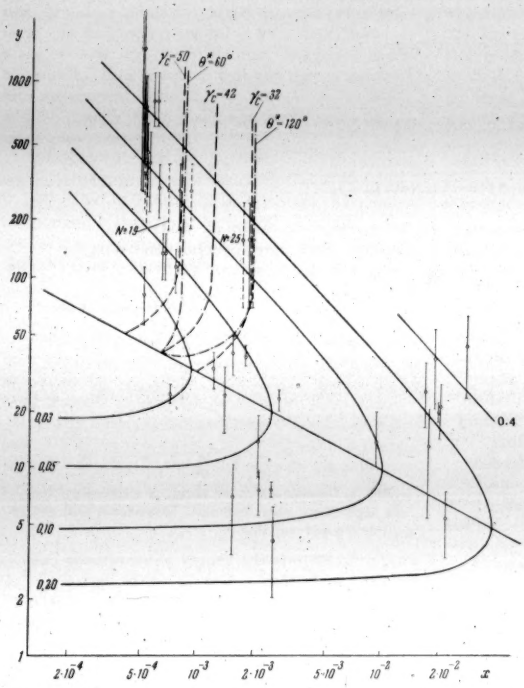

FIG. 2. Variation of y(x) for particles of the shower of De Benedetti et. al.[2] for $\gamma_c = 45$. For the particles No. 19 and 25 the points are plotted for 3 values of γ_c equal to 50, 45 and 40 respectively.

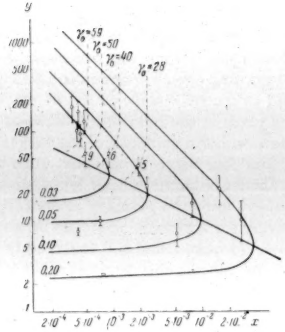

FIG. 3. The shower of Boos et. al.[3] The experimental points are plotted for $\gamma_c = 52$.

These curves for various values of γ_c are denoted in Figs. 2 and 3, by dashed curves. Analogous curves for different angles θ^* can be calculated using the same formula (3). In particular, the curves for the angles $\theta^* = 60°$ and $\theta^* = 120°$ are shown in Fig. 2.

Experimental data of references 2 and 3 are shown in Figs. 2 and 3. Comparing Fig. 2 with Fig. 7 of the article by Huzita, it is clear that the latter assumed that particles with the angles of emissions $\theta^* > \theta_0^*$ were produced as a result of a separate interaction. In Fig. 3 (shower observed by Boos et al.[3]), particles with angles of emission $\theta^* > \theta_0^*$ are also present. Their fraction in both cases is $\sim 20\%$ of the total number of particles, and increases, if among the shower particles, there are particles heavier than π mesons.

An analysis of showers using Eqs. (2) and (4) makes it possible to find the value of γ_c more accurately than determined by another method (for instance by the half-angle method). For this purpose, one draws curves (4) for various γ_c. Assuming the equality of the number of particles emitted in the forward and backward direction in c.m.s., we can determine the corresponding value of γ_c. Accounting for fluctuations of points near $\theta^* = 90°$, one can find the limits of possible values γ_c. It can be seen from Fig. 2 that the apparent lower limits of γ_c are equal to 50 and 32 correspondingly, the probable value of γ_c being equal to 42.2 (De Benedetti et al.[2] give the value of γ_c equal to 40 to 50). A more accurate value of γ_c can then be obtained by the method of consecutive approximations. It is sufficient, however, to do this only once, since the corrected value of γ_c almost does not change. Thus, if we assume $\gamma_c = 40$, the corrected value of γ_c is 40.5. (It is shown in Fig. 2 how the position of particles number 19 and 25 changes in dependence of γ_c). In an analogous fashion, for $\gamma_c = 50$, one obtains a more accurate value of 43.5.

Applying the same method to the shower of Boos et al.[3] we obtain the upper and lower limits $\gamma_c = 40$ and 28 with the probable value of 34.5.

The possible fluctuations of particle No. 6 leads to variation of the limits of γ_c (see Fig. 3).

The advantage of the above method lies in the fact that, for the more accurate values of γ_c, one takes into account the experimental data for the angular and energy distribution of shower particles in the l.s. We do not make use of the usually-made assumption of symmetry (or isotropy) of the angular distribution in the c.m.s., nor do we assume that the particles are monoenergetic, etc. Only the equality of the number of particles emitted in the forward and backward directions in the c.m.s. is essential.

In all analyzed cases, the proposed method has led to a lowering of γ_c as compared to the half-angle method. This is in agreement with the data of other authors.[4,5]

In conclusion, the authors would like to express their gratitude to J. S. Takibaev for his interest in the work and helpful advice.

[1] De Benedetti, Garelli, Tallone, and Vigone, Nuovo cimento **4**, 1142 (1956).

[2] H. Huzita, Nuovo cimento **6**, 841 (1957).

[3] Boos, Vinnitskiĭ, Takibaev, and Chasnikov, J. Exptl. Theoret. Phys. (U.S.S.R.) **34**, 622 (1958); Soviet Phys. JETP **7**, 430 (1958).

[4] Birger, Grigorov, Gusev, Zhdanov, Slavatinskiĭ, and Stashkov, J. Exptl. Theoret. Phys. (U.S.S.R.) **31**, 971 (1956); Soviet Phys. JETP **4**, 872 (1957).

[5] J. S. Takibaev, J. Exptl. Theoret. Phys. (U.S.S.R.) **35**, 277 (1958), Soviet Phys. JETP **8**, 191 (1959). A. I. Nikishov and I. L. Rozental', J. Exptl. Theoret. Phys. (U.S.S.R.) **35**, 165 (1958); Soviet Phys. JETP **8**, 115 (1959).

Translated by H. Kasha
217

NUCLEAR FORCES AND LEVELS OF THE LITHIUM ISOTOPES

V. V. BALASHOV

Institute of Nuclear Physics, Moscow State University

Submitted to JETP editor September 11, 1958

J. Exptl. Theoret. Phys. (U.S.S.R.) **36**, 1123-1128 (April, 1959)

A refinement is introduced in the intermediate coupling model of the nuclear shell theory by taking into account paired spin-orbit interaction between the nucleons. Calculations carried out for Li^6 and Li^7 yield better agreement with experiment than the usual intermediate-coupling model which takes into account only single particle spin-orbit interaction. Some indications are obtained with respect to the existence of different types of radial dependence for nuclear forces of different exchange nature.

1. INTRODUCTION

DURING the last few years many papers have appeared on the analysis of the energy levels of light nuclei, their purpose being to obtain information on the forces acting between nucleons.[1-3] Of special interest from this point of view is Li^6, which contains two p-nucleons beyond the filled $S^4_{1/2}$ shell corresponding to the He^4 nucleus. The energy spectrum of this nucleus has been thoroughly studied[4] and the first six levels have been reliably identified (see Fig. 1). A detailed analysis of the levels for Li^6 and Li^7 has been carried out by Soper[1] and Meshkov and Ufford.[2] In both papers the calculation has been carried out for the intermediate-coupling approximation.

As shown in reference 5, a consistent description of the p-shell nuclei, involving no assumptions whatsoever about the actual form of the paired nucleon interaction, requires the introduction of 12 independent parameters to describe this interaction. The use of a smaller number of parameters is tantamount to setting down additional conditions for these independent quantities, associated with assumptions about the form of the potential of the nucleon interaction. In describing nuclei with the aid of an intermediate-coupling model, and among these descriptions we can cite the work of Soper and Meshkov and Ufford, other assumptions are made, based on considerations of convenience in computation, in addition to such a physical assumption about the properties of the two-nucleon potential. Upon analysis of these additional limitations, it was deemed interesting to dispense with them and to carry out this analysis consistently from an original physical point of view. Such a program requires more complicated computations than those involving the intermediate-coupling model but which, however, are readily performed by the use of computer techniques.

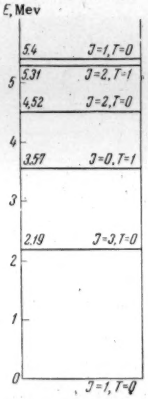

FIG. 1

In the present paper such an analysis is carried out on the basis of a computation for the nuclei of Li^6 and Li^7. We intend later to carry out computations for other p-shell nuclei, in particular for the nucleus of B^{10}, which has a very rich and thoroughly studied energy level spectrum.

2. CENTRAL NUCLEON INTERACTION

According to the intermediate coupling model the interaction of nuclei is described by paired central forces which have exchange terms and single-particle spin-orbit forces. Thus the Hamiltonian has the form

$$H = \sum_i \frac{p_i^2}{2m} + \sum_{i<j} V_{ij} + a \sum_i \mathbf{l}_i \mathbf{s}_i, \qquad (1)$$

where

$$V_{12} = (W + MP_x + BP_\sigma + HP_xP_\sigma) V(r_{12}). \qquad (2)$$

Here $\mathbf{P_X}$ and $\mathbf{P_\sigma}$ are the operators of interchange of space and spin coordinates; W, M, B, H are the coefficients that characterize the contribution of the Wigner, Majorana, Bartlett and Heisenberg forces to the central-interaction potential, satisfying the normalization condition

$$W + M + B + H = 1. \qquad (3)$$

In the analysis of the p-shell nuclei, all the integrals in $V(r_{12})$ can be expressed by two Slater integrals: direct (L) and exchange (K);[6] Therefore the central interaction as a whole is described by five independent parameters L, K and four coefficients W, M, B, H, connected by the additional relation (3).

The requirement of a common radial dependence of the various exchange terms of potential (2) is an additional limitation set on the central interaction of nuclei; this limitation follows neither from experiment nor from theory. Failure to use this limitation will lead to a substantial increase in the number of parameters when we set down the potential in its configurational presentation, while in the shell presentation[5] only one more parameter is required than in references 1 and 2. In this presentation the independent parameters of the central potential are matrix elements over the states of the two nucleons in the L-S coupling scheme, which are diagonal in L, S and T and are independent of the total momentum J:

$$F_1 = \langle p^2 : {}^1S_0^{T=1} | V_{12} | \rangle, \qquad F_2 = \langle p^2 : {}^3S_1^{T=0} | V_{12} | \rangle,$$
$$F_3 = \langle p^2 : {}^1P_1^{T=0} | V_{12} | \rangle, \qquad F_4 = \langle p^2 : {}^3P_J^{T=1} | V_{12} | \rangle,$$
$$F_5 = \langle p^2 : {}^1D_2^{T=1} | V_{12} | \rangle, \qquad F_6 = \langle p^2 : {}^3D_J^{T=0} | V_{12} | \rangle. \qquad (4)$$

Here no assumptions are made about the exchange nature of the interaction, about its dependence on the velocity, or about the form of the radial functions of the nucleons in the nucleus.

Having expressed the six matrix elements (4) in terms of L, K, W, M, B, and H it is easy to show that the additional relation involving F_1, $F_2, \ldots, F_6$:

$$F_1/F_2 = F_5/F_6. \qquad (5)$$

corresponds to the requirement of the common radial dependence of central forces of different nature.

3. SPIN-ORBIT INTERACTION OF NUCLEON

The dependence of the nucleon interaction on the velocity is shown in (1) in terms of single particle spin-orbit forces

$$V_{sl} = a \sum_i \mathbf{l}_i \mathbf{s}_i. \qquad (6)$$

A general analysis of the dependence of the interaction on the velocity is given in references 7 and 8. The basic term that describes such an interaction consists of the two particle spin-orbital forces

$$V_{sl}(1,2) = f(1,2)(\sigma_1 + \sigma_2)[(\mathbf{r}_2 - \mathbf{r}_1)(\mathbf{p}_2 - \mathbf{p}_1)]/\hbar$$
$$= f(1,2)(\mathbf{S}_{12}\mathbf{L}_{12}), \qquad (7)$$

where $\mathbf{S}_{12}$ and $\mathbf{L}_{12}$ are the total spin and orbital momentum for the relative motion of two nucleons. $f(1,2)$ consists of two exchange members — Wigner type and Heisenberg type.

The potential (7) leads to the same splitting of the interaction between the outer nucleon and the nucleons of the filled shell with $j = l + \frac{1}{2}$, as in (6).[9] Thus the single-particle spin-orbit forces (6) and the two-particle forces (7) are completely equivalent in the description of nuclei containing one nucleon or one "hole" in the unfilled shell. However, in the description of nuclei having a larger number of nucleons in the unfilled shell, there is no such simple correspondence. In this sense the accepted description of the nucleon interaction by means of potential (1), used in the intermediate-coupling model, where we account for the interaction of the external nucleons with the nucleons of the filled shells and neglect the spin-orbital interaction between them, is inconsistent, since this description does not correspond to any physical assumption about the nucleon interaction.

Going over to the center-of-mass system of two interacting nucleons, following Talmi,[10] it is easy to see that within the p-shell limits the potential (7) is characterized by two independent parameters α_1 and α_2, which correspond to the spin-orbit interaction of nucleons in the P and D states of relative motion:

$$\langle {}^3P_0^{T=1} | V_{sl}(1,2) | \rangle = 2\alpha_1, \qquad \langle {}^3D_1^{T=0} | V_{sl}(1,2) | \rangle = 3\alpha_2,$$
$$\langle {}^3P_1^{T=1} | V_{sl}(1,2) | \rangle = \alpha_1, \qquad \langle {}^3D_2^{T=0} | V_{sl}(1,2) | \rangle = \alpha_2,$$
$$\langle {}^3P_2^{T=1} | V_{sl}(1,2) | \rangle = -\alpha_1,$$
$$\langle {}^3D_3^{T=0} | V_{sl}(1,2) | \rangle = -2\alpha_2. \qquad (8)$$

In the simplest case of oscillator wave functions,

TABLE I

Parameters	$\alpha_2 = 0$	$\alpha_2 = 0.2$	$\alpha_2 = 0.4$	$\alpha_2 = 0.6$
F_2	−7.869	−7.263	−6.746	−6.314
F_6	−4.333	−3.690	−3.135	−2.667
Δ	2.33	2.03	1.73	1.43

TABLE II

$F_1(\alpha_1, \alpha_2)$

α_1	$\alpha_2 = 0$	$\alpha_2 = 0.2$	$\alpha_2 = 0.4$	$\alpha_2 = 0.6$
0	−3.710	−3.170	−2.762	−2.341
0.4	−3.759	−3.201	−2.761	−2.403
0.8	−3.803	−3.254	−2.802	−2.445
1.2	−3.842	−3.292	−2.838	−2.477
1.6	−3.876	−3.326	−2.869	−2.504

TABLE III

$F_5(\alpha_1, \alpha_2)$

α_1	$\alpha_2 = 0$	$\alpha_2 = 0.2$	$\alpha_2 = 0.4$	$\alpha_2 = 0.6$
0	−2.160	−1.502	−0.897	−0.370
0.4	−2.092	−1.389	−0.727	−0.029
0.8	−2.007	−1.248	−0.443	+0.926
1.2	−1.898	−1.042	+0.132	7.817
1.6	−1.752	−0.707	1.909	—

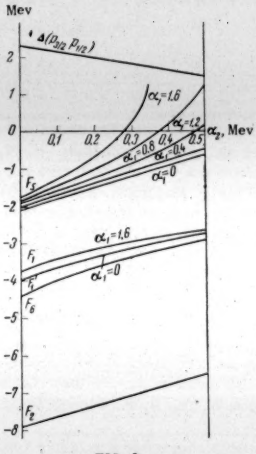

FIG. 2

which describe the nucleons of the s and p shells, the parameter a of the single-particle spin-orbital coupling is connected with α_1 are by the relation $a = 3\alpha_1$, and the magnitude of the spin-orbit splitting of the interaction of the p-nucleon with the $s^4_{1/2}$ shell can be expressed in terms of α_1:

$$\Delta(p_{3/2},\ p_{1/2}) = {}^9/_2\,\alpha_1. \qquad (9)$$

In a more rigorous approach, relation (9) should be considered only as approximate: the magnitude of the spin-orbit splitting $\Delta(p_{3/2}, p_{1/2})$ may be more sensitive to the fine terms of the radial wave functions and nucleon interaction, right down to multiple effects, than the interaction of the nucleons in the p-shell with each other. For this reason we shall consider $\Delta(p_{3/2}, p_{1/2})$ as an additional independent parameter. In this way the problem of the accuracy of relation (9), obtained from the more rigorous model assumptions, becomes an experimental problem while relation (9) itself becomes a criterion for the correctness of these model assumptions.

4. CALCULATION OF THE Li^6 and Li^7 LEVELS

In Tables I—III and in Fig. 2 we present the values for the parameters $\Delta(p_{3/2}, p_{1/2})$, F_1, F_2, F_5, and F_6 (in Mev) as a function of α_1 and α_2, determined from the spectrum of the excited Li^6 levels (Fig. 1).

The data are given for the particular case of $F_3 = F_4 = 0$, which corresponds to neglecting the interaction of nucleons in the P state of relative motion as compared with the interaction in the S state.[11]

From the values of parameters thus obtained, we compute the magnitude of binding energy for Li^6 (relative to He^4). Here the energy for the Coulomb interaction of the external proton with the He^4 core is determined from the isotope multiplets, He^5—Li^5 and He^6 (J = 0, T = 1)—Li^6 (J = 0, T = 1), and comes to 0.66 Mev in both cases. The binding energy of the $p_{3/2}$ nucleon with the $S_{1/2}$ shell is equal to −0.81 Mev, i.e., the binding energy of He^5 relative to He^4. As can be seen from Fig. 3, $\alpha_2 \cong 0.2$ Mev corresponds to the experimental value E = 3.70 Mev.

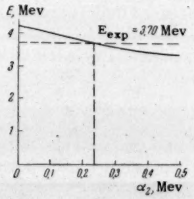

FIG. 3

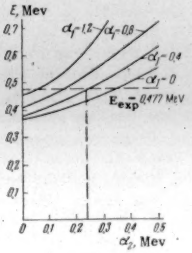

FIG. 4

In the energy-level spectrum of the Li^7 nucleus, identification has been made for levels with $J = \frac{1}{2}$, $T = \frac{1}{2}$ at $E = 0.477$ Mev and $J = \frac{5}{2}$, $T = \frac{1}{2}$ at $E = 7.46$ Mev. In Fig. 4 we give the results of the calculation for the energy of level $(\frac{1}{2}, \frac{1}{2})$ with the parameters determined for Li^6. We have chosen an energy scale for Li^7, after reference 1, by fixing the position corresponding to the 7.46-Mev level. $\alpha_1 \cong 0.4$ Mev corresponds to the experimental value for $E(\frac{1}{2}, \frac{1}{2}) = 0.477$ Mev; the ratio of the scales for Li^7 and Li^6 is 1.26. At this value of α_1, the first level with $J = \frac{7}{2}$, $T = \frac{1}{2}$ coincides with an unidentified level at $E = 4.61$ Mev, while the first level with $J = \frac{5}{2}$, $T = \frac{1}{2}$ corresponds to the level at $E = 5.5$ Mev (see Fig. 5).

The binding energy of Li^7 (relative to Li) for $\alpha_1 = 0.4$ and $\alpha_2 = 0.2$, comes to 7.06 Mev, while the experimental value is 7.15 Mev. On the other hand, the intermediate-coupling approximation gives a value of 9.15 Mev.

The calculation also includes, as a particular case, the intermediate-coupling approximation.

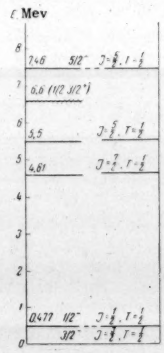

FIG. 5

For the latter the corresponding values are $\alpha_1 = 0$ and $\alpha_2 = 0$. The corresponding values $a = \frac{2}{3}$, $\Delta = 1.55$ Mev, $L = -(F_2 + 2F_6)/3 = 5.51$ Mev, and $K = -(F_2 - F_6)/2 = 1.18$ Mev coincide with those given by Soper.[1]

5. CONCLUSIONS

1. Accounting for the paired spin-orbit interaction between nucleons in the unfilled shell leads to a significant change in the parameters that describe the central interaction of the nucleons.

2. It follows from these calculations that a mixture of central (in a common form) and two-particle spin-orbital forces is a good approximation for the interaction between the nucleons in the nucleus. An analysis of the energy levels for the Li isotopes leads to the following values for the parameters of the paired nucleon interaction (Mev):

$$\Delta = 1.98, \quad \alpha_1 = 0.43, \quad \alpha_2 = 0.23,$$
$$F_1 = -3.12, \quad F_2 = -7.18,$$
$$F_5 = -1.28, \quad F_6 = -3.55. \qquad (10)$$

3. The values for the parameters $\Delta(p_{3/2}, p_{1/2})$ and α_1 are found to be in good agreement with relation (9) obtained by means of the oscillator functions for the s and p nucleons.

4. Relation (5), which holds for $\alpha_1 = 0$ and $\alpha_2 = 0$, does not hold for the parameters given by (10). This indicates the existence of a different radial dependence for nuclear forces of different exchange character. It should be pointed out that by the same token it becomes possible to explain the remarkably small value for the matrix element $\langle p_{3/2}: 21 | V | \rangle = 0.49$ Mev, obtained by the author[12] and Talmi and Thieberger[13] in connection with the analysis of the nuclear binding forces in the $p_{3/2}$ shell, which is completely impossible to obtain if relation (5) is satisfied.

The author expresses his deep gratitude to Yu. M. Shirokov for his continuous interest in the work and for valuable criticisms. The author is also very grateful to A. A. Samarskiĭ and V. Ya. Gol'din for many consultations during the computational work.

[1] I. M. Soper, Phil. Mag. **2**, 1219 (1957).

[2] S. Meshkov and C. Ufford, Phys. Rev. **101**, 734 (1956).

[3] D. Kurath, Phys. Rev. **101**, 216 (1956).

[4] F. Ajzbenberg and T. Lauritsen, Revs. Modern Phys. **27**, 77 (1955).

[5] Shirokov, Balashov, and Tumanov, J. Exptl. Theoret. Phys. (U.S.S.R.) **32**, 167 (1957), Soviet

Phys. JETP **5**, 136 (1957). Balashov, Dorofeiev, Kalitkin, Kaminskiĭ, Smirnov, Tumanov, and Shirokov, Ядерные реакции при малых и средних энергиях. Труды Всесоюзной конференции, ноябрь, 1957. (Trans. All-Union Conference on Low and Medium Energy Nuclear Reactions, Nov. 1957) Acad. Sci. Press, Moscow, 1958.

[6] E. Feenberg and E. Wigner, Phys. Rev. **51**, 95 (1937). E. Feenberg and M. Phillips, Phys. Rev. **51**, 597 (1937).

[7] Puzikov, Rindin, and Smorodinskiĭ, J. Exptl. Theoret. Phys. (U.S.S.R.) **32**, 592 (1957), Soviet Phys. JETP **5**, 489 (1957).

[8] S. Okubo and R. E. Marshak, Ann. of Phys. **4**, 166 (1958).

[9] J. Huges and K. Le Couteur, Proc. Phys. Soc. (London) **A63**, 1219 (1950). J. P. Elliott and A. M. Lane, Phys. Rev. **96**, 1160 (1954).

[10] I. Talmi, Helv. Phys. Acta **25**, 185 (1952).

[11] A. I. Baz', J. Exptl. Theoret. Phys. (U.S.S.R.) **31**, 831 (1956), Soviet Phys. JETP **4**, 704 (1957).

[12] V. V. Balashov, Ядерные реакции при малых и средних энергиях. Труды Всесоюзной конференции, ноябрь, 1957. (Trans. All-Union Conference on Low and Medium Energy Nuclear Reactions, Nov. 1957) Acad. Sci. Press, Moscow, 1958.

[13] I. Talmi and R. Thieberger, Phys. Rev. **103**, 718 (1956).

Translated by M. E. Zaret
218

ON RADIATIVE TRANSITIONS BETWEEN ROTATIONAL LEVELS IN SPIN 1/2 NUCLEI

D. F. ZARETSKIĬ

Submitted to JETP editor September 13, 1958

J. Exptl. Theoret. Phys. (U.S.S.R.) **36**, 1129-1132 (April, 1959)

The relative intensities of electric and magnetic transitions between rotational levels in spin $\frac{1}{2}$ nuclei are considered. The calculation is based on the coupling scheme previously proposed by the author. As an example the Tm^{169} nucleus is considered. It is shown that the observed intensity ratio does not contradict the proposed coupling scheme.

To calculate the probabilities for the magnetic dipole and electric quadrupole transitions between the rotational levels of deformed nuclei with spin $\frac{1}{2}$, we shall assume:

(1) These nuclei are in $\Sigma^{+}_{g,u}$ states, i.e., in the one-nucleon states described in Hund's coupling scheme b.[1] The indices g and u refer to the states $\frac{1}{2}^{+}$ and $\frac{1}{2}^{-}$, respectively.

(2) Correspondingly, we have, besides the trivial ones, the following integrals of the motion: the nucleon spin $\mathbf{s}$, the total rotational momentum $\boldsymbol{\kappa} = \mathbf{l} + \mathbf{R}$ ($\mathbf{R}$ is the moment vector of the collective rotation), the projection of the orbital momentum of the nucleon $\mathbf{l}$ on the nuclear axis $\Lambda = 0$, and the projection of the vector $\boldsymbol{\kappa}$ on the nuclear axis $\kappa_{z'} = 0$. The total angular momentum is $\mathbf{J} = \boldsymbol{\kappa} + \mathbf{s}$.

The wave function for these states can be written in the form

$$\Psi^{JM}_{\varkappa,s} = \varphi_0 \sum_{m,m_s} (\varkappa^1/_2\, m m_s | \varkappa^1/_2\, JM)\, Y_{\varkappa,m}\, \chi_{1/_2,m_s}, \qquad (1)$$

where φ_0 is the wave function describing the motion of the nucleon relative to the nuclear axes, and χ is the spin function of the extra nucleon in the laboratory system. The rotational quantum number runs through the values 0, 2, 4, ... for the states Σ^{+}_{g}, and through 1, 3, 5, ... for the states Σ^{+}_{u}.

The wave function (1) is conveniently written in a system of coordinates connected with the nuclear axes. For this purpose we note that

$$Y_{\varkappa,m}(\theta, \varphi) = \sqrt{(2\varkappa+1)/8\pi^2}\, D^{\varkappa}_{m,0}(\theta, \varphi, \psi), \qquad (2)$$

where (θ, φ, ψ) are the Eulerian angles defining the orientation of the nuclear axes in space. The function $D^{\kappa}_{m,\nu}(\theta, \varphi, \psi)$ describes the unitary transformation from the fixed system to the system of coordinates connected with the nucleus.

Noting that

$$\chi_{1/_2,m_s} = \sum_{m'_s} D^{1/_2}_{m_s m'_s} \chi_{1/_2,m'_s}, \qquad (3)$$

we can write the wave function (1) in the coordinates referred to the nuclear axes in the form

$$\Psi^{JM}_{\varkappa s} = \sqrt{(2\varkappa+1)/8\pi^2}\, \varphi_0 \sum_{m'_s} (\varkappa^1/_2 0 m'_s | \varkappa^1/_2 J m'_s)\, D^{J}_{M,m'_s}\, \chi_{1/_2,m'_s}. \qquad (4)$$

The calculation of the probabilities for electric quadrupole transitions between the rotational levels of spin $\frac{1}{2}$ nuclei with the help of the wave function (3) presents no difficulties. The result is the same as in the paper of A. Bohr and B. Mottelson,[2] where these probabilities were calculated for a different coupling scheme. It is now of interest to calculate the probabilities for magnetic dipole transitions. The operator for magnetic dipole transitions can be written in the form[2]

$$\mathfrak{M}(1, m) = \sum_{\nu} D^{1}_{m,\nu}\, \mathfrak{M}'(1, \nu), \qquad (5)$$

where

$$\mathfrak{M}'(1, \nu) = \nabla r Y_{1\nu} [(g_l - g_R)\mathbf{l} + (g_s - g_R)\mathbf{s} + g_R \mathbf{J}]$$

is the operator for a magnetic dipole transition in the coordinate system connected with the nuclear axes; g_l, g_s, and g_R are the gyromagnetic ratios for the single-nucleon and collective motions, respectively.

With the help of the wave function (4) one can without great difficulty compute the probability for a magnetic dipole transition between levels with the same rotational quantum number (transitions within a doublet). The expression for this probability is of the form

$$T(M1, J+1 \to J) = \frac{16\pi}{9\hbar} \left(\frac{\omega}{c}\right)^3 B_{\varkappa}(M1, J+1 \to J), \qquad (6)$$

where

$$B_{\varkappa}(M1, J+1 \to J) = \left(\frac{e\hbar}{2mc}\right)^2 (g_s - g_R)^2\, \frac{3}{16\pi}\, \frac{2J+1}{J+1}.$$

Another possible case is the transtion in which κ changes by two units. In this case the magnetic transition probability is zero, if the transition

operator (5) is used. This difficulty can be avoided in the case of nuclei with an extra proton by adding to the operator (5) a term arising from the spin-orbit coupling:[3]

$$\mathfrak{M}_{sl}(1, m) = \frac{\lambda}{mc^2}[\nabla U(\mathbf{r})(\mathbf{sr}) - \mathbf{s}(\mathbf{r}\nabla U)]\nabla r Y_{1m}\frac{e\hbar}{2mc}. \quad (7)$$

Here $\mathbf{r}$ is the radius vector of the odd proton, λ is the spin-orbit coupling constant, and $U(\mathbf{r})$ is the self-consistent potential of the nucleus.

Using the operator (7), relation (6), and the wave function (4), we can obtain the abovementioned probability for the magnetic dipole transition between states whose κ value differ by two units (and $\Delta J = 1$):

$$B(M1, J+1 \to J) = \frac{\lambda}{mc^2}\left\langle\left|(n_z^2 - n_x^2)\, r\frac{\partial U}{\partial r}\right|\right\rangle^2 \frac{3}{4\pi}\left(\frac{e\hbar}{2mc}\right)^2 \frac{2J+1}{2^4(J+1)}. \quad (8)$$

The diagonal matrix element appearing in this expression is taken between the wave functions φ_0 and can be determined from the magnitude of the doublet splitting in the rotational spectrum of the corresponding nucleus.[1,3] Writing the Hamiltonian related to the rotational terms in the form

$$H_{\text{coll}} = \hbar^2 \mathbf{x}^2/2I + \gamma \mathbf{x}\mathbf{s}, \quad (9)$$

where I is the moment of inertia of the nucleus, we obtain

$$\frac{\lambda}{mc^2}\left\langle\left|(n_z^2 - n_x^2)\, r\frac{\partial U}{\partial r}\right|\right\rangle = \frac{2\gamma}{3\sqrt{5/4\pi}\,\beta\hbar^2/I}$$

with β the deformation parameter.

It is known from experiment that the rotational levels of spin $\frac{1}{2}$ nuclei have doublet character. The transitions between the components of different doublets with $\Delta J = 1$ are essentially of the magnetic dipole type. The electric quadrupole admixture apparently does not exceed 10 to 20%.

To determine the possible order of magnitude of the probability for magnetic transitions, we calculate the ratio $T(M1)/T(E2)$ for a transition with an energy of 110 kev in the rotational spectrum of Tm^{169}.[4] For this nucleus $\beta \approx 0.3$ (reference 5) and $\gamma/(\hbar^2/I) = 0.24$ (reference 4). Using (8) and (9), we then obtain for the ratio $T(M1)/T(E2) \approx 4$.

It follows from this estimate that the spin-orbit effect can account for the observed ratio of the probabilities in these transitions with an odd proton. In the case of an extra neutron one must introduce an effective charge arising from the interaction of the neutron with the nuclear core.[6]

In any case, it should be noted that the magnetic moment,[3] the character of the rotational spectrum, and the electric transition probabilities for the nucleus Tm^{169} do not stand in contradiction to our proposed classification.

It is also interesting to note that data on the Coulomb excitation of the Yb^{171} nucleus have recently appeared.[7] This nucleus is a daughter of Tm^{171} in β decay, whose ground state has spin $\frac{1}{2}$. The Coulomb excitation gives rise to two levels of Yb^{171}. Their energies and spins are given in the figure. In the same figure we also give the energies and spins of the rotational levels of Tm^{171}, for comparison.[8]

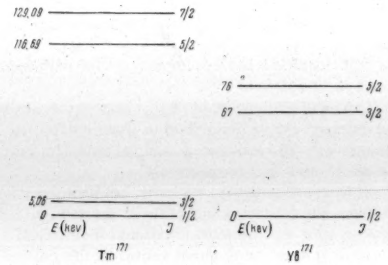

If our classification is correct, it follows necessarily from the form of the rotational spectra that the ground state of Tm^{171} corresponds to the Σ_u^+ one-nucleon term ($\frac{1}{2}^-$), and the ground state of Yb^{171} to the Σ_g^+ term ($\frac{1}{2}^+$). This corresponds to the fact that Tm^{171} changes its parity during β decay.

This classification in general does not contradict the available data on the rotational levels of spin $\frac{1}{2}$ nuclei. There is, however, some disagreement in the parities of the ground states of several nuclei, as given by our classification and that of Nilsson.[9] For example, we ascribe negative parity to the ground state of the Tm^{169} nucleus, while in the Nilsson scheme this nucleus has positive parity.[5]

In conclusion I express my gratitude to S. A. Baranov for a discussion of the experimental data, and also to D. P. Grechukhin for useful comments.

[1] D. F. Zaretskiĭ and A. V. Shut'ko, J. Exptl. Theoret. Phys. (U.S.S.R.) **32**, 370 (1957); Soviet Phys. JETP **5**, 323 (1957).

[2] A. Bohr and B. Mottelson, Kg. Danske Videnskab. Selskab, Mat.-Fys. Medd. **27**, No. 16 (1953).

[3] D. F. Zaretskiĭ, J. Exptl. Theoret. Phys. (U.S.S.R.) **36**, 869 (1959); Soviet Phys. JETP **9**, 612 (1959).

[4] Hatch, Boehm, et al., Phys. Rev. **104**, 745

(1957). S. A. Baranov and P. M. Polevoĭ, Атомная энергия (Atomic Energy) **3**, 256 (1957).

[5] B. Mottelson and S. Nilsson, Z. Physik **141**, 217 (1955).

[6] J. S. Bell, Nucl. Phys. **4**, 295 (1957).

[7] Elbek, Nielson, and Olesen, Preprint (1957).

[8] E. N. Hatch and F. Boehm, Phys. Rev. **108**, 113 (1957).

[9] S. Nilsson, Kgl. Danske Videnskab. Selskab, Mat.-Fys. Medd. **29**, No. 16 (1955).

Translated by R. Lipperheide
219

EQUATION OF STATE OF A PLASMA

A. A. VEDENOV and A. I. LARKIN

Moscow State University

Submitted to JETP editor October 1, 1958

J. Exptl. Theoret. Phys. (U.S.S.R.) **36**, 1133-1142 (April, 1959)

The free energy F of a completely ionized gas is given in terms of an expansion in the density n:

$$F = F_{\text{ideal}} + An^{3/2} + Bn^2 \ln n + Cn^2.$$

The term $An^{3/2}$ is identical with the familiar Debye-Hückel term. Expressions for B and C have been obtained. A diagram technique has been used to carry out the calculations.

THE equation of state of a system of particles which interact via Coulomb forces has been considered in a great number of papers. The usual formulas for the virial coefficients do not apply in this case. Because the Coulomb forces are long-range, even in the first term of an expansion of the thermodynamic quantities in powers of the gas density it is impossible to consider pair interactions alone. Debye and Hückel[1] have used a self-consistent field method for finding the first term in the expansion of the free energy in the density of the interacting particles n; this term was found to be proportional to $n^{3/2}$ (per unit volume). In the work of Glauberman and Yuchnovskiĭ at attempt was made to compute the following terms in the expansion, but the methods used in this work do not appear to be valid and lead to erroneous results.

In the present work, the first terms in the density expansion have been determined using a graphical method similar to the Feynman method in quantum electrodynamics.

1. DIAGRAM TECHNIQUE. GAS APPROXIMATION.

We consider a system of interacting particles in a volume V in a state of thermodynamic equilibrium at a temperature $T = 1/\beta$. The Hamiltonian for the system is $H = H_0 + H'$ where

$$H_0 = \sum_p \varepsilon_p a_p^+ a_p,$$

$$H' = \frac{1}{2V} \sum_{p_1 p_2 q} V_q a_{p_1}^+ a_{p_2}^+ a_{p_2+q} a_{p_1-q}, \qquad \varepsilon_p = p^2/2m.$$

Here a_p and a_p^+ are the particle annihilation and creation operators; $V_q = \int e^{i-qx} V(\mathbf{x})\, d\mathbf{x}$ where $V(\mathbf{x})$ is the potential for the pair interaction. In the case of a Coulomb interaction $V_q = 4\pi e^2/q^2$.

The partition function for a gas of interacting particles is given by the expression

$$Z = \operatorname{Sp} \exp\left\{-\beta H + \beta\mu \sum_p a_p^+ a_p\right\},$$

where μ is the chemical potential.

Matsubara has shown[3] that the ratio Z/Z_0 (where $Z_0 = \operatorname{Sp} \exp\{-\beta H_0 + \beta\mu \sum a_p^+ a_p\}$) can be computed conveniently by a method similar to that used in quantum electrodynamics for finding the S matrix. The quantity Z/Z_0 is given as the sum of all graphs which in electrodynamics serve for computation of the vacuum expectation value of the S matrix. The solid line corresponds to the zeroth Green's function

$$G_0(p, t_1 - t_2) = \frac{\operatorname{Sp} T \exp\{-\beta H_0 + \beta\mu \sum a_p^+ a_p\}\, a_p(t_1) a_p^+(t_2)}{\operatorname{Sp} \exp\{-\beta H_0 + \beta\mu \sum a_p^+ a_p\}}$$

$$= \begin{cases} (1 \mp n_p)\, e^{-(\varepsilon_p - \mu)\tau} & \tau > 0 \\ \mp n_p\, e^{-(\varepsilon_p - \mu)\tau} & \tau < 0 \end{cases}. \qquad (1)$$

Here the upper and lower signs refer respectively to Fermi and Bose particles, and T is an ordering operator which operates on the argument t,

$$\tau = t_1 - t_2; \quad a_p(t) = a_p e^{-(\varepsilon_p - \mu)t};$$

$$a_p^+(t) = a_p^+ e^{(\varepsilon_p - \mu)t}, \quad n_p = [e^{(\varepsilon_p - \mu)\beta} \pm 1]^{-1}.$$

The dashed line corresponds to $V_q \delta(\tau)$. Time increases going upward in the figure. Then all the dashed lines are horizontal. The solid line which goes upwards then corresponds to the factor $\mp n_p e^{-(\varepsilon_p - \mu)\tau}$, the line which goes downward corresponds to the factor $(1 \mp n_p)\, e^{-(\varepsilon_p - \mu)\tau}$.

As in quantum electrodynamics, the sum of graphs which give Z/Z_0, may be given in the form e^{-L}. The quantity L is the sum of all connected closed graphs and all the graphs considered below appear in the sum with the factor $(-1)^{r+1+k}/2k$ where k is the number of dashed lines in a given graph and r is the number of closed loops. All

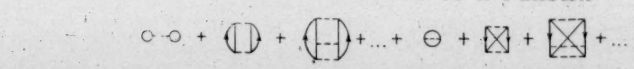

EIG. 1

the graphs being considered are closed; hence the factor $e^{\mu\tau}$ in Eq. (1) can be neglected.

The thermodynamic potential $\Omega = -T \ln Z$ is

$$\Omega = \Omega_0 + \Delta\Omega = \Omega_0 + TL, \qquad \Omega_0 = -T \ln Z_0.$$

In what follows we will assume that the gas is nondegenerate (so that departures from the Boltzmann distribution are small); we introduce the quantity n which is related to the chemical potential by the expression

$$n = e^{\beta\mu} (m/2\pi\hbar^2\beta)^{3/2}. \tag{2}$$

We first consider short-range forces. We will assume that the particles have no spin. In order to find the second virial coefficient it is necessary to sum all graphs which contain two solid lines which go in the upward direction and whose remaining lines go downward (Fig. 1). In these graphs we neglect n_p as compared with unity.

To the k-th order perturbation approximation there are k identical graphs which differ only in the way in which the pair of solid lines go upwards. Hence in each order we need consider only one graph and can neglect the factor 1/k. Then

$$-\beta\Delta\Omega = {}^1/_2 \int_0^\beta dt_2 \int_0^{t_2} dt_1 \, G_{p_1}(t_1 - t_2)\, G_{p_1}(t_1 - t_2)$$

$$[\Gamma(p_1 p_2 p_1 p_2\, t_2 t_1) + \Gamma(p_1 p_2 p_2 p_1\, t_2 t_1)]\, d^3p_1\, d^3p_2. \tag{3}$$

The factor $\Gamma(p_1 p_2 p_3 p_4 t_1 t_2)$ is the sum of graphs of the "ladder" type (Fig. 2) and satisfies the equation

$$\Gamma_g(pp'\, t_1 t_2) = V_{p-p'}\, \delta(t_1 - t_2)$$

$$-\int_{t_2}^{t_1} dt'\, d^3p_1 V_{p-p_1} G_{g/2+p_1}(t_1 t')\, G_{g/2-p_1}(t_1 t')\, \Gamma_g(p_1 p' t' t_2).$$

Here

$$d^3p = dp_x\, dp_y\, dp_z/(2\pi)^3,$$

$$\Gamma_g(pp') = \Gamma(g/2 + p,\, g/2 - p,\, g/2 + p',\, g/2 - p')$$

Introducing the variables $\tau = t_1 - t_2$, $\tau' = t' - t_2$ and making the substitution $G(p\tau) = e^{-\epsilon p^2}(\tau > 0)$, we have

$$\Gamma_g(pp'\tau) = V_{p-p'}\, \delta(\tau)$$

$$-\int_0^\tau d\tau'\, d^3p_1 V_{p-p_1} \exp\left\{-\frac{1}{m}\left(p_1^2 + \frac{g^2}{4}\right)(\tau - \tau')\right\} \Gamma_g(p_1 p' \tau')$$

FIG. 2

or, in the Laplace transform representation

$$\Gamma_\omega = \int_0^\infty e^{-\omega\tau}\, \Gamma(\tau)\, d\tau$$

$$\Gamma_{g\,\omega}(pp'\omega) = V_{p-p'} - \int d^3p_1 V_{p-p_1} \frac{\Gamma_{g\,\omega}(p_1 p'\omega)}{(p_1^2 + g^2/4)/m + \omega}.$$

The equation for

$$\chi_{g\,\omega}(pp'\omega) = \Gamma_{g\,\omega}(pp'\omega) \left/ \left[\frac{1}{m}\left(p^2 + \frac{g^2}{4}\right) + \omega\right]\right.$$

is in the form of an inhomogeneous Schrödinger equation with potential V_q:

$$\left(\frac{p^2 + g^2/4}{m} + \omega\right)\chi(p) + \int V_{p-p_1}\chi(p_1)\, d^3p_1 = V_{p-p'}.$$

Hence its solution is expressed in terms of the wave functions for the relative motion of the particles

$$\chi_{g\,\omega}(pp'\omega) = \int V_{p-p_1} \sum_k \frac{\psi_k(p_1)\,\psi_k^*(p')}{E_k + g^2/4m + \omega}\, d^3p_1$$

$$= \sum_k \psi_k(p)\,\psi_k^*(p') \frac{E_k - p^2/m}{E_k + g^2/4m + \omega}. \tag{4}$$

Substituting in Eq. (3)

$$G(p, \tau) = \exp[\mu\beta - (\beta + \tau)\varepsilon_p], \quad \tau < 0,$$

we find the Laplace transform of the function $\varphi(\beta) = -\beta\Delta\Omega e^{-2\mu\beta}$:

$$\varphi(\omega) = \int_0^\infty e^{-\beta\omega}\, \varphi(\beta)\, d\beta$$

$$= \int d^3p\, d^3g \frac{1}{(p^2/m + g^2/4m + \omega)^2}\, [\Gamma_g(p, p, \omega) + \Gamma_g(p, -p, \omega)].$$

Using Eq. (4) we have

$$\varphi(\omega) = -\int d^3p\, d^3g \frac{1}{p^2/m + g^2/4m + \omega}$$

$$\times \sum_k \psi_k(p)\,[\psi_k^*(p) + \psi_k^*(-p)] \frac{E_k - p^2/m}{E_k + g^2/4m + \omega}.$$

Inasmuch as $\psi_k(-p) = \pm\psi_k(p)$, corresponding to the states with positive and negative parity, this expression can be written in the form

$$\varphi(\omega) = -2\int d^3p\, d^3g \frac{1}{p^2/m + g^2/4m + \omega}$$

$$\times \sum{}' \psi_k(p)\,\psi_k^*(p) \frac{E_k - p^2/m}{E_k + g^2/4m + \omega},$$

where $\sum'$ is taken over even states. Returning to $\varphi(\beta)$, for the correction to $\Delta\Omega$ we obtain the expression

$$-\beta\Delta\Omega = \tfrac{1}{2} e^{2\mu\beta} \Big\{ 2 \sum_k{}' (e^{-\beta E_k} - e^{-\beta p^2/m})\, \psi_k(p)\, \psi_k^*(p)\, d^3p \times \int e^{-\beta g^2/4m}\, d^3g \Big\}$$

$$= \tfrac{1}{2} e^{2\mu\beta} \Big(\frac{m}{\pi\hbar^2\beta}\Big)^{3/2} \Big\{ \sum_k{}' e^{-\beta E_k} - \int e^{-\beta p^2/m}\, d^3p \Big\}, \qquad (5)$$

which coincides with that found in reference 4. For Fermi particles with spin $\frac{1}{2}$ we obtain a similar expression which differs only in that in place of the sum over even states $\sum'$ we have $\frac{1}{4}\sum' + \frac{3}{4}\sum''$, where $\sum''$ is the sum over odd states.

In the quasi-classical case the summation in Eq. (5) can be replaced by the integral

$$2 \sum_k{}' e^{-\beta E_k} = \int e^{-\beta E} \frac{dn}{dE}\, dE,$$

where

$$n(E) = \frac{2}{\pi} \int_0^\infty dr \int_0^{r\sqrt{E-U}} 2l\, dl \sqrt{m(E - l^2/mr^2 - U)}.$$

Substituting in Eq. (5) we have

$$-\beta\Delta\Omega = \frac{1}{2} n^2 \int_0^\infty (e^{-\beta U} - 1)\, 4\pi r^2\, dr, \qquad (5a)$$

where n is defined by Eq. (2), coinciding with the correction to $\Delta\Omega$ due to the second virial coefficient in the classical case.

2. SUMMATION OF GRAPHS IN THE CASE OF A COULOMB INTERACTION

It is shown in the Appendix that in order to find the thermodynamic potentials of the plasma it is sufficient to know Ω for $V_{q=0} \equiv V_0 = 0$: $\Omega_{V_0=0} = \Omega$. Hence it is possible to neglect the graphs with V_0 (for example the graph of Fig. 3a). Divergences arise in the first-order graphs (Fig. 3, b and c).

a b c

FIG. 3

Figure 3b gives a contribution equal to

$$-\frac{1}{4} \int d^3\boldsymbol{q} \int_0^\beta dt_1 \int_0^\beta dt_2\, V_q^2 \Pi_q^2(t_1 t_2), \qquad (6)$$

where

$$\Pi_q(t_1 t_2) = \int G_{p-q/2}(t_1 t_2)\, G_{p+q/2}(t_2 t_1)\, d^3p.$$

The integral in Eq. (6) diverges linearly in the region of small q. Hence it is convenient to give Π_q^2 in the form of a sum

$$\Pi_0^2 + \{2(\Pi_q - \Pi_0)\Pi_0 + (\Pi_q - \Pi_0)^2\},$$

where Π_0 is the value of Π_q at the point q = 0: $\Pi_0 \equiv \Pi_{q=0} = -n$.

If this expression is substituted in Eq. (6) the integral containing the brackets has no singularities and becomes

$$\tfrac{1}{4}\pi^{3/2} n^2 e^4 \beta^{1/2}\hbar\, m^{-1/2}. \qquad (7)$$

The divergence in the integral which contains Π_0 is due to the fact that it is not valid to neglect certain higher-order terms in the density. For example, when the contribution of the graphs of Fig. 4 is taken into account the integrand in the region of small q becomes larger than the corresponding expression for the graph in Fig. 3b.

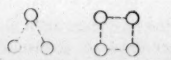

FIG. 4

Hence, in carrying out the integration over q it is necessary to sum the integrands in all the graphs in which each V_q has the same vector q. Since $\Pi_0 = -n$ is independent of t, the summation is carried out easily:

$$\tfrac{1}{4}(\beta\Pi_0 V_q)^2 + \tfrac{1}{6}(\beta\Pi_0 V_q)^3 \ldots$$

$$= \frac{1}{2} \int_0^1 \frac{d\lambda}{\lambda} [(\beta\Pi_0 V_q\lambda)^2 + (\beta\Pi_0 V_q\lambda)^3 + \ldots]$$

$$= \frac{1}{2} \int_0^1 \frac{d\lambda}{\lambda} \frac{\beta^2\Pi_0^2 V_q^2 \lambda^2}{1 - \beta\Pi_0 V_q \lambda}.$$

The integration over q and λ then gives

$$\Delta\widetilde{\Omega} = -\tfrac{2}{3}\sqrt{\pi\beta}\, e^3 (-\Pi_0)^{3/2}. \qquad (8)$$

The contribution from the graph of Fig. 3c gives an integral which diverges logarithmically in the region in which all the q are small:

$$\frac{1}{2} \int dq_1\, dq_2\, V_{q_1} V_{q_2} V_{q_1+q_2}\, I_{q_1 q_2};$$

$$I_{q_1 q_2} = \int_0^\beta dt_3 \int_0^{t_3} dt_2 \int_0^{t_3} dt_1 G_{p_1}(t_1 t_3) G_{p_2}(t_1 t_2)$$

$$G_{p_1+q_1}(t_3 t_2)\, G_{p_2-q_1}(t_3 t_2) G_{p_1-q_2}(t_2 t_1) G_{p_2+q_2}(t_2 t_1).$$

In carrying out the calculation it is convenient to give I in the form

$$I_{q_1 q_2} = \{I_{q_1 q_2} - \beta^3 n^2/6\,(1 + \lambda q_1^2)(1 + \lambda q_2^2)(1 + \lambda(q_1 + q_2)^2)\}$$

$$+ \beta^3 n/6\,(1 + \lambda q_1^2)(1 + \lambda q_2^2)(1 + \lambda(q_1 + q_2)^2) \qquad (9)$$

(where $\lambda = \beta\hbar^2/m$). The integral which contains the brackets has no singularities and is

$$1/3\,\pi an^2(\beta e^2)^3, \qquad (10)$$

where a is a numberical coefficient of order unity. We shall not make an exact computation of this coefficient for the following reasons. In the case of low or high temperatures (where we use correspondingly the quasi-classical or Born approximations for the electrons) the coefficient in front of the term of order n^2 in the expansion of Ω in the density turns out to be of order $(\hbar^2\beta/m)^{3/2}$, i.e., considerably larger than the quantity $(\beta e^2)^3$ which appears in Eq. (10). On the other hand, since the term of order n^2 is the smallest of those given in the present work, small corrections of order $(\beta e^2)^3$ to the coefficient for this term can be neglected.

In the remaining second term in $I_{q_1q_2}$ in carrying out the integration over $q_{1,2}$ we sum the contribution of those graphs of higher order in the density in which all the momenta $\mathbf{q}$ along the dashed lines correspond to one of the momenta, $\mathbf{q}_1$, $\mathbf{q}_2$, $\mathbf{q}_1+\mathbf{q}_2$. This summation means that we replace V_q by

$$V_q/(1-\beta\Pi_0V_q) = 4\pi e^2/(\mathbf{q}^2+\varkappa^2), \quad \varkappa^2 = -4\pi e^2\beta\Pi_0.$$

Under these conditions the integral of the second term in I converges. In order to compute this integral it is convenient to introduce the Fourier transform for q:

$$\frac{4\pi}{q^2+\varkappa^2}\frac{1}{1+\lambda q^2} = \int e^{i\mathbf{qr}}\,\frac{e^{-\varkappa r}-e^{-r\sqrt{\lambda}}}{r}\,\frac{1}{1-\lambda\varkappa^2}\,d\mathbf{r},$$

after which the integral assumes the form

$$\frac{1}{2}\,e^6\,\frac{\beta^3n^2}{6}\,4\pi\int\frac{dr}{r}\,(e^{-\varkappa r}-e^{-r/\sqrt{\lambda}})^3(1-\lambda\varkappa^2)^{-3}. \qquad (10a)$$

Computing this integral to accuracy of order $n^{5/2}$ in the density and neglecting the correction $(\beta e^2)^3$ in the quadratic term we have

$$(\pi/3)\,n^2(e^2\beta)^3\ln(\sqrt{\lambda}\varkappa). \qquad (10b)$$

Thus, to obtain the correct virial correction to $\Delta\Omega$ of this system with a Coulomb interaction it is necessary to correct the contributions from the lower-order graphs. The first terms in the expansion in powers of the interaction in (5) are replaced by the corrected expressions obtained by the methods indicated above.

In the quasi-classical case $e^2/\hbar v \gg 1$; thus, replacing the first terms of the expansion in e^2 in Eq. (52) by the corrected terms (8), (9), and (10a) we have:

$$-\beta\Delta\widetilde{\Omega} = \frac{n^2}{2}\int_0^\infty\left[\left(e^{-\beta e^2/r}-1+\frac{\beta e^2}{r}-\frac{(\beta e^2/r)^2}{2}+\frac{(\beta e^2/r)^3}{6}\right)\right.$$
$$\left.-\frac{(\beta e^2)^3}{6}\,\frac{e^{-\beta\varkappa r}}{r^3}\right]4\pi r^2\,dr+\frac{2}{3}\sqrt{\pi\beta^3}e^3n^{3/2}. \qquad (11)$$

Here we have not taken account of the quantum corrections since the contribution in (7) is neglected and we have assumed $\lambda = 0$. Limiting ourselves to the principal values of the expansion in n and computing the integral we have

$$-\beta\Delta\widetilde{\Omega} = \frac{2}{3}\sqrt{\pi\beta^3}\,e^3n^{3/2}+\frac{\pi}{3}\,n^2(\beta e^2)^3\ln\frac{1}{\beta e^2\varkappa}. \qquad (12)$$

3. EQUATION OF STATE OF THE PLASMA

We consider a system consisting of ions of charge z and electrons. We consider only classical ion motion.

It is necessary to make the following changes in Eqs. (8) to (10a) above: the quantity Π_0, which represents the contribution from the electron and ion loop, becomes

$$\Pi_0 = -(z^2n_i+n_e), \qquad n_{i,e} = e^{\beta\mu_{i,e}}(m_{i,e}/2\pi\hbar\beta)^{3/2}. \qquad (13)$$

Consequently, the quantity $\varkappa^2 = -4\pi\beta e^2\Pi_0$ becomes $4\pi\beta e^2(z^2n_i+n_e)$.

We consider two limiting cases.

a) $T \ll me^4/\hbar^2$

In this case the motion of both the ions and electrons is quasi-classical. The Debye term in $\Delta\Omega$ (proportional to $n^{3/2}$) is obtained from Eq. (8) by substituting Eq. (13) in place of Π_0. The next term in the expansion of Ω in powers of the density, which is proportional to $n^2\ln n$, is obtained from the graphs of Fig. 3c in which the solid lines may be considered electron and ion Green's functions. The contributions from the graphs containing two electron or two ion loops are obtained from the second term of Eq. (12) by replacing n^2e^6 by $n_e^2e^6$ and $z^6n_i^2e^6$ respectively. In computing the contribution from the graph with one electron and one ion loop from Eq. (11) we would obtain an integral which diverges exponentially at small values of r, since in this case the quantity e^2 in Eq. (11) is replaced by $-z^2e^2$. This results from the inapplicability of the classical expression (11) at small distances. Nonetheless in obtaining the term $n^2\ln n$ it is possible to use Eq. (11), limiting ourselves in the integration to the region in which (11) applies. We obtain (neglecting terms n_en_i):

$$-\frac{\pi}{3}(ze^2\beta)^3\,n_in_e\ln\frac{1}{\beta e^2\varkappa}. \qquad (14)$$

In computing the term of order n_in_e in Eq. (5) we keep only the first term in the sum; this term corresponds to the ground state of the electron in the field of an ion of charge z:

$$n_in_e\exp\{\beta z^2me^4/2\hbar^2\}.$$

We note that the error in the calculation of Eq. (14) is exponentially small as compared with this term; the other terms in Eq. (5) are also exponentially small.

Thus, in the quasi-classical case the expression for the potential Ω is of the form:

$$\beta\tilde{\Omega} = \beta\Omega_0 - \frac{2}{3}\sqrt{\pi\beta^3}\, e^3 (z^2 n_i + n_e)^{1/2} + \frac{\pi}{3}(\beta e^2)^3 (z^2 n_i - n_e)^2 \ln\frac{1}{\beta e^2 \varkappa} + \left(\frac{2\pi\hbar^2\beta}{m}\right)^{3/2} n_i n_e \exp\left\{\frac{\beta z^2 m e^4}{2\hbar^2}\right\}. \quad (15)$$

We may note that this expression applies when $T \ll z^2 me^4/\hbar^2$.

b) $T \gg z^2 me^4/\hbar^2$

In this case the electron-electron and electron-ion interactions considered in accordance with perturbation theory. The term proportional to $n^{3/2}$ remains unchanged. The ion-ion interaction leads to a correction in Ω which arises from the second term in Eq. (12) when n^2e^6 is replaced by $n_i^2 z^6 e^6$.

The "non-exchange" terms of the electron-electron interaction of second and third order in e^2 give the expressions in (7) and (10b) respectively, in which n must be replaced by n_e. The corresponding terms of the electron-ion interactions are obtained by the following substitution: in second-order it is necessary to replace n^2e^4 by $z^2 n_i n_e e^4$ and to add the factor $1/\sqrt{2}$ which arises because the reduced mass is increased by a factor of 2; in the third-order graph it is necessary to replace n^2e^6 by $-z^3 n_i n_e e^6$. The "exchange" terms arising in the electron-electron interaction (corresponding to the graphs in Fig. 5)

a b

FIG. 5

lead to the following contribution in the correction term to $\beta\Delta\Omega$: the first-order exchange term (Fig. 5a) is:

$$\frac{\beta}{2}\int V_q n_{p+q/2} n_{p-q/2} d^3p d^3q = \pi n_i^2 \beta^2 e^2 \frac{\hbar^2}{m},$$

the second-order term (Fig. 5b) is:

$$\frac{1}{2}\int_0^\beta dt_2 \int_0^{t_2} dt_1 \int G_{p+q/2+q_1/2}(t_1 t_2)\, G_{p-q/2+q_1/2}(t_2 t_1)\, G_{p-q/2-q_1/2}(t_1 t_2) \times G_{p+q/2-q_1/2}(t_2 t_1) V_q V_{q_1} d^3p\, d^3q d^3q_1;$$

replacing G by (1), we have

$$\pi^{1/2} \ln 2 \cdot n^2 e^4 \beta^{5/2}\hbar/\sqrt{m}.$$

Thus, in the case $T \gg z^2 me^4/\hbar^2$ the expansion of the thermodynamic potential $\tilde{\Omega}$ in terms of the density is

$$\beta\tilde{\Omega} = \beta\Omega_0 - {}^2/_3\sqrt{\pi\beta^3}e^3(z^2 n_i + n_e)^{3/2} + (\pi/3)(\beta e^2)^3[z^6 n_i^2 \ln(1/z^2\beta e^2\varkappa) + n_e^2 \ln(m^{1/2}/\hbar\beta^{1/2}\varkappa) - 2z^3 n_i n_e \ln(m^{1/2}/\hbar\beta^{1/2}\varkappa)] + {}^1/_4\pi^{3/2} n_e^2 \hbar^3 \beta^{3/2} m^{-3/2} + n_e^2\{-\pi e^2\hbar^2\beta^2 m^{-1} + \pi^{3/2}(\ln 2 + {}^1/_4) e^4 \hbar\beta^{3/2} m^{-1/2}) + n_i n_e (2^{-1/2}\pi^{3/2} z^2 e^4 \hbar\beta^{3/2} m^{-1/2}). \quad (16)$$

The terms ${}^1/_4 n_e^2 \hbar^3 (\pi\beta/m)^{3/2}$ in this expression is independent of the interaction and is due to the departure of the electron momentum distribution function from a Maxwellian distribution (due to the identity of the electrons).

Using the equations

$$\partial\tilde{\Omega}/\partial\mu_i = -N, \quad \partial\tilde{\Omega}/\partial\mu_e = -zN$$

we express μ_i and μ_e in terms of the atomic density $N/V \equiv n$; substituting in the formula

$$F = \Omega + \mu_i N + \mu_e z N,$$

we find the free energy per unit volume:

$$\beta F = \beta F_0 - \frac{2}{3}\sqrt{\pi\beta^3}e^3 [z(z+1)]^{3/2} n^{3/2} + \frac{\pi}{3}(\beta e^2)^3 z^2 (z^2-1)^2 n^2 \ln\frac{m^{1/2}}{\beta^{1/2}\hbar\varkappa} + n^2\left\{\frac{\pi^{3/2}}{4} z^2 \frac{\hbar^3\beta^{3/2}}{m^{3/2}} - \pi z^2 e^2 \frac{\beta^2\hbar^2}{m} + \left(\ln 2 + \frac{1}{4} + \frac{z}{\sqrt{2}}\right)\pi^{3/2} z^2 e^4 \frac{\hbar\beta^{3/2}}{m^{1/2}}\right\}. \quad (17)$$

4. CONCLUSIONS

Equation (17) represents an expansion of the free energy in terms of the density. The coefficient of the quadratic density term is a function of the parameter $ze^2\sqrt{\beta m}/\hbar$. The three first terms of the expansion involve this parameter. In the case in which $ze^2\sqrt{\beta m}/\hbar \sim 1$ the function is expressed in terms of the phase in the Coulomb field and can be computed. The term of the expansion of F in the density proportional to $n^{5/2}$ may also be expressed in terms of the phase; however, in order to find the higher order terms in the expansion in density it is necessary to know the wave functions of s system of three interacting Coulomb particles.

In conclusion the authors wish to thank L. D. Landau and V. M. Galitskiĭ for valuable comments.

APPENDIX

We find Ω for $V_0 \to \infty$, knowing the quantity $\tilde{\Omega} = \Omega_{V_0=0}$ computed in the text.

The interaction Hamiltonian is of the form

$$H' = \frac{1}{2V}\sum_{q} V_q \sum_{pp'} (a_p^+ a_{p'}^+ a_{p'-q} a_{p+q}$$

$$+ z^2 \alpha_p^+ \alpha_{p'}^+ \alpha_{p'-q} \alpha_{p+q} - 2z a_p^+ \alpha_{p'}^+ \alpha_{p'-q} a_{p+q}),$$

where a_p and α_p are the annihilation operators for electrons and ions respectively. The quantity Ω is given as a function of μ_e, μ_i and V_0 by (per unit volume)

$$\beta\Omega = -\frac{1}{V} \ln \mathrm{Sp} \exp\left\{-\beta\left(H_0 + H'\right.\right.$$

$$\left.\left. - \mu_e \sum_p a_p^+ a_p - \mu_i \sum_p \alpha_p^+ \alpha_p\right)\right\}.$$

Differentiating this expression with respect to V_0, μ_e and μ_i it is easy to find the relation (to terms which approach zero as $V \to \infty$):

$$\partial\Omega / \partial V_0 = -{}^1/_2 (z\partial\Omega / \partial\mu_i - \partial\Omega / \partial\mu_e)^2.$$

We introduce the variables

$$M = z\mu_e + \mu_i, \quad \mu = (z\mu_e - \mu_i) / 2z,$$

whence the equation assumes the form

$$\partial\Omega / \partial V_0 = -{}^1/_2 (\partial\Omega / \partial\mu)^2. \tag{I}$$

It is required to find the solution of this equation for the initial condition $\Omega(\mu, 0) = \widetilde{\Omega}(\mu)$. The general integral is of the form

$$\Omega = -\frac{a^2}{2} V_0 + a\mu + b(a), \tag{II}$$

where a is a function of μ and V_0 defined by the equation

$$-aV_0 + \mu + b'(a) = 0. \tag{III}$$

The function $b(a)$ is expressed so as to satisfy the initial condition

$$a(\mu, 0)\,\mu + b[a(\mu, 0)] = \widetilde{\Omega}(\mu). \tag{IV}$$

It is apparent from Eq. (III) that as $V_0 \to \infty$ the quantity $a(\mu, V_0)$ approaches zero as $(\mu + b'(0))/V_0$; hence $\Omega(\mu, \infty) = b(0)$ and is independent of the variable μ.

In order to find $b(0)$ we differentiate (IV) with respect to μ; then, using (III), we have $a(\mu, 0) = d\widetilde{\Omega}/d\mu$.

We define μ_0 by the equation

$$(d\widetilde{\Omega} / d\mu)_{\mu=\mu_0} = 0. \tag{V}$$

Substituting in Eq. (IV) $\mu = \mu_0$, we find $b(0) = \widetilde{\Omega}(\mu_0)$.

Thus,

$$\Omega(\mu, \infty) = \widetilde{\Omega}(\mu_0, 0), \tag{VI}$$

where μ_0 is defined by Eq. (V).

The free energy of the system if $F = \Omega + MN$ where M is found from the condition $\partial\Omega/\partial M = -N$. Returning to the variables μ_e and μ_i, taking account of Eqs. (V) and (VI) we have

$$F = \widetilde{\Omega} + z\mu_e N + \mu_i N,$$

where μ_i and μ_e are defined by the relations

$$\partial\widetilde{\Omega} / \partial\mu_i = -N, \quad \partial\widetilde{\Omega} / \partial\mu_e = -zN.$$

[1] P. Debye and E. Hückel, Physik Z. **24**, 185, 1923.

[2] A. E. Glauberman and I. R. Yukhnovskiĭ, J. Exptl. Theoret. Phys. (U.S.S.R.) 22, 564, 572, 1952. I. R. Yukhnovskiĭ, J. Exptl. Theoret. Phys. (U.S.S.R.) **34**, 379 (1958); Soviet Phys. JETP **7**, 263 (1958).

[3] T. Matsubara, Progr. Theoret. Phys. **14**, 351 1955.

[4] E. Beth and G. Uhlenbeck, Physica **4**, 915 (1937).

Translated by H. Lashinsky
220

ON THE THEORY OF DIRECT NUCLEAR REACTIONS INVOLVING POLARIZED PARTICLES

G. L. VYSOTSKIĬ and A. G. SITENKO

Physico-Technical Institute of the Academy of Sciences, Ukrainian S.S.R.; Khar'kov State University

Submitted to JETP editor October 2, 1958

J. Exptl. Theoret. Phys. (U.S.S.R.) **36**, 1143-1153 (April, 1959)

The theory of direct nuclear reactions (stripping and pick-up reactions) involving polarized particles is considered. The angular distributions and polarizations of the products of direct nuclear reactions induced by polarized particles in oriented nuclei are determined by the distorted wave method without inclusion of the spin-orbit coupling.

1. INTRODUCTION

THE theory of direct nuclear reactions (stripping and pick-up reactions) is widely used in nuclear spectroscopy to determine the properties of nuclei. The angular distribution of the products of the direct reactions permits the determination of the spin and the parity of the final state of the remaining nucleus, if the spin and the parity of the initial state of the initial nucleus are known. Additional information about the structure of the nucleus can be obtained in the investigation of the polarization phenomena accompanying the direct reactions.

Newns[1] was the first to point out the possibility of a polarization of the protons in stripping reactions. He also showed that the sign of the polarization of the proton determines the value of the total angular momentum of the captured neutron ($j_n = l + \frac{1}{2}$ or $j_n = l - \frac{1}{2}$). Assuming the nucleus to be completely black for protons, Newns found that the polarization is negative if the neutron is absorbed with $j_n = l + \frac{1}{2}$, and positive if $j_n = l - \frac{1}{2}$. The positive direction is taken along the vector $\mathbf{k}_d \times \mathbf{k}_p$. Horowitz and Messiah[2] determined the polarization of the protons in stripping reactions, using for the nucleus the model of a hard sphere. They obtained the same sign for the polarization as in reference 1. The experimental sign of the polarization was in disagreement with these predictions.[3]

Later Tobocman, and also Newns and Refai[4] showed that the correct sign of the polarization of the protons can be obtained if the scattering of the deuteron wave by the nucleus is taken into account. The experimental results[5,6] are in agreement with reference 4.

Cheston[7] and Sawicki[8] discussed the effect of the spin-orbit interaction on the polarization of the protons, which is, however, small.

Dalitz[9] and Lakin[10] considered the theory of the reactions of particles with spin 1. The stripping reaction with polarized deuterons was also investigated by Satchler.[11,12]

In the present paper we obtain the angular distribution and the polarization of the products of stripping and pick-up reactions in the interaction of polarized particles with arbitrarily oriented nuclei. The angular distribution of the protons produced in the stripping reaction with polarized deuterons has an azimuthal asymmetry. A study of this asymmetry leads to the possibility of determining the spin of the final state of the remaining nucleus. We also consider other possibilities of using the stripping reaction with polarized deuterons to obtain additional information about the structure of the nucleus. In particular, it will be possible to determine the reduced widths for states with different values of the orbital momentum of the absorbed neutron.

The formation of deuterons in the interaction of polarized protons with nuclei is also characterized by an angular distribution with an azimuthal asymmetry. The produced deuterons are polarized. The capture reaction with polarized nucleons can be used for the production of polarized deuterons.

We use the method of distorted waves. The spin-orbit interaction was neglected, since it gives a relatively small contribution to the cross section.[4] We also neglect Coulomb effects, which are insignificant for sufficiently high energies.

2. THE STRIPPING REACTION (d,p) WITH POLARIZED PARTICLES

We shall describe the polarization effects in the stripping reaction (d,p) with the help of a density matrix, whose elements completely determine the spin states of the particles participating in the reaction.

The density matrix of the total system in the initial state (deuteron + initial nucleus) is given in the form of the direct product of the density ρ^d and ρ^A, referring to the deuteron and the nucleus. The deuteron density matrix has three rows and columns: $\rho^d = \rho_{\mu_d\mu'_d}$ (μ_d and μ'_d are the possible values of the spin projection of the deuteron). The nuclear density matrix has $(2i+1)$ rows and columns: $\rho^A = \rho_{\mu_i\mu'_i}$ (i is the spin of the initial nucleus, μ_i and μ'_i are the possible values of the spin projection of the nucleus).

Instead of giving the elements of the density matrix, we can expand it in terms of spin-tensors. These form an orthogonal system of matrices which transform according to an irreducible representation of the rotation group when the system of coordinates is rotated. The spin states of the system are then given by the coefficients of this expansion. We expand the 3×3 deuteron density matrix $\rho_{\mu_d\mu'_d}$ in terms of the spin-tensors

$$T^{JM}_{\mu_d\mu'_d} = (-1)^{1+\mu'_d}(11\mu_d - \mu'_d \mid JM)$$

of rank J = 0, 1, and 2:

$$\rho_{\mu_d\mu'_d} = \sum_{JM} \langle T^{JM+}\rangle T^{JM}_{\mu_d\mu'_d}. \qquad (1)$$

The $(2i+1)$-rowed density matrix of the initial nucleus $\rho_{\mu_i\mu'_i}$ is expanded in terms of the spin-tensors $T^{LQ}_{\mu_i\mu'_i} = (-1)^{i+\mu'_i}(ii\mu_i - \mu'_i \mid LQ)$ of rank L = 0, 1, . . . , 2i:

$$\rho_{\mu_i\mu'_i} = \sum_{LQ} \langle T^{LQ+}\rangle T^{LQ}_{\mu_i\mu'_i}. \qquad (2)$$

The density matrix of the total system in the initial state is normalized to unity: Sp ρ = 1.

The density matrix of the system in the final state (proton + remaining nucleus), ρ', is connected with the initial matrix, ρ, by the relation

$$\rho' = S\rho S^*,$$

where S is the reaction matrix. It can be shown that, neglecting the spin-orbit interaction, the reaction matrix has the form

$$S_{\mu_p\mu_j;\ \mu_d\mu_i} = \sum_{lsm\mu_s\mu_n} (1/2\,1/2\mu_p\mu_n \mid 1\mu_d)$$

$$\times\ (i\,1/2\mu_i\mu_n \mid s\mu_s)(sl\mu_s m \mid j\mu_j)\sqrt{\gamma_{ls}}\,J^m_l, \qquad (3)$$

if the state of the captured neutron in the nucleus is given in the $l-s$ coupling scheme. Here l and m are the orbital angular momentum of the absorbed neutron and its projection, s and μ_s are the channel spin and its projection, j and μ_j are the spin of the remaining nucleus and its projection, μ_n and μ_p are the spin projections of the neutron and the proton in the deuteron, and γ_{ls} is the reduced width. The quantity J^m_l is defined by

$$J^m_l = \sqrt{\frac{4M\alpha}{n\hbar^2 R}} \int_{r>R} \psi^*_{\mathbf{k}_p}(\mathbf{r})\,\frac{k_l(k_n r)}{k_l(k_n R)}\,Y^*_{lm}(\vartheta,\varphi)\,\psi_{\mathbf{k}_d}(\mathbf{r})\,d\mathbf{r}.$$

$\psi_{\mathbf{k}_p}$ is the wave function of the liberated proton with the wave vector $\mathbf{k}_p$; $\psi_{\mathbf{k}_d}$ is the wave function of the incoming deuteron; $k_n = \sqrt{2M\,|\,E_n\,|}/\hbar$; E_n is the energy of the neuteron in the nucleus.

Using the expansions (1) and (2), we write the density matrix of the final state in the form

$$\rho'_{\mu_p\mu_j;\ \mu'_p\mu'_j} = \sum_{JM,\ LQ} \langle T^{JM+}\rangle \langle T^{LQ+}\rangle$$

$$\times \sum_{\mu_d\mu'_d\mu_i\mu'_i} S_{\mu_p\mu_j;\ \mu_d\mu_i}\, T^{JM}_{\mu_d\mu'_d}\, T^{LQ}_{\mu_i\mu'_i} S^*_{\mu'_d\mu_i;\ \mu'_p\mu'_j} \qquad (5)$$

Summing (5) over the spin projections of the remaining nucleus, we find the density matrix for the proton liberated in the stripping of the deuteron by the nucleus:

$$\rho'_{\mu_p\mu'_p} = \sum_{\mu_j} \rho'_{\mu_p\mu_j;\ \mu'_p\mu_j}.$$

The trace of the density matrix $\rho'_{\mu_p\mu'_p}$ determines the angular distribution of the protons. With the wave functions $\psi_{\mathbf{k}_p}$ and $\psi_{\mathbf{k}_d}$ normalized to unity in the incoming wave, we obtain for the reaction cross section

$$d\sigma/d\omega = (v_p/v_d)\,\mathrm{Sp}\,\rho',$$

where v_d and v_p are the velocities of the deuteron and the proton.

To find the polarization of the protons liberated in the stripping process, we must expand the density matrix (normalized to unity, $\rho'/\mathrm{Sp}\,\rho'$) in terms of the spin-tensors

$$T^{RT}_{\mu_p\mu'_p} = (-1)^{1/2+\mu'_p}(1/2\,1/2\mu_p - \mu'_p \mid RT)$$

of rank R = 0 and 1:

$$\rho'_{\mu_p\mu'_p}/\mathrm{Sp}\,\rho' = \sum_{RT} \langle T^{RT+}\rangle T^{RT}_{\mu_p\mu'_p}.$$

The coefficients of this expansion, $\langle T^{RT+}\rangle$, will then determine the spin states of the liberated protons.

Using the normalization condition for the spin-

tensors and the expression (3) for the reaction matrix, we obtain the coefficient $\langle T^{RT+}\rangle$ in the form

$$\langle T^{RT+}\rangle \operatorname{Sp}\rho' = \sum_{JM,\,LQ} \langle T^{JM+}\rangle \langle T^{LQ+}\rangle$$

$$\times \sum_{lsl's'm} \sqrt{\gamma_{ls}\gamma_{l's'}}\, J_l^m J_{l'}^{m+M+Q-T^*} \sum_{\mu_d\mu_n\mu_j} (-1)^{s/2+l+\mu_j-m-Q-T-M}$$

$$\times (1/2\,1/2\mu_d\ -\mu_n\mu_n \mid 1\mu_d)\,(i\,1/2\mu_j - m - \mu_n\ \mu_n \mid s\mu_j - m)$$

$$\times (s\ l\mu_j - m\ m \mid j\mu_j)\,(11\mu_d M - \mu_d \mid JM)$$

$$\times (ij\mu_j - m - \mu_n\ \ Q - \mu_j + m + \mu_n \mid LQ)$$

$$\times (1/2\,1/2\mu_d\ -\mu_n - T\ \ \mu_n + T - M \mid 1\mu_d - M)$$

$$\times (i\,1/2\mu_j - m - \mu_n - Q\ \ \mu_n + T - M \mid s'\mu_j - m + T - M - Q)$$

$$\times (s'l'\mu_j - m + T - M - Q\ \ m + M + Q - T \mid j\mu_j)$$

$$\times (1/2\,1/2\mu_d - \mu_n\ \ T - \mu_d + \mu_n \mid RT).$$

With the help of known sum rules[13] we carry out the summation over the spin projections μ_d, μ_n, and μ_j. We have

$$\langle T^{RT+}\rangle \operatorname{Sp}\rho' = \sum_{JM,\,LQ} \langle T^{JM+}\rangle \langle T^{LQ+}\rangle \sum_{ls\,l's'} \sqrt{\gamma_{ls}\gamma_{l's'}}$$

$$\times \sum_{r,\,P} (-1)^{-j-s+R-T+P}\ 3\,(2j+1)\,(2J+1)^{1/2}(2L+1)^{1/2}$$

$$\times (2R+1)^{1/2}(2s+1)^{1/2}(2s'+1)^{1/2}\ (2r+1)^{1/2}$$

$$\times (RJ - TM \mid rM - T)\,(LrQM - T \mid PQ + M - T)$$

$$\times W(ll'ss';\ Pj)\,X(1/2\,R\,1/2;\ \ 1/2\,r\,1/2;\ \ 1\,j\,1)\,X(1/2\,r\,1/2;\ \ iLi;\ \ sPs')$$

$$\times \sum_m (-1)^m (ll' - mm + M + Q - T \mid PM + Q - T)$$

$$\times J_l^m J_{l'}^{m+M+Q-T^*}, \qquad (6)$$

where X are the Fano functions.[14]

For R = 1 this formula determines the polarization of the protons. The components of the polarization vector **P** are related to the coefficients $\langle T^{RT+}\rangle$ by

$$P_x = \langle T^{11+}\rangle - \langle T^{1-1+}\rangle, \quad P_y = i\,(\langle T^{11+}\rangle + \langle T^{1-1+}\rangle),$$
$$P_z = -\sqrt{2}\,\langle T^{10+}\rangle. \qquad (7)$$

We note that $\langle T^{00+}\rangle = -1/\sqrt{2}$; with R = T = 0 we then find from (6) the angular distribution of the protons:

$$\operatorname{Sp}\rho' = \sum_{JM,\,LQ} \langle T^{JM+}\rangle \langle T^{LQ+}\rangle \sum_{ls\,l's'} \sqrt{\gamma_{ls}\gamma_{l's'}} \sum_P (-1)^{-j-s+J+P}$$

$$\times 3\,(2j+1)\,(2J+1)^{1/2}(2L+1)^{1/2}(2s+1)^{1/2}(2s'+1)^{1/2}$$

$$\times (LJQM \mid PQ + M)\,W(ll'ss';\ Pj)\,W(1\,1/2\,1/2\,1;\ \ J\,1/2)\,X$$

$$\times (1/2\,J\,1/2;\ \ iLi;\ \ sPs') \sum_m (-1)^m$$

$$\times (ll' - m\,m + M + Q \mid PM + Q)\,J_l^m J_{l'}^{m+M+Q^*} \qquad (8)$$

Formulas (6) and (8) are the most general formulas giving the angular distribution and the polarization of the protons liberated in the stripping process for arbitrary polarization of the incoming deuterons and the initial nuclei, given by the quantities $\langle T^{JM+}\rangle$ and $\langle T^{LQ+}\rangle$.

We now consider the simplest special cases of (8) and (6).

Nuclei and Deuterons Unpolarized. In this case

$$\langle T^{JM+}\rangle = \frac{1}{\sqrt{3}}\,\delta_{J0}\delta_{M0}, \qquad \langle T^{LQ+}\rangle = \frac{(-1)^{2l}}{\sqrt{2l+1}}\,\delta_{L0}\delta_{Q0}.$$

Substituting these expressions in (8) and (6), we obtain the following expressions for the angular distribution and the polarization of the protons:

$$(\operatorname{Sp}\rho')_0 = \frac{2j+1}{2\,(2l+1)} \sum_{ls} \frac{\gamma_{ls}}{2l+1} \sum_m |J_l^m|^2, \qquad (9)$$

$$\langle T^{RT+}\rangle_0 (\operatorname{Sp}\rho')_0 = \sum_{lss'} \sqrt{\gamma_{ls}\gamma_{ls'}}\ (-1)^{-l-j-s-s'-1/2-T}$$

$$\times \frac{2j+1}{2i+1} (2s+1)^{1/2}(2s'+1)^{1/2}$$

$$\times W(1/2\,1/2\,1/2;\ R1)\,W(1/2\,1/2ss';\ Ri)\,W(llss';\ Rj)$$

$$\times \sum_m (-1)^m (ll - mm - T \mid R - T)\,J_l^m J_l^{m-T^*}. \qquad (10)$$

If the scattering of the deuteron and proton waves in the field of the nucleus is neglected, the differential cross section will be given by the well-known Butler formula

$$\left(\frac{d\sigma}{d\Omega}\right)_B = \frac{2j+1}{2i+1}\frac{k_p}{k_d}\frac{4M\alpha R^3}{\hbar^2}\,\{\alpha^2 + (\mathbf{k}_d/2 - \mathbf{k}_p)^2\}^{-2}$$

$$\times \sum_{ls} \gamma_{ls} \left| \frac{dj_l(kR)}{dR} - j_l(kR)\,\frac{d}{dR}\ln k_l(k_n R) \right|^2 \qquad (11)$$

($\mathbf{k} = \mathbf{k}_d - \mathbf{k}_p$). In this approximation there is no polarization of the protons.

If the scattering of the deuteron and the proton waves in the field of the nucleus is taken into account, we obtain a somewhat different angular distribution from that given by (11):

$$\left(\frac{d\sigma}{d\Omega}\right)_0 = \frac{2j+1}{2i+1}\frac{k_p}{k_d} \sum_{ls} \frac{\gamma_{ls}}{2l+1} \sum_m |J_l^m|^2, \qquad (12)$$

Furthermore, the protons will be polarized.

It can be shown that the protons are polarized in the direction perpendicular to the plane of the reaction, i.e., in the direction of the vector $\mathbf{k}_d \times \mathbf{k}_p$. Indeed, the angular dependence of the wave functions $\psi_{\mathbf{k}_d}$ and $\psi_{\mathbf{k}_p}$ in the expression for J_l^m is given by

$$\psi_{\mathbf{k}_d}(\mathbf{r}) = \sum_{l_d m_d} R_{l_d}(r)\,Y_{l_d m_d}(\vartheta,\varphi)\,Y^*_{l_d m_d}(\vartheta_{\mathbf{k}_d},\varphi_{\mathbf{k}_d}),$$

$$\psi_{\mathbf{k}_p}(\mathbf{r}) = \sum_{l_p m_p} R_{l_p}(r)\,Y_{l_p m_p}(\vartheta,\varphi)\,Y^*_{l_p m_p}(\vartheta_{\mathbf{k}_p},\varphi_{\mathbf{k}_p}).$$

Substituting these expressions in J_l^m, choosing

the z axis along $\mathbf{k}_d \times \mathbf{k}_p$, and integrating over ϑ and φ, we obtain

$$J_l^m \sim \sum_{l_d l_p m_d m_p} A^l_{l_d l_p} (l_p l 00 \mid l_d 0)(l_p l m_p m \mid l_d m_d) \times Y_{l_p m_p}\left(\frac{\pi}{2}, \varphi_{k_p}\right) Y^*_{l_d m_d}\left(\frac{\pi}{2}, \varphi_{k_d}\right).$$

$Y_{lm}(\pi/2, \varphi)$ is different from zero for even $l+m$, or what is the same thing, for even $l-m$. Contributions to J_l^m come only from terms with even $l_p + m_p$ and $l_d - m_d$. On the other hand, the coefficient $(l_p l 00 \mid l_d 0)$ is different from zero only for even $l_p + l + l_d$. Therefore $l-m$ must also be even. Formula (10) contains the product $J_l^m J_l^{m-T*}$. The requirement that $l-m$ and $l-m+T$ be even limits the possible values of T to the single value T = 0. We therefore have for the polarization of the proton in this system of coordinates

$$\langle T^{11+} \rangle = \langle T^{1-1+} \rangle = 0, \qquad \langle T^{10+} \rangle \neq 0,$$

i.e., the polarization vector is directed along the vector $\mathbf{k}_d \times \mathbf{k}_p$,

$$P_z = \sqrt{\tfrac{2}{3}} \sum_{lss'} \sqrt{\gamma_{ls}\gamma_{ls'}}\, (-1)^{-l-l-s-s'-1/2+l} (2s+1)^{1/2} \times (2s'+1)^{1/2} (2l+1)^{-1/2}\, W(1/2\, 1/2\, s s'; 1i)\, W(llss'; 1j) \times \sum_m \frac{-m}{\sqrt{l(l+1)}} |J_l^m|^2 \Big/ \sum_{lsm} \frac{\gamma_{ls}}{2l+1} |J_l^m|^2. \qquad (13)$$

In the derivation of formula (13) we assumed that the l-s coupling scheme is valid for the neutron absorbed in the nucleus. In the case of j-j coupling we can obtain an expression for the polarization by using the relation between the reduced widths for the two types of coupling,[11]

$$\sqrt{\gamma_{ls}} = \sum_{j_n} (-1)^{l_n - l - 1/2} (2s+1)^{1/2} (2j_n+1)^{1/2} \times W(l^1/_2 l; s j_n) \sqrt{\gamma_{lj_n}}.$$

Substituting this expression in (13) and summing over s and s', we find

$$P_z = \frac{1}{3} \sum_{lj_n} \frac{\gamma_{lj_n}}{2l+1} \frac{j_n(j_n+1) - l(l+1) - 3/4}{l(l+1)} \times \sum_m m |J_l^m|^2 \Big/ \sum_{lj_n} \frac{\gamma_{lj_n}}{2l+1} \sum_m |J_l^m|^2. \qquad (14)$$

By measuring experimentally the sign of the polarization of the protons in a number of stripping reactions, we can uniquely determine the spin of the remaining nucleus.

Deuterons Polarized, Nuclei Unpolarized. In this case the general formulas can also be greatly simplified. Substituting in (6)

$$\langle T^{LQ+} \rangle = (-1)^{2l} (2i+1)^{-1/2} \delta_{L0} \delta_{Q0},$$

we find

$$\langle T^{RT+} \rangle \operatorname{Sp} \rho' = \sum_{JM} \langle T^{JM+} \rangle \sum_{lss'} \sqrt{\gamma_{ls}\gamma_{ls'}} \times \sum_p (-1)^{-l-l-s-s'-1/2+R-T}\, 3(2j+1)(2i+1)^{-1}(2J+1)^{1/2} \times (2R+1)^{1/2}(2s+1)^{1/2}(2s'+1)^{1/2}\, (RJ-TM \mid PM-T) \times W(1/2\, 1/2\, s s'; Pi)\, W(llss'; Pj)\, X(1/2\, 1/2\, R; 1J; 1/2\, 1/2\, P) \times \sum_m (-1)^m (ll-mm' \mid PM-T)\, J_l^m J_l^{m+M-T*}.$$

Using now equation (10) as the definition of $\langle T^{RT+} \rangle_0$, we obtain

$$\langle T_p^{RT+} \rangle \operatorname{Sp} \rho' = \left\{ -1/2 (3+R)^{1/2} (2-R)^{1/2} \langle T_d^{RT+} \rangle + \langle T_p^{10+} \rangle \times \left[\delta_{R1}\delta_{T0} + \sum_{J=1,2} (-1)^{R-J+1} 2 \cdot 3^{1/2} (2R+1)^{1/2} (R1T0 \mid JT) \times X(1/2\, R^1/_2; 1/2\, 1^1/_2; 1J1) \langle T_d^{JT+} \rangle \right] \right\} (\operatorname{Sp} \rho')_0. \qquad (15)$$

In particular, if R = T = 0, we have

$$\operatorname{Sp} \rho' = \{1 - 6 \langle T_p^{10+} \rangle_0 \langle T_d^{10+} \rangle\} (\operatorname{Sp} \rho')_0. \qquad (16)$$

Expression $\langle T_d^{10+} \rangle$ through the polarization vector of the deuteron $\mathbf{P}_d$, we obtain the following formula for the angular distribution of the protons produced in the stripping reaction with polarized deuterons:

$$d\sigma / d\omega = (1 + 3\mathbf{P}_p \mathbf{P}_d)(d\sigma / d\omega)_0. \qquad (17)$$

The study of the azimuthal asymmetry in the angular distribution of the protons in the stripping reaction with polarized deuterons leads to the same information about the structure of the nucleus as the polarization of the protons. The cross section is maximal if the polarization vectors $\mathbf{P}_p$ and $\mathbf{P}_d$ are parallel; it is minimal if they are in opposite directions. This dependence of the cross section on the mutual orientation of the polarization vectors can be easily understood by recalling the mechanism of the polarization. The polarization of the protons in the stripping reaction due to the scattering of the proton and the deuteron waves is related to the difference of the neutron absorption cross sections for the two possible spin orientations. Since the spins of the neutron and the proton in the deuteron are parallel, the direction of polarization of the protons will correspond to the orientation of the neutron spin leading to the greater absorption probability. The yield of the reaction becomes, of course, greater if the incoming deuterons are polarized. The direction of this polarization coincides with the direction of polarization of the protons in the stripping process.

The polarization of the protons produced by

polarized deuterons is given by the expression

$$\langle T_p^{1T+}\rangle = \{-\langle T_d^{1T+}\rangle + \langle T_p^{10+}\rangle_0 (\delta_{T0} + \sqrt{6(4-T^2)} \times \langle T_d^{2T+}\rangle)\}/(1 - 6\langle T_p^{10+}\rangle_0 \langle T_d^{10+}\rangle_0). \quad (18)$$

Hence the polarization of the protons depends not only on the polarization, but also on the alignment of the deuterons.

Deuterons Unpolarized, Nuclei Polarized. In this case the angular distribution and the polarization of the protons are given by the expressions

$$\mathrm{Sp}\,\rho' = \sum_{LQ} \langle T^{LQ+}\rangle \sum_{ll's's} \sqrt{\gamma_{ls}\gamma_{l's'}}(-1)^{-l+l+1/2} 2^{-1}(2j+1) \times (2s+1)^{1/2}(2s'+1)^{1/2} W(ll'ss'; L^1/_2)\, W(iss'; L^1/_2) \times \sum_m (-1)^m (ll'-mm+Q\,|\,LQ)\, J_l^m J_{l'}^{m+Q*}. \quad (19)$$

$$\langle T^{RT+}\rangle \mathrm{Sp}\,\rho'_i = \sum_{LQ} \langle T^{LQ+}\rangle \sum_{ll's's} \sqrt{\gamma_{ls}\gamma_{l's'}} \sum_P (-1)^{-l-s-T+P} \times (2j+1)(2L+1)^{1/2}(2R+1)^{1/2}(2s+1)^{1/2}(2s'+1)^{1/2} \times (LRQ-T\,|\,PQ-T)\, W(ll'ss'; Pj)\, W(^1/_2\,^1/_2\,^1/_2\,^1/_2; R1) \times X(^1/_2 R\,^1/_2; iLi; sPs') \times \sum_m (-1)^m (ll'-mm+Q-T\,|\,PQ-T)\, J_l^m J_{l'}^{m+Q-T*}. \quad (20)$$

These formulas can be considerably simplified for the actual values of the spin of the initial nucleus.

3. THE PICK-UP REACTION (p, d) WITH POLARIZED PARTICLES

We consider the polarization effects in the pick-up reaction (p, d). The spin of the initial nucleus is denoted by j, the spin of the remaining nucleus, by i. The density matrix of the total system in the initial state is written in the form

$$\rho_{\mu_p\mu_j;\,\mu_p'\mu_j'} = \sum_{RT,\,LQ} \langle T^{RT+}\rangle \langle T^{LQ+}\rangle T^{RT}_{\mu_p\mu_p'} T^{LQ}_{\mu_j\mu_j'},$$

where the expansion coefficients $\langle T^{RT+}\rangle$ (R = 0, 1) and $\langle T^{LQ+}\rangle$ (L = 0, 1, . . . , 2j) determine the initial spin states of the proton and the initial nucleus. The initial density matrix is normalized to unity: Sp ρ = 1.

Using the definition of the reaction matrix,

$$S'_{\mu_d\mu_i;\,\mu_p\mu_j} = 2S_{\mu_p\mu_j;\,\mu_d\mu_i},$$

we obtain the following expression for the deuteron density matrix in the final state:

$$\rho'_{\mu_d\mu_d'} = \sum_{RT,\,LQ} \langle T^{RT+}\rangle \langle T^{LQ+}\rangle \times \sum_{\mu_p\mu_p'\mu_j\mu_j'\mu_i} S'_{\mu_d\mu_i;\,\mu_p\mu_j} T^{RT}_{\mu_p\mu_p'} T^{LQ}_{\mu_j\mu_j'} S'^{*}_{\mu_d'\mu_i;\,\mu_p'\mu_j'} \quad (22)$$

The trace of this matrix determines the angular distribution of the deuterons produced in the pick-up process:

$$d\sigma/d\omega = (v_d/v_p)\,\mathrm{Sp}\,\rho'$$

The matrix (22), normalized to unity, is expanded in terms of the spin-tensors T^{JM} (J = 0, 1, 2). The expansion coefficients determine the polarization of the produced deuterons:

$$\rho'_{\mu_d\mu_d'}/\mathrm{Sp}\,\rho' = \sum_{JM} \langle T^{JM+}\rangle T^{JM}_{\mu_d\mu_d'}.$$

By calculations similar to those in the previous case we obtain the following general formulas for the angular distribution and the polarization of the deuterons formed in the pick-up reaction with polarized protons and oriented nuclei:

$$\mathrm{Sp}\,\rho' = \sum_{RT,\,LQ} \langle T^{RT+}\rangle \langle T^{LQ+}\rangle \sum_{ls l's'} \sqrt{\gamma_{ls}\gamma_{l's'}} \times \sum_p (-1)^{l+s+1/2-l'+L+T-Q+R} 12(2j+1)(2R+1)^{1/2}(2L+1)^{1/2} \times (2s+1)^{1/2}(2s'+1)^{1/2}(LRQT\,|\,PQ+T)\, W(ss'^1/_2\,^1/_2; Ri) \times W(^1/_2\,^1/_2\,^1/_2\,^1/_2; 1R)\, X(s'sR; l'lP; jjL) \sum_m (-1)^m \times (ll'-mm-T-Q\,|\,P-T-Q) J_l^{m*} J_{l'}^{m-T-Q}; \quad (23)$$

$$\langle T^{JM+}\rangle \mathrm{Sp}\,\rho' = \sum_{RT,\,LQ} \langle T^{RT+}\rangle \langle T^{LQ+}\rangle \sum_{ls l's'} \sqrt{\gamma_{ls}\gamma_{l's'}} \times \sum_p (-1)^{l+s+1/2-l'+J+L+T-Q} 12(2j+1)(2J+1)^{1/2}(2R+1)^{1/2} \times (2L+1)^{1/2}(2s+1)^{1/2}(2s'+1)^{1/2}(2p+1)^{1/2} \times (JR-MT\,|\,pT-M)\,(LpQT-M\,|\,PQ+T-M) \times W(ss'^1/_2\,^1/_2; pi)\, X(^1/_2\,^1/_2\,1; ^1/_2\,^1/_2\,1; RpJ)\, X(s'sp; l'lP; jjL) \times \sum_m (-1)^m (ll'-mm+M-T-Q\,|\,PM-T-Q) \times J_l^{m*} J_{l'}^{m+M-T-Q}. \quad (24)$$

We consider a few actual cases.

Nuclei and Protons Unpolarized. In this case the initial spin state of the system is characterized by the quantities

$$\langle T^{LQ+}\rangle = (-1)^{2j}(2j+1)^{-1/2}\delta_{L0}\delta_{Q0},$$
$$\langle T^{RT+}\rangle = -\delta_{R0}\delta_{T0}/\sqrt{2}. \quad (25)$$

Substituting these values in (23) and (24), we find

$$(\mathrm{Sp}\,\rho')_0 = 3\sum_{lms} \frac{\gamma_{ls}}{2l+1} |J_l^m|^2,$$

$$\langle T_d^{JM+}\rangle_0 (\mathrm{Sp}\,\rho')_0 = \sum_{lss'} \sqrt{\gamma_{ls}\gamma_{ls'}}(-1)^{-l+l+s-s'+1/2+J} 6(2s+1)^{1/2} \times (2s'+1)^{1/2}\, W(^1/_2\,^1/_2 ss'; Ji)\, W(^1/_2\,^1/_2\,11; J^1/_2)\, W(llss'; Jj) \times \sum_m (-1)^m (ll-mm+M\,|\,JM)\, J_l^{m+M} J_l^{m*}. \quad (26)$$

We note that $\langle T_d^{JM+}\rangle$ reduces to zero for J = 2.

The differential cross section for the pick-up reaction (p, d) is equal to

$$\left(\frac{d\sigma}{d\omega}\right)_0 = \frac{3}{2}\frac{k_d}{k_p}\sum_{lsm}\frac{\gamma_{ls}}{2l+1}\,|J_l^m|^2. \qquad (27)$$

The deuterons formed in the pick-up process are polarized in the direction perpendicular to the plane of the reaction:

$$P_d = \sum_{lss'}\sqrt{\gamma_{ls}\gamma_{ls'}}\,(-1)^{l-l+l+s-s'+1/2}2^{1/2}3^{-1/2}(2s+1)^{1/2}$$
$$\times(2s'+1)^{1/2}(2l+1)^{-1/2}\,W(1/2\,1/2ss';1i)\,W(llss';1j)$$
$$\times\sum_m\frac{m}{\sqrt{l(l+1)}}\,|J_l^m|^2\Big/\sum_{lsm}\gamma_{ls}(2l+1)^{-1}\,|J_l^m|^2. \qquad (28)$$

If the scattering of the deuteron and the proton waves is neglected, there is no polarization.

Protons Polarized, Nuclei Unpolarized. Substituting $\langle T^{LQ+}\rangle$ from (25) into (23) and (24), and using (26) as the definition of $\langle T_d^{JM+}\rangle_0$, we find

$$\mathrm{Sp}\,\rho' = (1-\langle T_p^{10+}\rangle\langle T_d^{10+}\rangle_0)(\mathrm{Sp}\,\rho')_0, \qquad (29)$$

$$\langle T_d^{JM+}\rangle = \{(-1)^J 2W(1/2\,1/2\,1;J^1/2)\langle T_p^{JM+}\rangle + [\delta_{J1}\delta_{M0}$$
$$+2(-1)^{J-M}3^{1/2}(2J+1)^{1/2}(J1-MM\,|\,10)$$
$$\times X(1/2\,1/2\,1;1/2\,1/2\,1;11J)\langle T_p^{1M+}\rangle]\langle T_d^{10+}\rangle_0\}$$
$$\times(1-\langle T_p^{10+}\rangle\langle T_d^{10+}\rangle_0)^{-1}. \qquad (30)$$

Thus the angular distribution of the deuterons formed in the pick-up process with polarized protons and unoriented nuclei is given by the cross section

$$\frac{d\sigma}{d\omega} = (1+{}^1/_2\mathbf{P}_p\mathbf{P}_d)\left(\frac{d\sigma}{d\omega}\right)_0, \qquad (31)$$

where P_d and $(d\sigma/d\omega)_0$ are determined by (28) and (27).

The polarization of the deuterons is given by the expressions

$$\langle T_d^{1M+}\rangle = (-{}^2/_3\langle T_p^{1M+}\rangle$$
$$+\langle T_d^{10+}\rangle_0\delta_{M0})/(1-\langle T_p^{10+}\rangle\langle T_d^{10+}\rangle_0); \qquad (32)$$

$$\langle T_d^{2M+}\rangle = -\sqrt{{}^2/_3(4-M^2)}$$
$$\times\langle T_p^{1M+}\rangle\langle T_d^{10+}\rangle_0/(1-\langle T_p^{10+}\rangle\langle T_d^{10+}\rangle_0). \qquad (33)$$

We note that the use of polarized protons in the pick-up reaction can lead to the formation of aligned deuterons.

Protons Unpolarized, Nuclei Polarized. In this case we have the following formulas for the angular distribution and the polarization of the deuterons:

$$\mathrm{Sp}\,\rho' = \sum_{LQ}\langle T^{LQ+}\rangle\sum_{ll's}\sqrt{\gamma_{ls}\gamma_{l's}}\,(-1)^{l'+s-Q}\,3\,(2j+1)\,W(ll'jj;Ls)$$
$$\times\sum_m(-1)^m(ll'-mm-Q\,|\,L-Q)\,J_l^{m*}J_{l'}^{m-Q}, \qquad (34)$$

$$\langle T^{JM+}\rangle\,\mathrm{Sp}\,\rho' = \sum_{LQ}\langle T^{LQ+}\rangle\sum_{ls\,l's'}\sqrt{\gamma_{ls}\gamma_{l's'}}$$
$$\times\sum_\mu(-1)^{l'+s+1/2-l'+L-Q}\,6\,(2j+1)$$
$$\times(2J+1)^{1/2}(2L+1)^{1/2}(2s+1)^{1/2}$$
$$\times(2s'+1)^{1/2}(LJQ-M\,|\,PQ-M)\,W(1/2\,1/2\,11;J^1/2)$$
$$\times W(1/2\,1/2ss';Ji)\,X(ll'P;ss'J;jjL)\sum_m(-1)^m$$
$$\times(ll'-mm-Q+M\,|\,PM-Q)\,J_l^{m*}J_{l'}^{m-Q+M} \qquad (35)$$

4. THE EXAMPLE $B^{11}(d,p)B^{12}$

As an example, we consider the angular distribution and the polarization of the protons produced in the reaction $B^{11}(d,p)B^{12}$ (reference 15). In the calculation we use the following parameters:

$$E_d = 8\ \text{Mev},\quad Q = 1.14\ \text{Mev},$$
$$R = 4.4\cdot10^{-13}\ \text{cm},\quad s = 2.23\ \text{Mev}.$$

The orbital angular momentum of the absorbed neutron is equal to unity, $l = 1$. The initial state of B^{11} is odd (−), the spin is $3/2$, the final state is even (+), with the possible spin values j = 0, 1, 2, 3.

In the calculation of the integrals J_l^m entering into the reaction matrix we choose for the wave function of the proton a plane wave $\psi_{\mathbf{k}_p} = e^{i\mathbf{k}_p\mathbf{r}}$; in the deuteron wave function, on the other hand, we take account of the scattering of the deuteron by the nucleus:

$$\psi_{\mathbf{k}_d}(\mathbf{r}) = e^{i\mathbf{k}_d\mathbf{r}} - 4\pi$$
$$\times\sum_{l_dm_d}\eta_{l_d}i^{l_d}h_{l_d}^{(1)}(k_dr)\,Y_{l_dm_d}^*(\vartheta_{k_d},\varphi_{k_d})\,Y_{l_dm_d}(\vartheta,\varphi).$$

Regarding the nucleus as a hard sphere of radius R, we have for the coefficients η_l:

$$\eta_{l_d} = j_{l_d}(k_dR)\,[j_{l_d}(k_dR)$$
$$-in_{l_d}(k_dR)]/[j_{l_d}^2(k_dR)+n_{l_d}^2(k_dR)].$$

Substituting these functions in the integral J_l^m, we obtain

$$J_l^m = \sqrt{\frac{4\alpha M}{\pi\hbar^2R}}\left\{\frac{4\pi i^lR^2}{k^2+k_n^2}\,Y_{lm}^*(\vartheta_k\varphi_k)\right.$$
$$\times\left[\frac{dj_l(kR)}{dR}-j_l(kR)\frac{d}{dR}\ln k_l(k_nR)\right]-(4\pi)^{1/2}\sum_{l_dl_p}\eta_{l_d}i^{l_d-l_p}$$
$$\times\sqrt{\frac{(2l+1)(2l_p+1)}{2l_d+1}}\,(ll_p00\,|\,l_d0)(ll_pmm_p\,|\,l_dm_d)$$
$$\left.\times J_{ll_pl_d}Y_{l_pm_p}(\vartheta_{k_p},\varphi_{k_p})\,Y_{l_dm_d}^*(\vartheta_{k_d},\varphi_{k_d})\right\},$$

where $\mathbf{k} = \mathbf{k}_d - \mathbf{k}_p$. We also introduced the notation

$$J_{ll_pl_d} = \int_R^\infty j_{l_p}(k_pr)\frac{k_l(k_nr)}{k_l(k_nR)}\,h_{l_d}^{(1)}(k_dr)\,r^2dr.$$

In the calculations we included the deuteron scattering states $l_d = 0, 1, 2, 3$, and 4.

The resulting angular distribution of the protons is given in the figure.

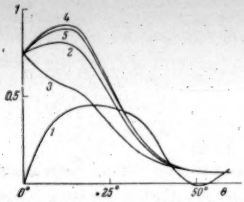

The function $m(\theta)$ (curve 1) and the angular distributions in arbitrary units for the reaction B^{11} (d, p) B^{12} with unpolarized deuterons (curve 2) and completely polarized deuterons (curves 3, 4, 5). The angular distributions were obtained under the assumptions $j = 1$, and $\beta = 0.1$ and ∞, respectively.

The polarization of the protons is in this case given by the expression

$$P = c(j)\, m(\theta), \quad m(\theta) = \sum_m m\, |J_1^m|^2 \Big/ \sum_m |J_1^m|^2.$$

The functional dependence of $m(\theta)$ is also shown in the figure. The coefficient $c(j)$ depends on the value of the spin of the nucleus in the final state. For different possible values of the nuclear spin this coefficient is equal to

$$c(0) = 1/6, \quad c(1) = \frac{\beta^2 + 2\sqrt{5}\beta - 3}{12(\beta^2+1)},$$

$$c(2) = -\frac{\beta^2 - 6\beta + 1}{12(\beta^2+1)}, \quad c(3) = 1/6,$$

where $\beta^2 = \gamma_{11}/\gamma_{12}$. We note that a measurement of the absolute value of the polarization makes it possible to determine the ratio of the reduced widths for a given spin of the final state.

We express our gratitude to Yu. Berezhnyĭ and V. Kharchenko for help in the numerical computations.

[1] H. Newns, Proc. Phys. Soc. **A66**, 477 (1953).
[2] J. Horowitz and A. Messiah, J. Phys. radium **14**, 731 (1953).
[3] P. Hillman, Phys. Rev. **104**, 176 (1956).
[4] H. Newns and M. Refai. Proc. Phys. Soc. **A71**, 627 (1958). W. Tobocman, Techn. Rep. 29, Case Institute of Technology (1958).
[5] A. Juveland and W. Jentschke, Phys. Rev. **110**, 456 (1958).
[6] Bokhari, Cookson, Hird, and Weesakul, Proc. Phys. Soc. **72**, 88 (1958).
[7] W. Cheston, Phys. Rev. **96**, 1590 (1954).
[8] J. Sawicki, Phys. Rev. **106**, 172 (1957).
[9] R. Dalitz, Proc. Phys. Soc. **A65**, 175 (1952).
[10] W. Lakin, Phys. Rev. **98**, 139 (1955).
[11] G. Satchler, Nucl. Phys. **6**, 543 (1958).
[12] G. Satchler, Preprint (1958).
[13] Biedenharn, Blatt, and Rose, Revs. Modern Phys. **24**, 249 (1952).
[14] H. Matsunobu and H. Takebe, Progr. Theoret. Phys. **14**, 589 (1955).
[15] J. Holt and T. Marsham, Proc. Phys. Soc. **A66**, 1032 (1953).

Translated by R. Lipperheide
221

THE MASS SPECTRUM OF MESONS IN HEISENBERG'S THEORY

Ya. I. GRANOVSKIĬ

Institute of Nuclear Physics, Academy of Sciences, Kazakh S.S.R.

Submitted to JETP editor October 4, 1958

J. Exptl. Theoret. Phys. (U.S.S.R.) **36**, 1154-1158 (April, 1959)

The mass spectrum of mesons is computed in Heisenberg's theory. The comparison of the results with the experimental data indicates that the scalar version of the nonlinear term leads to the best agreement in the first approximation of the Tamm-Dancoff method.

THE theory of elementary particles proposed by Heisenberg[1] makes use of the Lagrangian

$$L = \bar{\psi}\gamma_\mu \nabla_\mu \psi - {}^1/_2 l^2 (\bar{\psi}\psi)(\bar{\psi}\psi) \tag{1}$$

and the new commutator function

$$\frac{1}{2} S(q) = \frac{\varkappa^3}{q^3(q^2+\varkappa^2)}\left(\frac{\varkappa}{q^2}\gamma_\nu q_\nu - i\right). \tag{2}$$

The mass spectrum of the mesons, and the mass and electric charge of the nucleons were computed on this basis;[2,3] the results are quite close to what is observed in nature. It becomes necessary, in this connection, to investigate other versions of the theory in order to determine whether the simplest choice of the nonlinear term, as made in reference 1, is also the best.

The nonlinear term in (1) can have the form

$$\pm {}^1/_2 l^2 (\bar{\psi} O_n \psi)(\bar{\psi} O_n \psi), \tag{3}$$

where $O_n = 1$, γ_5, γ_μ, $i\gamma_5\gamma_\mu$, $i\gamma_\mu\gamma_\nu$ $(\mu \neq \nu)$ are matrices known from the theory of β decay. The form of the matrices O_n and the sign of (3) have to be chosen such that the consequences of the theory be in agreement with experiment.

1. MESONS IN THE MODEL WITH THE NONLINEAR TERM (3)

We choose the minus sign in front of the nonlinear term of the Lagrangian.

The integral form of the field equation,

$$\psi(x) = -\frac{1}{2} i l^2 \int G(x,u) O_n \psi(u) \cdot \bar{\psi}(u) O_n \psi(u)\, d^4u, \tag{4}$$

applied to the meson amplitude

$$\varphi(x,y) = \langle 0 | T\psi(x)\bar{\psi}(y) | \Phi \rangle, \tag{5}$$

leads to the equation

$$\varphi(p) = \frac{il^2}{8(2\pi)^4}\int d^4q [\, G(p+q) O_n \varphi(p) O_n S(q) - G(p+q) O_n S(q) \operatorname{Sp} O_n \varphi(p) - S(-q) O_n \varphi(p) O_n G(p+q) + S(-q) O_n G(p+q) \operatorname{Sp} O_n \varphi(p)], \tag{6}$$

where

$$\varphi(p) = \int \langle 0 | T\psi(x)\bar{\psi}(x) | \Phi \rangle e^{-ipx} d^4x. \tag{7}$$

Equation (6) is only approximate, since we neglected the amplitude $\langle 0 | N\psi(x)\psi(u)\bar{\psi}(u)\psi(u) | \Phi \rangle$ in its derivation, which corresponds to the first approximation in the Tamm-Dancoff method.

Substituting expression (2) and the Green's function

$$G(p+q) = 2(p+q)^{-2}\gamma_\mu(p_\mu + q_\mu), \tag{8}$$

into (6), we obtain

$$\varphi = \gamma_\mu O_n \varphi O_n \gamma_\nu J_{\mu\nu} + {}^1/_2 (\gamma_\mu O_n \varphi O_n - O_n \varphi O_n \gamma_\mu) J_\mu - \gamma_\mu O_n \gamma_\nu J_{\mu\nu} \operatorname{Sp} \varphi O_n - {}^1/_2 (\gamma_\mu O_n - O_n \gamma_\mu) J_\mu \operatorname{Sp} \varphi O_n, \tag{9}$$

where J_μ and $J_{\mu\nu}$ are momentum integrals:

$$J_\mu = \frac{l^2\varkappa^3}{(2\pi)^4}\int \frac{(p_\mu + q_\mu)\, d^4q}{q^3(q^2+\varkappa^2)(p+q)^2} = p_\mu B(p^2),$$

$$J_{\mu\nu} = \frac{il^2\varkappa^4}{(2\pi)^4}\int \frac{(p_\mu + q_\mu)\, q_\nu d^4q}{q^4(q^2+\varkappa^2)(p+q)^2} = \delta_{\mu\nu} C(p^2) + p_\mu p_\nu D(p^2), \tag{10}$$

which are expressed in terms of the functions B, C, and D introduced in reference 2.

In the center of mass system of the meson equation (9) simplifies if φ is expanded in terms of the 16 Dirac matrices:

$$\varphi = \frac{1}{4}\sum_{\rho=1}^{16} \varphi_\rho \Gamma_\rho, \tag{11}$$

since we can then use the following formulas:

$$O_n \Gamma_\rho O_n = A_\rho^{(n)} \Gamma_\rho, \quad \gamma_\mu \Gamma_\rho \gamma_\mu = \beta_\rho \Gamma_\rho, \quad \gamma_4 \Gamma_\rho \gamma_4 = \varepsilon_\rho \Gamma_\rho \tag{12}$$

(A_ρ, β_ρ, and ϵ_ρ are numbers; no sum over ρ). Multiplying (9) by Γ_ρ and taking the spur, we obtain the equation

$$\varphi_\rho = \varphi_\rho A_\rho (\beta_\rho C + \varepsilon_\rho p^2 D) + \varphi_\sigma A_\sigma \frac{1-\varepsilon_\sigma}{2} p_4 B - 4\left[\delta_{\rho n}(\beta_n C + \varepsilon_n p^2 D) + \delta_{\sigma n}\frac{1-\varepsilon_n}{2} p_4 B\right]\varphi_n, \tag{13}$$

where $\varphi_\rho = \operatorname{Sp} \varphi\Gamma_\rho$, $\varphi_\sigma = \operatorname{Sp} \varphi\Gamma_\sigma$, and $\Gamma_\sigma = \gamma_4\Gamma_\rho$.

This equation together with the equation for φ_σ forms a system of two homogeneous equations. By setting its determinant equal to zero, we obtain the equation

$$(a_\rho Dp^2 + b_\rho C - 1)(a_n Dp^2 + b_n C - 1) + eB^2 p^2 = 0, \quad (14)$$

which can be used to determine p^2. Its coefficients are given by the formulas

$$a_\rho = \varepsilon_\rho (A_\rho - 4\delta_{\rho n}), \qquad b_\rho = \beta_\rho (A_\rho - 4\delta_{\rho n}),$$
$$e = -\tfrac{1}{2}(1 - \varepsilon_\rho)(A_\rho - 4\delta_{\rho n})(A_n - 4\delta_{\rho n}) \quad (15)$$

and depend on the choice of the nonlinear term as well as on the spin and the parity of the emitted meson. All of them are easily computed with the help of (12).

The functions B, C, and D contain the constant $(4\pi/\kappa l)^2$ as a factor. We calculated them, following reference 2, by determining the mass of the proton and then identifying it with κ. Thereafter the functions B, C, and D were tabulated and Eq. (14) solved numerically, The results of the calculation and the values of the constant are given in Table I.

It should be noted, first of all, that our results for the scalar version are somewhat different from the data of Heisenberg, Kortel, and Mitter.[2] The reason for this is that these authors include only the first two terms of our equation (6), so that the coefficient e in (14) does not contain the factor $(1 - \epsilon_\rho)/2$. However, the term eB^2p^2 is relatively small, and the discrepancy does not exceed ~ 7 to 10%.

In the vector version the mesons are absent altogether. By changing the sign in front of the nonlinear term, i.e., going over to the Lagrangian

$$L' = \bar{\psi}\gamma_\mu \nabla_\mu \psi + \tfrac{1}{2} l^2 (\bar{\psi} O_n \psi)(\bar{\psi} O_n \psi), \quad (16)$$

we can change the sign of the interaction potential between the nucleon and the antinucleon, which also modifies the mass spectra of the mesons. The corresponding equations are obtained from those above by makeing the replacement $l^2 \to -l^2$. The results of the solution of these altered equations are given in the last column of Table I.

It is seen from these data that the masses of the pseudoscalar mesons, as a rule, exceed the observed masses by a factor of 2 to 3. It should be expected that the results of the theory could be improved by taking account of the isotopic properties of the field ψ.

2. MESONS IN THE "REALISTIC MODEL"

We introduce the isotopic properties of the field ψ in the framework of the "realistic model" of Heisenberg,[1] which makes use of the iso-scalar χ together with the iso-spinor ψ in defining the Lagrangian

$$L = \bar{\psi}\gamma_\mu \nabla_\mu \psi + \bar{\chi}\gamma_\mu \nabla_\mu \chi - l^2 (\bar{\psi} O_n \chi)(\bar{\chi} O_n \psi). \quad (17)$$

In the first approximation of the Tamm-Dancoff

TABLE I

Version	$\left(\frac{4\pi}{\kappa l}\right)^2$	Spin and parity	M/M$_p$ for L	M/M$_p$ for L′
S	2.897	0+	0.40 0.12	—
		0−	0.23	0.23
		1+	0.05	0.05
		1−	—	0.05
V	5.078	0+	—	0.45
		0−	—	—
		1+	—	0.30
		1−	—	0.07
T	4.738	0+	—	0.56
		0−	0.56	—
		1+	—	—
		1−	—	—
A	7.645	0+	0.06	0.35
		0−	0.68	0.68
		1+	<0.03	—
		1−	0.20	—
P	1.665	0+	—	0.386 0.392
		0−	0.55 0.71	0.55
		1+	0.43	—
		1−	0.16	—

method the meson amplitude $\varphi(x, y)$ satisfies the equation

$$\varphi(x, y) = \frac{il^2}{8}\int d^4u\,[G(x, u)\,O_n\chi(u, u)\,O_nS^{\psi}(u, y) + S^{\psi}(x, u)\,O_n\chi(u, u)\,O_nG(u, y)], \quad (18)$$

where

$$\chi(u, v) = \langle 0\,|\,T\chi(u)\,\bar{\chi}(v)\,|\,\Phi\rangle. \quad (19)$$

The equation for $\chi(u, v)$ is of an analogous form:

$$\chi(x, y) = \frac{il^2}{8}\int d^4u\,[G(x, u)\,O_n\,\mathrm{tr}\,\varphi(u, u)\,O_nS^{\chi}(u, y) + S^{\chi}(x, u)\,O_n\,\mathrm{tr}\,\varphi(u, u)\,O_nG(u, y)] \quad (20)$$

(tr denotes the spur with respect to the isotopic spin indices).

We retain the form (2) for the function S^{χ}, while S^{ψ} is taken to be[1]

$$\frac{1}{2}S^{\psi}(q) = \frac{\varkappa^3}{q^2(q^2+\varkappa^2)}\left[\frac{\varkappa}{q^2}\,\gamma_\nu q_\nu\tau_0 - i\tau_3\right], \quad (21)$$

where τ_0 is the unit matrix and τ_3 the third Pauli matrix in iso-space. Using these expressions, we go over to the momentum representation:

$$\varphi(p) = \gamma_\mu O_n\chi(p)\,O_n\gamma_\nu J_{\mu\nu}(p)\,\tau_0 + {}^1/_2[\gamma_\mu O_n\chi(p)\,O_n - O_n\chi(p)\,O_n\gamma_\mu]\,J_\mu(p)\,\tau_3, \quad (22a)$$

$$\chi(p) = \gamma_\nu O_n\,\mathrm{tr}\,\varphi(p)\,O_n\gamma_\nu J_{\mu\nu}(p) + {}^1/_2[\gamma_\mu O_n\,\mathrm{tr}\,\varphi(p)\,O_n - O_n\,\mathrm{tr}\,\varphi(p)\,O_n\gamma_\mu]\,J_\mu(p). \quad (22b)$$

Here $\varphi(p)$ and $\chi(p)$ denote the Fourier components of $\varphi(x, x)$ and $\chi(x, x)$ (see (7)), and the momentum integrals J_μ and $J_{\mu\nu}$ are given by the formulas (10).

It follows from the definition (5) that the isotopic structure of the amplitude $\varphi(p)$ is

$$\varphi = \begin{pmatrix} \langle p\bar{p}\rangle & \langle p\bar{n}\rangle \\ \langle n\bar{p}\rangle & \langle n\bar{n}\rangle \end{pmatrix} = \begin{pmatrix} \pi_0^1 & \pi^+ \\ \pi^- & \pi_0^2 \end{pmatrix}. \quad (23)$$

Comparing this expression with (22a), we conclude that the amplitudes of the charged mesons are in this version of the theory identically equal to zero:

$$\varphi_{\pi^\pm}(p) \equiv 0. \quad (24)$$

Since S^{χ} and S^{ψ} are diagonal in the isotopic spin indices, this result is preserved even in the higher approximations of the Tamm-Dancoff method.

For the amplitude of the neutral meson with isotopic spin $T = 0$ (reference 4),

$$\varphi_0(p) = (\langle p\bar{p}\rangle + \langle n\bar{n}\rangle)/\sqrt{2} = \mathrm{tr}\,\tau_0\varphi(p)/\sqrt{2}, \quad (25)$$

we obtain the following system of equations [see formulas (22a,b)]:

$$\sqrt{2}\,\varphi_0(p) = 2\gamma_\mu O_n\chi(p)\,O_n\gamma_\nu J_{\mu\nu}(p),$$
$$\chi(p) = \sqrt{2}\,\gamma_\mu O_n\varphi_0(p)\,O_n\gamma_\nu J_{\mu\nu}(p) + {}^1/_2\sqrt{2}\,[\gamma_\mu O_n\varphi_0(p)\,O_n - O_n\varphi_0(p)\,O_n\gamma_\mu]\,J_\mu(p). \quad (26)$$

Simplifying it by the method described in the previous section, we obtain

$$\begin{vmatrix} 2(A_\rho)^2(\beta_\rho C + \varepsilon_\rho p^2 D)^2 - 1 & (1-\varepsilon_\rho)\,A_\rho A_a(\beta_\rho C + \varepsilon_\rho p^2 D)\,p_4 B \\ (1-\varepsilon_a)\,A_\rho A_a(\beta_\rho C + \varepsilon_a p^2 D)\,p_4 B & 2(A_a)^2(\beta_a C + \varepsilon_a p^2 D)^2 - 1 \end{vmatrix} = 0 \quad (27)$$

(the coefficients A_ρ, β_ρ, and ϵ_ρ and the functions B, C, and D are defined in section 2).

For the pseudoscalar meson we have

$$\beta_\rho = -4, \quad \varepsilon_\rho = -1, \quad \beta_a = 2, \quad \varepsilon_a = -1, \quad (28)$$

and A_ρ depends on the choice of the version.

The constant $(4\pi/\kappa l)^2$ entering in (27) was also determined by computing the mass of the proton. All the necessary quantities together with the results of the numerical solution of equation (27) for the pseudoscalar meson are given in Table II.

The amplitude of the neutral meson with isotopic spin $T = 1$ (reference 4),

$$\varphi_1(p) = (\langle p\bar{p}\rangle - \langle n\bar{n}\rangle)/\sqrt{2} = \mathrm{tr}\,\tau_3\varphi(p)/\sqrt{2}, \quad (29)$$

is, according to (22a), given in the form

$$\varphi_1(p) = [\gamma_\mu O_n\chi(p)\,O_n - O_n\chi(p)\,O_n\gamma_\mu]\,J_\mu(p)/\sqrt{2}. \quad (30)$$

But since $\chi(p) \sim \varphi_0(p)$, the only non-zero Fourier components of $\varphi_1(p)$ are those, whose mass coincides with the mass of the isoscalar meson mentioned earlier. The comparison of the data of Table II with those of Table I shows that the masses of the pseudoscalar mesons are in all versions of the theory lowered, as was to be expected (see the remarks at the end of section 1).

TABLE II

Version	$(4\pi/\kappa l)^2$	A_ρ	A_a	M_{π^0}/M_p	Version	$(4\pi/\kappa l)^2$	A_ρ	A_a	M_{π^0}/M_p
S	3.345	1	1	0.19 0.30	T A	11.209 7.208	6 4	0 −2	<0.01 0.46
V	4.146	−4	2	0.42 0.61	P	2.470	1	−1	0.31 0.42

However, even in this case the disagreement between the theoretical and experimental results in the scalar version amounts to ~25% and even more in the other versions. We obtained a similar result in the calculation of the mass of the K meson.[5]

3. CONCLUSION

The above calculations of the mass spectrum of the mesons show that the scalar version of the nonlinear term is preferable to the others in the first approximation of the Tamm-Dancoff method. It should be kept in mind, however, that it is not obvious that the first approximation is sufficient. The comparison with experiment therefore is rather of a qualitative nature.

Taking account of the isotopic properties improves the results for the mass, but also leads to difficulties with the charged mesons. As long as the Lagrangian (17) is retained, this difficulty can only be removed by a complete change of the isotopic structure of the commutator function $S^{\psi}(q)$.

In conclusion I express my gratitude to Prof. W. Heisenberg and Dr. H. Mitter for making available the numerical calculations omitted in their paper.[2] I. G. Golyak was very helpful in the calculations of Sec. 1.

[1] W. Heisenberg, Revs. Modern Phys. **29**, 269 (1957).

[2] Heisenberg, Kortel, and Mitter, Z. Naturforsch. **10a**, 425 (1955).

[3] R. Ascoli and W. Heisenberg; Z. Naturforsch. **12a**, 177 (1957).

[4] H. A. Bethe and J. Hamilton, Nuovo cimento **4**, 1 (1956).

[5] Ya. I. Granovskii, Уч. зап. Каз. гос. ун-та (Scientific Papers of Kazakh State University) (in press)

Translated by R. Lipperheide
222

THE KINEMATICS OF ELEMENTARY INTERACTIONS

N. G. BIRGER and Yu. A. SMORODIN

P. N. Lebedev Physics Institute, Academy of Sciences, U.S.S.R.

Submitted to JETP editor October 4, 1958

J. Exptl. Theoret. Phys. (U.S.S.R.) 36, 1159-1167 (April, 1959)

Kinematic methods for the analysis of nuclear reactions of fast particles are considered. Application of such a method of analysis of the interactions observed in cloud chambers and photographic emulsions permits us to obtain angular and energy characteristics of the interaction in the center-of-mass system of the colliding particles.

STUDY of the interaction of particles of high energy ($> 10^9$ ev) with nucleons and nuclei are made difficult by two fundamental causes:

a) The absence of any sort of complete theory for the description of the processes of interaction of particles leads to the result that it is not possible to analyze the experimental data from a single point of view. In the majority of cases there are no theoretical representations at all which could be verified or refuted by experiment.*

b) Experimental setups currently used for the study of the interaction of high-energy particles, both in cosmic rays[1-4] and in accelerators,[5-7] as a rule do not yield exhaustive information on the observed processes.

Such a situation leads to the fact that at present partial methods are used for the analysis of the experimental data, which permit us to find individual phenomenological characteristics of the processes.

The purpose of the present research is the consideration of methods of analysis of the nuclear interactions that make use of kinematic relations. Such an analysis permits one to obtain separate particular characteristics of processes that are free from specific model representations.

1. APPLICATION OF CONSERVATION LAWS

In what follows we shall denote the total energy, momentum, angle of flight of the particle relative to the primary, and mass by E, p, θ, and M, respectively.

In the laboratory system of coordinates (l-system) we shall denote the first particle by the index 0, the more rapid of the two nucleons after the nucleon-nucleon collision by the index n, and the much slower nucleon by the index δ. The same system of characterization is preserved in the center-of-mass system of two colliding particles (c-system), but in this case all of the parameters are identified by an additional index c. In what follows we use a system of units in which the velocity of light $c = 1$.

Considering the kinematics of the interaction of fast particles, especially when the colliding particles possess the same mass, it is convenient in a number of cases to transform to the coordinate system of the center-of-mass of the colliding particles, inasmuch as in this system, in the mean, there should be symmetry relative to the plane that is perpendicular to the direction of motion of the primary particle. In a determination in a c-system, $\sum p = 0$, whence is easy to obtain γ_c — the Lorentz factor of the c-system for the case in which one of the interacting particles is at rest in the l-system:

$$\gamma_c = \frac{\gamma_0 + M_t/M_0}{\sqrt{2\gamma_0 M_t/M_0 + (M_t/M_0)^2 + 1}}; \quad \beta_c = \frac{\beta_0}{1 + M_t/M_0\gamma_0}, \quad (1)$$

where M_t is the mass of the target nucleus. In the particular case in which two nucleons interact,

$$\gamma_c = \sqrt{(\gamma_0 + 1)/2}; \qquad \beta_c = \beta_0/(1 + 1/\gamma_0). \quad (1')$$

the angles of flight of the secondary particles in the c-system are determined by the formula

$$\tan\theta_c = \frac{1}{\gamma_c}\frac{\sin\theta}{\cos\theta - \beta_c/\beta}. \quad (2)$$

For the determination of the angles θ_c, it is convenient to use a graphical representation of Eq. (2) put forth by Bradt et al.[9] Figure 1 shows a nomogram, with the help of which we can quickly carry out a transformation of the angles. The

*An exception is the statistical theory, the development of which has permitted a satisfactory description of the multiplicity of generation of particles in the region of energy of primary particles $10^9 - 10^{10}$ ev.[8]

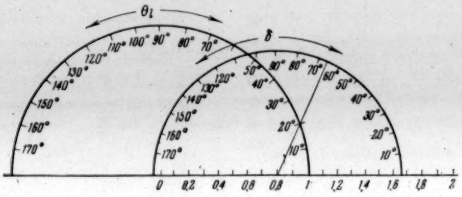

FIG. 1

values of the ratio β_c/β are marked along the horizontal diameter in units of the radius of the larger semicircle. The divisions on the larger semicircle correspond to the values of the angles θ_1. Setting the center of the smaller semicircle at the point corresponding to the given value of β_c/β, we draw a ray from its center to the point on the larger semicircle corresponding to the angle θ_1. The point of intersection of the ray with the smaller semicircle gives the value of the angle $\delta = \tan^{-1}(\gamma_c \tan\theta_c)$. To accelerate the transformation, it is best to draw the small semicircle on a separate sheet of transparent material and to mark the corresponding values of $\ln\tan\delta$ against the values of the angle δ.

Hereinafter, the only general laws that will be used in the analysis of the interaction of high-energy particles will be the laws of conservation of energy and momentum:

$$E_0 + M_t = \sum E_i,$$

$$p_0 = \sum p_i \cos\theta_i, \quad \sum p_i \sin\theta_i = 0. \tag{3}$$

The index i denotes all particles after the collision, independent of their nature.

Inasmuch as we are interested in interactions due to particles, whose energy is large in comparison with their rest mass, it is convenient to write (3) in the form

$$E_0 - p_0 + M_t = \sum (E_i - p_i \cos\theta). \tag{3'}$$

We write $E_i - p_i\cos\theta = \Delta_i$, while Δ is written in turn as the sum of two quantities ϵ and κp:

$$\varepsilon = E - p = p(\sqrt{1-(M/p)^2} - 1),$$

$$\varkappa = 1 - \cos\theta. \tag{4}$$

Then Eq. (3′) takes the form*

$$\sum \varepsilon_i + \sum \varkappa_i p_i = M_t + \varepsilon_0. \tag{5}$$

In Fig. 2 we have plotted the curves $\epsilon = \epsilon(p)$ for pions and nucleons. It is seen from the curve that when the primary particles are nucleons, we

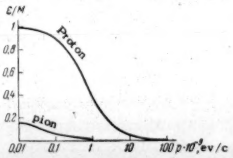

FIG. 2

can neglect ϵ_0 in comparison with M_n in Eq. (5) for all energies $E_0 > 5 \times 10^9$ ev (here $E_0 = 5 \times 10^9$, $\epsilon_0 = 0.1\,M_n$) and, consequently,

$$\sum \varepsilon_i + \sum \varkappa_i p_i = M_t. \tag{6}$$

In the case in which the interaction takes place on one of the nucleons of the nucleus, one must take account of the Fermi momentum of these nucleons. This inaccuracy in Eq. (6) is less than $0.1\,M_n$.

The laws of conservation of energy and longitudinal momentum, written in this fashion, can serve as an excellent criterion for discovering the lack of a nucleon-nucleon interaction. Actually, in a certain interaction produced by a primary nucleon, let the sum of all quantities Δ_i for all observable secondary particles exceed the value of the rest mass of the nucleon, $\sum \Delta_i > M_n$. In this case we can state unambiguously that the target is not a free nucleon and that the interaction takes place either simultaneously with several nucleons of the nucleus or that more than one consecutive reaction takes place inside the nucleus.* The opposite conclusion, that a nucleon-nucleon reaction apparently occurs if $\sum \Delta_i < M_n$, is not possible, since the summation is carried out only over the observed charged particles; and the presence of secondary neutral particles (neutron, π^0

*The conservation laws were first written in this form by S. N. Vernov.

*It should be noted that a strict application of the criterion (6) pertains to the nucleon-nucleus class of interactions and to the case in which evaporation of the nucleus takes place owing to the small energy transmitted to the nucleus in the interaction of the primary nucleon with one of the peripheral nucleons of the nucleus. In the analysis of similar case, it is possible to form the sum Δ_i, without considering the heavy nuclear fragments that are formed in the evaporation.

meson) can reverse the inequality sign. However, if it is known that there is a nucleon-nucleon interaction, and $\sum \Delta_i^{ch} < M_n$, then it can be verified that there are neutral particles among the secondary particles.

If it is assumed that only a single neutral particle is not found, then we have for it $\Delta_x = M_n - \sum \Delta_i$. The value of the quantity Δ_x can serve as an indication of the nature of the neutral particle.

In the case in which there are π^0 mesons as well as a slow neutron among the secondary neutral particles, the neutron makes the principal contribution to the total value of Δ. Actually, the value of ϵ for relativistic pions is small, as is also $\kappa p = p \sin\theta \tan(\theta/2)$, since $p \sin\theta \sim M_\pi$,[10] while the angular distribution of secondary pions is rather narrow for large values of E_0. Neglecting $\sum \Delta_i$ for neutral mesons and a fast nucleon, we can estimate Δ_δ for the δ neutron: $\Delta_\delta \lesssim M_n - \sum \Delta_i^{ch}$.

2. KINEMATICS OF A SLOW NUCLEON IN A NUCLEON-NUCLEON INTERACTION

A series of important conclusions on the nucleon-nucleon interactions can be made by considering the data applying to a nucleon emitted, in the center-of-mass system, in the direction opposite to the motion of the primary nucleon (δ nucleon). In the laboratory system, such a nucleon will be comparatively slow, whence it is easily shown that the range of permitted angles of emission is bounded from above. For the case in which only the number of secondary pions is known, the value for the limiting angle of emission of the δ nucleon in the laboratory system was obtained by Sternheimer.[11] The dependence of θ_{max} on E_0 is shown in Fig. 3 for various values of n_π calculated according to his formulas. Actually, the value of θ_{max} depends on the angular and momentum distribution of secondary pions in the laboratory system.

Let us look at the case in which the angles of emission and the values of the momentum of the relativistic particles are known, or at least if their lower boundary in the laboratory system is known. In this case, as was shown above, one can estimate the value of Δ for the slow neutron, $\Delta_\delta \leq M_n - \sum \Delta_i^{ch}$. The connection between the angle of emission θ_δ and the momentum p_δ in the laboratory system for a given value of Δ_δ is given by the relation

$$p_\delta = [\Delta_\delta \cos\theta_\delta \pm \sqrt{\Delta_\delta^2 \cos^2\theta_\delta - (1 - \Delta_\delta^2)\sin^2\theta_\delta}] / \sin^2\theta_\delta. \quad (7)$$

This dependence is shown graphically in Fig. 4. It is easy to see from the drawing that to each value of Δ_δ (the numbers on the curves given the value of Δ_δ, measured in nucleon masses) correspond a maximum possible angle of emission $(\theta_\delta)_{max}$ and a minimum momentum $(p_\delta)_{min}$. The analytic expression for these quantities can be represented by the formulas

$$\tan(\theta_\delta)_{max} = (\Delta_\delta^{-2} - 1)^{-1/2}, \quad (8)$$

$$(p_\delta)_{min} = (1 - \Delta_\delta^2)/2\Delta_\delta, \quad (9)$$

where Δ_δ is measured in nucleon masses. In the case in which Δ_δ is known precisely, Eqs. (7) – (9) give precise values for $p_\delta(\theta)$, $|p_\delta|_{min}$ and $|\theta_\delta|_{max}$.

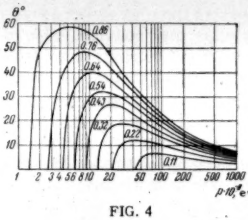

FIG. 4

However, only the highest value of Δ_δ is always found experimentally, inasmuch as the neutral particles are not included in $\sum \Delta_i$, while in certain cases, only the lower boundary is known for the values of Δ of observable particles in certain cases. This leads to the result that the value $|p_\delta|_{min}$, determined from the curves of Fig. 4, may prove to be only underestimated and the values of $|\theta_\delta|_{max}$ only overestimated in comparison with actual values. Particles emitted at angles exceeding $|\theta_\delta|_{max}$, determined by the formulas developed above, certainly cannot be nucleons.

For nucleon-nucleon collisions, it can be considered that, on average, the scattering of nucleons after the collision takes place symmetrically in the center-of-mass system. In this case, knowledge of the value of Δ_δ allows us to determine the character of the distribution of energy between the secondary particles of different types.

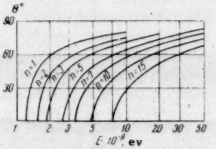

FIG. 3

We denote by α the fraction of the energy associated with the faster of the two nucleons after the interaction.

Let us consider a system of coordinates bound to the incoming nucleon (all quantities in this system are identified by the index s). Then the energy of a fast nucleon after the collision will be, in the laboratory system,

$$E_n = \gamma_0 (E_s + \beta_0 p_s \cos\theta_s)$$

and, if E_s and p_s are measured in nucleon masses,

$$\alpha = E_n/E_0 = E_s + \beta_0 p_s \cos\theta_s.$$

For all interactions in which multiple meson production takes place, we can set $\beta_0 = 1$. Then

$$\alpha = E_s + p_s \cos\theta_s. \qquad (10)$$

As a consequency of symmetry, the distribution of α in the s system will coincide with the distribution of the values of $\Delta_\delta = E_\delta - p_\delta \cos\theta_\delta$ in the laboratory system, while the mean value is

$$\bar{\alpha} = \bar{\Delta}_\delta. \qquad (11)$$

At the same time, as shown above, the quantity Δ_δ determines the maximum value of the angle of emission of the δ nucleon in the laboratory system. It then follows that the existence of δ nucleons, emitted at large angles, demonstrates the presence of interactions for which a significant fraction of the energy is connected with the fast nucleon. Thus, to interactions in which the δ nucleons are emitted at angles $\theta_\delta > 32°$, there should correspond interactions for which $\alpha \geq 0.5$ (see Fig. 4).* It must be emphasized that in separately chosen interactions there is no direct connection between the quantities Δ_δ and α, inasmuch as in the individual interaction the scattering of the nucleons after collision can also take place unsymmetrically.

We now find a connection between the energy spectrum of the δ nucleons in the laboratory system and the angular distribution of the nucleons in the center-of-mass system.

For simplicity, we assume that in the center-of-mass system the scattering of nucleons takes place isotropically. In this case it is easy to find the relative number of interactions in which δ nucleons emerge in the laboratory system with energy E_δ less than a certain value $E_{\delta a}$. Let the energy of the nucleons in the center-of-mass system be equal to $E_{\delta c}$; then all the nucleons lying within the cone of generating angle θ_{ac}, defined by the relation

$$\cos\theta_{ac} = (E_{\delta a}/\gamma_c - E_{\delta c})/\beta_c \sqrt{E_{\delta c}^2 - M_n^2},$$

will possess energies $\leq E_{\delta a}$ in the laboratory system. For the condition of isotropy, the relative number of such nucleons k will be determined by the fraction of the solid angle Ω ($\theta_{\delta c} \geq \theta_{ca}$) 4π.

Taking it into account that two nucleons take part in the interaction, we get

$$k = \frac{2}{4\pi} \int_{\theta_{ca}}^{180} d\Omega = 1 + (E_{\delta a}/\gamma_c - E_{\delta c})/\beta_c \sqrt{E_{\delta c}^2 - M_n^2}; \qquad (12)$$

k reaches a maximum value for $E_{\delta c} = \gamma_c / E_{\delta a}$:

$$k_{max} = 1 - \sqrt{\gamma_c^2 - E_{\delta a}^2}/\gamma_c \beta_c. \qquad (13)$$

The values of k_{max} for $E_0 = 3.5$ and 10 nucleon masses are given at the end of the article. We used here a value of 1.08 Bev for $E_{\delta a}$, which corresponds to a value $J/J_{min} = 2$, at which the proton still differs from the pions under experimental conditions.

3. APPLICATION OF THE RELATIONS OBTAINED TO EXPERIMENTAL DATA

a) We apply the criterion of non nucleon-nucleon collisions [Eq. (6)] to the interaction of nucleons with various nuclei: the light nucleus Be_4^9 and the nuclei in the composition of photoemulsions. Data on the interaction of protons of cosmic rays with nuclei of beryllium were taken by us from references 1 – 3, where Wilson cloud chambers located in a magnetic field were used.* For analysis of the interactions observed in photoemulsions,† sixty seven interactions were selected which were brought about by charged particles with $E_0 \sim 10^{10}$ ev, in which the secondary particles with ionizations exceeding seven fold were lacking and in which the number of "gray" tracks with ionizations with one half up to 7-fold did not exceed 1. The result of the analysis is shown in Table I.

It is seen from the table that in the interaction

*A. E. Chudakov first pointed out this relation between θ_δ and α.

*It should be observed that kinematic analysis can be rigorously applied in those cases in which the charged products of the interaction are observed. In Wilson chambers with plates there is a possibility of distortion of the results because of secondary processes in the plates.

†A survey and measurement of the angles and ionization of tracks of secondary particles were carried out in the Cosmic Ray Laboratory of the Physics Institute, Academy of Sciences, U.S.S.R. under the direction of G. B. Zhdanov, to whom the authors express their gratitude for making the experimental results available for the present analysis (prior to publication).

TABLE I

Target and reference	Energy of the primary nucleon E_0, 10^9 ev	Number of relativistic particles n_s	$N_g = 1$		$N_g = 0$	
			Total number of interactions	Number of non N–N interactions	Total number of interactions	Number of non N–N interactions
$Be^{1,2}$	~5	2–3	14	0	34	0
		⩾4	0	0	6	0
$Be^{3,4}$	5–50	⩾4	3	1	15	1
Nuclei of photoemulsions, G. B. Zhdanov et al.	9	$1 \leqslant n_s < 4$	17	12	25	—*
		⩾4	5	5	20	—*

*Lack of data on the momenta of relativistic particles prevents an application of criterion (6) to the interactions with $N_g = 0$.

TABLE II

Number of particles in the shower, n_s	$\sum \Delta_i^{ch}/M_m$	$(\Delta_\delta)_{max}/M_m$	$(\theta_\delta)^0_{max}$	Experimental date for particles whose nature has not been established from the moments and ionizations			
				θ	J/J_{min}	$p \cdot 10^9$ ev/c	Sign of charge
8	0.8	0.2	10	48	1	⩾13	?
				11	1	—	?
				25	1	⩾9	?
4	0.4	0.6	34	48	1	⩾9	?
7	0.5	0.5	30	32	1	12^{+6}_{-3}	+
7	0.4	0.6	34	45	1	—	
6	0.5	0.5	30	55	1	⩾3	?
				37	1	⩾3	?

of protons with nuclei of beryllium, the only insignificant fraction of the total number of interactions is not nucleon-nucleon. For interactions of protons with nuclei of the photoemulsion, there is a significantly different result: among the interactions which in most researches on photoemulsions are interpreted as nucleon-nucleon interactions, a significant fraction (not less than 0.5) are interactions of more than with a single nucleon of the nucleus.

b) In Sec. 1 it was shown that in the case in which the difference $M_n - \sum \Delta_i^{ch}$ for the interaction of nucleons with nucleons $\sum \Delta_i < M_n$ (the summation is taken over all observed charged particles) determines the maximum value of Δ for the δ nucleon.

Knowing $(\Delta_\delta)_{max}$, it is possible to find the value of $(\theta_\delta)_{max}$ from the curves of Fig. 4. Comparing the value of $(\theta_\delta)_{max}$ thus obtained with the experimental value, we can establish the nature of the particles emitted at large angles in the laboratory system.

The result of such an analysis carried out by us according to the data of reference 3, under the assumption that nucleon-nucleon interactions are generally absent in Be, is given in Table II. All the particles listed in the table were pions.

In the data of Fowler et al.,[5] the nature of the particles emitted at large angles in the interactions of neutrons of $\overline{E}_0 = 2.7$ Bev with protons was identified by means of the curves of Sternheimer (see Fig. 3). Application of the method that we have advanced would in this case permit a substantial reduction of the value of $(\theta_\delta)_{max}$ and at the same time determine the nature of the particles in most cases.

c) It was shown above that the distribution of values of Δ_δ should coincide with the distribution of values of α — the coefficient of elasticity for the interaction in which the pions are generated. The distribution of values of Δ_δ is plotted in Fig. 5 from the data of Smorodin.*

Out of a total number of 54 cases of production of one or more pions, in 6 cases, $n_s \geq 4$. In 14 of 48 cases with $n_s < 4$, showers were observed with a slow δ proton, the momentum of which was less than 700 Mev/c. The distribution of Δ_s for these cases is shown in Fig. 5 by the solid lines. In 10 cases, analysis based on the law of

*Only the research of Smorodin is used for such an analysis inasmuch as the operation of the Wilson chamber in this case was achieved by means of a system of counters which did not introduce any appreciable discrimination as to the character of the interaction.

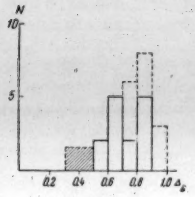

FIG. 5

conservation of electrical charge and of the quantity $M_n - \sum \Delta_i$ showed that in the interactions slow protons ought to be released, which are absorbed in the plate of Be. The value of Δ_δ in these cases exceeds 0.7. These cases are shown by the dashed lines. Thus, among showers with $n_s < 4$, in half the cases a proton is emitted with $p < 700$ Mev/c. It is natural to assume that in the remaining half of the cases with $n_s < 4$ the slow particle is a neutron. In showers with $n_s \geq 4$, not in a single case was a proton observed with increased ionization. This shows directly that even in these cases the momentum of the nucleon must be greater than 700 Mev/c, and consequently, $\Delta_\delta > 0.5$. Assuming that in these cases also, a δ proton is emitted in half of the interactions, we complete the histogram in Fig. 5 by three cases with $\Delta_\delta > 0.5$, distributing them conditionally in the interval from 0.3 to 0.5 (the shaded rectangle), since at $E_0 \sim 5 \times 10^9$ ev, α cannot be less than 0.3.

The value $\bar{\alpha} = 0.7$, which is obtained from the histogram, is in excellent agreement with the average value of the elastic coefficient obtained by Grigorov[12] from the analysis of the energy losses of the nucleon component of cosmic rays with energies $\sim 10^{10}$ ev in their passage through the atmosphere.

The demonstration obtained in reference 2 of the small value of the coefficient of elasticity in those showers in which a large number of pions is generated is confirmed by the research of reference 3, in which the interactions of rather high energy ($5 \times 10^9 - 5 \times 10^{10}$ ev) were separated. In this work, among 18 recorded showers with $n_s \geq 4$, only a single case was observed of a proton with $J/J_{min} > 2.0$ (Δ_δ in this case is equal to 0.64) and at the same time relativistic particles emitted at large angles (which could be identified with δ protons) were not observed. This circumstance suggests that the recorded cases are characterized by a small value of Δ_δ.*

*In reference 3, the coefficient of elasticity is determined in a different manner; the result obtained there agrees well with our conclusion.

The determination of the coefficient of elasticity in a fashion not connected with the determination of the energy of the primary particle at high energies of primary particles is of fundamental interest. We have considered the value of $\sum \Delta_i$ for showers described in the research of De Benedetti et al.[13] The shower, recorded in a photoemulsion, contained 39 relativistic particles whose momenta were measured. The authors of reference 13 estimated the energy of the primary particle to be $E_0 \sim 5 \times 10^{12}$ ev. The value of $\sum \Delta_i^{ch}$ was determined to be $0.7\,M_n$, while in this sum there were not taken into account two pions emitted at a large angle with respect to the axis of the shower. The momenta of these pions are not found in reference 13. We can consider this case to be interaction of two nucleons only if the number of emitted mesons is significantly smaller than one half the number of charged mesons. If this shower is the result of the collision of two nucleons, then $\Delta_\delta \leq 0.3\,M_n$, and consequently the coefficient of elasticity is small.

d) Kinematic analysis permits us to establish the fact that in the center-of-mass system, the nucleons are emitted anisotropically after the interaction, being concentrated in directions close to the direction of motion of the nucleons before the collision.

Let us write out the data taken from reference 2 for the values of k_{max}:

	Calculated			Experimental		
$E_0/M_n =$	3	5	10	3	5	
k_{max} (%) =	35	15	5	60 [4]	80	(13a)

In the calculation, the value of $E_{\delta a}$ was taken equal to 1.08 Bev. On the right we have given the values of k found by experiment (the data of reference 4 applied to the interaction of neutrons with mean energy ~ 2.7 Bev with hydrogen). From the data set forth it is evident that the observed number of slow nucleons does not agree with the assumption on the isotropic scattering of nucleons in the center-of-mass system. A similar conclusion was obtained earlier in the work of Grigorov.[12]

The anisotropy of the scattering of nucleons in the center-of-mass system after the interaction takes place is in accord with the results of reference 3, evidently in those cases also in which the number of pions generated is large.

In conclusion, the authors consider it their duty to note that individual aspects of the work were discussed with many co-workers in the Cosmic Ray Laboratories of the Physical Institute, Academy of Sciences, U.S.S.R. and the Scientific Research Institute for Nuclear Physics, to whom they express their acknowledgment.

[1] Baradzeĭ, Rubtsov, Smorodin, Solov'ev, Tolkachev, and Tulinova, Izv. Akad. Nauk SSSR, Ser. Fiz. **19**, 502 (1955), Columbia Tech. Transl. p. 453.

[2] Yu. A. Smorodin, Dissertation, Physics Institute, Academy of Sciences, U.S.S.R. 1958.

[3] Birger, Grigorov, Guseva, Zhdanov, Slavatinskiĭ, and Stashkov, J. Exptl. Theoret. Phys. (U.S.S.R.) **31**, 971 (1956), Soviet Phys. JETP **4**, 872 (1957).

[4] Birger, Guseva, Kotel'nikov, Maksimenko, Ryabikov, Slavatinskiĭ, and Stashkov, J. Exptl. Theoret. Phys. (U.S.S.R.) **31**, 982 (1956), Soviet Phys. JETP 4, 836 (1957).

[5] Fowler, Shutt, Thorndike, and Whittemore, Phys. Rev. **195**, 1026 (1954).

[6] Block, Harth, Cocconi, Hart, Fowler, Shutt, Thorndike, and Whittemore, Phys. Rev. **103**, 1484 (1956).

[7] Wright, Saphir, Powell, Maenchen, and Fowler, Phys. Rev. **100**, 1802 (1956).

[8] Belen'kiĭ, Maksimenko, Nikishov, and Rozental', Usp. Fiz. Nauk **62**, 1 (1957).

[9] Bradt, Kaplon, and Peter, Helv. Phys. Acta **23**, 24 (1950).

[10] G. B. Zhdanov, J. Exptl. Theoret. Phys. (U.S.S.R.) **34**, 856 (1958), Soviet Phys. JETP **7**, 592 (1958).

[11] R. M. Sternheimer, Phys. Rev. **93**, 642 (1954).

[12] N. L. Grigorov, Usp. Fiz. Nauk **58**, 599 (1956).

[13] Debenedetti, Garelli, Tallone, and Vigone, Nuovo cimento **4**, 1142 (1956).

Translated by R. T. Beyer
223

PROPERTIES OF THE SPECTRUM OF ELEMENTARY EXCITATIONS NEAR THE DISINTEGRATION THRESHOLD OF THE EXCITATIONS

L. P. PITAEVSKIĬ

Institute of Physics Problems, Academy of Sciences, U.S.S.R.

Submitted to JETP editor October 6, 1958

J. Exptl. Theoret. Phys. (U.S.S.R.) **36**, 1168-1178 (April, 1959)

The singularity of the Bose-liquid Green's function near the excitation disintegration threshold is investigated by quantum-field theory methods without assuming weakness of the interaction. It is shown that three possible types of decay thresholds exist. In the first case the excitation velocity at the threshold point $p = p_0$ equals that of sound, so that starting with this point the excitation can produce phonons, thus leading to damping proportional to $(p_0 - p)^3$. In the two other cases, excitation at the threshold can break up into two excitations with non zero momenta, which are either parallel to each other or form a definite angle. In either case, the spectrum curve ends at the threshold point, and the excitation velocity at this point equals that of each of the excitations produced in the decay. Scattering of neutrons in the liquid, involving the production of excitations near the threshold is considered.

1. STATEMENT OF THE PROBLEM. POSSIBLE TYPES OF DISINTEGRATION THRESHOLDS

THIS paper is devoted to an investigation of the properties of the spectrum of elementary excitations in a Bose liquid near its point of termination. As is known, at small momenta, the excitations in a Bose liquid are phonons, i.e., the excitation energy depends linearly on the momentum. As the momentum increases, the spectrum deviates from linear and its further course depends on the specific properties of the interaction between the liquid particles, and cannot be calculated theoretically in general form. Thus, the energy spectrum of liquid He^4 has a complex form with a minimum at $p = 2 \times 10^{-19}$ g-cm/sec. Upon further increase in momentum, the excitation energy reaches a certain threshold value, above which the excitation is unstable and may break up into two or more excitations with lower energies. This point is the end point of the spectrum, and at larger momenta undamped excitations no longer exist.* The end point is a singular point of the spectrum, and the work presented is devoted to a clarification of the character of this singularity.† We shall see later that this investigation can be carried out in general form, without assumption of weak interaction.

*This pertains to absolute zero temperature. At absolute zero, disintegration is the only mechanism of damping Bose excitations.

†This statement of the problem is due to L. D. Landau.[1]

When an excitation breaks up into two, the energy and momentum conservation laws must be satisfied, as given by

$$\varepsilon(p) = \varepsilon(q) + \varepsilon(|\mathbf{p} - \mathbf{q}|). \tag{1}$$

Here $\mathbf{p}$ and $\epsilon(p)$ are the momentum and energy of the excitation that breaks up, $\mathbf{q}$ and $\epsilon(q)$ are the momentum and energy of one of the excitations formed in the breakup, and $\mathbf{q}_1 = \mathbf{p} - \mathbf{q}$ and $\epsilon(|\mathbf{p} - \mathbf{q}|)$ are the momentum and energy of the second excitation produced. If Eq. (1) does not have solutions for $\mathbf{q}$ for a given $\mathbf{p}$, no disintegration is possible. The threshold of the disintegration [we denote the momentum of the excitation at the threshold point by $\mathbf{p}_0$, and the energy by $\epsilon_0 = \epsilon(p_0)$] is characterized by the fact that Eq. (1), when taken with respect to $\mathbf{q}$, has no solutions for $\epsilon < \epsilon_0$ and has a solution for $\epsilon = \epsilon_0$. It is obviously necessary for this that the right half of (1), when expressed as a function of $\mathbf{q}$, have a minimum at $p = p_0$ for certain values of $\mathbf{q}$. When $p = p_0$ the right half of (1) depends on two variables, q and $\cos\vartheta$, where ϑ is the angle between the vectors $\mathbf{p}$ and $\mathbf{q}$. For the foregoing expression to have a minimum with respect to ϑ, it is necessary that $\cos\vartheta$ have a maximum, i.e., that the angle ϑ be zero, or else that the function $\epsilon(|\mathbf{p} - \mathbf{q}|) = \epsilon(q_1)$ have a minimum with respect to $\cos\vartheta$ for certain $\vartheta = \vartheta_0$, and consequently, that it have a minimum with respect to its argument q_1 at a certain value $q_1 = p_0$.

In the former case, the excitations produced in the disintegration proceed "forward," i.e., along the direction of the vector $\mathbf{p}$, and have identical velocities v_c. (Otherwise the right half of (1) would contain terms linear in the increments of $\mathbf{q}$ and could not have a minimum). There are two possibilities here. First, one of the disintegration excitations may have a momentum as close to zero as desired. This corresponds to the case when the speed of excitation at the point p_c equals the velocity of sound c, and the excitation may produce a phonon (case a). Second, the two created excitations may have finite momenta (case b).

Let us proceed to the case of finite ϑ. In this case each of the excitations is produced with a momentum equal to p_0, at which the energy $\epsilon(q)$ is a minimum, i.e., it has in the vicinity of p_0 the "roton" form

$$\varepsilon(q) = \Delta + (q - p_0)^2/2\mu. \tag{2}$$

If the excitation energy is $\epsilon = \epsilon_c = 2\Delta$, the excitation breaks up into two rotons with $q = p_0$ and $\epsilon = \Delta$, emitted at an angle ϑ_0 such that the sum of the momenta is p_c (case c); it is naturally necessary for this that $p_c < 2p_0$. These three cases cover all types of thresholds of disintegration into two excitations.*

To investigate the form of the spectrum near the threshold we use the methods of quantum field theory. Specifically, we calculate the Green's function of the elementary excitations, the poles of which indeed determine the excitation spectrum. We consider here elementary excitations as being Bose particles capable of disintegrating. We also assume that the interaction between the excitations has a three-particle character, i.e., that the interaction Hamiltonian is in the form of a product of three ψ-operators. This assumption is made only to simplify the formulas. It is easy to verify that the result is not changed if the Hamiltonian contains terms with products of a larger number of operators. Let us note that the Bose liquid can be considered more rigorously by the technique developed by Belyaev,[4] in which the system is described not by one but by two Green's functions. It can be shown, however, that in our case both approaches lead to the same results. This is caused by the fact that both functions, as can be readily shown in the general case, have the same poles, so that any modification of the analysis given below reduces to the appearance of equations with not one but several terms having an identical analytical behavior.

*N. N. Bogolyubov[2] has shown that a nearly-ideal Bose gas would have a phonon spectrum with $(\partial^2\varepsilon/\partial p^2)_{p=0} > 0$. Such a spectrum would be unstable from the very outset. According to calculations by Belyaev,[3] the attenuation damping in this case is proportional to p^5 at small p. In real helium, however, $(\partial^3\varepsilon/\partial p^2)_{p=0} < 0$.

2. FORM OF THE SPECTRUM NEAR THE THRESHOLD POINT

To clarify the character of the singularity of the Green's function $G(p)$, we use the Dyson equation, the form of which is shown in Fig. 1.[5]

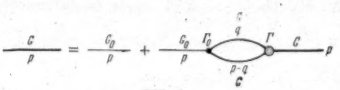

FIG. 1

The heavy line denotes here the complete Green's function G, and the thin line the free Green's function G_0, while the shaded circle denotes the complete vertex part Γ and the dot denotes the vertex point Γ_0 in the perturbation-theory approximation. In analytical form this expression becomes

$$G^{-1}(p) - G_0^{-1}(p) = i\int \Gamma(p; q, p-q) \times G(q)\, G(p-q)\, \Gamma_0(p; q, p-q)\, d^4q/(2\pi)^4. \tag{3}$$

Hereinafter p in the arguments of Green's functions and in the vertex parts will denote the energy-momentum 4-vector with components $\{\epsilon, \mathbf{p}\}$, and analogously $q = \{\omega, \mathbf{q}\}$ etc.

Near the thresholds of all three types listed in Sec. 1, the equations in (3) have properties that are entirely different, and we must consider each case separately.

a. Properties of the spectrum near the threshold of phonon creation. We consider the properties of the excitation spectrum near the point where the speed of excitation becomes equal to the speed of sound. Starting with this point, the excitation may create a phonon. The conservation law (1) becomes in this case

$$\varepsilon(p) = \varepsilon(|\mathbf{p} - \mathbf{k}|) + \omega(k), \tag{4}$$

where $\omega(k)$ is the phonon frequency, and k is its wave vector.* At small k, $\omega(k)$ becomes

$$\omega(k) = ck - \alpha k^2 \tag{5}$$

(c is the velocity of sound). We assume that $\alpha > 0$, i.e., that the phonon Spectrum is stable (see footnote in preceding column). The function $\epsilon(p)$ has a singularity at $p = p_c$. We assume, however (this will be con-

*We use a system of units in which $\hbar = 1$.

firmed later on), that this singularity appears only in terms of higher order of smallness than second, i.e., that

$$\varepsilon(p_c+\Delta p)\approx\varepsilon_c+c\Delta p+\beta(\Delta p)^2. \qquad (6)$$

(We have assumed the speed of the excitation to be c at $p=p_c$.)

When $p=p_c$ and $\cos\vartheta=1$ (ϑ is the angle between k and p) the right half of (4) becomes, taking (5) and (6) into account,

$$\varepsilon_c+(\beta-\alpha)k^2. \qquad (7)$$

The point $p=p_c$ is actually the threshold only if (7) has a minimum at $k=0$, i.e., if the inequality $\beta>\alpha$ is satisfied.

Since in this case the excitation can produce a phonon with $k\to 0$ when $p=p_c$, the region of small values of the argument of one of the Green's functions, say q, will be significant in the integral of (3). If $\omega\gg\epsilon_c$ and $q=k\ll p_c$, the Green's function G(q) is the propagation function of the phonon and has the form

$$G^{-1}(k)=B^{-1}[\omega^2(k)-\omega^2-i\delta]$$
$$\approx B^{-1}[(ck-\alpha k^2)^2-\omega^2-i\delta],\ \delta\to+0. \qquad (8)$$

When $p\approx p_c$ and $\epsilon\approx\epsilon_c$, the function $G^{-1}(p)$ has a singularity. We assume, however, that according to (6) $G^{-1}(p)$ has the following form near zero (i.e., near the pole of G)

$$G^{-1}(p)=A^{-1}[c\Delta p-\Delta\varepsilon+\beta(\Delta p)^2-i\delta]$$
$$(\Delta p=p-p_c,\ \Delta\varepsilon=\varepsilon-\varepsilon_c) \qquad (9)$$

plus certain terms of higher order, which we must determine.

At small k, the vertex portion Γ_0, as is known, has the form g_0k. We assume that when $k\to 0$, Γ is also proportional to k:

$$\Gamma(p,k,p-k)=gk \quad \text{for } k\to 0. \qquad (10)$$

In this case the integral equation (3) for G can be solved by successive approximation.

We separate the region of integration in (3) into two regions — one of large k and ω ($k\geq K$ and $\omega\geq\Omega$) and one of small values of k and ω ($k\leq K$ and $\omega\leq\Omega$), with

$$\Delta p\ll K\ll p_c,\quad \Delta\varepsilon\ll\Omega\ll\varepsilon_c. \qquad (11)$$

In the second region it is possible to use expressions (8) through (10) for G(k), G(p−k) and Γ. Assuming that the integral over large k and ω has no singularities, we obtain from (3)

$$G^{-1}\sim i\int\frac{k^3dkd(\cos\vartheta)\,d\omega}{[(ck-\alpha k^2)^2-\omega^2-i\delta][c(\Delta p-k\cos\vartheta)-\Delta\varepsilon+\omega+\beta(\Delta p-k)^2-i\delta]}. \qquad (12)$$

The symbol $\sim$ here and hereinafter denotes that the right half of the equality may differ from the left half by a coefficient that has no singularities and by an additive term. We shall henceforth drop the regular coefficients, without stating it specifically.

Small angles $\vartheta\ll 1$ are significant in the integral (12), and we can therefore put, with sufficient accuracy, $\cos\vartheta=1$ in the quadratic terms. The integration over ω can be extended to the interval $-\infty<\omega<+\infty$. As a result, the integration reduces to taking the residue with respect to ω at $\omega=ck-\alpha k^2$. We have

$$G^{-1}(p)\sim\int\frac{k^3dkd(\cos\vartheta)}{x+ck(1-\cos\vartheta)-2\beta\Delta pk-k^2(\alpha-\beta)}$$
$$\sim\int k^2\ln[x-2\beta k\Delta p+(\beta-\alpha)k^2]\,dk. \qquad (13)$$

We introduce here $x=c\Delta p+\beta(\Delta p)^2-\Delta\epsilon$. Factoring the expression under the logarithm sign and integrating, we get

$$G^{-1}(p)\sim a_1(k_1/2)^3\ln k_1+a_2(k_2/2)^3\ln k_2, \qquad (14)$$

where

$$k_{1,2}=\beta\Delta p\pm\sqrt{(\beta\Delta p)^2-(\beta-\alpha)x}.$$

It is seen from (14) that G^{-1} really has a singularity in terms of higher order than those used in Eq. (9), thus confirming the assumption made.

We determine $G^{-1}(p)$ in the direct vicinity of the pole of G(p), namely at

$$|x|\ll\beta(\Delta p)^2. \qquad (15)$$

In this case the term with k_2 can be neglected. We then obtain

$$G^{-1}\sim(\Delta p)^3\ln(-\Delta p) \qquad (16)$$

or, taking (9) into account,

$$G^{-1}(p)=A^{-1}[c\Delta p+\beta(\Delta p)^2$$
$$+a(\Delta p)^3\ln(-\Delta p)-\Delta\varepsilon]. \qquad (17)$$

Equation (17) determines the energy of the elementary excitation near the threshold:

$$\varepsilon(p)=\varepsilon_c+c(p-p_c)$$
$$+\beta(p-p_c)^2+a(p-p_c)^3\ln(p_c-p). \qquad (18)$$

Thus, when $p>p_c$, the excitation energy has a negative imaginary part equal to $-a\pi(\Delta p)^3$. This means that when $p>p_c$ the excitations are damped out, and their lifetime is inversely proportional to $(p-p_c)^3$. We note that the same result would have been obtained by perturbation theory, since the interaction with long-wave phonons is always weak, owing to the presence of the factor k in Γ.

Knowing the Green's function it is easy to verify that all the corrections to Γ have an order not less than k, thereby justifying the assumption that Γ is proportional to k.

b. Properties of the spectrum near the threshold of disintegration into two excitations with parallel non-zero momenta. In this case, when integrating over q in (3), the significant values of the 4-momentum q, as expected from physical considerations, are those with which the excitations are created near threshold. However, the values of the momentum and energy at which the excitations are created near threshold are not singular for the Green's functions. The only singularity of this point is that the given excitations may "coalesce" with the other in the vicinity of this point, a process which is impossible at absolute zero, owing to the absence of real excitations. Therefore the Green's functions under the integral in (3) have near the pole the usual form

$$G^{-1}(q) = A^{-1}[\varepsilon(q) - \omega - i\delta], \quad \delta \to +0. \tag{19}$$

This circumstance makes it much easier to investigate the problem.

Let us examine the right half of (3). The quantity Γ_0 in this equation has naturally no singularity at $p = p_c$. We also assume that the total vertex portion neither vanishes nor goes to infinity at the threshold.

Let us break up, as in the case of phonon production, the region of integration over q in Eq. (3) into a small one, near the values of momentum and energy q_0 and ϵ_0 with which the excitations are created*

$$|\mathbf{q} - \mathbf{q}_0| \leqslant K \ll p_c, \quad |\omega - \varepsilon_0| \ll \Omega \ll \varepsilon_c$$

and a large one. In the small region Γ and Γ_0 can be assumed constant. As a result

$$G^{-1}(p) \backsim i\int \frac{d\omega d^3\mathbf{q}}{[\varepsilon(q) - \omega - i\delta][\varepsilon(|\mathbf{p}-\mathbf{q}|) - \varepsilon + \omega - i\delta]} \backsim \int \frac{d^3\mathbf{q}}{\varepsilon(q)+\varepsilon(|\mathbf{p}-\mathbf{q}|)-\varepsilon}. \tag{20}$$

Since the expression $\epsilon(q) + \epsilon(|\mathbf{p} - \mathbf{q}|)$ should have a minimum at $p = p_c$, it has the following form at values of p close to p_c

$$\varepsilon(q) + \varepsilon(|\mathbf{p} - \mathbf{q}|) \approx \varepsilon_c + v_c\Delta p + \alpha(\mathbf{q} - \mathbf{q}_0)^2 + \beta(\mathbf{q} - \mathbf{q}_0, \mathbf{p}_c)^2/p_c^2, \tag{21}$$

where v_c is the velocity of each of the excitations produced at the threshold point, $\mathbf{q}_0 = \nu\mathbf{p}_c$ is the momentum of one of the created excitations, and α and β are coefficients that are determined by the type of the function $\epsilon(q)$ and $\epsilon(|\mathbf{q}-\mathbf{p}|)$:

*An important region in the integral of (3) is also the symmetrical region $q \approx p_c - q_0$, $\omega = \varepsilon_c - \varepsilon_0$. This region makes exactly the same contribution as the first one, and we shall not write down the corresponding terms.

$$\alpha = \frac{v_c p_c}{2q_0(p_c - q_0)},$$

$$\beta = \frac{1}{2}\left\{\left(\frac{\partial^2\varepsilon}{\partial q^2}\right)_{q=q_0} + \left(\frac{\partial^2\varepsilon}{\partial q^2}\right)_{q=p_c-q_0} - \frac{v_c p_c}{q_0(p_c - q_0)}\right\}.$$

Introducing a new variable $\mathbf{u} = \mathbf{q} - \mathbf{q}_0$, $\mathbf{up_c} = up_c \cos\psi$, we get

$$G^{-1} \backsim \int \frac{u^2 du\, d(\cos\psi)}{v_c\Delta p - \Delta\varepsilon + \alpha u^2 + \beta u^2\cos^2\psi} \backsim \sqrt{v_c\Delta p - \Delta\varepsilon}. \tag{22}$$

The square root in (22) should be taken with the plus sign, since when $v_c\Delta p - \Delta\epsilon > 0$, the integral in (22) is positive. Since the point $p = p_c$, $\epsilon = \epsilon_c$ is by definition a point of the spectrum, $G^{-1}(p)$ should vanish at $\Delta p = 0$ and at $\Delta\epsilon = 0$, and consequently at small values of $\Delta\epsilon$ and Δp the regular portion of $G^{-1}(p)$ should have the form $a'\Delta p + b'\Delta\epsilon$. Finally

$$G^{-1}(p) = A_1^{-1}[a\Delta p + \Delta\varepsilon + b\sqrt{v_c\Delta p - \Delta\varepsilon}]. \tag{23}$$

The excitation energy is determined by the equation

$$G^{-1}(p) = 0. \tag{24}$$

For this equation to have a solution at $p < p_c$, it is necessary to satisfy the inequality

$$(a + v_c)/b > 0. \tag{25}$$

Now the solution of the Eq. (24) is of the form

$$\varepsilon = \varepsilon_c + v_c(p - p_c) - \left(\frac{a + v_c}{b}\right)^2 (p - p_c)^2. \tag{26}$$

When $p > p_c$, Eq. (24) has no solutions at all for ϵ in the vicinity of ϵ_c, neither real nor complex. Thus, in this case the curve of the energy spectrum approaches the threshold point with a slope equal to v_c, and does not continue further. It is easy to verify then that all the corrections to Γ are finite, thus justifying the assumption that Γ is finite at the threshold point.

c. Disintegration into two excitations emitted at an angle to each other. In this case, as in the preceding one, the region of importance in the integration is of those values of q, with which the excitations are produced near the threshold point. In this region the Green's functions have the usual form (19). However, one cannot state now that the vertex Γ is finite when $\epsilon = \epsilon_c$. To clarify the character of the singularity $\Gamma(p; q, p-q)$ we express it in terms of $\Gamma_0(p; q, p-q)$ and an irreducible 4-particle vertex part $\gamma_1(q_1, p-q; q, p-q)$, i.e., the set of all the 4-particle diagrams, which cannot be divided between the end points $q_1, p-q_1$ and $q, p-q$ into two parts, connected only by one or two lines. In order to ex-

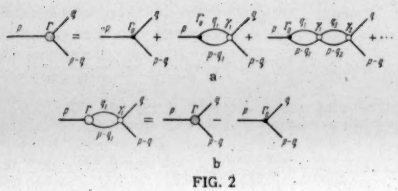

FIG. 2

press Γ in terms of Γ_0 and γ_1, it is necessary either to sum the series presented in Fig. 2a, or to solve the integral equation, shown in Fig. 2b, which is a result of this series. Theoretically this expression can be written in the following form*

$$\Gamma(p; q, p-q) - \Gamma_0(p; q, p-q) = i\int \Gamma(p, q_1, p-q_1)\, G(q_1)\, G(p-q_1) \times \gamma_1(q_1, p-q_1; p, p-q)\, d^4q_1/(2\pi)^4. \quad (27)$$

We emphasize that this is an exact equation.

Since the quantity γ_1 does not contain at all a singular integration of the type contained in Eq. (3) it is natural to assume that, like Γ_0, it remains finite at the threshold point.

We also assume that $\Gamma(p, q, p-q)$ has near the threshold a singularity only with respect to the first argument. (Each term of the series of Fig. 2a has this property.) All these assumptions should be verified in the future.

Separating in (27), as customary when integrating over the frequency ω_1, the region $|\omega_1 - \Delta| \ll \Delta$ and carrying out the integration, we obtain

$$\Gamma(p; q, p-q) - \Gamma_0(p; q, p-q) \sim \int \frac{\Gamma(p; q_1, p-q_1)\,\gamma_1(q_1, p-q_1; q, p-q)}{\varepsilon(q_1) + \varepsilon(|\mathbf{p}-\mathbf{q}_1|) - \varepsilon}\, d^3q_1. \quad (28)$$

When integrating over $\mathbf{q}_1$ we separate the following region: $|\mathbf{q}_1 - \mathbf{p}_0| \ll p_0$, $||\mathbf{q}_1 - \mathbf{p}| - p_0| \ll p_0$. In this region Γ and γ_1 can be considered independent of $\mathbf{q}_1$. Considering that in this region $\epsilon(q_1)$ and $\epsilon(|\mathbf{p}-\mathbf{q}_1|)$ have the form given by Eq. (2), we get

$$\Gamma(p) - \Gamma_0(p) \sim \Gamma(p) \times \int \frac{d^3q_1}{2\Delta - \varepsilon + (q_1 - p_0)^2/2\mu + (|\mathbf{q}_1 - \mathbf{p}| - p_0)^2/2\mu}. \quad (29)$$

*With the aid of Eq. (27) it is easy to determine $\Gamma(p; q, p-q)$ for case b. It turns out that in this case $\Gamma(p_c + \Delta p; q, p_c + \Delta p - q)$ is of the form

$$\Gamma \approx P + Q\sqrt{v_c \Delta p - \Delta\varepsilon}.$$

As is to be expected, this expression approaches the constant limit P when Δp and $\Delta\varepsilon$ go to zero.

(We recall that the symbol $\sim$ denotes equality with accuracy to a regular coefficient and a regular added term.)

Let us change to cylindrical coordinates q'_z, q'_ρ, and φ, in accordance with the following formulas (the z axis is aligned with p):

$$q_x = p_0 \cos\vartheta_1 + q'_z, \quad q_x = (p_0 \sin\vartheta_1 + q'_\rho)\cos\varphi, \quad q_y = (p_0 \sin\vartheta_1 + q'_\rho)\sin\varphi, \quad (30)$$

where the angle ϑ_1 is given by

$$2p_0 \cos\vartheta_1 = p. \quad (31)$$

Inserting (30) into (29) and neglecting the higher powers of q'_z and q'_ρ, we obtain

$$\Gamma(p) - \Gamma_0(p) \sim \Gamma(p) \int \frac{dq'_\rho\, dq'_z}{2\Delta - \varepsilon + (\sin^2\vartheta_1 q'^2_\rho + \cos^2\vartheta_1 q'^2_z)/\mu}$$

or, introducing the polar coordinates r and ψ,

$$\sin\vartheta_1 q'_\rho/\sqrt{\mu} = r\cos\psi, \quad \cos\vartheta_1 q'_z/\sqrt{\mu} = r\sin\psi,$$
$$\Gamma(p) - \Gamma_0(p) \sim \Gamma(p) \int \frac{r\,dr}{2\Delta - \varepsilon + r^2} \sim \Gamma(p) \ln(2\Delta - \varepsilon). \quad (32)$$

From (32) we find $\Gamma(p)$ at $|2\Delta - \epsilon| \ll \Delta$:

$$\Gamma(p; q, p-q) = P\left[1 + Q\ln\frac{2\Delta-\varepsilon}{\alpha}\right]^{-1} \approx \frac{P}{Q}\left[\ln\frac{2\Delta-\varepsilon}{\alpha}\right]^{-1} - \frac{P}{Q^2}\left[\ln\frac{2\Delta-\varepsilon}{\alpha}\right]^{-2}, \quad (33)$$

where P and Q are functions that have no singularities at $\epsilon = 2\Delta$. The expression (33) for Γ should be inserted into Eq. (3) to determine G(p). The integration in (3) is fully analogous to the integration in (27) and yields a term proportional to $\ln\frac{2\Delta-\epsilon}{\alpha}$. Thus

$$G^{-1} \sim [\ln(2\Delta - \varepsilon) + B']\left[1 + Q\ln\frac{2\Delta-\varepsilon}{\alpha}\right]^{-1} \sim \left(\ln\frac{2\Delta-\varepsilon}{\alpha}\right)^{-1}. \quad (34)$$

Finally, considering that by definition $G^{-1}(p_c) = 0$, we find

$$G^{-1}(p) = A_1^{-1}\left[(p - p_c) - a\left(\ln\frac{2\Delta-\varepsilon}{\alpha}\right)^{-1}\right]. \quad (35)$$

Thus, in this case the spectrum at $p < p_c$ has the form

$$\varepsilon(p) = 2\Delta - \alpha e^{-a/(p-p_c)}. \quad (36)$$

In this case, too, the curve $\epsilon(p)$ terminates at the point $p = p_c$ and has at this point a horizontal tangent of infinite order.

Knowing the Green's function, it is easy to check the assumption, made in the solution of Eq. (27), that the vertex part γ_1 is finite at the threshold point.

We note that in all the foregoing cases the

Green's function has a branch point at $\epsilon = \epsilon_c$, $p = p_c$.

The experimental data available at the present time do not permit an unambiguous answer to the question of how the phonon spectrum in He^4 is terminated. There probably occurs here either an emission of a phonon with zero momentum (case a) or a disintegration into two rotons with $\epsilon = \Delta$ (case c).

3. INELASTIC SCATTERING OF NEUTRONS WITH CREATION OF EXCITATIONS NEAR THE DISINTEGRATION THRESHOLD

The most effective method of investigating the excitation spectra is inelastic scattering of neutrons. In connection with this, we shall consider briefly the question of the probability of inelastic neutron scattering with a neutron energy loss $\epsilon \approx \epsilon_c$ and with a momentum loss $p \approx p_c$, i.e., with creation of excitations of energies close to their disintegration threshold.

In inelastic neutron scattering, the following energy and momentum conservations should be satisfied

$$P_1^2/2m = P_2^2/2m + \varepsilon, \tag{37}$$

$$\mathbf{p} = \mathbf{P}_1 - \mathbf{P}_2, \tag{38}$$

where m is the neutron mass, ϵ and $\mathbf{p}$ are the energy and momentum of the excitations created by the neutron, while $\mathbf{P}_1$ and $\mathbf{P}_2$ are respectively the initial and final momenta of the neutron. Squaring (38) we get

$$p^2 = 2m(E_1 + E_2 - 2\sqrt{E_1 E_2}\cos\varphi), \tag{39}$$

where E_1 and E_2 are neutron energies before and after scattering, and φ is the scattering angle. When $p \approx p_c$ and $\epsilon \approx \epsilon_c$, the neutrons are scattered through angles $\varphi \approx \varphi_c$, where φ_c is determined by

$$p_c^2 = 2m(2E_1 - \varepsilon_c - 2\sqrt{E_1(E_1 - \varepsilon_c)}\cos\varphi_c). \tag{40}$$

The energy and momentum transfer in the scattering angle are connected here by an equation that follows from (39) and (40):

$$p - p_c = \frac{m}{p_c}\left[\left(\sqrt{\frac{E_1}{E_1 - \varepsilon_c}}\cos\varphi_c - 1\right)(E_1 - E_2 - \varepsilon_c) + \sqrt{E_1(E_1 - \varepsilon_c)}\sin\varphi_c(\varphi - \varphi_c)\right] = \beta\varphi' + \nu\varepsilon' \quad (\varphi' = \varphi - \varphi_c, \quad \varepsilon' = \varepsilon - \varepsilon_c). \tag{41}$$

If the momentum transfer p is close to the threshold of photon creation, then the distribution of the scattered neutrons has a sharp line when $p < p_c$ and as $p \to p_c$ the intensity of this line has no singularity whatever. When $p > p_c$ the line starts broadening in proportion to $(p - p_c)^3$. The distribution of the scattered neutrons has in this case the form

$$dw = c\frac{a\pi(\beta\varphi' + \nu\varepsilon')^3}{[\varepsilon'(1 - \nu c) - \beta c\varphi']^2 + a^2\pi^2(\beta\varphi' + \nu\varepsilon')^6}\,d\varphi' d\varepsilon'. \tag{42}$$

We now proceed to scattering with creation of excitations near the threshold of disintegration into two excitations with finite momenta. To be specific, we shall treat the third type of disintegration. In this case, one excitation will be created at $\epsilon > 2\Delta$ and two excitations, each with energy $\geq \Delta$, will be created at $\epsilon > 2\Delta$. Graphically these processes are presented in Fig. 3. The wavy line corresponds here to the free neutron, the point $V(P, P_2; q, P_1 - P_2 - q)$ denotes the amplitude of the scattering of the neutron by the free atom, and $\gamma_2(q_1, p - q_1; q, p - q)$ denotes the aggregate of all 4-particle vertex diagrams, which cannot be separated between the terminals $q_1, p - q_1$ and $q, p - q$ into two parts joined by a single line only. We have taken into account here that the interaction between the free neutron and the atom can always be considered weak, and therefore we neglected all the graphs where the vertex V is encountered two times or more.

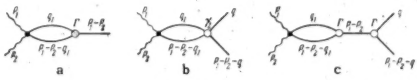

FIG. 3

When $\epsilon < 2\Delta$, when only one excitation can be created, ϵ and p are related by Eq. (36), which together with Eq. (41), in which we put $\epsilon_c = 2\Delta$, determines the energy lost by the neutron as a function of the scattering angle

$$E_1 - E_2 - 2\Delta = \alpha e^{-\alpha'/(\varphi_c - \varphi)},$$

$$\alpha' = ap_c/m\sqrt{E_1(E_1 - 2\Delta)}\sin\varphi_c. \tag{43}$$

The probability of neutron scattering in the momentum integral is given by the expression

$$dw = 2\pi|N_1 M|^2\,\delta(E_2 + \varepsilon - E_1)\,d^3\mathbf{P}_2/(2\pi)^3. \tag{44}$$

Here $M(\mathbf{P}_1, \mathbf{P}_2, \mathbf{P}_1 - \mathbf{P}_2)$ is the matrix element corresponding, in accordance with the usual rule, to the graph of Fig. 3a, and N_1 is the renormalization constant, equal to the square root of the negative residue of the Green's function of the created excitation at the point corresponding to the excitation energy. (Such a renormalization factor must be written down for each free end of the graph.) From (35) we find

$$N_1 = \sqrt{\frac{A(2\Delta-\varepsilon)}{a}}\left[-\ln\frac{2\Delta-\varepsilon}{\alpha}\right]. \quad (45)$$

As regards the matrix element M, it approaches, when ϵ approaches 2Δ, a constant limit, since the logarithm arising as a result of integration with respect to q (see Fig. 3a) is cancelled by the logarithm from the numerator in Γ (V, naturally, has no singularity). Therefore the behavior of dw is determined by the behavior of N_1, and the angular distribution of the neutrons (when $\varphi \le \varphi_0$) has the form

$$dw = C_1(\varphi_c - \varphi)^{-3}e^{-a'/(\varphi_c-\varphi)}\,d\varphi. \quad (46)$$

Thus, the probability of creation of excitation as $\varphi \to \varphi_c$ tends rapidly to zero.

We now proceed to scattering of neutrons with transfer of an energy greater than 2Δ. The scattering probability in this case has the form

$$dw = 2\pi|N_2^2 M_2|^2\,\delta(E_2+\varepsilon-E_1)\frac{d^3\mathbf{p}_2}{(2\pi)^3}\frac{d^3\mathbf{q}}{(2\pi)^3}. \quad (47)$$

Here M_2 is the sum of the matrix elements corresponding to the graphs of Figs. 3b and 3c. Now the normalization factors N_2, pertaining to excitations with energies close to Δ, have no singularities. Nor does the matrix element of the diagram in Fig. 3b have a singularity, since the vertex γ_2, like Γ, has a factor $[\ln(2\Delta-\epsilon)]^{-1}$, which, as can be readily seen, cancels out the integral with respect to q_1. The singularity of M_2 is therefore given by the graph of Fig. 3c. The matrix element of this graph has a maximum at $\varphi < \varphi_c$ and gives in this region the main contribution to the scattering. The corresponding probability has the form

$$dw = 2\pi\left|\int V(P_1,P_2,q_1,P_1-P_2-q_1)\right.$$
$$\times G(q_1)\,G(P_1-P_2-q_1)\,\Gamma(q_1,P_1-P_2-q_1,P_1-P_2)\left.\frac{d^4q_1}{(2\pi)^4}\right|^2$$
$$\times N_2^4|\Gamma(P_1-P_2;q,P_1-P_2-q)\,G(P_1-P_2)|^2$$
$$\times\delta(E_2+\varepsilon-E_1)\frac{d^3\mathbf{p}_2}{(2\pi)^3}\frac{d^3\mathbf{q}}{(2\pi)^3}. \quad (48)$$

The singularity of M_2 is contained in the term with the product ΓG. Integrating over q and using (33) and (35) we get

$$dw = C_2\,d\varphi\,dE_2\left\{\left[a-(p-p_c)\ln\left|\frac{2\Delta-E_1+E_2}{\alpha}\right|\right]^2\right.$$
$$\left.+\pi^2(p-q_c)^2\right\}^{-1}. \quad (49)$$

Inserting (41) into (49) we obtain the distribution of the scattered neutrons by angles and by energies

$$dw = C_2\,d\varepsilon'\,d\varphi'\left\{\left[a-\beta\varphi'\ln\frac{\varepsilon'}{\alpha}\right]^2+\pi^2\varphi'^2\beta^2\right\}^{-1}. \quad (50)$$

Let us describe qualitatively the scattering of the neutrons in this case. When $\varphi < \varphi_c$ there is a sharp line, corresponding to the creation of one roton, and its intensity tends to zero when $\varphi \to \varphi_c$. The creation of two rotons leads to a continuous spectrum of scattered neutrons, and the scattering intensity has a minimum at $\epsilon = 2\Delta$; when $\varphi < \varphi_c$ it has a smeared maximum at

$$\varepsilon' = \alpha e^{-a'/(\varphi_c-\varphi)}.$$

The calculations for the case of disintegration into two excitations with parallel momentum (case b) are analogous. We shall cite only the final formulas. The scattering probability with energy loss $\epsilon < \epsilon_c$ is

$$dw = C_1\sqrt{\varphi_c-\varphi}\,d\varphi. \quad (51)$$

The probability of scattering with $\epsilon' = \epsilon - \epsilon_c > 0$ is of the form

$$dw_1' = C_2 d\varepsilon' d\varphi'\,[(a+v_c)\varepsilon'$$
$$+b\sqrt{(v_c\nu-1)\varepsilon'-\beta\varphi'}]^{-2} \text{ for } (v_c\nu-1)\varepsilon'-\beta\varphi'>0,$$
$$dw = C_2 d\varepsilon' d\varphi'[(a+v_c)^2\varepsilon'^2$$
$$+b^2[(v_c\nu-1)\varepsilon'-\beta\varphi']\}^{-1} \text{ for } (v_c\nu-1)\varepsilon'-\beta\varphi'<0. \quad (52)$$

In this work we did not investigate the case when the threshold of disintegration into three excitations lies below the threshold of disintegration into two excitations. Although logically such a possibility does exist, it is of little likelihood.

Our entire investigations pertain naturally not only to the phonon spectrum of liquid He^4, but to any Bose excitation mode in condensed bodies. If, however, the interaction that leads to the excitation disintegration is weak, all the singularities described will appear only within a very small momentum interval near p_c, making it possible to determine them experimentally. It must also be borne in mind that in cases a and b, at weak interactions, the curve of the spectrum may, after a brief interaction, continue again with damping. Furthermore in the case of crystals the situation becomes greatly complicated by anisotropy.

In conclusion, the author expresses his gratitude to Academician L. D. Landau for valuable advice during the course of the work and to V. M. Galitskiĭ, L. P. Gor'kov, and I. E. Dzyaloshinskiĭ for useful discussions.

[1] L. D. Landau and E. M. Lifshitz, Статистическая физика (Statistical Physics), GITTL, 1951, ch. VI, p. 225.

[2] N. N. Bogolyubov, Izv. Akad. Nauk SSSR, Ser. Fiz. **11**, 67 (1947).

[3] S. T. Belyaev, J. Exptl. Theoret. Phys. **34**, 433 (1958), Soviet Phys. JETP **7**, 299 (1958).

[4] S. T. Belyaev, J. Exptl. Theoret. Phys. **34**, 417 (1958), Soviet Phys. JETP **7**, 289 (1958).

[5] Schweber, Bethe and de Hoffmann Mesons and Fields, Russ. Transl. vol. 1, ch. 24, p. 381, IIL, 1957 (Row, Peterson and Co., Evanston, Ill., 1955).

Translated by J. G. Adashko
224

ABSORPTION OF μ^- MESONS BY POLARIZED NUCLEI. ANGULAR DISTRIBUTION OF THE NEUTRONS

E. I. DOLINSKIĬ

Submitted to JETP editor October 8, 1958

J. Exptl. Theoret. Phys. (U.S.S.R.) 36, 1179-1184 (April, 1959)

The angular distribution of neutrons emitted in the absorption of unpolarized μ^- mesons by polarized nuclei is calculated.

I. INTRODUCTION

IN this article we consider the angular distribution of neutrons emitted in the absorption of unpolarized μ^- mesons by polarized nuclei. The shape of the angular distribution and, in particular, the asymmetry relative to the direction of polarization of the nucleus, depend on the variant of four-fermion interaction between μ mesons and nucleons, the degree of nonconservation of parity in μ^- capture, the degree of polarization of the nucleus and, of course, on specific properties of the nucleus considered. Results are calculated for nuclei in which the spin arises complete from a single proton outside filled proton subshells of the nucleus (this proton will be called the 'outer' proton in the future).

The process of nuclear absorption of μ^- mesons proceeds through an intermediate stage with formation of a mesic atom, and then through the reaction

$$\mu^- + P \to N + \nu, \qquad (1)$$

in which the proton (P) absorbs the μ^- meson and turns into a neutron (N) with emission of a neutrino (ν). In considering this effect, it is especially important to take into account the hyperfine structure of the μ^- meson in the K orbit of the mesic atom, since, owing to the slowness of the process[1] ($\tau \sim 10^{-6}$ to 10^{-7} sec),* unpolarized μ^- mesons falling into the K orbit of the mesic atom can acquire a substantial polarization in the direction of polarization of the atom because of the hyperfine structure, and, in the process, they depolarize the nucleus appreciably.* This leads, in particular, to an anisotropy in the angular distribution of neutrons emitted in the absorption of μ^- mesons by protons in closed subshells of the atom, which has the form

$$dW_\mu(E_N, \theta) \sim 1 + P_\mu \alpha(E_N) \cos\theta,$$

where θ is the angle between the direction of emission of the neutron and that of the polarization of the nucleus, and $\alpha(E_N)$ is the asymmetry coefficient calculated by L. D. Blokhintsev and the author.[1]

It should be noted that, together with the anisotropic angular distribution of neutrons emitted by the nucleus immediately after absorption by the μ^- meson ('direct' process), there will be an isotropic background of neutrons which are decay products of the compound nucleus formed in reaction.[1] However, as shown in reference 1, selection of neutrons of energies $E_N \gtrsim 3$ Mev significantly decreases the background.

Thus, the resulting angular distribution of neutrons of given energy E_N emitted in the absorption of unpolarized μ^- mesons by unpolarized nuclei, will have the form

*The frequency corresponding to the energy of hyperfine splitting ΔE in the K orbit of the mesic atom is equal to $\omega = \Delta E/\hbar \sim 10^{14} Z^3$ sec^{-1} so that $\tau\omega \gg 1$.

*It is easy to show that the degree of polarization acquired by the μ^- meson in the K orbit of a mesic atom is equal to $P_\mu = [4j/(2j+1)^2]P_i$, where P_i is the initial degree of polarization of the nucleus, and j is the spin of the nucleus. The resulting final polarization of the nucleus is equal to $P_f = [1-2/(2j+1)^2]P_i$. It should be noted that the hyperfine structure interaction can, in special cases, be important also for μ^- mesons in excited states of mesic atoms. However, if one tries to take this property into account, one meets a series of essential difficulties connected, in the main, with the absence of sufficiently reliable information about the initial stages of capture of μ^- mesons from the continuous spectrum into mesic atom orbits and about the way the μ^- meson makes transition from the excited states to the ground state.

$$dW(E_N, \theta) = dW_b(E_N) + dW_{nuc}(E_N, \theta) + dW_\mu(E_N, \theta), \quad (2)$$

where $dW_b(E_N)$ denotes the isotropic background, and $dW_{nuc}(E_N, \theta)$ and $dW_\mu(E_N, \theta)$ denote the angular distributions of neutrons, emitted from the nucleus as a result of the direct process on the outer proton and on the protons of the closed subshells, respectively. Formulas for dW_μ were given in reference 1.* The present work is devoted to consideration of $dW_{nuc}(E_N, \theta)$.

2. NEUTRON ANGULAR DISTRIBUTION

The Hamiltonian for the interaction between μ mesons and nucleons, the form of the wave functions of the particles, and the assumptions at the basis of the calculation coincide with those of Sec. 2 of reference 1. No difficulties arise in taking account of the hyperfine structure of the mesic atom. It is easy to show that, in the presence of hyperfine structure, the angular distribution of neutrons emitted in the absorption of unpolarized μ^- mesons by the outer proton of the nucleus, of spin j and projection j_z on the z axis, should be calculated from the formula

$$dW_{nuc}(E_N, \theta; njlIj_z) = {}^1/_2 \sum_{i_z} \sum_{l'} \left[C^{Ij_z}_{l i_z s_z}\right]^2 dW_{nuc}(E_N, \theta; Il'j_z + s_z), \quad (3)$$

where $dW_P(E_N, \theta; I\,l_z)$ is the angular distribution of neutrons emitted in μ^- capture by the outer proton of the mesic atom, in state with spin I and projection I_z; s_z is the projection of the μ^--meson spin, which is averaged over; summation is carried out over $I = j \pm {}^1/_2$; $s = {}^1/_2$.

The general formula for the angular distribution of neutrons emitted in absorption of unpolarized μ^--mesons by the outer proton of a polarized nucleus with arbitrary spin j, is rather complex and is given in the appendix [Eq. (A.1)]. In the special case of absorption of unpolarized μ^- mesons by polarized nuclei, the spin of which comes from the proton in state $n\,s_{1/2}$ ($j = {}^1/_2$, $l = 0$) Eq. (A.1) simplifies considerably, and has the form:†

$$dW_{nuc}(E_N, \theta; n\,{}^1/_2\,0) = \{(f_{11} + 3f_{22} + \gamma_v^2 f_{pp} - 2\gamma_v \mathrm{Re}\, f_{2p})\, a_n(E_N) + {}^1/_2 P^i_{nuc}[h_{11} + h_{22} + 2\,\mathrm{Re}\, h_{12} + \gamma_v^2 h_{pp} - 2\gamma_v \mathrm{Re}\,(h_{1p} + h_{2p})]\, b_n(E_N)\cos\theta\}\, dE_N d\Omega_N / 4\pi, \quad (4)$$

*Equation (9) in reference 1. Summation over n, j, l in Eqs. (A.2)–(A.4) is now carried only over the closed proton subshells.

†The notation used in this article is given in the appendix.

where $P^i_N = 2\langle j_z \rangle$ is the initial (previous to formation of the mesic atom) degree of polarization of the nucleus, and the quantities $a_n(E_N)$ and $b_n(E_N)$ are function of the neutron energy, depending also on properties of the nucleus considered. We note, for comparison, that in the case of μ^- capture by a free polarized proton, the neutron angular distribution is described by a formula analogous to Eq. (4), with $\gamma_\nu = 0.053$ and $a_n(E_N)/b_n(E_N) = 1$.

If the interaction between μ^- mesons and nucleons is described by the theory of Feynman and Gell-Mann,[2] which assumes vector (v) and pseudovector (a) variants of interaction, then the formula for the neutron angular distribution again simplifies considerably. Neglecting renormalization of the pseudovector coupling constant g_a, we obtain from Eq. (A.1):

$$dW_{nuc}(E_N, \theta; njl) = \frac{2}{\pi} |g|^2 [A_{1njl}(E_N, \theta) - A_{2njl}(E_N, \theta)]\, dE_N d\Omega_N, \quad (5a)$$

if $g_v = -g_a = g$, $g'_v = g_v$, $g'_a = g_a$;

$$dW_{nuc}(E_N, \theta; njl) = \frac{2}{\pi} |g|^2 [A_{1njl}(E_N, \theta) - B_{2njl}(E_N, \theta)]\, dE_N d\Omega_N, \quad (5b)$$

if $g_v = g_a = g$, $g'_v = g_v$, $g'_a = g_a$. In case $g'_v = -g_v$, $g'_a = -g_a$, the sign preceding $B_{2\,njl}$ should be changed from minus to plus in Eq. (5b). We remember that in the theory of Feynman and Gell-Mann for $|g_v| = |g_a|$, as noted in reference 1, the angular distribution of neutrons emitted in the absorption of polarized μ^--mesons by nuclei with zero spin is isotropic. Therefore, in Eq. (2), $dW_\mu = dW_\mu(E_N)$ and all of the dependence upon angle in the angular distribution of neutrons emitted in the absorption of unpolarized μ^- mesons by polarized nuclei will be contained in the term $dW_P(E_N, \theta)$, which arises from the absorption of the μ^--meson by the outer proton. Insofar as $A_{1\,njl}$ and $A_{2\,njl}$ are even functions of $\cos\theta$, and $B_{2\,njl}$ an odd function of $\cos\theta$, then it is clear from Eqs. (5a) and (5b) that in the case $g_v = -g_a$, there is no asymmetry in the angular distribution of neutrons relative to the direction of the polarization of the nucleus, and, in the case $g_v = g_a$, the indicated asymmetry occurs. In the case of μ^- capture by an $ns_{1/2}$ proton, Eqs. (5a) and (5b) take on the especially simple form

$$dW_{nuc}(E_N, \theta; n\,{}^1/_2\,0) = \frac{2}{\pi} |g|^2 a_n(E_N)\, dE_N d\Omega_N \quad (6a)$$

and

$$dW_{nuc}(E_N, \theta; n\,{}^1/_2\,0) = \frac{2}{\pi} |g|^2 [a_n(E_N) + {}^1/_2 P^i_{nuc}\, b_n(E_N)\cos\theta]\, dE_N d\Omega_N, \quad (6b)$$

i.e., for $g_V = -g_a$, the neutron angular distribution is isotropic, and for $g_V = g_a$, anisotropic.

We note the following, relevant to the absorption of polarized μ^- mesons by unpolarized nuclei. We assume that the neutrino is longitudinal (e.g., for definiteness, $g'_k = g_k$) and do not consider the pseudoscalar variant. We use the notation

$$x = |g_t + g_a| / |g_s + g_v|,$$

$$\Delta = \arg(g_t + g_a) - \arg(g_s + g_v).$$

Then, from Eq. (11) of reference 1 for the coefficient of asymmetry in the angular distribution of neutrons arising in the direct process of absorption of polarized μ^- mesons by nuclei with zero spin, we obtain the following expression

$$\alpha_0 = [(-1 + x^2) B_0 + 2x \sin\Delta \cdot G_0] [(1 + 3x^2) A_0]^{-1}. \quad (7)$$

On the other hand, from the results of the present work and those of reference 1 it is easy to show that the coefficient of asymmetry in the angular distribution of neutrons from the direct process of absorption of polarized μ^- mesons by unpolarized nuclei, the spin of which comes from a single proton in state $ns_{1/2}$ above filled proton subshells, is given by

$$\alpha_{1/2} = [(-1 + x^2) B_0 + 2x \sin\Delta \cdot G_0 + (1 + x^2 + 2x\cos\Delta) b_n] [(1 + 3x^2)(A_0 + a_n)]^{-1}. \quad (8)$$

In both cases the angular distribution has the form $1 + P_\mu \alpha \cos\theta$ ($\alpha = \alpha_0$ or $\alpha_{1/2}$) where P_μ denotes the polarization of the μ^- meson in the K orbit of the mesic atom.* The quantities A_0, B_0, G_0, a_n and b_n entering into Eqs. (7) and (8) can be calculated theoretically (we note that the quantities A_0, B_0 and G_0 in Eqs. (7) and (8) are, in general, different, since they refer to different nuclei).

Thus, measurement of the coefficients of asymmetry in the angular distribution of neutrons emitted in the direct part of the absorption of polarized μ^- mesons by nuclei of the type considered, would make it possible to determine the ratio of moduli and relative phase of the Fermi and Gamow-Teller constants for the interaction of μ^- mesons with nucleons.

In particular, for the interaction proposed by Feynmann and Gell-Mann (where $x = 1$ and $\Delta = 0, \pi$), $\alpha_0 \approx 0$ and $\alpha_{1/2} \sim (1 \pm x)^2$. Therefore, measurement of the coefficient of asymmetry of the angular distribution of the direct neutrons from the absorption of polarized μ^- mesons by unpolarized nuclei, the spin of which comes from a proton in the $ns_{1/2}$ state, would make it possible to differentiate directly between the case $g_V = -g_a$ ($\alpha_{1/2} \neq 0$).

*In the derivation of Eq. (8), we have assumed that the only depolarizing factor for the μ^- meson, falling into the K orbit of the mesic atom, is the interaction giving rise to the hyperfine structure of the mesic atom. In this case, for a nucleus of spin $j = \frac{1}{2}$, the μ^- meson falling into the K orbit of the mesic atom, depolarizes by 50%.

3. NUMERICAL ESTIMATES FOR μ^- CAPTURE IN F^{19}.

The quantities entering into Eq. (4) were evaluated for μ^- capture by the outer proton in the F^{19} nucleus. This proton was assumed to be in the state $2s_{1/2}$ ($n = 2$, $j = \frac{1}{2}$, $l = 0$). The assumptions in the calculation were the same as the assumptions noted in Sec. 3 of reference 1. The following parameters were used in the calculation: $R = 1.45 \times 10^{-13} A^{1/3}$ cm, $U_P = 44.7$ Mev, $U_N = 42$ Mev, $\xi = 0$ and -0.15, where R is the radius of the square-well potential, U_P and U_N are the potential depths for protons and for neutrons, ξ is the ratio of the imaginary part of the complex potential for the neutron to its real part.

The angular distribution, integrated over energy, for neutrons emitted in the absorption of unpolarized F^{19} nucleus, can be represented to a good accuracy as

$$dW_{nuc}(\theta) = \text{const}\,(1 + P^i_{nuc}\,\beta\alpha_H \cos\theta)\, d\Omega_N, \quad (9)$$

where α_H is the asymmetry coefficient for μ^- capture in mesic hydrogen, calculated including the hyperfine structure of the mesic atom [Eq. (A.16) of the appendix], and $\beta = 0.52$ for $\xi \approx 0$, $\beta = 0.76$ for $\xi = -0.15$. Eq. (9) also describes the angular distribution of the neutrons in the absorption of polarized μ^- mesons by the outer proton in unpolarized F^{19}, if P^i_N is replaced by $2P_\mu$, where P_μ is the polarization of the μ^- meson in the K orbit of the mesic atom. In so far as $2P_\mu$ is a quantity of order[3] ~ 0.2, and $0 \leq |\alpha_H| \leq 1$, then for $\beta \sim 0.7$ we find the upper limit of the quantity $|2P_\mu \beta \alpha_H|$ to be of the ~ 0.14. From the calculations given in reference 1, one can expect the maximum asymmetry in the angular distribution of direct neutrons from the absorption of polarized μ^- mesons in unpolarized F^{19} to be of the order of $\sim 5\%$.

The author would like to sincerely thank I. S. Shapiro for discussion of the results obtained in the present work.

APPENDIX

The probability of emission of a neutron in the direct process Eq. (1) with kinetic energy between

E_N and $E_N + dE_N$ into the solid angle $d\Omega_N$ at given angle θ to the direction of polarization of the nucleus, in the absorption of a μ^- meson by an outer proton in subshell (n, j, l) is of the form:

$$dW_{nljl}(E_N, \theta; njl) = \{|f_{11}A_1 + f_{22}(3A_1 - 2A_2) + \gamma_\nu^2 f_{pp}A_1 + 2\mathrm{Re}\, f_{12}\cdot A_2 - 2\gamma_\nu \mathrm{Re}\, f_{1p}\cdot A_3 - 2\gamma_\nu \mathrm{Re}\, f_{2p}\cdot(A_1 - A_2 + A_3)|$$
$$+ |h_{11}B_1 - h_{22}(B_1 + 2B_2) + \gamma_\nu^2 h_{pp}B_1 - 2\mathrm{Re}\, h_{12}\cdot B_2 + 2\mathrm{Im}\, h_{12}\cdot B_3$$
$$+ \gamma_\nu\cdot 2\mathrm{Re}\, h_{1p}\cdot B_2 - 2\gamma_\nu \mathrm{Re}\, h_{2p}\cdot B_1 - 2\gamma_\nu \mathrm{Im}\, h_{2p}\cdot B_3|\}\, dE_N d\Omega_N / 4\pi. \qquad (A.1)$$

where the following notation has been employed

$$A_m = A_{mnjl}(E_N, \theta) = \sum_{(k=0,\,1,\,2,\ldots)} a^{2k}_{mnjl}(E_N)\, f^{2k} P_{2k}(\cos\theta); \qquad (A.2)$$

$$B_m = B_{mnjl}(E_N, \theta) = \sum_{(k=0,\,1,\,2,\ldots)} b^{2k+1}_{mnjl}(E_N)\, f^{2k+1} P_{2k+1}(\cos\theta) \quad (m = 1, 2, 3); \qquad (A.3)$$

$$a^k_{1\,njl}(E_N) = [1 - k(k+1)/(2j+1)^2]\, W(jskj;\ jl) \sum_{LL'\Lambda} (-)^{(L+L')/2} (2\Lambda + 1)\, W(L\Lambda kl;\ lL')\, \mathrm{Re}\, F^k_{njlLsL'\Lambda}(E_N); \qquad (A.4)$$

$$a^k_{2\,njl}(E_N) = 3 \sum_{LL'\Lambda f} (-)^{(L+L')/2+1} (2\Lambda + 1)(2f + 1)\, W(L\Lambda kl;\ lL')\, V(jkf)\, X(jfjj;\ lkl;\ s1s)\, \mathrm{Re}\, F^k_{nflLsL'\Lambda}(E_N); \qquad (A.5)$$

$$a^k_{3\,njl}(E_N) = 3 \sum_{LL'\Lambda\Lambda'\tau fg} (-)^{(L+\Lambda+L'+\Lambda')/2} (2\Lambda + 1)(2\Lambda' + 1)(2f + 1)$$
$$\times (2g+1)\, C^{\tau 0}_{10\,10} C^{\tau 0}_{\Lambda 0\Lambda' 0}\, V(jkg)\, W(kg\tau 1;\ 1f)\, X(jgj;\ lfl;\ s1s)\, X(LkL';\ lfl;\ \Lambda\tau\Lambda')\, \mathrm{Re}\, F^k_{nflLsL'\Lambda'}(E_N); \qquad (A.6)$$

$$b^k_{1\,njl}(E_N) = 3^{1/2} \sum_{LL'\Lambda f} (-)^{(L+L'+1)/2} [(2\Lambda + 1)(2\Lambda + 2)(2\Lambda + 3)]^{1/2} (2f + 1)$$
$$\times V(jkf)\, W(jsfl;\ lj)\, X(LkL';\ lfl;\ \Lambda 1\Lambda + 1)\, \mathrm{Re}\, F^k_{njlLsL'\Lambda+1}(E_N); \qquad (A.7)$$

$$b^k_{2\,njl}(E_N) = 2\cdot 3^{1/2} [1 - k(k+1)/(2j+1)^2] \sum_{LL'\Lambda f} (-)^{(L+L'+3)/2}$$
$$\times [(2\Lambda + 1)(2\Lambda + 2)(2\Lambda + 3)]^{1/2} (2f + 1)\, X(jkj;\ lfl;\ s1s)\, X(LkL';\ lfl;\ \Lambda 1\Lambda + 1)\, \mathrm{Re}\, F^k_{nflLsL'\Lambda+1}(E_N); \qquad (A.8)$$

$$b^k_{3\,njl}(E_N) = 3[2(2k+1)]^{1/2} \sum_{LL'\Lambda f} (-)^{(L+L'+1)/2} [(2\Lambda+1)(2\Lambda+2)(2\Lambda+3)]^{1/2}$$
$$\times \varepsilon_l V(jkf)\, X(LkL';\ lkl;\ \Lambda 1\Lambda + 1)\, X(jfjj;\ lkl;\ s1s)\, \mathrm{Im}\, F^k_{nflLsL'\Lambda+1}(E_N); \qquad (A.9)$$

$$F^k_{nflLsL'\Lambda'}(E_N) = \tilde{C}j^k (2j+1) \binom{2k}{k} \left[\frac{(2k+1)(2j-k)!}{(2j+k+1)!}\right]^{1/2} (2L + 1)$$
$$\times (2L' + 1)\, C^{k0}_{L0L'0} C^{f0}_{L0\Lambda 0} C^{f0}_{L'0\Lambda' 0} [b^*_{L\Lambda njl}(E_\nu)\, b_{L'\Lambda' njl}(E_N)]\, \varrho_{njl}(E_\nu); \qquad (A.10)$$

$$V(jkf) = \sum_l (2l + 1)^2 W(jskl;\ lj)\, X(jfjj;\ lkl;\ s1s); \qquad (A.11)$$

$$\varepsilon_{k+1} = (2k + 3)[k/(k+1)]^{1/2}; \quad \varepsilon_{k-1} = -(2k - 1)[(k+1)/k]^{1/2}; \qquad (A.12)$$

$$f^k = j^{-k} \binom{2k}{k}^{-1} \sum_{j_z=-j}^{j} p_{ij_z} \sum_{r=0}^{r=k} (-)^r \frac{(j - j_z)!\,(j + j_z)!}{(j - j_z - r)!\,(j + j_z - k + r)!} \binom{k}{r}^2; \qquad (A.13)$$

$$a_n(E_N) = C \sum_{L=0}^{\infty} (2L + 1)\, |b_{LLn\frac{1}{2}0}(E_N)|^2 \varrho_{n\frac{1}{2}0}(E_N); \qquad (A.14)$$

$$b_n(E_N) = C \sum_{L=0}^{\infty} (2L + 2)\, \mathrm{Re}\, [b^*_{LLn\,\frac{1}{2}\,0}(E_N)\, b_{L+1L+1n\,\frac{1}{2}\,0}(E_N)]\, \varrho_{n\frac{1}{2}0}(E_N); \qquad (A.15)$$

$$\alpha_H = {}^1/_2 [h_{11} + h_{22} + \gamma^2 h_{pp} + 2\mathrm{Re}\, h_{12} - 2\gamma\, \mathrm{Re}\,(h_{1p} + h_{2p})]\, (f_{11}$$
$$+ 3f_{22} + \gamma^2 f_{pp} - 2\gamma\, \mathrm{Re}\, f_{2p})^{-1}; \quad \gamma = v_N / 2c = 0.053; \qquad (A.16)$$
$$g_1 = g_s + g_v, \quad g'_1 = g'_s + g' \quad g_2 = g_t + g_a, \quad g'_2 = g'_t + g'_a;$$

$$f_{ik} = g^*_i g_k + g'^*_i g'_k; \quad h_{ik} = g^*_i g'_k + g'^*_i g_k; \quad (i, k = 1, 2, p); \qquad \gamma_\nu \equiv \gamma^{njl}_\nu = E^{njl}_\nu / 2Mc^2; \quad C = (2M)^{3/2}\hbar^{-3}c^{-3}; \qquad (A.17)$$

where M is the nucleon mass, E^{njl}_ν is the neutrino energy.

In the case of a longitudinal neutrino ($g'_k = g_k$) we have: $\alpha_H = 1/2$ for s, v and p variants and $\alpha_H = 1/6$ for the t and a variants of interaction. The parameters f^k, which were introduced in reference 4, characterize the orientation of the nuclear spin; p_{j_z} is the probability of finding the nucleus in a state with spin projection on the z axis equal to j_z. The quantities $b_{L\Lambda njl}(E_N)$, $\rho_{njl}(E_N)$, W and X were given in the appendix to reference 1.

We note that for $f^1 \gg f^2, f^3, \ldots$ the neutron, angular distribution takes on the form: $1 + f^1 \alpha_{njl}(E_N) \cos\theta$, where f^1 is the degree of polarization of the nucleus, and $\alpha_{njl}(E_N)$ is a function of neutron energy only, depending on properties of the nucleus considered and on the properties of the nucleus considered and on the variant of interaction between μ^- mesons and nucleons.

[1] E. I. Dolinskiĭ and L. D. Blokhintsev, J. Exptl. Theoret. Phys. (U.S.S.R.) **35**, 1488 (1958), Soviet Phys. JETP **8**, 1040 (1959).

[2] R. P. Feynmann and M. Gell-Mann, Phys. Rev. **109**, 193 (1958).

[3] Egorov, Ignatenko, Khalupa and Chultém, Joint Institute of Nuclear Research, IV Session of the Scientific Conference, Dubna, May (1958).

[4] H. A. Tolhoek and J. A. M. Cox, Physica **19**, 101 (1953).

Translated by G.E. Brown
225

SOVIET PHYSICS JETP VOLUME 36(9), NUMBER 4 OCTOBER, 1959

EXCITATION OF ROTATIONAL NUCLEAR LEVELS BY CHARGED PARTICLES

A. D. PILIYA

Leningrad Physico-Technical Institute, Academy of Sciences, U.S.S.R.

Submitted to JETP editor October 9, 1958

J. Exptl. Theoret. Phys. (U.S.S.R.) **36**, 1185-1191 (April, 1959)

Scattering of charged particles by nuclei with large quadrupole moments is considered in the adiabatic approximation.

THE excitation of nuclei by charged particles has been thoroughly investigated both theoretically and experimentally[1] for the case when the energy of the incident particle is considerably lower than the Coulomb energy barrier B. For these conditions the nuclear forces are not involved and the excitation is controlled completely by the electromagnetic interaction, which usually may be considered as a small perturbation. Here, however, only the E2 transitions have a significant probability of occurrence (and E1 transitions occur rarely). Because of the fact that excitation cross-sections increase rapidly with an increase of collision energy, it is of interest to examine the excitation of nuclei by particles with energy close to the Coulomb barrier level. The interpretation of such experiments is complicated by two circumstances: firstly, the nuclear interaction becomes significant in this case, and secondly, the electromagnetic interaction between the particle and the nucleus may be not small. Nuclear interactions may be most simply accounted for by considering the level group excitation, when the internal structure of the nucleus remains unchanged. The nucleus in this case can evidently be described sufficiently well by a complex potential. On the other hand, the difficulties arising from the presence of a strong electromagnetic interaction will indeed be related to the group excitation, and expecially to the excitation of rotational levels.

In the present paper we have concentrated particularly on this aspect of the problem. We examine the scattering of protons or α particles by deformed nuclei for the conditions when the non-central portion of the electrical potential cannot be considered as a small perturbation and we confine ourselves to constructing a wave function for the scattered particle in a region outside the range of the nuclear forces. We neglect in this case the possibility of excitation of vibrational or any other (non-rotational) levels by the target nuclei. Consideration of nuclear interaction will be taken up in a later paper.

1. CONSTRUCTION OF THE WAVE FUNCTION OUTSIDE OF THE NUCLEUS

We set the origin of a fixed coordinate system at the center of gravity of the excited nucleus and set the z axis in the direction of the incident beam of particles.

We describe the orientation of the nucleus by Eulerian angles (θ_1) and the position of the incident particle by its radius vector $\mathbf{r}$ (r, θ, φ). We assume that the shape of the nucleus is axially symmetric. If the particle energy $E \cong B$, then the excitation of the low rotational levels may be considered from the adiabatic standpoint, that is, the particle is assumed scattered by a fixed nucleus. Indeed, the cross sections for Coulomb excitation obtained by perturbation theory depend on the excitation energy ΔE through the parameter $\eta \Delta E/2E$, where[2]

$$\eta = Z_1 Z_2 e^2 / \hbar v. \tag{1}$$

The condition for which the adiabatic approximation holds consists in this case of the requirement that

$$\eta \Delta E/2E \ll 1. \tag{2}$$

It can be seen that this condition is not connected with the application of perturbation theory and may therefore also be used for the general case. Let us note that since $2\eta = kR$ when $E = B$ (k is the wave number for the particle, and R is the nuclear radius), Eq. (2), will in our case be simultaneously the criterion for the applicability of the adiabatic approximation to nuclear scattering.[3]

Assuming for purposes of computation that $R = 1.2 \times 10^{-13} A_2^{1/2}$ cm (where A_2 is the atomic number for the target nucleus), we find that the left member of formula (1) (for $E = B$) is equal

to $0.08\sqrt{A_1 A_2 / Z_1 Z_2}\,\Delta E$ (Mev) and therefore inequality (1) is fulfilled for $\Delta E \leq 1$ Mev.

The scattering process of interest to us will therefore be described by the Schrödinger equation

$$\{-(\hbar^2/2m)\nabla^2 + V_n(r, \theta_i) + V_c(r, \theta_i) - E\}\Psi(r, \theta_i) = 0, \quad (3)$$

where V_n and V_c are respectively the nuclear and Coulomb potentials. The wave function Ψ of the particle for large values of r has the form

$$\Psi \to e^{ikr + i\eta \ln(kr - kr)} + \frac{f(\theta, \varphi, \theta_i)}{r} e^{i(kr - i\eta \ln kr}. \quad (4)$$

The amplitude b_{if} of the nuclear transition from the initial state with total momentum I_i, of its projection M_i on the fixed axis z, and of the projection K_i on the nuclear symmetry axis in the final state I_f, M_f, $K_f = K_i = I_i$ with the simultaneous scattering of the particle at solid angle $d\Omega$ is equal to

$$b_{if} = \int \tilde{D}^{I_f^*}_{M_f K_f}(\theta_i) f(\theta, \varphi, \theta_i) \tilde{D}^{I_i}_{M_i K_i}(\theta_i)\, (d\theta_i), \quad (5)$$

where $\tilde{D}^{I}_{MK}(\theta_i)$ is the normalized wave function for the rotational state (I, M, K).

For the total excitation cross section of the level with momentum I_f we have

$$\sigma_{if} = \frac{1}{2I_i + 1} \int d\Omega \sum_{M_i, M_f} |b_{if}|^2. \quad (6)$$

We examine Eq. (3) outside the region of nuclear force action. In this region $V_n = 0$ and V_c may be represented in the form

$$V_c = Z_1 Z_2 e^2 / r + \sum_{n=1}^{\infty} Z_1 Z_2 e^2 r^{-(2n+1)} Q^{(2n)} P_{2n}(\cos\theta'), \quad (7)$$

where P_n is a Legendre polynomial and θ' is the polar angle of the particle in the system of coordinates fixed with respect to the nucleus.

For multipole moments $Q^{(2n)}$ of highly deformed nuclei, we may take as an estimate

$$Q^{(2n)} \sim R^{2n}\beta^n, \quad (8)$$

where $\beta = \Delta R/R$ is the deformation parameter. If we make use of (8) it is not difficult to conclude that for $E \cong B$ the n-th member of summation (7) may be considered a perturbation in Eq. (3) if

$$\eta\beta^n < 1. \quad (9)$$

We shall assume henceforth

$$\eta\beta \sim 1, \quad (10)$$

$$\beta \ll 1 \quad (11)$$

and neglect in all cases quantities of order β compared with unity. Condition (10) denotes that we may consider only collisions of nuclei with protons and α particles, because for heavy ions $\eta\beta \gg 1$ at $E \cong B$, while for $E \ll B$ the adiabatic approximation is not applicable.

If condition (10) holds, then the first (quadrupole) member of summation (7) can no longer be considered a perturbation and must therefore be exactly accounted for in the solution of Eq. (3). On the other hand, the other members of this summation, in accordance with (8) and (11), remain small. With this condition in mind we substitute for potential (7) in Eq. (3) the expression

$$V_c' = {}^1/_2 Z_1 Z_2 e^2 [1/r_1 + 1/r_2], \quad (12)$$

where r_1 and r_2 are the distances from the particle to two points located on the major axis of the nucleus, symmetrically on opposite sides of the origin of coordinates at a distance d from the origin with

$$d = \sqrt{Q^{(2)}}. \quad (13)$$

Expanding Eq. (12) in Legendre polynomials in $\cos\theta'$, it is easy to prove that the first and second members of such a series coincide with the spherically symmetric and quadrupole terms of potential V_c and therefore V_c' differs from the exact potential only by a small quantity of the order of β.

Introducing the elliptical coordinates

$$\xi = (r_1 + r_2)/2d; \quad \mu = (r_1 - r_2)/2d; \ \varphi, \quad (14)$$

we can write Eq. (3) for the region outside the nucleus in the form

$$\frac{\partial}{\partial\mu}\left\{(1-\mu^2)\frac{\partial\Psi}{\partial\mu}\right\} + \frac{\partial}{\partial\xi}\left\{(\xi^2-1)\frac{\partial\Psi}{\partial\xi}\right\} + \left(\frac{1}{1-\mu^2} + \frac{1}{\xi^2-1}\right)\frac{\partial^2\Psi}{\partial\varphi^2} + \{k^2d^2(\xi^2-\mu^2) - 2\gamma_i kd\xi\}\Psi = 0. \quad (15)$$

This equation may be solved by separation of the variables and its particular solutions may be written as

$$\frac{R_{l\Omega}(\rho)}{\sqrt{\xi^2-1}}\Phi_{l\Omega}(\mu)e^{i\Omega\varphi},$$

for which $R_{l\Omega}$ and $I_{l\Omega}$ satisfy the equations

$$\frac{d}{d\mu}\left\{(1-\mu^2)\frac{d\Phi_{l\Omega}}{d\mu}\right\} + \left\{\frac{-\Omega^2}{1-\mu^2} - c^2\mu^2 + \Lambda_{l\Omega}\right\}\Phi_{l\Omega} = 0, \quad (16)$$

$$\frac{d^2R_{l\Omega}}{d\rho^2} + \left[1 - \frac{2\eta\rho}{\rho^2 - c^2} - \frac{\Lambda_{l\Omega} - c^2}{\rho^2 - c^2} - \frac{c^2(\Omega^2-1)}{(\rho^2-c^2)^2}\right]R_{l\Omega} = 0, \quad (17)$$

where $c^2 = k^2d^2$, $\rho = \xi c$, and $\Lambda_{l\Omega}$ are the eigen-

values of Eq. (16). If $c \to 0$, $\Lambda_{l\Omega} \to l(l+1)$, $\mu \to \cos\theta'$, and Eq. (16) is transformed into the equation for the associated Legendre polynomials.

We will consider $\Phi_{l\Omega}(\mu)$ normalized so that

$$\int_{-1}^{1} \Phi_{l'\Omega}(\mu)\,\Phi_{l\Omega}(\mu)\,d\mu = \delta_{ll'}, \tag{18}$$

$$\Phi_{l\Omega}(\mu)\,e^{i\Omega\varphi} \to Y_{l\Omega}(\theta'\varphi') \text{ for } c \to 0, \tag{19}$$

where $Y_{l\Omega}(\theta'\varphi')$ is a spherical function. It is convenient to represent the "angle" functions $\Phi_{l\Omega}$ in the form

$$\Phi_{l\Omega}(\mu)\,e^{i\Omega\varphi} = \sum_{n}{}' c^{\Omega}_{ln} Y_{n\Omega}(\arccos\mu, \varphi). \tag{20}$$

The prime on the summation sign indicates that n takes on values of only the same parity as l. Tables exist[4] for the eigenvalues of $\Lambda_{l\Omega}$ and for the coefficients c^{Ω}_{ln} (a more detailed solution of Eq. (16) is taken up in references 4 and 5).

The "radial" equations (17) have two linearly-independent solutions, $F_{l\Omega}(\rho)$ and $H_{l\Omega}(\rho)$ and at $\rho \to \infty$

$$F_{l\Omega}(\rho) \to \sin(\rho - l\pi/2 - \eta_l \ln 2\rho + \sigma_{l\Omega}), \tag{21}$$

$$H_{l\Omega}(\rho) \to \exp i\,(\rho - l\pi/2 - \eta_l \ln 2\rho + \sigma_{l\Omega}). \tag{22}$$

The nuclear and Coulomb potentials in Eq. (3) have inherently different symmetries (if, for example, we consider the nucleus to be a uniformly charged ellipsoid and the potential is taken as the approximation (12), then the surface of the nucleus will not be an equipotential). For this reason the "momentum" l is not conserved in scattering and the particular solutions for Eq. (3) describing the existence of a particle with a definite "momentum" in the incident wave will have the following form outside the nucleus

$$\Psi_{l\Omega} = F_{l\Omega}(\rho)\,\Phi_{l\Omega}(\mu)\,e^{i\Omega\varphi} + \sum_{l'}{}' b^{\Omega}_{ll'} H_{l'\Omega}\,\Phi_{l'\Omega} e^{i\Omega\varphi}. \tag{23}$$

The amplitudes of the nuclear scattering $b^{\Omega}_{ll'}$ are determined from the condition that (23) must be finite and continuous. A solution of Eq. (3) which goes asymptotically into (4) can be represented by the linear superposition of the functions (23).

$$\Psi = \sum_{l\Omega} a_{l\Omega}(\theta_i)\,\Psi_{l\Omega}. \tag{24}$$

The coefficients $a_{l\Omega}(\theta_i)$ can be easily found if we make note of the fact that for $r \to \infty$, $\mu \to \cos\theta'$ and therefore at great distances from the nucleus the entire dependence of function $\Psi_{l\Omega}$ on angles θ_i which characterize the nuclear orientation is contained in the spherical functions $Y_{n\Omega}(\theta', \varphi')$. [Here it is convenient to use form (20) for the functions $\Phi_{l\Omega}(\mu)$.]

If we examine in functions (24) and (5) the convergent wave and equate the coefficients of similar spherical functions we obtain

$$a_{l\Omega}(\theta_i) = 4\pi i^l e^{i\sigma_{l\Omega}} \sum_{n}{}' c^{\Omega}_{ln} Y^{*}_{n\Omega}(\theta_i). \tag{25}$$

In deriving formula (25) we use the fact that the coefficients c^{Ω}_{ln} form a unitary matrix.

Substituting (25) and (23) into (24) we obtain for the scattering amplitude,

$$f(\theta, \varphi, \theta_i) = \frac{2\pi}{ik} \sum_{ll'\Omega pn} (\delta_{ll'} + b^{\Omega}_{ll'})$$

$$\times \exp\{i(\sigma_{l\Omega} + \sigma_{l'\Omega})\} c^{\Omega}_{l'p} c^{\Omega}_{ln} Y^{*}_{p\Omega}(\theta_i)\, Y_{n\Omega}(\theta'\varphi'). \tag{26}$$

Integration in (6) and (7) and summation over M_i and M_f in (7) are now readily carried out, and we obtain finally

$$\sigma_{if} = \eta_i^2 \pi k^{-2} \sum_{L} (C^{I_f I_i}_{L\omega I_i\, I_f})^2 \{f_e^{(L)} + f_n^{(L)} + 2f_{nc}^{(L)}\}, \tag{27}$$

where $C^{\cdots}_{\cdots\cdots}$ are the Clebsch-Gordan coefficients and

$$f_e^{(L)} = \sum_{k,\,n} \left| \sum_{l,\,\Omega} c^{\Omega}_{lk} c^{\Omega}_{ln} e^{2i\sigma_{l\Omega}} C^{L\omega}_{k\Omega n-\Omega} \right|^2, \tag{28}$$

$$f_n^{(L)} = \sum_{k,\,n} \left| \sum_{ll'\Omega} c^{\Omega}_{l'k} c^{\Omega}_{ln} b^{\Omega}_{ll'} e^{i(\sigma_{l\Omega} + \sigma_{l'\Omega})} C^{L\omega}_{k\Omega n-\Omega} \right|^2, \tag{29}$$

$$f_{nc}^{(L)} = \sum_{k,\,n} \mathrm{Re}\left\{ \left(\sum_{l\Omega} c^{\Omega}_{lk} c^{\Omega}_{ln} e^{2i\sigma_{l\Omega}} C^{L\omega}_{k\Omega n-\Omega} \right) \right.$$

$$\left. \times \left(\sum_{ll'\Omega} c^{\Omega}_{l'k} c^{\Omega}_{ln} b^{\Omega *}_{ll'} e^{-i(\sigma_{l\Omega} + \sigma_{l'\Omega})} C^{L\omega}_{k\Omega n-\Omega} \right) \right\} \tag{30}$$

are dimensionless functions.

The first of these describes the purely Coulomb excitation of the nucleus, the second the excitation as a result of nuclear interaction, and the third the interference between these two processes. We will not compute here the nuclear amplitudes $b^{\Omega}_{ll'}$, however, it is immediately clear that, owing to the quasi-classical character of the problem, these amplitudes for $E \cong B$ decay rapidly (exponentially) with increasing l and l', and therefore the summations in (29) and (30) contain only a few terms. In (28) the convergence of the summation over l, with k and n fixed, depends inherently on the magnitude of the parameter $c = k\sqrt{Q^{[2]}}$ and improves rapidly with increasing k and n. Therefore the members of the summation over n decay as $1/n^3$ for $n > \eta$. For this reason for large values of η formula (28) is not convenient for the practical computation of $f_c^{(L)}$ and we shall obtain

below another expression for this function. In order to determine the phases $\sigma_{l\Omega}$ of the "radial" wave functions we may utilize the quasi-classical approximation, which when applied to Eq. (17) yields

$$\sigma_{l\Omega} = \left(l+\frac{1}{2}\right)\frac{\pi}{2} + \frac{\eta}{2}\ln\left[\gamma_l^2 + \Lambda_{l\Omega} - c^2\right] - \eta - \sqrt{\Lambda_{l\Omega}-c^2}\,\arcsin\left[1+\frac{\eta^2}{\Lambda_{l\Omega}-c^2}\right]^{-1/2} + \int_c^\infty \left[\left(1-\frac{2\eta\rho}{\rho^2-c^2}-\frac{\Lambda_{l\Omega}-c^2}{\rho^2-c^2}-\frac{c^2(\Omega^2-1)}{(\rho^2-c^2)^2}\right)^{1/2} - \left(1-\frac{2\eta}{\rho}-\frac{\Lambda_{l\Omega}-c^2}{\rho^2}\right)^{1/2}\right] d\rho. \quad (31)$$

Expression (31) reduces to an elliptic integral. However, since we already consider terms of the order of $\beta \cong c^2/\rho_0^2$ as small quantities, then, to compute the phases $\sigma_{l\Omega}$ to the same degree of accuracy, we can expand the integrand in (31) in powers of c^2/ρ^2 and use only the first two members of this series. For this case we obtain

$$\sigma_{l\Omega} = \left(l+\frac{1}{2}\right)\frac{\pi}{2} + \frac{\eta}{2}\ln\left[\gamma_l^2 + \Lambda_{l\Omega} - c^2\right] - \eta - \sqrt{\Lambda_{l\Omega}-c^2}\,\arcsin\left[1+\frac{\eta^2}{\Lambda_{l\Omega}-c^2}\right]^{-1/2} - \frac{c^2\eta}{\Lambda_{l\Omega}}\left(1-\frac{\eta}{\sqrt{\Lambda_{l\Omega}}}\arccos\frac{\eta}{\sqrt{\eta^2+\Lambda_{l\Omega}}}\right) - \frac{c^2(\Lambda_{l\Omega}+\Omega^2-1)}{4\Lambda_{l\Omega}^2} \times\left[(3\gamma_l^2+\Lambda_{l\Omega})\frac{1}{\sqrt{\Lambda_{l\Omega}}}\arccos\frac{\eta}{\sqrt{\eta^2-\Lambda_{l\Omega}}} - 3\gamma_l\right]. \quad (32)$$

2. SEMI-CLASSICAL COMPUTATION OF FUNCTION $f_c^{(L)}$

The functions $f_c^{(L)}$ actually depend on two dimensionless parameters, η and $\eta\beta$. In view of the fact that in many practically important cases $\eta \gg 1$, it would be interesting to obtain a limiting value of this function for $\eta \to \infty$ and for a set value of $\eta\beta$. It is difficult to make this transition to the limit in formula (28) because of the complicated character of the relation for the coefficients c_{ln}^{Ω} and the characteristic values $\Lambda_{l\Omega}$ of Eq. (16) as a function of the parameters of this equation. However, from the usual theory of Coulomb excitation[2] it is known that the limit for quantum-mechanical expressions for excitation cross sections at $\eta \to \infty$ coincides with the expressions obtained on the assumption of incident particles moving in classical trajectories. There is reason to believe that this coincidence is not connected with the use of perturbation theory and that, therefore, we can obtain by analogous means the limiting values of function $f_c^{(L)}$, (28), as well.

Let us, as before, consider conditions (2), (10), and (11) satisfied, and let us look into the collision of a charged particle moving in a classical trajectory with an even-even nucleus which is in the ground state ($I_i = 0$). The interaction of a particle with the nucleus is described by the potential (7). In view of condition (10) we can neglect the effect of the non-central portion of the Coulomb potential on the shape of the particle trajectory (this signifies neglecting corrections of the order of β), while in view of (11) we can neglect all the terms of summation (8) with $n \geq 2$. The adiabatic approximation used above is equivalent, when using this type of approach, to neglecting the kinetic energy of rotation of the nuclear target (because the adiabatic approximation signifies formally that the moment of inertia of the nucleus is considered infinite).

The motion of the nucleus is described therefore by the Schrodinger equation

$$i\hbar\partial\Psi(\theta_i)/\partial t = Z_1 Z_2 e^2 r^{-3}(t)\, Q^{(2)} P_2\left|\cos\theta'(t)\right|\Psi(\theta_i) \quad (33)$$

with initial conditions $\Psi = 1/\sqrt{4\pi}$ for $t = -\infty$. Here $r(t)$ and $\theta'(t)$ are specified time functions, determined by the classical laws of motion of a particle in a trajectory. These functions depend on the particle scattering angle as a parameter (or on the eccentricity of its hyperbolic orbit). The probability of exciting a level with momentum L by a particle scattered through an angle θ is equal to

$$w_L(\theta) = \sum_{M_f} \left|a_{LM_f}(\theta)\right|^2, \quad (34)$$

where

$$a_{LM_f} = \frac{1}{\sqrt{4\pi}}\int Y^*_{LM_f}(\theta'\varphi') \times \exp\left\{-i\frac{Z_1 Z_2 e^2 Q^{(2)}}{\hbar}\int_{-\infty}^{\infty}\frac{P_2\left|\cos\theta'(t)\right|}{r^3(t)}\,dt\right\} d\Omega. \quad (35)$$

In order to compute a_{LM_f} it is convenient to use a system of coordinates with an xy plane that coincides with the plane of particle motion, and an axis x directed along the axis of symmetry for the hyperbolic orbit of the incident particle. The integral in t in (35) is then expressed through the orbital integrals I_{20} and I_{22} known from the theory of Coulomb excitation (their explicit form is given in reference 1). To obtain the total excitation cross section corresponding to the level with momentum L we must multiply (34) by the cross section for Rutherford scattering and integrate it over θ.

Writing down this cross-section in the form

$$\sigma_L = \pi\gamma_i^2 k^{-2} f_c^{(L)}(x), \quad x = \gamma_i Q^{(2)}/2(Z_1 Z_2 e^2/2E)^2, \quad (36)$$

we obtain

$$f_c^{(L)}(x) = \frac{1}{\pi}\int_{-1}^{1}\sum_m \left|\int Y_{Lm}(\theta,\varphi)\right.$$

$$\times \exp\left\{ix z^2 \sin^2\theta\left[\frac{3}{1-z^2}\left(1-\frac{z\arccos z}{\sqrt{1-z^2}}\right)-\cos 2\varphi\right]\right\}$$

$$\left.\times \sin\theta d\theta d\varphi\right|^2 \frac{dz}{z^2}, \qquad (37)$$

where $z = \sin(\theta/2)$. Formula (36) refers to the excitation of the even-even nucleus ($I_i = 0$); in the general case the cross section for the transition $I_i \to I_f$, as can be easily shown, will be

$$\sigma_{if} = \frac{\pi\eta^2}{k^2}\sum_L (C^{I_f I_f}_{L0 I_i I_i})^2 f_c^{(L)}(x). \qquad (38)$$

In accordance with what has been said above we can assume that Eq. (38) is the first term of the series expansion of the exact expression (28) in powers of $1/\eta$ [moreover, it differs from (28) by a quantity of the order of β because it is derived with the use of a potential different from (12)]; it can be used in (27). The figure shows a plot of the functions $f_c^{(2)}$ and $f_c^{(4)}$. For $x \lesssim 1$ these functions can be conveniently represented as series in powers of x; for the functions $f_c^{(2)}$ and $f_c^{(4)}$ this series has the form

$$f_c^{(2)}(x) = 0.2279x^2 - 0.015x^4 - 0.0056x^6 + \ldots$$

$$f_c^{(4)}(x) = 0.00453x^4 - 0.000407x^6 + \ldots$$

It is worth noting that functions $f_c^{(L)}$ are the even functions, owing to the use of the adiabatic approximation.

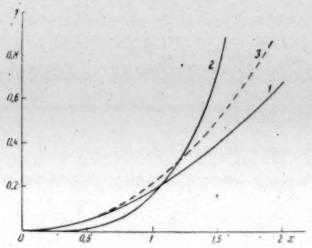

plots of functions $1 - f_c^{(2)}(x)$; $2 - f_c^{(4)}(x) \times 50$; $3 - f_c^{(2)}(x)$ by perturbation theory

In conclusion the author expresses his gratitude to K. A. Ter-Martirosyan for proposing the subject of the present paper and for helpful discussions.

[1] Alder, Bohr, Huus, Mottelson, and Winther. Revs. Modern Phys. **28**, 432 (1956).

[2] K. A. Ter-Martirosyan, J. Exptl. Theoret. Phys. (U.S.S.R.) **22**, 284 (1952).

[3] E. V. Inopin, J. Exptl. Theoret. Phys, (U.S.S.R.) **34**, 1455 (1958), Soviet Phys JETP, **7**, 1007 (1958).

[4] Stratton, Morse, Chu, and Hutner, Elliptic, Cylinder and Spheroidal Wave Functions, MIT, 1941.

[5] M. J. O. Strutt, Lamesche, Mathieusche und verwandte Funktionen in Physik und Technik, Springer, Berlin, 1932; Edwards, Ann Arbor, 1944. (Russ. Transl. Gostekhizdat, Khar'kov, 1935).

Translated by M. E. Zaret
226

STABILITY OF A PLANE POISEUILLE FLOW OF AN IDEALLY CONDUCTING FLUID IN A LONGITUDINAL MAGNETIC FIELD

E. P. VELIKHOV

Moscow State University

Submitted to JETP editor October 9, 1958

J. Exptl. Theoret. Phys. (U.S.S.R.) **36**, 1192-1202 (April, 1959)

The necessary and sufficient conditions for stability of a flow in a magnetic field have been found. It is shown that the critical value of the magnetic field that stabilizes the flow is $0.1\ V_0\sqrt{4\pi\rho}$ where V_0 is the velocity in the center of the channel and ρ is the fluid density.

1. INTRODUCTION

IN this paper we investigate the stability of flow of an ideally-conducting liquid in a longitudinal magnetic field with respect to infinitesimally small disturbances. We use here the asymptotic method of Heisenberg and Lin, the applicability of which was proven by Wasow and Tatsumi as well as by the agreement with the results of Thomas, obtained with a calculating machine. The physical interpretation of this method was confirmed in the experiments of Schubauer and Skramstad (see reference 1 and the literature therein). The inverse limiting case of poorly-conducting liquid was considered by Stuart.[2]

2. STATEMENT OF THE PROBLEM

The motion of an incompressible conducting liquid and of the field in it is described by the equations of magnetohydrodynamics

$$\rho\frac{d\mathbf{V}}{dt} = -\nabla P - \frac{1}{4\pi}\mathbf{B}\times\operatorname{curl}\mathbf{B} + \nu\nabla^2\mathbf{V};\ \operatorname{div}\mathbf{V} = 0;$$

$$d\mathbf{B}/dt = (\mathbf{B}\nabla)\mathbf{B} + \lambda\nabla^2\mathbf{B};\ \operatorname{div}\mathbf{B} = 0;\ \lambda = c^2/4\pi\sigma, \quad (2.1)$$

where ν is the kinetic viscosity and σ the conductivity of the liquid. The character of the flow is determined by the values of three dimensionless parameters: the hydrodynamic Reynolds number $R_g = V_c L/\nu$, the magnetic Reynolds number $R_m = V_c L/\lambda$, and the Alfven number $A = B_c/V_c\sqrt{4\pi\rho}$ (V_c is the characteristic velocity, B_c is the characteristic induction of the magnetic field, and L is the characteristic dimension of the flow).

At the critical values of these parameters the flow becomes absolutely unstable, i.e., infinitesimally small disturbances in the flow start increasing with time. To find the critical values of the parameters, we restrict ourselves to a consideration of the initial stage of the increase in disturbances, while they are still considerably smaller than the corresponding stationary values. We therefore seek all quantities in the form of large stationary terms and small disturbing increments

$$\mathbf{V} = \mathbf{V}_0 + \mathbf{v},\ \mathbf{B} = \mathbf{B}_0 + \mathbf{b},\ P = P_0 + p. \quad (2.2)$$

Inserting (2.2) into (2.1) we obtain a system of equation for the disturbances. The coefficients of this system are independent of the time. Its solutions are therefore of the form

$$f(\mathbf{r}, t) = f(\mathbf{r})\,e^{-i\omega t},$$

where ω is determined from the solution of the boundary-value problem for the system (2.1) with corresponding boundary conditions. The sign of the imaginary part of ω determines whether the disturbances increase or decrease with time.

We shall assume henceforth that the speed of flow and the field are directed along the x axis of a rectangular system of coordinates, and that all quantities depend only on z. The solutions have therefore the form

$$f(\mathbf{r}, t) = f(z)\exp(-i\omega t + ik_x x + ik_y y). \quad (2.3)$$

It was shown by Michael[3] that the most dangerous are two dimensional disturbances with $k_y = 0$. Using this, we obtain from (2.1) a sixth-order differential equation for the z component of the disturbance of the magnetic field.

In dimensionless symbols, it has the form

$$\left\{\left(w - \frac{\omega}{k}\right)^2 - A^2 - \frac{iw''}{kR_m}\right\}b_z'' + 2w'\left(w - \frac{\omega}{k}\right)b_z' - k^2\left\{\left(w - \frac{\omega}{k}\right)^2 - A^2 - \frac{iw''}{kR_m}\right\}b_z = -\frac{i}{k}\left\{\frac{(d^2/dz^2 - k^2)^2}{R_g}\left(w - \frac{\omega}{k}\right)b_z + \frac{(w-\omega/k)}{R_m}\times\left(\frac{d^2}{dz^2} - k^2\right)^2 b_z\right\} + \frac{1}{k^2R_mR_g}\left(\frac{d^2}{dz^2} - k^2\right)^3 b_z, \quad (2.4)$$

where $k = k_x$ and $w = V_0/V_c$. The z component of the velocity disturbance is connected with the z component of the disturbance of the magnetic field by the following relation

$$v_z = (w - \omega/k)\, b_z + (i/kR_m)(d^2/dz^2 - k^2)\, b_z. \qquad (2.5)$$

The boundary conditions at infinity consist of the vanishing of the disturbances of the velocity and of the field

$$\mathbf{v} = 0;\ \mathbf{b} = 0 \text{ for } z = \pm\infty.$$

On solid surfaces we need specify only the vanishing of the velocity disturbance

$$\mathbf{v} = 0 \text{ for } z = z_b. \qquad (2.6)$$

The magnitude of the field disturbance on a solid surface depends on the material of the solid. On a wall made of material with $\mu \sim 1$ and a conductivity σ_b, the boundary condition has the following form

$$b_z'/b_z = \pm(k^2 - i\omega\, 4\pi\sigma_b\, LV_0/c^2)^{1/2} \text{ for } z = \pm 1. \qquad (2.7)$$

It is obtained by joining the solution of the magnetohydrodynamic equations inside the flow with the solution of Maxwell's equation inside a thick wall.

Thus, the problem has been reduced to the determination of the eigenvalues of ω from the solution of the non-self-adjoint differential equation (2.4) with boundary conditions (2.6) and (2.7).

3. SUFFICIENT CONDITIONS OF STABILITY

For a well conducting liquid, $R_m \gg 1$. In most problems of practical interest the instability can be expected only at $R_g \gg 1$. Therefore all the terms in the right half of Eq. (2.4) are preceded by small parameters. However, it is dangerous merely to discard these terms, for this reduces the order of the differential equation and raises the paradox of vanishing dissipation.[1]

As is known, the dissipation is important not only in the thin boundary layer near the walls, where it is necessary to satisfy a larger number of boundary conditions than there are solutions for the "ideal" equation, but also near the singular points of this equation, obtained from Eq. (2.4) by going to the limits $R_g \to \infty$ and $R_m \to \infty$. At the point $z_0\,(w = \omega/k)$ phase resonance occurs between the disturbances and the flow, and at points z_1 and z_2 resonance occurs between the disturbances and the local Alfven wave.

However, as will be shown below, a strong magnetic field prevents such a resonance. Therefore in a strong magnetic field there should be no vanishing-dissipation paradox and the liquid can be considered as ideal. Eq. (2.4) now becomes

$$\frac{d}{dz}\left\{\left[(w - \omega/k)^2 - A^2\right]\frac{d}{dz}\, b_z\right\} - k^2\left[(w - \omega/k)^2 - A^2\right] b_z = 0 \qquad (3.1)$$

with boundary conditions $b_z = 0$ on the walls. If the characteristic velocity of flow is taken to be at a maximum, $V_c = \max V_0$, then $0 < w < 1$.

Let us multiply (3.1) by b_z^* and integrate between the walls. Integrating by parts, we obtain

$$\omega_i \int_{z_{b2}}^{z_{b1}} (w - \omega_r/k)\left(|b_z'|^2 + k^2|b_z|^2\right) dz = 0; \qquad (3.2)$$

$$\int_{z_{b2}}^{z_{b1}} \left[(w - \omega_r/k)^2 - A^2 - \omega_i^2/k^2\right]\left(|b_z'|^2 + k^2|b_z|^2\right) dz = 0, \qquad (3.2a)$$

where $\omega = \omega_r + i\,\omega_i$.

It follows from (3.2) that for disturbances that increase with time to exist it is necessary that the phase velocity of the disturbances coincide with the local velocity of the flow somewhere inside this flow. Therefore

$$0 < \omega_r/k < 1. \qquad (3.3)$$

Analogously, we obtain from (3.2a)

$$\omega_i^2/k^2 < \max\,(w - \omega_r/k)^2 - A^2 < 1 - A^2.$$

This leads to the sufficient condition for the stability of flow:

$$A^2 > 1. \qquad (3.4)$$

In this case resonant points z_1 and z_2 are outside the flow. For disturbances that increase with time to exist, it is apparently necessary that all three resonant points be present.

As expected, a strong field $(A > 1)$ stabilizes the flow no matter what the velocity of distribution. However, the critical value of the Alfven number A_{cr}, depends on the profile, particularly on whether this profile has a point of inflection, which determines the stability of flow of a non viscous liquid.

4. ASYMPTOTIC METHOD OF SOLUTION

We confine ourselves to an examination of monotonic distributions, symmetrical with respect to the point $z = 0$, of the speed of flow between solid surfaces at a distance $2L$ apart (at $z = \pm 1$, where z is a dimensionless vertical coordinate).

Equation (2.4) is now symmetrical with respect to the point $z = 0$. Its solutions therefore break up into a group of symmetrical and a group of antisymmetrical solutions, b_z^+ and b_z^-. We confine

ourselves to an examination of the symmetrical disturbances, which have a smaller number of zeros and lead to instability at lower values of R_g.

By solving the boundary-value problem we can obtain ω_i as a function of the parameters k, R_m, R_g, and A. The equation $\omega_i = 0$ determines the critical surface that separates the stability region from the instability region. To obtain this equation we put $\omega_i = 0$ in the original equations, i.e., we consider neutral disturbances.

It is obvious that the region of instability is bounded on the side of large k, since short-wave disturbances bend very strongly the lines of force and are, furthermore, attenuated by dissipation. This region is also bounded on the side of small R_g, since the field apparently cannot lead to a reduction in the critical value of this number.

Such limitations cannot be established for R_m and A, since they determine the influence of the field only in conjunction with each other. When $R_m < 1$ the role of electromagnetic retarding force, as shown by Stuart,[2] is determined by the product $R_m A^2$, and when $R_m \gg 1$, as we have seen, the flow is stable for $A > 1$.

Using these limitations, we seek approximate solutions of Eq. (2.4) in the form of asymptotic series in powers of the small parameters $1/kR_g$ and $1/kR_m$:

$$b_z(z) = \sum b_{z;\,p,\,n}\,(kR_m)^{-n}\,(kR_g)^{-p}.$$

For the zero approximation we obtain the second-order-equation

$$\frac{d}{dz}\left\{[(w-\omega/k)^2 - A^2]\,\frac{d}{dz}\,b_{z;\,0,\,0}\right\} - k^2\{(w-\omega/k)^2 - A^2\}\,b_{z;\,0,\,0} = 0. \qquad (4.1)$$

We seek a solution of this equation in the form of a convergent series in powers of k^2 (we shall henceforth drop the index z):

$$b_{00}^{+} = \sum_{n=0}^{\infty} q_n^{+} k^{2n}, \qquad b_{00}^{-} = \sum_{n=0}^{\infty} q_n^{-} k^{2n}, \qquad (4.2)$$

where

$$q_{n+1}^{\pm} = \int_0^z \frac{dz}{(w-\omega/k)^2 - A^2} \int_0^z \{(w-\omega/k)^2 - A^2\}\,q_n^{\pm}\,dz, \qquad (4.3)$$

$$q_0^{+} = 1, \qquad q_0^{-} = \int_0^z \frac{dz}{(w-\omega/k)^2 - A^2}. \qquad (4.4)$$

Thus, $b_{00}^{+} \approx 1 + k^2 q_1^{+}$. We shall call the solution b_{00}^{+} "ideal" and denote it by b_{id}^{+}. The four other linearly-independent solutions will be sought in the form

$$b_z = \exp\left\{\int g(z)\,dz\right\}. \qquad (4.5)$$

$$g(z) = \sqrt{kR_m}\,g_0 + g_1 + g_2/\sqrt{kR_m} + O(1/kR_m). \qquad (4.6)$$

For $g_0(z)$ we obtain the expression

$$g_0^2 = \frac{i}{2}\,(w-\omega/k) \pm \left[-\frac{(w-\omega/k)^2}{4} + \frac{R_g}{R_m}\{(w-\omega/k)^2 - A^2\}\right]^{1/2}. \qquad (4.7)$$

Away from the points $z = z_0$ and $z = z_1, z_2$, we have when $R_m/R_g \gg 1$

$$g_{0;\,3,\,4} = \pm\frac{1}{\sqrt{kR_m}}\left[ikR_g\,\frac{(w-\omega/k)^2 - A^2}{w-\omega/k}\right]^{1/2}; \qquad (4.8)$$

$$g_{0;\,5,\,6} = \pm\sqrt{i\,(w-\omega/k)}. \qquad (4.9)$$

The asymptotic expressions (4.8) and (4.9) are poor near the points $z = z_0$, z_1, and z_2. Approximate solutions near these points can be obtained, as in the WKB method, by expanding the coefficients of Eq. (2.4) in a series about the resonance points and by stretching the scale, so as to retain only the essential terms. For this purpose we make the change of variable

$$z - z_p = \varepsilon\eta, \qquad (4.10)$$

where

$$\varepsilon^{-3} = -e^{-3i\pi/2}\,2w_p'kR_g, \qquad w_p' \equiv w(z_p), \qquad (4.11)$$

$$\eta = -i\sqrt[3]{-2w_p'kR_g}\,(z - z_p). \qquad (4.12)$$

Inserting this new variable into Eq. (2.4) and putting $R_m = \infty$ in the same equation, we obtain, with accuracy to ϵ,

$$\frac{d}{d\eta}(\eta b_0' + b_0''') = 0. \qquad (4.13)$$

This equation has the following solutions:

$$b_{01} = 1 + O(\varepsilon); \quad b_{02} = \int S_{1,\,1/3}(^2/_3\eta^{3/2})\,\sqrt[3]{\eta}\,d\eta, \qquad (4.14)$$

$$b_{03} = \int h_1(\eta)\,d\eta, \qquad (4.15)$$

$$b_{04} = \int h_2(\eta)\,d\eta, \qquad (4.16)$$

where h is the Airy function (see reference 4) and S is the Lommel function (see reference 5).

The region of applicability of these asymptotic expressions differs from the region of applicability of expressions (4.8) and (4.9), for these are valid for fixed η and $kR_g \to \infty$, while (4.8) and (4.9) are valid for fixed z and $kR_g \to \infty$.

Away from the resonant points, the asymptotic representation of (4.15) and (4.16) coincides with (4.8), for in the sector

$$-\pi/6 < \arg\zeta < 7\pi/6 \qquad (4.17)$$

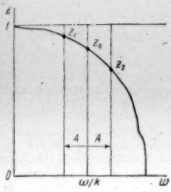

FIG. 1. Critical points on the velocity profile.

we have (see reference 4)

$$b_{03}(\zeta) \approx \zeta^{-1/4} \exp\{^2/_3 e^{-i\pi/4} \zeta^{3/2}\}[1 + O(\zeta^{-3/2})],$$

$$\zeta = (-2w'_p k R_g)^{1/3}(z - z_p). \qquad (4.18)$$

We thus have obtained asymptotic expressions for the linearly-independent solutions of Eq. (2.4). However, the resonant points are branch points of these functions.

Therefore, for neutral disturbances, it is necessary to find the correct path around the branch point. For disturbances that increase with time, the asymptotic expression for solutions (4.4), (4.8), and (4.9) has no singularities. If one considers a neutral disturbance as the limiting case of an increasing disturbances as $\omega_i \to 0$, this corresponds to going around the singular points in the complex z plane from above, since upon passing through the point $w = \omega_r/k$, the argument $w = \omega_r/k - i\omega_i/k$ (where $\omega_i > 0$) changes by $-\pi$ (see Fig. 1). If a neutral disturbances are considered as the limiting case of an attenuating disturbance, the phase changes by π. This paradox was resolved by Landau and Wasow. Landau[6] solved the initial-condition problem in an analogous case with the aid of a unilateral Laplace transformation, while Wasow[7] investigated the problem with allowance for dissipation. It was found in both cases that one must go around the resonant points from the $\omega_i > 0$ side. The same can be concluded from the condition (4.17), for when it is satisfied the four linearly-independent solutions of Eq. (4.13) go into two "ideal" solutions and two rapidly fluctuating ones.

As seen in Sec. 2, for neutral or increasing disturbances to exist it is necessary, apparently, that all three resonant points be located inside the flow. Therefore the point z_1 should be located near the wall. A numerical calculation for $z_1 > 1$ also discloses no neutral disturbances.

Since $\arg(w - \omega/k)$, $\arg(w - \omega/k - A)$, and $\arg(w - \omega/k + A)$ change by $-\pi$ in going about the resonant points, the real part of (4.7) does not reverse its sign. Therefore the solutions b_{04} and b_{06} increase exponentially from the wall inside the flow, and their contribution to the symmetrical combinations $a_1 b_{03} + a_2 b_{04}$ and $c_1 b_{05} + c_2 b_{06}$ is negligible near the wall. The point z_0 is separated from the boundary by a finite distance, and one can use for b_{05} the expression

$$b_{05} = \exp\left\{\int g_{05}\, dz\right\}. \qquad (4.19)$$

On an ideally conducting wall, the boundary conditions for b are of the form

$$b = 0; \quad b' = 0; \quad i\omega R_m b' + b''' = 0. \qquad (4.20)$$

Inserting (4.4), (4.15), and (4.19) into (4.20), and neglecting R_g/R_m compared with unity, we obtain the dispersion equation

$$b^+_{id}/b^{+'}_{id} = (b_{03}/b'_{03})\{1 + (b^{+''}_{id}/b^{+'}_{id})\, i\omega R_m\}. \qquad (4.21)$$

When $R_m = \infty$ (4.21) becomes

$$b^+_{id}/b^{+'}_{id} = b_{03}/b'_{03}. \qquad (4.22)$$

5. STABILITY OF PLANE FLOW FOR $R_m = \infty$

The right half of Eq. (4.22) is expressed in terms of the Airy function $h_1(0 - i\zeta)$:

$$\frac{b_{03}}{b'_{03}} = \frac{\int_{-\infty}^{\zeta} h_1(0 - i\zeta)\, d\zeta}{\zeta h_1(0 - i\zeta)}(z - z_1) = \Phi(\zeta). \qquad (5.1)$$

The function $\Phi(\zeta)$ is calculated by numerical integration and is shown in Table I and Fig. 2. It is important that the imaginary part of this function has a maximum equal to 0.387 at $\zeta \approx 2.4$, and tends to zero when $\zeta \to 1.5$ and $\zeta \to \infty$. This behavior of $\mathrm{Im}\,\Phi(\zeta)$ results in two branches of

TABLE I. The function $\Phi(\zeta)$

ζ	Re Φ(ζ)	Im Φ(ζ)	ζ	Re Φ(ζ)	Im Φ(ζ)
1.4	1.054	−0.03784	2.8	0.2316	0.3373
1.6	0.9677	0.09275	3.0	0.1644	0.2926
1.8	0.8476	0.2125	3.2	0.1190	0.2470
2.0	0.7195	0.3082	3.4	0.09002	0.2049
2.2	0.5789	0.3683	3.6	0.07436	0.1678
2.3	0.5087	0.3822	3.8	0.06408	0.1393
2.4	0.4421	0.3871	4.0	0.06026	0.1161
2.5	0.3803	0.3835	4.2	0.05917	0.09858
2.6	0.3241	0.3727			

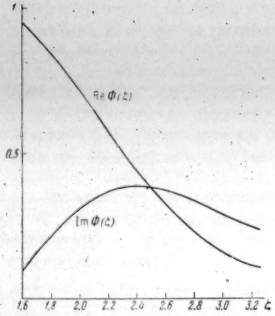

FIG. 2. The function $\Theta(\zeta)$.

the neutral curve. Asymptotically, when $\zeta \to \infty$,

$$\Phi(\zeta) \approx \zeta^{-3/2} e^{-i\pi/4} [1 + {}^{3}/_{4} \zeta^{-3/2} e^{i\pi/4} + \zeta^{-3} (-{}^{5}/_{64} + 2i)]. \quad (5.2)$$

The imaginary part of the "ideal" solution b_{id}^{+} equals the sum of the half residues at the resonant points z_1 and z_2. When going around these points, $\arg(w - \omega/k \pm A)$ changes by $-\pi$. Therefore

$$\operatorname{Im} b_{id}^{+} = \frac{k^2\pi}{2A} \left\{ \frac{1}{w_1'} \int_0^{z_1} [(w - \omega/k)^2 - A^2]\, dz \right.$$
$$\left. - \frac{1}{w_2'} \int_0^{z_2} [(w - \omega/k)^2 - A^2]\, dz \right\}. \quad (5.3)$$

It follows from Sec. 2 that the neutral disturbances are possible only when $A < 1$. Therefore Eq. (5.3) can be calculated approximately by expanding it in a series* in powers of A:

$$\operatorname{Im} b_{id}^{+} = \frac{k^2\pi}{w_1'} \left\{ \frac{w_1''}{w_1'^2} H_1 - \left(\frac{3w_1''^2}{w_1'^4} - \frac{w_1'''}{w_1'^3} \right) A + F_1 A^2 \right\},$$
$$H_1 = \int_0^{z_1} (w - \omega/k)^2\, dz, \quad (5.4)$$

where

$$F_1 = -\frac{12\, w_1'' w_1'''}{w_1'^5} H_1 + \frac{20\, w_1''^3}{w_1'^6} H_1 - \frac{2\, w_1^{(VI)}}{3\, w_1'^4} - \frac{2\, w_1'' z_1}{w_1'^2} + \frac{26}{3\, w_1'}.$$

The derivative of the symmetrical solution is

$$F \quad b_{id}^{+\prime} = \frac{k^3}{(w - \omega/k)^3 - A^2} \int_0^{z} [(w - \omega/k)^2 - A^2]\, dz. \quad (5.5)$$

Let us consider disturbances arising in a thin layer near the wall, i.e., let us put $1 - z_1 \ll 1$, which is not a limitation, since it follows from (5.6) that actually the distance between this point and the wall is always small. This permits us to express the critical values of the parameters in terms of the flow characteristics near the wall.

Inserting (5.4), (5.5), and (5.3) into (4.22) and considering that

$$(1 - z_1) \sim -(\omega/k - A)/w_b'; \quad (w_b' \equiv w'(1)), \quad (5.5a)$$

we get

$$-\frac{\pi w_b'}{w_1'^2} \frac{w_1'' H_1 + (w_1'''/w_1' - 3\, w_1''^2/w_1'^2) A}{H_b} \left(\frac{\omega}{k} + A \right)$$
$$= \operatorname{Im} \Phi(\zeta). \quad (5.6)$$

The left half of (5.6) increases with increasing ω/k, i.e., with decreasing z_1, provided

$$(w_1''' w_1' - 3\, w_1''^2)/w_1'^4 < 0. \quad (5.7)$$

This condition is satisfied for convex profiles of the Poiseuille-flow type. Therefore, the left half of (5.6) has a minimum at $z_1 = 1$ and equals

$$-(2\pi A/w_b'^2)[w_b''$$
$$+ A(w_b'''/w_b' - 3\, w_b''^2/w_b'^3)]. \quad (5.8)$$

If (5.8) is greater than max $\operatorname{Im} \Phi(\zeta) = 0.387$, the flow is stable. From this condition it is possible to determine the critical Alfven number

$$A_{cr}^{-1} = -8.12\, w_b''/w_b'^2$$
$$- [(66 + 48.7/H_b)\, w_b''^2/w_b'^4$$
$$- 16.2/H_b - w_b'''/w_b'^3]^{1/2}. \quad (5.9)$$

If $|\omega_b'''| \ll |\omega_b''^2/\omega_b'^2|$, we obtain from (5.9)

$$A_{cr}^{-1} = -(8.12 + \sqrt{66 + 48.7/H_b})\, w_b''/w_b'^2$$
$$\approx -21\, w_b''/w_b'^2, \quad (5.10)$$

since $H_b = \int_0^1 (w - \omega/k)^2\, dz \sim {}^{1}/_{2}$. Finally

$$A_{cr} \approx -0.05\, w_b'^2/w_b''. \quad (5.10a)$$

For a Poiseuille flow, it follows from (5.10) that

$$A_{cr}^{-1} \approx -20.6\, w_b''/w_b'^2 \approx 10.$$

A more exact numerical calculation given in Sec. 6 yields a value 9.8.

The smaller the critical magnetic Alfven number, the stronger the stabilizing influence of the field. It therefore follows from (5.10) that the greater the curvature of the profile, the more stable the flow and the less the field required for its stabilization. For example, when Poiseuille flow is established, the profile at the inlet of the tube is almost exponential near the wall, $|w''/w'^2| \sim 1$, and the critical Alfven number is half that of a steady-state parabolic profile.

If $A < A_{cr}$, then the flow is unstable when $R_g > R_g^{cr}(A)$. The curve of neutral stability $k(R_g)$ for flow in a field has a different asymp-

*Actually, it follows from the results [see (5.10)] that $A_{cr} \sim 1/10$.

totic value than without the field, since the "ideal" solution has no solutions with $k = 0$ and $\omega/k = A$.

Since $\operatorname{Im}\Phi(\zeta)$ is a function with a maximum, Eq. (5.6) has two solutions for $A < A_{cr}$, $\zeta = \zeta_1$ or ζ_2. The left half of Eq. (5.6) is bounded from below. Therefore $\infty > \zeta_1 > \zeta_2 > 0$ and $(1 - z_1) \sim (kR_g)^{-1/3}$, i.e., the resonant point z_1 is located at all times within a viscous layer near the wall. To find analytically the asymptote of the neutral-stability curve, we note that in the term $\sim \ln(1 - z_1)$ in the expression for $\mathrm{Re}\, b^+_{id}$ near the wall is particularly large. Therefore

$$\mathrm{Re}\, b^+_{id} \sim 1 - k^2 \frac{H_1}{2w'_1 A} \ln(1 - z_1),$$

$$(1 - z_1) \sim \exp\{2w'_b A / k^2 H_b\}. \qquad (5.11)$$

Since ζ is finite, we have

$$R_g = -\zeta^3 / 2kw'_1 (1 - z_1)^3 \sim \exp\{-6w'_b A / k^2 H_b\}. \qquad (5.12)$$

For Poiseuille flow $H \sim 8/15$ and $R_g \sim \exp(22.3\, Ak^{-2})$.

The critical Reynolds number is determined by the point where the two branches merge. The phase velocity ω/k of such "critical" disturbances is determined from (5.6), $\operatorname{Im}\Phi(\zeta) = 0.387$ where on the right side. The corresponding value of the wave number k is determined from Eqs. (4.22), (4.4), (5.1) and (5.5a) for $\zeta \sim 2.4$

$$\left(1 + k^2 \mathrm{Re} \int_0^1 \frac{dz}{(w - \omega/k)^2 - A^2} \int_1^z \left\{\left(w - \frac{\omega}{k}\right)^2 - A^2\right\} dz\right) \frac{\omega/k + A}{k^2 H_b} = -\frac{0.442}{w'_b}. \qquad (5.13)$$

The integral in (5.13) can be found approximately by using the transformation

$$J = \int_0^1 \frac{dz}{(w - \omega/k)^2 - A^2} \int_0^z \left\{\left(w - \frac{\omega}{k}\right)^2 - A^2\right\} dz$$

$$= \int_0^1 \frac{dz}{(w - \omega/k)^2 - A^2} \int_0^1 \left\{\left(w - \frac{\omega}{k}\right)^2 - A^2\right\} dz$$

$$- \int_0^1 \frac{dz}{(w - \omega/k)^2 - A^2} \int_{z_1}^1 \left\{\left(w - \frac{\omega}{k}\right)^2 - A^2\right\} dz. \qquad (5.14)$$

Since $\omega/k < 1$, the internal integral in the second term is small in the vicinity of the poles of the integrand. Therefore

$$J \approx \int_0^1 \frac{dz}{(w - \omega/k)^2 - A^2} H_b$$

$$\approx -\frac{H_b A^{-1}}{2w'_1} \ln \frac{\omega/k - A}{\omega/k - A - 4A/w'_1}; \qquad (5.15)$$

$$k = +\sqrt{-H_b / w'_1}$$

$$\times \left\{-\frac{1}{2A} \ln \frac{\omega/k - A}{\omega/k - A(1 + 4/w'_1)} + \frac{0.44}{\omega/k + A}\right\}^{-1/2}. \qquad (5.16)$$

In spite of the fact that k depends on the difference of the small quantities ω/k and A, the accuracy of the expression is not bad, since this dependence is logarithmic.

Using these expressions, it is possible to obtain from (4.18a), with accuracy to within the order of magnitude, the critical hydrodynamic Reynolds number

$$R_g^{cr} = \frac{\zeta^3_{cr}}{-2w'_1 k (1 - z_1)^3}$$

$$\approx \frac{13.8 w'^3_b}{2w'_1 k (\omega/k - A)^3} \sim \frac{\mathrm{const}}{(A_{cr} - A)^3}. \qquad (5.17)$$

We note that one cannot put $A = 0$ in any of the resultant expressions, for in this case the singular points will merge into one and the expansion in the vicinity of z_1 loses its meaning [see (4.13)].

6. STABILITY OF THE POISEUILLE FLOW. NUMERICAL METHOD

In conclusion let us give the results of the calculation of the stability of a parabolic velocity profile. In this case

$$b^+_{id} = 1 + k^2 \left\{\frac{z^3}{10} - \frac{1}{A}\left(\frac{2}{15} z_0^4 - \frac{A^2}{5}\right) \ln \left(\frac{z^3 - z_0^3 + A}{z^3 - z_0^3 - A} \frac{z_0^3 + A}{z_0^3 - A}\right)\right.$$

$$\left. - \frac{z_0^3}{15} \ln \frac{(z^3 - z_0^3)^2 - A^2}{z_0^4 - A^2} + \frac{2}{15} i\pi z_0^3\right\}. \qquad (6.1)$$

Inserting this expression into (4.21), we obtain

$$\frac{b^+_{id}}{b^+_{id}} = \{\mathrm{Re}\,\Phi(\zeta) - \mathrm{Im}\,\Phi(\zeta)\,\delta\}$$

$$+ i\{\mathrm{Im}\,\Phi(\zeta) + \mathrm{Re}\,\Phi(\zeta)\,\delta\}, \qquad (6.2)$$

where

$$\delta = -\frac{4}{kR_m} \left\{\frac{z_0^6 + 3z_0^4 - 9z_0^2 - A^2 z_0^2 + 5 + 3A^2}{(1 - z_0^2)(1 - z_1)^2 (1 + z_1)^2 (1 - z_0^2 + A)^2}\right.$$

$$\left. - \frac{1}{z_0^4 - 2z_0^2/3 - A^2 + 1/5}\right\},$$

and z_0^2 is the coordinate of the mean resonant layer $w = \omega/k$. This equation was solved numerically for $kR_m = \infty$, 10^8, 10^7, and 2×10^6.

The neutral curve for $A = 0.08$ and $kR_m = \infty$ is given in Table II and in Fig. 3. Table III and Fig. 3 contain the neutral curve for $kR_m = 10^8$ and the initial portions of the neutral curves for $kR_m = 10^7$ and 2×10^6. It is seen that as kR_m

TABLE II
Neutral curve at A = 0.08, $kR_m = \infty$

z_0^2	First branch		Second branch	
	k^2	$R_g^{1/3}$	k^2	$R_g^{1/3}$
0.919	0.130	3460	0.145	5230
0.918	0.148	1700	0.168	2550
0.915	0.183	663	0.210	971
0.910	0.222	325	0.260	445
0.905	0.255	214	0.299	293
0.900	0.286	159	0.334	211
0.895	0.316	128	0.365	164
0.890	0.346	107	0.394	131
0.885	0.380	92.1	0.420	108
0.880	0.400	84.4	0.439	90.2

TABLE III
Neutral curve at A = 0.08

z_0^2	k^2	$R_g^{1/3}$	k^2	$R_g^{1/3}$
$kR_m = 10^8$				
0.918	0.126	2210	0.129	2520
0.915	0.186	880	0.208	1185
0.910	0.222	330	0.258	462
0.905	0.255	214	0.299	293
0.900	0.286	159	0.334	211
0.895	0.316	128	0.365	164
0.890	0.364	107	0.394	131
0.885	0.380	92.1	0.420	108
0.880	0.400	84.4	0.439	90.2
$kR_m = 10^7$				
0.880	0.393	86.6	0.402	89.3
$kR_m = 2 \cdot 10^6$				
0.890	0.334	113	0.365	129

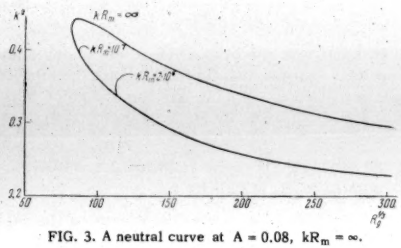

FIG. 3. A neutral curve at A = 0.08, $kR_m = \infty$.

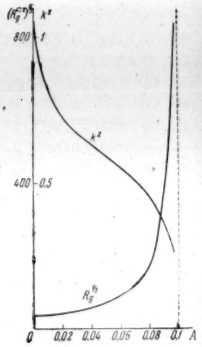

FIG. 4. Dependence of R_g^{cr} and of the wave number of critical disturbances on A.

decreases, the critical hydrodynamic Reynolds number increases. It is impossible to trace the reduction in the stabilizing influence of the field, owing to the limitations of the method.

The dependence of R_g^{cr} and of the wave number k of the critical disturbances on the Alfven number A is given in Table IV and in Fig. 4. The critical value of the Alfren number is 0.102, i.e., to stabilize the flow it is sufficient to have

$$B_c \geqslant V_c \sqrt{4\pi\rho}\, 0.102 \approx 0.36 V_c \sqrt{\rho}.$$

7. CONCLUSIONS

An analysis of infinitesimally small disturbances of plane flow in a magnetic field shows therefore that in the case of ideal conductivity of the liquid it is sufficient, to stabilize any flow, to have A > 1, i.e., $B_c^2/8\pi \geq \rho V_c^2/2$.

The field necessary for stabilization depends on the specific type of the velocity profile. The results of this work and of earlier research on stability are given below.

Arbitrary form of velocity profile A = 1
Tangential discontinuity of magnitude V_0 (reference 8) A = ½
Convex profile with maximum velocity V_0 $A = (\omega_b')^2/20|\omega_b|$.
Poiseuille flow A = 0.1

TABLE IV. Dependence of R_g^{cr} and of the wave number of critical disturbances on A

A	z_0^2	k^2	$(R_g^{cr})^{1/3}$	A	z_0^2	k^2	$(R_g^{cr})^{1/3}$
0.00		1.0845	17.45[1]	0.06	0.8608	0.5502	41.92
0.02	0.8266	0.7162	20.58	0.08	0.8784	0.4429	83.04
0.04	0.8438	0.8352	27.78	0.10	0.8956	0.2389	873.7

The difference in the magnitude of the stabilizing field is due to the fact that in flow with a tangential discontinuity the disturbances arise inside the entire layer, which is approximately replaced by the discontinuity, where the total velocity gradient is effective. In the case of a profile with an inflection or a kink, the disturbances arise between the point of inflection and the wall, and in the case of a convex profile they arise in the thin layer near the latter. Therefore the field need merely suppress the instability in this layer. If we insert in the Syrovatskiĭ[8] criterion, instead of the magnitude of the discontinuity, the speed of the extreme resonant layer for critical disturbances $z_2^2 = 0.8$, $\omega/k + A \sim 0.2$, we obtain for A_m^{cr} exactly the critical value

$$\frac{B_c^{cr}}{\sqrt{4\pi\rho}} \frac{1}{0.2 V_c} = \frac{1}{2} \text{ and } \frac{B_c^{cr}}{V_c \sqrt{4\pi\rho}} = 0.1.$$

The author is deeply grateful to S. I. Braginskiĭ for suggesting the problem and for valuable advice during the course of solution, and to D. A. Frank-Kamenetskiĭ for useful discussions.

[1] C. Lin, Theory of Hydrodynamic Stability (Russ. Transl.) M. IIL, 1958.

[2] I. T. Stuart, Proc. Roy. Soc. **A221**, 189 (1954).

[3] D. Michael, Proc. Cambr. Phil. Soc. **49**, 166 (1953).

[4] Tables of the Modified Hankel Functions of Order One-third and of their Derivatives, Cambridge, Mass., Harvard Univ. Press, 1945.

[5] Higher Transcendental Functions, Vol. 2, McGraw-Hill, 1953.

[6] L. D. Landau, J. Exptl. Theoret. Phys. (U.S.S.R.) **16**, 574 (1946).

[7] W. Wasow, Ann. Math. **58**, 222 (1953).

[8] S. I. Syrovatskiĭ, Труды ФИАН (Trans. Phys. Inst. Acad. Sci.) **8**, 13 (1956); J. Exptl. Theoret. Phys. (U.S.S.R.) **24**, 622 (1953).

Translated by J. G. Adashko
227

EFFECT OF IMPURITIES ON THE X-RAY SPECTRA OF TRANSITION METALS

I. B. BOROVSKIĬ and K. P. GUROV

Metallurgy Institute, Academy of Sciences, U.S.S.R.

Submitted to JETP editor October 10, 1958

J. Exptl. Theoret. Phys. (U.S.S.R.) **36**, 1203-1206 (April, 1959)

A method is proposed for an estimate of the effect of impurities on the parameters of transition-metal x-ray emission spectra. The method is applied to the case of dilute alpha-solid solutions with iron as the base.

SYSTEMATIC investigations carried out over the last few years for the study of dilute solid solutions with transition-group metals as a base have shown that a considerable influence is exerted by small impurities (of the order of 0.01 to 0.1% atomic) on some of the physical properties of these solutions. This influence is evidenced by changes in the x-ray emission and absorption spectra parameters, in the optical constants, in the diffusion coefficients, in the coefficient of linear expansion, in the electrical resistivity, etc.

A study of experimental data and a theoretical investigation of the subject have led us to a model of a physical mechanism describing the action of impurities on the electron energy spectrum for the transition metals and on the interatomic binding forces in theee metals.[1,2] We examine in the present paper the possibility of applying this model to a quantitative estimate of the wavelength changes in the emitted x-ray spectra.

The model can be described as follows.

Upon entering a metal, an impurity of substitution (or inclusion) loses its outer (valence) electrons, which are distributed in the conduction band of the base metal. The resultant positive charge on the impurity ion may be either greater or less than the positive charge on the remaining atomic cores, i.e., the impurity in the metal will possess an excess positive or negative charge. It turns out that the perturbing potential of this excess charge is active only with a finite radius, because of the shielding effect provided by the conduction electrons. The effective radius of the excitation potential comprises only a few coordination spheres around each impurity atom. The resultant polarization interaction leads to a distortion of the electron shells of the base-metal cores. In transition metals this effect also influences the defective (not fully built up) nd or nf shell. Since the corresponding energy band overlaps the conduction band, an equilization of electron energies takes place about the Fermi level, i.e., in the immediate vicinity of the impurity, electrons pass from the defective shell into the conduction band (or vice versa, depending on the sign of the excess charge of the impurity). Thus, in the vicinity of the impurity, the effective charge of the base-metal core changes, which is equivalent to the appearance of induced excess charges on these cores. These excess charges are always opposite in sign to the charge of the basic impurity. Therefore, an additional (polar) bond arises between the basic impurity and the surrounding cores. Thus, distinct reinforcement blocks appear and remain until the impurity concentration reaches a value such that the impurities develop strong interactions among themselves.

In Gurov's work[3] an investigation was made of the degree of validity of such a model and the limits within which it could be applied. It was shown that the model holds for those cases when an approximation of strongly bound electrons holds. The concepts thus developed are therefore applicable to all electrons of the atomic core including electrons of the "defective" shell, whereas if applied to the conduction electrons, they can cause considerable discrepancies.

Gurov[3] also showed that if the potential for the excess charge of the impurity drops off rapidly with distance and changes very little at distances on the order of the radius of the first coordination sphere (that is, practically constant over a range on the order of the dimensions of the core), then, the local deformation of the electron spectrum (isolated at each site) can be conveniently described by the "rigid band" approximation,[4] according to which

$$\Delta E = -eW(r), \tag{1}$$

where W is the potential of the excess impurity charge, e the absolute charge of the electron, and r the distance from the core of interest to the impurity. It is common practice to express W(r), after Mott,[5] in the following form (for a more precise form see reference 6)

$$W(r) = -(Ze/r)\,e^{-qr}. \qquad (2)$$

where Ze is the excess charge.

On the basis of the concepts described above and Moseley's law we can make an approximate evaluation of the influence of the impurities on the x-ray spectra of the transition metals. To illustrate how this evaluation is carried out, we examine the line shift of the x-ray emission spectrum of iron in dilute α-solid solution from the positions in the spectrum of pure α-iron.

We can consider the position of the Fermi level fixed for small impurity concentrations. For this case the change in effective charge takes place as a result of the "local deformation" of the 3d band and because of a corresponding leakage of electrons from the 4s band into the 3d band (or the reverse, as determined by the sign of the excess impurity charge). Thus, the mean change of effective charge, Δ Ze, per atom of the system is equal to the total change of effective charge in one block multiplied by the number of blocks, N_{imp}, for a given atomic concentration of impurity, c, and divided by the total number of atoms in the system, $N(c = 100\,N_{imp}/N)$. For an approximate computation, in view of the rapid falling off of potential of the excess impurity charge, the order of magnitude of the total change in effective charge in the block can be determined from the change of effective charge on the atomic cores situated on the first coordination sphere around the impurity. Therefore

$$\begin{aligned}|\Delta Ze| &= \left|\frac{N_{imp}}{N}\int\limits_{layer} e\,\{\rho_{3d}(\mathbf{r}, E_F) - \rho^0_{3d}(\mathbf{r}, E_F)\}\,d\tau\right| \\ &= \left|0.01\,ce\int\limits_{layer}\Delta E_F\,(\partial\rho/\partial E)_{E_F}\,d\tau\right| \\ &= \left|0.01\,cNe^2W(R_k)\,n^0_{3d}(E_F)\int\limits_{layer}|\psi_{3d}(\mathbf{r}, E_F)|^2\,d\tau\right| \\ &\approx 0.01\,ce^3|Z|\frac{N_k\exp(-qR_k)}{R_k}\,n^0_{3d}(E_F), \end{aligned} \qquad (3)$$

where ρ_{3d} and ρ^0_{3d} are the densities of the 3d electrons respectively in the dilute solid solution and in the pure metal, $n^0_{3d}(E_F)$ is the density (per atom) of the levels at the Fermi surface in the 3d band of the pure metal, N_k is the number of atomic cores on the first coordination sphere, and R_k is the radius of this sphere (for α-iron, $N_k = 8$, $R_k = 2.4 \times 10^{-8}$ cm). The integration is taken over a monatomic spherical layer which encompasses the atomic cores on the first coordination sphere; the transformations take into account the fact that in the approximation of strongly bound electrons

$$\int\limits_{layer}|\psi_{3d}(\mathbf{r}, E_F)|^2\,d\tau \approx N_k/N; \qquad (4)$$

the parameter q is connected with the effective radius of the blocks and may be approximated with the aid of the Friedel[4] scheme, or else empirically[7,8] from the position of the extremal points of the concentration curves for the diffusion coefficient or for the linear thermal expansion coefficient.[9,10] The concentration corresponding to the extremal point determines the concentration of impurity at which "dense packing" of the blocks takes place. This determines in turn the radius of a block and hence the parameter q. The theoretical and empirical values are of the same order of magnitude ($q \cong 0.5$ to 1.0×10^8 cm^{-1}). Estimates of the concentration that yields optimal action of impurities (c = 0.1% atomic), computed by this formula, lead to the following magnitude for the change of effective charge

$$|\Delta Ze| \approx 10^{-2}|Ze| \qquad (5)$$

(the density of levels in the 3d band at the Fermi surface in α-iron is taken from the Landolt-Bernstein tables: $n^0_{3d}(E_F) \cong 7 \times 10^{11}$ erg^{-1}).

We now estimate the change in the lines of the x-ray emission spectrum for iron. Let us take as the excess charge of the impurity a quantity on the order of unity (here and in all that follows, everything is expressed in units of electron charge) i.e., according to formula (5), $|\Delta Z| \cong 10^{-2}$.

The entire computation is carried out by means of Moseley's law in the following manner. We write Moseley's law in the form

$$\nu/R = \text{const}\cdot(Z_{nuc} - \sigma)^2, \qquad (6)$$

where Z_{nuc} is the absolute nuclear charge and σ is the shielding constant

$$\sigma = \sum_s B_s z_s, \qquad (7)$$

where each term indicates the contribution of a particular electron shell to the shielding (z_s is the charge of the corresponding electron shell). Evidently

$$\Delta(\nu/R) = -\,\text{const}\cdot 2\,(Z_{nuc} - \sigma)\,\Delta\sigma \qquad (8)$$

or

$$\Delta\nu/\nu = -\,2\,\Delta\sigma/(Z_{nuc} - \sigma). \qquad (9)$$

Let us estimate the value of $\Delta\sigma$. For the general case we have

$$\Delta\sigma = \sum_s B_s \Delta z_s + \sum_s z_s \Delta B_s. \quad (10)$$

A change in the charge of any one electron shell causes all the B_s to change, i.e. $\Delta B_s = F(\Delta z_1, \Delta z_2, \ldots)$ for any s. Moreover, it is evident that upon change in sign of any one Δz_j the signs of all the ΔB_s change, i.e., the $F(\Delta z_j)$ curves have inflection points at $\Delta z_j = 0$. Therefore, if we expand ΔB_s in powers of Δz_j the series will start with the $(\Delta z_j)^3$ term. For this reason we can neglect all the ΔB_s if $\Delta z_j \ll 1$. On the other hand, the terms which have been dropped become the dominant ones for $\Delta z_j \cong 1$.

In the scheme that we have investigated, the charge changes only in the 3d-shell, and $|\Delta z_{3d}| \cong 10^{-2} \ll 1$, so that

$$\Delta\sigma = B_{3d} \Delta z_{3d}. \quad (11)$$

The coefficient B_{3d} is determined by Sommerfeld's formula[11]

$$B_{3d} = a_n / a, \quad (12)$$

where a_n is the radius of the electron shell, with respect to which the screening is under consideration, and a is the atomic radius.

Let us investigate, for example, the shift of the K_{β_1} iron line (the 1s—3p transition). Here the determining quantity (of greater magnitude) will be a_{3p}, so that we must determine the radius of the 3p shell. This quantity can be found in the Landolt-Bernstein tables for a free iron atom (the radius of inner shells changes insignificantly for transitions in the metallic state). This radius is equal to $a_{3p} = 0.2 \times 10^{-8}$ cm (overestimated). For the atomic core of α-iron (metal), we find from the same tables $a = 0.4 \times 10^{-8}$ cm, so that

$$B_{3d} \approx 10^{-1}; \quad |\Delta\sigma| = B_{3d} |\Delta z_{3d}| \approx 10^{-3}. \quad (13)$$

It follows from the above that the estimated relative displacement of the K_{β_1} line is (bearing in mind the fact that $(Z_n - \sigma) \cong 20$)

$$|\Delta\nu / \nu| = |-2\Delta\sigma / (Z_{nuc} - \sigma)| \approx 10^{-4}. \quad (14)$$

Experimental data show a displacement of $\Delta\nu \cong 0.7$ ev for $\nu = 7 \times 10^3$ ev, i.e., of the same order of magnitude.

[1] I. B. Borovskiĭ and K. P. Gurov, Исследования по жаропрочным сплавам, (Investigation of Refractory Alloys), Vol. III, U.S.S.R. Acad. Sci. Press, 1958.

[2] Borovskiĭ, Gurov, Ditsman, Batirev, and Lobanova, Izv. Akad. Nauk SSSR, Ser. Fiz. **21**, 1401 (1957). Columbia Tech. Transl. p. 1389.

[3] K. P. Gurov, Доклады Высшей школы, серия физ.-мат. (Reports of the Higher Schools, Physics-Mathematics series), No. 3 (1958).

[4] T. Friedel, Advances in Physics **3**, 446 (1954).

[5] N. Mott, Progress in metal physics **3**, 76 (1952). N. Mott and H. Jones, The Theory of the Properties of Metals and Alloys, Oxford, 1945.

[6] L. Alfred and N. March, Phil. Mag. **46**, 759 (1955).

[7] I. B. Borovskiĭ and K. P. Gurov, Исследования по жаропрочным сплавам, (Investigation of Refractory Alloys), Vol. II, U.S.S.R. Acad. Sci. Press, 1957.

[8] I. B. Borovskiĭ and K. P. Gurov, Физика металлов и металловед. (Physics of Metals and Metal Res.) **4**, 187 (1957).

[9] Borovskiĭ, Gurov, and Miller, Dokl. Akad. Nauk SSSR **118**, 280 (1958), Soviet Phys "Doklady" **3**, 147 (1958).

[10] U. G. Miller, Dokl. Akad. Nauk SSSR **119**, 488 (1958), Soviet Phys. "Doklady" **3**, 409 (1958).

[11] A. Sommerfeld, Atomic Structure and Spectra (Russ. Transl.), Vol. 1, Gostekhizdat, 1956 [Atombau und Spektrallinien, Vieweg, Brunswick, 1951].

Translated by M. E. Zaret
228

A NONLINEAR VACUUM EFFECT IN GRAVITATION THEORY

N. V. MITSKEVICH

Uzbek State University

Submitted to JETP Editor October 14, 1958

J. Exptl. Theoret. Phys. (U.S.S.R.) **36**, 1207-1211 (April, 1959)

Second-quantization theory leads to a new interaction between gravitons through the virtual quanta of other fields. For the case of a scalar field in a slowly changing metric, a vacuum cosmological term arises, and can be obtained using Schwinger's method. This can be used to evaluate an additional scattering of gravitons by a Schwarzschild field in a scalar particle vacuum. For low-energy gravitons, the effect is comparable with the nonlinear effect in the classical theory.

1. INTRODUCTION

THE ideas of nonlinear field theory are gaining an ever increasing acceptance in physics. This theory is necessary for a unified description of physical fields, of the interactions between them, and of the structure of particles.[1-3] At the present time, the only widely accepted version of the theory is Einstein's theory of the gravitational field, which may turn out to be a consequence of a more fundamental unified theory of matter. However, nonlinear effects can also be analogous to a quantum-mechanical vacuum.[4,5] In lowest order of perturbation theory, the corresponding non-linear vacuum Lagrangians give effects which are known in high orders for the linear theory. In this connection, it should be emphasized that there is a fundamental difference between "bare" and vacuum nonlinearities. Both types of nonlinearity are serious obstacles to the realization of second-quantization program.[6,7] Hence it becomes necessary either to develop new methods for second quantization,[3] or to use known approximate methods which are useful in the theory of interacting fields.[8]

Leaving aside for the time being the unified field program, we will consider here interacting gravitational and scalar fields, and compare the bare and vacuum nonlinearities. The authors of an earlier work[9] tried adding a linear vacuum term to $\mathfrak{L}_g$; they also used an unusual Lagrangian for the scalar field $\mathfrak{L}_{sc}$. In calculating concrete effects, we use the interaction representation (as does Gupta[8]), but do not use tetrapods[10] but follow instead reference 11 in determining $\mathfrak{L}_g$ and various physical quantities. Following Piir,[12] we do not consider $\gamma = \delta_{\mu\nu}\gamma^{\mu\nu}$ to be independent we bear in mind the expansion

$$\sqrt{-g}\,g^{\mu\nu} = \delta^{\mu\nu} - k\gamma^{\mu\nu}, \tag{1}$$

where in cgs units the constant k is

$$k = \sqrt{2\varkappa} = \sqrt{16\pi G/c^2} = 6.1\cdot 10^{-14}\ \mathrm{cm}^{1/2}\cdot \mathrm{g}^{-1/2}, \tag{2}$$

G being Newton's gravitation constant). In the following we use, in addition to cgs units, natural ones ($c = 1, \hbar = 1$).

In the usual formalism for second quantization, in the interaction representation,[13] the field Lagrangians and other physical quantities are expanded in power series with respect to the constant k; only orders higher than the first are of interest to us. The Lagrangian $\mathfrak{L}_g$ for the gravitational field was expanded in reference 14; the first few terms of $\mathfrak{L}_{sc}$ are

$$\begin{aligned}\mathfrak{L}_{sc} &= {}^1/_2\sqrt{-g}\,(g^{\mu\nu}\varphi_{,\mu}\varphi_{,\nu} - m^2\varphi^2)\\ &= {}^1/_2(\delta^{\mu\nu}\varphi_{,\mu}\varphi_{,\nu} - m^2\varphi^2) + k({}^1/_4 m^2\gamma\varphi^2 - {}^1/_2\gamma^{\mu\nu}\varphi_{,\mu}\varphi_{,\nu})\\ &\quad + k^2 m^2\varphi^2({}^1/_8\gamma^{\mu\nu}\gamma_{\mu\nu} - {}^1/_{16}\gamma\gamma) + O(k^3).\end{aligned} \tag{3}$$

Since, in the interaction representation, the commutation relations are taken in the (linear) free-field approximation, they agree for the scalar (meson) field with those derived in reference 13. For the gravitational field they are

$$\left[\overset{(-)}{\gamma}{}^{\lambda\rho}(\mathbf{k}),\ \overset{(+)}{\gamma}{}^{\sigma\tau}(\mathbf{l})\right] = (\delta^{\lambda\rho}\delta^{\sigma\tau} - \delta^{\lambda\sigma}\delta^{\rho\tau} - \delta^{\lambda\tau}\delta^{\rho\sigma})\,\delta(\mathbf{k}-\mathbf{l}) \tag{4}$$

which is in accord with the form of the canonical energy-momentum quasi-tensor.[11] It is not difficult to verify that the spin of the gravitational field is two (we could equally well take the non-antisymmetrized spin of reference 11). Starting from a non-covariant Lagrangian for gravity,[12] Piir also obtained the relations (4).

2. THE VACUUM NON-LINEAR TERM IN $\mathfrak{L}_g$ (SCHWINGER'S METHOD)

In this section we obtain a vacuum correction (analogous to a cosmological term) to the Lagrangian of the gravitational field, i.e., we consider stationary fields only. This will give an interpretation of further conclusions to be drawn about cross sections.

Variation of the $g_{\mu\nu}$ in the action integral, constructed with the exact Lagrangian (3), gives

$$\delta W_{sc} = \frac{i}{2}\int (dx)\left[\left(\delta g^{\mu\nu}\ \frac{\partial^2}{\partial x^\mu \partial x^\nu} + m^2\delta\sqrt{-g}\right)D^c(x-y)\right]_{x\to y} \tag{5}$$

Introducing the notation

$$\mathfrak{D} = \sqrt{-g}\,(g^{\alpha\beta}\partial^2/\partial x^\alpha \partial x^\beta + m^2) \tag{6}$$

this expression can be written in the form

$$\delta W_{sc} = \frac{1}{2i}\delta\int_0^\infty ds\cdot s^{-1}\,\mathrm{Sp}\exp(-is\,\mathfrak{D}). \tag{7}$$

We have used here the following property of Green's functions:

$$\mathfrak{D}\,D^c(x-y) = \delta(x-y). \tag{8}$$

It should be noted that the δ function defined in this way should be a scalar density, which is in accord with invariance of the integral. In this way we are led to the assumption that the matrix elements

$$(x'|\exp(-i\mathfrak{D}\,s)|x'') = (x(s)'\,|\,x(0)''), \tag{9}$$

are scalar densities. According to the total differential (7), they enter into the vacuum Lagrangian of the gravitational field in the form

$$\mathfrak{L}_{vac}(x) = -\frac{i}{2}\int_0^\infty ds\cdot s^{-1}(x|\exp(-i\,\mathfrak{D}\,s)|x). \tag{10}$$

The calculation of the matrix elements (9) for a constant field is really no different from Schwinger's calculation.[4] The final result is:

$$(x(s)'\,|\,x(0)'') = \frac{-is^{-2}}{(4\pi)^2\sqrt{-g}}\exp\left[-\frac{i(x'-x'')^2}{4s\sqrt{-g}} - im^2 s\sqrt{-g}\right]. \tag{11}$$

Hence, the vacuum Lagrangian of the gravitational field is

$$\mathfrak{L}_{vac}(x) = -\frac{\sqrt{-g}}{32\pi^2}\int_{\tau_0}^\infty d\tau\cdot\tau^{-3}e^{-m^2\tau}, \tag{12}$$

where a cut-off at a minimal proper time τ_0 has been introduced to avoid a divergence. In contrast with electrodynamics[4] and mesodynamics,[5] we are faced here with a strong divergence in $\mathfrak{L}_{vac}$; it is impossible to cut off the integral correctly, and this makes our conclusions only qualitative. Since the sign of the quantity obtained agrees with the sign of Einstein's cosmological term,[2] (12) leads to the following value for the cosmological constant due to the vacuum

$$\Lambda_{vac} = \frac{\varkappa}{64\pi^2}\left[e^{-m^2\tau_0}(\tau_0^{-2} - m^2\tau_0^{-1} - m^4\ln\tau_0) - m^4(0.58 + \ln m^2)\right]. \tag{13}$$

Expression (12) leads formally to the gravitational equations, at least up to corrections linear in the $g_{\mu\nu}$, but since the multiplier $\sqrt{-g}$ has an infinite power series expansion in k, it must be interpreted in a nonlinear sense. Indeed, this term gives rise to a nonlinear effect in the scattering of gravitons by a Schwarzschild field, there being some extra scattering over and above that calculated previously.[14] It is clear that here we have to deal with the analogue of a mass term, although further difficulties arise, connected with the problem of quantizing the gravitational field, and due to the fact that Einstein's equations with a cosmological term have no solutions in empty space which differ but little from the Galilean ones.

3. THE SCATTERING OF GRAVITONS ON A SCHWARZSCHILD FIELD IN A SCALAR-PARTICLE VACUUM

The vacuum nonlinearity can be approached from another point of view, using the S-matrix formalism. The cosmological term does not enter into the usual theory, but on the basis of the results in Sec. 2, can be expected to affect the scattering in third order with respect to k. We examined the simplest processes giving scattering of gravitons on a Schwarzschild field (the cross section for the latter is given in reference 14, along with cross sections for scattering of other particles on this field). It is not possible to present all the complicated expressions here. We considered the interaction of gravitons with a vacuum of scalar particles having zero rest mass (for which it is relatively easy to calculate the total matrix element); a typical matrix element was also calculated for the interaction with vacuum meson of mass $m \neq 0$. In the first case, some of the terms, which describe processes where spin is not conserved in the intermediate states, diverge in an unusual way (the denominator vanishes identically because of the relativistic relation between energy and momentum for real particles). This

might be connected with the quantization difficulties mentioned above. In the interests of regularization, we introduced a graviton "mass" μ; the integrals were cut off at a maximum momentum L (cf. the earlier note on the minimum value of proper time). Considering only terms which do not violate spin conservation, the cross section in the first case (m = 0) can be written

$$d\sigma = \frac{4k^8M^2L^8}{3\,(8\pi)^6}\left(\frac{\mu^2+4k^2/3}{\mu^2+4k^2\sin^2(\theta/2)}\right)^2\frac{d\Omega}{k^4\sin^4(\theta/2)} \qquad (14)$$

while for the case $m \neq 0$

$$d\sigma = \frac{4k^8M^2m^4L^4}{(8\pi)^6}\frac{d\Omega}{k^4\sin^4(\theta/2)}. \qquad (15)$$

These can be compared with the expressions given in reference 14 because they have the same angular dependence at small θ. We see that for long graviton wave lengths the vacuum effect dominates over the classical one. The critical wavelength can easily be obtained. For example, from (15),

$$\lambda_c = (8\pi^2\hbar/kmL)\sqrt{\hbar/c}. \qquad (16)$$

The divergence of the cross section for scattering from a Schwarzschild field is characteristic of all particles with nonvanishing rest mass.[14] The mass of a graviton can be obtained by comparing our cross sections with those in the paper just quoted. According to (15), the mass in grams is

$$\mu = kmL/4\pi\sqrt{\hbar c} \approx 10^{-6}mL. \qquad (17)$$

The meson momentum is to be obtained from the radius of a nucleon, and the mass obtained does not contradict the astronomical data (taking into account the qualitative nature of the calculation). The result (17) can be understood in light of the deep analogy between the cosmological term and the mass term in Klein's quation. Then (13) leads to

$$\mu = k\sqrt{c}/8\pi\tau_0\sqrt{\hbar} \quad (m = 0). \qquad (18)$$

The mass μ could decrease or even vanish if account were taken of the interaction between gravitation and fields other than the scalar one considered. If the theory we started with had had a cosmological term, we could speak of its renormalization also.

In conclusion, the author would like to thank D. D. Ivanenko, M. M. Mirianashvili and A. M. Brodskiĭ for their interest in this work and for valuable discussions. He is also indebted to A. D. Danilov for his kind help in checking some of the calculations.

[1] A. Einstein, Scientific Autobiography. Russ. Transl. in Einstein and Contemporary Physics, GITTL, M. 1956.

[2] A. Einstein, The Meaning of Relativity, Princeton, 1945.

[3] W. Heisenberg, Revs. Modern Phys. **29**, 269 (1957).

[4] J. Schwinger, Phys. Rev. **82**, 664 (1951). W. Heisenberg and H. Euler, Z. Physik **98**, 714 (1936).

[5] M. M. Mirianashvili, Doctoral Dissertation, Tbilisi, 1958.

[6] A. A. Sokolov and D. D. Ivanenko, Квантовая теория поля, (Quantum Field Theory) GITTL M.-L. 1952.

[7] L. I. Schiff, Phys. Rev. **92**, 766 (1953).

[8] S. N. Gupta, Proc. Phys. Soc. (London) **A65**, 161, 608 (1952).

[9] D. D. Ivanenko and A. M. Brodskiĭ, Dokl. Akad. Nauk SSSR **92**, 731 (1953).

[10] F. Belinfante, Physica **7**, 449 (1940).

[11] N. V. Mitskevich, Ann. Physik **1**, 319 (1958).

[12] I. Piir, Report of the Institute for Physics and Astronomy, Acad. of Sciences, Estonian SSR, **5**, 41 (1957).

[13] N. N. Bogolyubov and D. V. Shirkov, Введение в теорию квантованных полей (Introduction to the Theory of Quantized Fields) GITTL, M. 1957.

[14] N. V. Mitskevich, J. Exptl. Theoret. Phys. (U.S.S.R.) **34**, 1656 (1958), Soviet Phys, JETP **7**, 1139 (1958).

Translated by R. Krotkov
229

CONNECTION BETWEEN STRUCTURAL AND MAGNETIC PARAMETERS OF THE TRANSITION METALS

F. M. GAL' PERIN

Submitted to JETP editor October 14, 1958; resubmitted January 10, 1959

J. Exptl. Theoret. Phys. (U.S.S.R.) 36, 1212-1223 (April, 1959)

The connection between the structural parameters (type of lattice, interatomic distances, coordinational number, etc.) and the magnetic parameters (atomic magnetic moment, Curie point, Curie constant) is considered for the pure transition elements Cr, Mn, Fe, Co, and Ni as well as for a number of their ferromagnetic ordered alloys and chemical compounds. These relations and the available experimental data on the crystalline and electronic structures of the metals are used to compute the magnetic parameters, which are found to be in good agreement with the experiments.

AFTER a detailed analysis of extensive experimental material, we noted the close connection between the structural and magnetic parameters of ferromagnets, which we expressed by means of semi-empirical relationships.[1,2] The latter, in conjunction with known optical data on the crystalline and electronic structures of the ferromagnets, were used to calculate the magnetic parameters of pure ferromagnetic metals, of the same metals in their alloys, and finally of the alloys themselves; the agreement with experiment was satisfactory.

Recent years have brought to light many new facts in ferromagnetism. Neutron-diffraction investigations have shown that the use of the Heitler-London-Heisenberg approximation (along with its natural extension, the polar model of Shubin and Vonsovskiĭ) is more suitable for the description of the interaction of the internal electrons (d) in ferromagnets than the collective-electron model (cf., e.g., references 3 — 6). Furthermore, neutron-diffraction and x-ray methods have shown that the electron structure of transition metals differs greatly from that previously suggested in the literature.[7-10]

In the present paper we attempt to improve the equations proposed by us for the purpose of (a) taking account of the results of the aforementioned new research and (b) extending these equations to include other transition metals (Cr and Mn) in the paramagnetic and ferromagnetic states, and not merely Ni, Co, and Fe in the magnetic state, as done essentially in the earlier investigations. In the first part we develop the concepts underlying the aforementioned relations. These are then applied to pure ferromagnetic metals and to their ordered alloys, and finally to Mn and Cr in ferromagnetic chemical compounds with a structure of the NiAs type and to Mn in ordered Geisler alloys of the type $MnCu_2Al$.

1. PRINCIPAL PREMISES

We consider the transition elements of the first long period of the periodic table, with atomic numbers Z from 21 to 29. Each of these is characterized by a constant, derived by us, which has the dimensionality of a length, equal to (Angstroms)

$$R = 0.13\,[(Z/2)^2 - 14.75\,Z + 235.5] \quad (\text{for } Z \geqslant 26), \quad (1)$$

$$R = 0.13\,[(Z/2)^2 - 13.75\,Z + 209.5] \quad (\text{for } Z \leqslant 26). \quad (2)$$

For lattices of metals of type A2 (cubic volume-centered, as in Fe) and of type A3 (hexagonal close-packed, as in Co) one consideres in the general case the first and second coordination zones of the lattice (i = 1 and i = 2, where i is the number of the zone).

We denote the interatomic distance and the number of neighbors of the atom by r_1 and n_1 for the first zone and by r_2 and n_2 for the second; $n_1 = 8$ and $n_2 = 6$ for lattices of type A2, and $n_1 = n_2 = 6$ for lattices of type A3. In the nearest-neighbor approximation, only the first zone is considered. An exception is Co, for which the neighbors of the second zone are also the nearest (because $r_2 \approx r_1$). For lattices of type A1 (cubic face centered, as in Ni) only the first zone was considered ($n_1 = 12$) because $r_2 = a \gg r_1$ (a is the lattice parameter).

We introduce the concept of the "effective" interatomic distance $r_{eff} = r_i - R$, where r_i is the equilibrium interatomic distance in the i-th zone. This concept is introduced so as to take into account, in the calculation of the magnetic param-

TABLE I. Structural Parameters of Ni, Co, and Fe

Metal (lattice type)	$n_1(r_1, A)$[11]	$n_2(r_2, A)$[11]	R, A	Class of metal	$r_1 - R$, A	$r_2 - R$, A	Δ	Δ_a	$N_d(n_2)$
Ni (A1)	$12(2.486_8)$	—	2.408_2	2	0.078_8	—	0.605_2	0.605_2	2 (2)
Co (A3)	$6(2.49_9)$	$6(2.50_7)$	2.53_8	1	-0.03_8	-0.03_1	0.26_9	0.26_9	3 (2)
Fe (A2)	$8(2.477_7)$	$6(2.861_9)$	2.733_2	1	-0.255_2	0.127_8	1.805_6	1.313_8	4 (2)

eters, only the magnetic electrons (of the unfilled electron shells that participate in the magnetism; the nonmagnetic electrons of the filled shells are also located at the interatomic distance r_1).

It is seen from Table I that the difference $r_1 - R$ is quite small for pure ferromagnetic metals.

Pure metals can be divided into two classes, depending on the sign of the difference $r_1 - R$. The first class (1) contains the metals (Co, Fe, Mn, and so on) for which this difference is negative, while the other (2) contains those (Ni etc) with a positive difference. This grouping of metals explains many experimental facts (see below).

Let us consider the law that governs r_{eff}. Let the abscissa (see the figure) represent the concentration C of the electrons (the number of the s and d electrons) of the isolated atom, first in ascending order (from C = 3 for Sc to C = 11 for Cu, left segment of the axis), followed by a descending order (right segment) along the same axis. Let the ordinates represent the difference $r_1 - R$. We plot the corresponding points for type A2 lattices over the left segment, and those for types A1 and A3 over the right segments. This results in the triangle shown in the figure.

An analogous picture is observed also for many binary ordered alloys of transition elements. The figure shows the dependence of the effective interatomic distance in the alloy lattice, $\bar{r}_{eff} = r_1 - \bar{R}$, on the mean concentration of the electrons of the alloy atom, $C = \lambda_a C_a + \lambda_b C_b$, where C_a and C_b are the concentrations of the electrons of the atoms of components a and b; λ_a and λ_b are the atomic concentration of the latter in the alloy; r_1 is the equilibrium interatomic distance in the first zone of the alloy lattice (it depends on the concentration of the alloy); $\bar{R} = \lambda_a R_a + \lambda_b R_b$; R_a and R_b are constants of the components a and b, calculated from (1) and (2). It is seen from the figure that the points of the alloys under consideration lie as a rule on the same triangle. Exceptions are certain alloys, particularly of manganese (Co-Mn, Ni-Mn, and others), whose points deviate from the triangle.

Along with the effective interatomic distance, one must consider also the number of neighbors of the atom in zone i, n_i; we introduce for this purpose the quantity $\sum n_i |r_i - R|$, which has the dimension of length. The change in the number Δ of magnetic electrons of the atom (with uncompen-

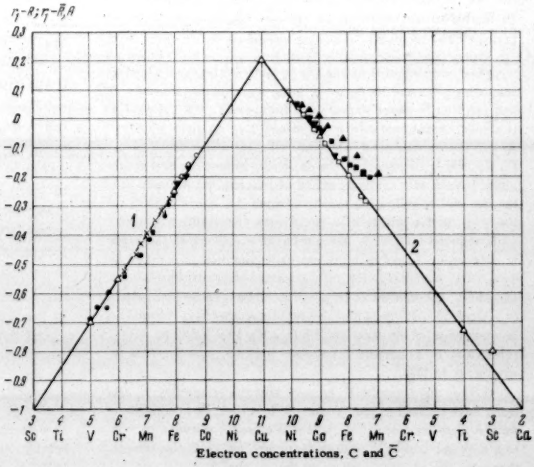

Curve 1 – type A2 lattice; 2 – type A1 and A3 lattices; Δ – pure metals, × – Fe-Cr, ● – Fe-V, ▼ – Fe-Ni, ■ – Co-Mn, □ – Ni-Cr, ▲ – Ni-Mn, ○ – Fe-Co.

sated spins) corresponding to this quantity, a change due to the fact that the outer portion of its electron shell (s and d) is substantially deformed in the crystalline state (compared with the shell of the isolated atom), is equal to*

$$\Delta = 0.642 \Sigma n_i (r_i - R). \quad (3)$$

In the nearest-neighbor approximation we use instead of (3)

$$\Delta_0 = 0.642 n_1 (r_1 - R).$$

An exception is Co, for which Δ is used in this approximation, and not Δ_0 (because $r_2 \approx r_1$).

It will be shown below that Δ or Δ_0 enters into the relation for all magnetic parameters, thus connecting the latter with the structural parameters.

Let us dwell on the question of the electronic structure of the considered transition elements, a structure which must naturally be taken into account when formulating the foregoing relations.

Isolated atoms of these elements, with the exception of Cr, have two s electrons each (Cr has one s electron) and either five (Cr, Mn), six (Fe), seven (Co), or eight (Ni) d electrons. The question of the distribution of these electrons in the atoms of the same elements in the crystalline state (transition metals) has been under discussion for many years.[12] It follows from recent experimental x-ray data† that the number of d electrons per atom of the metal is 0.2 ± 0.4 for Cr (A2), 2.3 ± 0.3 for Co (A3), 9.7 ± 0.3 for Ni (A1), and 9.8 ± 0.3 for Cu (A1). We see, first, that the electron distribution in a metal with an A2 lattice differs greatly from the distribution in isolated atoms: the d shell contains few electrons,† their number being equal to the number of Bohr magnetons (M_B) comprising the magnetic moments m of the atoms ($m = 2.20 M_B$ for Fe; according to neutron-diffraction data,[10] Cr is antiferromagnetic with an antiferromagnetic moment $m_{af} = 0.40 M_B$),* the d shell contains electrons of only one spin orientation. Second, the d shell of a metal with A1 or A3 lattice contains many electrons, $10 - m$ in number, where $m = 1.71$ for Co and 0.60 for Ni. A considerable portion of the s electrons, belonging to the s shell of the isolated atoms prior to formation of the crystal, shift to the d shell of the metal, and the electrons in the latter form two groups with opposite spin orientation.

Let us proceed to examine the connections between the foregoing crystal-structure, electron-structure, and magnetic parameters.

2. MAGNETIC PARAMETERS

Ferromagnetic Atomic Magnetic Moment

We first revise the concept of the number of electrons with uncompensated spins, participating in the spontaneous magnetization (ferromagnetic electrons[13]). The theory usually employs approximations for which e is an integer. For example, in the Bloch-Moller formula for the "three-halves" law, $e = 1$ for Ni and $e = 2$ for Fe.[14] In the experiments, however, judging from the new data on the electronic structure of pure ferromagnetic metals[7] and from their atomic magnetic moments, e becomes equal to m and is fractional. The same can be said of σ, the number of electrons that contribute to the paramagnetic moments of the same metals ($\sigma = 2.30$ for Fe, 0.90 for Ni, etc.). We shall give equations for both σ and e.

We write $n_d = C - n_s$, where $n_s = 2$ for all transition metals; $N_d = 10 - n_d$ for $n_d \geq 5$, and $N_d = n_d$ for $n_d < 5$ (see Table II). It is seen from the table that in the case of a ferromagnetic metal the integer portion m_0 of the experimental value of m is as a rule equal to $N_d - n_s$. Thus, $m = N_d - n_s + \epsilon$, where ϵ is the fractional increment of the moment (in M_B units), oriented, naturally, parallel to the integer portion of the moment [since $m > (N_d - n_s)$].

We note that $N_d - n_s = 2$ for Fe; on the other hand, the integral number of the electrons actually in the d shell, according to reference 7, is also equal to 2. Finally, in the Bloch-Moller formula, $e = 2$ for Fe. We assume that for all transition metals, which, like Fe, belong to the first class of metals, $e = N_d - n_s$ ($e = 1$ for Co, $e = 2$ for

*The coefficient 0.642 in (3) is justified by the following reasoning. Co and Ni have the same coordination numbers (12) and practically equal interatomic distances (2.50 and 2.49 A). However, their constants R (2.54 and 2.41 A) differ by 0.13 A, and the number of d electrons of their atoms differ by 1. On this basis, we propose the following generalization to include metals with arbitrary types of lattices, interatomic distances, and coordination numbers: when the interatomic distance r_1 in the lattice of a metal with coordination number 12 is reduced by 0.13 A, the number of electrons of the atom is reduced by 1, and if the interatomic distance is reduced not by 0.13 A, but by $(r_1 - R)$, for the same number of nearest neighbors, the number of its electrons changes by an amount $(r_1 - R)/0.13 = 7.7 (r_1 - R)$. The resultant quantity, referred to one neighbor of the atom, is $7.7 (r_1 - R)/12 = 0.642 (r_1 - R)$: referred to n_1 neighbors it becomes $0.642 n_1 (r_1 - R)$. This is analogous to (3).

†Lomer and Marschall[8] believe that the remaining d electrons have shifted to the s and p levels, thus accounting for the large number of conduction electrons, whereas in metals with A1 and A3 lattices there are few such electrons (because the s electrons go to the d shell).

*We shall drop henceforth the symbol M_B for the sake of brevity, since the magnetic moment is always expressed in units of M_B.

TABLE II. Atomic Magnetic Moments of Metals and Alloys

Metal	Lattice type	Experiment m	Experiment m_s	N_d	$N_d - n_s$	ε	m, calculated
Ni	A1	0.60*	0	2	0	0.60	0.60
Co	A3	1.71	1	3	1	0.69	1.69
Fe	A2	2.20	2	4	2	0.20	2.20
Fe (FeCo)	A2	2.80	2	4	2	0.96	2.96
Co (FeCo)	A2	1.98	1	3	1	0.96	1.96
Fe (Ni_3Fe)	A1	2.97	2	4	2	1.04	3.04
Ni (Ni_3Fe)	A1	0.62	0	2	0	0.51	0.51
Ni (Ni_3Mn)	A1	0.30	0	2	0	0.69	0.69
Mn (Ni_3Mn)	A1	3.18	3	5	3	0.55	3.55
Mn (MnAs)	NiAs	3.40	3	5	3	0.37	3.37
Mn (MnSb)	NiAs	3.53	3	5	3	0.55	3.55
Mn (MnBi)	NiAs	3.52	3	5	3	0.53	3.53
Cr (CrSb)	NiAs	2.70	2	4	2	0.71	2.71
Cr (CrTe)	NiAs	2.40	2	4	2	0.45	2.45
Cr (CrO_2)		2.07	2	4	2	—	—
Mn ($MnCu_2Al$)	A2	4.10		5	3	1.07	4.07
Mn ($MnCu_2Sn$)	A2	4.10		5	3	1.07	4.07
Mn ($MnCu_2In$)	A2	4.10		5	3	1.07	4.07
Number of electrons participating in the paramagnetism**							
Ni	A1	0.9	0	2	0	0.89	0.89
Co	A3	2.30		3	1	1.30	2.30
Fe	A2	2.30	2	4	2	0.30	2.30
Mn (MnAs)	NiAs	3.60	3	5	3	0.60	3.60
Mn (MnSb)	NiAs	3.20	3	5	3	0.20	3.20

*The values are rounded off; the exact ones are given in the text.

**The lower part of the table differs from the upper only in that the 3d, 4th, and 8th columns contain the number of paramagnetic electrons, σ, instead of the number of ferromagnetic electrons, m.

Fe, e = 3 for Mn, etc.), and for metals like Ni, which belong to class 2, e = 1, i.e., when writing the relation for the number, e, we start with its value as given by the Bloch-Moller formula, which at present gives the most accurate results.*

Going to the relation for the fractional added term ϵ, we consider that, according to the theory of Vonsovskiĭ and Vlasov,[15] the atomic magnetic moment of pure ferromagnetic metals is

$$m = N_d + 0.15 n_s (J_0/J - 4)/(1 - 2J_s/J), \qquad (4)$$

where J_0 and J are the exchange integrals between the s and d electrons in one lattice site and between its neighboring sites, respectively, and J_S is the transfer integral of the s electron. At the present state of the theory, as pointed out by the authors of the theory itself, these integrals cannot yet be evaluated and therefore (4) cannot be used for quantitative determination of the atomic magnetic moments.

In view of this, it makes no sense in practice to attempt to formulate semi-empirical relations for the magnetic parameters in terms of crystal-structure and electron-structure parameters of the metals, introduced in the first and this section. It is desirable here to be guided by the suggested analogy with Eq. (4) of Vonsovskiĭ-Vlasov for m and their relations for other magnetic parameters

By way of such a relation for ϵ (in the approximation of non-conducting ferromagnetic lattice: $J_S = 0$), we propose the following:

$$\varepsilon = n_s \left\{1 + 0.15 \left[\frac{1}{e}\left(1 + \frac{1}{\beta\gamma}\right) - 4\right]\right\}. \qquad (5)$$

By adding the difference $N_d - n_S$ to (5), we find a relation for m, analogous to (4). Here β characterizes the orientation of the s-electron spin relative to the unpaired d electrons of the atoms: when $n_d \geq 5$ we have $\beta = -1$ (antiparallel orientation), and when $n_d < 5$ we have $\beta = 1$. According to van Vleck, the spin of the electron temporarily "arriving" on the cation from the anion (during the process of indirect exchange in FeO or MnO)

*In view of the fact that a minimum number of arbitrary model assumption has been made in the derivation of this formula from the multi-electron spin-wave theory. Landau and Lifshitz have therefore proposed to evaluate the volume integral A by the Bloch-Moller formula, and not by rough approximate formulas (of Heisenberg and others), in which A is connected with the Curie point. The relation which we derived from this point of view for A (in particular, with allowance for the proposed relation for e) is in satisfactory agreement with experiment (see below).

is also oriented with respect to the cation. For Cu, Ni, Co, Fe, and Mn the first condition ($\beta = -1$) is satisfied, while $\beta = +1$ for Cr, V, etc. The form of γ depends on the class of the metal: $\gamma^{(1)} = N_d - n_s - \Delta$, $\gamma^{(2)} = N_d - n_s + \Delta$, where the superscript denotes the class of the metal, on which the sign of Δ depends (the sign as the same as that of $r_1 - R$, which, by definition, is negative for class 1 and positive for class 2); Δ is calculated from (3).

We note that the first term in the square brackets of (5) is similar to Vonsovskiĭ's equation[16] for the s-d exchange energy of the s electron:

$$E_{sd} = -\tfrac{1}{2} A(\xi)[1 + (\eta\mu)],$$

where η is the vector of the spin of the s electron ($\eta = \pm 1$), μ is the average magnetic moment of the d electrons per atom, $A(\xi)$ is the exchange integral between an s electron with quasi-momentum ξ and one (nearest) d electron. We see that a) μ has the same meaning and same numerical values as β in Eq. (5), b) the first term in the square brackets of (5), like A, is also referred to one magnetic electron (the expression in the round brackets is divided by e), and c) in the approximation of strongly-bound electrons, A depends on the number n of the nearest neighbors of the atom in the lattice. But Δ also contains n, and contains, furthermore, the effective interatomic distance, on which J must naturally depend. The coefficient $\frac{1}{2}$ in the expression for E_{sd} also enters into Δ, since $0.642 \approx 2^{1/3}/2$. Thus, not only the fact that the first term in the square brackets of (5) is located in the place occupied by the exchange-integral ratio J_0/J in Eq. (4), but also the considerations listed above give rise to the thought that this term is connected with the integral of the s-d exchange in the lattice. In view of this, the plus sign in front of this term (for the ferromagnetic state of pure ferromagnetic metals) must be replaced by a minus sign in the case of transition metals that are not ferromagnetic in pure form (Mn and Cr), but play the role of ferromagnetic metals in many alloys (cf. below and reference 16, p. 192).

A similar change in sign should be made also when going from the ferromagnetic state of pure ferromagnetic metals to the paramagnetic state.

We have seen that in calculating Δ from (3) for Ni (A1) and Co (A3), only the nearest neighbors of the atom are considered, and for Fe (A2) the following neighbors are also considered. The nearest neighbors (−) and those following (+) in a type A2 lattice correspond, apparently, to exchange integrals with signs opposite to those indicated in the parentheses. In fact, it was indeed this circumstance that the French authors (Neel, Fallot, and others) had in mind when they assumed that not the nearest neighbors of the Fe atom, but those following, participate in ferromagnetism. From our point of view, as shown above, both types of neighbors play a role in the spontaneous magnetization of a metal with a lattice of type A2. If we confine ourselves to the nearest neighbors (Δ_0) in a lattice of type A2 (see below) the sign of the exchange integral [and with it the sign of the first term in the square brackets of (5)] must be reversed (compared with the sign that corresponds to the case when both types of neighbors are considered). Let us cite several examples: 1) For Fe (as well as Co and Ni) in the paramagnetic state, it would be necessary to take the minus sign in the place indicated in Eq. (5) (instead of the plus sign for the ferromagnetic state); but the transition of Fe into the paramagnetic state differs from the analogous transition for Co and Ni in that in the case of Fe it is still necessary here to neglect the neighbors following the nearest ones (which are considered, as shown, in the ferromagnetic state). This causes another reversal of the sign (− into +), leaving the initial + sign in the place indicated in Eq. (5). 2) The alloy $MnCu_2Al$ also has an A2 type lattice. In view of the fact that its ferromagnetism is due to Mn, then according to the foregoing, the sign in (5) should be minus; but for this alloy, as for other Geisler alloys, it is necessary to adhere to the nearest-neighbor approximation (see below), and consequently the initial + sign is retained in Eq. (5). 3) In weak Fe-Cr and Co-Cr solid solutions the Cr is paramagnetic and has the same lattices as the solvents — A2 and A3 respectively. Therefore, in the nearest-neighbor approximation and at a concentration close to zero, the spin of its s electron should have antiparallel orientations (−1 for Fe-Cr and +1 for Co-Cr, as confirmed experimentally,[9] see reference 2).

Let us proceed to apply (5) to particular cases.

(a) Pure ferromagnetic metals. Considering the foregoing, we can rewrite (5) for pure ferromagnetic metals in the following form:

$$m^{(1)} = N_d + 0.15\, n_s\left[\frac{(N_d - n_s - \Delta) - 1}{(N_d - n_s)(N_d - n_s - \Delta)} - 4\right], \quad (6)$$

$$m^{(2)} = N_d + 0.15\, n_s\left[\frac{(N_d - n_s + \Delta) - 1}{(N_d - n_s + \Delta)} - 4\right]. \quad (7)$$

Δ is calculated from (3), and the initial data for this calculations are listed in Table I. Inserting the numerical values into (6) and (7) we obtain: $m^{(1)} = 2.20$ for Fe and 1.69 for Co (reference

16 gives 2.21_T and 1.71 respectively); $m^{(2)} = 0.60$ for Ni (0.60_5 in reference 16); the values of reference 16 are experimental. If we confine ourselves to the nearest neighbors for Fe, i.e., we put $\Delta_0 = 1.31$ in (6) (instead of $\Delta = 1.80$), we get $m = 2.73$; the latter differs from the moment of the neighboring Co ($m = 1.7$) by unity. The reason why the values of the moments of neighboring elements of class 1 (of which one has an A2 lattice and the other a different one) do not differ by unity (whereas their atomic numbers differ by unity) is, according to (6), that the neighbors following the nearest ones also participate in the spontaneous magnetization of a metal with lattice A2.

(b) Ferromagnetic ordered alloys. We find that (6) and (7) can be used to calculate also the individual magnetic moments of the components of the foregoing alloys. Let us consider those investigated by neutron-diffraction,[9,10] where it is possible to determine experimentally the difference in the aforementioned moments, and the individual moments can be evaluated from the results of saturation magnetization measurements.

The alloy FeCo has an A2 lattice (like Fe), which can be mentally subdivided into two simple cubic sublattices, one occupied by the iron atoms and the other by the cobalt. In each of the sublattices, an atom of a given kind is surrounded by six nearest neighbors of the same kind, at a distance $r_1 = a = 2.85$ A.[17] Since the condition $r_1 > R$ is satisfied for both components ($R_{Co} = 2.54$ A, $R_{Fe} = 2.73$ A), they are metals of class 2 (while pure Co and Fe are of class 1) and consequently, Eq. (7) is applicable to both. Inserting the numerical values into (3) we find $\Delta_{Co} = 1.19$, $\Delta_{Fe} = 0.46$. From Eq. (7) we obtain $m^{(2)} = 2.98$ and 1.96 for Fe and Co respectively (experiment[8] yields 2.80 and 1.98 respectively).

The alloy Ni_3Fe has an A1 lattice (like Ni). The Ni atoms are located in the centers of the faces, while the Fe atoms are at the corners of the elementary cell. The atom Ni [2] is surrounded by eight nearest-neighbor nickel atoms at a distance $r_1 = 2.508$ A, while Fe [2] is surrounded by six nearest-neighbor iron atoms at a distance $r_1 = a = 3.546$ A;[8] the class of the metal is indicated in the square brackets. According to Eq. (3), $\Delta = 3.13$ for Fe and 0.51 for Ni, and according to (7) $m^{(2)}$ is 3.04 and 0.51 for Fe and Ni respectively (experiment[9] yields 2.97 ± 0.15 and 0.62 ± 0.05 respectively). Here and in what follows, the constant R for the component is the same as for the pure metal, and is calculated from (1) and (2).

The alloy Ni_3Mn has the same lattice and the same arrangement of the atoms as the Ni_3Fe, except that manganese replaces the iron. Here $r_1 = 2.543$ A and $R = 2.408$ A for Ni [2]; $r_1 = a = 3.596$ A[19] and $R = 2.863$ for Mn [2]. From (3) we get $\Delta = 2.82$ for Mn and 0.69 for Ni. Inserting the numerical values in (7) we get $m^{(2)} = 0.67$ (experiment:[9] 0.30 ± 0.05) for nickel. As to Mn, which is not ferromagnetic in pure form, in virtue of the previous statements concerning similar elements, we tentatively place a plus sign in front of the first term in the square brackets of (6) and (7), and then use the latter to calculate the moment. The same applies also to Cr (see below). To avoid repetition, we make use of (6) and (7) in similar cases, with the proviso that the indicated preliminary sign reversal has been made. According to (7) we have for manganese $m^{(2)} = 3.55$ and $m_{Mn} - m_{Ni} = 2.88$ (experiment:[9] 3.18 ± 0.25 and 2.88 ± 0.20 respectively).

The calculated and experimental values are in satisfactory agreement in the case of the first two alloys. For the third alloy, such an agreement is found only for the difference in the moments of the components (we recall that only the difference is obtainable directly by neutron-diffraction), but the values of the moments themselves are greatly divergent. The calculated value of the moment for Mn (3.55) is practically the same as is frequently obtained experimentally (see below). The same can be said about the moment of nickel (0.67). On the other hand, the experimental value of the moment of nickel (0.30) is unreasonably small. We note also that in the calculation of the moments of the components we did not take into account the interaction with neighbors of different kind (say Co-Fe).

(c) Ferromagnetic chemical compounds with structure of the NiAs type. The compounds MnAs, MnSb, MnBi, CrSb, and CrTe contain only one transition element (Mn or Cr), which is responsible for their ferromagnetism. The atom of this element has two nearest neighbors at a distance r_1 and six following neighbors of the same kind at a distance $r_2 = a$ (a is the lattice parameter). For Mn in all the foregoing compounds, $N_d = 5$, and $n_s = 2$, while $N_d = 4$ and $n_s = 2$ for Cr.

In the compound MnAs, Mn [1] belongs to class 1 (in view of the fact that $r_1 = 2.84$ A $< R = 2.86$ A; $a = 3.71$ A[20]). According to (3), $\Delta = 3.30$, and according to (6) $m^{(1)} = 3.37$ (experiment[20] yields 3.40).

In MnSb, we have $r_1 = 2.89$ A for Mn [2] ($R = 2.86$ A; $a = 4.12$ A[20]). According to (3) $\Delta = 4.89$, and according to (7) $m^{(2)} = 3.55$ (experiment[20] yields 3.53).

In MnBi we have $r_1 = 3.06$ A for Mn [2] ($R =$

2.86 A, a = 4.30 A[20]). According to (3) $\Delta = 5.80$ and according to (7) $m^{(2)} = 3.53$ (experiment[20] yields 3.52).

In CrSb we have $r_1 = 2.726$ A for Cr [1] (R = 3.058 A; a = 4.127 A[10]). From (3), $\Delta = 4.54$. In view of what has been said above regarding crystalline chromium (p. 867) we find that we can calculate its moment from Eqs. (6) and (7), except that a plus sign must be placed in front of the 1 in the numerators and, as before, a minus sign must precede the terms in the square brackets, as is the case for all transition elements which are nonferromagnetic in pure form but ferromagnetic when alloyed. From (6), $m^{(1)} = 2.71$ (ecperiment[10] — 2.7 ± 0.2).

In CrTe we have $r_1 = 3.105$ A for Cr [2] (R = 3.058 A; a = 3.981 A[21]). From (3), $\Delta = 3.61$ and from (7) $m^{(2)} = 2.45$ (experiment[21] — 2.40).

(d) Ferromagnetic Geisler alloys $MnCu_2Al$, $MnCu_2Sn$, and $MnCu_2In$. In these alloys Mn [2] belongs to class 2 (since the distances between the nearest atoms of Mn, amounting to $r_1 = 4.17$, 4.35, and 4.39 A respectively,[22] are greater than R = 2.86 A). Each Mn atom is surrounded by twelve nearest atoms of the same kind. According to (3) $\Delta = 10.06$, 11.47, and 11.78 respectively. In view of statements made on p. 867, we obtain from (7) $m^{(2)} = 4.07$ (experiment[23] — 4.10).

(e) Ferromagnetic weak solid solutions. By way of an example, we consider the system Fe-Me with A2 lattice, where Me = V, Cr, α-Mn, Co, and Ni. For these we have, at 100 atomic percent of Me, $m_{Me} = 1 + \beta\,[(N_d - n_s)_{Me} - 0.642 \times 6\,(a - R_{Me})] + 0.642 \times 8\,(R_{Fe} - R_{Me})$, where the difference $a - R_{Me}$ is found from the diagram. For A2 lattices the difference $N_d - n_s$ equals the number of electrons actually contained in the d shell of the crystal atom. Assuming that $N_d - N_s = 0$ for the antiferromagnetic Cr and α-Mn and unity for V, then $m_{Me} = 0$ (0) for V and Cr, 0.2(0.2) for Mn, 1 (1.2) for Ni, and 3.1 (3.4) for Co; the parentheses contain the experimental values. These results do not agree with the premises of Lomer and Marschall,[8] who assume that the filling of the atomic shells begins with Cr, that Mn has one d electron, and V has none.

Paramagnetic atomic magnetic moment and Curie constant. The atomic magnetic moment of ferromagnetic metals in the paramagnetic state is $m_p = \sqrt{\sigma(\sigma+2)}$, where σ is the number of paramagnetic electrons (participating in the paramagnetism) per atom. We shall show that this number can be calculated from relations analogous to (6) and (7). Assume that only the nearest neighbors of the atom (Δ_0) contribute to the moment m_p of all transition metals. Nothing is different in this respect for metals having lattices other than A2 (for example Co and Ni), since only the nearest neighbors participate even in their spontaneous magnetization. However, this assumption changes matters substantially for metals with A2 lattices (say Fe), for as we have seen even the atoms following the nearest neighbors contribute to their spontaneous magnetization, but here (in the case of paramagnetism) these are neglected. In the case of iron, in particular, this necessitates a plus sign in front of the square brackets in (5), cf. p. 867, while in the case of Co and Ni a minus sign is necessary (instead of the plus for the ferromagnetic state). Next, for example, for pure ferromagnetic metals, the denominators of (6) and (7) contain the integral parts $[e^{(1)} = N_d - n_s$ or $e^{(2)} = 1]$ and the fractional parts $[\gamma^{(1)} = N_d - n_s - \Delta$ or $\gamma^{(2)} = N_d - n_s + \Delta]$* of the number of ferromagnetic electrons, m. Assume that the foregoing integral parts are retained also for the paramagnetic state. As to the fractional parts, it is obvious that they are quite different; they must now be replaced by the fractional parts of the numbers of electrons that do not participate in the ferromagnetism. We assume that the latter equal $n_s - \gamma^{(1)}$ or $n_s - \gamma^{(2)}$.

Finally, the signs in front of γ_0 and 1 in the sought relations for m_p should be the same as in (6) and (7), for they are determined by the class of metal and by the orientation of the s-electron spin (both of which remain unchanged).

Considering all the foregoing, we find

$$\sigma^{(1)} = N_d + 0.15 n_s \left[- \frac{n_s - N_d - \Delta_0 - 1}{(N_d - n_s)(2n_s - N_d + \Delta_0)} - 4 \right], \quad (8)$$

$$\sigma^{(2)} = N_d + 0.15 n_s \left[- \frac{n_s - N_d + \Delta_0 - 1}{2n_s - N_d - \Delta_0} - 4 \right]. \quad (9)$$

Inserting the numerical values in (8) and (9) we get: $\sigma^{(1)} = 2.34$ and $m_p^{(1)} = 3.19$ (experiment[24] — 3.20) for Co; $\sigma^{(1)} = 2.31$ and $m_p^{(1)} = 3.18$ (experiment[24] — 3.20) for Fe; $\sigma^{(2)} = 0.89$ and $m_p^{(2)}$ 1.60 (experiment[24] — 1.60) for Ni.

Let us find the same quantities for MnAs and MnSb (the latter are chosen because we know their Curie constants C_0 per gram atom, which are proportional to $m_p^{(2)}$). $\Delta_0 \approx 0$ for both com-

*For pure ferromagnetic metals, Eq. (5) and the relations written for $\gamma^{(1)}$ and $\gamma^{(2)}$ yield practically the same values; (5) is the more general. It is seen from this that ε (or, what is the same, $\gamma^{(1)}$ or $\gamma^{(2)}$) is a fraction of n_s; in view of this, it is assumed that the number of electrons not participating in the ferromagnetism is the remainder of n_s, i.e., $n_s - \varepsilon$ or $n_s - \gamma$.

pounds. From (8) we have $\sigma^{(1)} = 3.61$ and $(m_p^{(1)})^2 = 20.24$, $\sigma^{(2)} = 3.24$ and $(m_p^{(2)})^2 = 17$ for MnAs and MnSb respectively.

Inserting the numerical values into the following relation

$$C_0 = LM_B^2 m_p^2 / 3k \qquad (10)$$

(L is the number of atoms per gram-atom and k is Boltzmann's constant), we obtain $C_0 = 0.325$ (0.322^{25}), 1.267 (1.228^{25}), 1.250 (1.265^{25}), 2.565 (2.594^{20}), and 2.110 (2.085^{20}) for Ni, Co, Fe, MnAs, and MnSb, respectively. The parentheses contain the experimental values and the references).

Curie Points

According to the theory of Vonsovskiĭ and Vlasov, the ferromagnetic Curie point is

$$\Theta = \Theta_{dd} / [1 - 0.15\, n_0 J (J_0/J - 4)^2 / b (1 - 2J_s/J) N], \qquad (11)$$

where $\Theta_{dd} = b/2k$ is the Curie point produced by d-d exchange only, b is an exchange integral on the order of J, and n_0 and N are the numbers of s and d electrons per cubic centimeter. It is impossible to calculate Θ from (11). We propose in its stead the following semi-empiral relations:

$$\Theta^{(1)} = \frac{n(n-1)(1+N_d^2)}{1 - 0.15\, n_s (N_d - n_s - \Delta_0)\{4 + [1 - (N_d - n_s - \Delta_0)] / (N_d - n_s - \Delta_0))^2 / nn_d}, \qquad (12)$$

$$\Theta^{(2)} = \frac{n(n-1)(1+N_d^2)}{1 - 0.05\, n_s \Delta_0 \{4 + (1 - \Delta_0)]^2 / nn_d} - nn_s (n_s + 2)/3, \qquad (13)$$

where n is the number of nearest neighbors. According to (12) and (13), $\Theta^{(1)} = 1041°\,K$ (experiment[23] — 1043° K) for Fe and 1389° K (experiment[23] — 1393° K) for Co; $\Theta^{(2)} = 637°\,K$ (631° K^{23}) for Ni.

The paramagnetic Curie point is

$$\Theta_p^{(1)} = \frac{n(n-1)(1+N_d^2)}{1 - 0.15\, n_s (2n_s - N_d + \Delta_0)\{4 - [1 - (2n_s - N_d + \Delta_0)] / (2n_s - N_d + \Delta_0))^2 / nn_d}, \qquad (14)$$

$$\Theta_p^{(2)} = \frac{n(n-1)(1+N_d^2)}{1 - 0.05\, n_s (2n_s - N_d - \Delta_0)\{4 - [1 - (2n_s - N_d - \Delta_0)] / (2n_s - N_d - \Delta_0))^2 / nn_d} - nn_s (n_s + 2)/3. \qquad (15)$$

According to (14) and (15), $\Theta_p^{(1)} = 1116°\,K$ ($1101°\,K^{25}$) for Fe and 1435° K (1428 — 1403° K^{25}) for Co; $\Theta_p^{(2)} = 646°\,K$ ($650°\,K^{25}$) for Ni.

Exchange Energy

The exchange energy equals

$$A^{(1)}/k = (N_d - n_s - \Delta_0)\Theta^{(1)}/(N_d - n_s)^2 \qquad (16)$$

$$A^{(2)}/k = (1 - \Delta_0)\Theta^{(2)} - nn_s (n_s + 2)/3. \qquad (17)$$

According to (16) and (17), $A^{(1)}/k = 180$ (183^{26}, 207^{27}) for Fe and 1014 for Co; $A^{(2)}/k = 223$ (226^{26}, 220^{27}) for Ni.

[1] F. M. Gal'perin, J. Exptl. Theoret. Phys. (U.S.S.R.) **31**, 150 (1956), **32**, 381 (1957), **34**, 1000 (1958), Soviet Phys. JETP **4**, 147 (1957), **5**, 321 (1957), **7**, 690 (1958).

[2] F. M. Gal'perin, Izv. Akad. Nauk SSSR, Ser. Fiz. **21**, 1323 (1957), Columbia Techn. Transl. p. 1308.

[3] R. D. Lowde, Proc. Roy. Soc. **235**, 305 (1956).

[4] R. J. Elliott, Proc. Roy. Soc. **235**, 289 (1956).

[5] S. V. Vonsovskiĭ, Izv. Akad. Nauk SSSR, Ser. Fiz. **21**, 854 (1957), Columbia Tech. Transl. p. 854.

[6] N. N. Bogolyubov and S. V. Tyablikov, Izv. Akad. Nauk SSSR, Ser. Fiz. **21**, 849 (1957), Columbia Techn. Transl. p. 849.

[7] R. J. Weiss and J. J. DeMarco, Revs. Modern Phys. **30**, 59 (1958).

[8] W. M. Lomer and W. Marschall, Phil. Mag. **3**, 659 (1958).

[9] C. G. Shull and M. K. Wilkinson, Phys. Rev. **97**, 304 (1955). C. G. Shull, Colloque International de Magnetisme de Grenoble — 2 au 6 jouillet, 1958.

[10] A. I. Snow, Phys. Rev. **85**, 365 (1952). G. E. Bacon, Neutron Diffraction, Russ. Transl., p. 196, 1957 (Oxford, 1955).

[11] M. C. Neuburger, Z. Kristal. 93, **1** (1936).

[12] W. Hume-Rothery and B. R. Cole, Advanc. Phys. **3**, 149 (1954).

[13] E. I. Kondorskiĭ and A. S. Pakhomov, J. Exptl. Theoret. Phys. (U.S.S.R.) **32**, 323 (1957), Soviet Phys. JETP **5**, 269 (1957).

[14] F. Bloch, Z. Physik, **61**, 206 (1930). Ch. Moller, Z. Physik **82**, 559 (1933).

[15] S. V. Vonsovskiĭ and K. B. Vlasov, J. Exptl. Theoret. Phys. (U.S.S.R.) **25**, 327 (1953).

[16] S. V. Vonsovskiĭ and Ya. S. Shur, Ферромагнетизм (Ferromagnetism), M-L, GTTI,

1948; Современное учение о магнетизме (Modern Theories of Magnetism), M-L, GTTI, 1952.
[17] W. C. Ellis and E. S. Greiner, Trans. Am. Soc. Metals **29**, 415 (1941).
[18] Owen, Yates, and Sully, Proc. Phys. Soc. **49**, 315 (1937).
[19] W. Köster and W. Rauscher, Z. Metallkunde **39**, 178 (1948).
[20] Ch. Guillaud, Journ. de Phys. **12**, 223 (1951).
[21] Ch. Guillaud, Compt. rend. **222**, 12, 386 (1946).
[22] F. A. Hames and D. S. Eppelsheimer, J. Metals **1**, 495 (1943); Nature **162**, 968 (1948).
[23] R. Bozorth, Ferromagnetism, Van Nostrand, 1951 (Russ. Transl. 1956).
[24] W. Sucksmith and R. R. Pearce, Proc. Roy. Soc. **A167**, 189 (1938).
[25] Ya. G. Dorfman, Магнитные свойства и строение вещества (Magnetic Properties and Structure of Matter), GTTI, 1955.
[26] E. I. Kondorskiĭ and L. N. Fedotov, Izv. Akad. Nauk SSSR, Ser. Fiz. **16**, 432 (1952).
[27] M. Fallot, J. phys. et radium **5**, 153 (1944).

Translated by J. G. Adashko
230

EMPIRICAL REGULARITIES IN THE NUCLEON PAIR PRODUCTION ENERGIES IN NUCLEI

V. A. KRAVTSOV

Leningrad Polytechnic Institute

Submitted to JETP editor October 15, 1958

J. Exptl. Theoret. Phys. (U.S.S.R.) **36**, 1224-1232 (April, 1959)

The variation of the pairing energies of nucleons and of the energy of the residual n-p interaction of odd nucleons is investigated on the basis of the most recent experimental data. It is found that the pairing energy depends not only on the total angular momentum of the nucleons but also on the position of the pair in the nuclear shell and on the deformation of the nucleus. The decrease in pairing energy with mass number A is slower than predicted by the theory. The pairing energy remains almost constant if two nucleons of different types and added to the nucleus. The energy of the residual n-p interaction of the odd nucleons is not zero, decreases with A, and is smaller than the pairing energy.

MODERN theory of nuclear structure starts out, in the zero approximation, from the concept of a separate nucleon moving independently of all remaining nucleons in the averaged field of the nucleus. Mayer[1,2] was able to explain the existence of nuclear shells for a spherically symmetrical nuclear field, assuming the existence of a strong spin-orbit coupling. However, many experimental data indicate that the single-particle approximation is inadequate. The total nuclear angular momentum j, which is the sum of the orbital momentum l and the spin s, equals zero in all even-even nuclei. This experimental fact can be attributed to the presence of a residual interaction between the nucleons. Identical nucleons with equal but opposite j form pairs with zero angular momentum. The presence of this residual interaction and the production of pairs is confirmed by the fact that the joining energy of, say, an even neutron is always greater than the nucleon binding energy of the preceding odd neutron.

The difference in the nucleon binding energies between the even neutron and the preceding odd neutron is the energy of production of a pair of neutrons in the nucleus, and is called the pairing energy P_n of the neutrons. The proton pairing energy P_p is analogously defined.

Considering the residual interaction between identical nucleons with equal but opposite directions of j, Mayer and Jensen[1,2] calculated the pairing energy P. They used delta forces as the interaction forces. This yielded for the pairing energy

$$P = -C(2j+1)/A, \qquad (1)$$

where A is the mass number of the nucleus to which the pair is joined and C is a constant that depends on the type of potential. Expression (1) should be valid only near filled nuclear shells, since it considers the residual interaction of only two nucleons.

Birbrair and Sliv[3] have shown that the presence of spherical symmetry in even-even nuclei that are not very close to nuclei with filled shells is explained by the existence of pairing energies. They have also shown that in deformed nuclei the pairing energies are lower than in spherically-symmetrical nuclei.

The author of this paper[4] has attempted to ascertain the dependence of the pairing energy and the total angular momentum j. The experimental data of 1952 did not disclose this dependence. Quisenberry, Scolman, and Nier,[5] Johnson and Nier,[6] and Giese and Benson[7] also failed to find a dependence of the pairing energies on j in new, more accurate experimental data.

Nomoto[8] checked the experimental values of the pairing energy against the Mayer formula (1) for nuclei with mass numbers less than 115. Although the constant C was indeed calculated in reference 8, the curves show that the agreement between the experimental data and formula (1) is not good enough.

The purpose of this paper is an attempt to establish the principal regularities in the variation of pairing energies, using the latest experiments. It is proposed here not only to compare the principal theoretical laws of Mayer and of Birbrair and Sliv with experiment, but also to point to new regularities in regions where the existing theories

do not give satisfactory results.

1. EXPERIMENTAL DATA AND CALCULATION OF PAIRING ENERGIES

The initial experimental data for the calculation of the pairing energies are the masses of the atoms and binding energies of the nuclei calculated from them. For isotopes in the interval from hydrogen to zinc ($1 \leq Z \leq 30$) and from xenon to europium ($54 \leq z \leq 62$), use was made of masses and binding energies calculated from the values of the mass-spectrometric doublets by Quisenberry, Scolman, Nier, Giese, Benson, and Johnson[5-7,9-11] and from the reaction and decay energies. These masses and binding energies are listed in a review by the author.[12] The masses of the atoms and the binding energies from gallium to xenon ($31 \leq Z \leq 54$) are taken from the Wapstra mass tables.[13]

The nucleon binding energies of the last neutrons in the nuclei of the isotopes from gadolinium to lead ($64 \leq Z \leq 82$) are taken from the measurements of Johnson and Bhanot.[14,12] The atomic masses and the binding energies of the nuclei from thallium to uranium ($81 \leq Z \leq 92$) are taken from the tables of Huizenga.[15] The nucleon binding energy of the last neutrons and protons in the nuclei of the isotopes from uranium to fermium ($92 \leq Z \leq 100$) are taken from the survey of Hyde and Seaborg.[16]

The pairing energy of the N-th and the $(N-1)$-th neutrons in a nucleus with protons is

$$P_n(Z, N) = B_n(Z, N) - B_n(Z, N-1), \qquad (2)$$

where N is an even number and $B_n(Z, N)$ is the nucleon binding energy of the last N-th neutron to the nucleus with Z protons.

Analogously, the pairing energy for the Z-th and $(Z-1)$-th protons in a nucleus with N neutrons is

$$P_p(Z, N) = B_p(Z, N) - B_p(Z-1, N), \qquad (3)$$

where Z is an even number and $B_p(Z, N)$ is the energy of the binding of the last Z-th proton to the nucleus with N neutrons.

For a description of the total binding energy of the nuclei, $E(Z, N)$, use is made of a geometrical representation, namely the energy surface $E = f(Z, N)$ in the three-dimensional space E, Z, N. This surface has four branches: even-even (even Z and even N), even-odd (even Z and odd N), odd-even (odd Z and even N), and odd-odd (Z and N both odd).

After determining the joining energy of the last neutrons, we can express the pairing energy in the terms of the total binding energy of the nuclei $E(Z, N)$ as follows:

$$P_n(Z, N) = 2\{{}^1\!/_2[E(Z, N) + E(Z, N-2)] - E(Z, N-1)\},$$
$$P_p(Z, N) = 2\{{}^1\!/_2[E(Z, N) + E(Z-2, N)] - E(Z-1, N)\}. \qquad (4)$$

For even Z and N it is easy to verify that $P_n(Z, N)$ is twice the distance along the E axis between the even-even and even-odd energy surfaces. $P_p(Z, N)$ is the distance along the E axis between the even-even and odd-even energy surfaces. From the well-known Weizzäcker-Fermi semi-empirical formula for the binding energies,[17] we can express the pairing energy from (4) as follows

$$P = -2\delta A^{-3/4}. \qquad (5)$$

In the present paper we consider in addition to the pairing energy also the residual reaction between the odd neutrons and protons. To determine this interaction, we have calculated from the experimental data the value of R_{np}, the difference between the energy of simultaneous binding of a neutron and proton to an even-even nucleus (Z, N) and the sum of the energies of the binding of the neutron and proton separately to the same nucleus

$$R_{np}(Z+1, N+1) = B_{np}(Z+1, N+1) - B_p(Z+1, N) - B_n(Z, N+1),$$

where

$$B_{np}(Z+1, N+1) = E(Z+1, N+1) - E(Z, N). \qquad (6)$$

Here Z and N are even numbers.

We shall call the quantity R_{np} the residual n-p interaction. To calculate R_{np} it is more convenient to use other formulas:

$$R_{np}(Z+1, N+1) = B_p(Z+1, N+1) - B_p(Z+1, N) = B_n(Z+1, N+1) - B_n(Z, N+1). \qquad (7)$$

If B_n and B_p are considered negative, all values of the residual n-p interaction energy are always negative, within the limits of experimental errors.

Certain other authors[5-7] consider $P_n(Z, N)$ with odd Z and $P_p(Z, N)$ with odd N, and call these quantities pairing energies, too. In view of the presence of an odd nucleon of another type in the nucleus, these quantities depend also on the residual n-p interaction and therefore should not be called pairing energies; they are not considered in the present paper.

2. VARIATIONS OF PAIRING ENERGIES AND OF THE RESIDUAL n-p INTERACTION

To investigate the variation of the pairing energies we plotted the graphs shown in Figs. 1 – 5. The first three show the dependence of the pairing energy of the neutrons P_n on the number of neutrons N in the nucleus. All the points representing the pairing energies in the nuclei of isotopes of the same element are connected by straight lines. The broken lines thus formed are tagged with the symbol of the element. The fraction near each point represents the total angular momentum of the preceding odd neutron, known from experiment or assumed from the decay data; the values of j are taken from the tables of Dzhelepov and Peker[18] and from the paper by Peker.[19]

Figures 4 and 5 show the depencence of the pairing energy of protons P_p on the number of the protons Z in the nucleus. As in Figs. 1 – 3, the points representing the pairing energy in nuclei with equal number of neutrons are joined by a broken line, tagged with the number of neutrons in these nuclei. The fraction at each point indicates the value of j of the preceding odd proton, taken from references 18 and 19.

Everywhere in the intervals $4 \leq N \leq 40$ (Fig. 1) and $4 \leq Z \leq 30$ (Fig. 4), the errors in the pairing energies are less than the circles representing the points, with the exception of the cases represented by vertical segments. In the intervals $40 \leq N \leq 56$ (Fig. 1) and $32 \leq Z \leq 42$ (Fig. 4), the errors in the pairing energies increase approximately from ±0.30 Mev to ±0.60 Mev. In Fig. 2, in the interval $78 \leq N \leq 90$, the error in P_n fluctuates about ±0.15 Mev, and in the interval $92 \leq N \leq 126$ the error is ±0.03 Mev almost everywhere in the region of the heavy nuclei. In Figs. 3 and 5, the pairing energies have on the average errors from ±0.10 to ±0.30 Mev.

In the regions missing from the diagrams, the mass-measurement accuracy is insufficient for the calculation of the pairing-energy values suitable for the investigation of the regularities.

A study of the course of variation of the pairing energies with the number of nucleons in the nuclei and with their total angular momentum j shows that the pairing energies frequently depend on j. We see in Figs. 1, 3, and 4 that the pairing energy of nucleons with $j = 1/2$ is as a rule lower than that of nucleons with larger j (for example, in Fig. 1 for N = 8 and 16, in Fig. 3 for N = 126, in Fig. 4 for Z = 8, 16, and 40, and in other cases). There are exceptions, however; for example, in Fig. 1 at N = 40 the pairing energy for nucleons with $j = 1/2$ is higher than at N = 34 with $j = 3/2$, with the values of P_n for zinc being shown to a high degree of accuracy.

It is seen from the curves that most frequently the pairing energy increases with increasing j, but the increase in the pairing energy is apparently slower than $(2j + 1)$.

From an examination of the intervals $20 \leq N \leq 28$ $(j = 7/2)$ and $38 \leq N \leq 50$ $(j = 9/2)$ in Fig. 1 and of the intervals $20 \leq Z \leq 28$ $(j = 7/2)$ and $30 \leq Z \leq 40$ $(j = 5/2)$ in Fig. 4 it can be seen that for equal j, the pairing energy depends on the position of the pair in the shell. As the shell becomes filled, the pairing energy decreases. The pairing energy reaches a maximum value either at the middle of the shell, or at the beginning.

An examination of the curves for P_n in Figs. 1 – 3 shows that the neutron pairing energy P_n

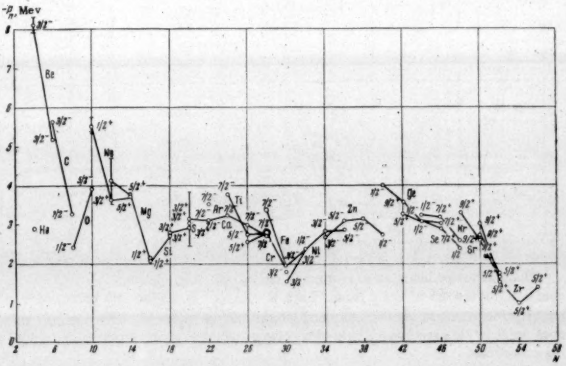

FIG. 1. Pairing energies of neutrons in nuclei with even atomic number Z, for the 4th to the 56th neutrons. Located near each point is the value of the spin of the preceding odd neutron, known from experiment. The broken lines are tagged with the symbol of the element in whose nucleus the pair is produced.

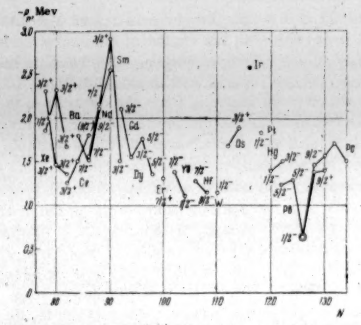

FIG. 2. Pairing energies of neutrons in nuclei with even atomic number Z for the 78th to 132d neutrons. All other data are as in Fig. 1: o – points for even-even nuclei, • – point for the 116th neutron, which produces a pair in the odd-even nucleus of iridium.

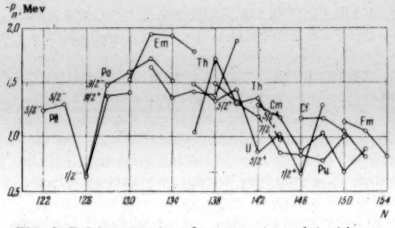

FIG. 3. Pairing energies of neutrons in nuclei with even atomic number Z for the 122d to 154th neutrons. The rest is as in Fig. 1.

depends little on the number of even protons in the nucleus, Z, since most frequently the spread of the points at given values of N barely exceeds the errors. As can be seen from Figs. 4 – 5, the pairing energy of the protons P_p also depends little on the number of even neutrons N in the nucleus, although in many cases the spread in the points, at the given Z, is somewhat greater than in the case of P_p. This experimental fact shows that the residual energy of the n-p interaction is small for the nucleons that produce the pairs.

In many cases, as indicated by Mayer,[1] when levels with large j are filled, the last odd nucleon may occupy the nearest level with small j, this being explained by the presence of a large pairing energy at large j. When the next even nucleon appears, the odd nucleon goes to a level with large j and a pair with large j in the opposite direction is produced. For example, in Fig. 1 in the interval $42 \leq N \leq 50$, according to the Mayer scheme, the level with $j = 9/2$ should be filled, but along with this j we find also $j = 1/2$. Here the $j = 1/2$ appear at the middle and at the start of the level, where P_n is large, and upon approaching the end of the shell, when P_n becomes smaller, the large $j = 9/2$ appear more frequently. This apparently confirms the Mayer hypothesis concerning the pairing energy and the appearance of individual nucleons at levels with small j.

The increase in pairing energy halfway between shells can explain to some extent the increased value of the pairing energy P_n at $N = 40$ (Fig. 1), for here we deal exactly with the middle of the shell, between $N = 28$ and $N = 50$.

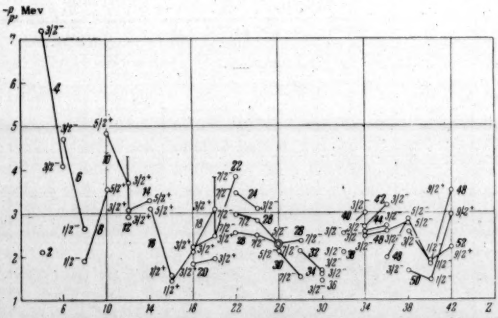

FIG. 4. Pairing energies of protons in nuclei with even number of neutrons, for the 4th to 42d protons. Each broken line is tagged with the number of neutrons in the nucleus in which the pair is produced. Near each point is the experimentally-known value of the spin of the preceding odd proton.

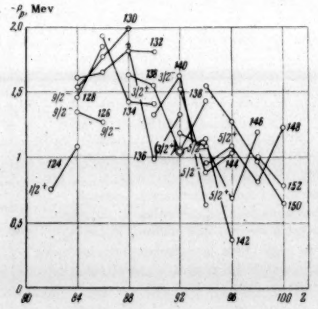

FIG. 5. Pairing energies of protons in nuclei with even number N, for the 82d to the 100th protons. The rest is as in Fig. 4.

The new mass values given in references 5 – 7 and 9 – 11 no longer give rise to the subshells mentioned by the author[20] for the case of N = 34, 40, etc. The same is confirmed by Zeldes,[21] who, using the new values of the masses, sought but could not find the same subshells. The decrease in P_p at Z = 40 is possibly due to the fact that the neutron shell N = 50 is filled in this region. This confirms the theoretical premise that the Mayer theory, including formula (1) for the pairing energy, is suitable only in the vicinity of nuclei with closed shells.

Figure 3 shows graphs for the variation of pairing energies in the region of deformed nuclei of rare-earth isotopes, the interval $90 \leq N \leq 114$. The neutron pairing energy rises sharply and reaches a maximum on the boundary of the region of deformed nuclei at N = 90. Within the region of deformed nuclei the neutron pairing energy drops toward the middle of the shell and reaches a minimum at N = 110 in tungsten. This is followed by a rise with a maximum at N = 116 in iridium (Z = 77). The point N = 116 was taken for an odd-even nucleus, since P_n was not measured for even Z for N = 116. On the basis of the experimental law indicated by Quisenberry et al.,[5] the residual interaction energy for even-even nuclei is always less than the pairing energy. Consequently, the point at N = 116 for the true pairing energy of even-even nuclei should lie above the point shown for iridium in the curve.

In the region of light deformed nuclei near magnesium on Fig. 1 at $10 \leq N \leq 14$ and on Fig. 4 at $10 \leq Z \leq 14$, it is also possible to observe a reduction in the pairing energy for deformed nuclei. For heavy deformed nuclei at $Z \geq 88$ in Figs. 3 and 5, we also note a drop in the pairing energies. The drops in the pairing energies in the region of the deformed light and heavy nuclei are not as clearly pronounced as in the rare-earth region. This reduction in the pairing energies for deformed nuclei was theoretically explained by Birbrair and Sliv.[3]

Figures 6 and 7 show the dependence of the residual n-p interaction (R_{np}) on the number of neutrons and on the number of protons for light and heavy nuclei. The ordinates represent R_{np} and the abscissas the number of neutrons in the nucleus N; the points pertaining to nuclei with the same Z are joined by straight lines. It is seen from the curves that R_{np} is everywhere negative, with two exceptions that do not exceed the errors. R_{np} diminishes with mass number A in the nucleus. If R_{np} is compared with the pairing energies we see that on the average, in nuclei with equal mass numbers, $|R_{np}| < |P|$, i.e., the energy of the residual n-p interaction is less in absolute magnitude than the pairing energy.

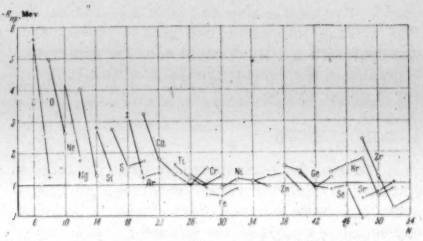

FIG. 6. Energy of residual n–p interaction of odd nucleons in nuclei of isotopes from carbon to zirconium, as a function of the number of neutrons N in the nucleus to which the nucleons are joined. Each broken line is tagged with the symbol of the element to whose nucleus the nucleons are joined.

Nomoto[8] compared the Mayer formula (1) for the pairing energy with the experimental data for nuclei with $10 \leq A \leq 120$. It is clearly seen from Nomoto's curves that the experimental values diminish more slowly than 1/A, as would follow from (1). Since the dependence of the pairing energy on j is also subject to doubt, the dependence on A was investigated for only one fixed j. A total momentum $j = 1/2$ was chosen, since almost all nucleons with $j = 1/2$ are found in nuclei close to nuclei with filled shells, and these nuclei fit the Mayer model better. The P_n at N = 40 were omitted in the investigation, since a nucleus with these values of P_n is relatively far away from the nuclei with filled shells. We considered the pairing energies of all spherical nuclei with $j = 1/2$, including heavy nuclei, but omitting $P_n(40)$. We calculated the products PA, $PA^{3/4}$, and

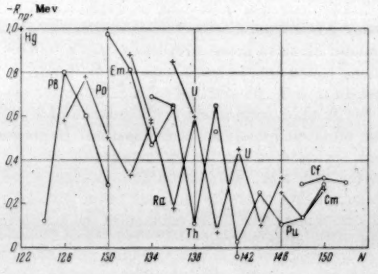

FIG. 7. Energy of residual n–p interaction of odd nucleons in nuclei of the isotopes from mercury to curium. The rest is the same as in Fig. 6.

$PA^{1/2}$. The smallest spread is in the product $PA^{1/2}$. Thus, the pairing energies of protons and neutrons with $j = 1/2$, located near the end or the beginning of the nuclear shells, diminish in inverse proportion to $\sqrt{A}$.

3. CONCLUSIONS

A study of the experimentally-obtained pairing energies of nucleons (mass-spectroscopic measurements, measurements of the reaction and decay energies) parmits the following conclusions:

1. The pairing energy is usually greater for nucleons with large total angular momenta j. The increase in pairing energy with j is slower than $(2j+1)$. A deviation from this rule is found only for nuclei with a number of nucleons that differ substantially from magic.

2. The pairing energy increases as the number of pairing nucleons deviates from magic.

3. The pairing energy of the neutrons depends little on the number of paired protons in the nucleus. The analogous rule for protons is less clearly pronounced.

4. The course of variation of the pairing energies and of j confirm the Mayer hypothesis that in even-odd nuclei the odd nucleons may temporarily occupy near-lying levels with small j, and that in even-even nuclei they again pass to the level with larger j.

5. The pairing energies have a large maximum at the beginning of the region of deformed nuclei, then drop to a minimum in the middle of the region of deformed nuclei, rising again towards the end of the region.

6. Residual n-p interaction energies different from zero exist for odd nucleons. The residual n-p interaction diminishes with increasing mass number A and is always less than the pairing energy.

7. The decrease in pairing energies with increasing mass number A is slower than 1/A. In nuclei close to those with filled shells, the pairing energy of nucleons with $j = 1/2$ diminishes in inverse proportion to $A^{1/2}$.

For further refinement of the course of variation of pairing energies it is desirable to obtain more accurate values for the masses of atoms heavier than zinc. Of particular importance are measurements of stable isotopes of molybdenum and ruthenium, and of the masses of the isotopes from gadolinium to lead.

In conclusion, I consider it my pleasant duty to thank B. L. Birbrair and L. A. Sliv for discussing the results of this investigation.

[1] M. Goeppert-Mayer and J. H. D. Jensen, Elementary Theory of Nuclear Shell Structure, Wiley, N. Y., 1955.

[2] M. Goeppert-Mayer, Phys. Rev. **78**, 16 (1950).

[3] B. Birbrair and L. Sliv, Мезисы докладов на Всесоюзной конференции по ядерным реакциям при малых и средних энергиях (Theses of Papers delivered at the All-Union Conference of Low and Medium Energy Nuclear Reactions), M., 1957, p. 74. B. Birbrair, J. Exptl. Theoret. Phys. **33**, 1235 (1957), Soviet Phys. JETP **6**, 951 (1957).

[4] V. Kravtsov, Izv. Akad Nauk SSSR, Ser. Fiz. **18**, 5, 1954.

[5] Quisenberry, Scolman, and Nier, Phys. Rev. **104**, 461 (1956).

[6] W. Johnson Jr. and A. Nier, Phys. Rev. **105**, 1014 (1957).

[7] C. Giese and J. Benson, Phys. Rev. **110**, 712 (1958).

[8] M. Nomoto, Progr. Theoret. Phys. **18**, 483 (1957).

[9] Quisenberry, Scolman, and Nier, Phys. Rev. **102**, 1071 (1956).

[10] Scolman, Quisenberry, and Nier, Phys. Rev. **102**, 1076 (1956).

[11] Quisenberry, Giese, and Benson, Phys. Rev. **107**, 1665 (1957).

[12] V. Kravtsov, Usp. Fiz. Nauk **65**, 451 (1958).

[13] A. Wapstra, Physica **21**, 385 (1955).

[14] W. Johnson Jr. and V. Bhanot, Phys. Rev. **107**, 1669 (1957).

[15] J. Huizenga, Physica **21**, 410 (1955).

[16] E. Hyde and G. Seaborg, Handbuch der Physik **42**, 294 (1957).

[17] E. Fermi, Nuclear Physics, Univ. of Chicago Press, 1950 (Russ. Transl. 1951).

[18] B. Dzhelepov and L. Peker, Схемы распада радиоактивных изотопов (Decay Schemes of Radioactive Isotopes). U.S.S.R. Acad. Sci. Press, 1957.

[19] L. Peker, Izv. Akad. Nauk SSSR, Ser. Fiz. **21**, 1029, 1957, Columbia Tech. Transl. p. 1030.

[20] V. Kravtsov, J. Exptl. Theoret. Phys. (U.S.S.R.) **30**, 408 (1956), Soviet Phys. JETP **3**, 297 (1956).

[21] N. Zeldes, Nucl. Phys. **7**, 27 (1958).

Translated by J. G. Adashko
231

DEVELOPMENT OF THE NUCLEAR-ACTIVE COMPONENT OF EXTENSIVE AIR SHOWERS

S. N. VERNOV, E. V. GORCHAKOV, I. P. IVANENKO, and G. B. KHRISTIANSEN

Institute of Nuclear Physics, Moscow State University.

Submitted to JETP editor October 16, 1958

J. Exptl. Theoret. Phys. (U.S.S.R.) **36**, 1233-1239 (April, 1959)

The spectrum of the nuclear-active particles in extensive atmospheric showers and the particle and absorption ranges are computed, and the rate of structure bursts is estimated, on the basis of certain simple assumptions regarding the nature of the elementary act. It is shown that the extensive atmospheric shower has certain characteristics that depend weakly on the nature of the elementary act, and certain characteristics that are sensitive to the latter.

THE Guzhavin's and Zatsepin[1] calculated the altitude variation of nuclear-active (n.a.) high-energy particles and of the number of high-energy muons at sea level. They also calculated the altitude variation of the nuclear-active and soft components of extensive atmospheric showers (e.a.s.). The elementary act for super-high energies was chosen in one of the variants of calculations after Landau.[2] In another variant it was assumed, in accordance with Vernov's hypothesis[3] that the nucleon always retains approximately 70% of the energy of the incident particle. The effective cross section for the collision was assumed constant for all energies and corresponding to a free path in air $\lambda_0 = 65 - 70$ g/cm^2.

It was found that the results of the calculations depended greatly on λ_0. We note that there is no known experimental value of λ_0 at energies $\gtrsim 10^{10}$ ev. We therefore undertook a calculation of various characteristics of nuclear-active component of extensive atmospheric showers, in which the magnitude of λ_0 is determined by the type of elementary act and by the experimental value of the absorption range of nuclear-active high-energy particles ($\approx 10^{12}$ ev). By making simple assumptions concerning the character of the elementary act, we calculated the spectrum of the n.a. particles in the e.a.s., the absorption ranges of n.a. particles, and the energy fluxes in the showers. We also estimated the probability of observation of one or two n.a. high-energy particles at a given level. The principal purpose of the calculation is to determine the e.a.s. characteristics that are sensitive to the character of interaction, by varying different parameters of the elementary act and the magnitude of λ_0.

Let us assume that upon collision between n.a. particles of energy ϵ' with an air nucleus, the probability of observing secondary n.a. particles of energies $\epsilon_1, \ldots, \epsilon_n$ is a function of only the ratios ϵ_i/ϵ', and can be written

$$\Phi(\varepsilon', \varepsilon_1, \ldots, \varepsilon_n) = \delta(\alpha_1 - \varepsilon_1/\varepsilon') \ldots \delta(\alpha_n - \varepsilon_n/\varepsilon'), \qquad (1)$$

where $\alpha_i = \text{const}$.

We assume that the energy carried away by the secondary n.a. particles amounts to $\sim 70 - 80\%$ of the energy of the incident particle. The assumed fraction of the energy retained by the secondary n.a. particles takes into account the transformation of a portion of the energy into π^0 mesons, and also considers to some extent the decay of the $\pi^\pm$ mesons. If we assume that the principal portion of the energy of the primary particle is carried away by π mesons and nucleons, their energy should be greater than $\sim 60\%$ of ϵ'. Analogous conclusions concerning the fraction of the energy remaining in the nuclear-active component were reached by Rozental' and Gerasimova in reference 5.

Taking this into account, we limit our analysis to the following three variants: 1) the collision produces one particle with energy $0.7\,\epsilon'$ ($\alpha_1 = 0.7$); 2) two particles of essentially different energies, $0.7\,\epsilon'$ and $0.1\,\epsilon'$ ($\alpha_1 = 0.7$, $\alpha_2 = 0.1$), are produced; 3) seven particles are produced, each with energy $0.1\,\epsilon'$ ($\alpha_1 = , \ldots = \alpha_7 = 0.1$).

We shall calculate the spectrum of the n.a. particles in the shower for each of the three variants. For this purpose it is necessary to know the range for the interaction, λ_0. Assuming that the range for the interaction is independent of the energy, we determine its magnitude, using

data on the absorption of high-energy n.a. particles in the atmosphere. It is known that if the spectrum of the secondary particles is written in form (1), and the spectrum of the primary cosmic radiation is in the form of a power law, the following relation holds[6]

$$\lambda_0 = \lambda\left(1 - \sum_{i=1}^{n} \alpha_i \gamma\right), \qquad (2)$$

where λ is the range for absorption of n.a. high-energy particles in the atmosphere, and γ is the exponent of the integral spectrum of the primary cosmic radiation.

By taking $\lambda = 120$ g/cm^2 (reference 4) and $\gamma = 1.6$ (reference 7), we obtain for the first case $\lambda_0 = 52.7$ g/cm^2, for the second case $\lambda_0 = 50.2$ g/cm^2, and for the third case $\lambda_0 = 99.0$ g/cm^2.

Knowing λ_0, we calculate the average number of n.a. particles, $N(\epsilon, x)$, in an e.a.s. with energy $\geq \epsilon$, at a depth x (ϵ is the energy of the n.a. particles as a fraction of the energy E_0 of the particle producing the shower). The depth of the atmosphere x is measured in units of λ_0.

The average number of particles with energy ϵ at a depth x can be written in the following form (see reference 8)

$$N(\varepsilon, x) = \sum_{k=0}^{\infty} \frac{x^k}{k!} e^{-x} F_k(\varepsilon),$$

where in the absence of decay

$$F_k(\varepsilon) = \int_{\varepsilon}^{1} F_{k-1}(\varepsilon') W(\varepsilon', \varepsilon)\, d\varepsilon'.$$

$W(\epsilon, \epsilon')$ is the probability of observing secondary particles with energies ϵ upon collision of a particle with energy ϵ' with a nucleus; this probability is determined as follows:

$$W(\varepsilon', \varepsilon)\, d\varepsilon = \int_0^{\varepsilon'} \dots \int_0^{\varepsilon'} \Phi(\varepsilon', \varepsilon, \varepsilon_2, \dots, \varepsilon_n)(\varepsilon')^{-n} d\varepsilon d\varepsilon_2 \dots d\varepsilon_n + \int_0^{\varepsilon'} \dots \int_0^{\varepsilon'} \Phi(\varepsilon', \varepsilon_1, \varepsilon, \varepsilon_3, \dots, \varepsilon_n)(\varepsilon')^{-n} d\varepsilon_1\, d\varepsilon d\varepsilon_3 \dots d\varepsilon_n + \dots + \int_0^{\varepsilon'} \dots \int_0^{\varepsilon'} \Phi(\varepsilon', \varepsilon_1, \dots, \varepsilon_{n-1}, \varepsilon)(\varepsilon')^{-n} d\varepsilon_1 \dots d\varepsilon_{n-1} d\varepsilon = \sum_{i=1}^{n} \delta\left(\alpha_i - \frac{\varepsilon}{\varepsilon'}\right)\frac{d\varepsilon}{\varepsilon'}. \qquad (3)$$

By calculating the e.a.s. produced by the primary particle of energy E_0, we obtain $F_0(\epsilon) = \delta(1 - \epsilon)$. Then in our case

$$F_1(\varepsilon) = \int_{\varepsilon}^{1} d\varepsilon' \delta(1 - \varepsilon') \sum_{i_1=1}^{n} \delta\left(\alpha_{i_1} - \frac{\varepsilon}{\varepsilon'}\right)\frac{1}{\varepsilon'} = \sum_{i_1=1}^{n} \delta(\alpha_{i_1} - \varepsilon),$$

$$F_2(\varepsilon) = \sum_{i_1=1}^{n} \sum_{i_2=1}^{n} \delta(\alpha_{i_1}\alpha_{i_2} - \varepsilon), \dots, F_k(\varepsilon) = \sum_{i_1=1}^{n} \dots \sum_{i_k=1}^{n} \delta(\alpha_{i_1} \dots \alpha_{i_k} - \varepsilon).$$

After calculating $F_k(\epsilon)$ we can determine the integral energy spectrum of n.a. particles at a given depth, since

$$N(\geqslant \varepsilon, x) = \int_{\varepsilon}^{1} N(\varepsilon', x)\, d\varepsilon' = \sum_{i=0}^{\infty} \frac{x^i}{i!} e^{-x} F_i(\geqslant \varepsilon), \qquad (4)$$

where

$$F_i(\geqslant \varepsilon) = \int_{\varepsilon}^{1} F_i(\varepsilon')\, d\varepsilon'.$$

The energy dependence of the average number of n.a. particles with energies $\geq \epsilon$ in e.a.s. at sea level, calculated from formula (1) for the three variants of the elementary act, is shown in Fig. 1.

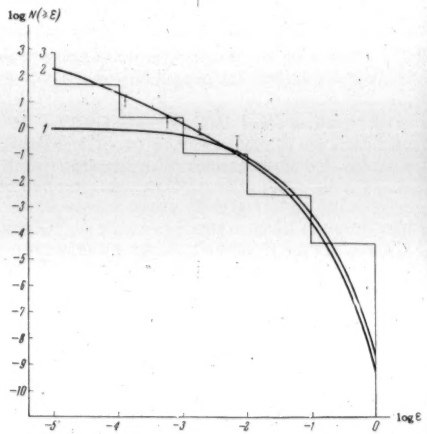

FIG. 1. Energy dependence of the average number of the nuclear-active particles with energy $\geq \varepsilon$ in e. a. s. at sea level. The curves are calculated from formula (4) for three respective variants of the elementary act. The points indicate the experimental results taken from reference 9.

To compare the resultant spectra with experiments, we used the data obtained in reference 9, shown as dots in Fig. 1. The authors of reference 9 measured the average number of n.a. particles with energies $\geq 10^{12}$ ev in showers with different numbers of particles, N_S, at sea level.

We assume that E_0 can be determined with sufficient accuracy from the number of shower particles.* We can then find E_0 with the aid of the relation $E_0 = kN_S$, derived by Cocconi[1] from an analysis of the altitude variation of the showers. At sea level we have $k = 10^{10}$ ev/particle.

*Estimates as well as calculations carried out by Grigorov and Shestoperov[10] show that this assumption is satisfactory when N_s is large ($\gtrsim 10^3$ particles).

As can be seen from Fig. 1, the variation of $N(\geq \epsilon)$, calculated according to the first variant, contradicts the experimental data, and will not be discussed further. $N(\epsilon)$, calculated with the aid of the second and third variants, agree with experiment. Our calculations show that variants intermediate between the second and third (for example, $\alpha_1 = 0.5$, $\alpha_2 = 0.12$, $\alpha_3 = 0.06$ and $\alpha_1 = 0.3$, $\alpha_2 = 0.2$, $\alpha_3 = 0.1$) also give good agreement with experiment. We note that spectra of n.a. particles at $10^{-5} \leq \epsilon \leq 1$ depend little on the presence of secondary low-energy particles during the collision. Thus, for example, if ten more particles are produced in the third variant, each with energy 0.01 of the energy of the incident particle, then $N(\geq 10^{-2})$ increases by the factor of 1.2, and $N(\geq 10^{-4})$ increases by 1.02 times. If still another 100 particles are formed with energies of 0.001 each, then $N(\geq 10^{-3})$ increases by 1.3 times.

The interaction of n.a. particles need not always occur in the same manner; for example, it may occur with a certain degree of probability in accordance with the second variant or according to the third. It is then to be expected that, with a suitable choice of λ_0, the calculated and experimental values will agree.

We note also that the function $N(\geq \epsilon, x)$ depends on the form of the function $W(\epsilon', \epsilon)$. Since the function $W(\epsilon', \epsilon)$ is obtained from Φ by formula (3) it may have the same form even if the function Φ has different forms. This will occur, for example, for

$$\Phi_1 = \delta(0.1 - \varepsilon_1/\varepsilon') \ldots \delta(0.1 - \varepsilon_7/\varepsilon')(\varepsilon')^{-7}$$

and

$$\Phi_2 = {}^1/_2\delta(0.1 - \varepsilon_1/\varepsilon') \ldots \delta(0.1 - \varepsilon_6/\varepsilon')(\varepsilon')^{-6} + {}^1/_2\delta(0.1 - \varepsilon_1/\varepsilon') \ldots \delta(0.1 - \varepsilon_8/\varepsilon')(\varepsilon')^{-8},$$

although in the first case seven particles are always produced in a nuclear collision, and in the second case six or eight particles may be produced, with probabilities of $\frac{1}{2}$.

Thus, an analysis of the spectrum of the n.a. particles in a shower for one level (if the value of λ_0 is not known from experiment and is determined from the absorption range of n.a. particles of energy $E \gtrsim 10^{12}$ ev) does not make it possible to determine, even approximately, the characteristics of the elementary act, if there is no possibility of observing the nuclear-active particles in the interval $0.1 \geq \epsilon \geq 1$. Therefore, in addition to calculating $N(\geq \epsilon)$ in e.a.s. for sea level, we performed analogous calculations for two other depths, 650 and 1250 g/cm^2.

On the basis of these calculations we obtained values of ranges for the absorption of n.a. particles, $\lambda_N(\geq \epsilon)$ with energies $\geq \epsilon$ and for the absorption of the energy $\lambda_E(\geq \epsilon)$ carried away by these particles (Fig. 2). As can be seen from the diagram, the quantities $\lambda_N(\geq \epsilon)$ and $\lambda_E(\geq \epsilon)$, calculated for the second and third variants, do not agree. Therefore an experimental measurement of these absorption ranges may prove important for the determination of the type of elementary act at super-high energies.

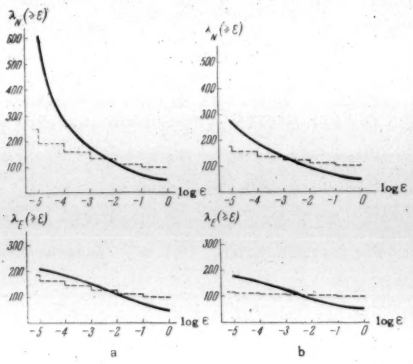

FIG. 2. Absorption ranges of nuclear-active particles $\lambda_N(\geq\varepsilon)$ with energy $\geq\varepsilon$, and absorption range $\lambda_E(\geq\varepsilon)$ for the energy carried by these particles: a – for the depth interval 650-1000 g/cm^2 for the second (solid) and third (dotted) interaction variants; b – the same for 1000 – 1250 g/cm^2.

Let us calculate, for the second and third variants, the probability of observing at a depth x_0 in a shower one particle $P(1, x_0)$ or two particles $P(2, x_0)$ of energy $\epsilon \geq 0.1$. For the second variant, the probability $P(1, x_0)$ can be written

$$P(1, x_0) = \int_0^{x_0} Q_1(x)\{Q_1(x_0 - x)\,Q_2(x_0 - x) + Q_2(x_0 - x)\,Q_4(x_0 - x)\}\,dx. \qquad (5')$$

Here $Q_1(x)\,dx = e^{-x}dx$ determines the probability of the primary particle interacting at a depth x, x+dx. As a result of this interaction there are formed at depth x two particles with energies $\epsilon = 0.7$ and $\epsilon = 0.1$. $Q_1(x_0 - x)$ determines the probability that a particle with energy $\epsilon = 0.1$ will traverse a distance $x_0 - x$ without interaction;

$$Q_2(x_0 - x) = 1 - (1 + \ldots + (x_0 - x)^5/5!)\exp\{-(x_0 - x)\}$$

determines the probability of a particle with energy $\epsilon = 0.7$ interacting more than five times

along a path $x_0 - x$ and reaching the observation level with energy $\epsilon < 0.1$. $Q_3(x_0 - x) = 1 - Q_1(x_0 - x)$ determines the probability of a particle with energy $\epsilon = 0.1$ interacting at least once and reaching the observation level with $\epsilon < 0.1$. $Q_4(x_0 - x) = 1 - Q_2(x_0 - x)$ is the probability of a particle with $\epsilon = 0.7$ interacting not more than five times along the path $x_0 - x$ and reaching the observation level with an energy $\epsilon > 0.1$.

Analogously, we obtain for $P(2, x_0)$ the expression

$$P(2, x_0) = \int_0^{x_0} Q_1(x) Q_1(x_0 - x) Q_4(x_0 - x)\, dx. \quad (6')$$

Calculating the integrals in (5′) and (6′), we get

$$P(1, x_0) = (2x_0 + x_0^3/2 + x_0^5/6 + x_0^4/24 + x_0^5/120 + x_0^6/720 - 12)\exp(-x_0) + (10x_0 + 4x_0^2 + x_0^3 + x_0^4/6 + x_0^5/60 + 12)\exp(-2x_0), \quad (5)$$

$$P(2, x_0) = 6\exp(-x_0) - (5x_0 + 2x_0^2 + x_0^3/2 + x_0^4/12 + x_0^5/120 + 6)\exp(-2x_0). \quad (6)$$

For the third variant, $P(1, x_0)$ can be written

$$P(1, x_0) = C_7^1 \int_0^{x_0} Q_1(x) Q_1(x_0 - x)[1 - Q_1(x_0 - x)]^6\, dx; \quad (7')$$

Since the interaction of the primary particle at the depth x, x+dx results in the production of seven particles with energy $\epsilon = 0.1$, the probability of at least one of the seven particles traversing a distance $x_0 - x$ without interaction is $C_7^1 Q_1(x_0 - x)$, and the probability that the remaining six particles will interact at least once is $[1 - Q_1(x_0 - x)]^6$. Analogously

$$P(2, x_0) = C_7^2 \int_0^{x_0} Q_1(x) Q_1^2(x_0 - x)(1 - Q_1(x_0 - x))^5\, dx. \quad (8')$$

Here C_7^1 and C_7^2 is the number of combinations of 7 elements one and two at a time.

After calculating the integrals contained in (7′) and (8′), we get

$$P(1, x_0) = (7x_0 - 17.15)\exp(-x_0) \text{ for } \exp(-x_0) \ll 1 \quad (7)$$

$$P(2, x_0) = 3.5\exp(-x_0) \text{ for } \exp(-x_0) \ll 1/6. \quad (8)$$

The value of $P(2, x_0)/[P(1, x_0) + P(2, x_0)]$, calculated at sea level, is found to be 5×10^{-5} and 0.06 for the second and third variants respectively. Thus, this quantity depends more strongly on the type of the elementary act than the ratio of the numbers of nuclear-active particles with energies greater than the given value.*

More detailed calculations of e.a.s. may disclose, apparently, other characteristics that depend strongly on the choice of the elementary act. In particular, various characteristics of the μ-meson component of an extensive atmospheric shower may be disclosed. Thus, the extensive atmospheric shower contains, along with nuclear-active component characteristics that depend little on the type of the elementary act, also characteristics that are quite sensitive to the character of the interaction. A detailed experimental study of these characteristics may yield important data on the elementary act.

[1] Guzhavina, Guzhavin, and Zatsepin, J. Exptl. Theoret. Phys. (U.S.S.R.) **31**, 819 (1956), Soviet Phys. JETP **4**, 690 (1957); V. V. Guzhavin and G. T. Zatsepin, J. Exptl. Theoret. Phys. (U.S.S.R.) **32**, 365 (1957), Soviet Phys. JETP **5**, 312 (1957).

[2] L. D. Landau, Izv. Akad. Nauk SSSR, Ser. Fiz. **17**, 51 (1953).

[3] Vernov, Grigorov, Zatsepin, and Chudakov, Izv. Akad. Nauk SSSR, Ser. Fiz. **19**, 493 (1955), Columbia Tech. Transl. p. 445.

[4] K. P. Ryzhkova and L. I. Sarycheva, J. Exptl. Theoret. Phys. (U.S.S.R.) **28**, 618 (1955), Soviet Phys. JETP 1, 572 (1955). Kaplon, Klose, Ritson, and Walker, Phys. Rev. **91**, 1573 (1953).

[5] I. L. Rozental', Dissertation, Phys. Inst. Acad. Sci. U.S.S.R., Moscow, 1958. N. M. Gerasimova, J. Exptl. Theoret. Phys. (U.S.S.R.) **33**, 637 (1957), Soviet Phys. JETP **6**, 488 (1958).

[6] G. T. Zatsepin, J. Exptl. Theoret. Phys. (U.S.S.R.) **19**, 1104 (1949).

[7] Barret, Bollinger, Cocconi, Eisenberg, and Greisen, Revs. Modern Phys. **24**, 133 (1952).

[8] G. T. Zatsepin, Dissertation, Phys. Inst. Acad. Sci. U.S.S.R., Moscow, 1954. N. L. Grigorov, Dokl. Akad. Nauk SSSR **94**, 835 (1954). G. T. Zatsepin and I. L. Rozental', Dokl. Akad. Nauk SSSR **99**, 369 (1954).

[9] Abrosimov, Dmitriev, Kulikov, Massal'skiĭ, Solov'ev, and Khristiansen, J. Exptl. Theoret. Phys. (U.S.S.R.) **36**, 751 (1959), Soviet Phys. JETP **9**, 528 (1959).

[10] N. L. Grigorov and V. Ya. Shestoperov, J. Exptl. Theoret. Phys. (U.S.S.R.) **34**, 1539 (1958), **33**, 1099 (1957); Soviet Phys. JETP **7**, 1061 (1958), **6**, 848 (1958).

[11] G. Cocconi, Handbuch der Physik **45**, Sec. 17.

Translated by J. G. Adashko
232

*Reference 10 contains the so called "association curves." The association curves are the results of the spectrum of nuclear-active particles in an extensive atmospheric shower and the spectrum of primary particles, and they are therefore not discussed separately in our paper. Let us note that it follows from our calculations that there is no need for introducing two types of elementary acts to explain the association curves.

ANGULAR DISTRIBUTION AND ANGULAR CORRELATION OF THE RADIATIONS FROM NUCLEI WITH ORIENTED ELECTRON SHELLS

V. A. DZHRBASHYAN

Institute of Physics, Academy of Sciences, Armenian S.S.R.

Submitted to JETP editor October 16, 1958

J. Exptl. Theoret. Phys. (U.S.S.R.) **36**, 1240-1245 (April, 1959)

The effect of an oriented electron shell on the angular correlation of nuclear radiations is investigated. The angular distribution due to this effect is obtained.

IF the lifetime of the intermediate nuclear level is not small as compared to the precession period of the nuclear moment in the field of the electron shell, the interaction with the electron shell leads to a redistribution of the m-sublevels of the nucleus; then a "perturbed" correlation of the nuclear radiations is observed.[1]

Alder[2] obtained a formula which takes account of this effect for the case of an electron shell which remains in a stationary state during the nuclear transitions. Later Coester[3] investigated the deviations from the Alder formula for the case when the stationary condition is not satisfied.

Owing to the large magnetic moment the electron shells orient themselves more easily than the nucleus. It is therefore meaningful to consider the effect of the oriented electron shell on the radiation of the nucleus.

In the present paper we investigate the angular correlation of two successive radiations of the nucleus; we study the correlation of the directions as well as the polarization effects with respect to the α, β, and γ rays and the conversion electrons[4] coming from an oriented electron shell. The basic formula for the correlation function is different from that used in the papers of Goertzel[1] and Alder,[2] since the correlation will also depend significantly on the hyperfine structure of the initial level of the nucleus in the presence of an orientation "of the k-th order."

THE CORRELATION FUNCTION

1. We consider the radiation from nuclei whose electron shells are oriented. In general, the correlation function will then depend not only on the directions of the radiations and on their polarizations, but also on the rotational symmetry axis of the total angular momenta of the electron shells η.

The probability for the emission of two rays in the nuclear cascade decay $A \to B \to C$ is given by the expression

$$W = \sum_{\beta\beta'} \mathcal{E}^{(1)}(\beta\beta') E^{(2)}(\beta'\beta), \tag{1}$$

where

$$\mathcal{E}^{(1)}(\beta\beta') = S_1 \sum_{\alpha\alpha'} a(m_{e\alpha}) \frac{(\beta \mid H_1 \mid \alpha)(\alpha \mid \alpha')(\alpha' \mid H_1 \mid \beta')}{1 + (\omega_{\alpha\alpha'}\tau_A)^2}, \tag{1a}$$

$$E^{(2)}(\beta'\beta) = S_2 \sum_{\gamma} \frac{(\beta' \mid H_2 \mid \gamma)(\gamma \mid H_2 \mid \beta)}{1 + (\omega_{\beta\beta'}\tau_B)^2}. \tag{1b}$$

S_i implies summation over all unchanged properties of the i-th radiation ($i = 1, 2$); $\omega_{\alpha\alpha'}$ and τ_A ($\omega_{\beta\beta'}$ and τ_B) give the hyperfine structure and the lifetime of the nuclear level A (B); $a(m_{e\alpha})$ is the probability that the projection of the total angular momentum of the electron shell before the beginning of the decay is $m_{e\alpha}$.

The denominators in (1a) and (1b) can be obtained from the descriptive discussions of Abragam and Pound.[5]

2. We choose η as the axis of quantization z. Then the matrix element $(\beta \mid H_2 \mid \gamma)$ can be written in the form

$$(\beta \mid H_2 \mid \gamma) \equiv (F_b m_b \mid H_2 \mid F_c m_c\, \Omega_2\sigma_2) = \sum_{L_2 M_2 \pi_2} (\Omega_2\sigma_2 \mid L_2 M_2 \pi_2)(F_b m_b \mid H_2 \mid F_c m_c L_2 M_2 \pi_2). \tag{2}$$

Here F_i is the quantum number of the total angular momentum of the nucleus (j_i) and the electron shell (j_e); m_i is the projection of F_i on the z axis. Ω_2 and σ_2 denote the direction and the polarization of the radiation; $(\Omega_2\sigma_2 \mid L_2\, M_2 \mid \pi_2)$ is the wave function of the radiation with a given angular momentum L_2, projection M_2, and parity π_2.

We now go over to the coordinate system of the radiation:

$$(\Omega_2\sigma_2 \mid L_2 M_2 \pi_2) = \sum_{\mu_2 M_2} D^{L_2}_{\mu_2 M_2}(R_2^{-1})(0\,\sigma_2 \mid L_2 \mu_2 \pi_2). \tag{3}$$

$D^{L}_{\mu M}$ is the irreducible representation of the three dimensional rotation group of dimension $2L+1$; R_2^{-1} implies a rotation from the direction of the radiation to the η axis.

We recall that the matrix element

$$(F_b m_b | H_2 | F_c m_c L_2 M_2 \pi_2) = \sum_{m m_2 m_e m'_e} (-1)^{j-l_e+m_b} (2F_b+1)^{1/2} \times \begin{pmatrix} j & l_e & F_b \\ m & m_e & -m_b \end{pmatrix} (jm\, l_e m_e | H_2 | l_2 m_2 l_e m'_e L_2 M_2 \pi_2) (-1)^{l_2-l_e+m_c} \times (2F_c+1)^{1/2} \begin{pmatrix} l_2 & l_e & F_c \\ m_2 & m'_e & -m_c \end{pmatrix}, \quad (4)$$

(where $\begin{pmatrix} \cdots \end{pmatrix}$ is the 3j symbol of Wigner[6]), and assume that the electron shell is stationary during the nuclear transitions. In accordance with the Eckart theorem,[7] this leads to

$$(jm\, l_e m_e | H_2 | l_2 m_2 l_e m'_e L_2 M_2 \pi_2) = (-1)^{L_2-l_2+m} (2j+1)^{1/2} \begin{pmatrix} L_2 & l_2 & j \\ M_2 & m_2 & -m \end{pmatrix} \delta_{m_2 m'_e} (j \| L_2 \| l_2). \quad (5)$$

Then expression (2) can be written as

$$(\beta | H_2 | \gamma) = \sum_{L_2 M_2 \tau_2 \mu_2} (-1)^{-l_2-l_e+L_2+m_b} (j \| L_2 \| l_2) (2j+1)^{1/2} (2F_b+1)^{1/2} \times (2F_c+1)^{1/2} \begin{Bmatrix} F_c & l_e & l_2 \\ j & L_2 & F_b \end{Bmatrix} \begin{pmatrix} F_c & L_2 & F_b \\ m_c & M_2 & -m_b \end{pmatrix} \times (0\sigma_2 | L_2 \mu_2 \pi_2) D^{L_2}_{\mu_2 M_2} (R_2^{-1}), \quad (6)$$

where the curly brackets stand for the 6j symbol of Wigner.[6] Formula (6) also determines

$$(\beta' | H_2 | \gamma) \equiv (F'_b m'_b | H_2 | F_c m_c \sigma'_2 \sigma'_2).$$

Using the properties of the matrix $D^{L}_{\mu M}$ (reference 7) and introducing the notation (y specifies the type of radiation)

$$C_{\nu_2 \tau_2} (L_2 L'_2 \pi_2 y) \equiv S_2 \sum_{\mu_2 \mu'_2} (-1)^{L_2+\mu_2} (2\nu_2+1)^{1/2} \times \begin{pmatrix} L_2 & L'_2 & \nu_2 \\ \mu_2 & -\mu'_2 & -\tau_2 \end{pmatrix} (0\sigma_2 | L_2 \mu_2 \pi_2)^* (0\sigma'_2 | L'_2 \mu'_2 \pi'_2), \quad (7)$$

we now apply the formulas for the contraction of the 3j and 6j symbols of Wigner. In the end we obtain for the density matrix

$$E^{(2)}(\beta'\beta) = \sum_{\substack{L_2 L'_2 \pi_2 \\ \nu_2 \rho_2 \tau_2}} (-1)^{j_2-l_e+L_2+F_b+F'_b+m_b} (j \| L'_2 \| j_2) \times (j \| L_2 \| j_2)^* (2j+1) (2\nu_2+1)^{1/2} \frac{(2F_b+1)^{1/2} (2F'_b+1)^{1/2}}{1+(\omega_{F_b F'_b} \tau_B)^2} \quad (8)$$

$$\times \begin{Bmatrix} j & l & \nu_2 \\ L'_2 & L_2 & j_2 \end{Bmatrix} \begin{Bmatrix} j & l & \nu_2 \\ F'_b & F_b & l_e \end{Bmatrix} \begin{pmatrix} F'_b & F_b & \nu_2 \\ m'_b & -m_b & \rho_2 \end{pmatrix} C_{\nu_2 \tau_2} (L_2 L'_2 \pi_2 y) D^{\nu_2^*}_{\tau_2 \rho_2} (R_2^{-1}).$$

3. The density matrix for the first transition is given by expression (1a).

Repeating the calculations of Sec. 2, we find

$$(\alpha | H_1 | \beta) = \sum_{\substack{L_1 M_1 \pi_1 \\ \mu_1 m_a m}} (-1)^{2l_e+l_1+L_1+m_b+m_a+m_1} (j_1 \| L_1 \| j) \times (2F_a+1)^{1/2} (2F_b+1)^{1/2} \begin{pmatrix} j_1 & l_e & F_a \\ m_1 & m_e & -m_a \end{pmatrix} \begin{pmatrix} L_1 & j & j_1 \\ M_1 & m & -m_1 \end{pmatrix} \times \begin{pmatrix} j & l_e & F_b \\ m & m_e & -m_b \end{pmatrix} (0\sigma_1 | L_1 \mu_1 \pi_1) D^{L_1}_{\mu_1 M_1} (R_1^{-1}), \quad (9)$$

where R_1^{-1} implies the rotation from the direction of the first radiation to the η axis, and

$$\mathcal{E}^{(1)}(\beta\beta') = \sum_{\substack{L_1 L'_1 \pi_1 \\ \nu_1 F_a F'_a}} (-1)^{2l_e+L'_1} (j_1 \| L'_1 \| j) (j_1 \| L_1 \| j) \times (2\nu_1+1)^{1/2} (2F_b+1)^{1/2} (2F'_b+1)^{1/2} \frac{(2F_a+1)(2F'_a+1)}{1+(\omega_{F_a F'_a} \tau_A)^2} \times \sum (-1)^{m_1+m'_1+M_1+m_2+m'_b} a m'_e \begin{pmatrix} j_1 & l_e & F'_a \\ m'_1 & m'_e & -m'_a \end{pmatrix} \begin{pmatrix} j_1 & l_e & F_a \\ m'_1 & m'_e & -m_a \end{pmatrix} \times \begin{pmatrix} j_1 & l_e & F'_a \\ m_1 & m_e & -m'_a \end{pmatrix} \begin{pmatrix} j & l_e & F'_b \\ m' & m'_e & -m'_b \end{pmatrix} \begin{pmatrix} j & l_e & F_b \\ m & m_e & -m_b \end{pmatrix} \times \begin{pmatrix} L'_1 & j & j_1 \\ M'_1 & m' & -m'_1 \end{pmatrix} \begin{pmatrix} L_1 & j & j_1 \\ M_1 & m & -m_1 \end{pmatrix} \begin{pmatrix} L_1 & L'_1 & \nu_1 \\ M_1 & -M'_1 & -\rho_1 \end{pmatrix} \times C_{\nu_1 \tau_1} (L_1 L'_1 \pi_1 x) D^{\nu_1^*}_{\tau_1 \rho_1} (R_1^{-1}). \quad (10)$$

The internal sum in (10) goes over the magnetic numbers m, m_1, m_e, m', m'_1, m'_e, m''_1, m''_e, M_1, M'_1, ρ_1, τ_1, m_a, and m'_a. The summation over the first six of these numbers is easily performed.

In order to apply Racah's formula for the contraction of the 3j symbols of Wigner in the sum

$$\sum_{M_1 M'_1} (-1)^{M_1} \begin{pmatrix} F_b & L_1 & F_a \\ m_b & M_1 & -m_a \end{pmatrix} \begin{pmatrix} F'_b & L'_1 & F'_a \\ m'_b & M'_1 & -m'_a \end{pmatrix} \begin{pmatrix} L_1 & L'_1 & \nu_1 \\ M_1 & -M'_1 & -\rho_1 \end{pmatrix},$$

which can also be written as

$$\sum_{M_1 M'_1 m''_b \rho} (-1)^{M_1} \begin{pmatrix} F_b & L_1 & F_a \\ -m''_b & M_1 & -m_a \end{pmatrix} \begin{pmatrix} F'_b & L'_1 & F'_a \\ m''_b & M'_1 & -m'_a \end{pmatrix} \times \begin{pmatrix} L_1 & L'_1 & \nu_1 \\ M_1 & -M'_1 & \rho \end{pmatrix} \delta_{-m_b m''_b} \delta_{m'_b m''_b} \delta_{-\rho_1 \rho}, \quad (11)$$

we replace the Kronecker symbols by the expressions

$$\delta_{m'_b m''_b} \delta_{-\rho_1 \rho} = \sum_{l x \lambda} \delta_{x\lambda} (2l+1) \begin{pmatrix} F'_b & \nu_1 & l \\ m''_b & \rho & -\lambda \end{pmatrix} \begin{pmatrix} F'_b & \nu_1 & l \\ m'_b & -\rho_1 & -x \end{pmatrix};$$

$$\delta_{-m_b m''_b} \delta_{x\lambda} = \sum_{k\sigma} (2k+1) \begin{pmatrix} F_b & l & k \\ m'_b & \lambda & -\sigma \end{pmatrix} \begin{pmatrix} F_b & l & k \\ -m_b & x & -\sigma \end{pmatrix}. \quad (12)$$

4. We further introduce the 9j symbol of Wigner,[6]

$$\begin{Bmatrix} F_b & L_1 & F_a \\ F_b' & L_1' & F_a' \\ \nu_2 & \nu_1 & k \end{Bmatrix} = \sum_l (-1)^{2l} \begin{Bmatrix} \nu_2 & F_b & F_b' \\ l & \nu_1 & k \end{Bmatrix} \begin{Bmatrix} F_a' & L_1' & F_b' \\ \nu_1 & l & L_1 \end{Bmatrix} \begin{Bmatrix} F_a & F_b & L_1 \\ l & F_a' & k \end{Bmatrix}, \quad (13)$$

and obtain for the correlation function, using the unitarity of the representation $D^{\nu}_{\tau\rho}$,

$$W = \sum (-1)^{j_1+j_2+L_2+F_a-F_b} (j_1 \| L_1 \| j)\,(j_1 \| L_1' \| j)\,(j \| L_2 \| j_2)\,(j \| L_2' \| j_2) \times C_{\nu_1\tau_1}(L_1 L_1' \pi_1 x)\, C_{\nu_2\tau_2}(L_2 L_2' \pi_2 y)\,(2j+1)\,(2\nu_1+1)^{1/2}(2\nu_2+1)^{1/2} \times (2k+1)^{1/2} \frac{(2F_a+1)\,(2F_a'+1)}{[1+(\omega_{F_a F_a'}\tau_A)^2][1+(\omega_{F_b F_b'}\tau_B)^2]} \begin{Bmatrix} j & j & \nu_1 \\ L_2 & L_2' & j_2 \end{Bmatrix} \times \begin{Bmatrix} j & j & \nu_2 \\ F_b & F_b' & j_e \end{Bmatrix} \begin{Bmatrix} L_1 & F_a & F_b \\ j_e & j & j_1 \end{Bmatrix} \begin{Bmatrix} L_1' & F_a' & F_b' \\ j_e & j & j_1 \end{Bmatrix} \begin{Bmatrix} k & F_a & F_a' \\ j_1 & j_e & j_e \end{Bmatrix} \times \begin{Bmatrix} F_b & L_1 & E_a \\ F_b' & L_1' & F_a' \\ \nu_2 & \nu_1 & k \end{Bmatrix} \langle |(j_e j_e) k0\rangle \begin{pmatrix} \nu_1 & \nu_2 & k \\ \rho & -\rho & 0 \end{pmatrix} D^{\nu_1}_{\rho\tau_1}(R_1)\, D^{\nu_2}_{-\rho\tau_2}(R_2), \quad (14)$$

where the summation goes over the corresponding quantum numbers; $\nu_1 + \nu_2 + k$ is an even number. $\langle |(j_e j_e) k0\rangle$ is the statistical tensor of Fano, which is proportional to

$$\langle |(j_e j_e) k0\rangle = \sum_{m_e} (-1)^{j_e - m_e} (2k+1)^{1/2} \begin{pmatrix} j_e & j_e & k \\ m_e & -m_e & 0 \end{pmatrix} a(m_e) = \begin{pmatrix} 2k \\ k \end{pmatrix} j_e^k \left[\frac{(2j_e+k+1)!}{(2k+1)\,(2j_e-k)!}\right]^{-1/2} j_k(j_e). \quad (15)$$

The matrix elements in (14) are chosen to be real, which is always possible[4] in view of the invariance under time reversal. This leads to the following normalization for the correlation function (14):*

$$(8\pi^2)^{-2} \int W\, d\Omega_1\, d\Omega_2\, d\chi_1\, d\chi_2 = \sum_{L_1 L_2} (j_1 \| L_1 \| j)^2\, (j \| L_2 \| j_2)^2. \quad (16)$$

The radiation parameters $C_{\nu\tau}(LL'\pi x)$ are given by Biedenharn and Rose.[4] Alder, Stech, and Winther[8] calculated these parameters for β decay including the possibility of parity non-conservation.

For $(\omega_{F_a F_a'}\tau_A)^2 \ll 1$, we sum over F_a and F_a' in (14) and obtain

$$W = \sum (-1)^{j_1+j+j_2+L_2+L_1'+L_2+j_e+F_b+\nu_2} (j_1 \| L_1 \| j)\,(j_1 \| L_1' \| j) \times (j \| L_2 \| j_2)\,(j \| L_2' \| j_2)\, C_{\nu_1\tau_1}(L_1 L_1' \pi_1 x)\, C_{\nu_2\tau_2}(L_2 L_2' \pi_2 y)\,(2j+1) \times (2\nu_1+1)^{1/2}(2\nu_2+1)^{1/2}(2k+1)^{1/2} \begin{Bmatrix} j & j & \nu_1 \\ L_1 & L_1' & j_1 \end{Bmatrix} \begin{Bmatrix} j & j & \nu_2 \\ L_2 & L_2' & j_2 \end{Bmatrix} \times \frac{(2F_b+1)\,(1F_b'+1)}{1+(\omega_{F_b F_b'}\tau_B)^2} \begin{Bmatrix} j & j & \nu_2 \\ F_b & F_b' & j_e \end{Bmatrix} \begin{Bmatrix} \nu_2 & k & \nu_1 \\ F_b & j_e & j \\ F_b' & j_e & j \end{Bmatrix} \langle |(j_e j_e) k0\rangle \times \begin{pmatrix} \nu_1 & \nu_2 & k \\ \rho & -\rho & 0 \end{pmatrix} D^{\nu_1}_{\rho\tau_1}(R_1)\, D^{\nu_2}_{-\rho\tau_2}(R_2). \quad (17)$$

If $(\omega_{F_b F_b'}\tau_B)^2 \ll 1$, expression (17) does not depend on the orientation of the electron shell, as was to be expected. It coincides in this case with the correlation function for the radiations from isolated nuclei:

$$W = \sum (-1)^{j_1-j_2+L_1'+L_2+\nu} (j_1 \| L_1 \| j)\,(j_1 \| L_1' \| j)\,(j \| L_2 \| j_2)\,(j \| L_2' \| j_2) \times (2j+1) \begin{Bmatrix} j & j & \nu \\ L_1 & L_1' & j_1 \end{Bmatrix} \begin{Bmatrix} j & j & \nu \\ L_2 & L_2' & j_2 \end{Bmatrix} C_{\nu\tau_1}(L_1 L_1' \pi_1 x)\, C_{\nu\tau_2} \times (L_2 L_2' \pi_2 y)\, D^{\nu}_{-\tau_2\tau_1}(R_2^{-1} R_1). \quad (18)$$

If the total angular momenta of the electron shells are randomly distributed [i.e., $a(m_e) = \text{const}$], (14) goes over into an expression which differs from (18) by the reducing factor

$$\sum_{F_b F_b'} \frac{(2F_b+1)\,(2F_b'+1)}{(2j_e+1)\,[1+(\omega_{F_b F_b'}\tau_B)^2]} \begin{Bmatrix} j & j & \nu \\ F_b & F_b & j_e \end{Bmatrix}^2$$

under the summation sign.*

5. It has been known that any interaction of the nucleus with the external field leads to a decrease in the anisotropy; in the limiting case $(\omega\tau)^2 \gg 1$ only the "hard core" remains.[9] The explanation for this has been that the external field leads to a redistribution of the m-sublevels in the intermediate state such that their population becomes more uniform.

It is seen from the example of the well-studied γ-γ cascade $^7/_2\,(1,2)\,^5/_2\,(2)\,^1/_2$ in Cd^{111} that the orientation of the shell leads to a weakening of this effect.

To obtain maximal anisotropy, we place the axis of orientation in (17) in the direction of the first quantum. Substituting the value $j_e = {}^3/_2$ for the total angular momentum of the electron shell, we obtain for the anisotropy:

$$A_{\text{unperturbed}} = -0.247; \quad A_{\text{unoriented}} = -0.103; \quad A_{\text{fully oriented}} = -0.149.$$

It turns out that in some cases the interaction between the nucleus and the oriented shell can lead to an increase of the anisotropy as compared to the case of an isolated nucleus. For example, using the same assumptions for the γ-γ cascade $^7/_2\,(1)\,^5/_2\,(2)\,^1/_2$, we obtain

*The rotation is defined by the Eulerian angles, φ, θ, and χ; the element of solid angle in the direction of the radiation is $d\Omega = \sin\theta\, d\theta d\varphi$; χ defines its transverse polarization.

*This is Alder's result.[2]

$$A_{\text{unperturbed}} = -0.1034; \quad A_{\text{unoriented}} = -0.0417; \quad A_{\text{fully oriented}} = -0.1557.$$

This can be explained in the following fashion. In the intermediate state the system nucleus + shell tends toward equilibrium. If the sublevels of the electron shell m_e are not uniformly populated, the non-uniformity of the population of the m-sublevels of the nucleus can be increased through the interaction.

ANGULAR DISTRIBUTION

Integrating (14) over $d\Omega_2 d\chi_2$, we obtain the angular distribution of the nuclear radiation:

$$W = \sum (-1)^{-j_1-j-L_1+F_a-F_a'-k} (j_1 \| L_1 \| j)(j_1 \| L_1' \| j)$$
$$\times C_{k\tau_1}(L_1 L_1' \pi_1 \pi) \frac{(2F_a+1)(2F_a'+1)}{1+(\omega_{F_a F_a'}\tau_A)^2} \begin{Bmatrix} L_1 & L_1' & k \\ j_1 & j_1 & j \end{Bmatrix} \begin{Bmatrix} F_a & F_a' & k \\ j_e & j_e & j_1 \end{Bmatrix}$$
$$\times \begin{Bmatrix} F_a & F_a' & k \\ j_1 & j_1 & j_e \end{Bmatrix} \langle (j_e j_e) k 0 \rangle D^k_{0\tau_1}(R_1). \qquad (19)$$

Expression (19) is normalized according to the condition

$$\frac{1}{4\pi} \int W \sin\theta \, d\theta \, d\chi = \sum (j_1 \| L_1 \| j)^2. \qquad (20)$$

It is seen from (19) that the distribution becomes isotropic if either the lifetime of the initial state is much smaller than the precession period of the nuclear moment in the field of the electron shell [$(\omega\tau_A)^2 \ll 1$], or the electron shell is not oriented [$f_k(j_e) = \delta_{k0}$].

If the transition under consideration is preceded by others, one must take into account the disorientation of the electron shell in these transitions. The corresponding expression for one such transition is obtained from (14) by integrating over $d\Omega_1 d\chi_1$.

In conclusion the author expresses his gratitude to K. A. Ter-Martirosyan for interest in this work.

[1] G. Goertzel, Phys. Rev. **70**, 897 (1946).
[2] K. Alder, Helv. Phys. Acta **25**, 235 (1952).
[3] F. Coester, Phys. Rev. **93**, 1304 (1954).
[4] L. C. Biedenharn and M. E. Rose, Revs. Modern Phys. **25**, 729 (1953).
[5] A. Abragam and R. V. Pound, Phys. Rev. **92**, 943 (1953).
[6] H. A. Jahn and J. Hope, Phys. Rev. **93**, 318 (1953).
[7] M. E. Rose, Multipole Fields, John Wiley and Sons, N. Y., 1955.
[8] Alder, Stech, and Winther, Phys. Rev. **107**, 728 (1957).
[9] M. Steffen, Adv. in Phys. **4**, 293 (1955).

Translated by R. Lipperheide
233

SOVIET PHYSICS JETP VOLUME 36 (9), NUMBER 4 OCTOBER, 1959

THE BASIC COMPENSATION EQUATION IN SUPERCONDUCTIVITY THEORY WHEN THE COULOMB INTERACTION IS TAKEN INTO ACCOUNT

CHEN CHUN-SIAN and CHOW SHIH-HSUN

Moscow State University

Submitted to JETP editor October 17, 1958

J. Exptl. Theoret. Phys. (U.S.S.R.) **36**, 1246-1253 (April, 1959)

Fröhlich's model is studied by the Bogolyubov method taking the Coulomb interaction into account. A partial summation of the perturbation theory series is performed by approximate second quantization in order to eliminate the infrared divergence. The basic compensation equation for dangerous diagrams and an expression for the renormalized single fermion excitation energy for the case when the Coulomb interaction is taken into account are obtained in explicit form as a result and are discussed.

1. INTRODUCTION

THE authors of recent papers on the microscopic theory of superconductivity have started from Fröhlich's model in which the Coulomb interaction between the electrons is not taken into account. At the same time it is undoubtedly impossible to assume the Coulomb repulsion to be small in real metals and the expediency of this essential simplification can only be discussed as the result of a detailed analysis of the consequences of Fröhlich's model, taking the Coulomb interaction explicitly into account. It is, however, perfectly obvious that in order to establish a criterion for the occurrence of superconductivity it is necessary to take the Coulomb interaction explicitly into account in Fröhlich's model as the principal competing factor with the electron-phonon interaction which makes the superconducting state, as is well known, the energetically more favorable. In other words, if the Coulomb effects are not taken into account, all metals described by the Fröhlich model will be superconductors which is in contradiction with the experimental facts. Bardeen, Cooper, and Schrieffer,[1] evading a mathematical consideration of this problem, assumed that a necessary condition for the occurrence of superconductivity in a given metal is the predominance of the interelectronic attraction caused by the electron-phonon interaction over the Coulomb repulsion (as an average effect in a well defined region of momentum space).

A mathematically rigorous consideration of the influence of the Coulomb interaction on superconductivity was given in the monograph by Bogolyubov, Tolmachev, and Shirkov.[2] A qualitative analysis shows that the criterion proposed in reference 1 does not correspond to reality and that the influence of the Coulomb interaction is appreciably weakened due to the collective interaction.

In the present paper we shall be engaged in a detailed investigation of the basic compensation equation, in particular of the expansion of the kernel of this integral equation in the region of the infrared divergence.

It is then essential to use a method of approximate second quantization to sum a special class of diagrams. Such a method was worked out by Bogoyubov, Tolmachev and Tyablikov and used by the authors in reference 3 to investigate the energy spectrum of a high density electron gas.

2. THE BASIC COMPENSATION EQUATION OF DANGEROUS DIAGRAMS

We start with an investigation of a dynamic system with the Hamiltonian of the Fröhlich model in the usual form, supplemented by the Coulomb interaction energy H_C:

$$H = \sum_{ks} (E(k) - \lambda) a_{ks}^+ a_{ks} + \sum_{|q|<q_D} \omega(q) b_q^+ b_q + H_{ph} + H_c, \quad (1)$$

where

$$H_{ph} = \sum_{\substack{kqs \\ k'-k=q}} (g^2 \omega(q)/2\Omega)^{1/2} [a_{ks}^+ a_{k's} b_q^+ + a_{k's}^+ a_{ks} b_q],$$

$$H_c = \sum_{\substack{pp'q \\ ss'}} \frac{v(q)}{2\Omega} a_{p+q,s}^+ a_{p'-q,s'}^+ a_{p's'} a_{ps},$$

a_{ks}^+ and a_{ks} are the creation and annihilation operators of an electron of momentum k and

spin s; $b_{\mathbf{q}}^{+}$ and $b_{\mathbf{q}}$ the creation and annihilation operators of a phonon with momentum $\mathbf{q}$, $\omega(q)$ and $E(k)$ the energy eigenvalues of the phonon and the electron respectively, λ the chemical potential, g the coupling constant, Ω the normalizing volume, and $\nu(q)$ the repulsive Coulomb potential in momentum representation.

One must note that the mathematical treatment of the Hamiltonian (1) is a very complicated problem. It is well known that the first convincing results for the Fröhlich model (without the term H_C) was obtained only recently in the well known paper of Bogolyubov's[4] thanks to a treatment by a new methematical method: "the principle of the compensation of dangerous diagrams." For an electron gas with a purely Coulomb interaction the situation is no less complicated and only recently has considerable success been achieved in the high-density approximation.[5]

According to the present-day formalism of perturbation theory the quantities characterizing any dynamical system can be constructed by means of the operator $R(E)$ only:

$$R(E) = H_{int} + H_{int}\frac{1}{E - H_0}H_{int} + \ldots \qquad (2)$$

We have, for instance, for the ground state energy and the energy of a one-fermion excitation

$$\begin{aligned} E_0 &= E(\Phi_V) + \Delta E, \quad E(k), \\ &= (E(\Phi_1) - E(\Phi_V)) + \bar{E}(k), \end{aligned} \qquad (3)$$

where

$$\Delta E = \langle \Phi_V | R(E(\Phi_V)) | \Phi_V \rangle_C, \quad \bar{E} = \langle \Phi_1 | R(E(\Phi_1)) | \Phi_1 \rangle_C;$$

$E(\Phi_V)$ and $E(\Phi_1)$ are respectively the energy of the ground state Φ_V and the energy of the one-particle excitation Φ_1 when there is no interaction. The index C indicates that in the averaging only connected diagrams are taken into account.

The basic difficulty is that the equations of the usual perturbation theory (3) do not give correct results if applied to the Hamiltonian (1) for two reasons. Firstly, the electron-phonon interaction, however small, is very important near the Fermi surface and changes the structure of the energy spectrum. Furthermore, as far as the Coulomb interaction is concerned, the different terms of the perturbation theory series diverge in the infrared region. The physical crux of such a situation was analyzed carefully in Bohm and Pines' papers on plasma theory. In references 3 and 5 rigorous mathematical methods were developed to overcome this difficulty in the high density approximation which essentially consists of a partial summation of the infinite series (3). In the present paper we shall overcome both difficulties mentioned.

Following the basic idea of Bogolyubov's[4] we shall first of all perform a canonical transformation in the Hamiltonian

$$a_{\mathbf{k}\,1/2} = u_{\mathbf{k}}\alpha_{\mathbf{k}0} + v_{\mathbf{k}}\alpha_{\mathbf{k}1}^{+}, \quad a_{-\mathbf{k}-1/2} = u_{\mathbf{k}}\alpha_{\mathbf{k}1} - v_{\mathbf{k}}\alpha_{\mathbf{k}0}^{+},$$
$$u_{\mathbf{k}}^2 + v_{\mathbf{k}}^2 = 1. \qquad (4)$$

The transformed Hamiltonian can be written in the form

$$H = U + H_0 + H_{ph} + H_c + H', \qquad (5)$$

where

$$U = 2\sum_{\mathbf{k}}(E(k) - \lambda)v_{\mathbf{k}}^2;$$

$$H_0 = \sum_{\mathbf{k}}\tilde{\varepsilon}(k)[\alpha_{\mathbf{k}0}^{+}\alpha_{\mathbf{k}0} + \alpha_{\mathbf{k}1}^{+}\alpha_{\mathbf{k}1}] + \sum_{\mathbf{q}}\omega(q)b_{\mathbf{q}}^{+}b_{\mathbf{q}};$$

$$H_{ph} = \sum_{\substack{\mathbf{kq}\\ \mathbf{k}'-\mathbf{k}=\mathbf{q}}}(g^2\omega(q)/2\Omega)^{1/4}(b_{\mathbf{q}}^{+} + b_{-\mathbf{q}})[M^{+}(\mathbf{k},\mathbf{k}')(\alpha_{\mathbf{k}0}^{+}\alpha_{\mathbf{k}'1}^{+} + \alpha_{\mathbf{k}1}\alpha_{\mathbf{k}'0}) + M^{-}(\mathbf{k},\mathbf{k}')(\alpha_{\mathbf{k}0}^{+}\alpha_{\mathbf{k}'0} + \alpha_{\mathbf{k}1}^{+}\alpha_{\mathbf{k}'1})];$$

$$H' = \sum_{\mathbf{k}}[(E(k) - \lambda)(u_{\mathbf{k}}^2 - v_{\mathbf{k}}^2) - \tilde{\varepsilon}(k)](\alpha_{\mathbf{k}0}^{+}\alpha_{\mathbf{k}0} + \alpha_{\mathbf{k}1}^{+}\alpha_{\mathbf{k}1}) + 2\sum_{\mathbf{k}}(E(k) - \lambda)u_{\mathbf{k}}v_{\mathbf{k}}(\alpha_{\mathbf{k}0}^{+}\alpha_{\mathbf{k}1}^{+} + \alpha_{\mathbf{k}1}\alpha_{\mathbf{k}0});$$

$$M^{+}(\mathbf{k},\mathbf{k}') = u_{\mathbf{k}'}v_{\mathbf{k}} + u_{\mathbf{k}}v_{\mathbf{k}'}, \quad M^{-}(\mathbf{k},\mathbf{k}') = u_{\mathbf{k}}u_{\mathbf{k}'} - v_{\mathbf{k}}v_{\mathbf{k}'}.$$

The transformed H_1 is a quartic expression in the Fermi operators $\alpha_{\mathbf{ks}}^{+}$, $\alpha_{\mathbf{ks}}$ with coefficients depending on $u_{\mathbf{k}}$ and $v_{\mathbf{k}}$.

Applying perturbation theory to the Hamiltonian (5) we get a series which contains divergences of two kinds. All terms which contain "vacuum-two fermion" type matrix elements diverge logarithmically near the Fermi surface. To overcome this difficulty the canonical transformation (4) was developed as well as the principle of the compensation of dangerous diagrams according to which we may put these "dangerous" terms equal to zero by an appropriate choice of the $u_{\mathbf{k}}$ and $v_{\mathbf{k}}$, namely by determining them from the equation

$$\langle \alpha_{\mathbf{k}_1} \alpha_{\mathbf{k}_0} R(0) \rangle = 0. \tag{6}$$

The renormalized fermion energy $\tilde{\epsilon}$ is determined from the condition that the radiative correction vanishes

$$\langle \alpha_{\mathbf{k}_0} R(\tilde{\epsilon}(k)) \alpha^+_{\mathbf{k}_0} \rangle = 0. \tag{7}$$

Equation (6) is the formal writing down of the basic compensation equation. It can, however, not be analyzed as long as $R(0)$ is in the form of an infinite series with divergent terms connected with the scattering by a Coulomb potential in the long-wavelength region. In the following we shall follow an idea of Gell-Mann and Brueckner and sum the most divergent terms of the series (6). This procedure enables us to remove the infrared divergence noted above and to evaluate accurately the main terms in the regular expansion in the dimensionless parameter $r_s = r_0/a$, where $r_0 = (4\pi N/3\Omega)^{-1/3}$ and a is the Bohr radius (r_s is small for high densities). This program can be carried out without special difficulties is the momentum $\mathbf{k}$ in Eqs. (6) and (7) corresponds to an energy $\tilde{\epsilon}(\mathbf{k}) \sim 0$. This assumption is perfectly legitimate, although it is not completely obvious that the expansion parameter is small, since, just in the immediate neighborhood of the Fermi surface where $\tilde{\epsilon}(\mathbf{k}) \sim 0$ the "vacuum-two fermion" type matrix elements become "dangerous." It follows therefore from the idea of the compensation of dangerous diagrams itself that we should investigate only the asymptotic behavior of Eq. (6) for $\tilde{\epsilon}(\mathbf{k}) \sim 0$.

Moreover, Eqs. (6) and (7) can, according to Shirkov's investigation (see reference 2), be written for $\tilde{\epsilon}(\mathbf{k}) \sim 0$ in the form

$$\langle \alpha_{\mathbf{k}_1} \alpha_{\mathbf{k}_0} R \rangle_c = 2\xi(k)\, u_{\mathbf{k}} v_{\mathbf{k}}$$
$$- (u^2_{\mathbf{k}} - v^2_{\mathbf{k}}) \sum_{\mathbf{k}'} Q(\mathbf{k}, \mathbf{k}')\, u_{\mathbf{k}'} v_{\mathbf{k}'} = 0, \tag{6'}$$

$$\langle \alpha_{\mathbf{k}_0} R \alpha_{\mathbf{k}_0} \rangle_c = \tilde{\epsilon}(k) - (u^2_{\mathbf{k}} - v^2_{\mathbf{k}})\, \xi(k)$$
$$- 2 u_{\mathbf{k}} v_{\mathbf{k}} \sum_{\mathbf{k}'} Q(\mathbf{k}, \mathbf{k}')\, u_{\mathbf{k}'} v_{\mathbf{k}'} = 0. \tag{7'}$$

We shall here not give the complicated formal expressions for $Q(\mathbf{k}, \mathbf{k}')$ and $\xi(\mathbf{k})$ in terms of variational derivatives with respect to Fermi amplitudes which were obtained in reference 2, since in the following we shall obtain explicit expressions for them using the simpler method of approximate second quantization.

Rigorously following a previous paper by the present authors[3] we shall write down the model Hamiltonian*

*In Wentzel's paper[6] a model Hamiltonian was considered which differed from (8) only in that there $(u_{\mathbf{k}}, v_{\mathbf{k}})$ everywhere took the trivial values (0,1).

$$\tilde{H} = \sum_{pq} \tilde{\omega}(p, q)\, B^+_{\mathbf{p}}(\mathbf{q})\, B_{\mathbf{p}}(\mathbf{q}) + \sum_{\mathbf{q}} \omega(q)\, b^+_{\mathbf{q}} b_{\mathbf{q}}$$
$$+ \sum_{\mathbf{p}\mathbf{p}'\mathbf{q}} (v(q)/2\Omega)\, [M^*(\mathbf{p}, \mathbf{p}+\mathbf{q})\, M^*(\mathbf{p}', \mathbf{p}'-\mathbf{q})$$
$$\times (B^+_{\mathbf{p}}(\mathbf{q})\, B^+_{\mathbf{p}'}(-\mathbf{q}) + B_{\mathbf{p}}(\mathbf{q})\, B_{\mathbf{p}'}(-\mathbf{q})) + 2M^*(\mathbf{p}, \mathbf{p}+\mathbf{q})\, M^*$$
$$\times (\mathbf{p}', \mathbf{p}'+\mathbf{q})\, B^+_{\mathbf{p}}(\mathbf{q})\, B_{\mathbf{p}}(\mathbf{q})] + \sum (g^2 \omega_q / 2\Omega)^{1/2} M^*(\mathbf{p}, \mathbf{p}+\mathbf{q})$$
$$\times [B^+_{\mathbf{p}}(\mathbf{q})\, (b^+_{-\mathbf{q}} + b_{\mathbf{q}}) + B_{\mathbf{p}}(\mathbf{q})\, (b_{-\mathbf{q}} + b^+_{\mathbf{q}})],$$

$$\omega(\mathbf{p}, \mathbf{q}) = \tilde{\epsilon}(\mathbf{p}+\mathbf{q}) + \tilde{\epsilon}(\mathbf{p}), \tag{8}$$

where $B^+_{\mathbf{p}}(\mathbf{q})$, $B_{\mathbf{p}}(\mathbf{q})$ are the Bose-amplitudes corresponding to the indecomposable complexes $\alpha^+_{\mathbf{p}+\mathbf{q},0}\, \alpha^+_{\mathbf{p}1}$. A rigorous solution of the problem with the Hamiltonian (8) is equivalent to a summation of all diagrams in which the electron-hole complex is not broken up (see the figure). The

←: electron, →: hole, wavy line: phonon

coefficients are chosen in such a way that the energy denominators and vertex parts in the model problem correspond to the corresponding elements in the summed diagrams of the exact problem. If $g^2 = 0$ and $(u_{\mathbf{k}}, v_{\mathbf{k}}) = (0, 1)$ the Hamiltonian $\tilde{H}$ goes over into the model Hamiltonian[3] for an electron gas with Coulomb interactions.

It is well known that the diagonalization of $\tilde{H}$ leads to the solution of a system of homogeneous linear equations for the functions $\varphi_{\mathbf{pq}}$ and $\alpha_{\mathbf{pq}}$, $\lambda_{\mathbf{q}}$ and $\mu_{\mathbf{q}}$:

$$(\tilde{\omega}(p\, q) + E)\ \chi_{\mathbf{pq}}$$
$$+ \frac{v(q)}{\Omega} M^*(\mathbf{p}, \mathbf{p}+\mathbf{q}) \sum_{\mathbf{p}'} [M^*(\mathbf{p}', \mathbf{p}'-\mathbf{q})\, \varphi_{\mathbf{p}', -\mathbf{q}}$$
$$+ M^*(\mathbf{p}, \mathbf{p}'+\mathbf{q})\, \chi_{\mathbf{p}', \mathbf{q}}]$$
$$+ (g^2 \omega_q / 2\Omega)^{1/2} M^*(\mathbf{p}, \mathbf{p}+\mathbf{q})\, (\lambda_{-\mathbf{q}} + \mu_{\mathbf{q}}) = 0,$$

$$(\tilde{\omega}(p, q) - E)\, \chi_{\mathbf{p}, \mathbf{q}}$$
$$+ \frac{v(q)}{\Omega} M^*(\mathbf{p}, \mathbf{p}+\mathbf{q}) \sum_{\mathbf{p}'} [M^*(\mathbf{p}', \mathbf{p}'-\mathbf{q})\, \chi_{\mathbf{p}', -\mathbf{q}}$$
$$+ M^*(\mathbf{p}', \mathbf{p}'+\mathbf{q})\, \varphi_{\mathbf{p}', \mathbf{q}}]$$
$$+ (g^2 \omega_q / 2\Omega)^{1/2} M^*(\mathbf{p}, \mathbf{p}+\mathbf{q})\, (\lambda_{\mathbf{q}} + \mu_{-\mathbf{q}}) = 0,$$

$$(\omega_q + E)\, \mu_{\mathbf{q}} + (g^2 \omega_q / 2\Omega)^{1/2} \sum_{\mathbf{p}'} (M^*(\mathbf{p}, \mathbf{q})\, \chi_{\mathbf{p}', \mathbf{q}}$$
$$+ M^*(\mathbf{p}', -\mathbf{q})\, \varphi_{\mathbf{p}', -\mathbf{q}}) = 0,$$

$$(\omega_q - E)\, \lambda_{\mathbf{q}} + (g^2 \omega_q / 2\Omega)^{1/2} \sum_{\mathbf{p}'} (M^*(\mathbf{p}', \mathbf{q})\, \varphi_{\mathbf{p}', \mathbf{q}}$$
$$+ M^*(\mathbf{p}', -\mathbf{q})\, \chi_{\mathbf{p}', -\mathbf{q}} = 0. \tag{9}$$

To determine the matrix element (7) we apply the "procedure of redefining the vacuum" developed in reference 3. We shall define two "vacuum functions" Φ_V, Φ'_V for the fermions α_{ps} and α'_{ps} respectively

$$\alpha_{ps}|\Phi_V\rangle = 0, \qquad \alpha'_{ps}|\Phi'_V\rangle = 0,$$

where

$$\alpha'_{p0} = \alpha_{p0}(1-\delta_{pk}) + \alpha^+_{p1}\delta_{pk}, \qquad \alpha'_{p1} = \alpha_{p1}(1-\delta_{pk}) - \alpha^+_{p0}\delta_{pk}.$$

The Fermi amplitudes a^+_{ps}, a_{ps} are expressed in terms of α'_{p0}, α'_{p1} by the equations

$$a_{p\,1/2} = u'_p\alpha'_{p0} + v'_p\alpha^+_{p1}, \qquad a_{-p-1/2} = u'_p\alpha'_{p1} - v'_p\alpha^+_{p0},$$

where

$$u_p = u'_p(1-\delta_{pk}) - v'_p\delta_{pk}, \qquad v_p = v'_p(1-\delta_{pk}) + u'_p\delta_{pk}.$$

One notes easily that Φ_V is the vacuum function of the α'_{ps} fermions and Φ'_V the state in which two fermions α_{k0} and α_{k1} are present. Then

$$\langle\alpha_{k0}R(\tilde{\varepsilon}(k))\alpha^+_{k0}\rangle$$

$$= {}^1/_2(\Delta E(\Phi'_V) - \Delta E(\Phi_V)) + \langle\alpha_{k0}H_c\alpha^+_{k0}\rangle. \qquad (10)$$

For a model Hamiltonian of the kind (8) $\Delta E(\Phi_V)$ can be evaluated exactly.[3] Thus, performing the canonical transformation (4) [or (4′)] in the exact Hamiltonian and comparing the indecomposable complexes with the Bose amplitudes $B^+_p(q)$ and $B_p(q)$ we shall obtain two model Hamiltonians $\tilde{H}$ and $\tilde{H}'$ which differ in that the functions (u_k, v_k) and (u'_k, v'_k) occur in them, respectively. The magnitude of the difference ΔE for the systems $\tilde{H}$ and $\tilde{H}'$ shall also be of interest to us.

The system (9) can easily be solved. The secular equation which determines the excited energy eigenvalues E_α is of the form

$$1 + D(q, E)f(q, E) = 0, \qquad (11)$$

where

$$D(q, E) = \Omega^{-1}\left(\nu(q) - \frac{g^2\omega_q^2}{\omega_q^2 - E^2}\right),$$

$$f(q, E) = \sum_p M^{+2}(p, p+q)\,\frac{2\omega(p, q)}{\omega^2(p, q) - E^2}.$$

For ΔE we have

$$\Delta E(\Phi_V) = -\sum E_\alpha[\chi^*_{p,q}(\alpha)\chi_{p,q}(\alpha) + \mu_q{}^*(\alpha)\mu_q(\alpha)], \qquad (12)$$

where $\chi_{p,q}(\alpha)$ and $\mu_q(\alpha)$ are determined from (9) and the normalization condition. After changing the sum into an integral and a number of elementary calculations (cf. reference 3)* we get

$$\Delta E(\Phi_V) =$$

$$-\sum_q \frac{1}{4\pi i}\int_\Gamma [\ln(1 + D(q, E)f(q, E)) - \frac{\nu(q)}{\Omega}f(q, E)]\,dE,$$

where the contour Γ encloses the real positive axis clockwise. $\Delta E(\Phi'_V)$ is obtained from $\Delta E(\Phi_V)$ by replacing (u_k, v_k) by (u'_k, v'_k). Subtracting $\Delta E(\Phi_V)$ from $\Delta E(\Phi'_V)$ we have

$$\tilde{\varepsilon}(k) = 2u_kv_k\sum_{k'}Q(k, k')\,u_{k'}v_{k'}$$

$$+ (u_k^2 - v_k^2)\left[\sum_{k'}(u_{k'}^2 - v_{k'}^2)F(k, k') + \sum_{k'}\frac{\nu(q)}{\Omega}v^2_{k'+q}\right], \qquad (13)$$

where

$$Q(k, k+q) = -\frac{1}{2\pi i}\int_\Gamma \frac{D(q, E)}{1 + D(q, E)f(q, E)}\,\frac{2\omega(k, q)}{\omega^2(k, q) - E^2},$$

$$F(k, k+q) = -\frac{1}{4\pi i} \qquad (14)$$

$$\times\int_\Gamma \frac{D(q, E)f(q, E)\nu(q)/\Omega + g^2\omega_q^2/(\omega_q^2 - E^2)}{1 + D(q, E)f(q, E)} \times \frac{2\omega(k, q)}{\omega^2(k, q) - E^2}\,dE$$

Comparing (13) with (7′) we find in our approximation the equation for the compensation of dangerous diagrams:

$$2\xi(k)u_kv_k - (u_k^2 - v_k^2)\sum_{k'}u_{k'}v_{k'}Q(k, k') = 0, \qquad (15)$$

where

$$\xi(k) = \sum_{k'}(u_{k'}^2 - v_{k'}^2)F(k, k') + \sum_{k'}\frac{\nu(q)}{\Omega}v^2_{k'+q}, \qquad (16)$$

and where $Q(k, k')$ is given by Eq. (14). Introducing $C(k)$ instead of (u_k, v_k) through the formula

$$C(k) = \sum_{k'}Q(k, k')\,u_{k'}v_{k'},$$

we can write Eqs. (13) and (15) in the more compact form:

$$C(k) = \frac{1}{2}\sum_{k'}Q(k, k')\,C(k')/\sqrt{C^2(k') + \xi^2(k')},$$

$$\tilde{\varepsilon}(k) = \sqrt{C^2(k) + \xi^2(k)}. \qquad (17)$$

The solution of Eq. (17) enables us to construct a microscopic theory of superconductivity and in particular a criterion for the occurrence of superconductivity in an electron-phonon system.

We shall now discuss the properties of $\xi(k)$ and $Q(k, k')$. $\xi(k)$ is by definition the energy

*When the sum is changed into an integral one must take the residue at infinity into account. We note in this connection that in Eq. (4) of reference 3 the constant term should be omitted.

of a one-fermion excitation from the ground state [C (**k**) = 0] taking corrections of all orders into account. After a few transformations we can write it in the form

$$\xi(k) = (E(k) - \lambda) + \sum_{|\mathbf{k}+\mathbf{q}|<k_F} \frac{\nu(q)}{\Omega} + \frac{1}{4\pi}\left[\sum_{|\mathbf{k}+\mathbf{q}|>k_F} - \sum_{|\mathbf{k}+\mathbf{q}|<k_F}\right] \int_{-\infty}^{+\infty} \left[\frac{\nu(q)\, f(q,\ u)/\Omega}{f(q,\ u) + D(q,\ u)} + \frac{\omega_q^2/\Omega\,(\omega_q^2 + u^2)}{1 + D(q,\ u)\, f(q,\ u)}\right] \frac{2\omega(\mathbf{k},\ \mathbf{q})}{\omega^2(\mathbf{k},\ \mathbf{q}) - u^2}\, du,$$

where

$$f(q,\ u) = \sum_{\mathbf{p}} \frac{2\omega(\mathbf{p},\ \mathbf{q})}{\omega^2(\mathbf{p},\ \mathbf{q}) + u^2}, \qquad D_q(u) = \Omega^{-1}\left(\nu(q) - \frac{g^2\omega_q^2}{\omega_q^2 + u^2}\right),$$

which for $g^2 = 0$ agrees exactly with the result of reference 3.

To study the asymptotic behavior of $Q(\mathbf{k}, \mathbf{k}')$ for small $\mathbf{q}$ we take the main term from (14) evaluating the residue at the pole $E = \omega(\mathbf{k}, \mathbf{q})$. We have then

$$Q(\mathbf{k},\ \mathbf{k}+\mathbf{q}) = Q_c(\mathbf{k},\ \mathbf{k}+\mathbf{q}) + Q_{ph}(\mathbf{k},\ \mathbf{k}+\mathbf{q}),$$

$$Q_c(\mathbf{k},\ \mathbf{k}+\mathbf{q}) = \frac{\nu(q)}{\Omega}\left[1 + \frac{\nu(q)}{\Omega} f(q,\ \omega(k,\ q))\right]^{-1} \approx \frac{4\pi e^2}{\Omega}\left[q^2 + k_F^2 \frac{r_s\alpha}{\pi}\left(1 - \frac{1}{2x}\ln\frac{1+x}{1-x}\right)\right]^{-1},$$

$$Q_{ph}(\mathbf{k},\ \mathbf{k}+\mathbf{q}) - \frac{1}{\Omega}\frac{g^2\omega_q^2}{\omega_q^2 - \omega^2(\mathbf{k},\ \mathbf{q})}\left[1 + \frac{k_F^2}{q^2}\frac{r_s\alpha}{\pi}\left(1 - \frac{1}{2x}\ln\frac{1+x}{1-x}\right)\right]^{-1},$$

where $x = k_F/(kt + \frac{1}{2}q)$, $t = (\mathbf{p}\cdot\mathbf{q})/pq$. It is then clear that $Q_c(\mathbf{k}, \mathbf{k}')$ is essentially the screened Coulomb interaction between the electrons. For small $\mathbf{q}$, $Q_{ph}(\mathbf{k}, \mathbf{k}') \sim 0$ which means the predominance of the effects of the Coulomb interaction in the long-wavelength region. These calculations completely confirm the qualitative considerations given in reference 2.

3. CONCLUSIONS

1. The influence of the Coulomb interaction on the occurrence of superconductivity has not been investigated sufficiently. Taking it into account is especially important from the point of view of establishing a criterion for the occurrence of superconductivity.

2. In Bogolyubov's new method in superconductivity theory the main difficulty in taking the Coulomb interaction into account is the infrared divergence of the basic quantities which occur in the equation of compensation of dangerous diagrams.

3. According to an idea of Gell-Mann and Brueckner and using the method of approximate second quantization we summed a special class of the most divergent diagrams giving a contribution to the main terms of an expansion in r_s, thus removing the infrared divergence and obtaining explicit expressions for the functions $\xi(k)$ and $Q(\mathbf{k}, \mathbf{k}')$ as the basic quantities in the compensation equation.

4. Equations (6′) and (7′) together with (14) and (15) form a closed system and a detailed investigation of it from the point of view of determining a criterion for the occurrence of superconductivity in an electron-phonon system remains a problem for further study. We must, however, note that to solve this physically very interesting problem one must clearly take the influence of the periodic field of the crystalline lattice into account in a more exact manner.

In conclusion the authors express their deep gratitude to N. N. Bogolyubov, V. V. Tolmachev, and D. V. Shirkov for suggesting to them the subject of this study and for their constant help and valuable discussions all the time while this paper was being completed.

[1] Bardeen, Cooper, and Schrieffer, Phys. Rev. **108**, 1175 (1957).

[2] Bogolyubov, Tolmachev, and Shirkov, Новый метод в теории сверхпроводимости (New Method in Superconductivity Theory), U.S.S.R. Acad. Sci. Press, 1958, Fortsch. Phys. **6**, 605 (1958).

[3] Chen Chun-Hsian and Chow Shih-Hsun, J. Exptl. Theoret. Phys. (U.S.S.R.) **34**, 1566 (1958), Soviet Phys. JETP **7**, 1080 (1958).

[4] N. N. Bogolyubov, J. Exptl. Theoret. Phys. (U.S.S.R.) **34**, 58 (1958), Soviet Phys. JETP **7**, 41 (1958).

[5] M. Gell-Mann and K. A. Brueckner, Phys. Rev. **106**, 364 (1957); K. Sawada, Phys. Rev. **106**, 372 (1957).

[6] G. Wentzel, Phys. Rev. **108**, 1593 (1957).

Translated by D. ter Haar
234

ON THE THEORY OF WEAK FERROMAGNETISM

E. A. TUROV

Institute for the Physics of Metals, Academy of Sciences, U.S.S.R.

Submitted to JETP editor October 24, 1958

J. Exptl. Theoret. Phys. (U.S.S.R.) **36**, 1254-1258 (April, 1959)

We have investigated a number of properties of weak ferromagnetics at low temperatures using Dzyaloshinskiĭ's theory which considers weak ferromagnetism to be the consequence of the magnetic symmetry of antiferromagnetic crystals of a well defined magnetic structure. We consider the case of "transverse" and of "longitudinal" weak ferromagnetism (in the first case the spontaneous magnetic moment is perpendicular, and in the second case parallel to the antiferromagnetic axis). We have evaluated the spin wave energy, the temperature dependence of the magnetization and its field dependence, and the spin part of the heat capacity.

1. To explain the nature of the weak ferromagnetism observed in $MnCO_3$ and $CoCO_3$, Borovik-Romanov and Orlova[1] suggested a model of ferromagnetism in which the directions of the magnetizations of the sublattices were not strictly antiparallel, but were rotated over a small angle with respect to one another. Dzyaloshinskiĭ[2] gave a group-theoretical justification of the possibility of such a magnetic state. He showed that weak ferromagnetism of compounds of the type α-Fe_2O_3 and $MnCO_3$ is a natural property of these magnetic substances in those states where the spins of the magnetic ions lie in the (111) planes and that the resulting spontaneous magnetic moment in that case is perpendicular to the antiferromagnetic axis ("transverse" weak ferromagnetism).

In the quoted paper by Borovik-Romanov and Orlova another possibility for weak ferromagnetism was also pointed out, which is produced by an incomplete compensation of the strictly antiparallel directed magnetic moments of the sublattices, due to a difference in their g-factors. This can, for instance, occur because the sublattices consist of magnetic ions (atoms) of different elements (in such a way that $N_1S_1 = N_2S_2$, but $g_1 \neq g_2$, where N_1, S_1, g_1 and N_2, S_2, g_2 are the number of ions, their spins and g-factors of the first and the second sublattice, respectively). Moreover, even for identical ions the g-factors may turn out to be different, if they occupy non-equivalent positions in the lattice so that the sites of the different sublattices have different environments. In that case, the resulting spontaneous magnetic moment of the crystal is parallel to the antiferromagnetic axis ("longitudinal" weak ferromagnetism).

Using Landau's theory of phase transitions and the most general expression for the magnetic energy which was allowed by the crystal symmetry, Dzyaloshinskiĭ investigated the behavior of weak ferromagnetics near the Curie point in its dependence on temperature and magnetic field. It is of interest to perform a similar analysis in the low temperature region where one can apply the spin wave approximation. In the present paper a first attempt in this direction is made.

2. We shall evaluate the energy of spin waves for rhombohedral crystals of the α-Fe_2O_3 and $MnCO_3$ type which are "transverse" weak ferromagnetics.

We shall describe the magnetic properties of the crystal with the aid of two magnetic moment densities $\mathbf{M}_1(\mathbf{r})$ and $\mathbf{M}_2(\mathbf{r})$ of the two magnetic sublattices respectively, and we shall assume that

$$\mathbf{M}_1^2(\mathbf{r}) = \mathbf{M}_2^2(\mathbf{r}) = \mathbf{M}_0^2 = \text{const}\ [3].$$

One can then write the energy density depending on the distribution of the magnetic moments in space up to terms of the second order in the direction cosines of $\mathbf{M}_1$ and $\mathbf{M}_2$ in the following form, following Dzyaloshinskiĭ[2] (see also reference 3):

$$\begin{aligned}\mathcal{H} = {} & (A/M_0^2)\, M_{1\alpha}M_{2\alpha} + (B/2M_0^2)(M_{1z}^2 + M_{2z}^2) \\ & + (B_1/M_0^2)\, M_{1z}M_{2z} + (D/M_0^2)(M_{1x}M_{2y} - M_{2x}M_{1y}) \\ & + (C_1/M_0^2)\, \nabla M_{1\alpha}\nabla M_{2\alpha} - (\mathbf{M}_1 + \mathbf{M}_2)\,\mathbf{H} \\ & + (C/2M_0^2)(\nabla M_{1\alpha}\nabla M_{1\alpha} + \nabla M_{2\alpha}\nabla M_{2\alpha}) \qquad (1)\end{aligned}$$

($\alpha \equiv x, y, z$; one sums over repeated indexes).

The first term here is the exchange energy between the sublattices, and the second and third terms are the usual magnetic anisotropy energy of a uniaxial crystal (trigonal axis along the z axis). The fourth term gives the magnetic energy typical for crystals of the symmetry considered here which is responsible for the weak ferromagnetism and which was taken into account for the first time by Dzyaloshinskiĭ using a correct analysis of the symmetry properties of magnetic crystals. The fifth and sixth terms take into account the change in the exchange energy produced by inhomogeneities of the magnetization where we have for the sake of simplicity only retained the isotropic part of this energy, while the last term is, finally, the energy of the magnetic substance in the external field **H**. A, B, B_1, D, C, and C_1 are quantities of the dimensions of an energy which enter as some phenomenological parameters.

The minimization of expression (1) shows that if $A > 0$, $B - B_1 > 0$, and $D > 0$ and with the field **H** in the basic XY plane the ground state of the system corresponds to those uniform distributions $\mathbf{M}_{01}$ and $\mathbf{M}_{02}$ of the magnetic moments for which they are situated in the same plane, almost antiparallel to one another, each deviating from the antiferromagnetic axis by a small angle θ such that

$$\sin\theta \approx (D + M_0 H)/2A \qquad (2)$$

($\sin\theta$ is determined by the ratio of the magnetic energy to the exchange energy and θ is thus, indeed, a very small angle). In view of the fact that the initial Hamiltonian (1) does not take the magnetic anisotropy in the basic plane into account, the position of the antiferromagnetic axis is fixed by the external field **H** which is perpendicular to that axis and parallel to the resulting magnetic moment. The magnitude of the latter is, according to (2) at $T = 0°K$ equal to

$$M(0, H) = 2M_0(H_D + H)/H_E, \qquad (2')$$

where $H_E = 2A/M_0$ is the effective field of the exchange forces (of the order of $10^6 - 10^7$ Oe), and $H_D = D/M_0$ some internal magnetic effective field (of the order of $10^3 - 10^4$ Oe) caused by the presence of the spontaneous magnetic moment at $H = 0$ which may be called the Dzyaloshinskiĭ field. The spontaneous magnetization $M_S(0) = 2M_0H_D/H_E$ is $0.01 - 1\%$ of the nominal one ($2M_0$).

Considering, further, weak oscillations $\Delta\mathbf{M}_j = \mathbf{M}_j - \mathbf{M}_{0j}$ ($j = 1, 2$) of the magnetic densities around their values corresponding to the ground state, one can by the usual means[3,4] obtain the energy of two kinds of spin waves

$$E_k^{(1)} = \{\mu^2(H_D + H)H + l^2k^2\}^{1/2}; \qquad (3)$$

$$E_k^{(2)} = \{\mu^2[H_0^2 + H_D(H_D + H)] + l^2k^2\}^{1/2}, \qquad (4)$$

where k is the spin wave vector, $\mu = ge\hbar/2mc$, $l^2 = 2A(C - C_1)\mu^2/M_0^2$, and $H_0 = \sqrt{2A(B - B_1)}/M_0$ is a third characteristic field the magnitude of which (of the order of $10^4 - 10^5$ Oe) is the geometric mean of the exchange forces field and the magnetic anisotropy field.

3. Using Eqs. (3) and (4) for the energy of the spin waves one can easily evaluate the temperature dependence of the magnetization. A standard calculation[3] gives

$$M(T, H) = M_s(T) + \chi(T)H, \qquad (5)$$

for the temperature range $\mu H_0 \ll \kappa T \ll \kappa\Theta_C$ (Θ_C: Curie temperature, κ: Boltzmann's constant), where the spontaneous magnetization is*

$$M_s(T) = (2M_0H_D/H_E)(1 - \alpha T^2),$$

$$\alpha = \mu^2 H_E \varkappa^2/24 M_0 l^3, \qquad (6)$$

and the susceptibility

$$\chi(T) = (2M_0/H_E)(1 - \alpha T^2). \qquad (7)$$

Borovik-Romanov and Orlova[1] obtained for $MnCO_3$ and $CoCO_3$ a two-term equation similar to (5) for the temperature and field dependence of the magnetization. As far as the specific form of the dependence of M_S and χ on the temperature is concerned one can for the moment only note the agreement of the theory with experiments as far as an increase of both quantities with a decrease of temperature is concerned and a tendency to saturation. For a more detailed verification of the theory it is necessary to extend the measurements to the region of very low temperatures (provided, of course, that there is in these substances no low-temperature transformation from the state of weak ferromagnetism to a truly antiferromagnetic state, such as, for instance, occurs in the case of hematite).

4. We shll begin the consideration of the "longitudinal" weak ferromagnetism with a discussion of the general case of a ferromagnetic with two magnetic sublattices, the magnetizations of which are antiparallel to one another in the ground state while $M_{01} \neq M_{02}$. The Hamiltonian of such a system is of the form [compare with Eq. (1)]

$$\mathcal{H} = (A_{12}/M_{01}M_{02})\,M_{1\alpha}M_{2\alpha} + (C_{12}/M_{01}M_{02})\nabla M_{1\alpha}\nabla M_{2\alpha}$$
$$+ (C_{11}/2M_{01}^2)\nabla M_{1\alpha}\nabla M_{1\alpha}$$
$$+ (C_{22}/2M_{02}^2)\nabla M_{2\alpha} - (\mathbf{M}_1 + \mathbf{M}_2)\mathbf{H}. \qquad (8)$$

*If H_0 is so large that $\mu H_0 \gg \varkappa T \gg \mu H$, μH_D, one must replace the coefficient α by $\alpha/2$ in Eq. (6).

if the anisotropy forces are not taken into account. The resulting magnetization in the ground state is equal to $M_{01} - M_{02}$ (if $A_{12} > 0$ and $M_{01} > M_{02}$) and directed along the field H. The spectrum of the eigenoscillations is given by the expression

$$E_k^{(1,2)} = \sqrt{(\varepsilon_1 + \varepsilon_2)^2/4 - \beta^2} \pm (\varepsilon_1 - \varepsilon_2)/2, \qquad (9)$$

where

$$\varepsilon_1 = (\mu_1/M_{01})(A_{12} + C_{11}k^2) + \mu_1 H,$$

$$\varepsilon_2 = (\mu_2/M_{02})(A_{12} + C_{22}k^2) - \mu_2 H,$$

$$\beta = (\mu_1\mu_2/M_{01}M_{02})^{1/2}(A_{12} + C_{12}k^2).$$

One sees easily that the necessary and sufficient condition that the spin wave energy have the linear dispersion law ($E_k \sim k$ if $H = 0$) characteristic for antiferromagnetics is the equation

$$M_{01}/\mu_1 = M_{02}/\mu_2. \qquad (10)$$

This equation allows a spontaneous magnetization to be present:

$$M_s(0) = M_{01} - M_{02} = \delta M_0,$$

where

$$\delta = \Delta\mu/\mu,\ \Delta\mu = (\mu_1 - \mu_2)/2,\ \mu = (\mu_1 + \mu_2)/2$$

$$\text{and } M_0 = (M_{01} + M_{02})/2.$$

We are here thus dealing with spin antiferromagnetism since, according to (10), $N_1S_1 = N_2S_2$, and with weak "longitudinal" ferromagnetism produced by a difference in g-factors of the magnetic ions of the different sublattices. The quantity δ which determines the possible value of the spontaneous magnetization of such hypothetical weak ferromagnetics can, generally speaking, vary within wide limits compared to the usual ferromagnetics; if we use the observed differences in g-factors for magnetic ions (atoms) of different elements or of one element, but in different compounds, we have $\delta \sim 10^{-3} - 10^{-1}$.

If for the sake of simplicity we restrict ourselves to the case $C_{11} = C_{22}$ we can write the energy of the spin waves (9) of a "longitudinal" weak ferromagnetic, taking (12) into account, in the form

$$E_k^{(1,2)} = \{\mu^2(\delta H_E H + \delta^2 H^2) + I^2k^2\}^{1/2} \pm \mu H. \qquad (11)$$

We note that the states considered by us, in which the antiferromagnetic axis is parallel to **H**, are stable only in the range $H \lesssim \delta H_E$ for the field. This range of stability is changed if we take the magnetic anisotropy energy into account in (8).*

*We shall not write down here the unwieldy equations for the spin wave energy taking magnetic anisotropy into account, since the latter does not change the conclusions which interest us in the following.

The evaluation of the temperature dependence of the magnetization (for $\kappa T \gg \mu\sqrt{\delta H_E H}$) gives again an expression of the form (5) where now, however,

$$M_s(T) = \delta M_0[1 - \mu^2 H_E(\varkappa T)^2/12M_0 I^3]; \qquad (12)$$

$$\chi(T) = \mu^2(\varkappa T)^2/3I^2. \qquad (13)$$

It is characteristic that that part of the magnetization which depends on the temperature $\Delta M(T, H) = -\mu^2(\kappa T)^2(\delta H_E - 4H)/12I^3$ must change its sign at $H = \delta H_E/4$.

5. On the basis of the calculations reported one can reach the following conclusions:

a) Both for "transverse" and for "longitudinal" weak ferromagnetics the spontaneous magnetic moment changes with temperature not according to a $T^{3/2}$ law, characteristic for ordinary ferromagnetics* but to a T^2 law.

b) The magnetic susceptibility $\chi(T)$ in a field H directed along the spontaneous magnetic moment is for "transverse" weak ferromagnetics the same as the usual perpendicular susceptibility of an antiferromagnetic and for "longitudinal" weak ferromagnetics as the usual parallel susceptibility of an antiferromagnetic [compare Eqs. (7) and (13) for $\chi(T)$ with the corresponding formulae for $\chi_\perp$ and $\chi_\parallel$ in the author's reference 6]. This fact can be one of the indications by which one can easily distinguish "transverse" weak ferromagnetism from "longitudinal."

c) Since for all weak ferromagnetics the spin wave energy obeys a linear dispersion law, namely, $E_k = Ik$ (for $\kappa T \gg \Delta E_0$ where ΔE_0 is the energy gap for the excitation of spin waves), their spin heat capacity C_S is proportional to T^3, as in antiferromagnetics. The corresponding expressions for C_S were, for instance, given in the papers by Kaganov and Tsukernik[4] and by the present author.[6]

To check the results of the present paper, it is necessary to have additional experimental data on the magnetization, heat capacity and magnetic resonance in known weak ferromagnetics, preferably on single crystal samples and at temperatures, low compared to the Curie temperature.

In conclusion I express my deep gratitude to S. V. Vonsovskiĭ for valuable advice and helpful discussions.

[1] A. S. Borovik-Romanov and M. P. Orlova,

*Vonsovskii and Seidov[5] obtained a T^2 law for ferromagnetic ferrites, thenks to the fact that the problem of two magnetic sublattices with $N_1S_1 \neq N_2S_2$ and $g_1 = g_2$ was in fact replaced by them by the problem with $N_1S_1 = N_2S_2$ and $g_1 \neq g_2$, which is not equivalent to it.

J. Exptl. Theoret. Phys. (U.S.S.R.) **31**, 579 (1956), Soviet Phys. JETP **4**, 531 (1957).

[2] I. E. Dzyaloshinskiĭ, J. Exptl. Theoret. Phys. (U.S.S.R.) **32**, 1547 (1957), Soviet Phys. JETP **5**, 1259 (1957); J. Exptl. Theoret. Phys. (U.S.S.R.) **33**, 1454 (1957), Soviet Phys. JETP **6**, 1120 (1958).

[3] E. A. Turov and Yu. P. Irkhin, Izv. Akad. Nauk SSSR, Ser. Fiz. **22**, 1168 (1958).

[4] M. I. Kaganov and V. M. Tsukernik, J. Exptl. Theoret. Phys. (U.S.S.R.) **34**, 106 (1958), Soviet Phys. JETP **7**, 73 (1958).

[5] S. V. Vonsovskiĭ and Yu. M. Seidov, Izv. Akad. Nauk SSSR, Ser. Fiz. **18**, 319 (1954) (Columbia Tech. Transl. p. 14).

[6] E. A. Turov, J. Exptl. Theoret. Phys. (U.S.S.R.) **34**, 1009 (1958), Soviet Phys. JETP **7**, 696 (1958).

Translated by D. ter Haar
235

ON THE SUPERFLUIDITY OF A SYSTEM OF POLAR BOSE EXCITATIONS

S. V. VONSOVSKIĬ and M. S. SVIRSKIĬ

Institute for Metal Physics, Academy of Sciences, U.S.S.R.

Submitted to JETP editor October 27, 1958

J. Exptl. Theoret. Phys. (U.S.S.R.) **36**, 1259-1266 (April, 1959)

We have investigated the possibility of a superconducting state in metals for which the elementary current excitations of the electronic system are (quasi-) bosons. This problem is solved, using Bogolyubov's method, in the framework of the "polar" many-electron model of a crystal. We have obtained criteria for a possible occurrence of a superconducting state in a system of charged bosons (low temperatures, low density of the quasi-particles, practically no "one-electron" transitions, and a negative sign of the exchange integral). The interaction between the current Bose particles, induced by the phonons, is attractive of character and opposes the appearance of superfluid properties of the latter. The critical temperature of a superconductor with boson current carriers depends differently on the isotopic mass of the crystal ions than for the case of metals with a Fermi electron spectrum. This difference can be used as the basis of an experimental method to distinguish superconductors of the "Fermi" and of the "Bose" type.

1. The latest developments in the microscopic theory of superconductivity in references 1 and 2 are connected with the assumption that the elementary current carriers obey Fermi statistics. An investigation of the interaction of these fermions with the phonons of the crystalline lattice made it possible to establish the presence of a state with the observed property of superfluidity below some critical temperature. It is, however, fully possible that there are cases where the current carriers in the system of interacting electrons in the crystal satisfy with sufficiently large accuracy Bose statistics.[3] It is in that connection of interest to study the presence of superconducting properties in a metal with a Bose-type energy spectrum of the current carriers. The idea itself of connecting the phenomenon of superconductivity with the Bose-Einstein condensation of a gas of charged bosons is not new, but a number of existing investigations in that direction (see, for instance, references 4 and 5) are, as a rule, methodic of character.[6] The reasons for this are, firstly, that the physical nature of the assumed charged bosons remains usually vague, and secondly that one considers a perfect boson gas, the thermodynamic properties of which differ from those observed in real superconductors (in particular, there is no phase transition of the second order in a perfect boson gas). These shortcomings are not present in the many-electron polar model[7,8] where, on the one hand, one does not postulate from the outset a gas of charged bosons, but obtains it in the appropriate limiting cases (predominance of the energy operator matrix elements corresponding to two-electron transitions[3]) through an analysis of the different kinds of interaction in the electron system, while, on the other hand, this gas turns out to be imperfect. It is therefore expedient to consider a system of charged polar Bose excitations, using the method applied by Bogolyubov in analyzing the properties of superfluidity of a weakly imperfect Bose-Einstein gas.[9]

2. In the case of a crystal where the energetically most favorable state is the one of maximum polarization[7,10] (the sites are either pairs or holes) while the matrix elements corresponding to two-electron transitions predominate over the matrix elements of the one-electron transitions ($|J_{qq'}| \gg |L_{qq'}|$, where $J_{qq'}$ is the integral of exchange between the orthonormal states θ_q and $\theta_{q'}$, and $L_{qq'}$ the corresponding transfer integral), the Hamiltonian of the polar model has in the second quantization representation according to (19) of reference 7 the following form:

$$\mathcal{H} = \sum_q^* \bar{G}(q,\ q)\, n_q + sA + {}^1/_2 \sum_{q \neq q'} B_{qq'} n_q n_{q'} + \sum_{q \neq q'} J_{qq'} (\Phi_q \Psi_q^+ \Phi_{q'}^+ \Psi_{q'} - \Phi_q \Phi_q^+ \Phi_{q'} \Phi_{q'}^+), \qquad (1)$$

where s is the number of pairs, A the energy eigenvalue of a pair, $B_{qq'}$ the integral of the mutual Coulomb repulsion of two valence elec-

trons in the states θ_q and $\theta_{q'}$, respectively, n_q the number of valence electrons in the state θ_q; $G(q, q)$ the energy of a valence electron in an isolated atom, corrected for its interaction with the other atomic cores, Φ_q and Φ_q^+ the operators of the annihilation and the corresponding creation of a pair in the state θ_q, and Ψ_q and Ψ_q^+ the corresponding operators for holes, satisfying according to reference 3 the plus-minus quantization relations:

$$[\Phi_q\Phi_q^+]_+ = [\Psi_q\Psi_q^+]_+ = 1,$$
$$[\Phi_q\Phi_{q'}^+]_- = [\Psi_q\Psi_{q'}^+]_- = 0 \qquad (\text{if} \quad q \neq q'),$$
$$[\Phi_q\Phi_{q'}]_- = [\Psi_q\Psi_{q'}]_- = [\Phi_q^+\Phi_{q'}^+]_- = [\Psi_q^+\Psi_{q'}^+]_- = 0. \quad (2)$$

Since in the case under consideration the condition of maximum polarization:

$$\Phi_q\Phi_q^+ + \Psi_q\Psi_q^+ = 1 \quad (3)$$

is satisfied, it is expedient to introduce instead of the operators Φ_q, Φ_q^+, Ψ_q, Ψ_q^+ the operators:

$$b_q = \Psi_q\Phi_q^+, \quad b_q^+ = \Phi_q\Psi_q^+, \quad (4)$$

which because of condition (3) also satisfy the commutation relations (2). The Hamiltonian (1) has in the new operators (4) the following form

$$\mathcal{H} = sA_1 + \sum_{q \neq q'} J_{qq'} b_q^+ b_{q'} + \sum_{q=q'} C_{qq'} b_q^+ b_q b_{q'}^+ b_{q'}, \quad (5)$$

where

$$A_1 = A + 2G(q, q) \text{ and } C_{qq'} = 2B_{qq'} - J_{qq'}. \quad (6)$$

Making in (5) the transition to wave vector space by means of the Fourier transformation

$$b_q = N^{-1/2} \sum_{\mathbf{k}} b_{\mathbf{k}} e^{i\mathbf{k}\mathbf{R}_q}, \quad b_q^+ = N^{-1/2} \sum_{\mathbf{k}} b_{\mathbf{k}}^+ e^{-i\mathbf{k}\mathbf{R}_q}, \quad (7)$$

where N is the number of lattice sites, we get

$$\mathcal{H} = \mathcal{H}_0 + \mathcal{H}_1, \quad (8)$$

$$\mathcal{H}_0 = \sum_{\mathbf{k}} (A_1 + \sum_{\mathbf{h}} J(h) e^{i\mathbf{k}\mathbf{h}}) b_{\mathbf{k}}^+ b_{\mathbf{k}} = \sum_{\mathbf{k}} \varepsilon_{\mathbf{k}} b_{\mathbf{k}}^+ b_{\mathbf{k}}, \quad (8_1)$$

$$\mathcal{H}_1 = \sum_{\mathbf{k}_1, \mathbf{k}_2, \mathbf{k}_3, \mathbf{k}_4} \delta(\mathbf{k}_2 - \mathbf{k}_1 + \mathbf{k}_4 - \mathbf{k}_3) \sum_{\mathbf{h}} C(h) e^{i\mathbf{h}(\mathbf{k}_4 - \mathbf{k}_3)} \times b_{\mathbf{k}_1}^+ b_{\mathbf{k}_2} b_{\mathbf{k}_3}^+ b_{\mathbf{k}_4}. \quad (8_2)$$

Here $\sum_{\mathbf{h}}$ denotes a sum over the radius vectors $\mathbf{h}$ performed from a fixed lattice site to the remaining lattice sites. According to reference 3, the operators $b_{\mathbf{k}}$ satisfy, when the ratio s/N is small, the commutation relations for Bose-operators approximately. If we restrict ourselves accordingly to the case* $s/N \ll 1$ ("poor" metal[11]) we must interpret $\mathcal{H}_0$ as the energy operator of a system of non-interacting quasi-bosons,* and $\mathcal{H}_1$ as the energy operator of their interaction. The Hamiltonian (8), (8_1), (8_2) has basically the same form as the Hamiltonian (3.63), (3.64) considered in reference 9. Following, accordingly, the reasoning given there we find in the first perturbation theory approximation

$$E\ldots n_{\mathbf{k}}\ldots = s\left[A_1 - \frac{1}{N}\sum_h C(h)\right] + \frac{s^2}{N}\sum_h C(h) + \sum_{\mathbf{k}} n_{\mathbf{k}} \sum_h J(h) e^{i\mathbf{k}\mathbf{h}} + \frac{1}{N} \sum_{\mathbf{k}_1 \neq \mathbf{k}_2} n_{\mathbf{k}_1} n_{\mathbf{k}_2} \sum_h C(h) e^{i\mathbf{h}(\mathbf{k}_1 - \mathbf{k}_2)}, \quad (9)$$

where

$$n_{\mathbf{k}} = b_{\mathbf{k}}^+ b_{\mathbf{k}}.$$

We find now the condition that the lowest level is the one with occupation numbers

$$n_{\mathbf{k}} = \begin{cases} s & \text{if} \quad \mathbf{k} = 0 \\ 0 & \text{if} \quad \mathbf{k} \neq 0, \end{cases} \quad (10)$$

i.e., the level

$$E_0 = s\left[A_1 - \frac{1}{N}\sum_h C(h)\right] + \frac{s^2}{N}\sum_h C(h) + s\sum_h J(h). \quad (11)$$

From (9) and (11) we find, if we use the nearest neighbor approximation and also restrict ourselves to considering the low temperature region, where $ka \ll 1$,[11]

$$E\ldots n_{\mathbf{k}}\ldots - E_0 = -J \sum_{\mathbf{k}} n_{\mathbf{k}} (ka)^2 + \frac{C}{N} \sum_{\mathbf{k}_1 \neq \mathbf{k}_2} n_{\mathbf{k}_1} n_{\mathbf{k}_2} [6 - (\mathbf{k}_1 - \mathbf{k}_2)^2 a^2]. \quad (12)$$

The expression within the square brackets is here positive by virtue of the condition $ka \ll 1$. Moreover, $C = 2B - J$ is also positive since B does not contain overlaps of the functions θ_q, while J contains two such overlaps. The second sum on the right hand side of (12) is thus positive. The first term on the right hand side of (12) is positive, if $J < 0$. If, however, $J > 0$, this term is negative and this coupled with the fact that in the case under consideration the interaction energy is assumed to be small compared to the kinetic energy, means that the right hand side of (12) will be negative. It is thus necessary that the exchange integral J be negative, if the energetically lowest state is to be the one for which all quasi-particles have $k = 0$, i.e., one for which condensation takes place.

*If there are only pairs and holes, (i.e., when the polarization is a maximum) the condition $s/N \ll 1$ can be satisfied if the number of electrons $2s$ is less than the number of lattice sites N, which shall be assumed to be the case in the following.

*We use in this case the term "quasi-bosons" to emphasize once again that for $s/N \ll 1$ the quasiparticles behave with a high degree of accuracy, but even so still only approximately, as bosons.

Restricting ourselves, therefore, in the following to the case $J < 0$, we have from (8_1)

$$\varepsilon_k = A_1 - 6|J| + p_k^2/2m_{\text{eff}}, \tag{13}$$

where

$$m_{\text{eff}} = \hbar^2/2|J|a^2. \tag{14}$$

We find now the energy necessary to take one quasi-particle from the system of quasi-particles moving all with the same wave vector $\mathbf{k}$. To do this, we use (9) and consider the difference ΔE between the energy $E_{\mathbf{k}_0}$ of the system moving with the wave vector $\mathbf{k}_0$ and the energy $E_{\mathbf{k}_0-\mathbf{g}}$ of a system of $(s-1)$ particles with wave vector $\mathbf{k}_0$ and one particle with wave vector $\mathbf{k}_0 - \mathbf{g}$:

$$\Delta E = E_{\mathbf{k}_0-\mathbf{g}} - E_{\mathbf{k}_0} \approx \sum_{\mathbf{h}} |J(h)| e^{i\mathbf{k}_0\mathbf{h}} - \sum_{\mathbf{h}} |J(h)| e^{i(\mathbf{k}_0-\mathbf{g})\mathbf{h}} + \frac{2s}{N}\sum_{\mathbf{h}} C(h)\cos(\mathbf{g},\mathbf{h}). \tag{15}$$

In the last term of (15) we have dropped 1 compared to s. Using the nearest neighbor approximation and (14), we can transform (15) to the form

$$\Delta E = E(\mathbf{g}) - (\mathbf{p}_g \mathbf{v}_0), \tag{16}$$

where

$$E(\mathbf{g}) = p_g^2/2m_{\text{eff}} + (2s/N)\sum_{\mathbf{h}} C(h)\cos(\mathbf{g},\mathbf{h}); \tag{17}$$

$$\mathbf{v}_0 = \mathbf{p}_0/m_{\text{eff}} \tag{18}$$

is the average velocity of the condensate corresponding to a quasi-momentum $\mathbf{p}_0 = \hbar\mathbf{k}_0$. In the nearest-neighbor approximation the ratio $E(\mathbf{g})/g$ has, according to (17), a minimum at the point:

$$(g_0 a)^2 = 1/(N|J|/12sC - {}^1/_0). \tag{19}$$

In order that this minimum occur in the region where the low temperature condition $ga \ll 1$ is satisfied, the inequality

$$s/N \ll |J|/2C, \tag{20}$$

must thus be satisfied, and this is the case; if the condition $s/N \ll 1$ is obeyed, which is used, anyway, in the present paper.

We introduce now the notation

$$E(\mathbf{g}_0)/g_0 = \hbar u, \tag{21}$$

whence

$$E(\mathbf{g}) \geqslant \hbar u g. \tag{22}$$

From (16) and (22) we find

$$\Delta E \geqslant p_g [u - v_0 \cos(\mathbf{p}_g, \mathbf{v}_0)], \tag{23}$$

or, since the maximum of cosine $(\mathbf{p}_g, \mathbf{v}_0) = 1$, we have

$$\Delta E \geqslant (u - v_0) p_g. \tag{24}$$

From this it follows that if $v_0 < u$ an excitation of the moving condensate of pairs is energetically unfavorable.

Applying Bogolyubov's method to the real Bose gas of the quasi-particles of the polar model we are thus able to establish the occurrence of the property of superfluidity of the electron system of the crystal, if the following conditions are satisfied: low temperatures $(ka \ll 1)$, poor metals $(s/N \ll 1)$, practically no one-electron transitions, and a negative exchange integral (positive effective mass).

3. The applicability of the results of the preceding section are, strictly speaking, restricted to the region of sufficiently large k (and satisfying at the same time the condition $ka \ll 1$),* when it has sense to use perturbation theory, assuming the interaction energy to be small compared to the kinetic energy. One can convince oneself of this by applying to the problem considered above the method of approximate second quantization.[9] Taking into account, namely, the fact that the main part of the quasi-particles is in the $k = 0$ state, and dropping accordingly in (8_2) the terms with triple and quadruple products of the b_k (for $k \neq 0$) one can transform the Hamiltonian of the system under consideration to the form:

$$\mathcal{H} = (s^2/N)\sum_{\mathbf{h}} C(h) + (A_1 - 6|J|)s + \sum_{\mathbf{k}} (|J| k^2 a^2 + \frac{2n_0}{N}\sum_{\mathbf{h}} C(h) e^{i\mathbf{h}\mathbf{k}}) b_{\mathbf{k}}^+ b_{\mathbf{k}} + (b_0^2/N) \times \sum_{\mathbf{k},\mathbf{h}} C(h) e^{i\mathbf{h}\mathbf{k}} b_{\mathbf{k}}^+ b_{-\mathbf{k}}^+ + (b_0^{+2}/N)\sum_{\mathbf{k},\mathbf{h}} C(h) e^{i\mathbf{h}\mathbf{k}} b_{\mathbf{k}} b_{-\mathbf{k}}, \tag{25}$$

where n_0 is the occupation number of the $k = 0$ state.

Now making the transition to the new Bose operators[9]

$$\beta_{\mathbf{k}} = b_0^+ n_0^{-1/2} b_{\mathbf{k}}, \quad \beta_{\mathbf{k}}^+ = b_0 n_0^{-1/2} b_{\mathbf{k}}^+ \tag{26}$$

and carrying out the canonical transformation[9]

$$\beta_{\mathbf{k}} = (\xi_{\mathbf{k}} + A_k \xi_{-\mathbf{k}}^+)/\sqrt{1 - A_k^2}, \quad \beta_{\mathbf{k}}^+ = (\xi_{\mathbf{k}}^+ + A_k \xi_{-\mathbf{k}})/\sqrt{1 - A_k^2}, \tag{27}$$

*From (29) it is clear that one can consider k, to be "large," $\sum_{\mathbf{h}}$ if it satisfies the condition $ka \gg 2(n_0/N|J|\sum_{\mathbf{h}} C(h) e^{i\mathbf{k}\mathbf{h}})^{1/2}$. The region of "large" k which do not violate the condition $ka \ll 1$ satisfies thus the inequalities $1 \gg ka \gg 2(n_0/N|J|\sum_{\mathbf{h}} C(h) e^{i\mathbf{k}\mathbf{h}})^{1/2}$. Since $n_0/N < s/N \ll 1$, and $\sum_{\mathbf{h}} C(h) e^{i\mathbf{k}\mathbf{h}}$ is of the same order of magnitude as $|J|$, such a region clearly exists.

where

$$A_k = (N/2n_0 \sum_h C(h)\, e^{i(kh)}\, |E(k) - |J|\, k^2 a^2 + \frac{2n_0}{N} \sum_h C(h)\, e^{i(kh)}], \quad (28)$$

one can verify that the Hamiltonian (25) is diagonalized, while one obtains for the energy of the quasi-particles the expression:

$$E(k) = \left[\frac{4n_0}{N} \sum_h C(h)\, e^{i(kh)}\, |J|\, k^2 a^2 + J^2 k^4 a^4\right]^{1/2}. \quad (29)$$

One sees from this easily that the result (17), obtained in Sec. 2 by perturbation-theory methods, is obtained for large values of k.

In the region of small k it follows from (29):

$$E(k) \approx 2\left[\frac{n_0}{N} \sum_h C(h)\, e^{i(kh)}\, |J|\right]^{1/2} ak, \quad (30)$$

i.e., one obtains phonon-type ($E \sim k$) excitations which leads also, as is well known, to the presence of the superfluidity property in a system of bosons.[9,12]

4. Since the method of approximate second quantization and the application of perturbation theory lead to the identical result for large k, we can take expression (21) for the critical velocity u.* Since the left hand side of (21) depends, according to (17) and (19), only on J, C, a, and s/N, it follows from this that in the case under consideration the critical velocity u does not depend on the isotopic mass M (if we neglect the possible, very weak dependence of the lattice constant a on M). In that respect a gas of bosons differs from a gas of fermions where the critical velocity of superfluidity is determined from the relation $u = \tilde{\omega} e^{-1/\rho} k_F^{-1}$, according to reference 1, and thus depends on the ionic mass according to a $u \sim M^{1/2}$ law, through $\tilde{\omega}$. It is in this connection of interest to elucidate in how far the results obtained above are influenced by taking the interaction of the gas of bosons with the vibrations of the crystalline lattice into account. Putting

$$J_{qq'} = J^0_{qq'} + (\Delta R_q - \Delta R_{q'})\, (\mathrm{grad}\, J_{qq'})_0 + \ldots, \quad (31)$$

where the index 0 indicates the equilibrium values of quantities, and expanding the displacement ΔR_q of the g-th lattice site, caused by the temperature vibrations, from its equilibrium position in plane waves

$$\Delta R_q = \frac{1}{\sqrt{N}} \sum_{t_j} \mathbf{p}_{t_j} [\xi_{t_j} e^{i(t_j R_q)} + \xi^+_{t_j} e^{-i(t_j R_q)}], \quad (32)$$

*The arguments given below are also applicable, if we begin the determination of u with (30).

where $\mathbf{p}_{t_j}$ is the unit polarization vector and $\mathbf{t}_j$ the wave vector, one can separate from (5) the following part of the Hamiltonian, which describes the interaction of the bosons with the lattice vibrations:[11]

$$H_{ph} = g \sum_{(k-k'=t)} i \sqrt{\frac{\hbar\omega_t}{2V}}\, b^+_k b_{k'} \alpha^+_t - g \sum_{(k-k'=t)} i \sqrt{\frac{\hbar\omega_t}{2V}}\, b^+_k b_{k'} \alpha_t, \quad (33)$$

where the α_t are the Bose operators for the phonons, V the volume of the system, and where the coupling constant $g = 2\pi J a^{3/2}/3v\sqrt{M}$ does not depend on M, since the sound velocity $v \sim M^{-1/2}$.

If we now apply Fröhlich's canonical transformation[13] we can separate a boson-boson interaction caused by the phonons of the form:

$$H_{b(ph)} = -\frac{1}{2} g^2 \sum_{t,\, k,\, k'} \frac{\hbar\omega_t}{2V} \frac{(1 + \Delta(k,\, t))\,(1 - \Delta(k,\, t))}{\varepsilon_{k'-t} - \varepsilon_{k'} + \hbar\omega_t} b^+_k b_{k-t} b^+_{k'-t} b_{k'} + \text{c.c.}, \quad (34)$$

where Δ has the same meaning as in reference 13. We note there that although an expression of the form (34) was obtained by Fröhlich* for fermions, it retains its validity also for bosons, since in deriving (34) the commutation relations for the quasi-particle operators were in reference 13 only used to obtain the relation (2.26):

$$a^+_k a^+_q a_r - a^+_q a_r a^+_k a_l = \delta_{lq} a^+_k a_r - \delta_{kr} a^+_q a_l,$$

and this relation retains its validity, as can easily be checked, also for Bose operators.

It is clear from (34) that if $|\varepsilon_{k'-t} - \varepsilon_{k'}| < \hbar\omega_t$ the interaction induced by the phonons is attractive in nature and impedes thus the establishment of the superfluidity property in a system of bosons. $H_{b\,(ph)}$ does here not depend on M, since in (34) there is a cancellation of ω in the numerator and the denominator.

In this respect there exists a similarity with the case of fermions where the interaction induced by the phonons is also by itself independent of M.[2] As far as the dependence on M of the critical velocity and of the critical temperature (isotope effect) is concerned, they occur in the case of fermions because the region of the effective attraction induced by the phonons is restricted to

*The interaction (34) was introduced by Fröhlich[13] without taking Coulomb forces into account, but it is also valid when they are taken into account, if we understand by g the "screened" coupling constant.[14]

the region $\hbar\omega$. In the case of bosons, however, when it is essential for the occurrence of superfluidity that the repulsion dominates over the attraction, a restriction of the consideration to the region of the effective phonon attraction is clearly not necessary. It follows that, although in this case the attraction induced by the phonons decreases the magnitude of u (through the effective decrease of the magnitude of C which, by the way, improves the applicability of perturbation theory methods, expounded in Sec. 2), the dependence of u on M is, apparently, in the case of bosons appreciably weaker than in the case of fermions.

To conclude this section we note that the above-mentioned restriction on the region of the effectiveness of the attraction induced by the phonons leads in the case of fermions not only to a dependence of different characteristics of the superconducting state on M, but also introduces according to Bogolyubov's theory[1] (in contradistinction to the theory of Bardeen, Cooper, and Schrieffer[2]) a dependence of the criterion for superconductivity itself on M. The Bogolyubov-Tolmachev criterion, $\rho > \rho_C [1 + \rho_C \ln (\tilde{E}_F/\tilde{\omega})]^{-1}$ depends, namely, on $\tilde{\omega}$ and thus on M, while the Bardeen, Cooper, and Schrieffer criterion $\rho > \rho_C$ does not depend on M. Thus, if one isotope of some metal is superconductive, all other isotopes of this metal will, according to the Bardeen, Cooper, and Schrieffer criterion, also possess the superconducting property. According to the Bogolyubov-Tolmachev criterion, however, it is possible in principle that the heavy isotopes of a given metal possess the superconducting property, while its light isotopes (having a relatively larger value of $\tilde{\omega}$) will not possess this property. It is accordingly possible that when we go to lighter isotopes of superconducting metals there is displayed a disappearance of the superconducting property itself, instead of an increase of T_{cr} following from the $T_{cr} \sim M^{-1/2}$ dependence. Such an effect, if it does occur, will be superficially analogous to the disappearance of the superfluidity observed when one goes from He_4 to the light isotope He_3. It is necessary, however, to note that in this case the disappearance of superfluidity is usually explained not through the lowering of M, but through the different statistics (He_4: bosons; He_3: fermions).

5. What we have stated above leads to the conclusion that the occurrence in a given metal of the superconducting property is apparently not yet a sufficient indication for a purely Fermi character of the energy spectrum of its electron system. It is fully possible that there are superconductors where the current carriers behave with sufficient accuracy as bosons. In the latter case, the dependence of the critical quantities on M must be appreciably weaker than in the case of fermions. Apart from that, the temperature dependence of the transport coefficients in the ground state of a metal with Bose current carriers must be different from that of a metal with Fermi current carriers.[11] These differences between Bose and Fermi conductors enable us to expect that a combined study of different properties of superconductors both above and below the critical temperature $T_{cr} \sim M^{-1/2}$ dependence) should give us the possibility to solve experimentally the problem of whether the energy spectrum of every real superconductor belongs to the Bose or to the Fermi type.

[1] N. N. Bogolyubov, J. Exptl. Theoret. Phys. (U.S.S.R.) **34**, 58, 73 (1958), Soviet Phys. JETP **7**, 41, 51 (1958); Bogolyubov, Tolmachev, and Shirkov, Новый метод в теории сверхпроводимости (A New Method in the Theory of Superconductivity) Moscow, 1958, Fortsch. Phys. **6**, 605 (1958).

[2] Bardeen, Cooper, and Schrieffer, Phys. Rev. **108**, 1175 (1957).

[3] S. V. Vonsovskiĭ and M. S. Svirskiĭ, J. Exptl. Theoret. Phys. (U.S.S.R.) **35**, 1447 (1958), Soviet Phys. JETP **8**, 1012 (1959).

[4] V. L. Ginzburg, Usp. Fiz. Nauk **48**, 25 (1952), Fortsch. Phys. **1**, 101 (1953).

[5] M. R. Schafroth, Phys. Rev. **100**, 463 (1955).

[6] V. L. Ginzburg, J. Exptl. Theoret. Phys. (U.S.S.R.) **30**, 1151 (1956), Soviet Phys. JETP **3**, 952 (1956).

[7] S. Schubin and S. Wonsowsky, Physik. Z. Sowjetunion **7**, 292 (1935).

[8] S. V. Vonsovskiĭ, Usp. Fiz. Nauk **48**, 289 (1952), Fortsch. Phys. **1**, 239 (1953).

[9] N. N. Bogolyubov, Лекции по квантовой статистике (Lectures on Quantum Statistics) Kiev, 1947.

[10] M. S. Svirskiĭ and S. V. Vonsovskiĭ, Физика металлов и металлов. (Phys. of Metals and Metal Research) **4**, 392 (1957).

[11] Vonsovskiĭ, Vlasov, and Sokolov, J. Exptl. Theoret. Phys. (U.S.S.R.) **21**, 1185 (1951).

[12] L. D. Landau and E. M. Lifshitz, Статистическая физика (Statistical Physics) Moscow-Leningrad, 1951; Engl. Transl., Pergamon Press, London, 1958.

[13] H. Fröhlich, Proc. Roy. Soc. **A215**, 291 (1952).

[14] J. Bardeen and D. Pines, Phys. Rev. **99**, 1140 (1955).

Translated by D. ter Haar
236

EFFECT OF SPECIMEN SHAPE ON FERROMAGNETIC RESONANCE IN A STRONG RADIO-FREQUENCY FIELD

G. V. SKROTSKIĬ and Yu. I. ALIMOV

Ural' Polytechnic Institute

Submitted to JETP editor October 28, 1958

J. Exptl. Theoret. Phys. (U.S.S.R.) **36**, 1267-1271 (April, 1959)

We analyze the exact solutions of the Landau-Lifshitz equations for nonspherical ferromagnetic specimens in a radio-frequency field of arbitrary amplitude. An expression is derived for the threshold field h_c, above which instability in the motion of the magnetization vector begins. The slow decrease of the magnetization component and the shift of the resonance field strengths $h_0 > h_c$ are explained. It is shown that for $h_0 > h_c$ the height of the absorption peak decreases and its width increases.

1. Experiments by Damon[1] and by Bloembergen and Wang[2] have shown that the magnetization component M_z in the direction of a constant magnetizing field H_0 decreases with increasing microwave power. This decrease is, however, much slower than expected from a theory based on the approximate solution of the equation of motion for the magnetization.

It has been found, furthermore, that for a radio-frequency field with amplitude greater than a certain threshold field h_0 (considerably smaller than the width H of the absorption line), the contour of χ'' begins to broaden, and the position of the resonant absorption maximum shifts while its magnitude decreases. If $h_0 > h_c$, a broad additional absorption peak appears in fields H_0 that are somewhat less than the resonant field H_r.

A successful attempt at explaining the principal results of these experiments was made by Suhl.[3,4] Calling attention to the nonlinear character of the magnetization equation of motion

$$\dot{\mathbf{m}} + \gamma[\mathbf{m}\times\mathbf{H}^{ef}] + \alpha[\dot{\mathbf{m}}\times\mathbf{m}] = 0,$$

$$\mathbf{m} = \mathbf{M}/M_s, \quad \alpha > 0, \quad \gamma > 0, \tag{1}$$

where in the case of a thin ferromagnetic disk

$$H_x^{ef} = h_x - N_\perp M_s m_x,$$

$$H_y^{ef} = h_y - N_\perp M_s m_y, \quad H_z^{ef} = H_0 - N_\parallel M_s m_z, \tag{2}$$

Suhl shows that starting with a certain critical field value

$$h_c = \Delta H\,(3.08\,\Delta H/4\pi M_s)^{1/2}, \tag{3}$$

the motion of the vector $\mathbf{m}$ becomes unstable close to ferromagnetic resonance.

Assuming further that the homogeneity of magnetization is disturbed in ferromagnetic specimens of spheroidal shape by thermal excitation, Suhl improved on Eq. (3).

The theory developed by Suhl is based to a considerable extent on the assumption that the magnetization vector deviates little from the equilibrium position ($m_z \approx 1$); as will be shown later, this theory is not suitable when $h_c \approx \Delta H$.

It is easy to dispense with the foregoing assumption by using the exact solutions of Eq. (1), as done in reference 5. It now becomes possible to find for the threshold field h_c an expression that is valid over the entire range of values of the parameters that characterize the system.

2. In a coordinate system rotating with a frequency ω about the direction of the constant field $H_0 = H_z$, Eq. (1) for steady motion becomes

$$[\mathbf{m}\times\boldsymbol{\xi}] + \mathbf{m}\times[\mathbf{m}\times\boldsymbol{\Omega}] = 0. \tag{4}$$

where

$$\boldsymbol{\xi} = (\gamma\mathbf{H}^{ef} - \boldsymbol{\omega})/\alpha\omega, \quad \boldsymbol{\Omega} = \boldsymbol{\omega}/\omega. \tag{5}$$

By choosing the axes of the rotating coordinate system such that the radio-frequency $\mathbf{h} = (h_0 \cos t, h_0 \sin t, 0)$ has only a component along the abscissa axis, and solving (4) for m_x and m_y, we obtain

$$m_x = a(\xi_0 - \xi_N m_z)m_z/[(\xi_0 - \xi_N m_z)^2 + m_z^2], \tag{6}$$

$$m_y = -am_z^2/[(\xi_0 - \xi_N m_z)^2 + m_z^2], \tag{7}$$

where

$$\xi_0 = \frac{\gamma H_0 - \omega}{\alpha\omega}, \quad a = \frac{\gamma h_0}{\alpha\omega}, \quad \xi_N = \gamma\frac{N_\parallel - N_\perp}{\alpha\omega}M_s. \tag{8}$$

It is now easy to determine χ' and χ'', the real and imaginary parts of the complex susceptibility

$$\chi' = \chi_0(\xi_0 - \xi_N m_z)m_z/[(\xi_0 - \xi_N m_z)^2 + m_z^2], \tag{9}$$

$$\chi'' = \chi_0 m_z^2 / [(\xi_0 - \xi_N m_z)^2 + m_z^2], \qquad (10)$$

where $\chi_0 = \gamma M_s / \alpha\omega$ is the value of χ'' at resonance in rf fields with $h_0 \leq h_c$, when

$$\gamma H_r = \omega + \gamma M_s (N_\parallel - H_\perp). \qquad (11)$$

It is readily seen that the half-width ΔH of the absorption line equals in this case $\alpha\omega m_z/\gamma$, where $m_z = (1 + \sqrt{1 - a^2})/2$. Thus, in weak fields, when $a^2 \ll 1$, the half-width is $\Delta H_0 = \alpha\omega/\gamma$. When $h_0 \leq h_c$ is increased, the half-width decreases to a value

$$\Delta H_c = {}^1/_2 \Delta H_0 \{[1 - (h_c/\Delta H_0)^2]^{1/2} + 1\}. \qquad (12)$$

This decrease in width is usually small, since $h_c < \Delta H_0$.

Using (6) and (7) together with the condition $m^2 = 1$ we obtain the equation

$$\xi_0 = m_z \left[\xi_N \pm \left(\frac{a^2}{1 - m_z^2} - 1\right)^{1/2}\right], \qquad (13)$$

in which we can analyze and plot the dependence of m_z on ξ_0 for various values of the parameter a (Fig. 1). For homogeneous strictly spherical specimens, $\xi_N = 0$ and the biquadratic equation (13) is readily solved[5] with respect to m_z. As the field h_0 (the parameter a) increases, the minima of the curves drop and shift along the dotted line $\xi_0 = \xi_N m_z$. The projection of the component of the magnetization vector on the line $\xi_0 - \xi_N m_z$ is $m_X = 0$ ($\chi' = 0$).

Equation (13) is correct for all values of ξ_N and $m_z \leq 1$, to the extent that the initial equation (1) is correct.

The approximate equation analogous to (13), used by Suhl, has the following form in our symbols

$$\xi_0 = m_z \xi_N \pm \left(\frac{a^2}{1 - m_z^2} - 1\right)^{1/2} \qquad (14)$$

and differs from (13) in that it does not contain the factor m_z in front of the parentheses.

3. As can be seen from the curves of Fig. 1, within a fixed range of values of ξ_0, $m_z(\xi_0)$ is not single valued after a certain value $a = a_c$ is reached. The critical value of the parameter a_c can be determined from the condition $d\xi_0/dm_z = 0$, which, according to (13), leads to the equation

$$a^4 - (1 - m_z^2)^2 [2 + \xi_N^2 (1 - m_z^2)] a^2 + (1 + \xi_N^2)(1 - m_z^2)^4 = 0,$$

the solutions of which are real if

$$1 - m_z^2 \geqslant 2 [\sqrt{1 + \xi_N^2} - 1] \xi_N^{-2}.$$

Since here $a^2 > 1 - m_z^2$, we have

$$a_c^2 = 2 [\sqrt{1 + \xi_N^2} - 1] \xi_N^{-2}. \qquad (15)$$

If $\xi_N \gg 1$, then

$$a_c = (2/\xi_N)^{1/2} \ll 1, \qquad (16)$$

which is the same expression found by Suhl.

4. When $a \leq a_c$, the motion of the magnetization vector is stable everywhere. When $a > a_c$, the motion is unstable on the sections of the curve of Fig. 1 marked 2—3—4. The variation of m_z with the external field H_0 (the parameter ξ_0) follows therefore the curve 1—2—4—5. In this case the minimum of m_z and the maximum of χ'' occur not at the point 3, but at the point 4, where $\chi' \neq 0$. Therefore the resonant field, determined from the position of the maximum of χ'', will correspond not to condition (11), as would appear from an analysis of (10), but to a value of ξ_0 other than $\xi_0 m_z$. The geometric locus of the points were χ'' has a maximum is shown in Fig. 1 by a dotted line passing through the discontinuities of m_z.

Thus, the discontinuity in the motion of the magnetization vector should cause a slower reduction in m_z at resonant with increasing amplitude of

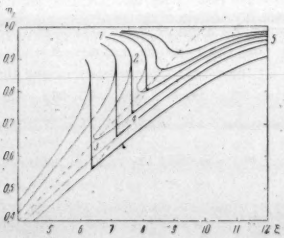

FIG. 1. Dependence of m_z on ξ for various values of the parameter a, at $\xi_N = 10$; the values of a (where $a^2 = 0.15$, 0.25, 0.36, 0.58, 1.0, and 2.0) are given in order of increasing gaps on the curves.

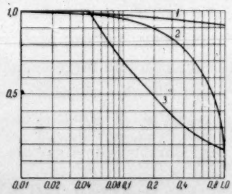

FIG. 2. Effect of non-sphericity of specimen on the character of the dependence of m_z on a^2 (curve 1) and of χ'' on a^2 (curve 3), for $\xi_N = 100$. The $m_z(a^2)$ curve for a homogeneously magnetized spherical specimen (curve 2) is shown for comparison.

the radio-frequency field h_0 than expected from condition (11) (Curve 1, Fig. 2).

In sufficiently weak fields, $a \leq a_c$, resonance occurs when condition (11) is satisfied. In this case $\chi'' = \chi_0$, i.e., constant. To ascertain the dependence of χ'' on a^2 when $a_c < a < 1$, we use the expression

$$\chi'' = \chi_0 (1 - m_z^2)/a^2, \qquad (17)$$

which is readily obtained from (10) and (13). According to the above, $1 - m_z^2$ increases more slowly than a^2. Therefore $\chi''(a^2)$ diminishes with increasing microwave power (a^2) when $h_0 > h_c$. A more rigorous analysis shows that the drop in $\chi''(a^2)$ begins with a value somewhat greater than h_c (Curve 3, Fig. 2). The greater $|\xi_N|$, the slower the drop in m_z and the faster the decrease in $\chi''(a^2)$.

It follows from (17) that the minimum of $m_z(\xi_0)$ for a given a corresponds to a maximum of $\chi''(\xi_0)$. Therefore, as the microwave power increases, the resonant frequency should shift. For $a \leq a_c$ this shift is determined by condition (11). When $a > a_c$ the shift can be determined graphically (dotted curve of Fig. 1).

By using (17) and (13) it is easy to plot curves of $\chi''(\xi_0)$ for various values of the parameter a. The width of the absorption line is found to increase with increasing $a > a_c$.

Thus, by accounting for the demagnetizing field in the specimen, it is possible to describe qualitatively the experimentally-observed peculiarities of ferromagnetic resonance in strong radio-frequency fields without making any assumptions whatever regarding the magnitude of M_z. However, certain details of the phenomenon are elusive and cannot be explained here. Thus, it does not follow directly from the analysis that an additional absorption maximum exists in fields where $a > a_c$, nor is it clear why the threshold field is small for specimens of nearly spherical shape.

Actually, for spherical specimens $N_{\parallel} = N_{\perp}$ and $\xi_N = 0$, and therefore $a_c = 1$. If the specimen is assumed spheroidal, even with a semi-axis ratio of 1.3, then according to Osborne[6] we have for nickel ferrite[3] ($\Delta H_0 = 50$ oe, $4\pi M_s/\Delta H_0 = 65$) $\xi_N = 6.6$ and $a_c = 0.51$, while the experimentally observed value is $a_c = 0.18$, corresponding to $\xi_N = 62$, which according to (8) can occur only for a thin disk. Thus, the assumption regarding the nonsphericity of the specimen cannot explain fully the small value of critical field observed in this case.

The presence of pores and of internal stresses, and the block-like nature of the specimen structure, may reduce substantially the value of the critical field. However, this problem has not been investigated experimentally.

To explain the smallness of the critical field in spheroidal specimens and the appearance of an additional absorption maximum it is necessary, according to Suhl, to take into account the presence of thermal magnetization fluctuations in the specimens. For this purpose it is necessary to include in the effective field (2) the fluctuation field, which disturbs the homogeneous precession. But in this case the peculiarities in the behavior of ferromagnets in a strong radio-frequency field can be described without the assumption that $m_z \approx 1$.

[1] R. W. Damon, Revs. Modern Phys. **25**, 239 (1953).
[2] N. Bloembergen and S. Wang, Phys. Rev. **93**, 72 (1954).
[3] H. Suhl, Proc. I.R.W. **44**, 1270 (1956).
[4] H. Suhl, J. Phys. Chem. Solids **1**, 209 (1957).
[5] G. V. Skrotskiĭ and Yu. A. Alimov, J. Exptl. Theoret. Phys. (U.S.S.R.) **35**, 1481 (1958), Soviet Phys. JETP 8, 1035 (1959).
[6] J. A. Osborne, Phys. Rev. **67**, 351 (1945).

Translated by J. G. Adashko
237

SOVIET PHYSICS JETP VOLUME 36 (9), NUMBER 4 OCTOBER, 1959

THE DISINTEGRATION OF UNSTABLE SHOCK WAVES IN MAGNETOHYDRODYNAMICS

G. Ya. LYUBARSKIĬ and R. V. POLOVIN

Physico-Technical Institute, Academy of Sciences, Ukrainian S.S.R.

Submitted to JETP editor October 30, 1958

J. Exptl. Theoret. Phys. (U.S.S.R.) **36**, 1272-1278 (April, 1959)

The fate of an unstable magnetohydrodynamic shock wave is considered; it is shown that such a wave must necessarily disintegrate into several waves among which there are fast and slow magnetoacoustic shock and similarity waves, Alfven discontinuities and a contact discontinuity. It is significant that disintegration of the unstable shock wave is accompanied by an increase in the entropy. The disintegration of a stable shock wave is impossible.

1. INTRODUCTION

ALTHOUGH the conditions for the stability of shock waves in ordinary and magnetohydrodynamics[1-3] are well known, it has not been explained what happens with an unstable magnetohydrodynamic shock wave if it is created in some fashion. This question is considered in the present paper in an example of a plane stationary shock wave in an ideal gas, on both sides of which the magnetic field makes a small angle with the normal to the plane of the discontinuity.

In Sec. 1, the qualitative picture of the disintegration is investigated. In Sec. 2, the problem of the disintegration is solved in zeroth approximation, with neglect of the small tangential magnetic field. In this case, the initial unstable shock wave disintegrates into two discontinuities. However, the approximate distance here between the discontinuities that are formed does not increase with time. Therefore, in making clear the possibility of such a disintegration, it is necessary to consider the following approximation. Consideration of the tangential magnetic field in first approximation is given in Sec. 3. In this approximation the initial shock wave disintegrates into four discontinuities. In Sec. 4, it is shown that in the consideration of a tangential magnetic field, the distances between the discontinuities which are formed continues to grow.

We note that, in order that the disintegration can actually take place, it is necessary not only that the distances between the discontinuities increase with time, but also that the discontinuities be stable. As follows from reference 2, satisfaction of the second condition automatically follows from the satisfaction of the first condition. Moreover, the process of disintegration must be accompanied by an increase in entropy. Satisfaction of this condition is also shown in Sec. 4.

We shall show that the value of the normal magnetic field H_x is such that on both sides of the discontinuity the Alfven velocity V_x is greater than the sound velocity c and the instability conditions are satisfied:[2,3]

$$V_{1x} < v_{1x}; \quad v_{2x} < V_{2x}, \tag{1}$$

where v_x is the velocity of the liquid relative to the front of the discontinuity; the index 1 refers to the region in front of the wave, the index 2 to that behind it. (The x-axis is directed perpendicularly to the plane of the discontinuity from the region 1 into region 2, the magnetic field lies in the xy plane, the plane of the discontinuity is at rest relative to the chosen system of coordinates, and the liquid moves parallel to the x axis in the positive direction.)

Such an unstable magnetohydrodynamic shock wave can be obtained if an ordinary stable hydrodynamic shock wave for which

$$v_{1x} > c_1; \; v_{2x} < c_2 \tag{1'}$$

is placed in a magnetic field (naturally, the liquid is assumed to be ideally conducting).

If such a wave disintegrates, then, in addition to the contact discontinuity, only plane shock and self-simulating waves* are formed. This results from the fact that a characteristic length is absent from the problem. The conditions for instability of the discontinuities that are formed superimposed restrictions on the possible picture of the

*Self-simulating in the narrow sense of this word applies to waves for which all the magnetohydrodynamic quantities depend upon the ratio x/t.

disintegration. As is well-known,[2] there exist three types of stable discontinuities: fast and slow magnetoacoustic shock waves, rotational (Alfven) discontinuities and three types of simple waves:[5] fast and slow magnetoacoustic, and rotational (magnetohydrodynamic).

The self-simulating waves are a special case of the simple waves. However, the rotational simple waves cannot be self-simulating, since the velocity in front of the front of a simple rotational wave is equal to the velocity of the back of the front; therefore, there exist only two types of self-simulating waves: fast and slow magnetoacoustic waves.

The velocity of all the enumerated waves are such that on each side there is propagated not more than three waves: in front, the fast magnetoacoustic (shock or self-simulating); behind, rotational discontinuity and, finally, the slow magnetoacoustic wave (shock or self-simulating). Waves traveling to the left are separated by the contact discontinuity from waves traveling to the right.

The amplitudes of these 7 waves should be determined such that the sum of the jumps of each of the seven magnetohydrodynamical quantities (ρ, p, v_x, v_y, v_z, H_y, H_z) on these waves is equal to the initial jump:

$$\sum_{i=1}^{7} \Delta_i \rho = \rho_2 - \rho_1; \quad \sum_{i=1}^{7} \Delta_i v_x = v_{2x} - v_{1x} \tag{2}$$

and so forth.

For simplification of the calculation, we shall assume that the initial magnetic field makes a small angle with the normal to the surface of discontinuity, i.e., that the tangential magnetic fields H_{1y} and H_{2y} are very small. Without limitation of generality, it can be assumed that $v_{1z} = v_{2z} = 0$, and the quantities v_{1y} and v_{2y} are small.

We note that even after the disintegration the component of the magnetic field H_z is identically equal to zero.

2. ZEROTH APPROXIMATION

We shall solve the problem of the disintegration by the method of successive approximations, neglecting in zeroth approximation the quantities H_{1y}, H_{2y}, v_{1y}, v_{2y}, and in the first approximation, the squares of these quantities.

In the determination of the type of waves being formed, it must be kept in mind that if a tangential magnetic field is absent in front of the fast magnetoacoustic wave, then the wave cannot be self-simulating. Actually, for each plane magnetoacoustic wave, the following relation is satisfied:[4,5]

$$dH_y / d\rho = u_\pm^2 H_y / \rho (u_\pm^2 - V_x^2), \tag{3}$$

where

$$u_\pm^2 = {}^1/_2 [V^2 + c^2 \pm \sqrt{(V^2 + c^2)^2 - 4c^2 V_x^2}\,], \quad V = H / \sqrt{4\pi\rho},$$

u_+ corresponds to the fast, and u_- to the slow acoustic wave.

Multiplying the relation (3) by H_y and noting that $u_-^2 < V_x^2 < u_+^2$, we find that $dH_y^2/d\rho > 0$ for the fast magnetoacoustic wave, and $dH_y^2/d\rho < 0$ for the slow magnetoacoustic wave. On the other hand, it is known[5-7] that the density decreases in self-simulating magnetoacoustic waves. From this it follows that in the fast magnetoacoustic wave, the magnetic field decreases, while in the slow, it increases. It is easy to show that the opposite conditions are satisfied in shock waves. Therefore, on the forward front of the fast magnetoacoustic self-simulating wave, the tangential magnetic field cannot be equal to zero.

From this it follows that the fast magnetoacoustic waves formed as a result of the disintegration are shock waves, if only they are not equal to zero in zeroth approximation.

It is easy to prove that the conditions (2) in zeroth approximation correspond to a disintegration into two shock waves traveling to the left,* while the magnetohydrodynamical quantities in the region included between these waves are equal to

$$\tilde{\rho} = \rho_1 v_{1x}^2 / V_{1x}^2; \quad \tilde{v}_x = V_{1x}^2 / v_{1x},$$

$$\tilde{p} = p_1 + \frac{\rho_1 (v_{1x}^2 - V_{1x}^2)}{3V_{1x}^2} (3c_1^2 + v_{1x}^2 - V_{1x}^2),$$

$$\tilde{v}_y = \eta \left[\frac{2}{3} \frac{v_{1x}^2 - V_{1x}^2}{v_{1x}^2} (4V_{1x}^2 - v_{1x}^2 - 3c_1^2) \right]^{1/2},$$

$$\tilde{H}_y = \eta \left[\frac{8\pi\rho_1}{3} \frac{v_{1x}^2 - V_{1x}^2}{V_{1x}^2} (4V_{1x}^2 - v_{1x}^2 - 3c_1^2) \right]^{1/2},$$

$$\eta = \pm 1. \tag{4}$$

If the velocity v_{1x} differs slightly from the velocity V_{1x} and $v_{2x} < u_{2-} = c_2$, then such a disintegration is possible only for $v_{1x} > V_{1x}$, i.e., only when the stability conditions[2,3] of the initial shock wave are not satisfied. It follows from this that for $v_{1x} < V_{1x}$ the expressions for $\tilde{H}_y$ and $\tilde{v}_y$ become imaginary.

The conditions (2) will also be satisfied when there is an Alfven discontinuity between the shock waves that are formed, making an angle π with the tangential magnetic field.

*This circumstance was noted by S. I. Syrovatskii in a lecture at the Conference on Applied Theoretical Problems of Magnetohydrodynamics.[8]

It can also be shown that there can be no other disintegrations of the initial wave which satisfy the equations (2) in zeroth approximation, if the quantity $\alpha = \sqrt{(v_{1x} - V_{1x})/V_{1x}}$ is sufficiently small and the amplitudes of all the waves are small except the slow magnetoacoustic wave traveling to the left.

We note that these waves are compressional waves, i.e., they satisfy the well-known condition of thermodynamic stability.[9-11]

The two waves found in the zeroth approximation lie at the boundary of the region of stability and have a velocity equal to zero. Therefore one cannot yet see at this stage of the calculation that the waves formed as a result of the disintegration of the initial wave are stable. In this connection, we proceed to the first approximation, i.e., we shall consider quantities of the order H_{1y}, v_{1y}, H_{2y}, v_{2y}.

3. FIRST APPROXIMATION

The schematic picture of the disintegration of the initial wave is shown in the drawing. The dotted line indicates the contact discontinuity. The fast and slow magnetoacoustic waves are located on either side of it. The Alfven discontinuities, indicated by the dashed lines, are located between the magnetoacoustic waves. The regions between the waves are denoted by the indices 1, 1′, 1″, 2‴, 2‴, 2″, 2′, 2. We shall denote the corresponding magnetohydrodynamical quantities by H_{1y}, H'_{1y}, ..., etc.

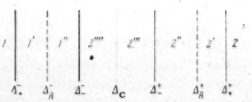

The discontinuities in the magnetohydrodynamical quantities on waves of small intensity are related among themselves in first approximation in the following way:

fast magnetoacoustic wave:

$$\Delta_+^+ v_y = -\Delta_+^+ H_y / \sqrt{4\pi\rho_2}; \tag{5}$$

slow magnetoacoustic wave:

$$\Delta_-^+ p = c_2^2 \Delta_-^+ \rho, \quad \Delta_-^+ v_x = \frac{c_2}{\rho_2} \Delta_-^+ \rho; \tag{6}$$

contact discontinuity:

$$\Delta_c \rho \neq 0.$$

Δ denotes the discontinuity undergone by the magnetohydrodynamical quantity in the passage of the wave. The upper index on Δ gives the direction of motion of the wave: the sign (+) to the right, the sign (−) to the left; the lower indices (+), (−), (A), and (c) correspond to the fast and slow magnetoacoustic waves, the Alfven wave and the contact discontinuity, respectively. All discontinuities not written down are equal to zero in the first approximation.

On the Alfven waves, the relations

$$H''_{1y} = \gamma_{i1} H'_{1y}, \quad v''_{1y} = v'_{1y} + V'_{1y}(\gamma_{i1} - 1); \tag{7}$$

$$H''_{2y} = \gamma_{i2} H'_{2y}, \quad v''_{2y} = v'_{2y} + V'_{2y}(1 - \gamma_{i2}). \tag{8}$$

are satisfied.

The remaining magnetohydrodynamical quantities do not change on Alfven discontinuities. The value of η_1 is equal to unity if the Alfven wave traveling to the left is absent, and is equal to -1 if this wave intersects the magnetic field at the angle π. The coefficient η_2 has analogous meaning for the Alfven wave traveling to the right.

The following general boundary conditions are satisfied on the two magnetoacoustic shock waves traveling to the left, whose intensity is not small:

$$\Delta[\rho(v_x - U)] = 0, \tag{9}$$

$$\Delta[H_x v_y - (v_x - U) H_y] = 0, \tag{10}$$

$$\Delta[\rho(v_x - U) v_y - H_x H_y / 4\pi] = 0, \tag{11}$$

$$\Delta[p + \rho(v_x - U)^2 + H_y^2 / 8\pi] = 0, \tag{12}$$

$$\Delta\left[\frac{5}{2}\frac{p}{\rho} + \frac{1}{2}(v_x - U)^2 + \frac{1}{2} v_y^2 + \frac{H_y}{4\pi\rho} - \frac{H_x H_y v_y}{4\pi\rho(v_x - U)}\right] = 0. \tag{13}$$

Let us consider in more detail Eqs. (9) — (13) on the fast magnetoacoustic wave traveling to the left. For simplicity of calculation, we shall consider the quantity α to be small in what follows. Introducing the notation $\delta H_y = H'_{1y} - \widetilde{H}_y$, $\delta\rho = \rho'_1 - \widetilde{\rho}$, ..., etc., we obtain from (9) — (13)

$$\delta\rho = \rho_1 \widetilde{v}_y \beta^{-2} \delta H_y / \sqrt{4\pi\rho_1} + O(\alpha H_{1y}),$$

$$\delta v_x = -V_{1x} \widetilde{v}_y \beta^{-2} \delta H_y / \sqrt{4\pi\rho_1} + O(\alpha H_{1y}),$$

$$U_+ = -\tfrac{1}{2} V_{1x} \widetilde{v}_y \beta^{-2} \delta H_y / \sqrt{4\pi\rho_1} + O(\alpha H_{1y}),$$

$$\delta v_y = \delta H_y / \sqrt{4\pi\widetilde{\rho}} - (\widetilde{v}_y^2 / 2\beta^2)\delta H_y / \sqrt{4\pi\rho_1} + v_{1y} - H_{1y} / \sqrt{4\pi\rho_1} + O(\alpha^2 H_{1y}), \tag{14}$$

where $\beta^2 = V_{1x}^2 - c_1^2$.

In order to find the quantities δH_y, U_-, $\Delta_{kc}\rho$, $\Delta_-^+\rho$, $\Delta_-^+ H_y$, we return to the five boundary conditions (9) — (13) on the slow magnetoacoustic shock wave traveling to the left. These equations lead to the following results:

$$U_- \sim \Delta_-^+ p \sim \Delta_c \rho \sim \alpha H_{1y}, \qquad \gamma_{i2} \frac{\Delta_+^+ H_y}{\sqrt{4\pi\rho_2}} = \frac{-2v_{1y} + 2V_{1y} + 2v_{2y} + 2V_{2y}(1-\eta_2) - \eta_2 V_{2y}\sqrt{\rho_2/\rho_1} + O(\alpha^2 H_{1y})}{2 + \sqrt{\rho_2/\rho_1}}, \tag{15}$$

$$\gamma_{i1} \frac{\tilde{v}_y^2}{2\tilde{v}^2} \frac{\delta H_y}{\sqrt{4\pi\rho_1}} = \frac{V_{1y} - v_{1y} + v_{2y} + V_{2y}}{1 + 2\sqrt{\rho_1/\rho_2}} + O(\alpha^2 H_{1y}). \tag{16}$$

Equations (15), (16), together with the formulas (4), (5), (6), (14) permit us to determine the values of the magnetohydrodynamical quantities in all regions for small α.

4. STABILITY OF ALL THE WAVES GENERATED

As we shall now show, the requirement of stability of the waves permits a unique determination of the values of the quantities η, η_1, and η_2.

We begin with the slow magnetoacoustic wave. For its stability, it is necessary that

$$v_{2x}' - U_- < u_{2-}';$$

$$v_{1x}' - U_- > u_{1-}'; \quad v_{1x}' - U_- < V_{1x}'. \tag{17}$$

The first and second of these inequalities reduce in zeroth approximation to the relations $v_{2X} < c_2$, $\tilde{V}_X > \tilde{u}_-$. The first of these is satisfied by virtue of (1′), and the second is an identity. In view of the smallness of H_{1y}, v_{1y}, H_{2y}, v_{2y}, these inequalities remain valid in higher approximations. The last inequality of (17) reduces to the relation

$$\gamma_i \gamma_{i1} (V_{1y} - v_{1y} + v_{2y} + V_{2y}) > 0. \tag{18}$$

for small α.

The conditions for stability of the fast magnetoacoustic wave traveling to the left have the following form

$$v_{1x}' - U_+ > u_{1+}', \quad v_{1x}' - U_+ < u_{1+}', \quad v_{1x}' - U_+ > V_{1x}'. \tag{19}$$

The first two inequalities of (19) reduce in zeroth approximation to the relations $v_{1X} > V_{1X}$, $\tilde{V}_X < \tilde{u}_+$. The first of these is satisfied by virtue of (1), while the second is an identity for $\tilde{H}_y \neq 0$. The last of the inequalities (19) reduces, for small α, to the expression

$$\gamma_i H_{1y} > 0 \quad \text{if} \quad \gamma_i = \operatorname{sign} H_{1y}. \tag{20}$$

We shall now consider the boundary conditions on the initial wave, connecting the quantities H_{1y}, v_{1y}, H_{2y}, v_{2y}. For small α, they reduce to the relations

$$v_{2y} - v_{1y} = V_{1y}; \; V_{2y} = -2\alpha^2 V_{1y}/(1 - \rho_1/\rho_2). \tag{21}$$

It follows from the relations (18), (21) that

$$\gamma_{i1} = 1, \tag{22}$$

i.e., the Alfven discontinuity traveling to the left is absent.

We note that upon satisfaction of the inequalities (17), (19), waves traveling to the left diverge.

Equations (15) and (21) show that $|H_{2y}'| \gg |H_{2y}|$. This increase in the magnetic field or in the fast magnetoacoustic wave is evidence that the latter is a shock and not a self-simulating wave. For such a wave and for small α, the relation

$$\Delta_+^+ p = (\Delta_+^+ H_y)^2/8\pi (V_{2x}^2 - c_2^2) < 0, \tag{22a}$$

is valid, indicating that this shock wave is a compressional wave. It then follows that it is thermodynamically stable. Proof of the mechanical stability of this wave is not carried out, since it requires the solution of the problem with account of quantities of the order H_{1y}^2. However, assuming that such stability does exist, we can determine the value of η_2. In fact, the tangential magnetic field has the same direction[7] on the two sides of the stable magnetoacoustic shock wave. This means that the quantities H_{2y} and $\Delta_+^+ H_y$ have the same sign. According to Eqs. (15), (21), this takes place for $\eta_2 = -1$.

Thus, the unstable shock wave under consideration disintegrates into four waves (if we neglect waves whose amplitudes are of the order of αH_{1y}): a fast magnetoacoustic shock wave traveling to the left with amplitude of the order α and velocity of the order V_{1y}; a slow magnetoacoustic shock wave traveling to the left with amplitude which differs slightly from the amplitude of the initial wave, and a velocity of the order αH_{1y}; an Alfven discontinuity traveling to the right and making an angle π with the magnetic field; and, finally, a fast magnetoacoustic shock wave traveling to the right with amplitude of the order H_{1y}.

The inequality $|U_+| \gg |U_-|$ leads to the result that the process of disintegration of the initial wave is accompanied by an increase in entropy. This means that the shock wave under consideration is unstable relative to disintegration not only from the viewpoint of mechanics but also in a thermodynamic sense.

In conclusion, we note that the case in which the magnetic field is strictly perpendicular to the initial unstable wave is excluded, since in this case the unstable wave cannot disintegrate spontaneously. However, upon collision of it with magnetoacoustic shock waves of small intensity, which are incident on it from two sides, it disintegrates into stable waves in which two of them have finite amplitude. This follows from the calculation carried out above; the boundary conditions (21) are replaced by the relations

$$v_{1y} = -V_{1y};\ v_{2y} = V_{2y}, \qquad (22b)$$

which hold for fast magnetoacoustic shock waves of low intensity and for $H_y \ll H_x$. The number of Alfven waves arising in the disintegration of an unstable wave is equal to zero, one or two, depending on the relation between V_{1y} and V_{2y}.

The authors take this opportunity to express their sincere gratitude to A. I. Akhiezer, A. S. Kompaneets, L. D. Landau and I. M. Lifshitz for discussions and useful advice.

[1] L. D. Landau and E. M. Lifshitz, Механика сплошных сред (Mechanics of Continuous Media) GITTL, Moscow, 1954.

[2] A. I. Akhiezer, G. Ya. Lyubarskiĭ and R. V. Polovin, J. Exptl. Theoret. Phys. (U.S.S.R.) **35**, 731 (1958); Soviet Phys. JETP **8**, 507 (1959).

[3] V. M. Kontorovich, "Conference on applied and theoretical problems of magnetohydrodynamics" (abstracts of papers). Academy of Sciences Latvian SSR Press, Riga, 1958, p. 8; J. Exptl. Theoret. Phys. (U.S.S.R.) **35**, 1216 (1958), Soviet Phys. JETP **8**, 851 (1959).

[4] A. I. Akhiezer, G. Ya. Lyubarskiĭ, and R. V. Polovin, Укр. физ. журн. (Ukr. J. Phys.) **3**, 433 (1958).

[5] A. G. Kulikovskiĭ, Dokl. Akad. Nauk SSSR **121**, 987 (1958); Soviet Phys. "Doklady" **3**, 743 (1958).

[6] G. Ya. Lyubarskiĭ and R. V. Polovin, J. Exptl. Theoret. Phys. (U.S.S.R.) **35**, 509 (1958), Soviet Phys. JETP **8**, 351 (1959).

[7] G. Ya. Lyubarskiĭ and R. V. Polovin, Укр. физ. журн. (Ukr. J. Phys.) **3**, 567 (1958).

[8] S. I. Syrovatskiĭ, "Conference on applied and theoretical problems of magnetohydrodynamics" (Abstracts of papers). Academy of Sciences Latvian SSR Press, Riga, 1958, p. 9; J. Exptl. Theoret. Phys. (U.S.S.R.) **35**, 1466 (1958); Soviet Phys. JETP **8**, 1024 (1959).

[9] S. V. Iordanskiĭ, Dokl. Akad. Nauk SSSR **121**, 610 (1958); Soviet Phys. "Doklady" **3**, 736 (1958).

[10] R. V. Polovin and G. Ya. Lyubarskiĭ, J. Exptl. Theoret. Phys. (U.S.S.R.) **35**, 510 (1958); Soviet Phys. JETP **8**, 351 (1959).

[11] R. V. Polovin and G. Ya. Lyubarskiĭ, Укр. физ. журн. (Ukr. J. Phys.) **3**, 571 (1958).

[12] L. D. Landau and E. M. Lifshitz, Электродинамика сплошных сред (Electrodynamics of Continuous Media) GITTL, Moscow, 1957.

Translated by R. T. Beyer
238

ANOMALOUS SPINORS AND BOSONS

A. M. BRODSKIĬ and D. D. IVANENKO

Moscow State University

Submitted to JETP editor November 5, 1958

J. Exptl. Theoret. Phys. (U.S.S.R.) 36, 1279-1285 (April, 1959)

A discussion is given of spinors and bosons which behave unusually under inversions and which in particular illustrate the anomalous commutation relations given by Gel'fand and Tsetlin. Possibilities of setting up such wave functions for various particles are indicated.

THE discovery of the isotopic-spin and strangeness properties of particles and the discovery of parity nonconservation in the weak interactions show the need for a more careful study of the properties of spinors and bosons under inversions. The usual representations of the Lorentz group are inadequate for the description of the whole extent of new properties of particles. In this connection the theory of isotopic space (three-dimensional or four-dimensional) has been developed.[1] Also it is found that the application of previously neglected possibilities of projective representations in the theory of spinors and "integrons" (particles of integer spin) even offers hopes of arriving at a description of isotopic spin and strangeness within the framework of ordinary space.[2] These questions acquire importance in applications of the method of fusion[3] and of compound-particle models,[4] and even in connection with the program of the nonlinear theory of matter,[5] in which unusual types of spinors have to be taken into account as possible elements of the field. Our problem is the analysis of the new types of spinors, and also the indication of unusual bilinear combinations and the examination of spin and statistics in this context.

We shall list the notations to be used:

$$ab = a_\mu b_\mu = a_i b_i - a_0 b_0, \quad (i = 1, 2, 3),$$

$$\gamma_i = -\gamma_i^+ = \begin{pmatrix} 0 & i\sigma_i \\ i\sigma_i & 0 \end{pmatrix}, \quad \gamma_0 = \gamma_0^+ = \begin{pmatrix} 0 & iE_2 \\ -iE_2 & 0 \end{pmatrix},$$

$$\gamma_5 = \begin{pmatrix} -iE_2 & 0 \\ 0 & iE_2 \end{pmatrix}. \tag{1}$$

The charge-conjugate spinor is best defined by the "anti-involution" relation

$$\psi^{C'} = \gamma_2 \psi^*, \quad \psi = -\gamma_2 \psi^{C'*} \tag{2}$$

It is also possible to use the more common relation[6]

$$\psi^C = i\gamma_0 \psi^{C'} = i\gamma_0 \gamma_2 \psi^* = C\psi^*, \quad \psi = i\gamma_0 \gamma_2 \psi^{C*}. \tag{2'}$$

In both cases the charge-conjugate spinors transform apart from sign like the original spinors. The definition (2) possesses an advantage in view of the theorem: "Under the substitution $\psi \to \psi^{C'}$ every bilinear combination $\psi^*\gamma\psi$, $\tilde{\psi}\gamma\psi$, etc. (γ is a 4×4 matrix) goes over into the complex-conjugate quantity" (in the case of (2') we get ± the complex conjugate for $\psi \to \psi^C$). Thus the change from ψ to $\psi^{C'}$ is a generalization of complex conjugation.

Let us denote the product of the three space reflections by P and the geometric time reversal by T^0. Lagrangians must be invariant with respect to P and the Schwinger inversion $T' = T^0 \times (\sim)$, where the tilde denotes transposition of operators in Hilbert space.[6] Invariance under T′ is in the last analysis equivalent to the condition of invariance under T^0 of the time-ordered T-products of operators in the Heisenberg representation. In virtue of the Hermitian property we have for the Lagrangian

$$T' = T^0 \times (\sim) = T^0 \times (*). \tag{3}$$

In its turn the operation of complex conjugation (*) reduces to two changes: first, replacement of operators by the charge-(complex)-conjugate operators in the sense of Eq. (2), and second, replacement of i by −i.

Let us list the various possibilities for the behavior of spinors under the geometrical reflections of the coordinates and the time (under rotations preserving the sense of the time all spinors have the same behavior), giving besides the previously known basic types I and II[6,9] the spinors of types III and IV that we have pointed out:[10]

"normal" spinors (type I)

$$\psi^{11} \to \pm \gamma_4 a_\mu \gamma_\mu \psi^{11}, \quad a^2 = \pm 1,$$

"pseudospinors" (type II)

$$\psi^{22} \to \pm a_\mu \gamma_\mu \psi^{22}, \quad a^2 = \pm 1,$$

"mixed" spinors (type III)

$$\psi^{12} \to \begin{cases} \pm \gamma_5 a_\mu \gamma_\mu \psi^{12}, & a^2 = +1 \\ \pm a_\mu \gamma_\mu \psi^{12}, & a^2 = -1, \end{cases} \tag{4}$$

and "mixed" spinors (type IV)

$$\psi^{21} \to \begin{cases} \pm a_\mu \gamma_\mu \psi^{21} & a^2 = +1 \\ \pm \gamma_5 a_\mu \gamma_\mu \psi^{21} & a^2 = -1 \end{cases}$$

(a_μ is the unit vector normal to the hypersurface with respect to which the reflection occurs; the first of the upper indices on the refers to space reflection, the second to time reflection).

We must further allow for the possibility of introducing additional factors $\pm i$ as well as ± 1 for space and time reflections (individually and collectively)* for all four fundamental types of spinors, in the same way as the factors ± 1, $\pm i$ were introduced earlier for space inversion of spinors of the type ψ^{11}.† Generalizing the Yang-Tiomno notation, we can introduce, for example, a spinor ψ^{1A2D} which transforms under space reflections by the matrix

$$+ \gamma_5 a_\mu \gamma_\mu, \quad a_\mu^2 = +1, \tag{5.1}$$

and under time reflection by the matrix

$$- i a_\mu \gamma_\mu, \quad a_\mu^2 = -1 \text{ and so on} \tag{5.2}$$

Thus one gets 64 distinct types of spinors. As can easily be verified, for all spinors of types A, B, (4) the square of a space reflection is $P^2 = -1$ (or a rotation through 2π), and the square of a time reflection is $T^2 = 1$; for spinors C, D, $P^2 = 1$, $T^2 = -1$; for spinors AC, AD, BC, BD, CA, etc. (for meanings of notations A, B, C, D see the paper of Yang and Tiomno[11]), $P^2 = T^2 = \pm 1$. Self-adjoint (Majorana) spinors that do not vanish identically can only be of types CD, DC, CC, DD, since in this case, following the inversion invariance, we can set

$$\psi = \Omega \psi^c = \Omega i \gamma_5 \gamma_2 \psi^*, \quad |\Omega|^2 = 1. \tag{6}$$

For the spinors of types I and II with homogeneous behavior (of any of the classes A, B, C, D)

$$PT = -TP,$$

but for the "mixed" spinors ψ^{12} and ψ^{21} (classes A, B, C, D)

$$PT = TP \tag{6'}$$

(one can choose $P = T$).

Thus we can say that our "mixed" spinors directly realize what can reasonably be called the "anomalous" (cf. reference 7) four-dimensional spinor representation; for them the operations P and T commute, whereas for the "normal" spinors ψ^{11} and ψ^{22} of types I and II (all classes A, B, C, D) these operators anticommute.*

"Normal" spinors of the class $\psi^{1A1\dot{A}}$ are ordinarily assigned to the electron-positron field.

Under space reflections the bilinear combinations

$$\psi^* \gamma_0 \gamma \psi, \tag{7}$$

$$\psi \gamma_2 \gamma_0 \gamma \psi, \tag{7'}$$

formed from spinors ψ^{11} (classes A, B) have, as is well known, the behavior of a scalar, a vector, an antisymmetric tensor, a pseudovector, and a pseudoscalar. Under time reflections ($a^2 = -1$) the covariants (7) and (7') (classes A, B) get an additional factor -1, i.e., the scalar behaves like a pseudoscalar, and so on. Combinations of the type (7) formed from spinors ψ^{11} of classes BC, AD, AC, and so on, transform in an analogous way under inversions. Meanwhile the combinations (7') formed from spinors of these latter classes get an additional factor -1 under an inversion.

Thus the Lagrangian of a linear theory formed in the usual way from spinors of type I will be a scalar with respect to the operation P and a pseudovector with respect to the operation T^0. Therefore in order for the Lagrangian to be unchanged under the operation T' it must get multiplied by -1 by the operation of transposition ($\sim$), or, what is the same thing, the operation of complex conjugation ($*$). As the result we get, as usual, the Lagrangian† (we have written out as an illustration the case of interaction with the electromagnetic field; the indices 11, AB, CD, etc. are omitted):

*Here it must be remembered that the cases $\pm i$, ± 1 refer to representations of the complete Lorentz group, as supplemented with the reflections in different ways.

†In a number of cases the transformation matrices of the various spinors are equivalent under unitary transformation, and we can speak only of a relative difference. For example, ψ^{11} (A) and ψ^{22} (A), etc., or ψ^{12} (A) and ψ^{21} (A), etc., are equivalent in the usual sense, with the unitary transformation matrix $u = (1 + \gamma_5)/2^{1/2}$. When, however, we take into account the antilinear relations associated with the antiparticle conjugation, the equivalence is destroyed. In fact, $CA^* = -AC$ for $A = a_\mu \gamma_\mu$, but $C'A'^* = +A'C'$ for $A' = a_\mu \gamma_\mu \gamma_5 = 2^{-1/2}(1+\gamma_5)A$. $2^{-1/2}(1-\gamma_5)$, $C' = 2^{-1/2}(1+\gamma_5)\, C \cdot 2^{-1/2}(1-\gamma_5)$. Examination of the auxiliary pseudospinors defined by Cartan in a space of an arbitrary number of dimensions is especially useful for the introduction of the "mixed" spinors.

*We note that the "mixed" spinors ψ^{12} and ψ^{21} the well known formal difficulties[8] with the construction of a spinor theory in a Riemannian space are absent.

†In Eq. (8) the expressions are equal part from a divergence. We set $\hbar = c = 1$.

$$L = {}^1/_2\Big[(\gamma_0\gamma_\lambda)_{\alpha\beta}\left(\psi^*_\alpha i\frac{\partial\psi_\beta}{\partial x^\mu} - i\frac{\partial\psi^*_\alpha}{\partial x^\mu}\psi_\beta\right) + m(\gamma_0)_{\alpha\beta}(\psi^*_\alpha\psi_\beta - \psi_\beta\psi^*_\alpha)$$
$$+ eA_\mu(\gamma_0\gamma_\mu)_{\alpha\beta}(\psi^*_\alpha\psi_\beta - \psi_\beta\psi^*_\alpha)\Big]$$
$$= {}^1/_2[\psi^+\ \gamma_0\gamma_\mu i\partial\psi/\partial x^\mu + \psi^{C+}\gamma_0\gamma_\mu i\partial\psi^C/\partial x^\mu$$
$$+ eA_\mu(\psi^+\gamma_0\gamma_\mu\psi - \psi^{C+}\gamma_0\gamma_\mu\psi^C) + m(\psi^+\gamma_0\psi - \psi^{C+}\gamma_0\psi^C)]$$
$$= {}^1/_2[(\psi^+\gamma_0\gamma_\mu i\partial\psi/\partial x^\mu + \psi^{C+}\gamma_0\gamma_\mu i\partial\psi^C/\partial x^\mu)$$
$$+ eA_\mu(\psi^+\gamma_0\gamma_\mu\psi - \psi^{C+}\gamma_0\gamma_\mu\psi^C) + m(\psi^+\gamma_0\psi + \psi^{C+}\gamma_0\psi^C)]. \quad (8)$$

As can be seen from the first form given in Eq. (8), L changes sign under the operation of transposition, and consequently if it were the commutator, and not the anticommutor, of ψ and ψ^* that is a c-number the entire Lagrangian would reduce to a c-number. The arguments given are equivalent to a proof of the theorem of the connection between spin and statistics.[6]

For type I spinors ψ^{1A1A}, etc., the Dirac equation has the usual form

$$-i\gamma_\mu\partial\psi/\partial x^\mu + eA_\mu\gamma_\mu\psi + m\psi = 0. \quad (9)$$

In the case of the type II* pseudospinors ψ^{2A2A}, etc., the space vector and pseudovector (7) will have the same structures as for ψ^{11}, whereas the space scalar and pseudoscalar (7) are interchanged. Accordingly a γ_5 enters the mass term of the expression (8), and an equation of the Dirac type is written in invariant form as follows:[9,10]

$$-i\gamma_\mu\partial\psi/\partial x^\mu + eA_\mu\gamma_\mu\psi + \gamma_5 m\psi = 0, \quad (10)$$

and here the Hermitian character of the Lagrangian is preserved (despite reference 9), and also the connection between energy-momentum and mass,

$$\varepsilon^2 - \mathbf{p}^2 - m^2 = 0. \quad (11)$$

For type II spinors, which are normal, the proof of their satisfying Fermi statistics goes through just as for type I spinors, since, as follows from Eq. (4), for them L is a scalar with respect to P and a pseudoscalar with respect to T^0.

Let us introduce the operation of charge (antiparticle) conjugation

$$C: \psi\to\psi^C, \quad e\to -e, \quad i\to i, \quad m\to -m,$$
$$A_\nu\to A_\nu, \quad \varphi\to\varphi^* \quad (12)$$

or in more usual form

$$C: \quad \psi\to\psi^C, \quad e\to -l, \quad i\to i,$$
$$m\to m, \quad \varphi\to\varphi^* \quad (13)$$

In its action on the Lagrangian C differs from complex conjugation, and consequently also from transposition, by a factor -1; symbollically we can write

$$(\tilde{\ }) = (^*) = C\times(-1). \quad (14)$$

For normal spinors the operations $(\tilde{\ })$ and $(^*)$ change the sign of L, so as to compensate for the change of sign produced by T^0. Thus linear-theory Lagrangians for spinors of types I and II are automatically invariant with respect to C (in any case if we do not include the four-fermion interactions). This fact forms a part, applicable to normal particles, of the PCT (or PT′) theorem of Lüders, where the Wigner inversion $T = CT'$ is the time inversion T^0 with multiplication by -1 (for Hermitian quantities).

Let us pass to the consideration of the mixed spinors, for which the space scalar and pseudoscalar will also behave like a scalar and pseudoscalar, respectively, under the operation T^0. At the same time, just as in the case of the normal spinors, the space vector and pseudovector will behave under T^0 like a pseudovector and vector, respectively. From this follows the impossibility of constructing, without additional assumptions, an inversion-invariant Lagrangian for the anomalous spinors with a mass term that does not reduce to a c-number, and also a violation of the Lüders theorem. In this connection there are three possibilities. First, we could renounce invariance with respect to P, while preserving invariance with respect to T′. Then, for example for ψ^{12}, we can write the Lagrangian in the form

$$L = {}^1/_2\Big[(\gamma_0\gamma_\mu)_{\alpha\beta}\left(\psi^*_\alpha i\frac{\partial\psi_\beta}{\partial x^\mu} - i\frac{\partial\psi^*_\alpha}{\partial x^\mu}\psi_\beta\right) + m(\gamma_0\gamma_5)_{\alpha\beta}(\psi^*_\alpha\psi_\beta - \psi_\beta\psi^*_\alpha)$$
$$+ eA_\mu(\gamma_0\gamma_\mu)_{\alpha\beta}(\psi^*_\alpha\psi_\beta - \psi_\beta\psi^*_\alpha)\Big]$$
$$= {}^1/_2[(\psi^+\gamma_0\gamma_\mu i\partial\psi/\partial x^\mu + \psi^{C+}\gamma_0\gamma_\mu i\partial\psi^C/\partial x^\mu)$$
$$+ m(\psi^+\gamma_0\gamma_5\psi + \psi^{C+}\gamma_0\gamma_5\psi^C) + eA_\mu(\psi^+\gamma_0\gamma_\mu\psi - \psi^{C+}\gamma_0\gamma_\mu\psi^C]$$
$$= {}^1/_8\sum_{\pm}\Big\{[(1\pm i\gamma_5)\psi]^+\gamma_0\gamma_\mu i\frac{\partial}{\partial x^\mu}[(1\pm i\gamma_5)\psi] + [(1\pm i\gamma_5)\psi]^{C+}$$
$$\times\gamma_0\gamma_\mu i\frac{\partial}{\partial x^\mu}[(1\pm i\gamma_5)\psi]^C + eA_\mu([(1\pm i\gamma_5)\psi]^+\gamma_0\gamma_\mu[(1\pm i\gamma_5)\psi]$$
$$- [(1\pm i\gamma_5)\psi]^C\gamma_0\gamma_\mu[(1\pm i\gamma_5)\psi]^C) \pm im([(1\mp i\gamma_5)\psi]^+\gamma_0$$
$$\times[(1\pm i\gamma_5)\psi] - [(1\mp i\gamma_5)\psi]^C\gamma_0[(1\mp i\gamma_5)\psi]^C)\Big\}. \quad (15)$$

The Lagrangian (15) is not invariant with respect to P, but is invariant with respect to the combined transformation PC (if C for two-component spinors is defined, for example, by $[(1+i\gamma_5)\psi]\to[(1+i\gamma_5)\psi]^C$). In the case of the choice of Eq. (15) the Fermi statistics is preserved for the anomalous spinors; the Dirac-type equation for ψ^{12} has the form (10), noninvariant under P, and

*Unlike the others, type II spinors ψ^{22}, etc., can be carried over into a five-dimensional space.[2]

that for ψ^{21} has the inversion-noninvariant form (9).

Second, we could renounce the invariance with respect to T′, replacing it with invariance with respect to T = T′ × C, and preserving invariance with respect to P. In this case, for example for ψ^{12}, the Lagrangian can be written in one of two possible forms

$$L = {}^1/_2\Big[(\gamma_0\gamma_\mu)_{\alpha\beta}\Big(\psi^*_\alpha i\frac{\partial\psi_\beta}{\partial x^\mu} + i\frac{\partial\psi_\beta}{\partial x^\mu}\psi^*_\alpha\Big) + m(\gamma_0)_{\alpha\beta}(\psi^*_\alpha\psi_\beta + \psi_\beta\psi^*_\alpha) + eA_\mu(\gamma_0\gamma_\mu)_{\alpha\beta}(\psi^*_\alpha\psi_\beta + \psi_\beta\psi^*_\alpha)\Big]$$

$$= {}^1/_2\Big[\Big(\psi^+\gamma_0\gamma_\mu i\frac{\partial\psi}{\partial x^\mu} - \psi^{C+}\gamma_0\gamma_\mu i\frac{\partial\psi^C}{\partial x^\mu}\Big) + m(\psi^+\gamma_0\psi - \psi^{C+}\gamma_0\psi^C) + eA_\mu(\psi^+\gamma_0\gamma_\mu\psi + \psi^{C+}\gamma_0\gamma_\mu\psi^C)\Big]. \quad (16)$$

Unlike the previous ones, the Lagrangian (16) is invariant with respect to transposition. Consequently, the particles described by it must obey not the Fermi, but the Bose statistics (Bose spinors). There is, however, also a possible way of writing the Lagrangian that corresponds to Fermi statistics; thus in this case the unique relation between spin and statistics is lost.

Finally, we only mention the third possibility for constructing a Lagrangian for the anomalous spinors; this is based on doubling the number of components. This possibility has been discussed in earlier papers;[2,7] it also can be associated with a violation of the usual unique realtion between spin and statistics.

In the formation of bilinear (multilinear) expressions account should be taken of the possibility of using spinors of all types (I, II, III, IV, A, B, C, D, etc.) and thus getting unusual combinations. For example, Mirianashvili[12] has used combinations of spinors (A, B, C, D) to obtain bosoms of "imaginary parity," which transform under inversions with a factor ±1.

In an analogous way one can obtain anomalous "bosons," or it is better to say particles of integral spin ("integrons" with anticommuting P and T), by using combinations of mixed and normal spinors. Since one cannot construct from such bosons inversion-invariant combinations, one must resort to doubling the number of quantities, adding a scalar to the pseudoscalar, and so on, these being quantities that are interchanged on reflections. If anomalous integrons are formed by means of anomalous boson spinors, they will be fermions.

In conclusion we present as an example a possible preliminary assignment of particles and fields. We shall suppose that: 1) spinors of the class $\psi^{1A1A} = \psi^e$ describe electrons and positrons; 2) self-adjoint spinors $\psi^{1C1C} = \psi_\nu$, corresponding to zero mass, describe neutrinos;* 3) spinors $\psi^{2A2A} = \psi_\mu$ describe μ mesons. It is also possible in all cases to replace class A by B and C by D. Then we have as an invariant with respect to the strong inversion PC the Hermitian effective interaction (different spinors are assumed to anticommute):

$$\varphi_\pi\psi^+_\mu\gamma_0(1 - i\gamma_5)\psi_\nu - \varphi_\pi\psi^{C+}_\mu\gamma_0(1 + i\gamma_5)\psi_\nu.$$

At the same time, for the same reasons that bring about the absence of a mass term in the neutrino Lagrangian, the μ-meson decay will necessarily be of vector or pseudovector character:

$$\psi^+_e\gamma_0\gamma_\mu(1 + \gamma_5)\psi_\mu\cdot\widetilde{\psi}_\nu\gamma_0\gamma_2\gamma_\mu i\gamma_5\psi_\nu + \text{Herm. adj.}$$
$$= {}^1/_4[\psi^+_e\gamma_0\gamma_\mu(1 + \gamma_5)\psi_\mu(\widetilde{\psi}_\nu(1 - i\gamma_5)\gamma_0\gamma_2\gamma_\mu(1 + i\gamma_5)\psi_\nu + \widetilde{\psi}_\nu(1 + i\gamma_5)\gamma_0\gamma_2\gamma_\mu(1 - i\gamma_5)\psi_\nu)] + \text{Herm. adj.}$$

or $\psi^*_e\gamma_0\gamma_\mu(1 - \gamma_5)\psi_\mu\widetilde{\psi}_\nu\gamma_0\gamma_2\gamma_\mu\psi_\nu$ + Herm. adj.

Thus according to this scheme if decay of a π meson gives a neutrino with a definite circular polarization, the decay of the μ meson gives two neutrinos with the opposite circular polarization.

From this point of view it is natural to characterize baryons by the anomalous representations,[2] and best simply to assign to them anomalous spinors. Then the first alternative, which is physically the most acceptable, gives a separation of a spinor into two two-component semispinors that do not transform into each other under PC and T′, and this can be associated with the existence of isotopic pairs, for example proton and neutron. This gives a possibility of interpreting the isotopic spin group in the framework of ordinary space.

On the other hand, one could characterize the baryons by spinors of the normal classes, using assignments to the classes A, B, C, D to introduce the baryon number.

In conclusion we express our gratitude to G. A. Sokolik for a discussion of the results.

[1] A. Pais, Physica **19**, 869 (1953). D. Ivanenko and H. Sokolik, Nuovo cimento **6**, 226 (1957).

[2] G. A. Sokolik, J. Exptl. Theoret. Phys. (U.S.S.R.) **33**, 1515 (1957), Soviet Phys. JETP **6**, 1170 (1958). J. C. Taylor, Nucl. Phys. **3**, 606 (1957). J. A. McLennan, Jr., Phys. Rev. **109**, 986 (1958).

[3] L. de Broglie, Théorie des Particules à Spin

*According to the invariant condition (6), where it is convenient to take $\Omega = \pm i$, so that by fusion of two neutrinos one can obtain fields with the properties of photons.

(Méthod de Fusion), 2-me ed., Gauthier Villars, Paris 1954.

[4] S. Sakata, Prog. Theor. Phys. **16**, 686 (1956). W. Heisenberg, Rev. Mod. Phys. **29**, 269 (1957).

[5] A. M. Brodskiĭ and D. D. Ivanenko, Dokl. Akad. Nauk SSSR **120**, 995 (1958), Soviet Phys. "Doklady" **3**, 608 (1958).

[6] J. Schwinger, Phys. Rev. **82**, 914 (1951).

[7] I. M. Gel'fand and M. L. Tsetlin, J. Exptl. Theoret. Phys. (U.S.S.R.) **31**, 1107 (1956), Soviet Phys. JETP **4**, 947 (1957).

[8] É. Cartan, La Théorie des Spineurs (Russ. transl., IIL, Moscow 1947).

[9] I. S. Shapiro, Usp. Fiz. Nauk **53**, 14 (1957); J. Exptl. Theoret. Phys. (U.S.S.R.) **23**, 412 (1952).

[10] A. M. Brodskiĭ and D. D. Ivanenko, J. Exptl. Theoret. Phys. (U.S.S.R.) **33**, 910 (1957), Soviet Phys. JETP **6**, 700 (1958).

[11] C. N. Yang and J. Tiomno, Phys. Rev. **79**, 495 (1950). V. B. Berestetskiĭ and I. Ya. Pomeranchuk, J. Exptl. Theoret. Phys. (U.S.S.R.) **19**, 756 (1949). G. F. Zharkov, J. Exptl. Theoret. Phys. (U.S.S.R.) **20**, 492 (1950).

[12] M. Mirianashvili, Dissertation, Tbilisi (Tiflis) University, 1958; Тр. Ин-та физики ГрузССР (Trans. Phys. Inst. Georgian S.S.R.) No. 4 (1958). F. Gürsey, Phys. Rev. Letters **1**, 98 (1958).

Translated by W. H. Furry
239

THE GREEN'S FUNCTIONS METHOD IN QUANTUM STATISTICS

E. S. FRADKIN

P. N. Lebedev Physics Institute, Academy of Sciences, U.S.S.R.

Submitted to JETP editor December 19, 1958

J. Exptl. Theoret. Phys. (U.S.S.R.) **36**, 1286-1298 (April, 1959)

A Green's function method in quantum statistics is developed. It is shown that the various methods of statistical physics and the many-body theory, and also their generalization to cases of non-zero temperature (e.g., the methods of Debye-Hückel, Hartree-Fock, Thomas-Fermi, Gell-Mann and Brueckner), are contained in simple form in the resultant equations. A transition to time-dependent Green's functions is considered, and a method is given for determination of the energy spectrum.

INTRODUCTION

RECENTLY, great attention has been paid to the development of methods that differ from the ordinary thermodynamic perturbation theory in statistics, and the usual perturbation theory of the many-body problem. We shall not now review all the researches in this direction,* but shall only remark that the existing methods are manifold and require considerable calculations for their establishment.

It is natural to attempt to find a more general approach to the solution of the problems of quantum statistics, not connected with perturbation theory which, in particular, would give in simple graphic approximation the results of the corresponding methods. Such an approach is given by the Green's function method which had already been applied successfully to the case $T = 0$.[2] Matzubara[3] was the first to formulate the method of Feynman and introduce the Green's function for the case $T \neq 0$. However, the problem of the derivation of closed equations for these Green's functions in x-space has not been brought to solution, and the transformation to p-space, which would facilitate the possibility of a practical solution of the equations, has not been considered.

On the other hand, the development of high-energy physics requires the development of the formalism of quantum statistics, generally with account both of relativistic corrections and the second quantization of the Hamiltonian of the system. Finally, for the investigation of the energy spectrum of the system, it is necessary to know the time dependence of the Green's function as well.

The present article* is devoted to the consideration of these problems (see also reference 5).

1. THE EQUATIONS FOR THE GREEN'S FUNCTION IN QUANTUM STATISTICS

The density matrix of the canonical ensemble has the form

$$\rho = \exp\{-\beta(\hat{H} - \mu\hat{N})\}, \tag{1.1}$$

where $\beta = 1/kT$, $\hat{H}$ is the total Hamiltonian of the system, consisting of the Hamiltonian of the free field (H_0) and the interaction Hamiltonian H_I; μ is the chemical potential, and $\hat{N}$ is the operator of an integral number of surviving particles (for example, the difference in the number of electrons and positrons).

Without limiting the generality, we shall carry out our subsequent analysis, for the case of the interaction of a single Fermi field ψ (mass m) with a Bose field (mass κ).

The Hamiltonian of the interaction in this case is equal to

$$\hat{H}_I = -\int j(x)\varphi(x)\,d^3x, \tag{1.2}$$

$$j(x) = {}^1/_2 ig\,\mathrm{Sp}\,\gamma[\bar{\psi}(x)\psi(x) - \psi(x)\bar{\psi}(x)],$$

$$\hat{N} = \frac{1}{2}\int \mathrm{Sp}\,\gamma_4[\bar{\psi}(x)\,\psi(x) - \psi(x)\bar{\psi}(x)]\,d^3x. \tag{1.3}$$

We shall not take a specific form for the interaction γ and the variance of the field φ (for example, for electrodynamics, $\gamma = \gamma_\mu$, $\varphi = A_\mu$). By the usual methods of field theory[3] we get

*For the corresponding literature references, see reference 1.

*The authors have been informed that similar questions are considered by Abrikosov, Gorkov and Dzyaloshinskiĭ.[12]

$$\rho(\beta) = \rho_0(\beta) S(\beta), \quad \rho_0(\beta) = \exp\{-\beta(\hat{H}_0 - \mu\hat{N})\},$$

$$S(\beta) = T\exp\left\{-\int_0^\beta dx_4 \int H_1(x_4, \mathbf{x})\, d^3x\right\},$$

$$H_1(\mathbf{x}, x_4) = -j(\mathbf{x}, x_4)\varphi(\mathbf{x}, x_4), \tag{1.4}$$

where T denotes the regular position of the operators from right to left in order of increase in time, while the operator $f(\mathbf{x}, x_4)$ is determined from the relation

$$f(\mathbf{x}, x_4) = \rho_0(-x_4) f(\mathbf{x}) \rho_0(x_4). \tag{1.5}$$

By analogy with quantum field theory,[4] we generalize the interaction Hamiltonian, including the additional interaction with external sources of Bose (J) and Fermi (η) fields, namely,

$$\tilde{H}_1(\mathbf{x}, x_4) = -\{[j(\mathbf{x}, x_4) + J(\mathbf{x}, x_4)]\varphi(\mathbf{x}, x_4) + \bar{\eta}(\mathbf{x}, x_4)\psi(\mathbf{x}, x_4) + \bar{\psi}(\mathbf{x}, x_4)\eta(\mathbf{x}, x_4)\}. \tag{1.6}$$

From (1.4) and (1.6), we get:

a) for x_4 in the interval from 0 to β:

$$\delta\rho(\beta)/\delta J(\mathbf{x}, x_4) = \rho_0(\beta) S(\beta) S(-x_4)\varphi(\mathbf{x}, x_4) S(x_4) = \rho(\beta)\hat{\varphi}(\mathbf{x}, x_4),$$

$$\delta\rho/\delta\bar{\eta}(\mathbf{x}, x_4) = \rho\hat{\psi}(\mathbf{x}, x_4), \quad \delta\rho/\delta\eta(\mathbf{x}, x_4) = \rho\hat{\bar{\psi}}(\mathbf{x}, x_4),$$

$$\delta^2\rho/\delta\bar{\eta}(\mathbf{x}, x_4)\delta\eta(\mathbf{x}', x_4') = \rho T(\hat{\psi}(\mathbf{x}, x_4)\hat{\bar{\psi}}(\mathbf{x}', x_4')) \text{ etc.}; \tag{1.7}$$

b) for x_4 outside the interval from 0 to β, all functional derivatives are equal to zero.

The arbitrary operator $f(\mathbf{x}, x_4)$ is connected with the operator $f(\mathbf{x})$ by the relation

$$\hat{f}(\mathbf{x}, x_4) = \rho^{-1}(x_4) f(\mathbf{x}) \rho(x_4). \tag{1.8}$$

Variation according to η and $\bar{\eta}$ is to be understood in the sense of variation to the right and left, respectively, i.e.,

$$\delta\rho = \int d^4x \left(\delta\bar{\eta}\frac{\delta\rho}{\delta\bar{\eta}} + \frac{\delta\rho}{\delta\eta}\delta\eta\right). \tag{1.9}$$

Using the commutation rule for ψ and φ, we can obtain[5] the following functional equations for the integral of the state:

$$(i\hat{\partial} + m - ig\gamma\delta/\delta J)\delta z/\delta\bar{\eta}(x) = \eta(x) z,$$

$$(-\partial^2/\partial x_\nu + x^2)\delta z/\delta J(x) = J(x) z - ig\,\mathrm{Sp}\,\gamma\delta^2 z/\delta\bar{\eta}(x)\delta\eta(x)), \tag{1.10}$$

where $z = \sum_n \Phi_n^* \rho \Phi_n = \mathrm{Tr}(\rho(\beta))$ (Φ_n is the wave function of the total Hamiltonian); $\hat{p} = \gamma_\nu\partial_\nu$; $\partial_4 = (\partial/\partial x_4) - \mu$; $\partial_k = \partial/\partial x_k$; $\hbar = c = 1$; $\nu = 1, 2, 3, 4$; $k = 1, 2, 3$. Here the functional derivatives differ from zero only for x_4 in the interval from 0 to β.

From (1.10), by the method of reference 6, we find the following operator solution for the state integral:*

$$z = z_0 \exp\left\{ig\,\mathrm{Sp}\,\gamma\int d^4x \frac{\delta}{\delta\eta(x)}\frac{\delta}{\delta\bar{\eta}(x)}\frac{\delta}{\delta J(x)}\right\} \times \exp\int\{J(x) D_0(x-y) J(y) + \bar{\eta}(x) G_0(x-y)\eta(y)\} d^4x d^4y, \tag{1.11}$$

where

$$z_0 = \prod_{rk}(1+\exp\beta(\mu-\varepsilon_r))(1+\exp[-\beta(\mu+\varepsilon_r)]) \times (1-\exp[-\beta\omega_k])^{-1}, \tag{1.12}$$

$$D_0(x-x') = (2\pi)^{-3}\int\frac{d^3\mathbf{k}}{2\omega_k}\{(f_k+1)\exp[i\mathbf{k}(\mathbf{x}-\mathbf{x}') - \omega_k|x_4-x_4'|] + f_k\exp[-i\mathbf{k}(\mathbf{x}-\mathbf{x}') + \omega_k|x_4-x_4'|]\};$$

$$G_0(x-x') = (i\hat{p}-m)(2\pi)^{-3} \times\int\frac{d^3\mathbf{k}}{2\varepsilon_k}\begin{cases}(N_k^+ - 1)\exp[i\mathbf{k}(\mathbf{x}-\mathbf{x}') - (\varepsilon_k-\mu)(x_4-x_4')] \\ N_k^+\exp[-i\mathbf{k}(\mathbf{x}-\mathbf{x}') - (\varepsilon_k-\mu)(x_4-x_4')] \\ +N_k^-\exp[-i\mathbf{k}(\mathbf{x}-\mathbf{x}') + (\varepsilon_k+\mu)(x_4-x_4')]\end{cases}, \quad x_4 > x_4',$$

$$+(N_k^- - 1)\exp[i\mathbf{k}(\mathbf{x}-\mathbf{x}') + (\varepsilon_k+\mu)(x_4-x_4')]\Big\}, \quad x_4 < x_4';$$

$$N_k^\pm = [1+\exp(\varepsilon_k \mp \mu)\beta]^{-1}; \quad f = [\exp(\omega_k\beta) - 1]^{-1};$$

$$\varepsilon_k = \sqrt{k^2+m^2}; \quad \omega_k = \sqrt{k^2+\varkappa^2}; \tag{1.13}$$

N_k^+ (N_k^-) is the mean number of electrons (positrons) in the state with energy ϵ_k. Eliminating the meson derivatives, we get from (1.11)

$$z = z_0\exp\int\left\{\left((J(x) + ig\gamma\frac{\delta}{\delta\eta(x)}\frac{\delta}{\delta\bar{\eta}(x)}\right)\frac{D_0(x-y)}{2}\left(J(y) + ig\gamma\frac{\delta}{\delta\eta(y)}\frac{\delta}{\delta\bar{\eta}(y)}\right)\right\} d^4x d^4y \times\exp\left\{\int\bar{\eta}(x) G_0(x-y)\eta(y)\, d^4x d^4y\right\}. \tag{1.14}$$

Differentiating ln z with respect to the charge, we get the following operator solution for the thermodynamic potential:

$$\Omega = \Omega|_{g=0} - \int_0^g\frac{idg'}{g'\beta z}\,\mathrm{Sp}\,\gamma\int d^4x\frac{\delta}{\delta\eta}\frac{\delta}{\delta\bar{\eta}}\frac{\delta}{\delta J}z, \tag{1.15}$$

Equations (1.11) and (1.15) can be expanded in power series in g, in which each term coincides with the corresponding approximation computed by the Feynman method.[3]

Our method is more suitable, especially for the higher approximations, since it is not necessary here to examine all possible Feynman diagrams; the entire problem reduces to the successive application of functional differentiation in the re-

*Here and below the integral over the fourth component extends from 0 to β.

quired order with respect to the charge, which is simple to perform.

The mean value of any T-regular function of the field operators $f(\psi\bar{\psi}\varphi)$ is calculated by the rule

$$\langle f\rangle = \frac{\mathrm{Tr}(\rho f)}{z} = \frac{1}{z} f\left(\frac{\delta}{\delta\bar{\eta}}\frac{\delta}{\delta\eta}\frac{\delta}{\delta J}\right) z\Big|_{J=\eta=0}, \qquad (1.16)$$

For example,

$$\langle T(\psi(x)\psi(x_1)\bar{\psi}(x')\bar{\psi}(x_1'))\rangle = \frac{1}{z}\frac{\delta^4 z}{\delta\bar{\eta}(x)\delta\eta(x_1)\delta\eta(x')\delta\bar{\eta}(x_1')}\Big|_{J=\eta=0}$$

We introduce the "one-particle" Green's function of fermions G and bosons D which, in accord with (1.16) can be written in the form*

$$G(x, y) = \frac{1}{z}\frac{\delta^2 z}{\delta\bar{\eta}(x)\delta\eta(y)}\Big|_{J=\eta=0},$$

$$D(x, y) = \frac{\delta^2 \ln z}{\delta J(x)\delta J(y)}\Big|_{J=\eta=0}. \qquad (1.17)$$

with the aid of (1.10), we obtain the following set of equations for G and D:

$$(i\hat{p} + m - ig\gamma\langle\varphi(x)\rangle)G(x, y) + \int\Sigma^*(x, z)G(z, y)d^4z = \delta(x-y), \qquad (1.18)$$

$$(-\partial^2/\partial x_\nu^2 + \varkappa^2)D(x, y) - \int\Pi(x, z)D(z, y)d^4z = \delta(x-y), \qquad (1.19)$$

$$(-\partial^2/\partial x_\nu^2 + \varkappa^2)\langle\varphi(x)\rangle = -\frac{ig}{2}\mathrm{Sp}\,\gamma[G(\mathbf{x}, x_4; \mathbf{x}, x_4-\varepsilon) + G(\mathbf{x}, x_4; \mathbf{x}, x_4+\varepsilon)]_{\varepsilon\to 0}, \qquad (1.20)$$

$$\Sigma^*(x, y) = g^2\int\gamma G(x, z)\Gamma(z, y, y')D(y', x)d^4zd^4y',$$

$$\Pi(x, y) = g^2\,\mathrm{Sp}\int\gamma G(x, z)\Gamma(z, y', y)G(y', x)d^4zd^4y',$$

$$\Gamma(x, y, y') = \gamma\delta(z-y')\delta(y-y') - \delta\Sigma^*(x, y)/\delta(ig\langle\varphi(y')\rangle). \qquad (1.21)$$

"One-particle" Green's functions are defined by the relations (1.19) – (1.21) for x_4 only in the interval from β to $-\beta$. Outside this interval, these functions can be defined in arbitrary fashion.

We apply the condition of periodicity (with period 2β) to the functions and expand them in Fourier series:

$$G(x) = \frac{1}{\beta(2\pi)^3}\sum_{p_4}\int d^3pG(\mathbf{p}, p_4)\exp(-ip_\nu x_\nu),$$

$$D(x) = \frac{1}{\beta(2\pi)^3}\sum_{p_4}\int d^3pD(\mathbf{p}, p_4)\exp(-ip_\nu x_\nu),$$

$$\Gamma(x, y, z) = \Gamma(x-z, y-z) = \beta^{-2}(2\pi)^{-6}\sum_{p_4, p_4'}\int\Gamma(p, p') \times\exp\{-ip_\nu(x-z)_\nu + ip_\nu'(y-z)_\nu\}d^3pd^3p'. \qquad (1.22)$$

It can be shown that: 1) the frequencies p_4 for the Fermi particles take the form $(2n+1)\pi/\beta$ while the frequencies p_4 for the Bose particles take* only the values $2\pi n/\beta$, where n runs through all integral values from $-\infty$ to $+\infty$; 2) for G and D, the following relations hold:

$$G(x_4 = \mp 0) = -G(x_4 = \pm\beta),\ \dot{D}(x_4 = \mp 0) = \dot{D}(x_4 = \pm\beta), \quad \left(\dot{D} = \frac{\partial}{\partial x_4}D\right).$$

This follows from the spectral representations for G and D, which have the form

$$G(x, x') = \frac{1}{z}\sum_{m, n}\psi_{m, n}(0)\bar{\psi}_{n, m}(0)\exp[(\mu N_m - E_m)\beta + (E_m - E_n + \mu N_n - \mu N_m)(x_4 - x_4') + i(\mathbf{p}_m - \mathbf{p}_n)(\mathbf{x} - \mathbf{x}')],\ x_4 > x_4',$$

$$G(x, x') = -\frac{1}{z}\sum_{m, n}\bar{\psi}_{n, m}(0)\psi_{m, n}(0)\exp[(\mu N_n - E_n)\beta + (E_m - E_n + \mu N_n - \mu N_m)(x_4 - x_4') + i(\mathbf{p}_m - \mathbf{p}_n)(\mathbf{x} - \mathbf{x}')],\ x_4 < x_4', \qquad (1.23)$$

$$D(x, x') = \frac{1}{z}\sum_{m, n}|\varphi_{n, m}(0)|^2\exp[-\beta E_n + (E_n - E_m)|x_4 - x_4'| + i(\mathbf{p}_n - \mathbf{p}_m)(\mathbf{x} - \mathbf{x}')]. \qquad (1.24)$$

The fact that we have only odd frequencies (in units of π/β) for the Green's functions G, and only even ones for the functions D, leads to the appearance of the Kronecker δ in the integration over x_4.† (The law of conservation of the "quasi-

*The first Green's functions for $T \neq 0$ were introduced by Matzubara.[3] Our Green's functions differ from his in that a complete symmetry is established between $\hat{H}$ and $\hat{N}$ i.e., all the quantities depend on $\hat{H} - \mu\hat{N}$ (while in Matzubara's case, x_4 enters only with the factor $\hat{H}$). As will be seen from what follows, this permits us to make the transformation to the p-representation in the equations for the Green's functions.

*The circumstance that, in the case $T \neq 0$, the thermodynamic quantities are expressed in the form of a series in $\varepsilon_n = \varepsilon(2n\pi/\beta)$ was shown by E. M. Lifshitz[7] in another connection.

†The author thanks I. M. Khalatnikov, who recently called our attention to the work of Ezawa, Tomozawa and Umezawa, where a Fourier expansion has been carried out for the case $\mu = 0$ in the matrix diagram technique. However, the Green's functions of Matzubara for $\mu \neq 0$ would have both even and odd frequencies, and therefore the integration over x_4 does not always lead to the Kronecker δ, and this transformation to the p-representation would not have been effective.

energy" at each angle of the Feynman diagrams.) In the p-representation, the set of equations for the Green's functions is appreciably simplified and takes the following form:[5]

$$[-ip_\nu\gamma_\nu-\gamma_4\mu+m+\Sigma^*(p)]\,G(p)=\sum_n\delta(p_4-(2n+1)\pi/\beta),$$

$$[k_\nu^2+\varkappa^2-\Pi(k)]\,D(k)=\sum_n\delta(k_4-2n\pi/\beta),$$

$$\Sigma^*(p)=\frac{g^2}{(2\pi)^3\beta}\int\sum_{k_4}\gamma G(p+k)\,\Gamma(p+k,\ p)\,D(k)\,d^3k,$$

$$\Pi(k)=\frac{g^2}{(2\pi)^3\beta}\,\mathrm{Sp}\int\sum_{p_4}\gamma G(p+k)\,\Gamma(p+k,\ p)\,G(p)\,d^3p,$$

$$\Gamma(p,\ p')=\sum_{n,\ m}\gamma^\delta(p_4-(2n+1)\pi/\beta)\,\delta(p_4-(2m+1)\pi/\beta)+\Lambda(p,\ p'), \tag{1.25}$$

where δ is the Kronecker symbol and Λ is the set of all diagrams of the vertex part, except the simple vertex.

As would be expected, it follows from (1.25) that the arguments p_4 and p_4' in $\Gamma(p, p', p-p')$ (which correspond to the "quasi-energies" of the Fermi particles) take on only the odd values $(2n+1)\pi/\beta$, and their difference (which corresponds to the "quasi-energy" of Bose particles) has only the even values $2n\pi/\beta$.

By means of (1.15), the thermodynamic potential (Gibbs function) is also expressed in terms of the "one-particle" functions

$$\Omega=\Omega|_{g=0}-\frac{V}{(2\pi)^3\beta}\sum_{k_4}\int_0^g\frac{\Pi(k)\,dg'}{g'(k^2-\Pi(k))}\,d^3k. \tag{1.26}$$

In concluding this section, we note that the transition to the non-relativistic approximation is contained in the following way: we must substitute $-i\gamma_\nu p_\nu-\gamma_\mu\mu+m$ for $-ip_4-\mu_1+p^2/2m$ and $G_{\alpha\beta}$ for $G\delta_{\alpha\beta}$ everywhere. In fact, it is easy to see from Eq. (1.25) that it suffices to consider the transition to the non-relativistic limit only for the Green's functions without the interaction:

$$G_0=\frac{\Sigma\delta(p_4-(2n+1)\pi/\beta)}{-i\gamma_\nu p_\nu-\gamma_4\mu+m}$$

$$=\frac{(i\gamma_\nu p_\nu+\gamma_4\mu+m)\,\Sigma\delta(p_4-(2n+1)\pi/\beta)}{(p_4-i\mu)^2+p^2+m^2}. \tag{1.27}$$

In the non-relativistic approximation, we have $\mu=m+\mu_1$; $\gamma=0$; $\gamma_4=\delta_{\alpha\beta}$; and all quantities are small relative to m. Leaving terms of first order of smallness, we obtain the following rule for transition to the non-relativistic case:

$$G_0=\frac{2m\delta_{\alpha\beta}\,\Sigma\delta(p_4-(2n+1)\pi/\beta)}{-2ip_4-m^2-2\mu_1 m+m^2+p^2}$$

$$=\frac{\delta_{\alpha\beta}\,\Sigma\delta(p_4-(2n+1)\pi/\beta)}{-ip_4-\mu_1+p^2/2m}. \tag{1.28}$$

2. METHOD OF OBTAINING THE TIME-DEPENDENT GREEN'S FUNCTION

Up to now we have been concerned with temperature dependent Green's functions which make it possible to compute all the thermodynamic characteristics of interest to us. However, for problems on the determination of the spectrum, etc., it is very important to know the time-dependent Green's function. For simplicity we shall carry out the following analysis for a nonrelativistic Hamiltonian.

Thus, our problem is to find the time dependent Green's function in quantum statistics; it is convenient to define the latter differently than was done by Landau,[8] namely

$$\overline{G}(x,t;x',t')=i\langle T(\psi(x,t)\psi^+(x',t'))\rangle, \tag{2.1}$$

where the dependence on time of any Heisenberg operator $f(xt)$ is generalized in the following way:

$$f(\mathbf{x},t)=e^{i(\hat H-\mu\hat N)t}f(\mathbf{x})e^{-i(\hat H-\mu\hat N)t}. \tag{2.2}$$

$\langle\ \rangle$ denotes averaging over the canonical ensemble. It is easy to write down the spectral representation for the time dependent function:[8]

$$\overline{G}(x,t;x',t')=\frac{i}{z}$$

$$\times\begin{cases}\sum\limits_{n,m}|\psi_{n,m}(0)|^2\exp[(\mu N_n-E_n)\beta+i(E_n-E_m\\ -\mu N_m+\mu N_m)(t-t')-i(\mathbf{p}_n-\mathbf{p}_m)(\mathbf{x}-\mathbf{x}')], & \text{for } t>t'\\ -\sum\limits_{n,m}|\psi_{n,m}(0)|^2\exp[(\mu N_m-E_n)\beta+i(E_n-E_m & \\ -\mu N_n+\mu N_m)(t-t')-i(\mathbf{p}_n-\mathbf{p}_m)(\mathbf{x}-\mathbf{x}')], & \text{for } t<t'.\end{cases} \tag{2.3}$$

Comparing (1.23) and (2.3), we see that the transition from G to $\overline{G}$ is connected with the analytic continuation of x_1, that is, $\overline{G}(\mathbf{x}-\mathbf{x}';\ t-t')$ in the interval $t-t'>0$ is the analytic continuation in $x_4\,(x_4\to it)$ of the function $G(\mathbf{x}-\mathbf{x}',\ x_4-x_4')$ in the interval $\beta>x_4-x_4'>0$ and the function $\overline{G}(\mathbf{x}-\mathbf{x}',\ t-t')$ in the interval $t-t'<0$ is the analytic continuation of $G(\mathbf{x}-\mathbf{x}';\ x_4-x_4')$ determined in the interval $0>x_4-x_4'>\beta$.

Thus the problem reduces to the establishment of the form of the Green's function in the intervals (0β) and $(-\beta 0)$. For this purpose, we make use of the spectral representation of the Green's function $G(x, x_4)$. According to (1.23), we have

$$G(\mathbf{p},p_4)=\frac{1}{z}$$

$$\times\sum_{n,m}|\psi_{n,m}^{(0)}|^2\frac{\exp(\mu N_n-E_n)\beta+\exp(\mu N_m-E_m)\beta}{-ip_4+(E_m-E_n)-\mu}, \tag{2.4}$$

where $p_4=(2n+1)\pi/\beta$, n is an arbitrary posi-

tive or negative number. It follows from (2.4) that it is always possible to represent G in the form

$$G(\mathbf{p}, p_4) = \int_{-\infty}^{+\infty} \frac{f(w, \mathbf{p})\, dw}{-ip_4 - \mu + w}. \qquad (2.5)$$

By means of (2.5) and (1.22), we can obtain $G(\hat{\mathbf{p}}, x_4)$ for the values of x_4 in the interval from $-\beta$ to β, that is,

$$G(\mathbf{p}, x_4) = \begin{cases} \int_{-\infty}^{+\infty} dw\, f(w, \mathbf{p}) \frac{\exp[-(w-\mu)x_4]}{1+\exp[-(w-\mu)\beta]}, & \text{when } \beta > x_4 > 0, \\ -\int_{-\infty}^{+\infty} dw\, f(w, \mathbf{p}) \frac{\exp[-(w-\mu)x_4]}{1+\exp(w-\mu)\beta}, & \text{when } 0 > x_4 > -\beta. \end{cases} \qquad (2.6)$$

We then get for the time-dependent Green's function

$$\overline{G}(\mathbf{p}, t) = i \begin{cases} \int_{-\infty}^{+\infty} dw\, f(w, \mathbf{p}) \frac{\exp[-i(w-\mu)t]}{1+\exp[-(w-\mu)\beta]} & \text{for } t > 0, \\ \int_{-\infty}^{+\infty} dw\, f(w, \mathbf{p}) \frac{\exp[-i(w-\mu)t]}{1+\exp(w-\mu)\beta} & \text{for } t < 0. \end{cases} \qquad (2.7)$$

Making a Fourier transformation in t, we get the time-dependent Green's function in the p-representation:*

$$\overline{G}(\mathbf{p}, p_4) = i \int_{-\infty}^{+\infty} dw\, f(w, \mathbf{p}) \left[\frac{\delta + (p_4 + \mu - w)}{1+\exp[-(w-\mu)\beta]} - \frac{\delta - (p_4 + \mu - w)}{1+\exp(w-\mu)\beta} \right], \qquad (2.8)$$

where

$$\delta_{\pm}(\alpha) = \int_0^{\infty} \exp(\pm i\alpha t)\, dt = \pi\delta(\alpha) \pm i/\alpha.$$

Here p_4 runs continuously through a series of values in the interval $-\infty$ to $+\infty$. We shall show that the energy spectrum can be found from the temperature dependent Green's function. In fact, the spectral function $f(w, \mathbf{p})$ is represented in the general case in the form†

$$f(w, \mathbf{p}) = \sum A_n(\mathbf{p})\, \delta(w - E_n(\mathbf{p})) + \rho(w, \mathbf{p}). \qquad (2.9)$$

Substituting (2.9) in (2.6), we get

$$G(\mathbf{p}, p_4) = \sum \frac{A_n(\mathbf{p})}{-ip_4 + E_n(\mathbf{p}) - \mu} + \int_{-\infty}^{+\infty} \frac{dw\, \rho(w)}{-ip_4 - \mu + w}, \qquad (2.10)$$

where $p_4 = (2m+1)\pi/\beta$.

On the other hand, it is evident that the poles of the time dependent Green's function are located at the points $p_4 = E_n - \mu$ where E_n gives the energy spectrum of the system. Hence we obtain the following rule: to find the poles of the time-dependent Green's function (and, consequently, the energy spectrum also) it suffices to find the zeros of the analytic continuation of $G^{-1}(\mathbf{p}, p_4)$ in the complex plane of p_4.

Consequently, E_n is determined from the following equation:

$$-E_n + \frac{p^2}{2m} + \Sigma^*(\mathbf{p}, p_4 = i(\mu - E_m)) = 0. \qquad (2.11)$$

In this case, the real part of E_n corresponds to the energy, and the imaginary part to the damping of the n-th excitation. As $\beta \to 0$, the levels with $E_n < \mu$ correspond to holes in the Fermi distribution, while the levels with $E_n > \mu$ correspond to the production of particles beyond the Fermi surface. It is also easy to determine the quantity

$$A_n(\mathbf{p}) = [1 - \partial\Sigma^*/\partial ip_4]^{-1}\big|_{ip_4 = E_n - \mu}. \qquad (2.12)$$

In the approximation, where the damping is small, i.e., $\Gamma_n \ll E_n^{(0)}$ ($E_n = E_N^{(0)} - i\Gamma_n$), we get from (2.11)

$$-E_n^{(0)} + \frac{p_2}{2m} + \Sigma_0^*(p, ip_4 = E_n^{(0)} - \mu) = 0; \quad \Sigma^* = \Sigma_0^* - i\Sigma_1^*,$$

$$\Gamma_n = \frac{\Sigma_1^*(p, p_4)}{1 - \partial\Sigma_0(p, p_4)/\partial ip_4}\Big|_{ip_4 = (E_n^{(0)} - \mu)} \qquad (2.13)$$

All these results are easily generalized to the case of Bose statistics:

$$\overline{D}(\mathbf{p}, p_4) = i \int_{-\infty}^{+\infty} dw\, f_1(w, \mathbf{p}) \times \left[\frac{\delta + (p_4 + \bar{\mu} - w)}{1 - \exp[-(w-\mu)\beta]} + \frac{\delta - (p_4 + \bar{\mu} - w)}{\exp[(w-\bar{\mu})\beta] - 1} \right], \qquad (2.14)$$

where $\bar{\mu}$ is the chemical potential of Bose particles. The poles of the time-dependent Green's function correspond to the poles of the analytic continuation (in p_4) of the temperature-dependent Green's function. Thus, for example, in the case $\bar{\mu} = 0$, we have the following equation for the spectrum of the energy E_n:

$$-E_n^2 + p^2 + \varkappa^2 - \Pi(p^2; -E_n^2) = 0. \qquad (2.15)$$

In the case of small damping, we have

$$\Gamma_n = \frac{\Pi_1(p^2; p_4^2)}{2E_n(1 - \partial\Pi^0/\partial p_4^2)}\Big|_{p_4^2 = -E_n^{(0)2}},$$

$$-E_n^{(0)2} + p^2 + \varkappa^2 - \Pi_0(p^2; p_4^2 = -E_n^{(0)2}) = 0, \qquad (2.16)$$

where $\Pi = \Pi_0 + i\Pi_1$, $E_n = E_n^{(0)} - i\Gamma_n$.

*It follows from (2.8) that the dispersion formula for $\overline{G}$, found by Landau,[8] is satisfied.

†The δ function can be spread out somewhat, because of the interaction, and the singularity takes the form of a pole for complex values of E_n.

3. A SYSTEM OF PARTICLES INTERACTING ACCORDING TO COULOMB'S LAW

Let us consider a system of electrons and ions, interacting according to Coulomb's law. In this case, the Hamiltonian of the interaction, with accuracy up to unimportant terms of the eigenenergy, can be written in the form

$$H_1 = -\frac{e^2}{2}\sum_{\lambda_1\lambda_2} z_{\lambda_1} z_{\lambda_2} \times \int \hat{j}_4^{(\lambda_1)}(\mathbf{x}) V(\mathbf{x}-\mathbf{x}') \hat{j}_4^{(\lambda_2)}(x')\, d^3x\, d^3x', \quad (3.1)$$

where z_λ is the charge of particles of type λ: $e^2/4\pi c = 1/137$; $\hbar = 1$. It is not difficult to see, according to Eq. (1.14), that the system under consideration is equivalent to a system of charged particles interacting with the fourth component of the vector field φ_μ, wherein

$$D^{(0)}(x-x') = V(\mathbf{x}-\mathbf{x}')\,\delta(x_4 - x_4'). \quad (3.2)$$

Therefore we can at once set down the equations for the Green's function for a system of particles interacting according to Coulomb's law.

Let us consider two limiting cases:

1) When the ions are uniformly distributed (a translationally invariant system). In this case, the set of equations for the Green's function has the form

$$[i\hat{p} - \gamma_4\mu_\lambda + m_\lambda - \Sigma_\lambda^*(p)]\, G_\lambda(p) = \sum_n \delta(p_4 - (2n+1)\pi/\beta), \quad (3.3)$$

$$D(k) = D_0(k) + D_0(k)\,\Pi(k)\,D(k), \quad (3.4)$$

$$\Sigma_\lambda^*(p) = \frac{e^2 z_\lambda^2}{(2\pi)^3\beta}\int \sum_{k_4} \gamma_4 G_\lambda(p+k)\,\Gamma_4^{(\lambda)}(p+k, p)\,D(k)\,d^3k, \quad (3.5)$$

$$\Pi(k) = \sum_\lambda \frac{e^2 z_\lambda^2}{(2\pi)^3\beta}\,\mathrm{Sp} \times \int \sum_{p_4} \gamma_4 G_\lambda(p+k)\,\Gamma_4^{(\lambda)}(p+k, p)\,G_\lambda(p)\,d^3p, \quad (3.6)$$

$$\Gamma_4^{(\lambda)}(p, p') = \gamma_4 + \Lambda^{(\lambda)}(p, p'), \quad (3.7)$$

When G_n is the "one-particle" Green's function of particles with charge z (for electrons, $z_\lambda = -1$); $D(k)$ is the distribution function of a longitudinal photon with the presence of plasma taken into account.

a) The self-consistent field approximation (Hartree-Fock) in terms of the equations just set forth corresponds to the following approximation: the mass operators are determined by Eq. (3.5) with neglect of Γ and Λ (i.e., it is assumed that $\Pi = \Lambda = 0$).

b) Because of the singularity $D_0(\mathbf{k}) = 1/\mathbf{k}^2$ for small momenta, there are essential and higher approximations (the so-called "correlation" contribution) and these eliminate the singularity in the $D(k)$ function at low momenta $(\mathbf{k})$.

In a practical case, we consider the principal part of the correlation energy by computing Π in first approximation, i.e.,

$$\Pi^{(1)}(k) = \sum_\lambda \frac{e^2 z_\lambda^2}{(2\pi)^3\beta}\,\mathrm{Sp}\int \sum_{p_4} \gamma_4 G_\lambda^{(0)}(p+k)\,\gamma_4 G_\lambda^{(0)}(p)\,d^3p. \quad (3.8)$$

With the help of $\Pi^{(1)}$ we can, by means of (1.26), obtain the following expression for the thermodynamic potential in this approximation:

$$\Omega = \Omega|_{e=0} + \frac{V}{2\beta(2\pi)^3}\sum_{k_4}\int \ln\left(1 - \frac{1}{\mathbf{k}^2}\Pi^{(1)}(k)\right) d^3k. \quad (3.9)$$

Separating the self-consistent part, i.e., $\Pi^{(1)}(\mathbf{k})/\mathbf{k}^2$, we obtain the following expression for the "correlation" part of the thermodynamic potential:

$$\Omega_{\mathrm{cor}} = \frac{V}{2(2\pi)^3\beta} \times \int \sum_{k_4}\left[\ln\left(1 - \frac{1}{\mathbf{k}^2}\Pi^{(1)}(k)\right) + \frac{1}{\mathbf{k}^2}\Pi^{(1)}(k)\right] d^3k. \quad (3.10)$$

In the classical limit $\hbar \to 0$ and $e^2\beta n^{1/3} \ll 1$, we obtain the Debye-Hückel theory. This corresponds to the approximation in which $\Pi_{(k)}^{(1)} = \Pi^{(1)}(0)$. In this case, we get the well-known expression for the Debye radius λ_D; it is determined by the expression

$$\lambda_D^{-2} = -\Pi^{(1)}(0) = -\frac{2e^2}{(2\pi)^3}\sum_\lambda \int \frac{\partial f^{(\lambda)}(k)}{\partial \epsilon_k^{(0)}}\,d^3k = e^2\sum_\lambda \frac{\partial n_\lambda}{\partial \mu_\lambda} z_\lambda^2, \quad (3.11)$$

where n_λ is the mean density of particles of type λ. Finding $\Pi^{(1)}$ we can, by means of (3.10), obtain not only the results of the Debye-Hückel theory, but also all subsequent corrections (in terms of the Debye-Hückel smallness parameter, i.e., $e^2\beta n^{1/3}$, to the thermodynamic potential.

c) It is important the other limiting case, where the Gell-Mann—Brueckner approximation is valid (the parameter of smallness is $me^2/\hbar^2 n^{1/3}$) also is contained in the given approximation of $\Pi^{(1)}$

In fact, carrying out the necessary calculations,* we get the following results from (3.10) in the nonrelativistic approximation:

*We note that the poles of the function $\cot(x\beta/2)[\tan(x\beta/2)]$ are located at $2n\pi/\beta[(2n+1)\pi/\beta]$; therefore, summation over the frequencies of the Bose (Fermi) fields can be changed to a calculation of the contour integral.

$$\Omega_{\varepsilon,\,\mathrm{cor}} = V\int\frac{d^3q}{2(2\pi)^3\beta}\sum_{n=-\infty}^{\infty}\left[\ln\left(1+\frac{2e^2}{q^2(2\pi)^3}\int\frac{w_p(f_p-f_{p+q})\,d^3p}{w_p^2+(2n\pi/\beta)^2}\right)\right.$$
$$\left.-\frac{2e^2}{q^2(2\pi)^3}\sum\int\frac{w_p(f_p-f_{p+q})}{w_p^2+(2n\pi/\beta)^2}\right], \qquad (3.12)$$

where $w_p = \epsilon_{p+q}^{(0)} - \epsilon_p^{(0)}$; $\epsilon_p^{(0)} = p^2/2m$; $f_p = [1+\exp(\epsilon_p^0-\mu)\beta]^{-1}$. By the usual methods, we find from (3.13) that for $\beta\to\infty$

$$E_{\varepsilon,\,\mathrm{cor}} = V\int\frac{d^4q}{2(2\pi)^4}\left\{\ln\left(1+\frac{2e^2}{(2\pi)^3}\int\frac{w_p(f_p^{(0)}-f_{p+q}^{(0)})\,d^3p}{w_p^2+q_4^2}\right)\right.$$
$$\left.-\frac{2e^2}{q^2(2\pi)^3}\int\frac{w_p(f_p^{(0)}-f_{p+q}^{(0)})\,d^3p}{w_p^2+q_4^2}\right\}, \qquad (3.13)$$

where

$$f_p^{(0)} = \begin{cases}0, & \text{when } \varepsilon_p^{(0)} > \mu,\\ 1, & \text{when } \varepsilon_p^{(0)} < \mu.\end{cases} \qquad (3.14)$$

Expanding (3.14) in the smallness parameter set forth above, we obtain the results of Gell-Mann and Bruekner.

By means of the method applied in Sec. 2, it is not difficult to establish the time dependence of the $\overline{D}$-function.

d) It is easy to verify that $\overline{D}$ has discrete poles, corresponding to the plasma. In this case, the equation for the determination of the poles a_n of the Green's function $\overline{D}$, according to (2.15), has the form

$$1+\frac{2e^2}{q^2(2\pi)^3}\int\frac{w_p(f_p-f_{p+q})\,d^3p}{w_p^2-w_n^2-i\delta} = 0. \qquad (3.15)$$

The continuous spectrum corresponds to pair production, and the discrete spectrum gives the energy of the plasma. Going on to the case $\beta\to 0$ we obtain the results we had previously.

In conclusion, we note that the best results for the Green's function in the case under consideration are obtained if we solve the set of equations (3.3) – (3.6), setting $\Gamma = \gamma$.

2) The other limiting case of interest to us is the one in which the ions are so correlated with their own electrons that an appreciable violation of the translational invariance takes place, which is the case for example, in the statistical theory of the atom. In this case, we can assume the ions are fixed in their lattice sites (atoms) in first approximation, and the problem can be reduced to the interaction of electrons with the scalar components of the electromagnetic field. [D_0 is determined as before by the equation $\nabla^2 D_0(\mathbf{x},\mathbf{y}) = \delta(\mathbf{x}-\mathbf{y})$]. Inasmuch as the distribution of the ions is essentially non-uniform, the "one-particle" Green's functions depend not only on the difference of the spatial coordinates (the dependence on the fourth components is differential, as before). The problem consists in obtaining a system of equations for the Green's function in the presence of an external field, which violates the translational invariance of the system. For simplicity, we consider an approximation in which $\Gamma = \gamma$ (in practice, this is the best approximation for atomic systems). It can be shown that in this case, the equations for the Green's function have the following form:

$$(-i(p_4 - i\mu + ie\langle\varphi(\mathbf{x})\rangle)\gamma_4 + \gamma\nabla_x)\,G(p_4,\mathbf{x},\mathbf{x}')$$
$$+\int\Sigma^*(p_4,\mathbf{x},\mathbf{y})\,G(p_4,\mathbf{y},\mathbf{x})\,d^3y$$
$$= \delta(\mathbf{x}-\mathbf{x}')\,\delta(p_4-(2n+1)\pi/\beta); \qquad (3.16)$$

$$\Delta\langle\varphi(\mathbf{x})\rangle = e\rho_1 + \frac{e}{\beta}\,\mathrm{Sp}\,\gamma_4\sum_{p_4}G(p_4,\mathbf{x},\mathbf{x}); \qquad (3.17)$$

$$-\Delta D(k_4,\mathbf{x},\mathbf{x}')$$
$$-\int\Pi(k_4,\mathbf{x},\mathbf{y})\,D(k_4,\mathbf{y},\mathbf{x}')\,d^3y = \delta(\mathbf{x}-\mathbf{x}'); \qquad (3.18)$$

$$\Sigma^*(p_4,\mathbf{x},\mathbf{y}) = \frac{e^2}{\beta}\sum_{k_4}\gamma_4 G(p_4+k_4,\mathbf{x},\mathbf{y})\,\gamma_4 D(k_4,\mathbf{y},\mathbf{x}); \qquad (3.19)$$

$$\Pi(k_4,\mathbf{x},\mathbf{y})$$
$$= \frac{e^2}{\beta}\,\mathrm{Sp}\sum_{p_4}\gamma_4 G(p_4+k_4,\mathbf{x},\mathbf{y})\,\gamma_4\,G(p_4,\mathbf{y},\mathbf{x}). \qquad (3.20)$$

We transform to the p-representation relative to the difference in coordinates, i.e.,

$$G(p_4,\mathbf{x},\mathbf{y}) = \frac{1}{(2\pi)^3}\int G(p_4,\mathbf{x},p)\,e^{ip(\mathbf{x}-\mathbf{y})}\,d^3p. \qquad (3.21)$$

Omitting the necessary calculations, we get the final form for the Green's function in the case being considered:

$$(-i\gamma_4 p_4 - \gamma_4\mu + m + e\gamma_4\langle\varphi(\mathbf{x})\rangle + \Sigma^*(\mathbf{x},\tilde{p}))\,G(\mathbf{x},p)$$
$$= \sum_n\delta(p_4-(2n+1)\pi/\beta); \qquad (3.22)$$

$$\Delta\langle\varphi(\mathbf{x})\rangle = e\rho_1 + \frac{e}{(2\pi)^3\beta}\,\mathrm{Sp}\int\gamma_4\sum_{p_4}G(\mathbf{x},p)\,d^3\mathbf{p}; \qquad (3.23)$$

$$[(\mathbf{p}-i\nabla)^2 - \Pi(\mathbf{x},\tilde{p})]\,D(\mathbf{x},p) = 1, \qquad (3.24)$$

$$\Sigma^*(\mathbf{x},p) = \frac{e^2}{(2\pi)^3\beta}\int\sum_{k_4}\gamma_4 G(\mathbf{x},\tilde{p}+k)\,\gamma_4 D(\mathbf{x},k)\,d^3k; \qquad (3.25)$$

$$\Pi(\mathbf{x},k) = \frac{e^2}{(2\pi)^3\beta}\sum_{p_4}\mathrm{Sp}\int\gamma_4 G(x,p+\tilde{k})\,\gamma_4 G(\mathbf{x},p)\,d^3p, \qquad (3.26)$$

where

$$\tilde{p}_k = p_k - i\nabla_k \text{ for } k = 1,2,3;\ \tilde{p}_4 = p_4.$$

Here the operator ∇ acts on the functions to its right.

a) The Hartree approximation in terms of these equations corresponds to $\Pi = \Sigma^* = 0$. In this case, we can write the following symbolic solution for G:

$$G(\mathbf{x}, p) = \frac{\sum_n \delta(p_4 - (2n+1)\pi/\beta)}{-i\gamma_\nu \tilde{p}_\nu - \gamma_4 \mu + m + e\gamma_4 \langle \varphi(\mathbf{x}) \rangle}. \quad (3.27)$$

It is not difficult to show that

$$-\frac{1}{\beta} \operatorname{Sp}\gamma_4 \sum_{p_4} G(\mathbf{x}, p) = 2(N^+ - N^-), \quad (3.28)$$

where

$$N^\pm = 1/(1 + \exp(\beta\tilde{\varepsilon}_p^\pm)),$$

$$\tilde{\varepsilon}_p^\pm = \sqrt{(\mathbf{p} - i\nabla)^2 + m^2} \mp (\mu - e\langle\varphi(\mathbf{x})\rangle). \quad (3.29)$$

(In the classical approximation, $\nabla = 0$).

Thus, in the Hartree approximation, we obtain the following symbolic equation for $\langle\varphi\rangle$:

$$-\Delta\langle\varphi(\mathbf{x})\rangle = -e\rho_1 + \frac{2e}{(2\pi)^3}\int \hat{\rho}(\tilde{\varepsilon}_p) d^3p, \quad (3.30)$$

where $\hat{\rho} = \hat{N}^+ - N^-$, $N^\pm$ and $\tilde{\epsilon}$ are determined by (3.29). We obtained the generalized Thomas-Fermi model with all the quantum and relativistic corrections.

In the nonrelativistic approximation, Eqs. (3.30) coincide in form with the operator equations obtained by Kirzhnits.[9]

b) Calculation of the exchange energy corresponds in our case to the calculation of the mass operator in first approximation (setting $D = D_0$). In this case we obtain the generalized Thomas-Fermi-Dirac model in operator form with all quantum and relativistic corrections (or the method of Hartree-Fock). The correlation corrections in our case, when the homogeneity of the spatial distribution of the charge is disrupted, have a still greater significance.[10] In order to find them, it suffices to compute the polarization operator in first approximation:

$$\Pi^{(1)}(\mathbf{x}\ p) = \frac{e^2}{(2\pi)^3\beta} \operatorname{Sp} \sum_{k_4} \int \gamma_4 G(\mathbf{x}, \tilde{p} + k)\gamma_4 G(\mathbf{x}, k) d^3k. \quad (3.31)$$

In this case the correlation part of the thermodynamic potential is obtained with the help of (1.26).

In conclusion, we note that in the case in which the potential $V(\mathbf{x} - \mathbf{x}')$ is short range, there are significant higher corrections to the function, and it is more appropriate to express the mass operator in terms of the two-particle Green's function G_{12}:

$$\int \Sigma^*(x, y) G(y, x') d^4y = g^2 \int V(\mathbf{x} - \mathbf{y}) \delta(x_4 - y_4) G_{12}(x, y, y, x') d^4y,$$

where $G_{12}(\mathbf{x}, \mathbf{y}, \mathbf{x}', \mathbf{y}') = \langle T(\psi(\mathbf{x})\psi(\mathbf{y})\bar{\psi}(\mathbf{x}') \times \bar{\psi}(\mathbf{y}'))\rangle$. It is not difficult to obtain the equation for G_{12} (in first approximation, this equation is of the Bethe-Salpeter type). Solving simultaneously for G and G_{12}, we obtain results corresponding to the Bruekner approximation (we obtain the "gaseous" approximation if we solve the equation for G_{12} approximately, setting $G = G_0$ in it). In this approximation superconductivity is also explained.

This question will be discussed by us in more detail in another paper.

The author is very grateful to I. E. Tamm, V. L. Ginzburg, and D. A. Kirzhnits for their interest in the research and for useful discussions of the results.

[1] E. W. Montroll and J. C. Ward, Phys. Fluids **1**, 55 (1958).

[2] V. M. Galitskiĭ and A. B. Migdal, J. Exptl. Theoret. Phys. (U.S.S.R.) **34**, 139 (1957); Soviet Phys. JETP **7**, 96 (1958).

[3] T. Matzubara, Prog. Theoret. Phys. **14**, 351 (1955).

[4] J. Schwinger, Proc. Nat. Acad. Sci. **37**, 452 (1951); E. S. Fradkin, Doklady Akad. Nauk SSSR **98**, 47 (1954).

[5] E. S. Fradkin, Doklady Akad. Nauk SSSR **125**, 311 (1959); Soviet Phys. "Doklady" **4**, in press.

[6] E. S. Fradkin, Doklady Akad. Nauk SSSR **100**, 897 (1955).

[7] E. M. Lifshitz, J. Exptl. Theoret. Phys. (U.S.S.R.) **29**, 94 (1955), Soviet Phys. JETP **2**, 73 (1956).

[8] L. D. Landau, J. Exptl. Theoret. Phys. (U.S.S.R.) **34**, 262 (1958), Soviet Phys. JETP **7**, 182 (1958).

[9] D. A. Kirzhnits, J. Exptl. Theoret. Phys. (U.S.S.R.) **32**, 115 (1957), Soviet Phys. JETP **5**, 64 (1957).

[10] D. A. Kirzhnits, J. Exptl. Theoret. Phys. (U.S.S.R.) **35**, 1198 (1958), Soviet Phys. JETP **8**, 835 (1959).

[11] Ezawa, Tomozawa, and Umezawa, Nuovo cimento **5**, 811 (1957).

[12] Abrikosov, For'kov, and Dzyaloshinskiĭ, J. Exptl. Theoret. Phys. (U.S.S.R.) **36**, 900 (1959), Soviet Phys. JETP **9** 636 (1959).

Translated by R. T. Beyer
240

Letters to the Editor

BETA DECAY OF STRANGE PARTICLES

V. M. SHEKHTER

Leningrad Physico-Technical Institute, Academy of Sciences, U.S.S.R.

Submitted to JETP editor December 7, 1958

J. Exptl. Theoret. Phys. (U.S.S.R.) **36**, 1299-1301 (April, 1959)

So far no decays of hyperons into nucleons and leptons (of the type $\Lambda^0 \to p + e^- + \tilde{\nu}$) have been observed. This contradicts the assumption that the four-fermion interaction constant F, responcible for this type of processes, is the same as that of the usual β decay or μ meson decay ($G = 1.41 \times 10^{-49}$ erg-cm^3).[1] The decrease in the magnitude of F may be due to either renormalization effects due to strong interactions which must exist in hyperon decay[2,3] or to a difference in the nonrenormalized constants. In either case an estimate of the order of magnitude of F is of interest. One way to obtain such an estimate is to study the K_{e3} and $K_{\mu 3}$ decays whose probability is determined by a matrix element of the same interaction that is supposed to lead to the β decay of hyperons. Phenomenologically we may write this matrix element as follows[4,2,5]

$$(\bar{u}_\mu + \bar{u}_e, [if(\hat{p}_K + \hat{p}_\pi) + ig(\hat{p}_K - \hat{p}_\pi)] \times (1 + \gamma_5) u_\nu) / \sqrt{4E_K E_\pi}, \quad (1)$$

where f and g are real functions of the invariant

$$Q^2 = -(p_K - p_\pi)^2 = m_K^2 + m_\pi^2 - 2m_K E_\pi; \; m_{\mu,e} \leqslant Q \leqslant m_K - m_\pi. \quad (2)$$

Using Eq. (1) we obtain for the probabilities for K_{e3} and $K_{\mu 3}$ decays in which the π meson has an energy E_π in the K meson rest system the following formulas (in the case of K_{e3} one may, of course, set $m_e = 0$)

$$dW(E_\pi) = (m_K P_\pi dE_\pi / 48\pi^3)(Q^2 - m_{\mu,e}^2)^2 Q^{-6} \{4f^2 P_\pi^2 \times (2Q^2 + m_{\mu,e}^2) + 3(m_{\mu,e}/m_K)^2 [f(m_K^2 - m_\pi^2) + gQ^2]^2\}. \quad (3)$$

To obtain the total decay probability one must integrate (3) over E_π from $m_{\mu,e}$ to $(m_K^2 - m_\pi^2 - m_{\mu,e}^2)/2m_K$.

So far the energy distribution of π mesons in K_{e3} and $K_{\mu 3}$ decays has not been studied so that the dependence of f and g on Q^2 is not known. One may assume that within the range of Eq. (2) this dependence is weak. Then f and g may be replaced by some average values $\bar{f}$ and $\bar{g}$ and these quantities may be obtained from the total probabilities of K_{e3} and $K_{\mu 3}$ decays. We assume that the $K^\pm$ meson lifetime is equal to[6] 1.224×10^{-8} sec and denote the branching ratios for the $K_{\mu 3}$ and K_{e3} decays relative to the total number of K decays by β_μ and β_e respectively. Integrating (3) over E_π gives

$$\bar{f}/G = 0{,}57\sqrt{\beta_e}, \quad \bar{g}/G = -2.0\sqrt{\beta_e} + \sqrt{17.6\beta_\mu - 7.8\beta_e}. \quad (4)$$

The dependence of $\bar{g}/\bar{f}$ on β_μ/β_e is shown in the figure as well as the experimental value of β_μ/β_e taken from references 6 – 9. None of the

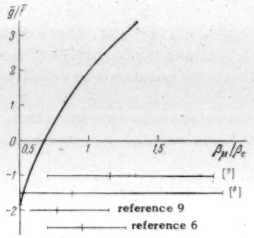

The dependence of the ratio of the constants $\bar{g}/\bar{f}$ on the ratio of the probabilities of $K_{\mu 3}$ and K_{e3} decays.

experiments are in contradiction with a value of β_μ/β_e between 0.7 and 1, i.e., $\bar{g}/\bar{f}$ between 0 and 2 and, in particular, $\bar{g} = 0$ (in which case $\beta_\mu/\beta_e = 0.7$). With $g = 0$ and $f = \bar{f} = \text{const}$, the interaction leading to (1) is in coordinate representation given by

$$H = \bar{f}\left(\varphi_{\pi^0}^* \frac{\partial \varphi_{K^-}}{\partial x_\lambda} - \frac{\partial \varphi_{\pi^0}^*}{\partial x_\lambda} \varphi_{K^-}\right)(\bar{\psi}_\mu + \bar{\psi}_e, \gamma_\lambda(1 + \gamma_5)\psi_\nu), \quad (5)$$

where, according to Eq. (4), $\bar{f} = 0.13\,G$ (here we take $\beta_e = 0.051$).[9] On the other hand, it was shown by Feynman and Gell-Mann[1] that decays of the form $\pi^- \to \pi^0 + e^- + \tilde{\nu}$ should exist, analogous to the K_{e3} decays and described by a direct interaction

$$H' = G\left(\varphi_{\pi^0}^* \frac{\partial \varphi_{\pi^-}}{\partial x_\lambda} - \frac{\partial \varphi_{\pi^0}^*}{\partial x_\lambda} \varphi_{\pi^-}\right)(\bar{\psi}_e, \gamma_\lambda(1 + \gamma_5)\psi_\nu). \quad (6)$$

A comparison of the constants shows that $\bar{f}$ is eight times smaller than the G appearing in Eq. (6). If one assumes, in analogy with Eq. (6), that $\bar{f}$ is of the same order as F, where F is the constant (more correctly, some sort of an average form factor) giving the strength of the four fermion interaction responsible for hyperon β

decay, then one would expect F to be an order of magnitude smaller than G. An analogous quenching takes place in the form factor responsible for the $K_{\mu 2}$ decay.[6]

Probabilities of hyperon decays

Decay mode	W	$10^{10}\tau$ [*]	$W\tau$
$\Lambda^0 \longrightarrow p + e^- + \tilde{\nu}$	$5.8 \cdot 10^5$	0.277	$1.6 \cdot 10^{-4}$
$\Lambda^0 \longrightarrow p + \mu^- + \tilde{\nu}$	$9.4 \cdot 10^4$	0.277	$2.6 \cdot 10^{-5}$
$\Sigma^- \longrightarrow n + e^- + \tilde{\nu}$	$3.4 \cdot 10^8$	0.167	$5.7 \cdot 10^{-4}$
$\Sigma^- \longrightarrow n + \mu^- + \tilde{\nu}$	$1.5 \cdot 10^8$	0.167	$2.5 \cdot 10^{-4}$
$\Xi^- \longrightarrow \Lambda^0 + e^- + \tilde{\nu}$	$1.2 \cdot 10^8$	~1	$1.2 \cdot 10^{-3}$
$\Xi^- \longrightarrow \Lambda^0 + \mu^- + \tilde{\nu}$	$3.2 \cdot 10^5$	~1	$3.2 \cdot 10^{-4}$
$\Xi^- \longrightarrow \Sigma^0 + e^- + \tilde{\nu}$	$1.4 \cdot 10^5$	~1	$1.4 \cdot 10^{-4}$
$\Xi^- \longrightarrow \Sigma^0 + \mu^- + \tilde{\nu}$	$2.1 \cdot 10^3$	~1	$2.1 \cdot 10^{-6}$

In the table are shown hyperon decay probabilities calculated on the assumption of an A-V interaction only with a constant F = 0.1 G. The results of the calculation using the exact formula[10] (the decay probabilities given in reference 10 for F = G are somewhat high due to a mistake in the coefficient) are for all practical purposes the same as those obtained from an approximate formula; for example for the decay $\Lambda^0 \rightarrow p + \mu^- + \tilde{\nu}$ one may use

$$W = \frac{F^2}{15\pi^3}(m_\Lambda - m_p)^5 \left(\frac{m_p}{m_\Lambda}\right)^{1/2} \Phi\left[\left(\frac{m_\mu}{m_\Lambda - m_p}\right)^2\right],$$

$$\Phi(x) = (1 - 4.5x - 4x^2)\sqrt{1-x} + \frac{15}{4}x^2 \ln\left|\frac{1+\sqrt{1-x}}{1-\sqrt{1-x}}\right| \qquad (7)$$

(for the electron modes $x \ll 1$ and $\Phi \approx 1$). It is seen from the table that the product $W\tau$ (τ = experimental hyperon lifetime), which gives the fraction of leptonic decays relative to the total number of decays, for F = 0.1 G is of the order of 2×10^{-4} for Λ^0 and 10^{-3} for Σ^- and Ξ^- (in the last case the estimate is complicated by the absence of exact data on Ξ^- lifetime). In view of the fact that the number of Λ and Σ decays investigated so far is much less than $1/W\tau$, the absence of leptonic modes among them is not surprising.

[1] R. P. Feynman and M. Gell-Mann, Phys. Rev. **109**, 193 (1958).

[2] M. L. Goldberger and S. B. Treiman, Phys. Rev. **110**, 1478 (1958).

[3] V. M. Shekhter, J. Exptl. Theoret. Phys. (U.S.S.R.) **36**, 581 (1959), Soviet Phys. JETP **9**, 403 (1959).

[4] Furuichi, Kodama, Sugahara, and Yonezawa, Progr. Theoret. Phys. (Japan) **16**, 64 (1956).

[5] I. Yu. Kobzarev and I. E. Tamm, J. Exptl. Theoret. Phys. (U.S.S.R.) **34**, 899 (1958), Soviet Phys. JETP **7**, 622 (1958). F. Zachariasen, Phys. Rev. **110**, 1481 (1958).

[6] M. Gell-Mann and A. Rosenfeld, Ann. Rev. Nucl. Sci. **7**, 407 (1957).

[7] Alexander, Johnston, and O'Ceallaigh, Nuovo cimento **6**, 478 (1957).

[8] Birge, Perkins, Peterson, Stork, and Whitehead, Nuovo cimento **4**, 834 (1956).

[9] Bruin, Holthuizen and Jongejans, Nuovo cimento **9**, 422 (1958).

[10] V. M. Shekhter, J. Exptl. Theoret. Phys. (U.S.S.R.) **35**, 458 (1958), Soviet Phys. JETP **8**, 316 (1959).

Translated by A. M. Bincer
241

ON THE ROTATION OF THE PLANE OF POLARIZATION OF ELASTIC WAVES IN A MAGNETICALLY POLARIZED MEDIUM

K. B. VLASOV and B. Kh. ISHMUKHAMETOV

Institute for the Physics of Metals, Academy of Sciences, U.S.S.R.

Submitted to JETP editor October 20, 1958

J. Exptl. Theoret. Phys. (U.S.S.R.) **36**, 1301-1303 (April, 1959)

LET us consider the propagation of plane elastic waves in a magnetically polarized medium (i.e., one located in a constant, uniformly polarized magnetic field H_0, or one which contains a constant, uniform magnetization polarization I_0) with uniaxial symmetry. Let us study the case in which a constant polarizing field H_0 is oriented along the axis of symmetry, which we shall take to be the axis x_3. Neglecting magneto-mechanical effects (i.e., magnetostriction and gyromagnetic effects) the non-equilibrium elastic processes are described by the relation:[1]

$$\sigma_f = c_{fg}\varepsilon_g + c^*_{fq}\omega_q, \qquad \varepsilon_g = (\partial u_i/\partial x_j + \partial u_j/\partial x_i)/2,$$

$$\omega_q = (\partial u_i/\partial x_j - \partial u_j/\partial x_i)/2, \qquad (1)$$

where $\sigma_f = \sigma^*_{ij} = \sigma^*_{ji}$ are the components of the mechanical stress tensor, u_i are the components of the displacement vector, and the non-zero components of the dynamic elastic modulus tensor, under the given conditions, are c_{fg} and c^*_{fq} (which depend on H_0 or I_0), given in reference 1. Here f, g, and q are the customary symbols for index pairs in the theory of elasticity.

Let us consider the propagation of elastic waves along the direction of the polarizing field H_0. Taking the solution of the equations of the theory of elasticity $\rho\ddot{u}_i = \partial\sigma^*_{ij}/\partial x_j$ in a form proportional to $\exp\{i(\omega t - kx_3)\}$, and neglecting absorption and the relativistic corrections to Ohm's law for the currents in a moving medium, we obtain the proper frequencies

$$\omega^{(1)} = k(c_{33}/\rho)^{1/2},\ \omega^{(2,3)} = k(c_{44}/\rho + k^2B^2/4\rho)^{1/2} \pm k^2B/2\rho. \quad (2)$$

Here it has been assumed that

$$c_{45} = -c_{54} = i\omega c'_{45};\ c^*_{45} = c^*_{54} = i\omega c^{*\prime}_{45};$$

$$c^*_{44} = (d_{2323} - d_{3232})/4 = 0,$$

and the notation $B = c''_{45} - c^{*\prime}_{45}$ has been introduced. The frequency $\omega^{(1)}$ corresponds to a longitudinal wave, and $\omega^{(2)}$ and $\omega^{(3)}$ correspond to two circularly polarized transverse waves; i.e., $(u^0_1/u^0_2)^{(2,3)} = \mp i$.

From Eq. (2) it follows that in the propagation of plane polarized transverse elastic waves, travelling along the direction of a constant magnetic field, one may expect a rotation of the plane of polarization of the elastic waves through an angle

$$\varphi = \varkappa H_0 x_3 = Bk^{(0)2} x_3/2(\rho c_{44})^{1/2}, \quad (3)$$

where $k^{(0)} = (k^{(1)} + k^{(2)})/2$.

We estimate the possible magnitude of the rotational constant χ, based on the microscopic model which has been proposed. We assume that the elastic medium is a metal, and use the free-electron model. According to Pippard,[2] when a transverse elastic wave passes through a metal it sets up alternating electric fields and currents in it, determined by the displacements. By working out the Lorentz force acting on the resulting current $(\mathbf{J}_e - Ne\dot{\mathbf{u}})$, where $\mathbf{J}$ and $(-Ne\dot{\mathbf{u}})$ are the electric currents due to electrons and ions respectively, it can be shown that the quantity

$$B = -Ne(1-g)H_0 l/c(k^2 + gk_0^2), \quad (4)$$

acts like a component of the elastic modulus tensor. Here $k_0^2 = 4\pi i\omega Ne^2\tau/c^2 m$; when $\omega\tau < 1$ the quantity g is equal to $g \approx 1 - (kl)^2/5$ if $kl \ll 1$, and $g = 3\pi/(4kl)$ if $kl \gg 1$; c is the speed of light, N is the number of free electrons in one cubic centimeter, and l and τ are the length and time of the free path. Note that in deriving the expression (4) no account was taken of the effect of the constant magnetic field H_0 in calculating the magnitude of the electric current. Hence it may be used either if the radius of curvature of the electron orbits in the magnetic field $r_0 \gg l$, or if the current due to electrons can be neglected in comparison with the ion currents. It follows from the work of Pippard that the latter conditions holds if $k^2 > k_0^2$ and $kl \gg 1$. Furthermore, we have not taken into account the effect of the magnetic field on the distribution function (these considerations are discussed in reference 3).

Generally speaking, the constant B may itself be complex, as can be seen from Eq. (4), for example. Hence in calculating φ (or χ) the real part of B must be used. The imaginary part of B gives the different absorption coefficients for the left-handed and right-handed circularly polarized waves. Consequently in the transmission of linearly polarized waves we should expect, in addition to a rotation of the plane of polarization, the appearance of some ellipticity (circular magnetic dichroism of transverse elastic waves). The axial ratio of the ellipse in this case is expressed in the following form:

$$b/a = \pm\tanh \operatorname{Im}\{Bk^{(0)2} x_3/[2(\rho c_{44})^{1/2}]\}.$$

The greatest value of the rotational constant χ is obtained under the conditions $k^2 > k_0^2$ and $kl \gg 1$. In this case, according to Eqs. (3) and (4), if we assume that $N \sim 10^{22}$ cm^{-3}, $\rho \sim 10$ g cm^{-3}, and $v_t \sim 10^5$ cm sec^{-1}, we obtain $\chi = Ne/(2\rho c v_t) \sim 10$ rad cm^{-1} oe^{-1}, where $v_t = (c_{44}/\rho)^{1/2}$.

It is interesting to note that the propagation of transverse waves along the x_1 axis, with their plane of polarization parallel to the x_2 axis, must be accompanied by the propagation of a longitudinal wave. In this case $u^0_1/u^0_2 = -2i\omega(c''_{16} - c^{*\prime}_{16})/(c_{11} - c_{12})$. In the free electron model which has been used for the metal, $c''_{16} - c^{*\prime}_{16} = -B$.

In conclusion the authors would like to express their thanks to S. V. Vonsovskiĭ for his continued interest in the work.

[1] K. B. Vlasov, Физика металлов и металловедение (Phys. of Metals and Metal Research) **5**, 385 (1957); Izv. Akad. Nauk SSSR, Ser. Fiz. **22**, 1159 (1958).

[2] A. B. Pippard, Phil. Mag. **46**, 1104 (1955).

[3] K. B. Vlasov, Физика металлов и металловедение (Phys. of Metals and Metal Research) **7**, 447 (1959).

Translated by D. C. West
242

SIMPLIFICATION OF THE FORMULAS FOR STATISTICAL WEIGHT CALCULATIONS

Ya. I. GRANOVSKIĬ

Institute for Nuclear Physics, Academy of Sciences, Kazakh S.S.R.

Submitted to JETP editor October, 24, 1958

J. Exptl. Theoret. Phys. (U.S.S.R.) **36**, 1303-1304 (April, 1959)

THE calculation of statistical weights has been the subject of consideration in many papers (see, for instance, references 1 and 2). The most complete results (in series form) are quoted in the review by Belen'kiĭ et al.[2] These calculations can be considerably simplified.

By definition

$$W_N = \int d\mathbf{p}_1 \dots d\mathbf{p}_N\, \delta\Big(\sum \mathbf{p}_k - \mathbf{P}_0\Big)\delta\Big(\sum E_k - E_0\Big)$$

$$= (2\pi)^{-4}\int d^4\tau \exp\{-i\tau_\mu \mathbf{P}_\mu^0\}\prod_k \int d\mathbf{p}_k \exp\{i(\tau \mathbf{p}_k - \tau_0 E_k)\} \quad (1)$$

(here summation over repeated indices is to be understood, and $\tau_\mu p_\mu^0 = \boldsymbol{\tau}\cdot\mathbf{P}_0 - \tau_0 E_0$). The basic difficulty in evaluating the integral (1) is that the momentum integrals are very cumbersome, since $E_k = \sqrt{\mathbf{p}_k^2 + m_k^2}$. The difficulty is removed if we go over to the four-dimensional relativistically invariant functions

$$J_k = \int d\mathbf{p}_k \exp\{i(\tau \mathbf{p}_k - \tau_0 E_k)\}$$

$$= (2\pi)^3 \frac{\partial}{\partial \tau_0}[\Delta(\tau_0^2 - \boldsymbol{\tau}^2) + i\Delta_1(\tau_0^2 - \boldsymbol{\tau}^2)] \quad (2)$$

(see the definition of the Δ function in reference 3). The next step usually consists in substituting for the Δ-functions their expressions in terms of Hankel functions,[2] after which, in practice, the only acceptable way to use the integral (1) is to expand it in series.

If, however, we take advantage of the well-known parametric representation of the Δ function[3]

$$\Delta = \frac{1}{2\pi^2}\int_0^\infty \cos[\alpha(\tau_0^2 - \boldsymbol{\tau}^2) + m_k^2/4\alpha]\, d\alpha,$$

$$\Delta_1 = -\frac{1}{2\pi^2}\int_0^\infty \sin[\alpha(\tau_0^2 - \boldsymbol{\tau}^2) + m_k^2/4\alpha]\, d\alpha, \quad (3)$$

we obtain for J_k

$$J_k = -8\pi i\tau_0 \int_0^\infty \alpha_k d\alpha_k \exp[-i\alpha_k(\tau_0^2 - \boldsymbol{\tau}^2) - im_k^2/4\alpha_k]. \quad (4)$$

Now the integration with respect to τ in Eq. (1) is carried out without any preliminary series expansion of the integrand, making use of the following formula:[4]

$$\int d^4\tau \exp(-i\tau P + ia\tau^2) = (\pi^2/ia^2)\exp(-iP^2/4a). \quad (5)$$

As a result we obtain

$$W_N = (2\pi)^{-4}\frac{\pi^3}{i}\Big(-8\pi\frac{\partial}{\partial E_0}\Big)^N \int_0^\infty \frac{\alpha_1 d\alpha_1 \dots \alpha_N d\alpha_N}{(\alpha_1 + \dots + \alpha_N)}$$

$$\times \exp\Big\{-i\frac{\mathbf{P}_0^2 - E_0^2}{4(\alpha_1 + \dots + \alpha_N)} - \frac{i}{4}\sum_k \frac{m_k^2}{\alpha_k}\Big\}. \quad (6)$$

By a change of variables, this formula can be put into a different form:

$$W_N = \frac{1}{i\pi^2}\Big(-\frac{\pi}{2}\frac{\partial}{\partial E_0}\Big)^N (E_0^2 - \mathbf{P}_0^2)^{2N-2}\int_0^\infty \frac{\beta_1 d\beta_1 \dots \beta_N d\beta_N}{(\beta_1 + \dots + \beta_N)^2}$$

$$\times \exp\Big\{\frac{i}{\beta_1 + \dots + \beta_N} - \frac{i\nu_1^2}{\beta_1} - \dots - \frac{i\nu_N^2}{\beta_N}\Big\}, \quad (7)$$

where

$$\nu_k^2 = m_k^2/(E_0^2 - \mathbf{P}_0^2). \quad (8)$$

For $\nu_k^2 = 0$ (the ultra-relativistic case), there is no branch point in the integral (7), and a straightforward calculation leads to the well-known expression[1,5]

$$W_N^{(0)} = \Big(\frac{\pi}{2}\Big)^{N-1}\frac{(4N-4)!}{(3N-4)!}\frac{E_0^{2N-4}}{(2N-2)!\,(2N-1)!} \quad (9)$$

(Here $\mathbf{P}_0$ has been put equal to zero, i.e., the center-of-mass system is used).

A correction to this formula, taking into account the fact that $\nu_k^2 \neq 0$, can be calculated if $\exp(-i\Sigma\nu_k^2/\beta_k)$ is expanded in a series broken off at the second term:

$$W_N^{(1)} = -\Big(\frac{\pi}{2}\Big)^{N-1}\frac{(4N-6)!}{(3N-6)!}\frac{E_0^{2N-4}}{(2N-3)!\,(2N-2)!}\sum_{k=1}^{N}(\nu_k)^2. \quad (10)$$

There are no logarithmic terms present in this case, either, due to the presence of the β_k factors in the denominator of the integrand. However, they do make their appearance in the next approximation ($\sim \nu^4$).

Thus, Eq. (6) [or (7)] appears to be a suitable starting point for approximate representations of statistical weights.

---

[1] R. H. Milburn, Revs. Modern Phys. **27**, 1 (1955).

[2] S. Z. Belen'kiĭ, V. M. Maksimenko, A. I. Nikishov, and I. L. Rozental', Usp. Fiz. Nauk **62** (2), 1 (1957).

[3] D. D. Ivanenko and A. A. Sokolov, Классическая теория поля, (Classical Field Theory), Gostekhizdat, Moscow (1951).

[4] J. Schwinger, Phys. Rev. **75**, 651 (1949).

[5] I. L. Rozental', J. Exptl. Theoret. Phys.

(U.S.S.R.) 28, 118 (1955), Soviet Phys. JETP 1, 166 (1955).

Translated by D. C. West
243

STATISTICAL ELECTRON CAPTURE MECHANISM IN BETATRONS

M. SEIDL

Institute for Vacuum Electronics, Prague, Czechoslovakia

Submitted to JETP editor November 21, 1958

J. Exptl. Theoret. Phys. (U.S.S.R.) 36, 1305-1306 (April, 1959)

RECENT papers have shown that the capture of injected electrons into orbits is due to the Coulomb interaction and that the capture of part of the electrons becomes possible as a result of the loss of the remaining ones. Kovrizhnykh and Lebedev succeeded by an ingenious formulation of the kinetic equations in obtaining some general result.[1] However, the mathematical difficulties of integrating the kinetic equations hide the physical picture of the process.

Physically, the considered capture mechanism, which was proposed by Matveev,[2,3] is of importance in the initial phases of the capture process, although it in itself cannot lead to capture. This is a direct consequence of Poincare's theorem on conservative systems, if the following experimental data are considered.

1) The time dependence of the magnetic field does not have an important influence on the capture. A direct experimental proof is contained in our earlier work,[4,5] where all experiments on the capture were carried out in a dc magnetic field.

2) The capture takes place also on the flat portion of the injection pulse.[6] In contrast to Logunov et al., we find[5] that the pulse fronts do not seem to be important in the injection into a dc field.

3) The captured charge increases with increasing injection pulse length and reaches its maximum value at a pulse length corresponding to several tens of revolutions. The larger the injection current the sooner saturation sets in. However, if the injection time is of the order of one revolution the captured charge is very small even for very large injection currents.[5]

From this one obtains the following picture of the process of injection into a dc magnetic field. A few revolutions after the begin of the injection there appears a stationary state in the doughnut — the number of the injected electrons almost equals the number of lost electrons. Let us take a look at the Hamiltonian for an arbitrary electron which moves in the field of all the other electrons. As long as we do not take into account the microstructure of the charge distribution, the Hamiltonian does not depend on the time. If the electron does not strike the walls it will hit the injector after a few revolutions.

The system is not conservative if one takes into account the statistical fluctuations of the charge density. As a result of the collective interaction of the electrons, their density distribution approaches statistical equilibrium.

The author[7] has investigated the equilibrium state of a toroidal electron beam employing several simplifying assumptions. The equilibrium state is determined by two parameters:

$$a = 2kT/E_0, \qquad b = P/P_0, \tag{1}$$

where k is Boltzmann's constant, kT is the mean kinetic energy of the transversal electron motion, $E_0 = qV$ (q = electron charge, V = injection voltage) is the energy of the azimuthal motion, and $P = I/V^{3/2}$, where I = beam current; $P_0 = 3.33 \times 10^{-5}$ amp/(volt)$^{3/2}$.

In the case $a \gg b$ the effective radius of the beam cross section is (in terms of the radius of the equilibrium orbit, r_0) $\rho_0 = \sqrt{a}$ and the distribution of the charge density is given by

$$\sigma/\sigma_{max} = (b/\rho_0^2) \exp\{-(\rho/\rho_0)^2\}, \tag{2}$$

where ρ is the relative distance from the beam center and $\sigma_{max} = 2\epsilon_0 V/r_0^2$ is the maximum possible charge density (in MKS units). Experiments show that the distribution of the charge density agrees well with Eq. (2) and becomes established a short time after the injection. The figure shows the experimentally-observed equal-density curves in percent of σ_{max}; the values shown in a and b were measured after 20 and 100 revolutions after the termination of the injection, respectively.

The statistical electron capture mechanism can be understood if one considers the cooling process of the beam. The loss of electrons to the walls and to the injector does not only decrease the number of the electrons in the beam but also decreases the mean transversal energy of the remaining electrons. As a result of this cooling the cross section of the beam decreases. The change of the number of electrons, ΔN, and the temperature parameter, Δa, during the time

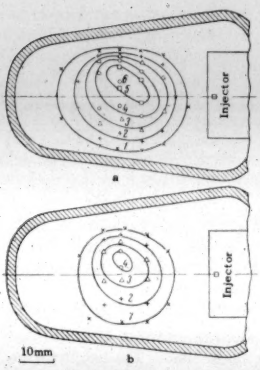

Curves of equal charge density. a—measured after 20 revolutions; b—measured after 100 revolutions after termination of injection. The numbers at the curves denote the charge density in percent of the maximum possible charge density.

interval Δt is approximately given by the expressions

$$\frac{\Delta N}{N} = -e^{-u}\frac{\Delta t}{\tau_p}, \qquad \frac{\Delta a}{a} = -\frac{ue^{-u}}{1-e^{-u}}\frac{\Delta t}{\tau_p}, \tag{3}$$

where $u = (\rho_m/\rho_0)^2$, ρ_m is the smallest relative distance of the doughnut walls from the beam center, and τ_p is the relaxation time. For the conditions of our experiment $\tau_p \sim 1$ μsec.

The following capture picture emerges from the foregoing. The injected electrons, which start out in a nonequilibrium distribution, try to approach the equilibrium distribution. As a result of the described cooling mechanism, the beam cross section decreases. Since the relaxation time is much larger than the time of one revolution, the number of the captured electrons depends on the mean life of the injected electrons. Matveev's mechanism increases this lifetime. For small values of the injected current this time increases, owing to a suitable ratio of the frequency of the betatron oscillations[5] and the orbital frequency.

[1] L. M. Kovrkzhnykh and A. N. Lebedev, J. Exptl. Theoret. Phys. (U.S.S.R.) **34**, 984 (1958), Soviet Phys. JETP **7**, 679 (1958).

[2] A. N. Matveev, J. Exptl. Theoret. Phys. (U.S.S.R.) **34**, 1331 (1958), Soviet Phys. JETP **7**, 918 (1958).

[3] A. N. Matveev, J. Exptl. Theoret. Phys. (U.S.S.R.) **35**, 372 (1958), Soviet Phys. JETP **8**, 259 (1959).

[4] M. Seidl, Czechosl. J. Phys. (in press).

[5] M. Seidl, Inst. for Vacuum Electronics, Prague, Report 27.32.58.

[6] Logunov, Ovchinnikov, and Rusanov, J. Tech. Phys. (U.S.S.R.) **27**, 1135 (1957), Soviet Phys. JTP **2**, 1023 (1957).

[7] M. Seidl, Czechosl. J. Phys. (in press).

Translated by M. Danos
244

ANISOTROPY OF THE ABSORPTION OF ULTRASOUND IN METALS IN A MAGNETIC FIELD

A. A. GALKIN and A. P. KOROLYUK

Institute of Radiophysics and Electronics; Physico-Technical Institute, Academy of Sciences, Ukrainian S.S.R.

Submitted to JETP editor December 12, 1958

J. Exptl. Theoret. Phys. (U.S.S.R.) **36**, 1307-1309 (April, 1959)

THE absorption of ultrasound in metals at low temperatures has been the subject of relatively few investigations, and principal attention has been paid to an investigation of the difference in absorption coefficients in the superconducting and normal states.[1,2] It has been noted that for longitudinal sound, the coefficient of absorption in tin depends on the magnetic field, but if the field is perpendicular to the sound wave vector **k**, a weakly pronounced maximum of absorption is observed in certain fields. A similar phenomenon was observed in polycrystalline copper[3] and in indium[4] and was not observed in zinc.

We report in this communication experiments set up to study the influence of the magnetic field on the absorption of ultrasound in single-crystal specimens of very pure metals. We prepared tin specimens with a residual resistivity less than 1.6×10^{-5} and of zinc with $R_{4.2}/R_{300} = 2 \times 10^{-4}$. The specimens were 12 mm in diameter and 12 and 15 mm long, respectively. The absorption coefficients were measured by known[5] pulse techniques at 17.3, 23.3, 51, and 70 Mcs.

Figure 1 shows the measured values of the coefficient of absorption of longitudinal sound in tin and zinc as a function of the magnetic field intensity at 4.2°K. The magnetic field is perpendicular to the wave vector. The ordinates represent the difference in the absorption coefficients with

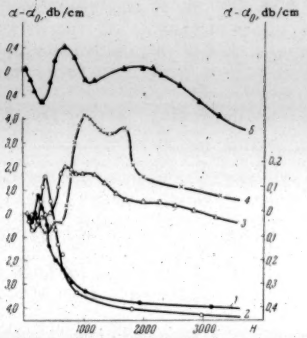

FIG. 1. Dependence of the coefficient of ultrasound absorption on the magnetic field H. Curves 1, 2, 3, 4 – tin; frequencies 17.3, 23.3, 51, and 70 Mcs. Curve 5 – zinc, 70 Mcs. Temperature 4.2°K. The vertical scale for curves 1 and 2 is on the right.

and without the field. It should be noted that when the temperature is reduced to 2° K the values of the absorption maxima increase, particularly in strong fields. A similar effect is produced by increasing the sound frequency. The value of the magnetic field at the maximum depends linearly on the ultrasound frequency, and the peak on the absorption curve is proportional to the square of the frequency. The effect is observed also in the case when the magnetic field is directed along the wave vector, but its magnitude is substantially smaller.

If the magnetic field is rotated in a plane perpendicular to the specimen axis, the character of the curves is substantially changed: the positions and magnitudes of the maxima change; in some directions the maxima smear out and disappear, while in others the maxima exist only at angles from 15 to 20°. Figures 2 and 3 (curves a) show

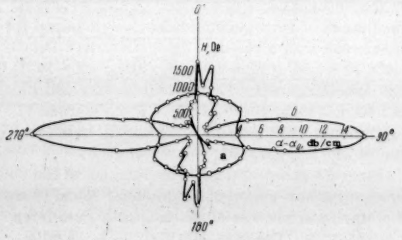

FIG. 2. a – rotation diagram of the maximum absorption of sound at 70 Mcs in tin, b – the same for the limiting absorption coefficient.

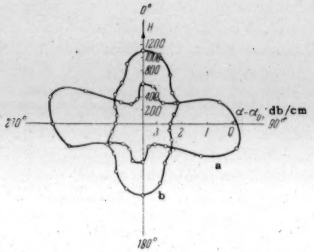

FIG. 3. a – rotation diagram for maximum absorption of sound at 70 Mcs in zinc, b – the same for the limiting absorption coefficient.

rotation diagrams for the first absorption maximum for tin or zinc. The length of the radius vector represents here the value of the field at the maximum. In tin the specimen axis makes 65° with the tetrangonal axis and lies in a plane making an angle of 62° with the (100) plane. The angle $\varphi = 0$ on the diagram corresponds to a field directed along this plane. In zinc the cylinder axis is perpendicular to the hexagonal axis and is inclined 7°30′ to the binary axis, while $\varphi = 0$ corresponds to a field along the hexagonal axis.

At frequencies on the order of 70 Mcs the coefficient of absorption of ultrasound tends to saturation at fields on the order of 5000 or 6000 oe, while its limiting value depends on the orientation of the specimen in the field. The results of the experiments made to determine the dependence of $\alpha - \alpha_0$ on the specimen orientation in a field of 10,000 oe at 70 Mcs are shown in Figs. 2 and 3 (curves b).

The irregularity of the coefficients of ultrasound absorption in a magnetic field and the presence of effects for both the longitudinal and transverse sound, as well as the existence of an effect for $\mathbf{H} \| \mathbf{k}$ indicate that the qualitative explanation offered by Pippard is inadequate for most observed phenomena.

It is possible that the observed effects can be attributed to diffraction scattering of the electrons by the space lattice, produced by the high-frequency fields. In this case the conditions to reflection or scattering under conditions when the Pippard relations[6] holds will be different than the scattering conditions in the absence of a field or in large fields. The presence of several absorption maxima and their anisotropy may be due to the existence of a series of effective electron masses $(0.2 - 1.0\ m_0)$.

The rotation diagram for limiting values of the

coefficients of absorption in large fields apparently describes the anisotropy of electric conductivity in a magnetic field.

[1] H. E. Bömmel, Phys. Rev. **100**, 758 (1955).
[2] H. E. Bömmel, Proc. Fifth International Conference on Low Temperature Physics and Chemistry, Madison, Wis., Aug. 26-31 (1957).
[3] Morse, Bohm, and Gavenda, Phys. Rev. **109**, 1394 (1958).
[4] R. W. Morse and H. V. Bohm. Proc. Fifth International Conference on Low Temperature Physics and Chemistry, Madison, Wis., August 26-31, 1957.
[5] S. Ya. Sokolov, Usp. Fiz. Nauk **40**, 3 (1950).
[6] A. B. Pippard, Phil. Mag. **2**, 1147 (1957).

Translated by J. G. Adashko
245

RANGES OF MU-MESIC ATOMS IN HYDROGEN CHAMBERS

S. S. GERSHTEĬN

Leningrad Physico-Technical Institute, Academy of Science, U.S.S.R.

Submitted to JETP editor December 15, 1958

J. Exptl. Theoret. Phys. (U.S.S.R.) **36**, 1309-1311 (April, 1959)

IN the experiments of Alvarez et al.,[1] who observed nuclear reactions catalyzed by μ^- mesons in a hydrogen chamber, the origin of the track of a μ^- meson that had carried off energy from a nuclear reaction was often separated from the point at which the μ^- meson was stopped by a "fissure" on the order of 1 mm in size. The same kind of fissure not infrequently separates the point at which the μ^- meson was stopped from the beginning of the track of the electron generated in the μ^- meson decay. Alvarez et al.[1] attribute the appearance of the fissure to the recoil energy (of the order of $\frac{1}{3} \times 135$ ev $\simeq 45$ ev) of the mesic deuterium atom during the capture of the μ^- meson from the proton by the deuteron. They believe that this energy creates a gap equal to the fissure. This view is confirmed by the effective cross sections for $d_\mu + p$ and $d_\mu + d$ scattering computed by Cohen et al.[2] The effective $d_\mu + p$ cross section is small, and, as calculations have shown, a d_μ mesic atom with an energy of 45 ev actually does travel a distance on the order of 1 mm in hydrogen. Therefore, for a slight increase in the concentration of deuterium, the fissure is observed more often, because then a greater number of μ^- mesons are captured by the deuterons. When the deuterium concentration is increased still more (to about 4.3%[1]), the d_μ track becomes very short (on the order of a few hundredths of a millimeter) because of $d_\mu + d$ collisions (whose effective cross section are computed to be large[2]), and the fissure is not observed. (Here the essential thing is that in collisions of d_μ atoms with protons at rest the d_μ atoms are not deflected into angles exceeding 30°, while in $d_\mu - d$ scattering the angle of deflection may be as great as 90°.)

In $p_\mu - p$ scattering, transitions may occur between levels of the hyperfine structure of the mesic atom. For energies considerably exceeding that of hyperfine dissociation ($\Delta\epsilon \approx 0.183$ ev) an analytic expression can easily be provided for the $p_\mu + p \rightarrow p_\mu + p$ cross section calculated by Cohen et al.[2] The cross section for p_μ scattering by protons is

$$\sigma = 2\pi \left(\frac{1}{4} \frac{\lambda_g^2}{1 + k^2\lambda_g^2} + \frac{3}{4} \frac{\lambda_u^2}{1 + k^2\lambda_u^2} \right), \qquad (1)$$

where* $k^2 = (M_p\epsilon)^{1/2}/\hbar$, ϵ is the energy of the relative motion of p_μ and p in the center-of-mass system, and λ_g and λ_u are the scattering lengths of protons by the mesic molecular potentials $E_q(R)$ and $E_u(R)$, which correspond respectively to symmetric and antisymmetric wave functions (in the proton coordinates) for the 1s σ_g and the 2p σ_μ system (in the first the total spin of both protons is equal to zero and in the second, equal to 1). The potentials $E_g(R)$ and $E_u(R)$ which include a correction for the influence of μ meson motion,[4] accurate to order m_μ/M_p, can be approximated accurately by a Morse potential and an exponential.[5] The scattering lengths λ_g and λ_u are easily expressed in terms of the parameters of these functions.[6] However, the approximation given formerly by this author[6] is too rough; more exact values have been obtained for these parameters by Zel'dovich et al.[5] (in their Fig. 2 the value of α has been rounded off to 0.67 from 0.673). If the more accurate values are employed, then $\lambda_g \approx -17.3$ and $\lambda_u \approx 5.25$ (in mesic atom units). When $kR_0 < 1$, the $pp\mu$ mesic molecular level and cross section (1) are in good agreement with the computations published by Cohen et al.[2] The rather large value for λ_g can be attributed to the presence of a virtual level near zero[6,7] in

the system. Because of this condition, cross section (1) has a resonance character for low energies.

For energies comparable to the energy $\Delta\epsilon$ of the hyperfine structure the scattering cross section varies according to which of the hyperfine states in p_μ is occupied. As was shown earlier,[6] the scattering cross section for a $F = 1 \rightarrow F = 0$ transition is very large (the transition probability for the more exact parametric values is $W \approx 5 \times 10^9\ \text{sec}^{-1}$). Therefore, p_μ mesic atoms pass to the state $F = 0$ in a time $t \simeq 2 \times 10^{-10}$ sec and acquire an energy $\frac{1}{4}\Delta\epsilon \approx 0.1$ ev. The elastic scattering cross section of p_μ in the $F = 0$ state can be obtained in a way analogous to that reported earlier,[6]

$$\sigma_{el} = 2\pi \left| \frac{(\lambda_g + 3\lambda_u) + 4ik_2\lambda_u\lambda_g}{4 + ik_1(\lambda_g + 3\lambda_u) + ik_2(3\lambda_g + \lambda_u) - 4k_1k_2\lambda_u\lambda_g} \right|^2, \quad (2)$$

where $k_1 = \sqrt{M_p\epsilon}$, $k_2 = \sqrt{M_p(\epsilon - \Delta\epsilon)}$, and ϵ is the energy in the center-of-mass system. It is important to note that the value of $\lambda_g + 3\lambda_u$, which with the values of λ_g and λ_u given above determines the elastic cross section, is very small (while the value of $\lambda_g - \lambda_u$ entering into the inelastic cross section is large). Therefore, the elastic scattering cross section is very small:† for $\epsilon = 0$, $\sigma_{el} \approx 1.7 \times 10^{-22}$, and for $\epsilon = \frac{1}{4}\Delta\epsilon$, $\sigma_{el} \approx 2.2 \times 10^{-22}\ \text{cm}^2$.

For $\epsilon = \frac{1}{4}\Delta\epsilon$, the inelastic cross section for the process by which $pp\mu$ mesic molecules are formed is[5] $\sigma_{inel} = W_{pp\mu}/Nv \approx 2.4 \times 10^{-22}\ \text{cm}^2$. Thus, the mean free path of a mesic atom that has passed from $F = 1$ to $F = 0$ is $\lambda \approx 1/N\sigma_{tot} \approx 0.5$ mm, i.e., a noticeable "fissure" can be observed even in pure hydrogen.

The $d_\mu + d$ cross section for energies greater than the hyperfine structure level is analogous to Eq. (1):

$$\sigma = 2\pi\left(\frac{2}{3}\frac{\lambda_g^2}{1 + k^2\lambda_g^2} + \frac{1}{3}\frac{\lambda_u^2}{1 + k^2\lambda_u^2}\right);\ \lambda_g = 6.7;\ \lambda_u = 5.7.$$

This cross section is two times smaller than the one obtained by Cohen et al.[2] We note that in the case of $d_\mu + d$ collisions a transition to a lower state of the d_μ ($F = \frac{1}{2}$) hyperfine structure is also possible (although the probability of this is considerably less than for the resonance transition in p_μ). This circumstance could, roughly speaking, triple the probability of $\mu^- + d \rightarrow n + n + \nu$ capture in comparison to the value computed by A. Rudik,[8] if it is assumed that the capture of a μ^- meson from the $F = 3/2$ state is very much suppressed. However, the formation of $dd\mu$ molecules causes the blending of the $F = 1/2$ and $F = 3/2$ states, and subsequent catalysis of the $d + d$ reaction would appear to make experiments for the study of the $\mu^- + d \rightarrow n + n + \nu$ reaction in deuterium impracticable.

*Assuming that $kR_0 \ll 1$ [R_0 is the interaction radius of the potentials $E_g(R)$ and $E_u(R)$].

†It should be noted that actually the cross section may be quite different from these values because of the sensitivity of the resonance value for λ_g on the exact form of the potential.

[1] Alvarez, Bradner, Crawford, et al., Phys. Rev. **105**, 1127 (1957).

[2] Cohen, Judd, and Riddel Jr., Phys. Rev. **110**, 1471 (1958).

[3] V. B. Belyaev and B. N. Zakhar'ev, J. Exptl. Theoret. Phys. (U.S.S.R.) **35**, 996 (1958), Soviet Phys. JETP **8**, 699, (1959).

[4] Bates, Ledsham, and Stewart, Phil. Trans. Roy. Soc. **A246**, 215 (1953); A. Dalgarno and R. McCarrol, Proc. Roy. Soc. **237**, 383 (1956).

[5] Ya. B. Zel'dovich and S. S. Gershteĭn, J. Exptl. Theoret. Phys. (U.S.S.R.) **35**, 649 (1958), Soviet Phys. JETP **8**, 453 (1959).

[6] S. S. Gershteĭn, J. Exptl. Theoret. Phys. (U.S.S.R.) **34**, 463 (1958), Soviet Phys. JETP **7**, 318 (1958).

[7] Ya. B. Zel'dovich, Dokl. Akad. Nauk SSSR **95**, 493 (1954).

[8] A. Rudik, Dokl. Akad. Nauk SSSR **92**, 739 (1953).

Translated by A. Skumanich
246

FLUCTUATIONS OF ATOMIC STRUCTURE IN LIQUID HELIUM

V. K. PROKHORENKO and I. Z. FISHER

Belorussian State University

Submitted to JETP editor December 18, 1958

J. Exptl. Theoret. Phys. (U.S.S.R.) **36**, 1311-1312 (April, 1959)

A detailed investigation of the atomic structure of liquid helium was carried out[1] by studying the scattering of slow neutrons. It was found that the packing of the atoms is quite dense, with an average coordination number of approximately eight units. However, the average distance between nearest atoms exceeded considerably the distance to the minimum on the curve of potential energy

of interaction of the atom pair, owing to the zero-point vibrations of the atoms. It was furthermore found that the atomic structure in the vicinity of ~ 2 — 5° K is little sensitive to changes in temperature and does not change upon transition through the λ point.

In view of the specific nature of liquid helium, it is interesting to study not only its average atomic structure, but also the fluctuations of this structure. We have obtained[2] an equation for the quadratic fluctuations of the coordination number in the liquid

$$(\delta z)^2 \equiv \overline{(\Delta z)^2} = \bar{z} + \frac{N\pi^2}{v^2}\int_0^{r_1}\int_0^{r_1} g(r)\,g(\rho)\left\{\int_{r-\rho}^{r+\rho}(g(t)-1)\,t\,dt\right\} r\,dr\rho\,d\rho, \qquad (1)$$

where g(r) is the radial distribution function, v the average volume per particle, r_1 the abscissa of the first minimum of g(r), and $\bar{z}$ the average coordination number

$$\bar{z} = \frac{4\pi}{v}\int_0^{r_1} g(r)\,r^2\,dr. \qquad (2)$$

In the derivation of (1) we used the superposition approximation from the theory of liquids, in which the triple distribution function is replaced by a product of binary distribution functions. At the present time it is well known that the superposition approximateion gives a higher order than actually exists in the liquid. One can therefore think that a calculation based on (1) should lead to values of δz that are too low.

We have calculated δz using Eq. (1) for liquid helium with the aid of an experimental function g(r) (from reference 1), which is the average of several series of measurements at temperatures below 2.25° K. The curves given in reference 1 for T = 4.24 and 5.04° K differ quite insignificantly from that selected by us and lead to the same results, within the accuracy limits possible in practical numerical integration. When r_1 = 4.6 A, Eq. (2) yields $\bar{z}$ = 8.4, which is in good agreement with the value indicated in reference 1, where another method of calculation is used, while Eq. (1) yields δz = 1.47. Thus, the relative mean-squared fluctuation of the number of nearest neighbors of a certain atom is 18% and, as indicated above, this number is apparently too low. We obtain a relatively high fluctuation level for the microstructure of liquid helium.

If the distribution of the number of nearest neighbors of a selected atom, W(z), is assumed to be approximately Gaussian, a knowledge of $\bar{z}$ and δz makes it possible to plot this distribution. The estimates obtained above for $\bar{z}$ and δz then

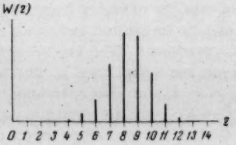

lead to the distribution W(z) shown in the diagram, where the ordinates are plotted in an arbitrary scale. The noticeable magnitude of fluctuations of z is seen here quite clearly.

One must indicate, however, that the foregoing results for liquid helium do not differ substantially from analogous results obtained for other liquids.[2]

[1] D. G. Hurst and D. G. Henshaw, Phys. Rev. **100**, 994 (1955).

[2] V. K. Prokhorenko and I. Z. Fisher, Журнал физической химии (J. Phys. Chem.) **31**, 2145 (1957).

Translated by J. G. Adashko
247

DIRECT PROOF OF THE APPLICABILITY OF THE MASSEY ADIABATIC CRITERION TO PROCESSES OF DOUBLE CHARGE EXCHANGE

Ya. M. FOGEL', V. F. KOZLOV, A. A. KALMYKOV, and V. I. MURATOV

Physico-Technical Institute, Academy Sciences, Ukrainian S.S.R.; Khar'kov State University

Submitted to JETP editor December 20, 1958

J. Exptl. Theoret. Phys. (U.S.S.R.) **36**, 1312-1314 (April, 1959)

AN investigation of the dependence of the effective cross sections for double charge exchange of H^+ and F^+ on their velocity has shown that two maxima are observed on the $\sigma_{1-1}(v)$ curves for these ions.[1] In reference 1 this fact was treated from the point of view of the Massey adiabatic criterion, according to which the maximum cross section of an inelastic process with a resonance defect ΔE is observed when a $|\Delta E|/hv_{max} \approx 1$. The presence of two maxima on the $\sigma_{1-1}(v)$ curves for the processes $H^+ \rightarrow H^-$ and $F^+ \rightarrow F^-$ is explained either by the formation of slow excited doubly-charged ions (the $H^+ \rightarrow H^-$ process)

or by the fact that the primary beam may contain admixtures of ions in excited metastable states (the $F^+ \rightarrow F^-$ process). The two maxima on the $\sigma_{1-1}(v)$ curves were explained by the fact that the process $F^+ \rightarrow F^-$ is also accompanied by the process $F^{+*} \rightarrow F^-$ with a resonance defect different from that of the former process, but having the same value of the constant a. The excitation energies of the F^+ ions, calculated on the basis of this assumption, agree within the limits of errors with the energy values known from spectroscopic investigations (cf. Table II, reference 1).

To check the correctness of these assumptions, we investigated the processes $B^+ \rightarrow B^-$ in Xe, Kr, and H_2 and $O^+ \rightarrow O^-$ in Xe. The $\sigma_{1-1}(v)$ curves displayed three maxima for $B^+ \rightarrow B^-$ and two maxima for $O^+ \rightarrow O^-$. The observed maxima, as can be seen from the accompanying table,

Process	Calculated excitation energy, ev	Ion term	Term energy, ev
$B^+ - Kr$	5.6±1.6	$2s2p\ ^3P^0$	4.6
$B^+ - Kr$	11.7±1.6	$2p^2\ ^3P$	12.1
$B^+ - Xe$	5.0±0.9	$2s2p\ ^3P^0$	4.6
$B^+ - Xe$	11.3±1.0	$2p^2\ ^3P$	12.1
$B^+ - H_2$	4.4±0.3	$2s2p\ ^3P^0$	4.6
$B^+ - H_2$	11.0±2.0	$2p^2\ ^3P$	12.1
$O^+ - Xe$	24.2±0.5	$2s2p^4\ ^2S$	24.4

which compares the calculated excitation energies of B^+ and O^+ with the tabulated data,[2] are due to the presence of B^+ ions in the excited states $2s\,2p\,^3P^0$ and $2p^3\,^3P$ and of O^+ ions in the $2s\,2p^4\,^2S$ state in the primary beam. The good agreement between the calculated and tabulated values of the excitation energy of the B^+ and O^+ ions gives further confirmation of the correctness of the premises used to explain the presence of several maxima on the $\sigma_{1-1}(v)$ curves. However, as indicated in reference 1, it is possible to prove directly the applicability of the Massy adiabatic criterion to an evaluation of the forms of the $\sigma_{1-1}(v)$ curves. For this purpose it is necessary to compare the forms of these curves in two cases: a) when it is known with certainty that the beam emerging from the source has no excited ions (thermionic source), and b) when the beam may contain excited ions (high-frequency ionic source).

To make such a comparison, we measured the effective cross section σ_{1-1} for $Li^+ \rightarrow Li^-$ in Kr, A, and H_2 using Li^+ beams from a thermionic and a high-frequency source.* The resultant $\sigma_{1-1}(v)$ curves are shown in the diagram. The curve (dotted) obtained with the aid of a thermionic source (described in reference 3) shows only one maximum connected with the $Li^+ \rightarrow Li^-$ process for the Li^+ ion in the ground state. The curve obtained with the high-frequency source (solid line) shows an additional maximum due to the Li^+ ions in excited states $2s\ ^3S$ and $2s\ ^1S$, with excitation energies 59 and 60.7 ev, contained in the beam. The arrows on the diagram indicate the positions of the maxima† for the processes $Li^+(^3S) \rightarrow Li^-$ and $Li^+(^1S) \rightarrow Li^-$, calculated on the basis of the Massey criterion under the assumption that the constant a for these processes has the same value, on the order of 1.5 A, as for the $Li^+ \rightarrow Li^-$ process, which determines the position of the main maximum. As seen from the diagram, the additional maxima for Kr and A, within the limits of experimental error, appear in the locations called for by the Massey criterion.‡ It follows from this fact that the assumption that the constant a has the same value for double charge-exchange processes for unexcited and excited ions is correct. The results of the investigation of the $Li^+ \rightarrow Li^-$ process prove directly the possibility of applying the adiabatic Massey criterion to double charge exchange of these ions, and also confirm the correctness of the explanation of the nature of additional maxima on the σ_{1-1} curves for the processes $F^+ \rightarrow F^-$, $B^+ \rightarrow B^-$, and $O^+ \rightarrow O^-$.

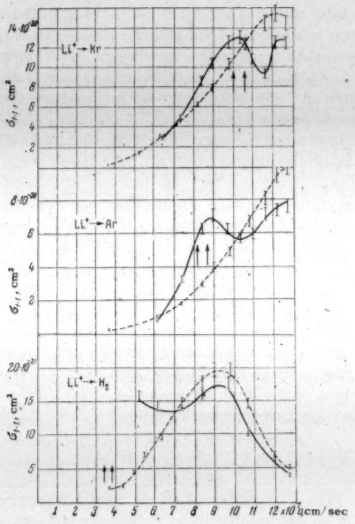

We express our gratitude to A. D. Timofeev, who participated in the initial stage of the investigation of double charge exchange of lithium ions

from a thermionic source.

*We have designed for this purpose a high-frequency source operating with LiCl vapor. This source will be described elsewhere.

†In view of the small energy difference between the terms $2s^3S$ and $2s^1S$, the additional maxima connected with these states are not separated.

‡We could not establish the position of the additional maximum on the $\sigma_{1-1}(\nu)$ curve for H_2 because of the low intensity of the Li^+ beam at low energies; it is clear from the course of the curve, however, that this maximum does not exist.

[1] Fogel', Mitin, Kozlov, and Romashko, J. Exptl. Theoret. Phys. (U.S.S.R.) **35**, 565 (1958), Soviet Phys. JETP **8**, 390 (1959).

[2] C. E. Moore, Atomic Energy Levels, National Bureau of Standards, 1949.

[3] Ya. M. Fogel' and A. D. Timoveev, Тр. физ.-мат. фак-та ХГУ; (Trans. Phys.-Math. Faculty, Khar'kov State University) **7**, 177 (1958).

Translated by J. G. Adashko
248

ELECTRON-NEUTRINO ANGULAR CORRELATION IN THE BETA DECAY OF THE FREE NEUTRON

Yu. V. TREBUKHOVSKIĬ, V. V. VLADIMIRSKIĬ, V. K. GRIGOR' EV, and V. A. ERGAKOV

Submitted to JETP editor December 25, 1958

J. Exptl. Theoret. Phys. (U.S.S.R.) **36**, 1314-1316 (April, 1959)

We have determined the electron-neutrino angular correlation in the β decay of the free neutron by studying the decay-electron spectrum for a fixed recoil proton momentum. Figure 1 shows a schematic diagram of the apparatus. A collimated neutron beam 35 mm in diameter from the heavy-water reactor of the U.S.S.R. Academy of Sciences passed into an aluminum vacuum chamber which contained detectors and magnetic lenses to focus the decay electrons and recoil protons.

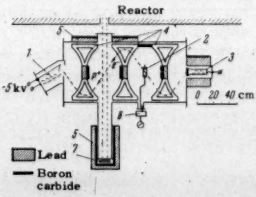

FIG. 1. Experimental setup: 1 – electron multiplier; 2 – Geiger-Mueller counter; 3 – photomultiplier; 4 – magnetic lenses; 5 – shield; 6 – device for filling the Geiger-Mueller counter; 7 – monitor.

The selection of electrons by momentum was done by the two consecutive toroidal magnetic lenses[1] pictured in the drawing to the right of the neutron beam. The resolving power of this system of spectrometers is ±3%. At the intermediate focus of the spectrometers there was a thin-walled (3 mg/cm^2 terelene) Geiger-Mueller counter filled with methylal at 110 mm Hg with forced gas circulation. At the second focus the electrons were detected by a counter consisting of a plastic scintillator 90 mm in diameter and 1 mm thick, a light pipe, and a BS photomultiplier.

With the help of this design only those electrons which passed through both detectors were chosen by means of a double coincidence with 0.2 μsec resolving time. The use of two consecutive lenses to detect electrons permitted us to reduce considerably the background of accidental coincidences and to limit the volume in which the detected decay occurred.

The separation of protons by momentum was done by a single toroidal spectrometer. An electron multiplier described in reference 2 was used to count the protons.

In the experiment we studied triple coincidences between the proton and electron detectors. To compensate for the flight time of the proton, pulses from the double coincidence circuit were delayed by 1.3 μsec relative to pulses from the proton detector. The resolving time of the triple coincidence circuit was 0.7 μsec.

In taking the data we regularly checked the efficiency of the electron multiplier with a calibrated α source and the operation of the Geiger-Mueller counter and the photomultiplier with the help of a Sr^{90} source.

The flow of neutrons was controlled with a monitor. The results of the measurements are shown in Fig. 2. The solid lines show the calculated forms of the electron spectra for different values of the electron-neutrino angular correlation coefficient.

The experimental points are shown with their standard errors. The results, worked out by the method of least squares, give the value $\lambda = -0.06 \pm 0.13$. Only statistical errors are given here. Possible systematic errors are being studied. The value we found is slightly different from the value of λ obtained by Robson[3] ($\lambda = +0.07 \pm 0.12$). If we assume that in β decay the main contribu-

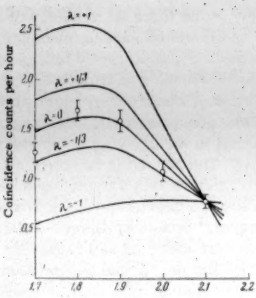

FIG. 2

tions are from the axial vector and vector interactions,[4-7] then our value for λ corresponds to

$$R = g_A^2/g_V^2 = 1.3^{+1.5}_{-0.13}.$$

The large statistical errors do not make it possible to state with assurance that the value R = 1.4 is confirmed, which would follow from the measurements of the neutron lifetime.[8]

In conclusion the authors consider it their duty to express their gratitude to the Academician A. I. Alikhanov for his valuable advice; to E. K. Tarasov for the theoretical calculations; to a group of co-workers, D. P. Zharkov, G. K. Tumanov, and N. I. Afanas'ev for their help in carrying out the experiment; to V. E. Nesterov for help in setting up the equipment; and to the chief engineer of the heavy-water reactor, S. A. Gavrilov, and his co-workers for the uninterrupted operation of the reactor.

[1] Vladimirskiĭ, Tarasov, and Trebukhovskiĭ, Приборы и техника эксперимента (Instruments and Meas. Engg.) **1**, 13 (1956).

[2] Trebukhovskiĭ, Ergakov, and Nesterov, Приборы и техника эксперимента (Instruments and Meas. Engg.) **1**, 75 (1956).

[3] J. M. Robson, Can. J. Phys. **36**, 1450 (1958).

[4] Herrmannsfeldt, Maxson, Stähelin, and Allen, Phys. Rev. **107**, 641 (1957).

[5] Goldhaber, Grodzins, and Sunyar, Phys. Rev. **109**, 1015 (1958).

[6] Herrmannsfeldt, Burman, Stähelin, Allen, and Braid, Phys. Rev. Letters **1**, 61 (1958).

[7] N. A. Burgov and Yu. V. Terekhov, J. Exptl. Theoret. Phys. (U.S.S.R.) **35**, 932 (1958), Soviet Phys. JETP **8**, 651 (1959).

[8] Sosnovskiĭ, Spivak, Prokof'ev, Kutikov, and Dobrynin, J. Exptl. Theoret. Phys. (U.S.S.R.) **35**, 1059 (1958), Soviet Phys. JETP **8**, 739 (1959).

Translated by Genevra Gerhart

249

THE PERMANENT STRUCTURE OF SHOCK WAVES WITH JOULE DISSIPATION

V. A. BELOKON'

Institute for Chemical Physics, Academy of Sciences, U.S.S.R.

Submitted to JETP editor December 30, 1958

J. Exptl. Theoret. Phys. (U.S.S.R.) **36**, 1316-1317 (April, 1959)

IF the only factor which changes the entropy of a composite medium is the Joule heat, then the equations of magnetohydrodynamics describing the time-independent uniform flow across magnetic lines of force (see reference 1) determine the evolution of the thermodynamic parameters in accordance with the continuity of mass and momentum flow

$$d\,(RT/V + H^2/8\pi)/dV \equiv dp/dV = -(\rho u)^2 = -(\rho u)^2_{\pm\infty} \qquad (1)$$

and the condition for heat balance is

$$\rho u T\, dS/dx = (c^2/16\pi^2\sigma)\,(dH/dx)^2 \geqslant 0. \qquad (2)$$

Magnetohydrodynamic shock waves, in their proper coordinate system, always represent a transition from hypersonic flow at $x = -\infty$ to a flow at $x = +\infty$ which is moving more slowly than adiabatic sound.[2] A trivial consequence of this is the fact that uninterrupted evolution of the thermodynamic parameters within the shock wave according to Eq. (1) would imply a maximum in the entropy within the compression wave, since at some points the speed of flow will be equal to the local adiabatic speed of sound; on the (p, V) diagram the isentropic lines, which are convex downward, will be tangent to the straight lines (1) at these points for any arbitrary amplitude. Any subsequent decrease in the entropy $S_{max} \to S_{+\infty}$ is impossible in view of (2). More than this, the whole region where $S \geq S_{+\infty}$ along the line (1) turns out to be forbidden, since in this region it is not possible to reach the final state. On the other hand, it is noteworthy that an attempt to construct a continuous solution would lead to a so-called "backlash" of the wave: (1) and (2) give

$$-(u/V)^3 T\, dS/dV = (c^2/16\pi^2\sigma)\,(dH/dV)^2\, dp/dx. \qquad (3)$$

When $dS/dV > 0$, i.e., when the entropy decreases as the material is compressed, the pressure tends to its final value with a negative gradient, implying an absurd triple-valued nature for the parameters of the flow in space.

In view of the absurdity of a continuous solu-

tion, we consider it unavoidable to postulate a Riemann "isentropic discontinuity"[3] in the flow parameters within a compression wave of any amplitude, by analogy with the isothermal discontinuity for purely heat-conducting gases.[4] At such a discontinuity, those gradients whose effect on the dissipation can be ignored must become infinite; i.e., at the discontinuity only the entropy and the magnetic field strength may not change abruptly. Inclusion of the thermal conductivity can smooth out the discontinuity only at sufficiently small amplitudes, above which an isothermal discontinuity sets in,[5] abruptly lowering the entropy. (The isomagnetic discontinuity is discussed in a number of papers,[2,5,6] which show that it must occur for sufficiently large amplitudes; the relationship between the field discontinuity and the entropy discontinuity is discussed in the work of Golitsyn and Stanyukovich,[7] but only in connection with the variation of the shock-front thickness.) If dissipation occurs by way of viscosity in addition to Joule heating, then the isentropic discontinuity mentioned above will be smoothed out for all amplitudes, since for vanishing viscosity the curves for continuous evolution of the flow parameters pass arbitrarily close to the isentropic line S_{max}, coinciding with it only in a single point, at $+\infty$. Even if there is no viscosity, structural continuity is still guaranteed in a shock wave in a heat-conducting medium if there is a sufficiently high density of radiation after the liquidation of the isothermal discontinuity.[8] For discussions of the present work the author is indebted to his coworkers in the Theoretical Section of the Institute of Chemical Physics, in particular to K. E. Gubkin.

[1] L. D. Landau and E. M. Lifshitz, Электродинамика сплошных сред, (Electrodynamics of Continuous Media) §§51 and 52, GITTL, M. (1957).

[2] W. Marshall, Proc. Roy. Soc. **A233**, 367 (1955).

[3] B. Riemann, Coll. Works, GITTL, 1948, pp. 383-385.

[4] L. D. Landau and E. M. Lifshitz, Механика сплошных сред, (Mechanics of Continuous Media), Gostekhizdat, M., 1954, §88.

[5] W. Marshall, Phys. Rev. **103**, 1900 (1956).

[6] G. S. Golitsyn and K. P. Stanyukovich, J. Exptl. Theoret. Phys. (U.S.S.R.) **33**, 1417 (1957), Soviet Phys. JETP **6**, 1090 (1958).

[7] G. S. Golitsyn and K. P. Stanyukovich, J. Exptl. Theoret. Phys. (U.S.S.R.) **35**, 828 (1958), Soviet Phys. JETP **8**, 575 (1959).

[8] V. A. Belokon', J. Exptl. Theoret. Phys. (U.S.S.R.) **36**, 341 (1959), Soviet Phys. JETP **9**, 235 (1959).

Translated by D. C. West
250

THE K_{e3} AND $K_{\mu 3}$ DECAYS

S. G. MATINYAN and L. B. OKUN'

Institute of Theoretical and Experimental Physics, Academy of Sciences, U.S.S.R. and Institute of Physics, Academy of Sciences, Georgian S.S.R.

Submitted to JETP editor December 31, 1958

J. Exptl. Theoret. Phys. (U.S.S.R.) **36**, 1317-1319 (April, 1959)

THE A-V interaction scheme[1,2] has recently had a series of experimental confirmations in the phenomena of β decay, μ and π decays, and decays of strange particles (decay of the Λ^0 hyperon, $K_{\mu 2}$ decay).[3-5] In connection with this, it is of interest to investigate the three-particle lepton K decays $K \to l + \nu + \pi$, where l denotes the electron or μ meson.

The matrix element for this process in the theory of universal A-V interaction, in which the electron and μ meson have the same status, has the following form (in the rest system of the K meson):

$$M^{-1/2} E_\pi^{-1/2} \left\{ \frac{m_l}{M} X (\bar{l}(1+\gamma_5)\nu) + Y (\bar{l}\gamma_4(1+\gamma_5)\nu) \right\}, \quad (1)$$

where E_π is the total energy of the π-meson, m_l and M are the mass of the lepton and K meson, respectively, while X and Y are real functions of the π-meson energy E_π, and are identical in K_{e3} and $K_{\mu 3}$ decays. If we neglect dependence of X and Y on E_π, assuming that X = const and Y = const, then it is possible to determine these quantities from experiment.

Such considerations were carried out by Gatto.[6*] Calculating the probabilities of $K_{\mu 3}$ and K_{e3} decays from Eq. (1) and comparing them with experimental values for the decay probabilities, Gatto obtained two possible pairs of values for X and Y, for which the ratio was either X/Y = 4.2 (solution I) or X/Y = −0.34 (solution II).

Knowing the constants X and Y, one can calculate the μ-meson energy spectrum for each

of the possible solutions I and II and, using the experiments, choose one of them. However, as follows from Gatto's work, the μ-meson energy spectra turn out to be very complex, and this makes the selection difficult. We would like to remark that the task of choosing between the two indicated solutions can be greatly simplified if the longitudinal polarization of the μ mesons in $K_{\mu 3}$ decay is measured.

It follows from Eq. (7) of reference 9 that the longitudinal polarization $\overline{P}$ of the μ meson is the following function of μ-meson energy in the A-V interaction scheme

$$\overline{P} = \frac{v - \alpha - 2\alpha \frac{X}{Y}\frac{m_\mu}{M}\frac{m_\mu}{E_\mu} - \left(\frac{X}{Y}\right)^2 \left(\frac{m_\mu}{M}\right)^2 (v+\alpha)}{1 - v\alpha + 2\frac{X}{Y}\frac{m_\mu}{M}\frac{m_\mu}{E_\mu} + \left(\frac{X}{Y}\right)^2 \left(\frac{m_\mu}{M}\right)^2 (1+v\alpha)},$$

$$\alpha = \frac{\sqrt{E_\mu^2 - m_\mu^2}}{M - E_\mu}, \qquad (2)$$

where v is the μ-meson velocity in the rest system of the K particle, E_μ is the μ-meson energy, and c = 1.

Figure 1 shows $\overline{P}$ as a function of the kinetic energy of the μ meson ($\kappa = E_{kin}/E_{kin}^{max}$) for the experimental value $\nu \equiv \tau(K_{e3})/\tau(K_{\mu 3}) = 0.96$. It is seen from the figure that solutions (I) and (II) give opposite signs and a completely different behavior for the longitudinal polarization as a function of energy. This makes it possible to determine X and Y unambiguously.

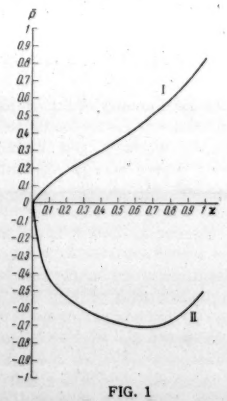

FIG. 1

Since the ratio ν is not accurately determined, it is of interest to investigate how $\overline{P}$ changes with ν (i.e., with X/Y) for given μ-meson energy. In

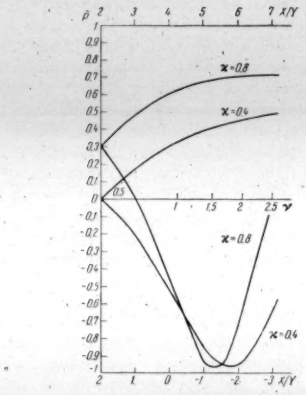

FIG. 2

Fig. 2, P is given as a function of ν (and X/Y) for $\kappa = 0.4$ and 0.8; for convenience, both abscissa axes corresponding to values of X/Y smaller and larger than 2 (X/Y = 2 corresponds to the limiting value $\nu = 1/2$) are laid off to the right of the ordinate.

If the experimental measurement of $\overline{P}$ gives results in disagreement with predictions, then (for a well-determined ν) this will mean that either the assumption of the weak energy dependence of X and Y is incorrect, or that the A-V interaction does not apply to K decays.

*Similar considerations were also given in reference 7 (see also reference 8).

[1] R. P. Feynman and M. Gell-Mann, Phys. Rev. **109**, 193 (1958).

[2] R. E. Marshak and E. C. Sudarshan, Phys. Rev. **109**, 1860 (1958).

[3] Proceedings of the Geneva Conference on High-Energy Physics, 1958.

[4] Fazzini, Fidecaro, Merrison, Paul, and Tollestrup, Phys. Rev. Letters **1**, 247 (1958).

[5] Impeduglia, Plano, Prodell, Samios, Schwartz, and Steinberger, Phys. Rev. Letters **1**, 249 (1958).

[6] R. Gatto, Phys. Rev. **111**, 1426 (1958).

[7] A. Fujii and M. Kawaguchi, Preprint.

[8] F. Zachariasen, Phys. Rev. **110**, 1481 (1958).

[9] L. Okun', Nucl. Phys. **5**, 455 (1958) (see also J. Werle, Nucl. Phys. **4**, 171, 693 (1957); S. W. McDowell, Nuovo cimento **6**, 1445 (1957)).

Translated by G. E. Brown
251

NUCLEON INTERACTION CROSS SECTIONS AT 9 Bev ENERGY

V. S. BARASHENKOV and HUANG NEN-NING

Joint Institute for Nuclear Research

Submitted to JETP editor January 3, 1959

J. Exptl. Theoret. Phys. (U.S.S.R.) **36**, 1319-1321 (April, 1959)

BOGACHEV et al.[1] obtained a value $\sigma \sim 40$ mbn for the total effective cross section of the NN interaction at E = 9 Bev. However, a more exact value of σ can be obtained by using the experimental value of the mean range of the proton in photoemulsion.

We consider first the mean range of a proton in an Ilford G-5* emulsion at E = 5.7 Bev.[2] The theoretical value of this range, calculated on the basis of the optical model, is in good agreement with the mean experimental value L = 37.6 cm, if the density distribution of the nucleons in the nucleus is taken from experiments on the scattering of fast electrons by nuclei,[3] and if a value $\overline{\sigma} \approx 32$ mbn is taken for the cross section of interaction between the incident nucleon and the nucleon in the nucleus, a value also in good agreement with the experimental value $\sigma = 31.3 \pm 1.5$ mbn at E = 6.15 Bev.[4] Detailed calculations made by us, on the basis of the optical model, for other cases,[5] also show that in the energy region E $\gtrsim$ 1 Bev good agreement can be obtained with experiment if the density of the distribution of the nucleons in the nuclei is obtained from experiments on the scattering of fast electrons by these nuclei. With accuracy to several percent, we have here $\overline{\sigma} = \sigma$, where σ is the interaction cross section of free nucleons.[6] Similar conclusions were reached by Elton and Bazhenov.[7]

It is natural to assume that these conclusion remain in force also at E = 9 Bev. The diagram shows the calculated values of the mean range $L(\sigma)$ of a proton in a NIKFI-R photoemulsion at $\overline{\sigma} = \sigma$ with E = 9 Bev.[1] Calculations show that this curve differs only by a few percent from the analogous curve for $L(\overline{\sigma})$, calculated for $\sigma = 30$ mbn.

The theoretical value of the range equals the experimental value L = 37.1 ± 1.0 cm (reference 1) if $\overline{\sigma} = \sigma = 30^{+1}_{-0.5}$ mbn. For a rougher value, L = 34.7 ± 1.5 cm (reference 8), we obtain from the figure a value $\overline{\sigma} = \sigma = 33^{+5}_{-3}$ mbn for the proton-nucleon cross sections. The values obtained for σ are close to the total cross

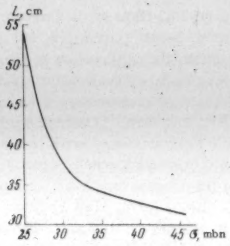

section for proton-proton interaction at E = 6.5 Bev.[4]

The calculated cross sections σ_{in} for the elements C, N, O, Br, and Ag at E = 9 Bev are respectively equal to 240, 260, 290, 900, and 1070 mbn (see references 1, 6, and 9 concerning the cross sections σ_{in} and σ_{el} for hydrogen).

Thus, the results obtained, together with the results of reference 9, show that the optical model can be successfully used to describe the interaction of elementary particle in the energy region E > 1 Bev.

We note that at E $\gtrsim$ 1 Bev the cross sections for the interaction between a nucleon and the nuclei become sensitive to the diffuseness of the nuclear boundary. In this case the principal contribution is made by interactions with impact parameters on the order of the nuclear radius. This uncovers new possibilities for an experimental investigation of the diffuseness of the nucleus.

We are grateful to P. Markov, K. Tolstoĭ, É. Tsyganov, and M. Shafranova for numerous evaluations of the photoemulsion experiments, and also to N. Bogachev for valuable comments.

*The calculations were based on the following photoemulsion composition (number of atoms N × 10^{-22} per cubic cm). N_H = 3.37, 2.93; N_C = 1.36, 1.39; N_N = 0.29, 0.37; N_O = 1.02, 1.06; N_{Br} = 1.02, 1.02, and N_{Ag} = 1.02, 1.02 for the Ilford G-5 and NIKFI-R emulsions, respectively.

[1] Bogachev, Bunyatov, Merekov, and Sidorov, Dokl. Akad. Nauk SSSR **121**, 617 (1958), Soviet Phys. "Doklady" **3**, 785 (1958).

[2] Cavaugh, Haskin, and Schein, Phys. Rev. **100**, 1263 (1955).

[3] R. Hofstadter, Ann. Rev. Nucl. Sci. **7**, 231 (1957).

[4] Cork, Wentzel, and Causey, Phys. Rev. **107**, 859 (1957).

[5] A. E. Brenner and R. W. Williams, Phys. Rev. **106**, 1020 (1957). T. Cook, Phys. Rev. **98**, 1369 (1955). W. O. Lock and P. V. March, Proc. Roy. Soc. **A230**, 215 (1955). L. W. Smith, Phys.

Rev. **92**, 851 (1953). Bowen, Di Corato, Moore, and Tagliaferri, Nuovo cimento **9**, 908 (1958).

[6] V. S. Barashenkov, Оптический анализ взаимодействия быстрых нуклонов с нуклонами и ядрами (материалы конференции в Ужгороде 2–6 октября 1958 г., в печати). [Optical Analysis of Interaction of Fast Nucleons with Nucleons and Nuclei (Proc. Conference in Uzhgorod, October 2–6, 1958)] (in press).

[7] L. R. B. Elton, Revs. Modern Phys. **30**, 557 (1958). R. B. Bazhenov, J. Exptl. Theoret. Phys. (U.S.S.R.) **34**, 775 (1958), Soviet Phys. JETP **7**, 534 (1958).

[8] Bogachev, Wang Shu-Fen, Gramenitskiĭ, et al. Атомная энергия (Atomic Energy) **3**, 281 (1958).

[9] B. S. Barashenkov and Huang Nen-Ning, J. Exptl. Theoret. Phys. (U.S.S.R.) **36**, 832 (1959), Soviet Phys. JETP 9, 587 (1959).

Translated by J. G. Adashko
252

BETA INTERACTION AND NUCLEON FORMFACTOR

V. B. BERESTETSKIĬ and I. Ya. POMERANCHUK

Submitted to JETP editor January 6, 1959

J. Exptl. Theoret. Phys. (U.S.S.R.) **36**, 1321-1322 (April, 1959)

ONE of the characteristic features of β-interaction is the rapid increase with energy of processes induced by it. However the existence of strong interactions leads to the acquisition of a formfactor by nucleons which may substantially change the energy dependence of β processes. The study of β transitions at high energies, for example the transformation of an electron into a neutrino

$$e + p \to n + \nu, \tag{1}$$

can be used for the measurement of this formfactor.

At the present time one may, apparently, consider as established[1,2] the fact that β interaction consists of the vector and axial-vector interactions. The general expression for the matrix element for the process (1) should have the following form:[3,4]

$$M = \frac{g}{\sqrt{2}} (\bar{u}_\nu \gamma_\mu (1+\gamma_5) u_e) \cdot$$
$$\times \left\{ \bar{u}_n \left[a\gamma_\mu + i\frac{b}{M} \hat{q}\gamma_\mu + \gamma_5 \left(c\gamma_\mu + \frac{id}{M} q_\mu \right) \right] u_p \right\}. \tag{2}$$

Here u_ν, u_e, u_n, u_p are the neutrino, electron, neutron, and proton amplitudes respectively; q is the electron-neutrino momentum difference; a, b, c and d are real functions of q^2 determining the vector (a, b) and axial vector (c, d) vertex functions of the nucleon. If the Gell-Mann and Feynmann hypothesis[1] is correct, then the vector β-interaction vertex function is identically the same as the electro-magnetic vertex function. Therefore the functions $a(q^2)$ and $b(q^2)$ may be determined from electron scattering experiments.[5]

The differential cross section for process (1) is

$$d\sigma = \frac{g^2}{(4\pi)^2} d\omega \frac{1}{\varepsilon^2 + M^2} \frac{1}{f} \left\{ (a^2 + c^2) \left(4f^4 - 2f^2 q^2 + \frac{q^4}{2} \right) \right.$$
$$- (a^2 - c^2) M^2 q^2 + (ac + 2bc)(q^4 - 4f^2 q^2)$$
$$\left. + b^2 \left(q^4 + \frac{4q^2 f^4}{M^2} - \frac{2f^2 q^4}{M^2} \right) + 2abq^4 \right\},$$
$$q^2 = \varepsilon^2 (1 - \cos\vartheta), \quad f^2 = \varepsilon^2 (1 + \sqrt{1 + M^2/\varepsilon^2}),$$

where M is the nucleon mass, ϵ and θ are the energy and scattering angles in the barycentric systems. We have assumed that the electron energy is high compared to the electron rest mass. In that case the last term in (2), containing the function $d(q^2)$, does not contribute to the cross section.

[1] R. P. Feyman and M. Gell-Mann, Phys. Rev. **109**, 193 (1958).

[2] E. C. G. Sudarshan, R. E. Marshak, Proc. of the Padua-Venice Conf. (1957); Phys. Rev. **109**, 1860 (1958).

[3] Akhiezer, Rozentsveĭg, and Shmushkevich, J. Exptl. Theoret. Phys. (U.S.S.R.) **33**, 765 (1957), Soviet Phys. JETP **6**, 588 (1958).

[4] M. Goldberger and S. Treiman, Phys. Rev. **110**, 1478 (1958).

[5] Hofstadter, Bumiller, and Yearian, Revs. Modern Phys. **30**, 482 (1958).

Translated by A. M. Bincer
253

GEODESICS IN FRIEDMAN-LOBACHEVSKY SPACE

I. G. FIKHTENGOL' TS

Leningrad Institute of Precision Mechanics and Optics

Submitted to JETP editor January 6, 1959

J. Exptl. Theoret. Phys. (U.S.S.R.) **36**, 1322-1323 (April, 1959)

We consider the equations for the geodesics in the space in which the square of the line element ds has the form

$$ds^2 = H^2\left(dx_0^2 - dx_1^2 - dx_2^2 - dx_3^2\right), \qquad (1)$$

where H is some function of the variables x_0 and $r = \sqrt{x_1^2 + x_2^2 + x_3^2}$.

Taking the time coordinate x_0 as the independent parameter, the equations for the geodesics are then written in the form (see, e.g., reference 1)

$$\ddot{x}_l - \dot{x}_l\Gamma^0_{\alpha\beta}\dot{x}_\alpha\dot{x}_\beta + \Gamma^l_{\alpha\beta}\dot{x}_\alpha\dot{x}_\beta = 0 \qquad (i = 1, 2, 3). \qquad (2)$$

Here $\Gamma^\nu_{\alpha\beta}$ is the Christoffel symbol of the second kind; the dot denotes the derivative with respect to the variable x_0; greek indices run through the values 0, 1, 2, 3, and identical indices are understood to be summed from 0 to 3.

Starting with formula (1), we obtain the following expressions for the Christoffel symbol of the second kind:

$$\Gamma^0_{00} = \frac{1}{H}\frac{\partial H}{\partial x_0}, \quad \Gamma^l_{00} = \Gamma^0_{0l} = \frac{1}{rH}\frac{\partial H}{\partial r}x_l, \quad \Gamma^l_{0k} = \Gamma^0_{ik} = \frac{1}{H}\frac{\partial H}{\partial x_0}\delta_{ik},$$
$$\Gamma^l_{ik} = \frac{1}{rH}\frac{\partial H}{\partial r}\left(x_i\delta_{kl} + x_k\delta_{il} - x_l\delta_{ik}\right). \qquad (3)$$

In these expressions $\delta_{ik} = 1$ for $i = k$, and $\delta_{ik} = 0$ for $i \neq k$; the Latin indices i, k, l run through the values 1, 2, 3.

With the expressions (3), the equations in (2) now take the form

$$\ddot{x}_l + \frac{1 - \dot{r}^2}{H}\left(\frac{1}{r}\frac{\partial H}{\partial r}\dot{x}_l + \frac{\partial H}{\partial x_0}\dot{x}_l\right) = 0. \qquad (4)$$

If we now set[1] $H = H(S)$, where $S = \sqrt{x_0^2 - r^2}$, then we finally obtain, according to (4),

$$\ddot{x}_l + \frac{\dot{r}^2 - 1}{S}\frac{H'}{H}\left(x_l - \dot{x}_l x_0\right) = 0, \qquad (5)$$

where the prime denotes the derivative with respect to the variable S.

It is seen immediately that the relations

$$x_l = \dot{x}_l x_0 \qquad (6)$$

yield $\dot{x}_l = \text{const}$; the functions x_l defined by them are therefore particular solutions of (5).

The relations (6) are used in a well-known way for the explanation of the phenomenon of the "recession of the galaxies," by regarding the quantities $\dot{x}_l$ as the coordinates of the corresponding mass in the accompanying system of coordinates.

[1] V. A. Fock, Теория пространства, времени и тяготения (The Theory of Space, Time, and Gravitation), GTTI, 1955.

Translated by R. Lipperheide
254

ON THE PRODUCTION OF PION AND MUON PAIRS BY THE ANNIHILATION OF HIGH-ENERGY POSITRONS

A. I. NIKISHOV

P. N. Lebedev Physics Institute, Academy of Sciences, U.S.S.R.

Submitted to JETP editor January 8, 1959

J. Exptl. Theoret. Phys. (U.S.S.R.) **36**, 1323-1324 (April, 1959)

The study of the processes $e^+ + e^- \rightleftarrows \mu^+ + \mu^-$ and $e^+ + e^- \rightleftarrows \pi^+ + \pi^-$ is of interest in connection with the possibility of detecting deviations from local theory at distances $\sim 10^{-13}$ cm. If we describe the deviation by a factor $F(q^2)$ in the expression for the transition current, we get the cross-sections for these processes from the corresponding expressions of local theory by simply multiplying by the squares of the form factors $F(q^2)$ for the particles in question. Since in the annihilation of two particles $q^2 = -4E^2$ (in the center-of-mass system), the introduction of the form factors does not change the angular distributions for these processes. The values of the form factors for $q^2 < 0$ (annihilation of particles) cannot be obtained from the values of $F(q^2)$ for $q^2 > 0$ (scattering).*

The absolute squares of the matrix elements in the center-of-mass system, averaged over the initial spin states and summed over the final (for those particles having spin), are as follows:†

$$|M|^2(e^+ + e^- \rightleftarrows \mu^+ + \mu^-) = \frac{1}{16E^4}\left\{1 + \left(\frac{\mu}{E}\right)^2 + \frac{p_\pi^2}{E^2}\cos^2\vartheta\right\},$$

$$|M|^2(e^+ + e^- \rightleftarrows \pi^+ + \pi^-) = \frac{p_\pi^2}{32E^4}\sin^2\vartheta.$$

We note that the matrix elements for the processes involving π mesons are small for nonrela-

tivistic values of the velocities v_π. The maximum of the angular distribution for this process lies in the plane perpendicular to the line of impact.

The corresponding differential cross-sections in the center-of-mass system are:

$$d\sigma(e^+ + e^- \to \mu^+ + \mu^-) = F_\mu^2 F_e^2 \frac{r_0^2}{16\gamma^2}\left\{1 + \left(\frac{\mu}{E}\right)^2 + \frac{p_\mu^2}{E^2}\cos^2\vartheta\right\} d\Omega,$$

$$d\sigma(e^+ + e^- \to \pi^+ + \pi^-) = F_\pi^2 F_e^2 \frac{r_0^2}{32\gamma^2}\frac{p_\pi^3}{E^3}\sin^2\vartheta\, d\Omega,$$

$$d\sigma(\mu^+ + \mu^- \to e^+ + e^-)$$

$$= F_\mu^2 F_e^2 \frac{r_0^2}{8\gamma^2}\frac{1}{v_{rel}}\left\{1 + \left(\frac{\mu}{E}\right)^2 + \frac{p_\mu^2}{E^2}\cos^2\vartheta\right\} d\Omega,$$

$$d\sigma(\pi^+ + \pi^- \to e^+ + e^-) = F_\pi^2 F_e^2 \frac{r_0^2}{\gamma^2}\frac{v_\pi}{32}\sin^2\vartheta d\Omega,$$

$r_0 = 2.8 \times 10^{-13}$ cm; $\gamma = E/m$; μ and m are the masses of meson and electron; E is the energy of a particle; $v_{rel} = 2v_\mu$ is the relative velocity of the mesons in the beam; v_π, p_π are the velocity and momentum of a π meson; ϑ is the angle between the colliding and emerging particles; $q^2 = -4E^2$; $\hbar = c = 1$.

In the limit v_π, $v_\mu \approx c$ we get for the cross sections integrated over the angles

$$\sigma(e^+ + e^- \to \mu^+ + \mu^-)/\sigma(e^+ + e^- \to \pi^+ + \pi^-) = 4F_\mu^2/F_\pi^2.$$

We note that the probability for decay of the bound system $\mu^+\mu^-$ into e^+e^- is given by

$$w = |\psi(0)|^2 (v_{rel}\sigma)_{v_{rel}=0} = 4 \cdot 10^{11}\ \text{sec}^{-1} \approx w_{\mu^+ + \mu^-} \to 2\gamma.$$

Because of the small velocities v_π the corresponding probability $w(\pi^+ + \pi^- \to e^+ + e^-)$ is vanishingly small.

If for an estimate we set $F = 1$ for all particles, the largest values of the total cross-sections are of the order $10^{-30} - 10^{-31}$ cm^2.

Finally we note that if in the process $\pi + N \to N + e^+ + e^-$ the angular characteristics of the pair do not differ strongly from those for the process $\pi^+ + \pi^- \to e^+ + e^-$, then it may be possible to distinguish it experimentally, in spite of the very large background of pairs from the decay $\pi^0 \to e^+ + e^- + \gamma$.

In conclusion I express my gratitude to I. Ya. Pomeranchuk, I. L. Rozental', and E. L. Feĭnberg for fruitful discussions.

*It is possible that this bears a relation to the fact that the average multiplicity of the mesons from the annihilation of antinucleons is somewhat larger than the value given by the statistical theory with $R = 1.4 \times 10^{-13}$ cm.[1]

†The production of meson pairs by the annihilation of positrons was first discussed by I. Ya. Pomeranchuk and V. B. Beresterskiĭ.[2] In their paper a factor 4 is omitted from the expression for $\sigma(e^+ + e^- \to \mu^+ + \mu^-)$.

[1] Belen'kiĭ, Maksimenko, Nikishov, and Rozental', Usp. Fiz. Nauk **62**, No. 2, 1 (1957).

[2] V. B. Berestetskiĭ and I. Ya. Pomeranchuk, J. Exptl. Theoret. Phys. **29**, 864 (1955), Soviet Phys. JETP **2**, 580 (1956).

Translated by W. H. Furry
255

ON PAIR PRODUCTION BY THE COLLISION OF TWO CIRCULARLY POLARIZED GAMMA-RAY QUANTA

F. S. SADYKHOV and B. K. KERIMOV

Moscow State University

Submitted to JETP editor January 10, 1959

J. Exptl. Theoret. Phys. (U.S.S.R.) **36**, 1324-1326 (April, 1959)

THE present note presents the results of a calculation of the electron-positron pair production in the collision of two circularly polarized γ-ray quanta, with account taken of the longitudinal polarization of the pair particles. An examination of this problem is of definite interest, since beams of γ-rays of high energy are now available ($E_\gamma \sim 0.5 - 1$ Bev).[1,2] The circularly polarized γ-rays are produced in the deceleration radiation of longitudinally polarized high-energy electrons,[3] and also in nuclear β-decay processes.[4]

The equation that describes the process $\gamma + \gamma' \to e^- + e^+$ is of the form

$$D\psi_2 = \{U(\varkappa) D^{-1} U(\varkappa') + U(\varkappa') D^{-1} U(\varkappa)\}\psi_0, \qquad (1)$$

where ψ_0 is the wave function of the initial state and ψ_2 that of the final state, D is the Dirac operator, and $U(\varkappa)$ and $U(\varkappa')$ are the operators for the interaction of electrons with the quanta having the momenta $\hbar\varkappa$ and $\hbar\varkappa'$. The polarization vectors $\mathbf{a}_l \equiv \mathbf{a}_l(\varkappa)$ and $\mathbf{a}'_{l'} \equiv \mathbf{a}_{l'}(\varkappa')$ of the quanta are taken in the form[5,6]

$$a_l = (\beta + il[\varkappa^0\beta])/\sqrt{2}, \quad a_{l'} = (\beta + il'[\varkappa'^0\beta])/\sqrt{2}. \qquad (2)$$

Here β is a unit vector perpendicular to the momenta of the γ-ray quanta, $\varkappa^0 = \varkappa/\varkappa$, and $\varkappa'^0 = \varkappa'/\varkappa'$. In the case $l = l' = 1$ we have quanta with right-handed polarization (the spins of the quanta are in the direction of motion), and for $l = l' = -1$ we have left-handed polarization (spin opposite to motion). Using Eqs. (21) and (15) of reference 5 for the total cross sections for electron-positron

pair production, with inclusion of the spin states of the particles, we find

$$\sigma = (\pi/8)(e^2/\hbar c)^2 \{(1 + s_-s_+)(1 + ll')F_1 + (1 - s_-s_+)(1 - ll')F_2 - (1 + s_-s_+)F_3 + s_-s_+(1 - ll')F_4 + (s_- + s_+)(l + l')F_5\}, \quad (3)$$

where

$$F_1 = 2k/K^3 + {}^1/_2(k^2/K^4 - 1/K^2)q,$$

$$F_2 = -k/K^3 + {}^1/_2(1/K^2 + k^2/K^4)q,$$

$$F_3 = k(3k_0^2 + 2k^2)/K^5 + (k^4/2K^6 + k^2/K^4 - 3/2K^2)q,$$

$$F_4 = (3k_0^2 + 2k^2)/kK^3 + (k^2/2K^4 + 1/K^2 - 3/2k^2)q,$$

$$F_5 = k^2/K^4 + qkk_0^2/2K^5,$$

$$q = \ln(K + k)/(K - k), \quad K = \sqrt{k^2 + k_0^2}.$$

Here $p_- = p_+ = \hbar k$ is the momentum of the electron (positron); $k_0 = m_0c/\hbar$ corresponds to the rest mass of the electron; $s_\pm = \pm 1$, with $s_- = 1$ (or $s_+ = 1$) for the state of the electron (or positron) with right-handed polarization, and $s_- = -1$ (or $s_+ = -1$) for the state of left-handed polarization.

From Eq. (3) it follows that: 1) in the collision of two right-handed ($l = l' = 1$) or two left-handed ($l = l' = -1$) quanta there can be production of an electron and positron with right-handed ($s_- = s_+ = 1$) or with left-handed ($s_- = s_+ = -1$) longitudinal polarization, the probabilities being different for the two polarizations. In such collisions, however, there cannot be production of an electron with right-handed ($s_- = 1$) and a positron with left-handed ($s_+ = -1$) polarization, or vice versa ($s_- = -1$, $s_+ = 1$), since the cross-section σ for this is zero. 2) In the collision of two quanta, one with right-handed ($l = 1$) and the other with left-handed ($l = -1$) polarization (or vice versa, $l = -1$, $l' = 1$) there can be production of: a) an electron and positron with right-handed ($s_- = s_+ = 1$) or with left-handed ($s_- = s_+ = -1$) polarization, the probabilities for the two results being equal; or b) an electron with right-handed ($s_- = 1$) and a positron with left-handed ($s_+ = -1$) polarization, or vice versa ($s_- = -1$, $s_+ = 1$), with equal probabilities.

In the ultrarelativistic case (κ and $k \gg K_0$) the expression (3) goes over into the following:

$$\sigma = \frac{\pi}{4}\left(\frac{e^2}{\hbar c}\right)^2 \frac{1}{k^2}\left\{(1 + s_-s_+)ll' + (1 - ll')\left[s_-s_+ - (1 - s_-s_+)\left(\frac{1}{2} - \ln\frac{2k}{k_0}\right)\right] + \frac{1}{2}(s_- + s_+)(l + l')\right\}. \quad (4)$$

The analysis given above can also be carried through for Eq. (4).

By averaging Eq. (3) over the polarizations of the quanta and summing over the spin states of the electron and positron, we get the cross-section for pair production by the collision of two unpolarized quanta:

$$\sigma_0 = \frac{\pi}{2}\left(\frac{e^2}{\hbar c}\right)^2 \times \left\{\frac{k}{K^3} - \frac{k(2k^2 + 3k_0^2)}{K^5} + \left(\frac{3}{2K^2} - \frac{k^4}{2K^6}\right)\ln\frac{K + k}{K - k}\right\}. \quad (5)$$

In conclusion we express our gratitude to Professor A. A. Sokolov for his constant interest in this work and for valuable comments.

[1] De Wire, Jackson, and Littauer, Phys. Rev. **110**, 1208 (1958).

[2] P. C. Stein and K. C. Rogers, Phys. Rev. **100**, 1209 (1958).

[3] Goldhaber, Grodzins, and Sunyar, Phys. Rev. **109**, 1015 (1958).

[4] H. Schopper, Phil. Mag. **2**, 710 (1957).

[5] A. A. Sokolov and D. D. Ivanenko, Квантовая теория поля, (The Quantum Theory of Fields), Part 1, GITTL 1952.

[6] B. K. Kerimov and I. M. Nadzhafov, Izv. Akad. Nauk SSSR, Ser. Fiz. **22**, 886 (1958), Columbia Tech. Transl., p. 879.

Translated by W. H. Furry
256

ON THE MECHANISM OF THE LEPTONIC DECAY OF HYPERONS

V. V. TUROVTSEV

Institute of Nuclear Physics, Moscow State University

Submitted to JETP editor January 13, 1959

J. Exptl. Theoret. Phys. (U.S.S.R.) **36**, 1326-1327 (April, 1959)

THE best confirmation of the universal V-A interaction[1] is now coming from nuclear β-decay experiments and from the study of the branching ratios for the different decay modes of the π meson.[2] This interaction also explains to a certain degree the equality of the probabilities for the K_{e3} and $K_{\mu 3}$ decays and the absence of the K_{e2} decay.[3] However, in the calculation of the leptonic decay rates of the Σ^- and Λ^0 hyperons,[4] (which, admittedly, were obtained without account of the form factor and the renormalization constant), the V-A interaction leads to values for these

rates which are too high in comparison with the upper limits set by experiment. Taking account of the form factor with an accuracy including the first two terms in its expansion in powers of $(p/M)^2$ lowers the rate of, e.g., the $\Sigma^- \to p + e + \nu$ decay by a factor of 2.5 (reference 5). In the leptonic decays of the hyperons, therefore, either the unknown form factor plays an important role, or the decay mechanism is different from the four-fermion V-A interaction.

In the present note we consider the decay of a hyperon at rest into leptons via a virtual K meson whose spin is assumed to be zero (this should lead to a lower decay rate than that obtained with the local four-fermion interaction). We calculate the ratio, R, of the energy spectrum of the nucleons for the $Y \to n + \mu + \nu$ decay (a) and the corresponding spectrum for the $Y \to n + e + \nu$ decay (b). The experimental determination of R for the purpose of identifying the decay mechanism is, of course, much more difficult than the determination of the ratio of the decay rates. On the other hand, neither the absolute values of rates of the decays (a) and (b), nor their ratio can be computed exactly.

Without recourse to perturbation theory, we can write the matrix element for the decay process in the form

$$M = f(\varepsilon)(\bar{u}_n G \Gamma u_\gamma)(\bar{u}_\mu \Gamma (g + g'\gamma_5) u_\nu) \qquad (1)$$

(the indices specifying the parity of the K meson are omitted), where Γ is either 1 or γ_5, and $f(\epsilon)$ is some unknown function of the nucleon energy, which also depends on G and the masses M_Y, M_n, M_K, m_π, but not on either m_e or m_μ; G and g, g' are the strong and weak coupling constants, where $gfG \to g_S$ (or g_P) for $M_K \to \infty$. These expressions for M correspond to the S and P variants of the theory of the four-fermion interaction. According to (1), we obtain for the energy dependent (i.e., the nucleon energy) decay rate

$$dW/d\varepsilon = \text{const} \cdot |f|^2 \sqrt{\varepsilon^2 - 1}$$
$$(\varepsilon_{max} - \varepsilon)^2 (\varepsilon \pm 1)/(1 + M_Y^2 - 2M_Y\varepsilon), \qquad (2)$$

$\epsilon_{max} = (M_Y^2 - m^2 + 1)/2M_Y$ is the maximal energy of the nucleon in units of $M_n c^2$. The signs ± refer to a scalar and pseudoscalar virtual meson, respectively. It is seen from (2) that the ratio R is independent of the parity of the meson and of the factor f. It is connected with the analogous ratio F, obtained from the V-A variant without account of the energy form factor and the renormalization constant, in the following way:

$$F = R\left[m_\mu^2 + M_Y\left(1 - \frac{M_Y(\varepsilon^2-1)}{3(M_Y-\varepsilon)(M_Y\varepsilon-1)}\right)\right]$$
$$\times \left[m_e^2 + M_Y\left(1 - \frac{M_Y(\varepsilon^2-1)}{3(M_Y-\varepsilon)(M_Y\varepsilon-1)}\right)\right]^{-1} \equiv RH(\varepsilon), \qquad (3)$$

ϵ^μ_{max} and ϵ^e_{max} are the maximal energies of the leptons for the decays (a) and (b), respectively. We note that the factor $H(\epsilon)$, which determines the deviation of R from F near the upper limit of the energy spectrum of the nucleons, reaches the values ~2.5, ~2.0, and ~2.6 for the leptonic decays of the Λ^0, Σ^-, and Ξ^- hyperons, and is close to unity at the beginning of the spectrum.

In conclusion I thank I. S. Shapiro for suggesting the topic of the present note and for interest in this work.

[1] R. P. Feynman and M. Gell-Mann, Phys. Rev. **109**, 193 (1958). E. C. G. Sudarshan and R. E. Marshak, Phys. Rev. **109**, 1890 (1958).

[2] Fazzini, Fidecaro, Merrison, Paul, and Tollestrup, Phys. Rev. Lett. **1**, 247 (1958). Impeduglia, Plano, Prodell, Samios, Schwartz, and Steinberger, Phys. Rev. Lett. **1**, 249 (1958).

[3] I. Yu. Kobzarev and I. E. Tamm, J. Exptl. Theoret. Phys. (U.S.S.R.) **34**, 899 (1958); Soviet Phys. JETP **7**, 622 (1958).

[4] V. M. Shekhter, J. Exptl. Theoret. Phys. (U.S.S.R.) **35**, 458 (1958); Soviet Phys. JETP **8**, 316 (1959).

[5] A. Sirlin, Phys. Rev. **111**, 337 (1958).

Translated by R. Lipperheide
257

ASYMMETRY OF ANGULAR DISTRIBUTION OF $\mu^+ \to e^+$ DECAY ELECTRONS IN A 27,000 GAUSS MAGNETIC FIELD

C. A. ALI-ZADE, I. I. GUREVICH, Yu. P. DOBRETSOV, B. A. NIKOL'SKIĬ, and L. V. SURKOVA

Submitted to JETP editor February 1, 1959

J. Exptl. Theoret. Phys. (U.S.S.R.) **36**, 1327-1329 (April, 1959)

IT is known that the angular distribution of $\mu \to e$ decay electrons is given by

$$4\pi dN/d\omega = 1 - a\cos\theta, \quad a = \lambda P/3 = a_0 P, \qquad (1)$$

where $\lambda = 3a_0 = -\cos(V, A)$ determines the rela-

tive contribution of the vector and pseudovector interactions in the $\mu \to e$ decay; P is the μ-meson polarization. The maximum possible value of the coefficient a, namely $\frac{1}{3}$, corresponds to cos (V, A) = −1 (V-A interaction). The different values of a (0 − 0.26) obtained with the aid of electronic apparatus are explained by the depolarizing action of the medium in which the μ meson is slowed down and then decays. Such a determination of the coefficient a has that shortcoming, that not all the $\mu \to e$ decay electrons are registered with equal efficiency. Experiments on the observation of $\pi \to \mu \to e$ decays in photoemulsion permits registration of electrons of any energy with equal efficiency. However, the photoemulsion is a strongly depolarizing medium. The value of the coefficient a for the NIKFI type R emulsion was found[1] to be $a = 0.092 \pm 0.018$, while the average value of a for the Ilford G-5 emulsion can, according to data of many investigations, be assumed to be[2] equal to 0.14.

Swanson[3] combined the results obtained by electronic means for various substances (including emulsion) with the results of the measurement of the asymmetry of $\mu \to e$ decay in emulsion and in propane, and found for graphite values reaching $a = 0.303 \pm 0.048$, i.e., reaching almost the maximum value.

The depolarizing action of the medium decreases in the observation of μ-meson decay in a magnetic field having the same direction as the μ-meson polarization. When observing $\mu \to e$ decay in a longitudinal magnetic field, the increase in the coefficient a due to this effect can be found from the following formula:[4]

$$a = a_0\left[1 - \frac{0.5}{1 + (\mu H / \Delta E)^2}\right], \qquad (2)$$

where a_0 is the value of a in the absence of depolarization and ΔE is the energy of the hyperfine splitting of the μ-mesic atom in the 1S state. It follows from Eq. (2) that in practice a becomes equal to a_0 at fields $H \geq 8000$ Gauss. Equation (2) is not sufficiently reliable, for it does not take into account the electron exchange between the μ-mesic atom and the medium after production of the μ meson. Experiments aimed at verifying Eq. (2) where performed by several workers[4-6] for fields up to 14,000 Gauss, and it was shown that qualitatively a(H) behaves like Eq. (2) in the case of many substances used to slow down μ mesons, including photoemulsion.

In the present investigation we determined the value of the coefficient a in Eq. (1) by observing the $\pi \to \mu \to e$ decay in an emulsion placed in a magnetic field with H = 27,000 Gauss. In scanning we selected the $\pi \to \mu \to e$ decay events in which the μ meson was emitted at an angle $\theta_\mu = 0 - 30°$ or $\theta_\mu = 180 - 150°$ with the direction of the field. A total of 11,166 such $\pi \to \mu \to e$ decay events was observed.

Particular attention was paid in the scanning to elimination of systematic errors due to the unequal efficiency of registering different $\pi \to \mu \to e$ decay events. Only such $\pi \to \mu \to e$ decay events were considered, in which the end of the μ meson was not closer than 15 μ to the surface of the developed emulsion layer. In only 47 events (0.42% of all the $\mu \to e$ decay events) was no $\mu \to e$ decay electron observed.

We measured the angle of emission of the $\mu \to e$ decay electron relative to the direction of the magnetic field. The electron-emission angle was measured from the direction of the magnetic field if the μ meson traveled "along the field" ($\theta_\mu = 0 - 30°$) and from the opposite direction when the travel was "against the field" ($\theta_\mu = 180 - 150°$). The value of a was determined from the relation

$$a = 2(N_{back} - N_{forward})/(N_{back} + N_{forward}),\ \delta a = 2/\sqrt{N}.$$

The corresponding values of the coefficient a were found to be

$a_1 = 0.315 \pm 0.026$ for the case $\theta_\mu = 0—30°$;
$a_2 = 0.295 \pm 0.027$ for the case $\theta_\mu = 150—180°$.

The total value of a, averaged over both direction of emission of the μ meson, was found to be $a_3 = 0.305 \pm 0.019$.

The value of a in Eq. (1) exceeds somewhat the values of a_1, a_2, or a_3, owing to the depolarization of the muons by precession of the muon spin about the direction of the field H. Obviously $a_{true} = a_3\sqrt{\cos\theta_\mu}$. For the selected $\pi \to \mu$ decay events we found $\cos\theta_\mu = 0.940$, hence $a_{true} = a_3/0.940 = 0.324 \pm 0.020$.

It follows from this value that $|\lambda|\, P = 0.972 \pm 0.06$, i.e., with accuracy to within the statistical error (6%), $|\lambda|$ reaches its maximum value, and consequently $P \approx 1$. A determination of the sign of λ, i.e., the choice between the V − A and V + A variants of interaction, is impossible because the direction of the μ-meson polarization is unknown. The value obtained for $|\lambda|$ agrees with the Feynman-Gell Mann theory[7] of universal (V-A) interaction.

A strong magnetic field eliminates the polarization completely. Equation (2), which gives a = f(H), is quite inaccurate. Work continues on improving the obtained value of a and on

measuring a in photoemulsions placed in various magnetic fields.

An analogous result, $a \approx 1/3$ was obtained by Vaĭsenberg et al. and Lynch et al.[2,8] for emulsions placed in strong magnetic fields.

In conclusions, the authors express their gratitude to B. S. Neganov and B. V. Sokolov for aid in the irradiation of the photoemulsions, to D. M. Samoĭlovich for developing the emulsion, and also to V. M. Kutukova, A. M. Alpers, and G. V. Pleshivtseva for help with the work.

[1] Gurevich, Kutukova, Mishakova, Nikol'skiĭ, and Surkova, J. Exptl. Theoret. Phys. (U.S.S.R.) **34**, 280 (1958), Soviet Phys. JETP **7**, 195 (1958).

[2] Vaĭsenberg, Rabin, and Smirnitskiĭ, J. Exptl. Theoret. Phys. (U.S.S.R.) **36**, 1680 (1959), Soviet Phys. JETP **9**, in press.

[3] R. A. Swanson, Phys. Rev. in press (preprint).

[4] Orear, Harris, and Bierman, Phys. Rev. **107**, 323 (1957).

[5] Sens, Swanson, Telegdi, and Iovanovitch, Phys. Rev. **107**, 1465 (1957).

[6] Barkas, Giles, and Heckman, Phys. Rev. **107**, 911 (1957).

[7] R. P. Feynman and M. Gell-Mann, Phys. Rev. **109**, 193 (1958); E. S. Sudarshan and R. E. Marshak, Phys. Rev. **109**, 1860 (1958).

[8] Lynch, Orear, and Rosendorff, Phys. Rev. Lett. **1**, 471 (1958).

Translated by J. G. Adashko
258

BROADENING OF SPECTRAL LINES IN STRONGLY IONIZED PLASMA

M. A. MAZING and S. L. MANDEL'SHTAM

Lebedev Physical Institute, Academy of Sciences, U.S.S.R.

Submitted to JETP editor February 12, 1959

J. Exptl. Theoret. Phys. (U.S.S.R.) **36**, 1329-1331 (April, 1959)

MEASUREMENTS of the width of spectral lines are often used to determine the density of charged particles in a plasma; at the same time, the investigation of line broadening in a plasma is by itself an interesting physical problem, since under plasma conditions the emitting atoms are subjected to extremely strong rapidly-changing inhomogeneous fields of the surrounding particles, fields which cannot be achieved by other means. Until recently, only the line widths were usually studied; considerably greater information can be obtained if the line widths are measured simultaneously with the line shifts.

The results of our preliminary measurements of line widths and shifts in the plasma of a spark discharge[1] show a drastic qualitative disagreement with the existing Weisskopf-Lindholm theory, according to which the ratio of width to shift must have for all lines a constant value 1,6 and must depend on Stark's constant C_4 as $C_4^{2/3}$ (C_4 determines the line shift in a constant electric field, $\Delta\nu = F^2C_4/e^2$, where e is the charge of the electron, $\Delta\nu$ is expressed in cm^{-1}, and F is in electrostatic cgs units). On the basis of these measurements, a new non-stationary theory of line broadening due to charged particles has been developed by Vaĭnshteĭn and Sobel'man,[2] according to which the broadening and shift substantially depend on the parameter $\beta \simeq (Z\mu/m)(\Delta E/kT) \times (S/3ga_0^2)^{1/2}$. Here Z is the charge, μ is the mass of the perturbing particle, m is the mass of the electron, ΔE is the separation between the level under consideration E_1 and the nearest excited level E_2 (only one excited level is assumed to exist), and S is the oscillator strength of the line corresponding to the transition between the levels E_1 and E_2. The ratio of the width to the shift also depends on β and is not the same for all lines.

We have measured, with a considerably improved accuracy the widths and shifts of 50 lines of A II and several lines of He I in the plasma of the spark discharge in argon and helium (U = 14 kv, C = 0.02 μf, L = 10 μh) at temperatures of $3 \times 10^4 - 4 \times 10^4$ °K and an electron density of $\sim 10^{17}$ cm^{-3}. Spectra were photographed by means of a spectrograph with a dispersion of 2 A/mm. The line widths γ were measured in the usual manner, the line shifts Δ in the spectrum of the spark were measured relative to the same lines in the discharge spectrum of a hollow cathode, where the lines could be considered unshifted. The accuracy of the width measurements was 5 to 10%, the smallest definitely detectable shift was ≈ 0.03 A.

The results of measurements have confirmed the preliminary conclusions. In the accompanying table we give data for 6 lines of A II; they are typical for the rest of the lines measured. The constants C_4 are calculated from the measurements of Minnhagen[3] and Maissel[4] in a homogeneous field. The ratio γ/Δ varies from 2 to

λ, A	10^{-11} γ, sec^{-1}	10^{-11} Δ, sec^{-1}	γ/Δ	$10^4 C_4$, $cm^4 \cdot sec^{-1}$	ΔE, cm^{-1}	β
4579.4	5.1	0.45	11.5	0.5	10000	0.31
4460.4	3.8	0.66	5.8	0.5	8000	0.22
4598.8	8.4	2.7	3.1	7.8	122	$2.6 \cdot 10^{-2}$
3561.0*	12	5.0	2.4	9.2	100	$2.2 \cdot 10^{-2}$
3559.5*	13	5.6	2.3	2.0	40.5	$8.5 \cdot 10^{-4}$
4474.8	15	7.8	1.9	5.5	13.5	$2.6 \cdot 10^{-4}$

*ΔE has been calculated for these lines.

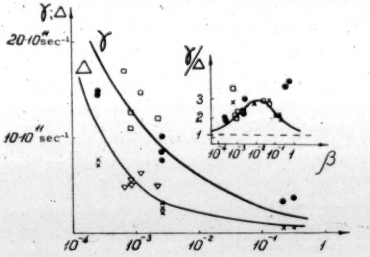

Dependence of the width γ and the shift Δ on β. The curves give theoretical results; • and × are experimental γ and Δ for the lines with known ΔE; □ and ▽ are experimental γ and Δ for the lines with calculated ΔE. The insert gives the dependence of the ratio γ/Δ on β. The dashed line represents the results of the stationary theory; the solid curve represents the results of the non-stationary theory; • and □ are for the lines of A II; ○ are authors' measurements for the lines of He I; × are for the lines of He I after Wulff.[5]

10, and the width changes only by a factor of 3 or 4 when C_4 changes by two orders of magnitude.

The accompanying figure gives a comparison of experimental results with the results of the non-stationary theory. In our case the data necessary for the calculation of β (ΔE and S) are available for only 7 lines. For the remaining lines, in view of the incomplete term level diagram of A II, the values for ΔE are unknown. We have estimated these quantities by using the data on the shift in a homogeneous field,[4] assuming that the oscillator strengths are approximately the same for all lines. In the upper picture (dependence of γ/Δ on β) we have also plotted Wulff's[5] data for He I lines, for which we have calculated the β values (ΔE and S are known).

As can be seen from the figure, the agreement of the experiment with the non-stationary theory is quite good. It should, however, be noted that for several lines the experimental values γ/Δ ≈ 10 considerably exceed the theoretical values; in a number of cases this can be apparently explained by the existence of two or more excited levels.

By way of a practical conclusion it may be mentioned that it is advantageous to use line shifts for determining the electron density, since additional data on second-order collision cross sections are required for the calculations from the widths. Corresponding measurements for the plasma which we have investigated gave $n_e \approx 1.5 \times 10^{17}$ cm^{-3} for argon and $n_e \approx 7 \times 10^{16}$ cm^{-3} for helium in good agreement with the estimates obtained on the basis of line intensities of A II and A III with the aid of Saha's formula.

In concluding, we should like to remark that previously we used γ/Δ = 1.6 for the lines of Ca I in the plasma of an arc.[6] For the investigated lines the non-stationary theory gives only minor corrections, and the conclusions of this investigation remain valid.

[1] Vaĭnshteĭn, Koloshnikov, Mazing, Mandel'shtam, and Sobel'man, Izv. Akad. Nauk SSSR, Ser. Fiz. **22**, 718 (1958) [Columbia Tech. Transl., in press]; Mazing, Mandel'shtam, and Koloshnikov, Сб. памяти акад. Г. С. Ландсберга (Anthology in Memory of Academician G. S. Landsberg), 1959 (in press).

[2] L. A. Vaĭnshteĭn and I. I. Sobel'man, Оптика и спектроскопия (Optics and Spectroscopy) **6**, No. 4 (1959).

[3] L. Minnhagen, Arkiv Mat. Astr. Fys. **A35**, 16 (1958).

[4] L. Maissel, J. Opt. Soc. Am. **48**, 835 (1958).

[5] H. Wulff, Z. Physik **150**, 614 (1958).

[6] M. A. Mazing and S. L. Mandel'shtam, Оптика и спектроскопия (Optics and Spectroscopy) **2**, 276 (1957).

Translated by O. Jefimenko
259

ELECTRONIC PARAMAGNETIC RESONANCE SPECTRA OF FROZEN OH RADICALS

S. D. KAĬTMAZOV and A. M. PROKHOROV

P. N. Lebedev Physics Institute, Academy of Sciences, U.S.S.R.

Submitted to JETP editor February 12, 1959

J. Exptl. Theoret. Phys. (U.S.S.R.) **36**, 1331-1332 (April, 1959)

THE observation of an electronic paramagnetic resonance spectrum of radicals obtained by freezing the electric discharge products in H_2O or H_2O_2 vapor, was reported previously.[1,2] Subsequent investigation of these radicals* did not permit identification of the radicals obtained from the discharge.

To determine these radicals, we decided to investigate in detail the spectrum of the radicals obtained by ultraviolet irradiation of frozen H_2O_2 and to compare these spectra. We assume that the radicals obtained by ultraviolet† irradiation of frozen H_2O_2 ($T = 77°K$) are OH radicals, since the spectrum of the mercury arc lamp employed by us (SVDSh-1000) contains no quanta capable of breaking the O—H bond (110 Kcal/mole). Since the spectrum of the radicals does not depend on the peroxide concentration in 5 to 98% aqueous solutions, it is assumed that there are no secondary reaction.

We observed the electronic paramagnetic resonance spectra at 12,000, 9400, 2600, 1300, and 850 Mcs. At all these frequencies, the spectrum of the OH radicals coincided with the spectrum of the radicals obtained from the discharge. Consequently, the radical obtained by freezing the discharge products in H_2O and H_2O_2 vapor is essentially the OH radical.

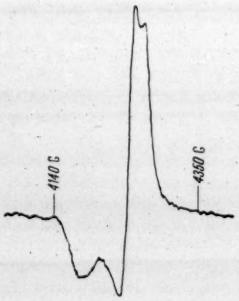

At 850 Mcs there is a clearly pronounced doublets with a distance of 12 ± 1 Gauss between components, produced by the nuclear moment of the hydrogen proton.

At 12,000 Mcs the shape of the spectrum is determined essentially by the anisotropic broadening ($g_\perp \neq g_\parallel$). The derivative absorption line for 12,000 Mcs is shown in the figure. The shape of the observed line is readily explained by the presence of anisotropic broadening and the presence of hyperfine splitting. From this curve, we estimate that $g_\perp \approx 2.00$ and $g_\parallel \approx 2.03$.

*The investigation was made by us in collaboration with A. B. Tsentsiper, and the results will be published.

†Ingram[3] also observed the electronic-magnetic resonance spectrum of the radical obtained by ultraviolet irradiation of the peroxide at 9400 Mcs.

[1] Kaĭtmazov, Prokhorov, Tsentsiper, and Gorbonev, Журнал физической химии (J. of Phys. Chem.) **31**, 515 (1957).

[2] Livingston, Ghormley, and Zeldes, Chem. Phys. **24**, 483 (1956).

[3] G. J. E. Ingram, Nature **176**, 1227 (1955).

Translated by J. G. Adashko
260

ON ELECTRON OSCILLATIONS IN A PLASMA

A. A. ZAĬTSEV, G. S. LEONOV, and I. A. SAVCHENKO

Moscow State University

Submitted to JETP editor February 19, 1959

J. Exptl. Theoret. Phys. (U.S.S.R.) **36**, 1332-1334 (April, 1959)

THE oscillations of the electrons in a plasma have been observed in numerous experiments, although many details of these oscillations remain obscure. Experiments with a plasma and a beam, independent of the plasma, have been described in a number of papers. To some degree there is a contradiction between the different results obtained. According to Looney and Brown,[1] regular oscillations are impossible without the formation of standing waves, while the paper by Kojima et al.[2] confirms Bohm and Gross' theory.[3]

In the present research oscillations were observed in inert gases. We could change the pres-

sure from 3×10^{-1} to 5×10^{-4} mm Hg. The oscillations were detected by a superheterodyne system with a separate decimeter range generator and a separate amplifier of an intermediate frequency, the frequency and passband of which were 30 and 10 Mcs, respectively. The amplifier could be varied within wide limits,

It turned out that the upper limit of the pressure for which regular oscillations could still be observed was different for different gases. We established that this limit was for He about 2×10^{-1}, for A about 10^{-2}, and for Xe about 6×10^{-3} mm Hg. The total effective cross sections for the interaction of the atoms with the primary electrons, taken for the above mentioned gases and pressures and taking the velocity of the electrons in the beam into account, were approximately equal (they differed by less than 25%).

A very important problem from the point of view of elucidating the mechanism of exciting the oscillations is that of the distribution of the oscillations along the axis of the discharge. The results obtained in this direction up to now are not free from distortions produced by the probe.[4] The elimination of the influence of the probe should therefore give a truer picture.

The distribution of the oscillations was studied in a cylindrical tube of diameter 7 cm, a distance of 2.2 cm between the cathodes, and a pressed powder cathode with a 3 mm diameter. A cylindrical probe of 0.1 mm diameter could be moved along the axis of the tube to any position between the cathode and anode, and its position was noted after every 0.5 or 1 mm by a reading microscope with an accuracy of 0.2 mm. When the probe moved into the beam itself, the perturbation of the beam by the probe was observed, and the measurement was thus performed under such conditions that the probe only touched the beam and that there is no noticeable influence, whatever on the beam. This was attained by turning the edge, on which the cathode was mounted slightly asymmetrically, round.

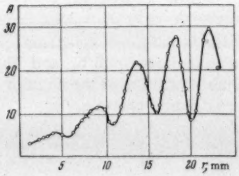

In the figure we have given a picture of an intensity distribution of the oscillations which is typical for pressures when the mean free path of the primary electrons is larger than the distance between the electrodes (the intensity of the oscillations A in arbitrary units is given along the ordinate axis, and the distance r of the probe from the cathode in mm along the abscissa axis). It is clear that the measurement of the intensity along the axis of the discharge is detected by the detector in the form of a periodic function, the zero value of which increases in the direction towards the anode. The intensity of the oscillations and the coefficient of its increase increase with decreasing pressure. The intensity of the oscillations could be varied along the beam by more than a factor of one thousand in order to determine the conditions in the discharge. For sufficiently high pressures, when the mean free path of the electrons was less than the distance between the electrodes, the oscillations were damped in the direction towards the anode, and only one maximum could be observed.

The measurements showed that the spatial period can be well approximated by the formula $l = 2\pi v_0/\omega$, where v_0 is the velocity of the electrons in the beam in cm sec^{-1} and ω the cirular frequency of the observed oscillations; the deviation of the measured period from the one calculated from the formula is always in the lower direction and was less than 10 — 25%. Visually we could not observe any periodic inhomogeneity along the beam in the discharge glow. The discharge was often characterized by well distinguished inhomogeneities, caused by the non-uniform emission from the pressed powder cathode, along the cross section of the beam.

In the region where sufficenly strong oscillations start the anomalous scattering of the primary bean was observed visually. This scattering could occur both before and after the narrowing of the beam produced by the focusing action of the positive space charge. When the anomalous scattering took place before the narrowing, we clearly distinguished smaller beams in the primary beam against the general background different. When the scattering occurred after the narrowing, the beam was nearly uniform. In the first case, the convergence of the beams stopped at the position of the scattering so that no nodes could form; in the second case, there was in general not observed any tendency to form later nodes.

[1] D. H. Looney and S. C. Brown, Phys. Rev. **93**, 965 (1954).

[2] Kojima, Kato, and Hagiwura, J. Phys. Soc. Japan **12**, 1276 (1957).

[3] D. Bohm and E. P. Gross, Phys. Rev. **75**, 1851 (1949).

[4] R. A. Bailey and K. G. Emeleus, Proc. Roy. Irish Acad. **A57**, 53 (1955).

Translated by D. ter Haar
261

POSSIBILITY OF DETERMINING THE CHIRALITY OF THE MUON BY MEANS OF δ-ELECTRON CASCADES FROM MAGNETIZED IRON

A. I. ALIKHANOV and V. A. LYUBIMOV

Institute of Theoretical and Experimental Physics, Academy of Sciences, U.S.S.R.

Submitted to JETP editor February 21, 1959

J. Exptl. Theoret. Phys. (U.S.S.R.) **36**, 1334-1335 (April, 1959)

IT is known that the violation of spatial parity in weak interaction causes the muons produced by pion (or $K_{\mu 2}$-meson) decay to be polarized. However, the direction of muon polarization has not been experimentally determined to date. We propose here a method for measuring both the direction and magnitude of muon polarization, and consider possible experiments with accelerators and cosmic rays to solve this problem.

Berestetskiĭ (private communication) derived a formula for the cross section for the scattering of a polarized muon by polarized electrons

$$\sigma d\varepsilon = \sigma_0 d\varepsilon + \mathbf{P}_e \mathbf{P}_\mu \sigma_1 d\varepsilon$$

$$= 2\pi r_0^2 \frac{mdz}{\beta^2 \varepsilon^2}\left[1 - \beta^2 \frac{\varepsilon}{\varepsilon_m} + \frac{1}{2}\frac{\varepsilon^2}{E^2} - \mathbf{P}_e \mathbf{P}_\mu \frac{\varepsilon}{E}\left(1 - \frac{\varepsilon}{\varepsilon_m} + \frac{\varepsilon}{2E}\right)\right],$$

where m, β, and r_0 are the rest energy, velocity, and classical radius of the electron; ϵ and ϵ_m are the energy and maximum energy transferred to the electron by collision with the muon; E is the muon energy; $\mathbf{P}_e$ and $\mathbf{P}_\mu$ are the electron and muon polarization vectors. It is seen from this formula that σ_1/σ_0, the relative magnitude of the cross section that is sensitive to the polarization, will be noticeable, if large energy transfers to electrons colliding with high-energy muons are separated out. This can be done by registering δ cascades with specified number of particles, produced by muons in magnetized iron.

The probability of a cascade with more than n electrons being produced by a polarized muon in magnetized iron can be calculated from cascade theory:[1]

$$b(E, n) = \int_0^{\varepsilon_m(E)} f(\varepsilon, n)\,\sigma(E, \varepsilon)\,d\varepsilon$$

$$= b_0(E, n) + \mathbf{P}_e \mathbf{P}_\mu b_1(E, n),$$

where $f(\epsilon, n)$ is the probability of producing a cascade with more than n particles by a δ electron of energy ϵ, and b_0, b_1 are the polarization-sensitive and polarization-insensitive probability of cascade occurrence.

To obtain a specified accuracy in the measurement of muon polarization it is necessary to register, in minimum time, such cascade in which the number of particles is greater $n_0 = n_0(E)$, a value at which the expression $b_1(E, n)/\sqrt{b_0(E, n)}$ has a maximum.

We give here the values of b_0 and $P_e b_1/b_0$ at 8% polarization of electrons in magnetized iron, as a function of the muon energy, for cascades with more than n_0 particles

$E_{\text{Bev}}^{-1} =$	1.8	3.3	4.6	6.5	8.7	12
$n_0 =$	1	2	3	4	5	6
$P_e b_1/b_0 =$	2.6%	2.8%	3.0%	3.0%	3.0%	3.0%
$10^2 b_0 =$	8.6	7.5	6.6	6.6	6.6	6.6

If we register δ cascades with more than n_0 particles, produced in iron magnetized along and opposite the direction of motion of muons in an accelerator beam, then, to measure muon polarization with 30% accuracy at $P_\mu = 100\%$, it is necessary to have 1.5×10^6 muons pass through the apparatus.

The proposed method can also be used to measure the chirality of muons from cosmic rays. If the muons are not separated by energies, but by sign, the probability of producing a shower with more than n cosmic muons can be found as

$$b(n) = \int_0^{\varepsilon_m(E)} \int_E^\infty f(\varepsilon, n)\, S(E)\, \sigma(E, \varepsilon)\, d\varepsilon dE$$

$$= b_0(n) + P_e P_\mu b_1(n),$$

where $S(E)\,dE$ is the muon spectrum.

We give here the values of b_0 and $P_e b_1/b_0$ for $P_e = 8\%$ as a function of the number of particles in the registered shower:

$n =$	1	2	4	6
$b_0 =$	$2.2 \cdot 10^{-2}$	$5.8 \cdot 10^{-3}$	$1.4 \cdot 10^{-3}$	$6.4 \cdot 10^{-4}$
$P_e b_1/b_0 =$	1.4%	2.1%	3.0%	3.3%

If the aperture ratio of the apparatus is such that it transmits $\sim 10^3$ muons per minute with polarization $P_\mu > 30\%$, approximately 30 days

of measurement would be needed for the performance of the experiment.

We are grateful to V. B. Berestetskiĭ for discussions.

[1] S. Z. Belen'kiĭ, Лавинные процессы в космических лучах, (Cascade Processes in Cosmic Rays), M-L, 1948.

Translated by J. G. Adashko
262

CORRECTION TO THE PAPER BY V. Ya. EĬDMAN "RADIATION OF AN ELECTRON MOVING IN A MAGNETO-ACTIVE PLASMA"

Submitted to JETP editor January 10, 1959

J. Exptl. Theoret. Phys. (U.S.S.R.) **36**, 1335-1336 (April, 1959)

In a paper of the author by this title J. Exptl. Theoret. Phys. (U.S.S.R.) **34**, 131, 1958, Soviet Phys. JETP **7**, 91 (1958) the normalization of the polarization vector $\mathbf{a}_{j\lambda}$ has not been carried out completely. These vectors should be written in the form:

$$\mathbf{a}_{j\lambda} = \zeta_j \{1/\sqrt{2};\ i\alpha_j/\sqrt{2};\ i\beta_j/\sqrt{2}\},$$

where

$$\zeta_j^2 = 2n_{j\lambda}^2 \Big/ \Big[\Big(1-\frac{V}{1-u}\Big)(1+\alpha_j^2) + (1-V)\beta_j^2 - \frac{2V\sqrt{u}}{1-u}\alpha_j\Big],$$

$$\alpha_j = K_j \cos\theta + \gamma_j \sin\theta;\quad \beta_j = -K_j \sin\theta + \gamma_j \cos\theta;$$

$$K_j = \frac{2\sqrt{u}\,(1-V)\cos\theta}{u\sin^2\theta \mp \sqrt{u^2\sin^4\theta + 4u\,(1-V)^2\cos^2\theta}},$$

$$\gamma_j = \frac{V\sqrt{u}\,\sin\theta + K_j u V \cos\theta \sin\theta}{1-u-V\,(1-u\cos^2\theta)}.$$

Taking account of the above correction leads to the appearance of the factor ζ_j in Eq. (7) and the factor $|\zeta_j|^2$ in Eqs. (10), (12) – (17), (24), (25) and the formula following Eq. (22). Hence the last equation in the paper should contain the factor $|\zeta_1|^2/|\zeta_2|^2$. Furthermore, in addition to the expression for W_{1j} [Eq. (24)], we must introduce the expression

$$W_{-1j} = \frac{Te^2\omega_{-1}^2\, d\Omega\,[v_1(-1+\alpha_j) - \beta_j\omega_{-1}n_{j\lambda}r_0\beta_2\sin\theta]^2\,|\zeta_j|^2}{16\pi c^3\,|\,1-\beta_2\cos\theta\,(n_{j\lambda}+\omega_{-1}\partial n_{j\lambda}/\partial\omega)\,|},$$

$$\omega_{-1} = \frac{\Omega_0}{|1-\beta_2 n_{j\lambda}\cos\theta|}.$$

Translated by H. Lashinsky
263

SOVIET PHYSICS JOURNALS

Published in English by the American Institute of Physics

Soviet Physics – JETP

A translation, beginning with 1955 issues of "Journal of Experimental and Theoretical Physics" of the USSR Academy of Sciences. Leading physics journal of Soviet Union. Similar to "The Physical Review" in quality and range of topics. Outstanding new work is most likely to appear in this journal.

Twelve issues, approximately 3,500 pages. $75 domestic, $79 foreign. Libraries $35 domestic, $39 foreign. Single copies, $8.*

Soviet Physics – SOLID STATE

A translation, beginning with 1959 issues of "Fizika Tverdogo Tela" of the USSR Academy of Sciences. Offering results of theoretical and experimental investigations in the physics of semiconductors, dielectrics, and on applied physics associated with these problems. Also publishes papers on electronic processes taking place in the interior and on the surface of solids.

Twelve issues, approximately 2,000 pages. $55 domestic, $59 foreign. Libraries $25 domestic, $29 foreign. Single copies, $8.*

Soviet Physics – TECHNICAL PHYSICS

A translation, beginning with the 1956 issues of the "Journal of Technical Physics" of the USSR Academy of Sciences. Contains work on plasma physics and magnetohydrodynamics, aerodynamics, ion and electron optics and radio physics. Also publishes articles in mathematical physics, the physics of accelerators and molecular physics.

Twelve issues, approximately 2,000 pages, $55 domestic, $59 foreign. Libraries $25 domestic, $29 foreign. Single copies, $8.*

Soviet Physics – ACOUSTICS

A translation, beginning with 1955 issues of "Journal of Acoustics" of USSR Academy of Sciences. Devoted principally to physical acoustics but includes electro, bio, and psycho acoustics. Mathematical and experimental work with emphasis on pure research.

Four issues, approximately 400 pages. $12 domestic, $14 foreign. (No library discounts) Single copies, $4.

Soviet Physics – DOKLADY

A translation, beginning with 1956 issues of "Physics Sections" of Proceedings of USSR Academy of Sciences. All-science journal offering four-page reports of recent research in physics and borderline subjects.

Six issues, approximately 1,500 pages. $35 domestic, $38 foreign. Libraries $15 domestic, $18 foreign. Single copies Vols. 1 and 2, $5; Vol. 3 and later issues, $7.*

Soviet Physics – CRYSTALLOGRAPHY

A translation, beginning with 1957 issues of the journal "Crystallography" of USSR Academy of Sciences. Experimental and theoretical papers on crystal structure, lattice theory, diffraction studies, and other topics of interest to crystallographers, mineralogists, and metallurgists.

Six issues, approximately 1,000 pages. $25 domestic, $27 foreign. Libraries $10 domestic, $12 foreign. Single copies, $5.*

SOVIET ASTRONOMY – AJ

A translation, beginning with 1957 issues of "Astronomical Journal" of USSR Academy of Sciences. Covers various problems of interest to astronomers and astrophysicists including solar activity, stellar studies, spectroscopic investigations of radio astronomy.

Six issues, approximately 1,100 pages. $25 domestic, $27 foreign. Libraries $10 domestic, $12 foreign. Single copies, $5.*

Soviet Physics – USPEKHI

A translation, beginning with September, 1958 issue of "Uspekhi Fizicheskikh Nauk" of USSR Academy of Sciences. Offers reviews of recent developments comparable in scope and treatment to those carried in "Reviews of Modern Physics." Also contains reports on scientific meetings within the Soviet Union, book reviews, and personalia.

Six issues, approximately 1,700 pages. (Contents limited to material from Soviet sources.) $45 domestic, $48 foreign. Libraries $20 domestic, $23 foreign. Single copies, $9.*

*For libraries of non-profit degree-granting academic institutions.

Subscription prices subject to annual variation depending on size of Russian originals.

Please send orders and inquiries to

American Institute of Physics

335 East 45 Street, New York 17, N. Y.

CONTENTS

	Page	Russian Reference
Oscillations of a Plasma in a Magnetic Field at Frequencies Close to the Cyclotron Frequency ... V. N. Lazukin	685	36, 969
Structure of the Core and of the Central Region of An Extensive Air Shower at Sea Level ... S. N. Vernov, Ya. S. Babetskiĭ, N. N. Goryunov, G. V. Kulikov, Yu. A. Nechin, Z. S. Strugal'skiĭ, and G. B. Khristiansen	691	36, 976
Determination of Charged Particle Mass from Scattering and Residual Range in Multiplate Cloud Chambers ... F. R. Arutyunyan	697	36, 985
Lateral Distribution of the Energy Flux of the Electron-Photon Component of Extensive Air Showers ... V. A. Dmitriev, G. V. Kulikov, E. I. Massalskiĭ, and G. B. Khristiansen	702	36, 992
Determination of the Ionization Potential of Uranium by a Surface Ionization Method ... I. N. Bakulina and N. I. Ionov	709	36, 1001
Production of Strange Particles in the Interaction between 9-Bev Protons and Emulsion Nuclei ... N. I. Kostanashvili and O. A. Shakhulashvili	713	36, 1006
Measurement of the Neutron Half-life ... A. N. Sosnovskiĭ, P. E. Spivak, Yu. A. Prokof'ev, I. E. Kutikov, and Yu. P. Dobrynin	717	36, 1012
Low Energy Positrons from the $\mu^+ - e^+$ Decay ... A. O. Vaĭsenberg	722	36, 1019
Magneto-Optical Resonance in Nickel at Infrared Frequencies ... G. S. Krinchik and R. D. Nuralieva	724	36, 1022
Anomalous Electron Scattering and the Excitation of Plasma Oscillations ... M. D. Gabovich and L. L. Pasechnik	727	36, 1025
He^3 Cryostats ... V. P. Peshkov, K. N. Zinov'eva, and A. I. Filimonov	734	36, 1034
Measurement of the Resistance of High Purity Tin at Helium Temperatures ... V. B. Zernov and Yu. V. Sharvin	737	36, 1038
Millisecond Half-Life Isomers Produced in Reactions Involving 14-Mev Neutrons ... V. L. Glagolev, O. M. Kovrizhnykh, Yu. V. Makarov, and P. A. Yampol'skiĭ	742	36, 1046
Effect of Atomic Ordering on Exchange Interaction in the Fe_3Pt Alloy ... K. P. Belov and Z. D. Sirota	752	36, 1058
The Magnetization and Magnetocaloric Effect of Manganese Phosphide ... I. G. Fakidov and V. P. Krasovskiĭ	755	36, 1063
Interaction between $10^{11} - 10^{12}$ ev Particles and Iron Nuclei ... N. L. Grigorov, V. S. Murzin, and I. D. Rapoport	759	36, 1068
Observation of the $\pi \rightarrow e^- + e^+ + e^- + e^+$ Decay ... Yu. A. Budagov, S. Viktor, V. P. Dzhelepov, P. F. Ermolov, and V. I. Moskalev	767	36, 1080
Contribution to the Theory of Ferroelectric Polarization Curves ... N. S. Akulov	772	36, 1085
New Dispersion Relations in Quantum Field Theory ... L. A. Khalfin	774	36, 1088
Polarization in Pair Production by Circularly Polarized Quanta ... I. G. Ivanter	777	36, 1093
A New Class of Representations of the Full Lorentz Group ... G. A. Sokolik	781	36, 1098
Dispersion Relations and Chew-Low Type Equations for Inelastic Meson Processes in the Fixed Source Case ... W. Zoellner	784	36, 1103
Wall Probe in a Magnetic Field ... I. K. Fetisov	789	36, 1110
On the Analysis of High-Energy Showers ... Ya. I. Granovskiĭ and I. Ya. Chasnikov	795	36, 1119
Nuclear Forces and Levels of the Lithium Isotopes ... V. V. Balashov	798	36, 1123
On Radiative Transitions between Rotational Levels in Spin $\frac{1}{2}$ Nuclei ... D. F. Zaretskiĭ	803	36, 1129
Equation of State of a Plasma ... A. A. Vedenov and A. I. Larkin	806	36, 1133
On the Theory of Direct Nuclear Reations Involving Polarized Particles ... G. L. Vysotskiĭ and A. G. Sitenko	812	36, 1143
The Mass Spectrum of Mesons in Heisenberg's Theory ... Ya. I. Granovskiĭ	819	36, 1154
The Kinematics of Elementary Interactions ... N. G. Birger and Yu. A. Smorodin	823	36, 1159
Properties of the Spectrum of Elementary Excitations near the Disintegration Threshold of the Excitations ... L. P. Pitaevskiĭ	830	36, 1168
Absorption of μ^--Mesons by Polarized Nuclei. Angular Distribution of the Neutrons ... E. I. Dolinskiĭ	838	36, 1179
Excitation of Rotational Nuclear Levels by Charged Particles ... A. D. Piliya	843	36, 1185
Stability of a Plane Poiseuille Flow of an Ideally Conducting Fluid in a Longitudinal ... E. P. Velikhov	848	36, 1192
Effect of Impurities on the X-Ray Spectra of Transition Metals ... I. B. Borovskiĭ and K. P. Gurov	856	36, 1203

(Contents continued on inside back cover)

CONTENTS—continued

	Page	Russian Reference
A Nonlinear Vacuum Effect in Gravitation Theory . . . N. V. Mitskevich	859	36, 1207
Connection between Structural and Magnetic Parameters of the Transition Metals . . . F. M. Gal'perin	862	36, 1212
Empirical Regularities in the Nucleon Pair Production Energies in Nuclei . . . V. A. Kravtsov	871	36, 1224
Development of the Nuclear-Active Component of Extensive Atmospheric Showers . . . S. N. Vernov, E. V. Gorchakov, I. P. Ivanenko, and G. B. Khristiansen	877	36, 1233
Angular Distribution and Angular Correlation of the Radiations from Nuclei with Oriented Electron Shells . . . V. A. Dzhrbashyan	881	36, 1240
The Basic Compensation Equation in Superconductivity Theory when the Coulomb Interaction Is Taken into Account . . . Chen Chun-Sian and Chow Shih-Hsun	885	36, 1246
On the Theory of Weak Ferromagnetism . . . E. A. Turov	890	36, 1254
On the Superfluidity of a System of Polar Bose Excitations . . . S. V. Vonsovskiĭ and M. S. Svirskiĭ	894	36, 1259
Effect of Specimen Shape on Ferromagnetic Resonance in a Strong Radio-Frequency Field . . . G. V. Skrotskiĭ and Yu. I. Alimov	899	36, 1267
The Disintegration of Unstable Shock Waves in Magnetohydrodynamics . . . G. Ya. Lyubarskiĭ and R. V. Polovin	902	36, 1272
Anomalous Spinors and Bosons . . . A. M. Brodskiĭ and D. D. Ivanenko	907	36, 1279
The Green's Function Method in Quantum Statistics . . . E. S. Fradkin	912	36, 1286

LETTERS TO THE EDITOR

Beta Decay of Strange Particles . . . V. M. Shekhter	920	36, 1299
On the Rotation of the Plane of Polarization of Elastic Waves in a Magnetically Polarized Medium . . . K. B. Vlasov and B. Kh. Ishmukhametov	921	36, 1301
Simplification of the Formulas for Statistical Weight Calculations . . . Ya. I. Granovskiĭ	923	36, 1303
Statistical Electron Capture Mechanism in Betatrons . . . M. Seidl	924	36, 1305
Anisotropy of the Absorption of Ultrasound in Metals in a Magnetic Field . . . A. A. Galkin and A. P. Korolyuk	925	36, 1307
Ranges of Mu-Mesic Atoms in Hydrogen Chambers . . . S. S. Gershteĭn	927	36, 1309
Fluctuations of Atomic Structures in Liquid Helium . . . V. K. Prokhorenko and I. Z. Fisher	928	36, 1311
Direct Proof of the Applicability of the Massey Adiabatic Criterion to Processes of Double Charge Exchange . . . Ya. M. Fogel', V. F. Kozlov, A. A. Kalmykov, and V. I. Muratov	929	36, 1312
Electron-Neutrino Angular Correlation in the Beta Decay of the Free Neutron . . . Yu. V. Trebukhovskiĭ, V. V. Vladimirskiĭ, V. K. Grigor'ev, and V. A. Ergakov	931	36, 1314
The Permanent Structure of Shock Waves with Joule Dissipation . . . V. A. Belokon'	932	36, 1316
The K_{e3} and $K_{\mu 3}$ Decays . . . S. G. Matinyan and L. B. Okun'	933	36, 1317
Nucleon Interaction Cross Sections at 9 Bev Energy . . . V. S. Barashenkov and Huang Nen-Ning	935	36, 1319
Beta-Interaction and Nucleon Formfactor . . . V. B. Beresteskiĭ and I. Ya. Pomeranchuk	936	36, 1321
Geodesics in Friedman-Lobachevsky Space . . . I. G. Fikhtengol'ts	937	36, 1322
On the Production of Pion and Muon Pairs by the Annihilation of High-Energy Positrons . . . A. I. Nikishov	937	36, 1323
On Pair Production by the Collision of Two Circularly Polarized Gamma-Ray Quanta . . . F. S. Sadykhov and B. K. Kerimov	938	36, 1324
On the Mechanism of the Leptonic Decay of Hyperons . . . V. V. Turovtsev	939	36, 1326
Asymmetry of Angular Distribution of $\mu^+ \rightarrow e^+$ Decay Electrons in a 27,000 Gauss Magnetic Field . . . C. A. Ali-Zade, I. I. Gurevich, Yu. P. Dobretsov, B. A. Nikol'skiĭ, and L. V. Surkova	940	36, 1327
Broadening of Spectral Lines in Strongly Ionized Plasma . . . M. A. Mazing and S. L. Mandel'shtam	941	36, 1329
Electronic Paramagnetic Resonance Spectra of Frozen OH Radicals . . . S. D. Kaĭtmazov and A. M. Prokhorov	944	36, 1331
On Electron Oscillations in a Plasma . . . A. A. Zaĭtsev, G. S. Leonov, and I. A. Savchenko	944	36, 1332
Possibility of Determining the Chirality of the Muon by Means of δ-Electron Cascades from Magnetized Iron . . . A. I. Alikhanov and V. A. Lyubimov	946	36, 1334
Correction to the Paper by V. Ya. Eĭdman "Radiation of an Electron Moving in a Magneto-Active Plasma"	947	36, 1335